THE JOURNAL
OF
CHEMICAL PHYSICS

VOLUME 21, NUMBER 9 SEPTEMBER, 1953

A Model of Metal-Ammonia Solutions, with Reference to Electron Spin Resonance Experiments

J. KAPLAN AND C. KITTEL
Department of Physics, University of California, Berkeley, California
(Received May 28, 1953)

An explanation is given of the extreme sharpness of the electron spin resonance line in solutions of potassium in liquid ammonia, as reported by Hutchison and Pastor. Motional narrowing of the width associated with dipolar and hyperfine interactions results from the rotation and diffusion of ammonia molecules. The model of metal-ammonia solutions used in the calculation is shown to be supported by thermal, magnetic, volumetric, and conductivity data. The model pictures the electrons removed from the potassium atoms as located in cavities in the liquid, the cavities having approximately the volume of two to four ammonia molecules. The electrons in the cavities are in equilibrium with respect to the reaction $2e \rightleftarrows e_2 + 0.2$ ev, where e_2 represents two electrons in a singlet state in one cavity. The electrons in cavities may perhaps be thought of as in molecular orbital states on the protons of the adjacent NH_3 molecules.

I. INTRODUCTION

SOLUTIONS of potassium in liquid NH_3 have, according to Hutchison and Pastor,[1] the sharpest electron spin resonance line ($\sim$0.02 oe) yet reported for a liquid or solid; this characteristic promises to be useful for the calibration of magnetic fields, particularly below 1000 oe. We consider in the present paper the origin of the line width in these solutions. The major part of the investigation is concerned actually with the development of a satisfactory physical model of metal-ammonia solutions, as there has not been general agreement on the nature of the solutions.[2,3] It turns out to be quite possible to substantiate a well-defined model which accounts at least approximately for the outstanding features of these remarkable solutions. The model has been proposed in all essentials previously; some of the details go back to the work of Kraus and others are due to Ogg. Our contribution is to exhibit fully the compatibility of this particular model with the experimental data and to apply the model to the resonance results. The model, as illustrated by Fig. 1, has these central features: (A) The potassium atoms are ionized in solution. (B) The electrons removed from the potassium atoms are located in cavities in the liquid, the cavities having approximately the volume of two to four ammonia molecules. (C) The electrons in the cavities are in equilibrium with respect to the following reaction, where e_2 represents two electrons in a singlet state (antiparallel spins) in one cavity:

$$2e \rightleftarrows e_2 + 0.2 \text{ ev}; \qquad (1)$$

that is, the dissociation energy of a cavity containing two electrons (e_2 center) with respect to two cavities containing one electron each (e centers) is 0.2 ev. (D) The electrons associated with cavities may be thought of as in molecular orbital states on the protons of the NH_3 molecules adjacent to the cavities. (E) There is a conduction band about 1 ev above the cavity states.

In Sec. II below we review the salient features of the existing experimental data on alkali metal solutions in NH_3, indicating the connection between the data and the assumed properties of our model. The spin resonance data are discussed in Sec. III.

II. SUMMARY OF EXPERIMENTAL FACTS

Detailed reviews of the physical properties of metal-ammonia solutions are given by Kraus[4] and by Yost

[1] C. A. Hutchison, Jr. and R. C. Pastor, Phys. Rev. **81**, 282 (1951); Revs. Modern Phys. **25**, 285 (1953); see also M. A. Garstens and A. H. Ryan, Phys. Rev. **81**, 888 (1951); Levinthal, Rogers, and Ogg, Phys. Rev. **83**, 182 (1951).
[2] S. Freed and N. Sugarman, J. Chem. Phys. **11**, 354 (1943); E. Huster, Ann. Physik **33**, 477 (1938).
[3] R. A. Ogg, J. Chem. Phys. **14**, 114, 295 (1946); J. Am. Chem. Soc. **68**, 155 (1946).
[4] C. A. Kraus, J. Franklin Inst. **212**, 537 (1931); *The Properties of Electrically Conducting Systems* (Chemical Catalog Company, New York, 1922).

and Russell.[5] We limit the present summary to the properties of dilute solutions directly related to the specification of a model.

(1) The volume of a dilute solution of an alkali metal in liquid ammonia is greater than the sum of the volume of the constituents by about $72A^3$ per alkali atom.[6] To estimate the volume associated with an electron in the solution, we should add to this the difference, for sodium, of $36A^3$ between the atomic volume of metallic sodium and the sodium ion. Lipscomb suggests that we should add also about $35A^3$ for the electrostrictive effect of the Na^+ ion, whereby the neighboring solution is squeezed together about the Na^+ ion. It seems clear that there is a volume of the order of 100 to $150A^3$ associated with each electron stripped from the alkali atom on entering into solution. The volume associated with an NH_3 molecule is $41A^3$, so that the electron displaces perhaps 2 to 4 NH_3 molecules. Hutchison and Pastor[1] have pointed out that the paramagnetic part of the susceptibility of the solutions (as deduced from the intensity of the spin resonance line) agrees within the experimental error with that part of the total static susceptibility which may be attributed to the solute.

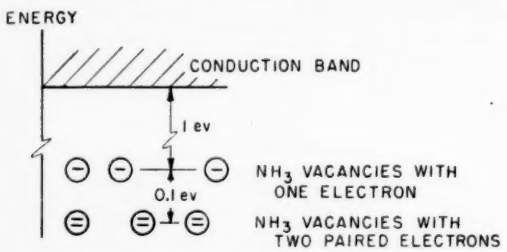

FIG. 1. Proposed energy level diagram of metal-ammonia solutions. Two e centers are formed in the decomposition of one e_2 center, with an energy difference of 0.2 ev.

This places an upper bound on the diamagnetic susceptibility of the e and e_2 centers. Estimating the experimental error at 50×10^{-6} per mole, the radius of a cavity containing one or two electrons must be not greater than about $4A$, in agreement with Lipscomb's volume estimate.

(2) The electrical conductivity of the solutions is almost entirely independent of the particular alkali metal used as solute, and the slight differences in conductivity which do exist are probably caused by differences in the contribution of the alkali ions. The mobility of the electrons is close to the general order of magnitude of ionic mobilities and is definitely not compatible with electronic mobilities in a conduction band. At low concentrations the equivalent conductance of the electrons is reported by Kraus as about 1000 mhos, so that the mobility is

$$\mu\approx1000/(6\times10^{23})(1.6\times10^{-19})\cong0.01 \text{ cm}^2/\text{volt-sec}.$$

The minimum mobility expected for untrapped thermal electrons in a conduction band would be determined by taking a minimum mean free path of the order of $1A$, as there is no plausible mechanism in a conduction band which would lead to a shorter mean free path. Thus, near the boiling point

$$\mu_{\min}\approx e\Lambda/mv\approx(5\times10^{-10})(10^{-8})/(10^{-27})(10^7)(300)$$
$$\approx2 \text{ cm}^2/\text{volt-sec}.$$

It is seen that the observed mobility is smaller by a factor of the order of 10^2 than the smallest mobility which might be reasonably associated with an electron in a conduction band. This suggests that we are concerned here with ionic type conduction processes, rather than conduction band processes.

We support this viewpoint by a rough estimate of the mobility which would result from one electron trapped in a mobile cavity in liquid ammonia. We make the estimate by the use of Stokes' law, supposing the liquid flows relative to the cavity. At low concentrations we have to deal largely with e centers, rather than e_2 centers: this follows from mass action considerations, as will be seen below. Then

$$eE=6\pi\eta Rv, \tag{2}$$

where η is the viscosity, R the radius of the cavity, and v the drift velocity of the cavity. The mobility is

$$\mu=e/6\pi\eta R\approx(5\times10^{-10})/(19)(0.0025)(3\times10^{-8})(300)$$
$$\approx0.001 \text{ cm}^2/\text{volt-sec},$$

using $\mu=0.0025$ poise as the viscosity at the boiling point (-33°C) and taking $R=3A$. This estimate gives a result smaller than the observed value by a factor of ten; one should not be surprised at the difference as it may be supposed plausibly that an e center permits much easier passage of ammonia molecules than is characteristic of the bulk solution; a lowering of the ammonia barrier energy by a factor of about two is all that is needed to account for the estimate, and such a change is quite reasonable; further, we should not expect Stoke's law to be accurate at atomic dimensions. At low concentration the mobility is observed to increase with increasing temperature, in agreement with the experimental results. At concentrations greater than about one molar the electrical conductivity increases very rapidly with increasing concentration. There is every indication that in the high-concentration region the conductivity mechanism is of the type normally associated with electrons. At one molar the average spacing of the electron centers is of the order of only $10A$; this is small enough to permit conductivity by tunneling of an electron from one center to an adjacent center. The process has been discussed by L. Farkas.[7] A saturated solution (≈5 mole l^{-1}) of K in NH_3 solution at the boiling point has a conductivity of 4500 mhos, corresponding to a mobility of 10 cm^2/volt-sec; this is

[5] D. M. Yost and H. Russell, *Systematic Inorganic Chemistry* (Prentice-Hall, Inc., New York, 1944), p. 136.

[6] The volume increase is discussed in detail by W. N. Lipscomb, J. Chem. Phys. **21**, 52 (1953).

[7] L. Farkas, Z. physik. Chem. **A161**, 355 (1932).

compatible with a conduction band mechanism in a disordered solid. The onset of conduction band processes at high concentrations are reminiscent of the sudden changes which occur in doped silicon and germanium as the impurity concentration is increased.

(3) The magnetic susceptibility per mole of alkali metal in solution is strongly dependent on the concentration of the solution, even at such low concentrations that exchange effects cannot be significant (Fig. 2). The susceptibility per mole of solute is higher at low concentrations than at high concentrations, in agreement with the law of mass action for the reaction Eq. (1). The susceptibility decreases as the temperature is lowered, suggesting that the e_2 centers are in singlet states (paired spins) and are lower in energy than the the e centers.

The concentration dependence of the susceptibility may be understood quantitatively in the following way: The susceptibility per atom of solute is given by

$$\chi_A = n_1\mu_B^2/nkT, \tag{3}$$

where n_1 is the number of e centers and n the number of solute atoms. The problem of the determination of n_1 is solved in the Appendix, Eq. (A.1). For concentrations low enough so that n may be neglected in comparison with the total number N of potential lattice sites, but high enough so that most of the e_2 centers are not ionized, we have

$$n_1 \cong (Nn)^{\frac{1}{2}} e^{-W/kT}. \tag{4}$$

Then

$$\chi \cong \left(\frac{N}{n}\right)^{\frac{1}{2}} \frac{\mu_B^2 e^{-W/kT}}{kT}, \tag{5}$$

so that the atomic susceptibility is inversely proportional to the square root of the concentration of solute atoms. The experimental results plotted in Fig. 2 are seen to be in general accord with the theoretical expectation. The agreement is a quite good test of the features of the present model. The best fit is obtained for $W=0.1$ ev or $2W=0.2$ ev. Calorimetric measurements by Coulter[8] *et al.* give $2W \approx 0.2 \pm 0.05$ ev, in satisfactory agreement with our analysis of the susceptibility variation.

(4) Jolly[9] has found a strong absorption in sodium-ammonia solutions at 1.5 microns (0.8 ev). He interprets the absorption as arising from the ionization of an e_2 center, one of the electrons being excited to a conduction band in the solution. This suggestion seems quite plausible, although he has not actually shown that the excited state permits easy conductivity.

III. INTERPRETATION OF SPIN RESONANCE RESULTS

We are concerned here primarily with the interpretation of the width of the spin resonance line in metal ammonia solutions, although the sign of the g shift follows correctly from our model. The general idea is that at low concentrations the line width is caused by motionally narrowed hyperfine interactions of the e-center electron with the nuclei of the molecules which border the vacancy. The problem is somewhat similar to the problem of spin resonance line widths in colored alkali halide crystals; there it is known[10] that hyperfine interactions account for the width of the resonance line, but there is no motional narrowing.[11]

The N–H bond is partly ionic, with the nitrogen negatively charged and the hydrogen positively charged. It is likely for electrostatic reasons that the protons are more important in the formation of the e centers than are the nitrogen ions; further, the magnetic moment of N^{14} is only about 15 percent of the magnetic moment of the proton, and there are three protons for every nitrogen nucleus. It is evident that we may neglect the

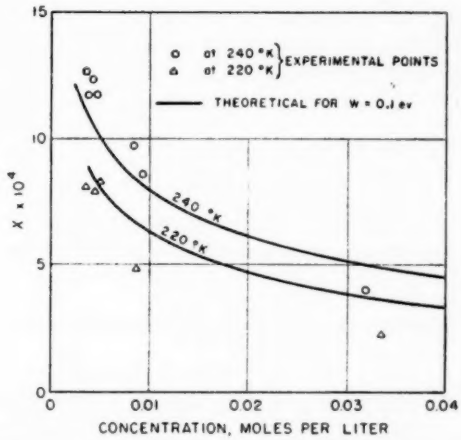

FIG. 2. Experimental magnetic susceptibility of potassium-ammonia solutions as a function of concentration compared with the calculated susceptibility using the law of mass action and the Langevin equation. The susceptibility per mole of solute is given. The experimental data have been corrected for the diamagnetism of the solvent (Hutchison and Pastor, reference 1).

influence of the nitrogen nuclei on the line width. We may perhaps think of the e-center electron as in a molecular orbital state on the P protons adjacent to the cavity:

$$\Psi = P^{-\frac{1}{2}} \sum_{i=1}^{P} \psi_i, \tag{6}$$

where P may be of the order of 50, and ψ_i may resemble a $1s$ atomic orbital on the ith proton, but with strong mixtures of higher states because of electrostatic polarization effects.[12] As with F centers, the g value is expected to be slightly less than the free electron value;

[8] Coulter, Wolsky, Zdanuk, and Monchick; Abstract 101, page 50P, 119th meeting American Chemical Society, 1951.
[9] W. L. Jolly, University of California Radiation Laboratory Report No. UCRL-2008 (1952), unpublished.
[10] Kip, Kittel, Levy, and Portis, Phys. Rev. (to be published).
[11] The theory of motional narrowing is due to Bloembergen, Purcell, and Pound, Phys. Rev. **73**, 679 (1948); see also J. H. Van Vleck, Phys. Rev. **74**, 1168 (1948); P. W. Anderson and P. R. Weiss, Revs. Modern Phys. **25**, 269 (1953).
[12] A. H. Kahn and C. Kittel, Phys. Rev. **89**, 315 (1953).

this is the observed direction, as reported by Hutchison and Pastor ($\Delta g \approx -0.001$). We shall introduce later the rotational motion of the NH_3 molecules, but if we were to introduce molecular motion at this stage the wave function would be time-dependent and would be written as

$$\Psi(t) = (P')^{-\frac{1}{2}} \sum_{i=1}^{P'} \psi_i(t), \tag{7}$$

the sum including perhaps twice the number of protons included in Eq. (6).

We first make an estimate of the contribution of hyperfine interactions to the line width on the assumption that the neighboring ammonia molecules are frozen rigidly in place; we shall later have to correct this estimate for the effects of motional narrowing. The s components of the ψ_i are the components principally effective in the hyperfine interaction. We denote the fractional effective s character of ψ_i by ξ, in the sense that in the solution the value of $|\psi_i|^2$ at a proton is equal to ξ times the free hydrogen atom value

$$|\psi(0)|^2 = \frac{1}{\pi a_H{}^3} = 2.1 \times 10^{24} \text{ cm}^{-3}, \tag{8}$$

for the $1s$ state. The mean square width follows from Eq. (6) above and from Eq. (13) of reference 10:

$$\langle (\Delta H)^2 \rangle_{\text{Av}} = \frac{64\xi^2}{9P} \cdot \frac{\mu_p{}^2}{a_H{}^6} = \frac{\xi^2}{N} (94)^2 \text{ oersteds}^2. \tag{9}$$

If we take the number of neighboring protons $P \approx 50$,

$$\langle \Delta H \rangle_{\text{rms}} \approx 13\xi \text{ oersteds}. \tag{10}$$

When the perturbation responsible for the line width fluctuates with a characteristic frequency ω_e considerably higher than the calculated static width $\Delta\omega_0$, the actual line width $\Delta\omega$ may be estimated by the following prescription:[11]

$$\Delta\omega = (\Delta\omega)_0{}^2/\omega_e. \tag{11}$$

In terms of magnetic fields,

$$\Delta H \approx (\Delta H)_0{}^2/H_e. \tag{12}$$

In the present problem ω_e may be estimated from the Debye relation for rotational dipolar relaxation:

$$\omega_e \approx kT/3\eta V, \tag{13}$$

where V is the volume of the molecule which is supposed to be spherical. In this way we estimate

$$\omega_e \approx 1.1 \times 10^{11} \text{ radians/sec}, \tag{14}$$

for ammonia at the boiling point. Direct dielectric measurements of the relaxation frequency do not appear to be available; in any event it is not clear to what extent Eq. (13) may be applicable to the molecules adjacent to a cavity. The magnetic field equivalent to Eq. (14) is

$$H_e \approx 6 \times 10^3 \text{ oersteds}. \tag{15}$$

Thus, combining Eqs. (10), (11), and (15), we have

$$\Delta H \approx 0.03\xi^2 \text{ oersteds}. \tag{16}$$

This result is of the correct order of magnitude, taking $\xi^2 \approx 1$. The experimental width at low concentrations is about 0.025 oersted at 28°C and 0.05 oersted at the boiling point (−33°C), according to Hutchison and Pastor. The width is expected on this model to vary with temperature inversely as the relaxation frequency; this is roughly the observed behavior. The inversion motion of the NH_3 pyramid may reduce the temperature dependence. It would be reasonable to expect $\xi \approx \frac{1}{2}$ and to expect that the effective viscosity for molecular rotation to be greater than the bulk viscosity because of the polarizing effect of the e center on the molecules. These two changes affect the width in opposite directions and tend to cancel each other.

We do not propose that the detailed numerical results of the line-width calculation are to be taken very seriously: there are too many imperfectly known quantities entering the calculation—the effective number of neighbors, the s character of the atomic orbitals, and the effective viscosity—for the final result to have any significance other than as a qualitative explanation of the unusual sharpness of the observed line. It should be possible by investigation of the line width in dilute solutions of potassium in deuterated ammonia to check the proposed explanation. The deuteron magnetic moment is only about 0.3 of the proton magnetic moment, so that the line should be significantly sharper, unless differences in motional narrowing work the other way. Because of the differences in the moment of inertia of NH_3 and ND_3 the line widths should probably be compared at temperatures such that the dielectric relaxation frequencies are equal in NH_3 and ND_3. The inversion frequency in ND_3 is less than 0.1 that in NH_3; this will tend to broaden the spin resonance line in the ND_3 solutions.

We must consider finally the possible effects on the line width of magnetic dipolar interactions among the e-centers. Abrahams and Kittel[13] find for N electrons per cm^3 distributed at random on a simple cubic lattice,

$$\Delta H_0 \approx N \times 10^{-19} \text{ oersted}.$$

The measurements of Hutchison and Pastor go down to about 0.01 mole l^{-1}; at this point $N \approx 6 \times 10^{18}$ per cm^3, so that $\Delta H \approx 0.6$ oersted, which is considerably wider than the observed line. Here again, however, it is necessary to take account of motional narrowing. The rapid diffusion of e centers will reduce the line width. The magnitude of the final line width in these circumstances may be taken from an estimate by Bloembergen,

[13] C. Kittel and E. Abrahams, Phys. Rev. **90**, 238 (1953).

Purcell, and Pound,[11] with appropriate changes:

$$\Delta H = 3\pi g^3 \mu_B{}^3 N/20aD. \tag{17}$$

Here the diffusion coefficient D is to be calculated from the observed mobility using the Einstein relation $\mu kT = eD$, and a is the cavity radius. For 0.01 mole l^{-1}, we have $\Delta H \approx 3\times 10^{-3}$ oersted. This result shows that dipolar interactions are not important below concentrations of the order of 0.1 mole l^{-1}; the observed increase in width above this concentration may be ascribed plausibly to dipolar interactions.

ACKNOWLEDGMENT

We are greatly indebted to Professor C. A. Hutchison, Jr. for advance communication and discussion of his results. Dr. W. L. Jolly has kindly discussed with us the general status of experiments on liquid ammonia solutions, and Professor R. A. Ogg has contributed to our interest in the problem. This research has been supported in part by the U. S. Office of Naval Research.

APPENDIX

We give a brief derivation of the equilibrium concentrations for the reaction $2e \leftrightarrows e_2 + 2W$. We suppose that $n = n_1 + 2n_2$ electrons are distributed on N potential lattice sites, with n_1 electrons forming e centers and n_2 pairs of electrons forming e_2 centers. The number of arrangements of n_1+n_2 electrons one to a site is

$$\frac{N!}{(n_1+n_2)!(N-n_1-n_2)!}.$$

The number of arrangements of n_2 electrons one to a site already singly populated is

$$(n_1+n_2)!/n_1!n_2!.$$

The number of spin arrangements is 2^{n_1}. The total number of arrangements is given by the product of these three factors:

$$\frac{N!2^{n_1}}{n_1!n_2!(N-n_1-n_2)!}.$$

Using the Stirling approximation, the entropy is

$$S/k = n_1 \log 2 + N \log N - n_1 \log n_1 - n_2 \log n_2 - (N-n_1-n_2)\log(N-n_1-n_2).$$

The free energy $F = U - TS$ is given by

$$F = n_1 W - kT[n_1 \log 2 + N \log N - n_1 \log n_1 - \tfrac{1}{2}(n-n_1)\log \tfrac{1}{2}(n-n_1) - (N-\tfrac{1}{2}n-\tfrac{1}{2}n_1)\log(N-\tfrac{1}{2}n-\tfrac{1}{2}n_1)].$$

This is a minimum with respect to n_1 when

$$W = kT[\log 2 - \log n_1 + \tfrac{1}{2}\log \tfrac{1}{2}(n-n_1) + \tfrac{1}{2}\log(N-\tfrac{1}{2}n-\tfrac{1}{2}n_1)],$$

so that we have the result

$$\frac{n_1{}^2}{(n-n_1)(2N-n-n_1)} = e^{-2W/kT}, \tag{A.1}$$

which may be written at low concentrations as

$$n_1{}^2/n_2 N \cong e^{-2W/kT}. \tag{A.2}$$

On the Presence of Free Chlorine in Sodium Chloride Crystals Containing Color Centers and Color Center Precursors

MICHAEL HACSKAYLO,* DUMAS OTTERSON, AND PHILIP SCHWED
National Advisory Committee for Aeronautics, Lewis Flight Propulsion Laboratory, Cleveland, Ohio
(Received March 10, 1953)

Measurements have been carried out of the free chlorine content of NaCl crystals subjected to electrolysis before and after exposure to x-rays, as well as the free chlorine content of normal NaCl crystals after irradiation. It has been found that crystals which have not been irradiated contain no free chlorine, whereas those exposed to x-rays contain between 0.1 and 0.6 free chlorine atom per vacancy pair.

IN investigating the nature of such nonequilibrium states of alkali halide crystals as those associated with color centers and color center precursors,[1,2] it is obviously important to determine the chemical composition of the substance being studied. It is well known, for instance, that certain absorption bands in such crystals are related to the presence of small quantities of chemical impurities[3] or to a stoichiometric excess of the alkali metal.[4] More recently it has been shown that inducing color centers in a normal NaCl crystal by irradiation with x-rays changes its chemical behavior in such a fashion that a solution made by dissolving an irradiated crystal is more basic than one made by dissolving a normal crystal;[1,2] this, despite the fact that the total chemical composition of the two crystals is obviously the same. It was suggested that consequent to the rearrangement of the structure of the crystal connected with the formation of the color centers, the crystal, while dissolving, behaves as if it contained a certain number of free sodium atoms together with an equal number of free chlorine atoms instead of being composed entirely of the corresponding ions.[2] If this hypothesis is correct, it is significant not only with regard to the state of crystals colored by irradiation, but also for the interpretation of the amount of excess alkali found in crystals in other nonequilibrium states. We therefore decided to investigate whether any "free" chlorine was liberated upon the solution in water of NaCl crystals in various nonequilibrium states.

For this purpose we made use of a spectrophotometric method based upon the coloration[5] produced by the reaction between *o*-tolidine and free chlorine in aqueous solution. In every case the degree of coloration was measured by determining the optical absorption coefficient of the solution at 435 mμ with a Beckman Model B spectrophotometer. An indicator stock solution containing 0.1 percent (by weight) of *o*-tolidine in 0.1 N HCl was prepared. To determine the "free" chlorine content of a crystal, it was first weighed and then dissolved in 5 ml of distilled water. One ml of indicator stock solution was added and the total volume of the resulting solution brought up to 10 ml with distilled water. The measurement of optical density was then carried out. Preliminary experiments showed that no appreciable amount of chlorine was detected with the use of this method either in the

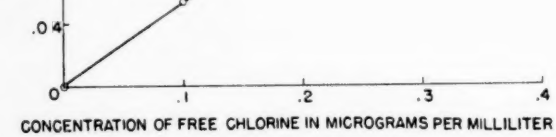

FIG. 1. Calibration curve for the spectrophotometric determination of free chlorine.

TABLE I. Amount of free chlorine and its relation to the number of vacancies for various states of NaCl crystals.

Color	Uncolored	Nonpermanently colored	Permanently and nonpermanently colored		Permanently colored
State	Metastable state	Irradiated in normal state	Irradiated in metastable state	Irradiated after being colored by electrolysis	Colored by electrolysis
Measured no. free Cl atoms/cm³ $\times 10^{-17}$	0	15±4	5.6±2	7.6±2	0
Vacancy pairs/cm² $\times 10^{-17}$	3.6±1	25±6	53±6	68±6	4.2±1
Ratio of free Cl atoms to vacancy pairs	...	0.6	0.1	0.1	...
Ratio of free Na atoms to vacancy pairs*	1.3	.12	.12	.19	2.3
Calculated no. free Na atoms/cm² $\times 10^{-17}$	4.6	3.0	6.1	13	9.9

* Taken from reference 2.

* Now at The Harshaw Chemical Company, Cleveland, Ohio.

[1] M. Hacskaylo, and G. Groetzinger, Phys. Rev. **87**, 789 (1952).
[2] M. Hacskaylo, and D. Otterson, J. Chem. Phys. **21**, 552 (1953).
[3] E. Rexer, Z. Physik **106**, 70 (1937).
[4] Z. Gyulai, Z. Physik **37**, 889 (1926).
[5] F. D. Snell and C. T. Snell, *Colorimetric Methods of Analysis* (D. Van Nostrand Company, Inc., New York, 1941), Vol. 1, pp. 538–539.

distilled water or in solutions of NaCl of the concentration used in our measurements when prepared from normal NaCl crystals. Since the indicator reaction is based on the oxidizing properties of the free chlorine, it was expected that the presence of free sodium would not affect the results. To verify this expectation, NaCl crystals containing a known excess of sodium were dissolved in distilled water at the usual concentrations and it was shown that no appreciable free chlorine could be detected by the indicator method. As a further check, an NaCl crystal containing a known excess of sodium was dissolved in a solution of known chlorine content and the chlorine concentration of the resulting solution was determined by this method. The result agreed to within 10 percent with that obtained for a sodium free solution of chlorine of the same concentration. In order to calibrate the method, a solution of hyperchlorous acid made by dissolving chlorine in distilled water at a concentration of around 0.04 N was standardized by titration of the iodine liberated upon addition of potassium iodide with standard thiosulfate.[6] By dilution of this solution, standards of known chlorine concentration were prepared and used in obtaining the curve of optical density versus concentration under the conditions employed here which is given in Fig. 1. This curve is linear within 10 percent.

Measurements of chlorine content were carried out for crystals irradiated with x-rays in the normal state, in the metastable state, and in the state resulting from coloration by electrolysis, as well as for crystals in the latter two states which had not been subjected to any irradiation. The number of additional vacancy pairs in these crystals was measured by the change of density method.[1] The results are shown in Table I which also contains the number of "free" chlorine atoms per additional vacancy pair, and for purposes of comparison, the number of "free" sodium atoms per additional vacancy pair found previously for crystals in various states.[2] Perhaps the most significant result is that there were found of the order of one chlorine and 0.1 sodium atom per vacancy pair in the case of normal NaCl crystals subjected to irradiation with x-rays. It thus appears that in this case most of the electrons trapped in negative vacancies do not return to the chlorine atom when the crystal is dissolved, and consequently, there is a "free" chlorine atom† for each F center. If this is correct, there should likewise be a "free" sodium atom for each F center. However, the method used to detect free sodium atoms depends upon the assumption that a hydroxyl radical is produced for each free sodium atom present in the crystal. In fact, a large proportion of the hydroxyls produced in this fashion are neutralized by the hydrogen ions resulting from the dissociation of the hypochlorous and hydrochloric acid produced when the "free" chlorine dissolves. A rough calculation shows that there should be about one unneutralized hydroxyl produced for each nine sodium atom-chlorine atom pairs dissolved. This is in fair agreement with the ratio 1:6 found experimentally.

Crystals subjected to electrolysis and thus brought into the metastable or electrolytically colored state show no "free" chlorine so that the amount of sodium found presumably represents the true excess above the stoichiometric quantity. Crystals subjected to irradiation after electrolysis contain, consequently, a true excess of sodium which is introduced by the electrolysis and which contributes to the measured free sodium. For this reason, the ratio of the number of free sodium atoms to the number of free chlorine atoms is much greater for such crystals than it is for crystals irradiated in the normal state.

Thanks are due Dr. Gerhart Groetzinger for valuable discussions.

[6] I. M. Kolthoff and E. B. Sandell, *Quantitative Inorganic Chemistry* (The Macmillan Company, New York, 1943), revised edition, p. 627.

† To show that the presence of the excess chlorine is connected with the coloration, crystals containing temporary color centers were annealed and the amount of free chlorine measured. None could be detected.

The Interaction with Molecular Rotation of the Nuclear Electric Quadrupole Moments of Two Nuclei Having Spins 3/2*

G. WILSE ROBINSON† AND C. D. CORNWELL‡
Department of Chemistry and Chemical Engineering, State University of Iowa, Iowa City, Iowa
(Received February 23, 1953)

The theory of nuclear electric quadrupole effects in molecules is applied to the particular case of a molecule containing two nuclei each having spin 3/2. The matrix elements of the first-order Hamiltonian of interaction between the nuclear electric quadrupole moments and the molecular rotational angular momentum are determined in the $I_1I_2IJFM_F$ representation. In one particular case the secular equations may be solved explicitly for the energy levels in terms of J, and the general solutions as well as their numerical values for $J \leqslant 12$ are given. For the other cases, higher-order secular equations must be solved, and to facilitate this, coefficients in the expanded secular determinants have been computed. The method for obtaining relative line strengths for transitions is described, and numerical values of these are given for some transitions. Applications to the analysis of rotational spectra are also discussed.

INTRODUCTION

THE theory of the interaction of the nuclear electric quadrupole moments of a single nucleus or of multiple nuclei with the molecular rotational angular momentum has been developed previously by a number of authors.[1–10] Molecules containing a single nucleus with quadrupole moment (spin $>\frac{1}{2}$) have been studied extensively in the microwave region of the spectrum, and a few molecules containing more than one such nucleus have also been studied.[11] Heretofore, however, there has been very little work done on molecules containing two identical or "nearly identical" nuclei of this type.[12,13] This may be partly owing to the fact that certain of the quadrupole computations are somewhat tedious, and because these molecules are generally asymmetric tops.

For the double nucleus problem, the $I_1JF_1I_2FM_F$ representation,[5] where

$$\boldsymbol{I}_1+\boldsymbol{J}=\boldsymbol{F}_1$$
$$\boldsymbol{F}_1+\boldsymbol{I}_2=\boldsymbol{F},$$

is the most convenient when the two nuclei have widely different coupling,§ since the smaller effect may be treated as a perturbation upon the larger. For two nuclei having identical coupling, however, the $I_1I_2IJFM_F$ scheme where

$$\boldsymbol{I}_1+\boldsymbol{I}_2=\boldsymbol{I}$$
$$\boldsymbol{I}+\boldsymbol{J}=\boldsymbol{F},$$

described first by Foley,[8] is the simplest to use since the secular equations factor into a symmetrical and an antisymmetrical part. For other cases, including the case of "nearly identical" coupling, which may arise in a molecule containing two isotopic nuclear species having identical spins, higher-order equations must be solved.

From a practical standpoint, a particularly interesting double-coupling problem is that where each nucleus has a spin of 3/2 since there is an abundance of interesting molecules of this type, and the secular equations are of sufficiently low order to be solved readily. The purpose of this paper then is to present the computed quantities necessary for the microwave study of molecules containing two nuclei having spins of 3/2. The $I_1I_2IJFM_F$ representation will be used throughout.

THE MATRIX ELEMENTS OF H_Q

The matrix elements of the Hamiltonian[14]

$$\begin{aligned}H_Q=&[(eQ_1\langle(\partial^2V/\partial z^2)_1\rangle_{Av})/2J(2J-1)I_1(2I_1-1)]\\&\times[3(\boldsymbol{I}_1\cdot\boldsymbol{J})^2+(3/2)(\boldsymbol{I}_1\cdot\boldsymbol{J})-I_1^2J^2]\\&+[(eQ_2\langle(\partial^2V/\partial z^2)_2\rangle_{Av})/2J(2J-1)I_2(2I_2-1)]\\&\times[3(\boldsymbol{I}_2\cdot\boldsymbol{J})^2+(3/2)(\boldsymbol{I}_2\cdot\boldsymbol{J})-I_2^2J^2],\end{aligned}\quad(1)$$

for the first-order interaction between the electric

* This paper is based in part on a thesis submitted by G. Wilse Robinson in partial fulfillment of the requirements for the degree of Doctor of Philosophy at the State University of Iowa. The work was made possible by the support extended the State University of Iowa by the U. S. Office of Naval Research under ONR contract N8onr-79400.

† Present address: Department of Chemistry, University of Rochester, Rochester, New York.

‡ Now at the University of Wisconsin, Madison, Wisconsin.

[1] H. B. G. Casimir, *On the Interaction Between Atomic Nuclei and Electrons* (Teyler's Tweede Genootschap, E. F. Bohn, Haarlem, 1936).

[2] Kellogg, Rabi, Ramsey, and Zacharias, Phys. Rev. **57**, 677 (1940).

[3] Dailey, Kyhl, Strandberg, Van Vleck, and Wilson, Phys. Rev. **70**, 984 (1946).

[4] D. K. Coles and W. E. Good, Phys. Rev. **70**, 979 (1946).

[5] J. Bardeen and C. H. Townes, Phys. Rev. **73**, 97 (1948).

[6] J. K. Bragg, Phys. Rev. **74**, 533 (1948).

[7] J. K. Bragg and S. Golden, Phys. Rev. **75**, 735 (1949).

[8] H. M. Foley, Phys. Rev. **71**, 747 (1947).

[9] R. Bersohn, J. Chem. Phys. **18**, 1124 (1950).

[10] M. Mizushima and T. Ito, J. Chem. Phys. **19**, 739 (1951).

[11] For a summary of experimental work prior to 1952 see P. Kisliuk and C. H. Townes, National Bureau of Standards Circular 518, June 23, 1952.

[12] R. J. Myers and W. D. Gwinn, J. Chem. Phys. **20**, 1420 (1952).

[13] G. W. Robinson, "The Microwave Spectrum of Phosgene" (to be published).

§ In this paper the term *coupling* refers to the quantity $eQ\langle\partial^2V/\partial z^2\rangle_{Av}$.

[14] See, for example, reference 5.

quadrupole moments Q_1 and Q_2 of two nuclei with the molecular rotational angular momentum J, may be obtained from the matrix elements of $I_1 \cdot J$ and $I_2 \cdot J$ given by Foley,[8] in conjunction with the rotationally dependent $eQ\langle \partial^2 V/\partial z^2 \rangle_{Av}$'s determined by the method of Bragg and Golden.[7] Here I_1 and I_2 are the nuclear spin angular momentum operators for the two nuclei, e is the electronic charge, and V is the electrostatic field produced at a nucleus by all charges external to that nucleus. z is a space-fixed axis and the average is taken over the rotational state in the representation which diagonalizes the rotational energy matrix. In the first-order problem, the matrix of H_Q is diagonal in $I_1 I_2 JF$ and M_F and, in the forthcoming discussion, these indexes will be dropped wherever possible. The elements $(I|H_Q|I)$ and $(I|H_Q|I\pm 2)$ originally given by Foley[8] for identical coupling have recently been corrected by Myers and Gwinn.[12] These elements were independently verified by the authors and, for the sake of completeness, have been repeated here in somewhat different form. The first off-diagonal elements $(I|H_Q|I\pm 1)$, not presented in any previous work and nonvanishing when the coupling is different, have also been determined.

For the purpose of discussing the matrix elements it is convenient to introduce the following quantities:

$$X^{\pm}=\tfrac{1}{2}[eQ_1\langle(\partial^2 V/\partial z^2)_1\rangle_{Av}\pm eQ_2\langle(\partial^2 V/\partial z^2)_2\rangle_{Av}], \quad (2)$$

$$R=X^-/X^+, \quad (3)$$

$$\Phi(I)=F(F+1)-J(J+1)-I(I+1), \quad (4)$$

$$\Psi(I)=\left[\frac{(2I_1+1)^2-I^2}{4I^2-1}\right](F+I-J)(F+J-I+1)\times(F+I+J+1)(I+J-F). \quad (5)$$

When $I_2=I_1$ the matrix elements may be written in the form

$$(I|H_Q|I)=\{X^+/J(2J-1)I_1(2I_1-1)\}\times\{(3/16)[\Phi^2(I)+\Psi(I)+\Psi(I+1)+2\Phi(I)]-I_1(I_1+1)J(J+1)\}, \quad (6)$$

$$(I|H_Q|I+1)=\{3X^+R/8J(2J-1)I_1(2I_1-1)\}\times\{\Psi^{\frac{1}{2}}(I+1)[\Phi(I)-I]\}=(I+1|H_Q|I), \quad (7)$$

$$(I|H_Q|I+2)=\{3X^+/16J(2J-1)I_1(2I_1-1)\}\times\{\Psi^{\frac{1}{2}}(I+1)\Psi^{\frac{1}{2}}(I+2)\}=(I+2|H_Q|I). \quad (8)$$

The other nonvanishing elements, $(I|H_Q|I-1)$ and $(I|H_Q|I-2)$ may be obtained from the above since the matrix is symmetrical. The matrix consists of $4I_1+1$ submatrices labeled by F; one of order $2I_1+1$ and two each of descending orders, except for $J<2I_1$, where some values of F are not possible.

Everything that has thus far been said about the matrix of H_Q may be applied to a problem involving any two nuclei of like spins. Substitution of $I_1=3/2$ into Eqs. (6), (7), and (8) gives the required matrix for the present problem. The values of the energy E are then found by diagonalizing this matrix. Since the quantity X^+ factors out of the total matrix, the energy may be written

$$E\epsilon_{JF}=X^+\lambda\epsilon_{JF}, \quad (9)$$

and the quantities $\lambda\epsilon_{JF}$ are the ones which will be ultimately tabulated. The quantity $\epsilon=0$, 1, 2, or 3 is a pseudo spin quantum number which, along with the quantum numbers F and J, labels the energy states. For identical coupling the labeling of states is unambiguous in some cases, but where it is not, the labeling is carried out in such a way that the approximate selection rule $\Delta\epsilon=0$ holds best. As long as the difference in coupling is not large the concept of ϵ is still useful, but for extreme nonidentical coupling the states are best labeled by F_1 and F of the $I_1 J F_1 I_2 F M_F$ representation. The correlation between the two schemes is shown in Table I. F is identical in both representations.

The following discussion treats the cases of identical and nonidentical coupling separately.

TABLE I. Correlation between the ϵJFM_F and the $I_1 J F_1 I_2 F M_F$ schemes for the case $I_1=I_2=3/2$.

ϵ	F	F_1	ϵ	F	F_1
3	$J+3$	$J+(3/2)$	3	$J-2$	$J-(3/2)$
3	$J+2$	$J+(1/2)$	3	$J-3$	$J-(3/2)$
3	$J+1$	$J+(1/2)$	2	$J+2$	$J+(3/2)$
1	$J+1$	$J+(3/2)$	2	$J+1$	$J-(1/2)$
3	J	$J-(1/2)$	2	J	$J+(3/2)$
1	J	$J-(3/2)$	0	J	$J+(1/2)$
3	$J-1$	$J-(3/2)$	2	$J-1$	$J-(1/2)$
1	$J-1$	$J+(1/2)$	2	$J-2$	$J-(1/2)$

Case I. Identical Coupling

In this case, $eQ_1\langle(\partial^2 V/\partial z^2)_1\rangle_{Av}=eQ_2\langle(\partial^2 V/\partial z^2)_2\rangle_{Av}$; the quantity X^- vanishes and the resulting matrix contains no first off-diagonal elements. The submatrices (seven for $I_1=I_2=3/2$) reduce to first and second order by rearrangement of rows and columns, and thus the energy levels may be obtained as explicit functions of J. These, as well as their numerical values for $J\leqslant 12$, are tabulated in Appendix I. The resulting first- and second-order submatrices lead to symmetric or antisymmetric levels depending upon whether $\epsilon=1$, 3 or $\epsilon=0$, 2, respectively. If the molecule exhibits a C_2 symmetry axis some of these levels may be actually missing, or as the case may be, their relative populations will depend upon the number of pairs of nuclei exchanged by the operation C_2. For example, in the molecule $COCl_2$ (C_{2v} symmetry) the two chlorines are exchanged by a rotation of 180° about the intermediate axis of inertia. The total wave function must be antisymmetric with respect to this operation. Thus, for a totally symmetric electronic-vibrational state, only symmetric nuclear levels exist for antisymmetric rota-

tional states; and, conversely, only antisymmetric nuclear levels exist for symmetric rotational states. In other molecules such as CH_2Cl_2 (C_{2v} symmetry) other pairs of nuclei with spin $\geqslant\frac{1}{2}$ may be exchanged in addition to the two nuclei of interest. In these cases no levels are missing but the relative populations of the levels are determined by the type of exchanged pairs. Of course if other nuclei having relatively large quadrupole moments are present in the molecule, the theory as presented here is not applicable.

Case II. Nonidentical Coupling

In this case X^- does not vanish and the matrix contains first off-diagonal elements which are functions of the rotationally dependent quantity R. The expanded secular equations will have the form

$$\sum_{j=0}^{n}\lambda^{n-j}(a_{n-j}{}^{F}+b_{n-j}{}^{F}R^2)=0, \tag{10}$$

where $n=1$, 2, 3, or 4; $a_n{}^F=1$; $b_n{}^F=0$. Except for $J<3$, there will be two equations of first order, two of second order, two of third order, and one of fourth order to be solved for each rotational state of interest. The first- and second-order equations may be solved explicitly in terms of J and R, and these roots have been listed in the first part of Appendix II. The solution of the third- and fourth-order equations may be carried out on a computer. Where a computer of the required type is not available, solution of the equations is facilitated by a table in Appendix II of the explicit forms of the JF dependent coefficients a^F and b^F. Numerical values of these for $J\leqslant 12$ have also been given in the second part of Appendix II. Experimentally determined values of R and X^+ for various rotational states are sufficient to determine the quadrupole coupling constants for each of the two nuclei.

The above results are applicable to any double-coupling problem where the spins of the two nuclei are 3/2. For instance, if $eQ\langle\partial^2/\partial z^2\rangle_{Av}$ for one nucleus vanishes, then $|R|$ equals unity and the energy levels revert to those for the single nucleus problem.

LINE STRENGTHS

It can be shown[15] that the square root of the line strength $S(\epsilon JF\gamma,\ \epsilon' J'F'\gamma')$ for a transition from the primed state to the unprimed state in the $\epsilon JF\gamma$ representation may be written

$$S^{\frac{1}{2}}(\epsilon JF\gamma,\ \epsilon' J'F'\gamma')=\sum_I(\epsilon JF\gamma|IJF\gamma)[S^{\frac{1}{2}}(IJF\gamma,\ IJ'F'\gamma')]\times(IJ'F'\gamma'|\epsilon' J'F'\gamma'), \tag{11}$$

where γ includes the rotational quantum numbers and the electronic and vibrational quantum numbers. The transformation matrix $||(\epsilon JF\gamma|IJF\gamma)||$ is that which diagonalizes the quadrupolar perturbation to first order. This matrix is diagonal in J, F, and γ but contains elements for which $\epsilon=I$, $I\pm1$, $\epsilon\pm2$. The $\epsilon=I\pm1$ terms depend upon R, and, for $|R|\ll1$, may be safely neglected in the determination of line strengths.

The quantities $S^{\frac{1}{2}}(IJF\gamma,\ IJ'F'\gamma')$ must be assigned the proper phase.[16] They are composed of a factor related to the relative line strengths within a multiplet originating in the level $IJ'F'\gamma'$, and a factor $(J\gamma\vdots\mu\vdots J'\gamma')$ which may be shown to be related to the Cross, Hainer, King[17] rotational line strengths $\lambda_{J\tau,J'\tau'}$ in the following way:

$$|(J\gamma\vdots\mu\vdots J'\gamma')|^2=\lambda_{J\tau',J'\tau'}/(2J+1)\Xi(J,J'), \tag{12}$$

where

$$\Xi(J,J+1)=(J+1)(2J+3),$$
$$\Xi(J,J)=J(J+1),$$
$$\Xi(J,J-1)=J(2J-1).$$

Tables of $S^{\frac{1}{2}}(IJF\gamma,\ IJ'F'\gamma')$ in terms of $(J\gamma\vdots\mu\vdots J'\gamma')$ as well as numerical values (for $J\leqslant6$) of a quantity related to it are given by Condon and Shortley.[15]

It is convenient to compute the relative quantities defined by

$$L(\epsilon JF\gamma,\epsilon' J'F'\gamma')=S(\epsilon JF\gamma,\epsilon' J'F'\gamma')/(2J+1)\Xi(J,J')|(J\gamma\vdots\mu\vdots J'\gamma')|^2, \tag{13}$$

since multiplication by the appropriate Cross, Hainer, King line strengths gives the proper line strength for any member of a multiplet originating in the $\epsilon' J'F'\gamma'$ level. Values of L for $R=0$ have been tabulated in Appendix III for some low J transitions. Except for very low J, these quantities are given approximately by $L(IJF\gamma,IJ'F'\gamma')$ with $\epsilon=$I, because of the manner in which the energy states were labeled. The selection rule $\Delta\epsilon=0$ is thus approximated except for $|R|\gg0$ or for very low J, where the $\Delta\epsilon=\pm2$ transitions may be of importance. Also, as $|R|$ deviates considerably from zero the $\Delta\epsilon=\pm1$ transitions start becoming important for all J values. Since F retains its identity as a good quantum number for any value of R, the selection rules on F are the same as for single coupling, that is, the strongest transitions are those for which $\Delta F=\Delta J$.

If $|R|\sim1$, as is the case for two nuclei having widely different coupling, line strengths are most easily found in the $I_1JF_1I_2FM_F$ scheme. For other values of R, line strengths may be roughly approximated by interpolation between the two extreme cases or found exactly from Eq. (11).

APPLICATION TO ANALYSIS OF SPECTRA

If approximate values of the quadrupole coupling constants can be obtained from other molecules and if approximate structural parameters of the molecule are

[15] See, for example, E. U. Condon and G. H. Shortley, *The Theory of Atomic Spectra* (Cambridge University Press, Cambridge, 1951), Chap. IX.

[16] Reference 15, p. 277.

[17] Cross, Hainer, and King, J. Chem. Phys. **12**, 210 (1944).

known, approximate hyperfine patterns may be constructed by using the results obtained on the preceding pages. These approximate patterns may then be used to identify observed patterns and thus to arrive at the rotational analysis of the spectrum.

Q transitions in a molecule where R vanishes are the most useful for this purpose since, for the strongest components ($\Delta F=0$), $\lambda_{\epsilon JF}$ is identical in initial and final states. The hyperfine pattern will then be equivalent to the energy level pattern multiplied by the difference of X^+ for the two states. Symmetrical triplets arise from symmetrical rotational transitions in the $COCl^{35}Cl^{35}$ type molecules and are very easy to detect experimentally, especially for low J transitions. This fact in itself facilitates sorting transitions of different rotational symmetry for this type molecule. The patterns resulting from antisymmetric rotational transitions are quite unsymmetrical in appearance. Other kinds of Case I molecules present unsymmetrical patterns for both rotational symmetries, but the effect, for instance, of the interchange of the two hydrogen atoms in the methylene chloride type molecule may again be used to sort transitions of different rotational symmetry, if intensity measurements are reliable. Precise frequency measurements of the components of the unsymmetrical groups are themselves sufficient to assign the J value to the transition since the ratio of the splittings is a function only of J in a given molecule.

P and R transitions, on the other hand, present a less ideal situation since the patterns change irregularity with slight changes in the coupling constants and rotational parameters. If the Q transitions have been assigned, however, the coupling constants as well as part of the rotational parameters are known accurately, and the P and R transitions may then be assigned without too much difficulty.

The Case II molecules are more difficult than the above. If, however, the coupling is nearly identical, the patterns are not changed much from Case I, except that the symmetry arguments no longer hold. Also, for $|R|\sim 1$, the analysis is similar to that for the single coupling case. Intermediate cases are at best tedious unless the rotational assignment can be obtained easily as in symmetric-top or slightly asymmetric-top molecules.

The authors wish to thank Professor George Glockler, Director of The Microwave Project at the State University of Iowa, for his continued interest in the work. They are also indebted to the Office of Naval Research for its support of the research.

APPENDIX I[a]

ϵ	F	$\lambda_{\epsilon JF}$ as explicit functions of J for identical coupling $\lambda_{\epsilon JF}$	
3	$J+3$	0.5	
3	$J+2$	$-\dfrac{3}{2J}$	
3	$J+1$	$\dfrac{-(2J^2+5J-9)-[(2J^2+5J-9)^2+24J(2J-1)]^{\frac{1}{2}}}{4J(2J-1)}$	
1	$J+1$	$\dfrac{-(2J^2+5J-9)+[(2J^2+5J-9)^2+24J(2J-1)]^{\frac{1}{2}}}{4J(2J-1)}$	
3	J	$\dfrac{6-[36+(2J-1)(2J+3)(J+3)(J-2)]^{\frac{1}{2}}}{2J(2J-1)}$	$J\neq 1$
1	J	$\dfrac{6+[36+(2J-1)(2J+3)(J+3)(J-2)]^{\frac{1}{2}}}{2J(2J-1)}$	$J\neq 1$ $\lambda=1.0$ for $J=1$
3	$J-1$	$\dfrac{-(2J^2-J-12)+[(2J^2-J-12)^2+24(2J+3)(J+1)]^{\frac{1}{2}}}{4J(2J-1)}$	$J\neq 1$
1	$J-1$	$\dfrac{-(2J^2-J-12)-[(2J^2-J-12)^2+24(2J+3)(J+1)]^{\frac{1}{2}}}{4J(2J-1)}$	$J\neq 1$ $\lambda=-2.0$ for $J=1$
3	$J-2$	$\dfrac{3(2J+3)}{2J(2J-1)}$	$J\neq 1,2$
3	$J-3$	$\dfrac{(2J+3)(J+1)}{2J(2J-1)}$	$J\neq 1,2$

APPENDIX I[a]*—continued.*

$\lambda_{\epsilon JF}$ as explicit functions of J for identical coupling

ϵ	F	$\lambda_{\epsilon JF}$	
2	$J+2$	0	
2	$J+1$	0	
2	J	$\left[\frac{(J+1)(2J+3)}{4J(2J-1)}\right]^{\frac{1}{2}}$	
0	J	$-\left[\frac{(J+1)(2J+3)}{4J(2J-1)}\right]^{\frac{1}{2}}$	
2	$J-1$	0	$J\neq 1$
2	$J-2$	0	$J\neq 1$

Numerical values for $1 \leqslant J \leqslant 12$ and $J=\infty$ for identical coupling

		J												
ϵ	F	1	2	3	4	5	6	7	8	9	10	11	12	∞
3	$J+3$	0.5	0.5	0.5	0.5	0.5	0.5	0.5	0.5	0.5	0.5	0.5	0.5	0.5
3	$J+2$	−1.5	−0.75	−0.5	−0.375	−0.3	−0.25	−0.21429	−0.18750	−0.16676	−0.15	−0.13636	−0.125	0
3	$J+1$	−0.82288	−1.0	−0.90990	−0.83223	−0.77627	−0.73545	−0.70471	−0.68086	−0.66187	−0.64642	−0.63363	−0.62286	−0.5
1	$J+1$	1.82288	0.25	0.10990	0.06437	0.04294	0.03090	0.02339	0.01836	0.01481	0.01221	0.01025	0.00873	0
3	J	...	0	−0.38310	−0.48887	−0.52588	−0.54019	−0.54555	−0.54700	−0.54665	−0.54545	−0.54387	−0.54215	−0.5
1	J	1.0	1.0	0.78310	0.70315	0.65921	0.63110	0.61148	0.59700	0.58586	0.57703	0.56984	0.56388	0.5
3	$J-1$	...	1.21825	0.44244	0.21160	0.11897	0.07473	0.05081	0.03661	0.02756	0.02146	0.01717	0.01404	0
1	$J-1$	−2.0	−0.71825	−0.54244	−0.49731	−0.48564	−0.48382	−0.48487	−0.48661	−0.48834	−0.48988	−0.49120	−0.49230	−0.5
3	$J-2$	...	...	0.9	0.58929	0.43333	0.34091	0.28022	0.23750	0.20588	0.18158	0.16234	0.14674	0
3	$J-3$	...	...	1.2	0.98214	0.86667	0.79545	0.74725	0.71250	0.68627	0.66579	0.64935	0.63587	0.5
2	$J+2$	0	0	0	0	0	0	0	0	0	0	0	0	0
2	$J+1$	0	0	0	0	0	0	0	0	0	0	0	0	0
2	J	1.58114	0.93541	0.77460	0.70076	0.65821	0.63066	0.61125	0.59687	0.58578	0.57697	0.56980	0.56386	0.5
0	J	−1.58114	−0.93541	−0.77460	−0.70076	−0.65821	−0.63066	−0.61125	−0.59687	−0.58578	−0.57697	−0.56980	−0.56386	−0.5
2	$J-1$	...	0	0	0	0	0	0	0	0	0	0	0	0
2	$J-2$	...	0	0	0	0	0	0	0	0	0	0	0	0

[a] *Notes to Appendix* I.—The corresponding energy values are found by multiplying λ by the appropriate value of X^+ as explained in the text. The values for $J=0$ have been omitted since in this case the energy is identically equal to zero. For $J=1,2$ some combinations of g and F are not possible, and the general solutions are not valid for these J values. This has been indicated in the right-hand margin of the general solutions section along with the correct value of λ when it exists. In the numerical section the missing values are indicated by dots.

APPENDIX II[a]

$\lambda_{\epsilon JF}$ as explicit functions of J for nonidentical coupling

ϵ	F	$\lambda_{\epsilon JF}$	
3	$J+3$	0.5	
3	$J+2$	$\frac{-3-[9+4J(J+3)R^2]^{\frac{1}{2}}}{4J}$	
3	$J-2$	$(2J+3)\frac{3+[9+4(J+1)(J-2)R^2]^{\frac{1}{2}}}{4J(2J-1)}$	$J\neq 1,2$
3	$J-3$	$\frac{(2J+3)(J+1)}{2J(2J-1)}$	$J\neq 1,2$
2	$J+2$	$\frac{-3+[9+4J(J+3)R^2]^{\frac{1}{2}}}{4J}$	
2	$J-2$	$(2J+3)\frac{3-[9+4(J+1)(J-2)R^2]^{\frac{1}{2}}}{4J(2J-1)}$	$J\neq 1,2$ $\lambda=0$ for $J=2$

APPENDIX II[a]—*continued.*

The coefficients a^F and b^F in terms of J

$$b_0^{J+1}=-\frac{(J+3)(J-2)(2J+3)}{8J^2(2J-1)}$$

$$a_1^{J+1}=-\frac{3}{2J(2J-1)}$$

$$b_1^{J+1}=-\frac{2J^3-J^2-6J+18}{4J^2(2J-1)}$$

$$a_2^{J+1}=\frac{2J^2+5J-9}{2J(2J-1)}$$

$$a_0^{J}=\frac{(J+1)(2J+3)^2(J+3)(J-2)}{16J^3(2J-1)^2}$$

$$a_1^{J}=\frac{3(J+1)(2J+3)}{2J^2(2J-1)^2}$$

$$b_1^{J}=\frac{9(2J+3)}{4J^3(2J-1)^2}$$

$$a_2^{J}=-\frac{(2J+3)(J^2+J-3)}{2J^2(2J-1)}$$

$$b_2^{J}=-\frac{9(4J^2+4J-7)}{4J^2(2J-1)^2}$$

$$a_3^{J}=4a_1^{J+1}$$

Not valid for $J=1$.
See numerical values at end of this appendix.

$$b_0^{J-1}=-2a_0^{J}$$

$$a_1^{J-1}=-a_1^{J}$$

$$b_1^{J-1}=-\frac{(2J+3)(2J^3+7J^2+2J-21)}{4J^2(2J-1)^2}$$

$$a_2^{J-1}=a_3^{J}+(1/2)$$

Not valid for $J=1$.
See numerical values at end of this appendix.

Numerical values of the coefficients a^F and b^F for $1 \leqslant J \leqslant 12$

	J = 1	2	3	4	5	6	7	8	9	10	11	12
b_0^{J+1}	2.5	0	−0.15	−0.17188	−0.17333	−0.17046	−0.16680	−0.16328	−0.16013	−0.15737	−0.15496	−0.15285
a_1^{J+1}	−1.5	−0.25	−0.1	−0.05357	−0.03333	−0.02273	−0.01648	−0.01250	−0.00980	−0.00790	−0.00649	−0.00544
b_1^{J+1}	−3.25	−0.375	−0.25	−0.23661	−0.23667	−0.23864	−0.24058	−0.24219	−0.24346	−0.24447	−0.24528	−0.24592
a_2^{J+1}	−1	0.75	0.8	0.76786	0.73333	0.70455	0.68132	0.66250	0.64706	0.63421	0.62338	0.61413
a_0^{J}	...	0	0.18	0.16881	0.15022	0.13559	0.12464	0.11634	0.10989	0.10477	0.10062	0.09720
a_1^{J}	...	0.875	0.24	0.10523	0.05778	0.03616	0.02464	0.01781	0.01346	0.01051	0.00843	0.00691
b_1^{J}	...	0.21875	0.03	0.00789	0.00289	0.00129	0.00066	0.00037	0.00022	0.00014	0.00010	0.00007
a_2^{J}	...	−0.875	−0.9	−0.83482	−0.78000	−0.73864	−0.70722	−0.68281	−0.66340	−0.64763	−0.63459	−0.62364
b_2^{J}	...	−1.06250	−0.41	−0.20950	−0.12556	−0.08316	−0.05896	−0.04391	−0.03393	−0.02699	−0.02197	−0.01822
a_3^{J}	...	−1	−0.4	−0.21429	−0.13333	−0.09091	−0.06593	−0.05000	−0.03922	−0.03158	−0.02597	−0.02174
b_0^{J-1}	...	0	−0.36	−0.33761	−0.30044	−0.27118	−0.24928	−0.23268	−0.21979	−0.20955	−0.21025	−0.19439
a_1^{J-1}	...	−0.875	−0.24	−0.10523	−0.05778	−0.03616	−0.02464	−0.01781	−0.01346	−0.01051	−0.00843	−0.00691
b_1^{J-1}	...	−1.3125	−1.02	−0.79624	−0.66444	−0.58110	−0.52451	−0.48391	−0.45348	−0.42990	−0.41112	−0.39582
a_2^{J-1}	...	−0.5	0.1	0.28571	0.36667	0.40909	0.43407	0.45000	0.46078	0.46842	0.47403	0.47826

Note: For $J=1$ the secular equation reads $\lambda^3-\lambda^2-(2.5+2.25R^2)\lambda+2.5=0$.

Note: For $J=1$, $\lambda=-2.0$.

[a] *Notes to Appendix II.*—The irregularities for $J=1,2$ have been explained in the notes to Appendix I.

APPENDIX III[a]

Numerical values of $L(\epsilon JF\gamma, \epsilon' J'F'\gamma')$ in identical coupling.

$\Delta J=0$	initial state		J					approx.	
	ϵ	F	1	2	3	4	6	6	12
$\Delta F=0$									
$\Delta\epsilon=0$	3	$J+3$	1.88	1.76	1.62	1.52	1.39	1.39	1.22
	3	$J+2$	0.10	0.74	0.98	1.07	1.12	1.12	1.11
	3	$J+1$	1.07	0.44	0.71	0.85	0.97	0.91	1.03
	1	$J+1$	0.70	0.75	0.97	1.03	1.06	1.13	1.05
	3	J	...	0.06	0.32	0.54	0.76	0.73	0.93
	1	J	0.25	0.34	0.72	0.84	0.92	0.95	0.98
	3	$J-1$	...	0.20	0.11	0.37	0.67	0.60	0.88
	1	$J-1$	0	0.45	0.58	0.66	0.76	0.82	0.88
	3	$J-2$	...	...	0.02	0.23	0.52	0.52	0.79
	3	$J-3$	...	...	0	0.21	0.47	0.47	0.74
	2	$J+2$	1.56	1.50	1.41	1.35	1.26	1.26	1.15
	2	$J+1$	0.14	0.70	0.90	0.99	1.04	1.04	1.05
	2	J	0.57	0.56	0.77	0.86	0.93	0.86	0.98
	0	J	0.57	0.56	0.77	0.86	0.93	1.00	0.98
	2	$J-1$	...	0.05	0.36	0.55	0.73	0.73	0.89
	2	$J-2$	...	0	0.29	0.46	0.65	0.65	0.83
$\Delta F=+1$									
$\Delta\epsilon=0$	3	$J+2$	1.13	0.44	0.23	0.14	0.07	0.07	
	3	$J+1$	0.26	0.40	0.25	0.16	0.08	0.11	
	3	J	...	0.42	0.29	0.20	0.10	0.13	
	1	J	0.10	0.27	0.13	0.08	0.04	0.02	
	3	$J-1$	...	0.26	0.25	0.16	0.07	0.13	
	1	$J-1$	0.33	0.08	0.04	0.01	0.003	0.02	
	3	$J-2$	...	...	0.25	0.17	0.08	0.11	
	3	$J-3$	...	...	0.14	0.12	0.07	0.07	
	2	$J+1$	0.78	0.30	0.16	0.10	0.05	0.05	
	2	J	0.38	0.20	0.11	0.07	0.03	0.07	
	2	$J-1$	...	0.18	0.11	0.07	0.03	0.07	
	2	$J-2$	...	0.20	0.14	0.09	0.05	0.05	
$\Delta F=0$									
$\Delta\epsilon=-2$	3	$J+1$	0.02	0.11	0.03	0.01	0.003	0	
	3	J	...	0.15	0.02	0.007	0.001	0	
	3	$J-1$	...	0.0005	0.01	0.01	0.003	0	
	2	J	0.06	0.06	0.02	0.006	0.001	0	
$\Delta F=+1$									
$\Delta\epsilon=-2$	3	J	...	0.05	0.05	0.04	0.02	0	
	3	$J-1$	...	0.14	0.09	0.06	0.03	0	
	3	$J-2$	...	...	0.02	0.03	0.03	0	
	2	$J-1$	...	0.18	0.11	0.07	0.03	0	
$\Delta F=-1$									
$\Delta\epsilon=-2$	3	$J+2$	0.85	0.22	0.11	0.07	0.03	0	
	3	$J+1$	0.32	0.02	0.004	0.002	0.0005	0	
	3	J	...	0.07	0.06	0.06	0.05	0	
	2	$J+1$	0.38	0.20	0.11	0.07	0.03	0	

[a] *Notes to Appendix III.*—The dots indicate that at least one of the levels does not exist as explained in the notes to Appendix I. Since L is symmetrical between initial and final states, the roles of these may be interchanged to obtain L for other transitions. In most cases only $\Delta F=\Delta J$ transitions will be observed for high J values. For this reason the weaker transitions have been omitted for $J=11$, 12 and have been sharply rounded off in the other cases. The approximate quantity $L(IJF\gamma, IJ'F'\gamma')$ is useful for $J\sim 5$ or higher as indicated in the tabulation.

APPENDIX III[a]—*Continued.*

$\Delta J=+1$	initial state		J					approx.	
	ϵ	F	1	2	3	5	5	11	
$\Delta F=+1$									
$\Delta\epsilon=0$	3	$J+3$	2.20	1.86	1.67	1.46	1.46	1.24	
	3	$J+2$	1.13	1.26	1.26	1.22	1.22	1.14	
	3	$J+1$	0.75	0.94	1.01	1.06	1.02	1.06	
	1	$J+1$	0.63	1.10	1.13	1.11	1.15	1.07	
	3	J	...	0.50	0.69	0.85	0.84	0.96	
	1	J	0.53	0.75	0.89	0.96	0.97	0.99	
	3	$J-1$	...	0.17	0.45	0.72	0.68	0.89	
	1	$J-1$	0.33	0.57	0.67	0.78	0.82	0.90	
	3	$J-2$	...	...	0.27	0.56	0.56	0.81	
	3	$J-3$	...	...	0.14	0.45	0.45	0.74	
	2	$J+2$	1.80	1.57	1.44	1.31	1.31	1.16	
	2	$J+1$	0.93	1.07	1.10	1.10	1.10	1.07	
	2	J	0.63	0.84	0.91	0.96	0.92	0.99	
	0	J	0.63	0.84	0.91	0.96	1.00	0.99	
	2	$J-1$	...	0.40	0.60	0.76	0.76	0.90	
	2	$J-2$	...	0.20	0.43	0.64	0.64	0.83	
$\Delta F=0$									
$\Delta\epsilon=0$	3	$J+3$	0.67	0.31	0.18	0.08	0.08		
	3	$J+2$	0.56	0.33	0.20	0.09	0.13		
	3	$J+1$	0.33	0.36	0.24	0.12	0.16		
	1	$J+1$	0.35	0.17	0.10	0.04	0.03		
	3	J	...	0.23	0.19	0.07	0.15		
	1	J	0.25	0.03	0.02	0.003	0.03		
	3	$J-1$	...	0.28	0.23	0.10	0.13		
	3	$J-2$	...	...	0.16	0.08	0.08		
	2	$J+2$	0.47	0.21	0.12	0.06	0.06		
	2	$J+1$	0.29	0.15	0.09	0.04	0.08		
	2	J	0.23	0.14	0.09	0.004	0.008		
	2	$J-1$	...	0.20	0.12	0.06	0.06		
$\Delta F=-1$									
$\Delta\epsilon=0$	3	$J+3$	0.08	0.02	0.007	0.002	0.002		
	3	$J+2$	0.23	0.06	0.02	0.004	0.005		
	3	$J+1$	0.13	0.06	0.02	0.002	0.007		
	1	$J+1$	0.002	0.0001	0.0002	0.0005	0.0006		
	3	J	...	0.10	0.03	0.006	0.007		
	3	$J-1$	...	0.14	0.03	0.004	0.004		
	2	$J+2$	0.03	0.007	0.002	0.0005	0.001		
	2	$J+1$	0.15	0.03	0.008	0.002	0.002		
	2	J	0.10	0.01	0.003	0.0005	0.001		
$\Delta F=+1$									
$\Delta\epsilon=+2$	1	$J+1$	0.01	0.003	0.003	0.001	0		
	1	J	0.23	0.0003	0.0004	0.002	0		
	1	$J-1$	0.003	0.02	0.03	0.01	0		
	0	J	0.04	0.007	0.002	0.0004	0		
$\Delta F=+1$									
$\Delta\epsilon=-2$	3	$J+1$	0.41	0.03	0.005	0.0005	0		
	3	J	...	0.07	0.008	0.008	0		
	3	$J-1$	...	0.001	0.003	0.001	0		
	2	J	0.04	0.007	0.002	0.0004	0		
$\Delta F=0$									
$\Delta\epsilon=+2$	1	$J+1$	0.22	0.08	0.05	0.03	0		
	1	J	0.002	0.17	0.08	0.04	0		
	1	$J-1$	...	0.003	0.02	0.03	0		
	0	J	0.23	0.14	0.09	0.004	0		
$\Delta F=0$									
$\Delta\epsilon=-2$	3	$J+2$	0.32	0.14	0.08	0.04	0		
	3	$J+1$	0.02	0.001	0.002	0.0005	0		
	3	J	...	0.10	0.08	0.06	0		
	2	$J+1$	0.29	0.15	0.09	0.04	0		
$\Delta F=-1$									
$\Delta\epsilon=+2$	1	$J+1$	0.46	0.04	0.01	0.002	0		
	1	J	...	0.04	0.006	0.001	0		
	1	$J-1$	...	0.001	0.002	0.001	0		
	0	J	0.10	0.01	0.003	0.0005	0		
$\Delta F=-1$									
$\Delta\epsilon=-2$	3	$J+3$	0.05	0.01	0.003	0.001	0		
	3	$J+2$	0.10	0.01	0.003	0.0005	0		
	3	$J+1$	0.05	0.01	0.006	0.002	0		
	2	$J+2$	0.03	0.007	0.002	0.0005	0		

Empirical Considerations of Entropy. I. The Entropies of the Oxy-Anions and Related Species*

JAMES W. COBBLE
Radiation Laboratory and Department of Chemistry and Chemical Engineering, University of California, Berkeley, California

(Received April 7, 1953)

The partial molal entropies for oxy-anions and related species have been correlated as a function of the charge, interatomic distance, and certain structural factors. An equation is given by which the entropy for unknown species can now be estimated fairly accurately. In the few cases where the method does not give good agreement, the data are open to suspicion as indicated by other independent observations. Some applications and extensions of the method are indicated for future study.

INTRODUCTION

RECENTLY Powell and Latimer[1] have demonstrated that it is possible to correlate the entropies of the monatomic aqueous ions in a simple manner as a function of their mass, charge, and crystalline radii. The correlation is so striking that it suggested the possibility that a similar situation might exist for more complex aqueous ions. Such a correlation would be generally useful in predicting the properties of as yet undetermined species, as well as indicating upon what types of ions further study might be fruitful. One might also hope that such an empirical treatment could provide some additional basis for a better understanding of the theory of ionic interactions in aqueous media. To this end, it has been found possible to correlate the entropies of aqueous complex ions similar to the methods of Latimer *et al.*,[1,2] and this communication describes the method and results obtained for the oxygenated anions and related species.

Powell and Connick[3] have also recently developed a theory for the oxygenated anions based upon different reasoning, but which, except in the case of large molecules, leads to quite similar results. The comparison of these two theories will be the subject of a future communication.

THE GENERAL METHOD

The equation proposed for the entropy of the oxygenated anions is of the form

$$\bar{S}^0 - 3/2R \ln M = a - b(Z/\rho), \qquad (1)$$

where $\bar{S}^0$ is the partial molal entropy (based upon $\bar{S}^0_{(H^+)} \equiv 0$), a and b are general constants for all of the oxy-anions, M is the ionic mass, Z the absolute integral charge, and ρ the *effective* ionic radius (in angstroms). The necessity for the linear dependence of the entropy on the charge Z has been previously discussed,[1] and is in apparent disagreement with the Born[4] electrostatic model. Attempts to fit the data to any other power of Z than unity were not successful. We have also observed that in the particular method we have chosen of assigning the effective radii to the ions, the data seem to agree better with a $1/\rho$ rather than a $1/\rho^2$ dependence. This is in disagreement with the model for simple ions[1] where it was observed that an inverse square-power of the radii rather than the inverse first power seemed to fit the data better. The differences may arise from the lesser amount of ion interaction of the oxygenated species with surrounding water dipoles. The effect of hydrogen bonding between the peripheral oxygen atoms of the ion and the solvent will, of course, be greater although the net interaction must surely be smaller.

THE EFFECTIVE IONIC RADII

The key to the problem was in the assignment of an effective ionic radius to the ion. Powell and Latimer[1] used the Pauling[5] ionic crystal radii for the simple ions plus an added one (for anions) and two (for cations) angstroms for the effects of hydration. No such well-defined set of radii is available for oxygenated ions. Further, one cannot simply add up either the appropriate covalent or ionic radii of the ion since the observed crystal interatomic distances usually lie somewhere between these two values. It is also clear that the effective ionic radius will be different for the linear ions than that for tetrahedral ions, and in general will be expected to depend in some manner on the structure of the ion. Finally, the effective radii will not be equal to the distance from the center of the central atom to the periphery of the outer oxygen atom, since this radius would not allow for penetration of the ion by water molecules. Indeed, this distance could not be easily and accurately calculated, since the oxygen diameter will be some function of its formal charge, and the crystal data in general would only give the interatomic distances. After trying various schemes, it was decided to fit the data using the *interatomic* distance

* This work was performed under the auspices of the U. S. Atomic Energy Commission.

[1] R. E. Powell and W. M. Latimer, J. Chem. Phys. **19**, 1139 (1951).

[2] L. V. Coulter and W. M. Latimer, J. Am. Chem. Soc. **62**, 2557 (1940).

[3] R. E. Powell and R. E. Connick (private communication).

[4] M. Born, Z. Physik **1**, 45 (1920).

[5] L. Pauling, *The Nature of the Chemical Bond* (Cornell University Press, Ithaca, 1939).

TABLE I. Comparison of some observed and calculated interatomic distances.

Ion	Observed (A)[a]	Calculated (Pauling's method)[b]
ClO_4^-	1.48–1.56	1.48
MnO_4^-	1.52–1.86	1.81
ReO_4^-	1.80–2.02	1.97
SeO_4^{-2}	1.61	1.66
CrO_4^{-2}	1.60–1.98	1.86
PO_4^{-3}	1.56	1.56
SiO_4^{-4}	1.62	1.63
CO_3^{-2}	1.26	1.24
NO_3^-	1.21–1.26	1.21
BrO_3^-	1.54–1.78	1.67
NO_2^-	1.13–1.23	1.23
CNS^-	1.42	1.37
SO_3^{-2}	1.39	1.34

[a] Some of these values for the ions containing heavier elements may be in error by 0.1A or more.
[b] See reference 7.

between the central atom and the peripheral oxygen atom, although it was obvious that this distance would be somewhat too small for the effective radius of some ions. These data are readily available in Wyckoff,[6] although the values observed for the distance, r_{12}, usually vary about 0.1–0.2A depending upon the cationic species involved in the crystal. We have found it convenient, therefore, to use the values of r_{12} calculated by the method of Pauling.[7] In practically all of the cases these calculated r_{12} values fall between the various observed values, except in cases where there is not enough data on various cationic forms to obtain a good average value for r_{12} (see Table I). Further, experimental r_{12} values are not always available, and may never be for some ions. The method must be used with reservation for the estimation of interatomic distances between non-oxygen bonds.

THE EMPIRICAL EQUATION AND STRUCTURAL FACTORS

The equation for the oxy-anions has been found by inspection to be

$$\bar{S}^0 - 3/2R \ln M = 66 - 81(Z/\rho), \qquad (2)$$

where ρ is related to the interatomic crystal distance, r_{12}, by a suitable structural constant, f:

$$\rho = r_{12}/f.$$

It is to be expected for reasons already discussed that f will be a function of the ion structure, and this has been found to be the case. It was also found that within the limits of experimental error all of the ions of one structural class (except in one case to be discussed) have the same structural factor. If this were not so, of course, the method proposed here would be of little value. The exception occurs in the tetrahedral class, where we find that the -3 ions require a somewhat different factor than the -1 or -2 ions. This need is probably *not* due to the failure of Eq. (1) since a linear dependence on Z was observed for the simple, highly charged ions.[1] We have also observed the linear Z dependence in the case of the highly charged non-oxygenated complex ions, which will be discussed in the second paper of this sequence.

The structural parameters, their average deviation, and the ions from which they were determined are given in Table II. The f values were obtained by dividing the calculated value of r_{12} by the value of ρ necessary to fit the mass-corrected entropy to Eq. (2).

It may seem that the desirability of basing a structural factor in some cases only on the data of a few ions is questionable. This practice has been used, however, since the method suggests a structural dependence, and we wish to keep it as flexible as possible. Some values may have to be revised slightly as new data become available, and yet the agreement obtained using the calculated values of r_{12}, the factors in Table II, and Eq. (2) is good, as is shown in Fig. 1. The average deviation is about 3 eu for some 30 experimental values, and some 12 estimates taken from Latimer. Considering that an error in r_{12} (or ρ) of ± 0.05A can cause in some cases an error of up to 15 eu, this agreement is as good as one could expect.

It is interesting that placing a proton on the ions reduces the need for further structural differentiation, since the hydrogenated ions now fall in groupings dependent upon only the total number of hydrogen atoms in the ion. We have used the same r_{12} values as calculated for the completely dissociated ions, ignoring the effect of the hydrogen atom on r_{12}. This is usually in agreement with the crystal structure data.

TABLE II. Structural classes and factors.

Ion class	f[a]	Ions[b]
Tetrahedral, -1, -2	0.74 ± 0.04	ClO_4^-, MnO_4^-, ReO_4^-,[c] CrO_4^{-2}, SO_4^{-2}, SeO_4^{-2}
Tetrahedral, -3	0.83 ± 0.02	PO_4^{-3}, AsO_4^{-3}
Tetrahedral, -4	(0.9)[d]	...
Pyramidal	0.74 ± 0.01	SO_3^{-2}, SeO_3^{-2}, ClO_3^-, BrO_3^-
Plane-triangular	0.68 ± 0.03	CO_3^{-2}, NO_3^-
Triatomic V-shaped	0.87 ± 0.11	NO_2^-, ClO_2^-
Triatomic linear	0.96 ± 0.02	BeO_2^{-2}(BO_2^-, AlO_2^-)[c]
Complex shape	0.77 ± 0.02	$N_2O_2^{-2}$, $Cr_2O_7^{-2}$, $C_2O_4^{-2}$ [f]
Linear related species	0.69 ± 0.01	CNO^-, N_3^-
Diatomic	1.34 ± 0.01	ClO^-, OH^-
Monohydrogen acid ions	0.91 ± 0.05	HCO_3^-, HSO_4^-, $HSeO_3^-$, HPO_4^{-2}, $HAsO_4^{-2}$, HSO_3^-
Dihydrogen acid ions	1.13 ± 0.02	$H_2BO_3^-$, $H_2PO_4^-$, ($H_2PO_3^-$)
Trihydrogen acid ions	(1.34)[g]	...
Tetrahydrogen acid ions	(1.55)[g]	...

[a] Deviations correspond to average deviations of all the ions in that class.
[b] Entropy data from W. M. Latimer, *Oxidation Potentials* (Prentice-Hall, Inc., New York, 1952), except as indicated.
[c] Cobble, Smith, and Oliver (to be published).
[d] Estimated from di- and trivalent tetrahedral ions.
[e] Values in parenthesis are from estimated values in reference b.
[f] For $M_2O_4^{-2}$ ions, $r_{12} = r_{M-O} + \frac{1}{2} r_{M-M}$.
[g] Estimated from the mono- and dihydrogen acid ions.

[6] R. W. G. Wyckoff, *Crystal Structures* (Interscience Publishers, Inc., New York, 1951), Vols. I and II.
[7] L. Pauling, J. Phys. Chem. **56**, 361 (1952); covalent radii from reference 5 except for the case of the first row elements, where we have used the values recommended by Schomaker and Stevenson (J. Am. Chem. Soc. **63**, 37 1941). Where covalent radii were not available, the metallic radii were used. For the special case of hydroxyl ion, the value of 1.40A observed in solid hydroxides has been used [A. F. Wells, *Structural Inorganic Chemistry* (Clarendon Press, Oxford, 1945)]; this is not exactly equivalent to the interatomic distance, but this latter quantity becomes difficult to define in aqueous solution for this species.

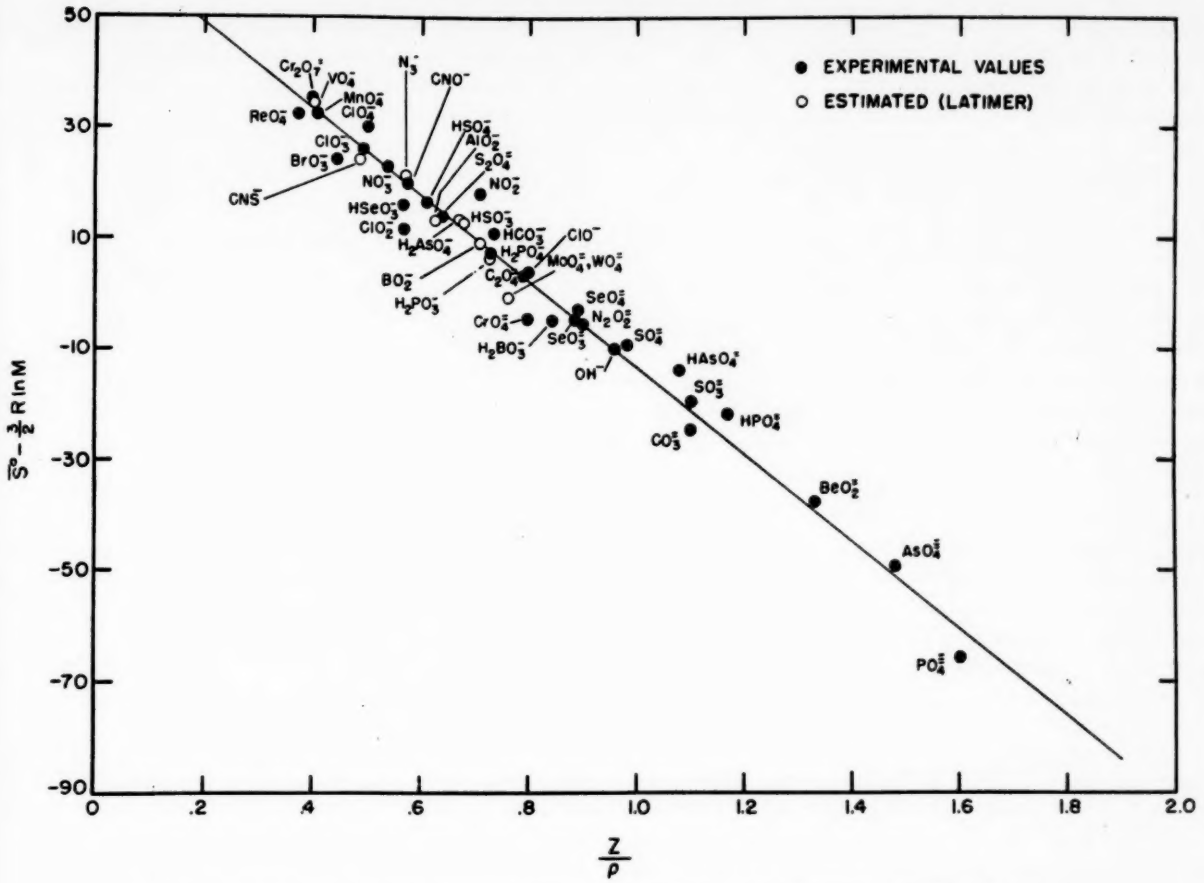

FIG. 1. Correlation of the mass corrected aqueous entropies with the charge to effective radius ratio.

It is believed that one of the entropies of the two triatomic shaped ions is incorrect, since a much larger deviation in f is observed for this class. It is further believed that nitrite ion is the one in error since the independent method proposed by Powell and Connick also indicates this discrepancy. Until other data for this class are available, however, we have no recourse but to average the values for both species.

There are a few isolated cases where the data cannot be made to fit on the curve in Fig. 1. These are IO_3^-, $HSeO_4^-$, and $HCrO_4^-$. In view of the fact that Crouthamel *et al.*[8] have found IO_4^- to exist in aqueous solution at room temperatures largely as the hydrated species, $H_4IO_6^-$, it is clear that IO_3^- cannot be considered as a failure of the method. Indeed, this is a case where the theory might seem to be useful in interpreting the data. Hall and Alexander[9] have also reported that O^{18} will exchange between aqueous IO_3^- and the solvent, suggesting that some hydration equilibrium does exist for this ion. No such exchange was observed for ClO_3^- where the entropy seems to be normal. Further, the Raman spectra of the aqueous solution also indicate the formula for the iodate species in aqueous solution is not simple.[10] The data for $HSeO_4^-$ and $HCrO_4^-$, if correct, indicate a similar situation in that the formula written simply does not correspond to the species present. The oxygen exchange data are in agreement with the hypothesis that hydration equilibria exist for these ions also.

THE ENTROPY OF IONIZATION

Powell and Latimer[1] have also proposed that the entropy of neutral species in water can be represented by the equation

$$\bar{S}^0 = S_{\text{int}} + 3/2R\ln M + 10 - 0.22V_m. \quad (3)$$

If one examines the weak acids, in general, it is found that they can be represented fairly well by the equation

$$\bar{S}^0 - 3/2R\ln M \approx 30 \pm 5. \quad (4)$$

Combining Eq. (4) with (2) it can then be shown that for the first ionization of a weak electrolyte, the entropy change is given by

$$\Delta S_{\text{ioniz}} = 36 - \frac{81}{r_{12}}. \quad (5)$$

We have taken an average value of f for the various species. Equation (5) is an extension of Pitzer's rule[11] in which the entropy of ionization of a weak electrolyte

[8] Crouthamel, Hayes, and Martin, J. Am. Chem. Soc. **72**, 82 (1951).

[9] N. F. Hall and O. R. Alexander, J. Am. Chem. Soc. **62**, 3455 (1940).

[10] J. H. Hibben, *The Raman Effect and its Chemical Applications* (Reinhold Publishing Corporation, New York, 1939), p. 381.

[11] K. S. Pitzer, J. Am. Chem. Soc. **59**, 2365 (1937).

is about -22 eu. Equation (5) predicts values between -17 and -25 eu for r_{12} values between 1.6–1.4A. The agreement of the experimental data with Eq. (5) is fair, although the equation $\Delta S_{\text{ion}12}=20-59/r_{12}$ fits the data better to an average deviation of 2–3 entropy units. The real interest in Eq. (5) is that it predicts the correct trend, so that low values of ionization (H_2SeO_3, $\Delta S=-15$) and high values (H_3BO_3, $\Delta S=-31$) are now somewhat easier to understand.

It can also be shown that the entropies of successive ionizations will also depend upon $1/r_{12}$ in general agreement with the few experimental observations available. These results should be generally useful in estimating entropies of various ionic and hydrated species, especially where the entropy for one member of the pair is available.

CONCLUSION

The method given here may not necessarily be unique in systematizing the aqueous entropy data, but for methods involving the charge to radius ratio (Z/ρ) it seems to work very well. For example, one can also use an equation of the type proposed by Powell and Latimer[1] for the simple ions in which 1.00A is added to the interatomic distance in a $Z/(r+1.00)^2$ term, but the fit is not as good, nor can the acid ions be treated simply in this manner. Another method which gives fair results is to use the "thermodynamic" radii of Kapustinskii and Yatsimuskii[12] obtained from lattice energy calculations. The fit becomes poorer for highly charged species, which is what one might expect from their treatment of the crystal energies.

There seems to be no *a priori* reason why oxygenated cationic species should not take on the same structural factors as their negative counterparts, but the data are not available to test this hypothesis.

It should also be interesting to test the large amount of entropy of activation data available from kinetic studies to see whether the observed values for the transition states are in agreement with those calculated by the method presented here.

ACKNOWLEDGMENTS

The author would like to thank Professors R. E. Powell and R. E. Connick for the opportunity of examining their manuscript prior to publication and also thank Professors W. M. Latimer, R. E. Powell, and K. S. Pitzer for their helpful and interesting discussions of the problem.

Note added in proof:—It should be noted that the numerical values of the structural factors and constants of Eq. (2) are purely arbitrary, and thus no unique interpretation can necessarily be placed on the effective radius ρ. The relative values of the structural factors do illustrate, however, the *differences* in the behavior of the various structural classes, and it was for this reason that a different factor was assigned to each class. With very little loss in accuracy, many of the classes can be combined to reduce the number of different arbitrary constants required to fit the data by a factor of two or more, but such a procedure is not necessarily advantageous, and indeed, de-emphasizes one of the main points of this communication.

It has also been recently called to the author's attention that it may not be correct to use a mass-correction term in describing entropies of ionic species. While there are some specific cases among the oxy-anions which favor this point of view, there are simply not yet enough data of sufficient accuracy to test the mass dependence.

[12] A. F. Kapustinskii and K. B. Yatsimuskii, Zhur. Obshchei Khim. **19**, 2191 (1949).

THE JOURNAL OF CHEMICAL PHYSICS VOLUME 21, NUMBER 9 SEPTEMBER, 1953

Empirical Considerations of Entropy. II. The Entropies of Inorganic Complex Ions*

JAMES W. COBBLE
Radiation Laboratory and Department of Chemistry and Chemical Engineering, University of California, Berkeley, California

(Received April 7, 1953)

A method is proposed by which the partial molal entropies of aqueous complex ions can be correlated in a simple manner as a function of the ratio of their charge to interatomic distance. The agreement obtained between the observed values and those calculated by this method has been shown to be within the accuracy of the experimental data. It is also demonstrated that when the complexing agent is water alone (i.e., no complexing) the proposed equation reduces to an expression similar to that previously obtained by Powell and Latimer for simple monatomic ions.

INTRODUCTION

WITH the success of Powell and Latimer[1] in correlating the entropies of simple ions, and the recent treatments of Powell and Connick[2] and Cobble[3] in correlations for the oxy-anions, it seemed desirable to search for a similar method of treating aqueous complex ions, if, indeed, any such correlation existed. Al-

* This work was performed under the auspices of the U. S. Atomic Energy Commission.

[1] R. E. Powell and W. M. Latimer, J. Chem. Phys. **19**, 1139 (1951).

[2] R. E. Powell and R. E. Connick, (private communication).

[3] J. W. Cobble, J. Chem. Phys. **21**, 1443 (1953), preceding paper.

though there are a large number of complex species which have been identified, there are few which have been characterized by accurate determinations of stability constants, and still fewer for which heat or temperature coefficient data are available so that entropy values can be calculated. In addition, many of the reported values are subject to large errors inherent in the conditions required for their study (i.e., high ionic strength), and frequently large discrepancies exist between values reported by different observers. We have, however, observed a correlation which is believed to be generally applicable to positively and negatively charged complex ions alike. A treatment for neutral nondissociated complex ions is also presented.

THE PROPOSED METHOD

Since the previous entropy treatments of aqueous ions have involved functions of the charge to radius ratio,[3] it was of interest to try a similar function for the complex ions. By "complex" ions, we mean in this communication those ions in which "simple" ions have associated to form a "complex." Thus, sulfate ion would not normally be thought of as a union of *aqueous* S^{+6} and O^{-2} ions, although substances such as $Fe(CN)_6^{-4}$ and $FeBr^+$ are easily formed in this manner. Further, partial complexing of these ions to give species such as SO_3^{-4}, SO_2^{-6}, etc., has not been observed. Our definition is occasionally troublesome in the case of a few very stable ions (such as $PtCl_6^{-2}$). In general, however, the distinction is clear, and for the majority of ions little ambiguity exists in assigning them to either the oxy-anion or complex ion class. It is also clear that one would expect the oxy-anions to differ from "complex ions" since their immersion in water will not disturb the structure of the solvent as much as non-oxygenated species of the same Z/r_{12} ratio. It will be seen, however, that the hydroxy complexes ($M(OH)^{+n}$) fit well into the treatment proposed for the "complex" ions, but did not agree with the method proposed for the oxy-anions. This is probably related to the supposition that the bond distances are greater in the $M(OH)^{+n}$ ionic complexes than in partially covalent oxy-ions. In any event, our original classification which is, in reality, based upon ease of dissociation, is as probably useful as any other.

In Fig. 1 the partial molal entropy[4] has been plotted against the ratio of the charge to interatomic distance

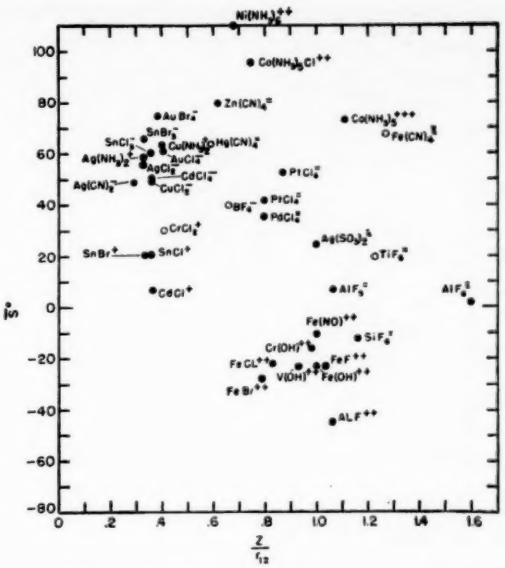

FIG. 1. Illustration of the absence of correlation of the aqueous entropies of complex ions with the charge to radius ratio.

($r_{12} \equiv r_1 + r_2$) for the ion, since this function had been found to be useful with the oxy-anions.[3] The interatomic distances were computed from the sum of the appropriate ionic[5] and covalent[6] radii. In cases where the magnetic evidence was not available to make such a classification, the decision has been based upon chemical reasoning. The distinction will cause little ambiguity in the r_{12} values except in those cases where the complexing agent is molecular (NH_3, SO_3^{-2}, CN^-, and NO). It can be seen that the method illustrated in Fig. 1 is of little use in classifying or comparing the species, since there is no obvious separation into groups dependent upon such variables as radii, charge, number of ions making up the complex, or structure. For example, AlF^{+2} and $Co(NH_3)_5^{+3}$ have about the same Z/r_{12} values, yet they differ in entropy by 120 entropy units; $Zn(CN)_4^{-2}$ and SiF_6^{-2} have the same charge, but differ by 92 e.u.; $Co(NH_3)_5^{+3}$ and $Fe(CN)_6^{-4}$ have the same entropy but no other obvious similarities, etc.

It thus appeared that little, if any, correlation existed until the observation was made that the entropies of highly complexed species ($CO(NH_3)_5Cl^{+2}$, $AuBr_4^-$, $Zn(CN)_4^{-2}$) appear to be uniformly more positive than the entropies for lesser complexed ions ($FeBr^{+2}$, AlF^{+2}). This situation indicates, of course, less interaction of a restrictive nature between the highly complexed ion and the solvent molecules, than with the lesser complexed ions, and suggests that this fact should be con-

[4] Values obtained mostly from W. M. Latimer, *Oxidation-Potentials* (Prentice-Hall, Inc., New York, 1952), 2nd edition; data for the aluminum fluoride complexes are from Latimer, private communication (to be published); $AgCl_2^-$ from J. H. Jonte and D. S. Martin, J. Am. Chem. Soc. **74**, 2053 (1952); $SnCl^+$, $SnCl_2^0$, $SnCl_3^-$ from C. E. Vanderzee and D. E. Rhodes, J. Am. Chem. Soc. **74**, 3552 (1952); $SnBr^+$, $SnBr_2^0$, $SnBr_3^-$ from C. E. Vanderzee, J. Am. Chem. Soc. **74**, 480 (1952); $V(OH)^{+2}$ calculated from the ΔS value given by S. C. Furman and C. S. Garner, J. Am. Chem. Soc. **72**, 1785 (1950), and assuming that $\bar{S}^0$ of V^{+3}, aq., is −66 eu (calc from reference 1); FeF^{+2} calculated from N. Uri, Chem. Revs. **50**, 375 (1952); $TlCl^0$, $TlBr^0$ from E. L. Anderson, Jr., and H. W. Dodgen, Abstracts Am. Chem. Soc. Meeting, Los Angeles, California, March 15–19, 1953; FeF_3^0 from L. Heppler (private communication).

[5] Ionic Radii from compilation of R. W. G. Wyckoff, *Crystal Structures* (Interscience, Publishers, Inc., New York, 1951), Vol. I; this compilation is more complete for ionic radii than reference 6.

[6] Covalent radii from L. Pauling, *Nature of the Chemical Bond* (Cornell University Press, Ithaca, 1938); for the radii of molecules, we have used the radius of NH_4^+ for NH_3 (1.48A) and ~1.1A for NO; the value of 1.40A for OH^- and 1.92A for CN^- are from A. F. Wells, *Structural Inorganic Chemistry* (Clarendon Press, Oxford, 1945).

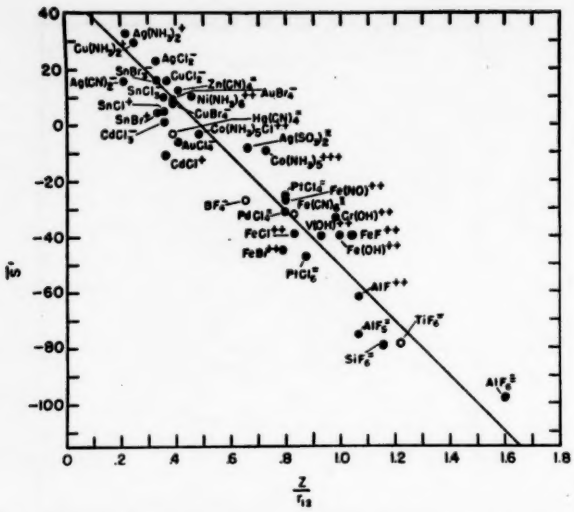

FIG. 2. Correlation of the hydration corrected entropies of complex ions with the charge to radius ratio.

sidered in the thermodynamic entropies under consideration.

Therefore, we have defined a quasi-thermodynamic function, the "corrected" partial molal entropy, $\bar{S}'$, which arises from the following considerations. In the complexing of a simple ion,

$$Fe^{+2}, \text{aq.}, +6CN^-, \text{aq.} = Fe(CN)_6^{-4}, \text{aq.}, \quad (1)$$

the entropy change for the process is measurable, and the entropy of the complex ferrocyanide is given by

$$\bar{S}^0 \text{ complex} = \Delta S + 6\bar{S}^0(CN^-, \text{aq.}) + \bar{S}^0(Fe^{+2}, \text{aq.}). \quad (2)$$

$\bar{S}^0$ represents the "normal," partial molal entropies for ionic species commonly in use. One can, however, also treat Eq. (1) as a replacement of the water in a fully coordinated aquated ferrous ion by cyanide ions, thus:

$$Fe(H_2O)_6^{+2}, \text{aq.} + 6CN^-, \text{aq.} = Fe(CN)_6^{-4}, \text{aq.} + 6H_2O, \quad (3)$$

for which

$$\Delta S = \bar{S}'(Fe(CN)_6^{-4}, \text{aq.}) + 6\bar{S}^0(H_2O) - 6\bar{S}^0(CN^-, \text{aq.}) - \bar{S}^0Fe^{+2}, \text{aq.} \quad (4)$$

and

$$\bar{S}' \text{ complex} = \Delta S + 6\bar{S}^0(CN^-, \text{aq.}) + \bar{S}^0(Fe^{+2}, \text{aq.}) - 6S^0(H_2O), \quad (5)$$

where $\bar{S}'$ refers to the "corrected" entropy.

ΔS is the same in both cases, being an experimental observation, and the corrected entropy, $\bar{S}'$, is related to the "normal" entropy, $\bar{S}^0$, by the relation

$$\bar{S}' = \bar{S}^0 - nS^0(H_2O), \quad (6)$$

where n represents the number of water molecules replaced from the normal coordinated aquated ion by the complexing agent.[7,8] In general, whether the complex ion can be formed by simple replacement or not is immaterial, as long as one is consistent in using the same (and correct) "n" value for a particular ion.†

In Fig. 2, the corrected entropy values, $\bar{S}'$, have been plotted as before against the same Z/r_{12} values, and it can be seen that there is a linear relationship between $\bar{S}'$ and Z/r_{12} which is, by inspection,

$$\bar{S}' = 49 - 99(Z/r_{12}). \quad (7)$$

This equation strictly holds only for complex ions which contain monatomic ions as ligands, and not molecules. To fit the molecularly complexed species, it was necessary to introduce a structural factor, f, so that $r_{12} = (r_1 + r_2)/f$. This procedure was necessary in the case of the oxy-anions[3] and would be expected to be necessary in comparing the complexes involving complicated groups (NO, NH_3, etc.) with monatomic ions (e.g., halides, etc.). The need for the structural factor for the former is undoubtedly related to the fact that these complexes have a more "open" structure. The center of gravity of the complexing molecule as a whole cannot approach the central ion as closely as a monatomic ion can because the charge distribution of the former is not uniform. Thus the calculated interatomic distance does not represent the effective radius of the ion, being too small. At present, neither the abundance nor accuracy of the data requires but a single structural factor ($f = 0.65$) for all of the known molecularly complexed ions for which data are available: (NO, NH_3,

[7] This value of "n" is similar to the "characteristic" and "maximum" coordination numbers of J. Bjerrum, Chem. Revs. **46**, 381 (1950).

[8] Since this paper was written, Professor Latimer has also independently, although earlier, used a similar method in treating the entropies of hydration in the aluminum fluoride complexes [see J. Am. Chem. Soc. **75**, 1548 (1953)].

† A more rigorous thermodynamic treatment can be given to the method by noting the identity

$$\bar{S}'_{MA_y{}^z(H_2O)_x} \equiv \bar{S}^0_{MA_y{}^z, \text{aq.}} + x\bar{S}^0_{H_2O,l}.$$

Equation (6) can therefore be considered as correlating the entropies of species written in their fully coordinated form: $MA_y{}^z(H_2O)_x$. In this interpretation, one should add $(6-y)\bar{S}^0_{H_2O,l}$ entropy units to the entropies of complex ions to "correct" for hydration instead of subtracting $y\bar{S}^0_{H_2O,l}$ units as above. The absolute values for the entropies as given by Eq. (6) are thus too low by a constant factor of $6\bar{S}^0_{H_2O,l}$ or 100.2 eu. It is obvious, however, that this constant will merely shift the scale of Fig. 2, and the calculated entropy for the ions as normally written ($MA_y{}^z$, aq.) will not be affected. Implicit in this treatment is the assumption that all positive ions have the same coordination number (6) inasmuch as the entropy is used as a criterion for coordination. A similar reasoning is implied in the treatment given the simple ions by Powell and Latimer (reference 1) in which a constant factor is added to the radii of all of the cations to obtain a suitable correlation. In this respect, the data reported by Taube and Posey [J. Am. Chem. Soc. **75**, 1463 (1953)] for an isomeric "outer-sphere" cobalt complex are extremely interesting:

$$Co(NH_3)_5SO_4^+ + H_2O = Co(NH_3)_5H_2OSO_4^+ \quad \Delta S = -13 \text{ eu.}$$

The entropy change is almost exactly equal to that which would be predicted by our model for the disappearance of one molecule of water, −16.7 eu. Thus the entropies of the two complex ions are essentially equal, and one has further verification that to a good approximation, the first six coordinating groups are all that need be considered in the entropy calculations.

CN^-, SO_3^{-2}). This approximation may have to be revised at some future date. It was not necessary to use the factor for hydroxy complexes $[M(OH)^{+n}]$ because, apparently, of the small size of the hydrogen atom.

The average deviation of the data given in Fig. 2 is about eight entropy units. It should be noted that the experimental determinations of the entropies of complex ions are subject to much larger errors than are the entropies of the simple ions or oxy-anions. Many of the entropy values have been obtained from equilibrium studies at different temperatures in high ionic strength media. In an excellent review article, Young[9] has pointed out the various difficulties in obtaining *true* thermodynamic constants from such studies, since the values at infinite dilution are required to calculate the $\bar{S}^0$ (and hence, $\bar{S}'$) values. Further, while the stability constants determined by cells with liquid junctions are usually more accurate and reproducible, the potentials may also suffer from unknown junction potentials as well as high ionic strength corrections. Thus, the ΔS data for cadmium chloride obtained by King[10] in solubility studies were for 3 molar chloride solutions, but absolute entropies were calculated using standard state partial molal entropies for the Cd^{+2} and Cl^- ions. These entropy values reported seem rather low in Fig. 1, and we would assume that when the proper corrections can be made, the cadmium chloride values will correspond more closely to those predicted by Eq. (7).

Further, we have no accurate means by which to evaluate the true interatomic distances for aqueous complex species, and most certainly the r_{12} value for $SnCl_3^-$, for example, is not the same as that in $SnCl^+$, although this had to be assumed in calculating (Z/r_{12}). In general, however, the radii are probably more accurate than the experimental errors and not greatly affected by solvation. Considering these difficulties, it is believed that the average deviation corresponds rather well to what one expects from the accuracy of most of the data.[4]

There are four ions which cannot be treated by the proposed method, and were omitted from Fig. 2: AlF_2^+, AlF_4^-, $HgBr_4^{-2}$, and $Au(CN)_2^-$. In the case of the latter, the value reported[11] for the potential leads to a value for the dissociation constant of 10^{-39}, which seems remarkably low [$Cu(CN)_2^-$: 1×10^{-16}; $Ag(CN)_2^-$: 1.8×10^{-19}]. If it is assumed that the heat of formation is correct ($\Delta H_f^0 = 58.4$ kcal mole^{-1}),[12] then the predicted value of the entropy of 64 eu (exp value calc: 29.5 eu) leads to a much lower value of K ($\sim10^{-30}$). This value is still small but seems corrected in the right direction.

The data of Sherill[13] on the halide complexing of mercury do not, in the case of the chloride complexes, agree with the more recent values of Johnson, Quarfort, and Sillen.[14] If the data for the $HgBr_4^{-2}$ are also incorrect, then the entropy value calculated for this species by Latimer[4] is also incorrect, as indeed, Eq. (7) predicts (exp 84 eu, calc: 39 eu).

Table I. Neutral aqueous complex ions.

Species	r_{12}(A)	$\bar{S}^0$ obs	$\bar{S}^0$ calc	$\bar{S}'$ calc
$SnBr_2^0$	2.98	47	46	13
$CdCl_2^0$	2.79	17	38	5
$AgCl^0$	2.77	37	21	4
$SnCl_2^0$	2.82	39	40	7
FeF_2^0	2.00	8	5	−45
AlF_3^0	1.88	−6	−6	−56
$TlBr^0$	3.46	50	47	30
$TlCl^0$	3.30	48	42	25

In the case of the two aluminum fluorides, no apparent explanation seems very satisfactory in view of the fact that the entropies of AlF_6^{-3}, AlF_5^{-2}, AlF^{+2}, BF_4^-, SiF_6^{-2}, TiF_6^{-2}, and FeF^{+2} seem to fit the proposed treatment. Unless these species are dimerized or further hydrated, we are unable to account at present for this apparent discrepancy: AlF_4^-, obs: 5 eu, calc: 62; AlF_2^+, obs: −23 eu, calc: 28.

It is of interest to note that the oxy-cations UO_2^{+2}, UO_2^+ are also in agreement with the present treatment (not shown in Figs. 1, 2). This may be accidental, and much more data will be required to see if this class in actuality represents a complex ion of the type under discussion.[15]

We have also included in Fig. 2 some estimates made by Latimer[4] which are based on only partially complete thermodynamic data.

NEUTRAL SPECIES

The same general method can be extended to neutral species and seems to correlate reasonably the few data which are available. Table I contains the calculated and observed entropies for eight neutral halide complex ions. The calculated values are from the equation obtained by inspection:

$$\bar{S}' = 132 - 354/r_{12}. \qquad (8)$$

Table II. Calculated values of $\bar{S}^0$ for some monatomic cations.

Species	$\bar{S}^0$(obs)	$\bar{S}^0$(calc)[a]
Cs^+	32	20
Na^+	14	15
Ag^+	18	14
Sr^{++}	−9	−15
Gd^{+++}	−43	−49
Al^{+++}	−70	−75
Pu^{++++}	−87	−83

[a] Calc from Eq. (13) using ionic radii of reference 5, and $r_2 = 2.0$A.

[9] T. F. Young, *Annual Reviews of Physical Chemistry* (Annual Reviews, Inc., Stanford, California), Vol. III, p. 275.
[10] E. L. King, J. Am. Chem. Soc. **71**, 322 (1949).
[11] G. Bodländer, Ber. deut. chem. ges. **36**, 3933 (1903).
[12] National Bureau of Standards, "Selected values of chemical thermodynamic properties" (1948).
[13] M. S. Sherill, Z. physik. Chem. **43**, 735 (1903); **47**, 103 (1904).
[14] Johnson, Quarfort, and Sillen, Acta. Chem. Scand. **1**, 46, 473 (1947).
[15] See also R. E. Connick and Z. Z. Hugus, J. Am. Chem. Soc. **74**, 6012 (1952).

The mean deviation of the calculated and observed values is ~7 eu, although if the $CdCl_2^0$ data are not used for reasons already given, then a revised equation can be used with a much smaller average deviation. Much more data on these species will have to be collected before the general validity of Eq. (8) can be established.

GENERAL EQUATIONS FOR COMPLEX ION FORMATION

The general equation for the complexing of a simple ion by ionic ligands can be written

$$xM^a(H_2O)_y + zN^{-b} = M_xN_z(H_2O)_{(y-z)}{}^{(xa-bz)} + zH_2O. \quad (9)$$

Powell and Latimer[1] have proposed for the simple ions the expression

$$\bar{S}^0 = 3/2R \ln M + 37 - 270Z/r_e^2, \quad (10)$$

for which we can substitute without any loss of generality and little in accuracy

$$\bar{S}^0 = 49 - 270Z/r_e^2, \quad (11)$$

where $r_e = r_N + 1.00$A for anions, and $r_M + 2.00$A for cations. Combining Eq. (11) with (7) we obtain for the reaction in Eq. (9)

$$\Delta S = 49 + 16.7z - 49(z+x) - \frac{99(xa-bz)}{r_{12}} + 270\left[\frac{bz}{(r_2+1)^2} + \frac{xa}{(r_1+2)^2}\right]. \quad (12)$$

$xa \neq bz$

Differentiation of this expression with respect to any one of the five variables (x, a, y, z, b) results in still complicated expressions which contain more than one term and frequently four variables. It thus appears that any "rules" or generalizations for entropy charges on complexing, in order to be accurately in agreement with Eq. (12) are not simply formulated, since the sign of the differential will depend upon the relative magnitudes of the various terms. This expression should be useful in comparing ΔS values of one cationic sequence and a particular anion complexing agent, with another series of the same cationic sequence and a different anion. In these cases, it might be hoped that the expression would be applicable even in nonideal situations of high ionic strength.

One generalization is evident, however, from our replacement model: The entropies of complex ions of the same cation-anion pair which have the same charge will differ by the difference in their number of ligands times the entropy of water, the more highly complexed species having the larger entropy; thus, $\bar{S}^0_{(SnBr_3^-)} - \bar{S}^0_{(SnBr^+)} = 2S^0_{(H_2O)} = 33$ eu, (obs 45); $\Delta S(SnCl_3^- - SnCl^+) = 33$ eu, (obs 39); $\Delta S(AlF_5^{-2} - AlF^{+2}) = 67$ e.u., (obs 52). If the general hypothesis of hydration which has been outlined here is valid, then it ought to be possible to calculate the entropies of the monatomic, aqueous ions by our same general method. For these ions, $\bar{S}^0 \equiv \bar{S}$ by Eq. (6) since $n=0$. Thus the general expression (7) becomes

$$\bar{S}^0 = 49 - 99\left(\frac{Z}{r_{12}}\right), \quad (13)$$

which we can compare to the modified Powell and Latimer Eq. (11) for monatomic ions. These two equations are strictly compatible only if $270(Z/r_e^2) \approx 99(Z/r_{12})$. Identifying r_{eff} with r_{12} gives $r_e \approx 2.7$A; since $r_e = r_1 + 2$A for the cations, then $r_1 \approx 0.7$A for which these two expressions are exactly equivalent. However, Eq. (11) is somewhat insensitive to changes in r_1, and since most of the simple ions have radii lying between 0.55 (Al^{+3}) and 1.70 (Cs^+)A, Eq. (13) effectively (though not as accurately) also reproduces the entropies for most of the monatomic ions. This fact is illustrated in Table II. The agreement is obviously poor for extreme r_1 values.[16]

The general usefulness of the method will perhaps be greatest in obtaining bond strengths for complex species from equilibrium measurements at single temperatures. Thus, it is now possible to estimate heats of formation for many complex ions for which only free-energy data at one temperature are now available. It is also possible that the method may be useful in aiding the extrapolation of thermodynamic functions to infinite dilution.

Although the heats of formation will be in error by only a few kilocalories due to an error of 5–10 eu in the estimation of ΔS values, the need for much more accurate entropy determinations (and redeterminations), properly corrected to standard state conditions is obvious from the scatter of the data in Fig. 2 and lack of agreement in the literature between various observers for some species.

ACKNOWLEDGMENT

The author would like to thank Professor W. M. Latimer, for his values on the entropies for the fluoride complexes of aluminum prior to publication, and Professor R. E. Connick for helpful discussions of the problem.

[16] Better agreement can be obtained if the mass correction term is incorporated in Eq. (13).

Empirical Considerations of Entropy. III. A Structural Approach to the Entropies of Aqueous Organic Solutes and Complex Ions*

JAMES W. COBBLE
Radiation Laboratory and Department of Chemistry and Chemical Engineering, University of California, Berkeley, California

(Received April 7, 1953)

A method for estimating the entropy of complex aqueous organic solutes and related species has been developed by a structural extension of a method of Powell and Latimer for simple solutes. The agreement between calculated and observed values is, in general, good, although systematic deviations begin to occur for very complicated and large solutes. The method is extended to the calculation of the entropies of charged organo-metallic complex ions with good success, and possible applications to systems of biological interest are indicated.

Subsequent to the development of the general method for estimating the entropies of aqueous solutes, an empirical equation is also given for calculating gaseous entropies of both inorganic (ionic) and organic molecules from their structures.

INTRODUCTION

THE success of our previous attempts, as well as others,[1,2] to correlate and calculate the entropies of aqueous inorganic ions[3] has led to an investigation of a similar correlation for organic aqueous species. These molecules are of particular interest due to current interest in organic complexing and chelating agents[4] and are much more general and abundant and varied than inorganic species. Further, the accumulation of the thermodynamic data for many types of organic compounds[5] has now provided a sizable amount of information with which (when combined with suitable solubility determinations) one can estimate the absolute entropies for aqueous complexing agents. In some cases of neutral solutes, the activity coefficients and thermochemical heats of solution are also available so that as a class the data for *neutral* organic species are as accurate as that available for inorganic solutes.

An attempt is also made to correlate the data available for metallo-organic complexes and chelates, although the data for this particular species are probably the least accurate yet treated. Nevertheless, we can semiquantitatively illustrate some general principles which, it is believed, will be generally applicable and useful.

STRUCTURAL DEPENDENCE

One can conclude from the previous treatments that the size of an aqueous solute is primarily responsible for the magnitude and sign of its partial molal entropy. While the charge is also important, this is probably due to the effect of orientation of nearby water molecules, which can be looked upon as a change in the effective size of the solute. In the inorganic ions, the size of an ion could be related to rather well-defined interatomic distances in the ion. This method proved successful probably because of the inherent simplicity and limited number of atoms in the inorganic ions. Further, those ions of larger size (i.e., complex ions) usually possessed high symmetry ($PtCl_6^{-2}$, $Fe(CN)_4^{-4}$) and could also be well defined by a single interatomic distance. With organic ions, the simplicity and symmetry rapidly disappears with increasing numbers of atoms, and it was clear that some other method would have to be used for organic solutes. One perhaps could effectively use the partial molal volumes, but these data are not generally available. A possible solution can be found in the recent treatment that Powell and Latimer[1] have proposed, which bases the aqueous entropy upon the molar volume of the pure liquid state of the solute. The equation which they give is

$$\bar{S}^0 = 10 + \tfrac{3}{2}R \ln M + S_{(\text{int})} - 0.22Vm, \qquad (1)$$

where $\bar{S}^0$ is the partial molal entropy at 25° for the hypothetical one molal ideal solution of a solute of mass M which has a molar volume, Vm, in the pure liquid state at 25°C. $S_{(\text{int})}$ is the internal entropy of the molecule, which is assumed to be the same for the dissolved solute as for that of the gaseous molecule, and is thus given by the total entropy, $S^0_{(g)}$, less the translational entropy, $\frac{3}{2}R \ln M + 26.00$. The gaseous entropy, $S^0_{(g)}$, can be approximated by the entropy of the pure substance plus its entropy of vaporization, but the entropy of vaporization is not always available for substances which are solids at ordinary temperatures, or which decompose easily when heated (sugars, amino acids, etc.). Therefore, use has been made of the observations previously made by others that the entropies of pure organic compounds are generally additive in some simple manner depending upon the number of atoms in

* This work was performed under the auspices of the U. S. Atomic Energy Commission.

[1] R. E. Powell and W. M. Latimer, J. Chem. Phys. **19**, 1139 (1951).

[2] R. E. Powell and R. E. Connick (private communication, 1952).

[3] J. W. Cobble, J. Chem. Phys. **21**, 1443, 1446 (1953), papers I and II of this sequence.

[4] A. E. Martell and M. Calvin, *Chemistry of the Metal Chelate Compounds* (Prentice-Hall, Inc., New York, 1952).

[5] Summarized in Volumes I–III, *Annual Reviews of Physical Chemistry* (Annual Reviews, Inc., Stanford, 1950–1952).

TABLE I. Structural correction entropy values.

Structure	$S^0_{(s)}$(e.u.)
double-bond	3.5
triple-bond	4.5
ring	14
branched chain	3.0
≥ 3 Adjacent $-OH$ groups	16

the molecule, and in the way in which it is put together.[6-8] Theoretical justifications for these empirical treatments have been discussed by others.[9,10] An equation which will reproduce the entropies of *gaseous* molecules (standard state: ideal gas at unit fugacity, 25°C) has been found by inspection of the entropies for a wide variety of compounds:

$$S^0_{(g)} = S^0_{(\text{trans})} + 9.2(N) - S^0_{(s)}$$
$$= \tfrac{3}{2}R \ln M + 26.00 + 9.2(N) - S^0_{(s)}, \qquad (2)$$

where N represents the number of "skeletal" bonded atoms in the compound (total bonded atoms minus hydrogens), M is the mass of the molecule, and $S^0_{(s)}$ is the entropy loss computed empirically from the observation that double bonds, rings, and branched chains all lower the entropy from an equivalent "normal" linear molecule. The entropy-loss values are given in Table I. It seems to make little difference whether N is a nitrogen, sulfur, hydrogen, or oxygen atom instead of carbon, and Eq. (2) will, for $N=0$, reduce to that required for monatomic gases. Electronic contributions to the ground states of atoms and molecules have been ignored.

The origin of the required subtraction of 16 e.u. for molecules possessing ≥ 3 neighboring $-OH$ groups is interesting. It was first noticed by inspection of the solution data and thought to be due to some special type of interaction of the solute molecule with the solvent. Actually, however, it can be demonstrated that the effect is also present in the gaseous molecule, and therefore probably does not constitute a bona-fide deviation from Eq. (1). Thus, the calculated value for the entropy of gaseous glycerin without the correction is 92 eu and, with it, 76 eu. The observed value (calculated from vapor pressure measurements and the entropy of liquid glycerin) is 80 eu.

The empirical constants given are based upon the following general considerations: (a) A cyclic ring in a compound is treated as a single atom when computing branched chains; thus methyl benzene and dimethyl benzenes would be considered as having no branched chains, while trimethyl benzene would have one. (b) A branched (but not terminal) NH_2 group is ignored in computing "N" and $S^0_{(s)}$, but not in "M," the molecular weight (this effect has long been observed by others, and we have also invoked this special exception). (c) The number of double and triple bonds in related compounds are determined by classical structures:

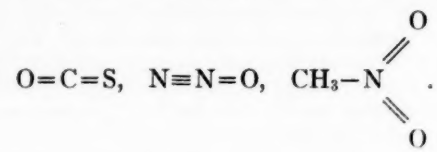

The justification for all of these "rules" is purely empirical. One could, of course, formulate so many rules that while the entropies could then be exactly calculated to a high precision, the method would soon lose its generality and usefulness. With the above few generalizations, all of the known gaseous entropies have been reproduced to an average deviation of a few entropy units.[11]

Combining Eqs. (1) and (2) the following expression is obtained:

$$\bar{S}^0 = 10 + \tfrac{3}{2}R \ln M + 9.2(N) - S^0_{(s)} - 0.22Vm. \qquad (3)$$

This equation is a structural extension of Eq. (1), but generally more useful in the above form since the entropies for many species can now be calculated for which no detailed information is available on the gaseous state. A test for Eq. (3) is afforded by Table II in which the observed and calculated partial molal entropies for a wide variety of species have been summarized. The average deviation is about 3 eu, the largest uncertainty frequently resulting from the necessity of approximating the molar volume, but this can usually be done for simple molecules by the parachor method, by estimation from the solid (by decreasing the density of the solid by $\sim$10 percent), or from the densities of concentrated solutions. Fortunately, the low coefficient, 0.22, removes the necessity for knowning Vm very accurately, although some exceptions to this generalization will be found in a later section on metallo-organic ions.

Since the deviations of palmitic acid ($N=18$) and sucrose ($N=23$) are both in the same direction, we would conclude that the proposed treatment becomes invalid for extremely large aqueous solutes. This deviation probably is due to the entropy of solution factors, or failure of the original Powell and Latimer equation (1), since our empirical equation for gaseous species agrees well with what experimental data are available for large gaseous molecules. If one plots the function $\bar{S}^0 - \tfrac{3}{2}R \ln M + S^0_{(s)} + 0.22Vm$ against "N," a smooth

[6] G. S. Parks and H. M. Huffman, *The Free Energies of Some Carbon Compounds* (Chemical Catalogue Company, New York, 1932).

[7] H. M. Huffman and E. L. Ellis, J. Am. Chem. Soc. **57**, 46 (1935); **59**, 2150 (1937).

[8] National Bureau of Standards and American Petroleum Institute Circular C-461, "Selected Values of Properties of Hydrocarbons," Washington, D. C., 1947.

[9] M. L. Huggins, J. Chem. Phys. **8**, 181 (1940).

[10] K. S. Pitzer, Chem. Revs. **27**, 39 (1940).

[11] It should be pointed out that the applicability of Eq. (2) is not limited to organic molecules. Thus, we compare the observed and calculated values for the gaseous entropies at 25° for a wide variety of inorganic compounds: BBr_3: 77.49, 77; KCl: 57.2, 57; IBr: 61.8, 60; O_4O_4: 65.6, 69; GeO: 52.6, 54; $B_3N_3H_3$: 73.7, 80; Re_2O_7: 100, 94; SO_3: 61.24, 62; CO: 47.3, 51.

TABLE II. Comparison of calculated and observed aqueous partial molal entropies at 25°C.

ΔS^0 reference	Species	S^0_{298}[a]	ΔS^{0b}	$\bar{S}^0$(obs)[b]	$\bar{S}^0$cal	Δ[c]
d	$He_{(g)}$	30.13	−18.5	11.6	12	0
d	$Rn_{(g)}$	42.10	−26.3	15.8	16	0
e	$HF_{(g)}$	41.47	−15.5	*26*	24	2
e	$H_2S_{(g)}$	49.15	−20.0	29.2	23	6
e	$NH_{3(g)}$	46.01	−19.7	26.3	24	2
d, f	$CH_{4(g)}$	44.50	−23.8	23.5	21	3
d	$C_2H_{2(g)}$	47.997	−17.6	30.4	28	2
d	$C_2H_{4(g)}$	52.45	−23.3	29.2	28	1
d, f	$C_2H_{6(g)}$	54.85	−28.4	26.5	26	−1
d	$CH_3Cl_{(g)}$	55.97	−25.6	30.4	29	0
e	$HCN_{(g)}$	48.23	−17.4	*30.8*	33	−2
d	$CH_3OH_{(g)}$	56.8	−27.0	31.6	30	2
d	$NO_{(g)}$	50.339	−21.4	28.9	30	−1
d	$O_{2(g)}$	49.003	−23.3	25.7	23	3
d	$CO_{(g)}$	47.30	−21.8	25.5	29	−3
e	$CO_{2(g)}$	51.061	−22.1	29.0	31	−2
e	$SO_{2(g)}$	59.40	−21.4	*38*	36	2
g	$CNI_{(g)}$	61.26	−23.4	37.9	37	1
e	HClO, aq.			*42*	37	5
e	$HCOOH_{(l)}$	30.82	8.3	39.1	36	3
d	$C_2H_5OH_{(g)}$	67.4	−32.8	34.6	36	−1
f	$C_3H_{8(g)}$	64.51	−32.0	32.5	32	0
d	$COS_{(g)}$	55.34	−27.1	28.2	32	−4
e	$H_2N_2O_2$, aq.			*52*	50	2
g	$(NH_2)_2CO_{(c)}$	25.00	16.6	41.6	42	0
f	$C_4H_{10(g)}$	74.10	−33.4	40.7	38	3
d	$(CH_3)_2CO_{(g)}$	[h]72.7	−27.1	45.6	43	3
d	$i\text{-}C_3H_7OH_{(g)}$	[h]78.3	−35.5	42.8	43	0
d	$CHCl_{3(g)}$	70.86	−35.8	35.1	40	−5
e	$CH_3COOH_{(l)}$	38.2	4.8	43.0	39	−4
d	$n\text{-}C_4H_9OH_{(g)}$	[i]86.7	−44.0	42.7	49	−6
d	tert.-$C_4H_9OH_{(g)}$	[i]78.0	−39.6	38.4	42	−4
d	$CCl_{4(g)}$	73.95	−30	44	44	0
d	$(C_2H_5)_2O_{(g)}$	[i]83.3	−42.5	40.8	49	−7
j	$CH_2(NH_2)COOH_{(c)}$	31.6	9.5	41.1	38	3
e	H_3PO_4, aq.			*42.1*	46	−4
d	$CH_3COOC_2H_{5(g)}$	85.6	−35.1	50.6	51	−1
k	glycerol$_{(l)}$	49.7	−4.7	45.0	46	−1
l	$C_6H_{6(l)}$	41.30	−5.6	35.7	34	2
j	$p\text{-}C_6H_4Cl_{2(c)}$	41.9	4.4	46.3	49	−3
m	$CH_3C_6H_{5(l)}$	52.48	−8.1	44.4	43	1
m	$C_2H_5C_6H_{5(l)}$	60.99	−11.1	49.9	46	4
m	*p*-xylene$_{(l)}$	59.12	−11.0	48.1	47	1
j	phenol$_{(s)}$	34.0	8.6	42.6	42	1
j	*d, l* leucine$_{(c)}$	[n]49.5	1.3	50.8	50	1
m	$C_6H_5COOH_{(c)}$	40.8	5.95	46.8	49	2
l	naphthalene$_{(c)}$	38.89	8.6	47.5	43	5
l	biphenyl$_{(c)}$	49.2	4.8	54.0	52	2
j	*l*-sorbose$_{(c)}$	[o]52.8	11	64	66	−2
j	mannitol$_{(c)}$	57.0	18	75	77	−2
j	*l*-tyrosin$_{(c)}$	[n]53.0	6.9	59.9	62	−2
j	*l*-cystine$_{(l)}$	[n]68.5	−13.5	55.0	56	−1
j	Palmitic acid$_{(c)}$	113.7	−9	105	120	−15
k	Sucrose$_{(c)}$	86.1	10.1	96.2	127	−31

[a] Values taken from references 7, 8, e, and g unless otherwise indicated.

[b] Italicized values indicate that $\bar{S}^0$ was calculated from sources other than the entropy of solution.

[c] $\Delta \equiv \bar{S}^0$(obs) $-\bar{S}^0$(calc).

[d] J. A. V. Butler, Trans. Faraday Soc. **33**, 229 (1937); Butler's standard state ($N_2=1$, and $p=1$ mm Hg) requires the subtraction of 21.2 eu to conform to the one used in this paper.

[e] W. M. Latimer, *Oxidation Potentials* (Prentice-Hall, Inc., New York, 1952), 2nd ed.

[f] W. F. Claussen and M. F. Polglase, J. Am. Chem. Soc. **74**, 4817 (1952); corrected to our standard state by subtraction of 8.0 eu.

[g] National Bureau of Standards, "Selected Values of Chemical Thermodynamic Properties," Washington, D. C., 1949.

[h] S. C. Schumann and J. G. Aston, J. Chem. Phys. **6**, 480 (1938).

[i] Gaseous entropies estimated from entropies of liquids given in references indicated and vapor pressure data summarized in J. Timmermans, *Physico-Chemical Constants of Pure Organic Compounds* (Elsevier Publishers, New York, 1950).

[j] ΔS values estimated from solubility-temperature data given in A. Siedell, *Solubilities of Organic Compounds* (D. Van Nostrand Company, Inc., New York, 1941) 3rd ed.; supplement, 1952; for phenol and mannitol, heat of solution from I.C.T., Vol. 5, 1st ed., p. 150.

curve can be drawn through the values and is linear [in agreement with Eq. (3)] below $N \approx 14$. With such a "working" curve, values can still be accurately estimated for large "N" values even though our original expression is no longer valid.

It is of interest that poorer agreement is obtained between calculated and observed aqueous entropies if the cyclic structure of sugars had been ignored:

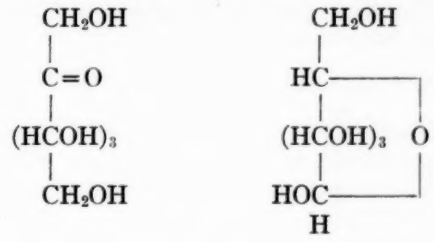

calc: 76 eu calc: 66 eu

(*l*-Sorbose: obs: 64 eu).

The amino acids also present a special class of compounds, but are formally well represented in the present treatment by assuming the "zwitterion" is in effect a cyclic compound, by partial charge cancellation:

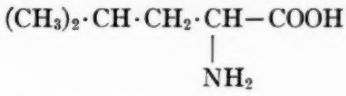

calc: 64 eu.

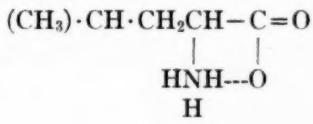

calc: 50 eu

(*d, l*, leucine, obs: 50.8 eu).

The contribution of the NH_2 itself has, in accord with our previous "rules," been ignored. Conversely, the general applicability of the treatment may also be of help to identify the structure of the solute when its entropy is known.

It might be pointed out that a consequence of Powell and Latimer's original equation is that the entropy of solution of a gaseous solute is given by

$$\Delta S^0 = -(16+0.22Vm). \quad (4)$$

[k] Solubility and activity coefficient data from Scatchard, Hamer, and Wood, J. Am. Chem. Soc. **60**, 3067 (1938); heat of solution data from I.C.T., Vol. 5, 1st ed., p. 150.

[l] R. L. Bohon and W. F. Claussen, J. Am. Chem. Soc. **73**, 1571 (1951). These authors give ΔS instead of ΔS^0 values and their data have been recalculated; the $\Delta \bar{H}$ values from which ΔS^0 is calculated for naphthalene and diphenyl are given for the equilibria involving supercooled liquids and have been corrected to the stable crystalline reference state by the heats of fusion of these compounds and the specific heats given in Spaght, Thomas, and Parks, J. Phys. Chem. **36**, 883 (1932).

[m] V. Jones and H. N. Parton, Trans. Faraday Soc. **48**, 8 (1952).

[n] See reference 7.

[o] G. W. Jack and G. Stegeman, J. Am. Chem. Soc. **63**, 2121 (1941).

This equation can then be used to test ΔS data for which the absolute entropy of the solute is not available. In general, the agreement between calculated and experimental values is excellent except in the cases of solutes with large molar volumes which have somewhat larger $-\Delta S$ values than predicted.

IONIC ORGANIC SPECIES

The treatment given above can be extended to ionic species by differentiating Eq. (3):

$$d\bar{S}^0 = 9.2dN - dS^0{}_{(s)} - 0.22dVm + \tfrac{3}{2}Rd\ln M. \quad (5)$$

Thus, the entropy of some member of an ionic homolog can be calculated from another simpler member by adding the entropy required by Eq. (5) for their differences in structure, numbers of atoms, and molar volumes. For example, we calculate from acetate ion ($\bar{S}^0 = 20.8$ eu) 30 eu for benzoate ion (obs: 27.9).[11] Formate ion was not used since it does not possess a "hydrocarbon" group, but from its entropy of 22.7 eu, bicarbonate is calculated to be 26 eu (obs: 22.7). The difference between CNO^- and $CN\bar{S}$ is calculated to be 2.9 eu (obs: 2.7 eu). The entropy of malonate ion is estimated to be 17.6 eu, from oxalate ion, 10.6 eu, etc. When more data are available, this method can be tested more exactly for its general applicability. (See also reference 3.)

METALLO-ORGANIC IONS: COMPLEXES AND CHELATES

In a previous paper[3] it was demonstrated that the entropies of complex inorganic ions could be correlated when the "corrected" entropies ($\bar{S}'$) were considered:

$$\bar{S}' = \bar{S}^0 - nS^0(H_2O), \quad (6)$$

where n represents the number of water molecules replaced from the central ion on complexing, and $\bar{S}^0$ is the partial molal entropy as normally used. It is with some assurance, therefore, that the same method can be applied to the organic ions, and these entropies can now be calculated in the following manner: As the simple ion is covered with organic ligands, the polar parts of the molecule will be oriented towards the central ion, so that the organic complex now presents a hydrocarbon "shell" to the solvent. The net effect is to screen or insulate the charge of the central ion, provided the organic ligand has a chain which is 2–3 atoms long. The entropy can be calculated by then assuming the complex is made up of hydrocarbon equivalent atoms by use of Eq. (2). This entropy is to be identified with $\bar{S}'$, $\bar{S}^0$ being finally calculated by Eq. (6). It should be noted that when organic molecules form chelates, *two* molecules of water per ligand are replaced, cyclic structures being formed in the process. Thus, n cannot be simply determined by the number of molecules in the complex ion, although usually values are reported for the

TABLE III. Comparison of observed and calculated entropies for metallorganic ions.

System	ΔSobs (e.u.)	$\bar{S}^0$ligand (e.u.)	$\bar{S}^0$complex (e.u.)		$\bar{S}'$complex calc (e.u.)	"n" (number of H_2O's replaced)	$\bar{S}^0 = \bar{S}' + nS^0(H_2O)$ (e.u.)
$6CH_3NH_2 + Ni^{++}$[a]	73	29	222		94	6	194
Triene[b] + Ni^{++}	24		84				
Zn^{++}	43	85	102	92	49	2	82
Mn^{++}	12		77	±10			
Cd^{++}	38		108				
Diene + Ni^{++}[b]	10.2		57				
Zn^{++}	15.9	72	62	54	69	2	98
Mn^{++}	5.2		55	±6			
Fe^{++}	−1.3		44				
3 en[c] + Ni^{++}	41	46	154		63	6	163
3 triene[b] + 2 Mn^{++}	0		215		125[e] (4 rings)	4	190
3 triene[b] + 2 Cd^{++}	0	85	225	209			
3 triene[b] + 2 Fe^{++}	−12		189	±10	−40[e] (14 rings)	12	160
3 triene[b] + 2 Co^{++}	2		207				
2 diene[b] + Mn^{++}	−3.7		120				
Fe^{++}	−7.7	72	109	114	83	4	150
Co^{++}	−5.4		114	±3			
Ni^{++}	−6.0		113				
3 Dipy[d] + Fe^{++}	~0	52	~130		50[e]	6	150
Dipy[d] + H^+	13	52	65		38	2	71

[a] See reference 13.
[b] Jonassen, Hurst, LeBlanc, and Meibohm, J. Phys. Chem. **56**, 16 (1952).
[c] F. Basolo and R. K. Murmann, J. Am. Chem. Soc. **74**, 5243 (1952), see also reference 16.
[d] J. H. Baxendale and P. George, Trans. Faraday Soc. **46**, 55 (1950).
[e] The entropies for these species were estimated from the expression $\bar{S}^0 = 10 + 3/2R\ln M + 10.1(N) - 0.1(N)^2 - S^0{}_{(s)} - 0.22Vm$ instead of Eq. (3) which is no longer valid for large "N" values (see text). In the case of $Fe(dipy)_3^{+2}$, the value predicted by Eq. (3) is approximately 100 eu too large.

maximum coordination, from which the structure (simple coordination or chelation) can then be inferred.

There are so few absolute entropies for organic complex ions available that it seems desirable to test the method proposed here by the *entropy change* data, ΔS^0, which are more available.[12] There are two ways this can be done: calculate ΔS^0 from estimations of the entropies of both the ligand and complex species, or, estimate the entropy of the ligand and calculate $\bar{S}^0$ for the complex. The latter will be used since it has several advantages, not the least being that it illustrates the large positive entropies which are involved.

As an example, consider the ΔS^0 value reported by M. Calvin[13] for the following:

$$Ni^{+2}, aq. + 6CH_3NH_2, aq. = Ni(CH_3NH_2)_6^{+2}$$
$$\Delta S = 73 \text{ e.u.}$$

From Eq. (3) the entropy of CH_3NH_2, aq. is estimated to be 29 eu, which is probably accurate to a few entropy units. Using -25 eu for Ni^{+2}, aq.,[14] the entropy of $Ni(CH_3NH_2)_6^{+2}$ is calculated to be 222 eu (compared to $Ni(NH_3)_6^{+2}$, $\bar{S}^0 = 111$ eu). The value can easily be in error by 10–15 eu due to the entropy of CH_3NH_2, aq., and ΔS is probably accurate only to ± 10 eu. Thus the entropy of $Ni(CH_3NH_2)_6^{+2}$ is only accurate to about 20 eu; 222 ± 20. Large errors are, in general, to be expected in these systems, since most entropy values for organic complex ions have been obtained from temperature coefficient data, and previous experience on inorganic species indicates that such calculated values frequently differ from direct calorimetric determinations by sizable amounts; further, little attempt has been made by investigators in this field to correct their data to zero ionic strength. As Young has recently pointed out,[15] such data not corrected cannot be considered but as an approximation to the correct thermodynamic properties. Nevertheless, the data are semiquantitatively useful since such large numbers are involved and ± 20 eu in 200 eu is only a 10 percent error. The calculated value is obtained from Eq. (2) with $N = 13$, and considering the $CH_3-NH_2-Cu^{+2}-NH_2-CH_3$ to have four branched NH_2-CH_3 groups. To approximate the molar volume, a value can be obtained by assuming the volume of six CH_3NH_2 molecules remains unchanged when added to the Cu^{+2} ion, but that its added mass changes the density and hence lowers the molar volume. Thus,

$$Vm \approx 6(40)/1.3 \approx 184 \text{ cc.}$$

$\bar{S}'$ is then calculated to be about 94 eu, and $\bar{S}^0 = 94 + 6S^0(H_2O) \approx 194$ eu. Comparison of this value with the one observed above, 222 ± 20, seems to be satisfactory in view of the fact that the latter was obtained from data not corrected to infinite dilution.

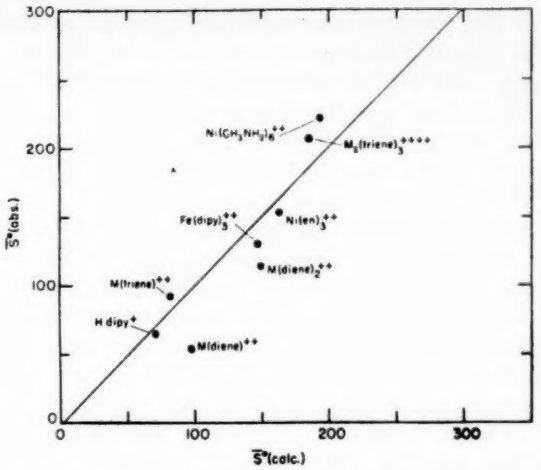

FIG. 1. Comparison of observed and calculated partial molal entropies for organo-metallic complex ions and chelates.

In a similar manner, entropies have been calculated for other species and are given in Table III. No attempt has been made to include all of the data available, and Table III contains only some selected systems to illustrate the principles involved. Since many of the values reported by various observers are frequently in disagreement,[16] it is believed that the average agreement obtained of 10–20 percent is all one can *expect*. The method proposed here for the calculation of entropy cannot be rigorously tested until the true thermodynamic constants are available, including calorimetric data on complexing.

The determination of the densities of pure complex species or similar species will also be necessary for the close estimation of the molar volumes, especially for the more complex ions where the term $0.22Vm$ becomes important.

There are a few interesting features to be noted in Table III. A criterion for internal consistency of a sequence of cations with a given complexing agent can be found in the constancy of the sum of the ΔS value and the entropy of the ion being complexed. This results from the fact that the theory does not distinguish between ions forming the same type of complex, except for the small changes in Vm caused by differences in mass. This is borne out by the experimental results in

[12] It seems remarkable, however, with the large number of stability constants known, that only a dozen or so ΔS values have been reported for organo-metallic species.

[13] As reported in H. S. Frank and M. W. Evans, J. Chem. Phys. 13, 507 (1945).

[14] Estimated by the method given in reference 1; (for comparison: Cu^{+2}, -23.6 eu; Mn^{+2}, -20 eu; Fe^{+2}, -27.1 eu).

[15] T. F. Young, *Annual Review of Physical Chemistry* (Annual Reviews, Inc., Stanford, California, 1952), Vol. 3, p. 275.

[16] To illustrate this point, M. Calvin and R. Bales (J. Am. Chem. Soc. 68, 953 (1946)) report $\Delta S = 2$ eu for the reaction $Ni^{+2} + 3\ en = Ni(en)_3^{+2}$, while F. Basolo and R. K. Murmann (J. Am. Chem. Soc. 74, 5243 (1952)) report $\Delta S = 41$. Further, Basolo and Murmann obtain 34 eu for the reaction $Ni^{+2} + 2en = Ni(en)_2^{+2}$, while H. Irving (private communication in previous reference) reports -27 eu. We find it hard to understand the small or negative entropies of reactions for these systems and have accordingly used Basolo's and Murmann's results in Table III. The value they report for similar Cu^{+2} ion complexing is also in agreement. (See also reference 15.)

Table III. Further, the requirement that the structure of the ion need be known in detail is not crucial, especially with chelate compounds. In these latter compounds further coordination is aided by the gain of 2(16.7 eu) per two water molecules released, but hindered by the loss of 14 eu per chelate ring formed. Also, in some structures, the entry of the metallic ion into further coordination may produce more than one ring with the net result being little change in the total entropy of the compound, as illustrated in Table III by the M_2 triene$_3$ chelates. As one proceeds to smaller and fewer organic ligands, the observed entropies will in general be smaller than the calculated values because our original hypothesis of "burying" the charge of the ion in a hydrocarbon matrix is no longer valid. The data have also been summarized in Fig. 1.

COMPLICATED SYSTEMS

It is of interest to extend the trestment to some very complex species. Klotz and Curme[17] have reported on the successive complexing of bovine serum albumin by cupric ions, from which we shall choose the reaction

$$\text{protein} + 16\ Cu^{++} = \text{protein}(Cu^{++})_{16} \quad \Delta S = 380 \text{ eu}.$$

While this value is very large, it represents only a very small change in the total entropy of the protein: ($\bar{S}^0_{(est)} \sim 2 \times 10^4$ eu). Nevertheless, the ΔS value can be thought of as involving the creation of a ring with each Cu^{+2} ion that goes on the protein molecule with a loss of two water molecules per bound ion. Therefore, the calculated value for ΔS above is 16(9), change in numbers of atoms, minus 16(14), formation of rings, plus 32(16.7), loss of water molecules from Cu^{+2} ions, giving $\Delta S = 454$ eu, compared to 380 observed. The discrepancy probably lies in our inability to compute accurately the small molar volume change, although even a very small change in this value might affect the entropy markedly for such macro-molecules. Nevertheless, we believe that the average entropy change per cupric ion, 28 eu (obs: 29–18), is in reasonable agreement with the observed values, especially when it is considered that the solutions may be extremely non-ideal. The method should be generally useful in estimating temperature coefficients for systems of biological interest.

[17] I. M. Klotz and H. G. Curme, J. Am. Chem. Soc. **70**, 939 (1948).

CONCLUSION

An extension has been developed to the equation of Powell and Latimer for the calculation of the entropy of aqueous solutes from structural considerations. The applicability and accuracy of the proposed method have been demonstrated and some applications have been made to the calculation of the entropies of organometallic complex ions and biological systems.

ACKNOWLEDGMENT

The author would like to express his thanks to Professor R. E. Powell, who has kindly discussed the problem at length and has offered many helpful suggestions.

Vibrational Spectra of Fluorinated Aromatics. III. 1,4-Difluorobenzene*

E. E. Ferguson, R. L. Hudson,† J. Rud Nielsen, *Department of Physics, University of Oklahoma, Norman, Oklahoma*

AND

D. C. Smith,§ *Naval Research Laboratory, Washington, D. C.*

(Received March 20, 1953)

The infrared absorption spectra of gaseous and liquid 1,4-difluorobenzene have been obtained in the regions 2–22μ and 2–38μ, respectively, with the aid of LiF, NaCl, KBr, and KRS-5 prisms. The Raman spectrum of the liquid phase has been photographed with a three-prism glass spectrograph of linear dispersion 15A/mm at 4358A. Depolarization ratios have been measured for the stronger Raman bands. A complete assignment of fundamental vibration frequencies has been made, and the spectra have been interpreted in detail. The nonplanar frequencies have been calculated with the aid of force constants determined for related molecules

INTRODUCTION

SINCE 1947 a joint investigation of the vibrational spectra of fluorinated hydrocarbons has been under way in these laboratories. Spectral data for nine fluorinated aromatics were reported in NRL Report 3567.[1] Included are the infrared spectrum of the liquid from 2–22μ, the Raman spectrum of the liquid but not polarization measurements, and a tentative assignment of seventeen of the thirty fundamental vibration frequencies of 1,4-difluorobenzene. Since then the infrared spectrum of the vapor has been obtained and that of liquid 1,4-difluorobenzene has been extended into the KRS-5 region. Also, Raman polarization measurements have been made for the liquid state.

In the meantime Delsemme[2] has published infrared and Raman data for this compound and has assigned fundamental vibration frequencies. However, Delsemme did not observe the infrared spectrum beyond 25μ, reported no Raman polarization measurements, and observed considerably fewer Raman and infrared bands than were found in the present work. On the other hand, Delsemme and Duchesne[3] also investigated the near-ultraviolet absorption spectrum of 1,4-difluorobenzene vapor.

The fundamental vibration frequencies of benzene have been given by Ingold *et al.*[4] and have been slightly revised by Mair and Hornig.[5] The infrared and Raman spectra of 1,3,5-trifluorobenzene, assignments of fundamentals, and a normal coordinate analysis of the nonplanar vibrations, have been reported in previous papers of this series.[6,7] The new spectral data for 1,4-difluorobenzene are presented in the present paper together with a complete assignment of fundamentals and a detailed interpretation of the spectra. The values of the nonplanar vibration frequencies are checked by normal coordinate analysis utilizing previously determined force constants for 1,3,5-trifluorobenzene[7] and benzene.[8] Spectral data and assignments for 1,2,4,5-tetrafluorobenzene, 1,3-difluorobenzene, fluorobenzene, and several other aromatics will be presented in future papers.

EXPERIMENTAL

The sample of 1,4-difluorobenzene was kindly supplied by Dr. G. C. Finger of the Illinois State Geological Survey, and is believed to be of high purity. The spectra indicate that a slight trace of fluorobenzene may be present and possibly a slight trace of 1,2,4-trifluorobenzene. The spectral measurements were made with the same instruments and in the same manner as described in earlier papers.[9,10]

RESULTS

The infrared absorption of gaseous and liquid 1,4-difluorobenzene between 2 and 22μ are shown in Figs. 1 and 2. The wave numbers of the observed absorption maxima are listed in Table I. The relative intensities, and in some cases the sharpness, of the bands are indicated by means of the previously used abbreviations.[9] The observed Raman shifts for liquid 1,4-difluorobenzene are given in the first column of Table II. The relative intensities and the depolarization ratios of the more intense Raman bands are listed in the second and third columns, and the exciting Hg lines are listed in the fourth column.

INTERPRETATION

The 1,4-difluorobenzene molecule undoubtedly has the symmetry V_h. The normal vibrations therefore divide themselves into symmetry species in the following

* A part of this work was supported by the U. S. Atomic Energy Commission under contract No. AT-(40-1)-1074 and by the U. S. Office of Naval Research under contract N7onr-398, T.O.I.

† Present address: Ethyl Corporation, Baton Rouge, Louisiana.

§ Present address: Phillips Petroleum Company, Bartlesville, Oklahoma.

[1] Smith, Nielsen, Berryman, Claassen, and Hudson, Naval Research Lab. Report 3567, September 15, 1949.

[2] A. H. Delsemme, J. Chem. Phys. **18**, 1680 (1950).

[3] A. H. Delsemme and J. Duchesne, Compt. rend. **234**, 612 (1952).

[4] C. K. Ingold *et al.*, J. Chem. Soc. **1936**, 912; **1946**, 222.

[5] R. D. Mair and D. F. Hornig, J. Chem. Phys. **17**, 1236 (1949).

[6] Nielsen, Liang, and Smith, Disc. Faraday Soc. **9**, 177 (1950).

[7] Eldon Ferguson, J. Chem. Phys. **21**, 886 (1953).

[8] F. A. Miller and B. L. Crawford, Jr., J. Chem. Phys. **14**, 282 (1946).

[9] Nielsen, Liang, and Smith, J. Chem. Phys. **20**, 1090 (1952).

[10] Nielsen, Crawford, and Smith, J. Opt. Soc. Am. **37**, 296 (1947).

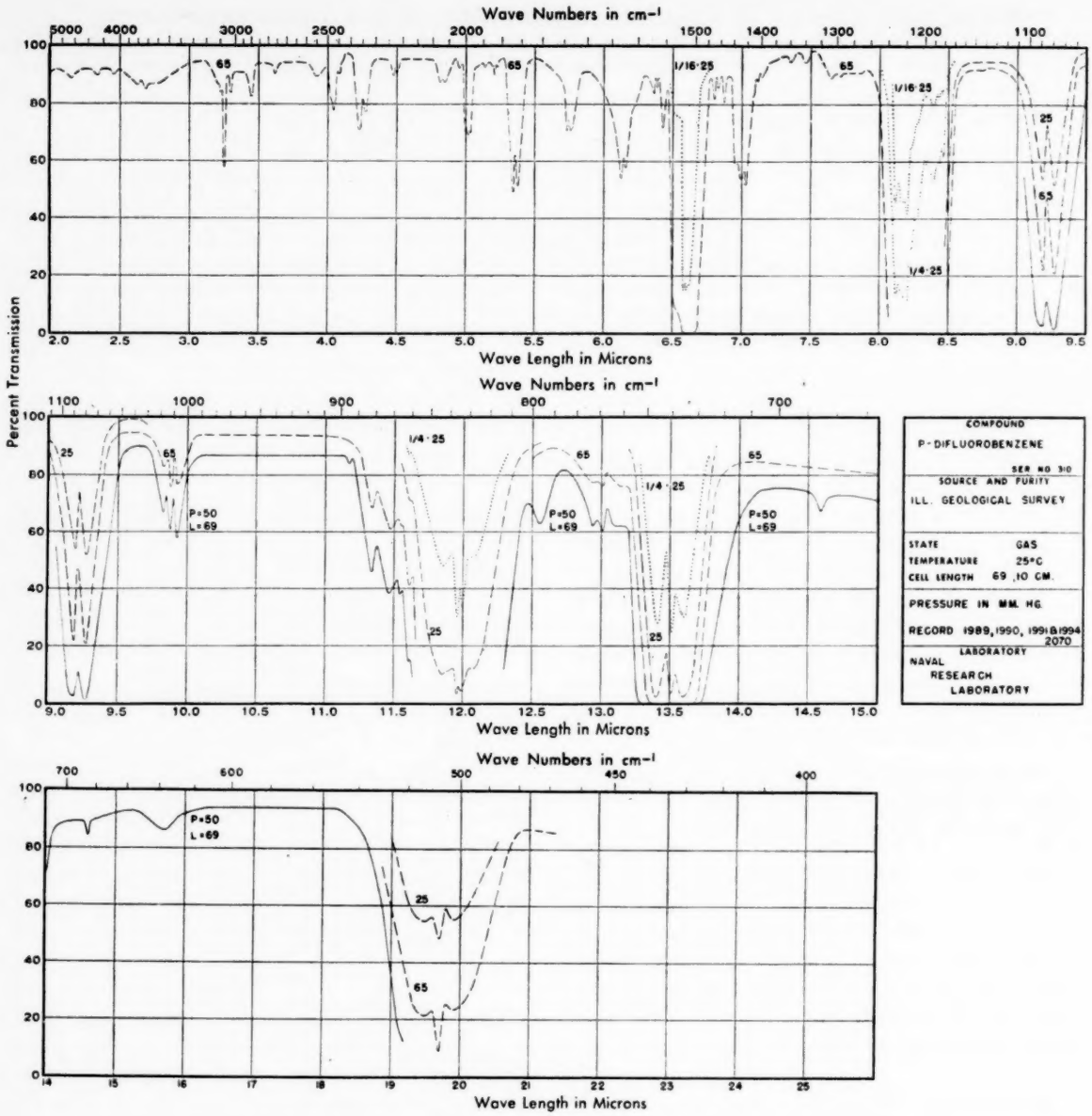

FIG. 1. Infrared spectrum of gaseous 1,4-difluorobenzene.

manner: $6a_g+1b_{1g}+5b_{2g}+3b_{3g}+2a_u+5b_{1u}+3b_{2u}+5b_{3u}$. The vibrations of the g species are Raman active, those of species a_g giving rise to polarized and the others to depolarized Raman bands. The species b_{1u}, b_{3u}, and b_{2u} vibrations are infrared active and give rise to type A, B, and C bands of Badger and Zumwalt,[11] respectively. The two vibrations of species a_u are inactive as well in infrared absorption as in the Raman effect.

RAMAN-ACTIVE FUNDAMENTALS

Species a_g

The very strong, polarized Raman band at 3084 cm^{-1} undoubtedly represents an a_g fundamental corresponding to symmetric C−H stretching. The intense polarized Raman bands at 1245 cm^{-1} and 451 cm^{-1} must also represent totally symmetric fundamentals. The first may be characterized roughly as a C−F stretching mode and the latter as a symmetric ring deformation mode. The medium intensity Raman band at 1617 cm^{-1} with a measured depolarization ratio of 0.73 is assumed to be an a_g fundamental. These assignments are all in agreement with the assignments of Delsemme. The remaining two a_g fundamentals are assumed to be represented by the very strong polarized pair of Raman bands at 840 and 858.5 cm^{-1}. Delsemme assigned 859 cm^{-1} as an a_g fundamental but lacking polarization measurements assigned the band at 840 cm^{-1} to species b_{1g}.

[11] R. M. Badger and L. R. Zumwalt, J. Chem. Phys. **6**, 711 (1938).

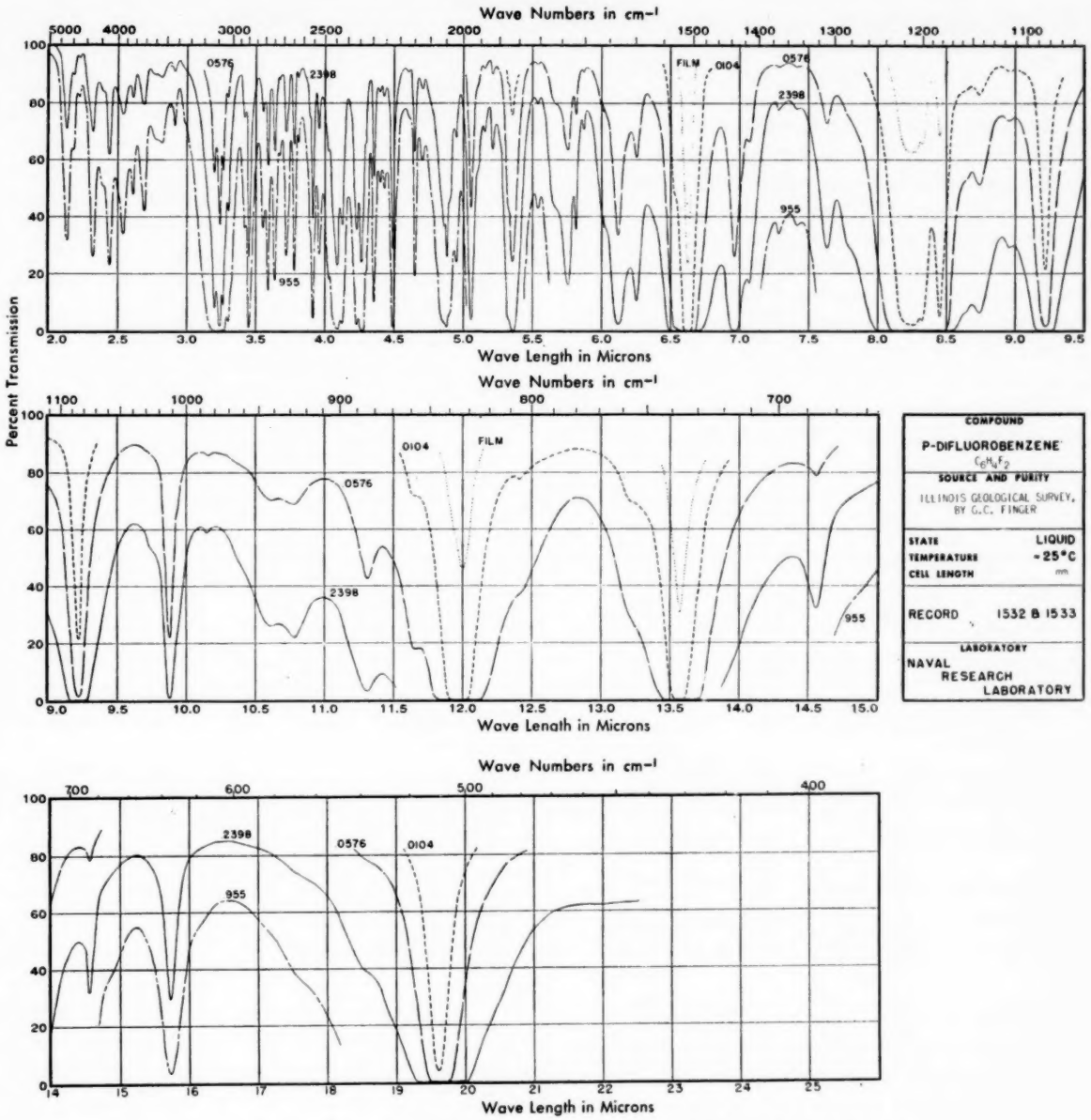

FIG. 2. Infrared spectrum of liquid 1,4-difluorobenzene (KRS-5 region not shown).

Species b_{1g}

The single normal vibration of species b_{1g} is a nonplanar wagging of the hydrogen atoms, the fluorine atoms remaining fixed with respect to the carbon ring. This fundamental corresponds to the e_{1g} fundamental of benzene which occurs at 850 cm^{-1} and, to the approximation that hydrogen bending force constants are transferable, should have the same frequency in 1,4-difluorobenzene. The weak Raman band at 800 cm^{-1} is assigned as this fundamental with considerable certainty. The appearance of weak Raman bands for nonplanar hydrogen bending vibrations has been previously observed in the case of 1,3,5-trifluorobenzene[7] and other fluorinated benzenes studied in this laboratory.

Species b_{3g}

The three nonplanar vibrations of species b_{3g} may be designated approximately as one ring-bending, one fluorine-bending, and one hydrogen-bending mode. Their frequencies have been calculated, using force constants obtained by Miller and Crawford[8] for benzene and in a previous investigation of 1,3,5-trifluorobenzene.[7] The assumptions underlying the choice of potential function were that hydrogen-bending and ring-bending valence force constants could be transferred from benzene, that the valence fluorine-bending constant could be transferred from 1,3,5-trifluorobenzene, and that the bending interaction constant between two *para*-related fluorines was negligible.

With these approximations, the calculated values for the three b_{3g} fundamental frequencies are 322, 714, and 915 cm^{-1}. A very weak Raman band at 887 cm^{-1} is interpreted as the highest fundamental of this species, i.e., the hydrogen-bending mode. Delsemme apparently did not resolve this band from the very intense band at 858.5 cm^{-1} and assigned a very weak band at 1087 cm^{-1} as this fundamental. The band at 1087 cm^{-1} can be readily interpreted as either of two binary sums as shown in Table II. The intermediate frequency of this species is assigned, in accordance with Delsemme, as 692 cm^{-1} where a weak Raman band occurs. The low value 0.69 of the measured depolarization ratio is probably a result of the large error of such measurements for weak Raman bands, although overlapping of the polarized combination band 186+508=694 A_g could be responsible for the low depolarization ratio.

The medium intensity Raman band at 375 cm^{-1} is undoubtedly the lowest b_{3g} fundamental. The agreement with the calculated frequency in this case (322 cm^{-1}) is quite poor.

Species b_{2g}

One of the five b_{2g} fundamentals is a hydrogen stretching mode which is assumed to overlap the very strong, broad a_g fundamental at 3084 cm^{-1}. Delsemme has assigned a frequency 3051 cm^{-1} to this mode. He reports Raman bands at 3051 cm^{-1} and 3130 cm^{-1} which have not been observed in the present work. Since the very strong band reported here at 3084 cm^{-1} is given the frequency 3090 cm^{-1} by Delsemme, it may be that his reported shifts of 3051 and 3130 cm^{-1} are actually the Hg lines at 5026A and 5046A which occur 3046 and 3125 cm^{-1}, respectively, from the 4358A Hg line.

The medium intensity Raman band at 635 cm^{-1}, and the weak band at 1285 cm^{-1}, are taken to be b_{2g} fundamentals with considerable certainty. These assignments are in agreement with those of Delsemme, as is also the assignment of the very weak Raman band at 507 cm^{-1} as a b_{2g} fundamental.

The remaining fundamental of this species is taken to be the medium intensity Raman band at 1142 cm^{-1} with a measured depolarization ratio of 0.66. This low

TABLE I. Infrared absorption spectrum of 1,4-difluorobenzene.

Gas Wave number	Gas Description	Liquid Wave number	Liquid Description	Interpretation
		~265	s	451−186=265 B_{2u}
		~288	w?	635−350=285 B_{1u}; 737−451=286 B_{1u}
		350	vs	b_{3u} fundamental
~502				
508	s, sh	509	vs	b_{2u} fundamental
~513				
~637	w, b	636	ms	451+186=637 B_{2u}
~685	w, sh	687	m	impurity?[a]
735				
740	vs, sh	737	vs, sh	b_{1u} fundamental
746				
		~757	m	370+375=745 B_{3u}?
~763				
769	w, sh			
773				
~796	w	~806	m	350+451=801 B_{3u}
~827				
834	vs, sh	833	vs	b_{2u} fundamental
836	vs, sh			
~844				
861	m, sh	~858	m	350+507=857 B_{1u}
867	m			
~872	m			
~882	m	884	m	692+186=878 B_{1u}
~894	w			
		928	w	1285−350=935 B_{1u}
		943	w	a_u fundamental?
		985	vw	350+635=985 B_{1u}
1010				
1012	m, sh	1012	ms	b_{1u} fundamental
1017				
1079	s			
1088	s	1085	s, sh	b_{3u} fundamental
		1117	w	375+737=1112 B_{2u}
		1144	w	b_{2g} fundamental?
1182	s	1183	vs, sh	b_{1u} fundamental
1186	s			451+737=1188 B_{1u}
1192	vs			350+840=1190 B_{3u}
1199	s			
~1208		~1202	vs, sh	509+692=1201 B_{1u}
~1218		~1212	vs, vb	b_{3u} fundamental
1220	vs			350+858=1208 B_{3u}
1225	vs			
1232	vs, sh			
		~1285	w	451+833=1284 B_{2u}
1297				
1307		1311	m	509+800=1309 B_{3u}
1339	w			
		1350	w	509+840=1349 B_{2u}
1361	w			509+858=1367 B_{2u}
		1374	w	635+737=1372 B_{3u}
1399	w			1012+375=1387 B_{2u}
1404	w			
		1414	w	692+737=1429 B_{2u}?
1422				
1429	m, sh			186+1245=1431 B_{2u}
~1438		1437	m, sh	b_{3u} fundamental
1456	w, sh			
1464	w, sh			451+1012=1463 B_{1u}
1471	w, sh			
1515	vs, sh	1511	vs, sh	b_{1u} fundamental
1520	vs, sh			
~1530	s	~1530	s	451+1085=1536 B_{3u}; 692+833=1525 B_{1u}
1555	w, sh			1183+375=1558 B_{2u}
1565	w, sh			
1572	w, sh			
~1605	w	1600	m, sh	350+1245=1595 B_{3u}; 737+858=1595 B_{1u}
1623	mw			
1631	mw	1634	ms, sh	350+1285=1635 B_{1u}; 1183+451=1634 B_{1u}

TABLE I.—*Continued.*

Gas Wave number	Gas Description	Liquid Wave number	Liquid Description	Interpretation
		~1665		451+1212=1663 B_{3u}
		1704	vw	887+833=1720 B_{1u}
		1720	w, sh	635+1085=1720 B_{1u}; 1212+507=1719 B_{1u}
~1733	w	1737	mw	800+935=1735 B_{1u}
1742	w, sh			
		~1760	w	509+1245=1754 B_{2u}
		1805	w	
1859	m			840+1012=1852 B_{1u}
1869	m	1868	m, sh	858+1012=1870 B_{1u}
		~1878		737+1142=1879 B_{3u}; 692+1183=1875 B_{2u}
1912				
1919	vw, sh	1919	w	840+1085=1925 B_{3u}
1923				
1946	vw	~1940	w	858+1085=1943 B_{3u}
		~1960		451+1511=1962 B_{1u}
		1978	m	737+1245=1982 B_{1u}
1988				
1992	w, sh			
2000				800+1212=2012 B_{2u}
2020	w	2021	w	737+1285=2022 B_{3u}; 840+1183=2023 B_{1u}
		~2040		858+1183=2041 B_{1u}
		2049	m	1212+840=2052 B_{3u}
2062	w	2056	w	1212+859=2071 B_{3u}
2075	w			635+1437=2072 B_{1u}
		~2125	vw	
		2151	w	635+1511=2146 B_{3u}
		~2172	vw	
2222	w			
2232	w	2228	m	1085+1142=2227 B_{1u}
		2257	vw	1012+1245=2257 B_{1u}
		2273	vw	840+1437=2277 B_{3u}
		2296	w	1012+1285=2297 B_{3u}; 858+1437=2295 B_{3u}
2342	w	2345	w	840+1511=2351 B_{1u}; 737+1617=2354 B_{1u}
2364	w	2365	w	858+1511=2369 B_{1u}; 1085+1285=2370 B_{1u}
		2424	w	1183+1245=2428 B_{1u}
2445	w, sh	2444	w	1212+1245=2457 B_{3u}
2475	w, sh	2481	vw	1183+1285=2468 B_{3u}
		2527	w	
~2550	w	2554	w	
		2627	vw	1012+1617=2629 B_{1u}
		2646	w	1142+1511=2653 B_{3u}
		2687	w	1245+1437=2682 B_{3u}
		2722	vw	1285+1437=2722 B_{1u}
		2749	w	1245+1511=2756 B_{1u}
2762	w			
		2786	w	1285+1511=2796 B_{3u}
		2813	vw	1183+1617=2800 B_{1u}
2899	w	2898	w	
		2924	w	
3030	w, sh	3028	mw	b_{1u} fundamental
		3064		1437+1617=3054 B_{3u}
3077	w, sh	3088	m	b_{3u} fundamental
		3124	m	1511+1617=3128 B_{1u}
		3436	vw	350+3084=3434 B_{3u}
		3550	vw	451+3088=3539 B_{3u}
3717	w	3720	w	635+3088=3723 B_{1u}
3802	w			
		3830	w	737+3084=3821 B_{1u}
		3940	w	858+3088=3946 B_{3u}
4274	w			
		4310	vw	1212+3084=4296 B_{3u}
		4500	vw	
		4590	vw	1511+3080=4591 B_{3u}
		4690	w	1617+3088=4705 B_{3u}

[a] Could be the result of fluorobenzene impurity.

value may be due to overlapping of 635+507=1142 A_g. Delsemme assigned the frequency 1397 cm^{-1} to this fundamental. The weak Raman band observed by him at 1397 cm^{-1} undoubtedly corresponds to the weak band reported here at 1385 cm^{-1} with a measured depolarization ratio of 0.39. It must belong to a totally symmetric vibration and is satisfactorily interpreted as the overtone, 2×692=1384 A_g.

INFRARED-ACTIVE FUNDAMENTALS

Species b_{1u}

The thirteen infrared-active fundamentals must be distinguished largely on the basis of the band contours in the spectrum of the gas. The five b_{1u} fundamentals should yield bands with type *A* contours. The strong band at 740 cm^{-1} has definitely a type *A* contour and is therefore taken to be a b_{1u} fundamental. One C—H stretching mode belongs to this species, and this is assumed to be the sharp weak band at 3028 cm^{-1}. The very strong band at 1192 cm^{-1} is definitely not a type *B* band and lies too high to be a b_{2u} fundamental. It is therefore assigned as a b_{1u} fundamental. The medium intensity band at 1012 cm^{-1} and the very strong band at 1517 cm^{-1} show some evidence of having type *A* contours and are chosen as the remaining b_{1u} fundamentals.

Species b_{3u}

The five fundamentals of species b_{3u} should have type *B* contours. One of these is a C—H stretching mode which is taken to be the band observed at 3077 cm^{-1}. The band at 1083 cm^{-1} is definitely of type *B* and is interpreted as a b_{3u} fundamental. The band at 1429 cm^{-1} shows slight evidence of a *B*-type contour and is also assigned to this species as a fundamental, as is the very strong band at 1225 cm^{-1} of uncertain contour. The remaining b_{3u} fundamental is taken to be the very strong band observed in the liquid at 350 cm^{-1}. In this assignment a pair of fundamentals are interchanged between species b_{1u} and b_{3u} as compared to the assignment of Delsemme. The resolution of Delsemme's infrared spectrometer was less than that available on the re-

search instrument at the Naval Research Laboratory, so that better contours were available for the present assignment.

Species b_{2u}

The three b_{2u} fundamentals correspond to nonplanar vibrations and should give infrared bands of type *C* contour. The strong infrared bands occurring at 508 and 836 cm^{-1} have such contours and are readily assigned to this species as was done by Delsemme. The calculated values are 543 and 767 cm^{-1}. The remaining b_{2u} fundamental offers the most perplexing problem presented by the assignment of fundamentals for this molecule. A strong infrared band is observed in the liquid spectrum at 265 cm^{-1} with KRS-5 prism and no very satisfactory explanation can be offered for this band, except as the lowest b_{2u} fundamental. However, a normal coordinate calculation yields the value 156 cm^{-1} for this frequency and the discrepancy seems quite unreasonable. Delsemme did not have infrared data beyond 25μ. He assumed this fundamental to be around 180 cm^{-1} but gave no basis for this estimate. A value of 186 cm^{-1} has been tentatively adopted for this b_{2u} fundamental, since it allows an explaination of the absorption maximum at 265 cm^{-1} as $451-186=265$ B_{2u}, while the corresponding sum $451+186=637$ B_{2u} occurs as an otherwise unexplained band. In addition the choice of the value 186 cm^{-1} explains the medium intensity infrared band at 884 cm^{-1} and two very weak Raman bands at 1414 cm^{-1} and 3198 cm^{-1}. A weak band occurs in the Raman spectrum of *p*-fluorotoluene at 152 cm^{-1} which has been suggested to be the corresponding fundamental.[1] The spectrum of *p*-fluorotoluene would be expected to resemble that of 1,4-difluorobenzene very closely and an examination of the spectrum indicates that this is indeed the case. Since *p*-fluorotoluene does not strictly have the symmetry V_h of 1,4-difluorobenzene, all fundamentals are both infrared and Raman active.

TABLE II. Raman spectrum of 1,4-difluorobenzene (liquid).

Wave number	Description	Depolarization	Exciting Hg lines	Interpretation
165 cm^{-1}	vw, d	~0.7	*e*	$509-350=159$ B_{1g}
239	vvvw		*e*	Impurity?[a]
375	m	0.82	$\pm e$	b_{3g} fundamental
451	m	0.43	$\pm e$	a_g fundamental
507	vvvw		*e*	b_{2g} fundamental
635	m, sh	0.86	$\pm ek$	b_{2g} fundamental
692	w, sh	0.69	*ek*	b_{3g} fundamental; $186+508=694$ A_g
800[b]	w, b	~0.8	*e*	b_{1g} fundamental
840	vs, sh	0.0	$\pm efgki$	a_g fundamental
858.5	vs, sh	0.0	$\pm efgki$	a_g fundamental
887	vvw		*e*	b_{3g} fundamental
1015	w, b	*p*	*e*	$2\times508=1016$ A_g; $833+186=1019$ A_g
1070	vvw		*e*	$375+692=1067$ A_g
1087	vvw		*e*	$451+635=1086$ B_{2g}; $350+737=1087$ B_{2g}
1142	m, sh	0.66	*eki*	b_{2g} fundamental; $635+507=1142$ A_g
1245	vs	0.13	*efki*	a_g fundamental
1285	w	0.75	*ek*	b_{2g} fundamental
1385	w	0.39	*e*	$2\times692=1384$ A_g
1414	vvvw		*e*	$1212+186=1398$ B_{1g}
1473	vvvw		*e*	$2\times737=1474$ A_g; $635+840=1475$ B_{2g}
1605	vvw		*e*	$2\times800=1600$ A_g
1617	m	0.73	*e*	a_g fundamental; $1437+186=1623$ B_{1g}
1668	vvvw		*e*	$2\times833=1666$ A_g; $375+1285=1660$ B_{1g}
1691	vvvw		*e*	$451+1245=1696$ A_g
1849	vvvw		*e*	$833+1012=1845$ B_{3g}
1885	vvvw		*e*	$635+1245=1880$ B_{2g}
2282	vvvw		*e*	$1085+1183=2268$ B_{2g}
2296	vvvw		*e*	$2\times1142=2284$ A_g
2367	vvvw		*e*	$2\times1183=2366$ A_g; $1437+935=2372$ B_{3g}
2393	vvvw		*e*	$1142+1245=2387$ B_{2g}
2420	vvvw		*e*	$2\times1212=2424$ A_g; $800+1617=2417$ B_{1g}
2464	vvvw		*e*	$858+1617=2475$ A_g
2492	vvvw		*e*	$2\times1245=2490$ A_g
2899	vvw		*e*	$1285+1617=2902$ B_{2g}
2914	vvvw		*e*	
3005	w, sh	*p*?	*ei*	$2\times1511=3022$ A_g
3084	vs, b	0.30	*ekil*	a_g+b_{2g} fundamentals
3198	vvw		*e*	$186+3028=3214$ B_{3g}
3230	vvw	*p*?	*e*	$2\times1617=3234$ A_g

[a] May be 1,2,4-trifluorobenzene or fluorobenzene impurity.
[b] Overlapped by 858.5 cm^{-1} band excited by 4348A Hg line.

Species a_u

The two inactive nonplanar fundamentals of species a_u can only be calculated very roughly, since the valence force constants for ring bending occur in combinations not previously encountered in benzene, whereas for each of the three b_{2u} and b_{3g} fundamentals it is possible to choose the symmetry coordinates so that the same combinations of ring-bending valence force constants occur as in Miller and Crawford's[8] treatment of benzene. The frequencies calculated for the a_u fundamentals are 450 and 1040 cm^{-1}. Both of these values seem too high. The benzene-ring-bending fundamental corresponding to the low a_u fundamental has a frequency 404 cm^{-1}. It seems reasonable to assume that the frequency would be somewhat lower for 1,4-difluorobenzene than for benzene, and a frequency 370 cm^{-1} is therefore chosen for this fundamental. This can be utilized in explaining one otherwise uninterpreted infrared band. The high a_u fundamental corresponds to a hydrogen-bending mode which has a frequency 955 cm^{-1} in benzene and is given a value 935 cm^{-1} in 1,4-difluorobenzene, since hydrogen bending frequencies appear to be little affected by substitution and since the value 935 cm^{-1} can be used to explain one otherwise uninterpreted infrared band. One of the weak infrared bands at 928 cm^{-1} and 943 cm^{-1} may be this high a_u fundamental appearing because of a breakdown of the selection rules for the liquid state. The band at 943 cm^{-1} is not otherwise explained.

DISCUSSION

The fundamental frequencies assigned are listed in Table III. The interpretations of the Raman and infrared spectra are included in Tables I and II. Since most of the bands to be explained are observed in the

liquid spectra, the liquid frequencies are used in the interpretations. Where the infrared active fundamentals are observed in both liquid and gas spectra, the frequency differences are generally small, the largest being 13 cm^{-1} for the band at 1212 cm^{-1}.

Of the thirty-nine Raman bands observed for the liquid state, only two extremely weak bands lying at 239 cm^{-1} and 2914 cm^{-1} have not been interpreted. Also, Delsemme reports a weak Raman shift of 145 cm^{-1} which has not been observed here. A possible explanation of the band at 239 cm^{-1} is either as a fluorobenzene impurity or as a 1,2,4-trifluorobenzene impurity. An examination of the infrared and Raman spectra of the compounds indicates that either might have been present as a trace in the 1,4-difluorobenzene sample.

Of the eighty-four observed infrared maxima for the liquid state, nine have not been explained as binary sum bands or as reasonable binary difference bands, and one additional band observed in the gas spectrum at 769 cm^{-1} has not been interpreted. These are all quite weak bands except one medium intensity band observed at 687 cm^{-1} in the liquid and also occurring very weakly in the spectrum of the gas. This band could be caused by a slight trace of fluorobenzene. The very weak unexplained bands may represent ternary combinations, which have not been invoked since the large number of possible combinations would make such assignments meaningless.

The only infrared band observed by Delsemme and not observed here which seems worthy of mention is the weak band at 412 cm^{-1} in the gas. Delsemme has assigned this as a b_{3u} fundamental. The gas spectrum was not observed in this region in the present investigation and the liquid spectrum reveals a very strong band at 350 cm^{-1}, which is interpreted as the low b_{3u} fundamental, and no absorption near 412 cm^{-1}.

TABLE III. Fundamental vibration frequencies for 1,4-difluorobenzene (values for liquid).

Approximate motion	Species a_g	b_{1g}	b_{2g}	b_{3g}	a_u	b_{1u}	b_{2u}	b_{3u}
C–H stretching	3084		~3080			3028		3088
C–F stretching	1245					1183		
C–C stretching	1617		1285			1511		1437
C–C breathing	858.5					737		1212
C–F bending			635	692			509	350
C–H bending	840	800	1142	887	(935)	1012	833	1085
C–C–C bending	451		507	375	(370)		(186)	

The calculated values of the seven active nonplanar frequencies have an average deviation of 8 percent from the observed frequencies. Although this is not very good agreement, it is good enough to be useful in checking assignments in several cases. The poorest agreement is in the case of the two low ring-bending modes of vibration, for which the discrepancies are 14 and 16 percent. Since all force constants have been borrowed from other molecules, it seems quite certain that one could determine two ring-bending constants and possibly the fluorine-bending interaction constant, here assumed to be zero, and fit the seven active fundamental frequencies quite closely.

ACKNOWLEDGMENT

The writers wish to acknowledge their indebtedness to Dr. G. C. Finger for the gift of the sample.

Vibrational Spectra of Fluorinated Aromatics. IV. 1,2,4,5-Tetrafluorobenzene*

E. E. Ferguson, R. L. Hudson,† and J. Rud Nielsen
Department of Physics, University of Oklahoma, Norman, Oklahoma

AND

D. C. Smith‡
Naval Research Laboratory, Washington, D. C.

(Received, June 22, 1953)

The infrared absorption spectra of gaseous and liquid 1,2,4,5-tetrafluorobenzene have been obtained in the region 2–22μ with the aid of LiF, NaCl, and KBr prisms. The Raman spectrum of the liquid phase has been photographed with a three-prism glass spectrograph of linear dispersion 15 A/mm at 4358A. Relative intensities and depolarization ratios have been measured for the stronger Raman bands. A complete assignment of fundamental vibration frequencies is made and the spectra are interpreted in detail. The values of the nonplanar fundamental frequencies are checked by normal coordinate analysis.

INTRODUCTION

In previous papers[1–3] of this series the infrared and Raman spectra of 1,3,5-trifluorobenzene and 1,4-difluorobenzene have been reported. In the present paper spectral data will be given for 1,2,4,5-tetrafluorobenzene. The fundamental vibration frequencies are assigned and the spectra are interpreted in detail. The nonplanar frequencies are calculated by transferring force constants from benzene and 1,3,5-trifluorobenzene. No previous spectral studies seem to have been made of this compound.

EXPERIMENTAL

The sample of 1,2,4,5-tetrafluorobenzene was kindly supplied by G. C. Finger of the Illinois Geological Survey. No information was available about its purity. The spectra indicate the presence of a trace of 1,2,4-trifluorobenzene in the sample. The infrared and Raman spectral data and the Raman polarization data were obtained in the manner previously described.[3]

RESULTS

The infrared absorption of gaseous and liquid 1,2,4,5-tetrafluorobenzene are shown in Figs. 1 and 2. The wave numbers of the observed absorption maxima are listed in Table I. The relative intensities, and in some cases the sharpness, of the bands are indicated by means of the previously used abbreviations. The observed Raman shifts for liquid 1,2,4,5-tetrafluorobenzene are given in the first column of Table II. The relative intensities and depolarization ratios of the Raman bands are listed in the second and third columns, and the exciting mercury lines are given in the fourth column.

ASSIGNMENT OF FUNDAMENTALS

The molecule of 1,2,4,5-tetrafluorobenzene undoubtedly has the symmetry V_h and hence normal vibrations that divide themselves into symmetry species in the following manner: $6a_g+2a_u+1b_{1g}+5b_{2g}+3b_{3g}+5b_{1u}+3b_{2u}+5b_{3u}$. The g vibrations are Raman-active, those of species a_g giving rise to polarized and the others to depolarized Raman bands. The vibrations of species b_{1u}, b_{2u}, and b_{3u} are infrared active, giving rise to type B, C, and A bands, respectively. The vibrations of species a_u are inactive as well in infrared absorption as in the Raman effect.

INFRARED-ACTIVE FUNDAMENTALS

Species b_{1u}

The five fundamentals of species b_{1u} should give rise to infrared bands with type B contours and $P-R$ branch separations of approximately 6.4 cm^{-1}. The four bands at 700, 960, 1229 and 1439 cm^{-1} are all definitely of type B contour with measured $P-R$ separations of 7, 6, 8 and 6 cm^{-1}, respectively. These are all extremely strong bands except the one at 960 cm^{-1} which is moderately strong. They are therefore taken with considerable certainty to be b_{1u} fundamentals. The fifth b_{1u} fundamental corresponds to a C–H stretching mode and evidently occurs at 3089 cm^{-1}.

Species b_{2u}

The three b_{2u} vibrations are out-of-plane motions corresponding approximately to one hydrogen bending, one fluorine bending, and one ring-bending mode. They should yield infrared bands having type C contours. The very strong bands at 867 and 459 cm^{-1} are readily assigned as b_{2u} fundamentals on the basis of their contours and intensities. The third fundamental of this species, namely the nonplanar ring bending, lies too low to be observed here.

* A part of this work has been supported by the U. S. Atomic Energy Commission under contract No. AT-(40-1)-1074 and by the U. S. Office of Naval Research under contract N7onr-398, T.O.I.

† Present address: Ethyl Corporation, Baton Rouge, Louisiana.

‡ Present address: Phillips Petroleum Company, Bartlesville, Oklahoma.

[1] Nielsen, Liang and Smith, Disc. Faraday Soc. **9**, 177 (1950).

[2] Eldon Ferguson, J. Chem. Phys. **21**, 886 (1953) to be published.

[3] Ferguson, Hudson, Nielsen, and Smith, J. Chem. Phys. **21**, 1457 (1953).

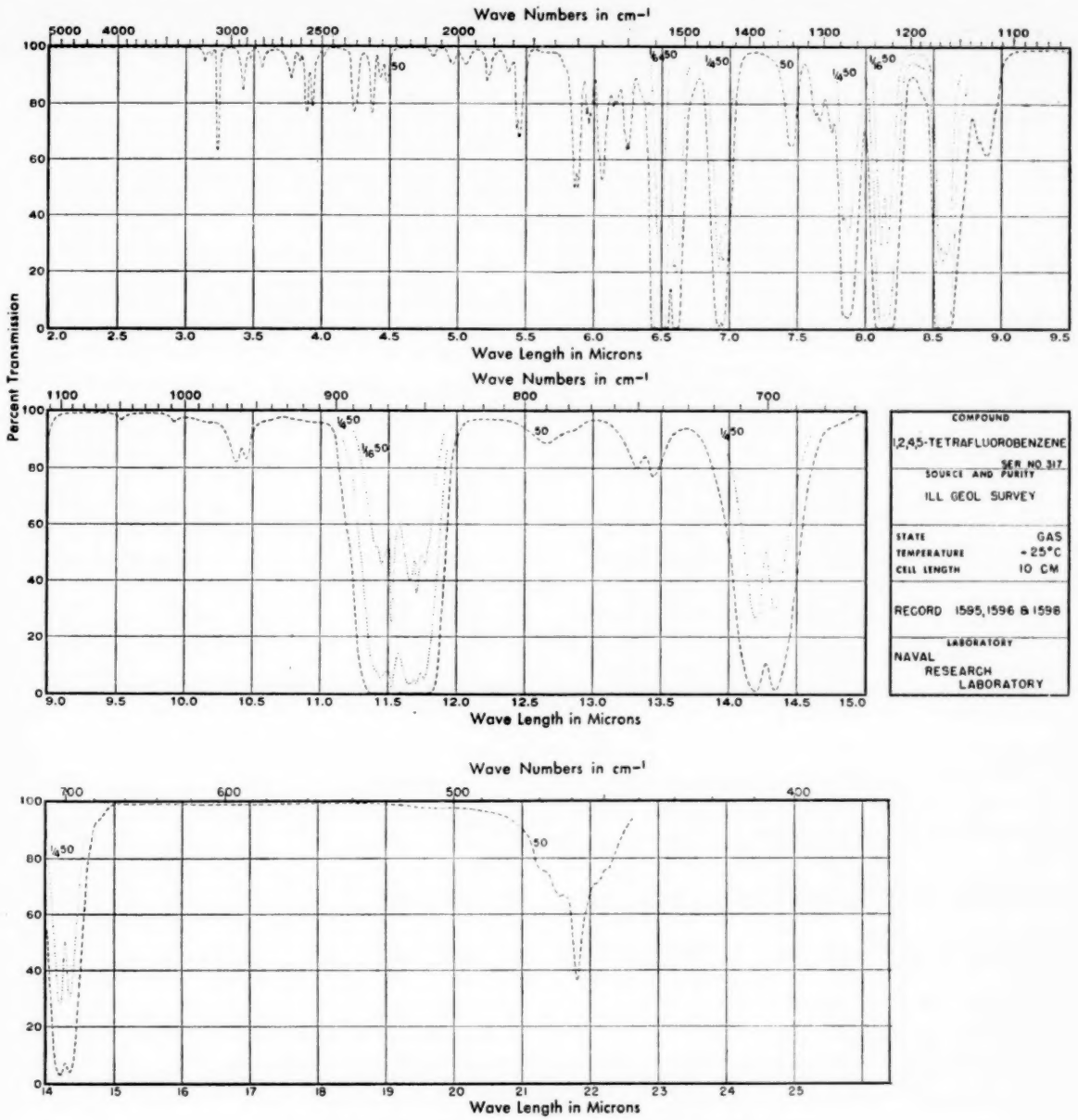

FIG. 1. Infrared spectrum of gaseous 1,2,4,5-tetrafluorobenzene.

In order to calculate the nonplanar frequencies of 1,2,4,5-tetrafluorobenzene, two frequencies must be used to determine two unknown fluorine bending interaction constants, the remaining force constants being borrowed from Miller and Crawford's[4] work on benzene, and from the previous work on 1,3,5-trifluorobenzene.[2] The intermediate b_{2u} fundamental and the b_{1g} fundamental were chosen for this and the remaining seven nonplanar frequencies were calculated. No attempt was made to determine force constants and frequencies precisely, so that the calculated and observed frequencies for the b_{1g} and the intermediate b_{2u} fundamental do not check exactly. A rather laborious algebraic approximation procedure was required, and with the approximations being made the fit seemed as good as was warranted. The highest b_{2u} fundamental frequency was calculated to be 880 cm^{-1}, agreeing to within two percent of the observed frequency. The lowest unobserved fundamental was calculated to be 223 cm^{-1}. A value 240 cm^{-1} was adopted for this frequency because it can be used to interpret seven infrared bands not otherwise explained.

Species b_{3u}

The five fundamentals of species b_{3u} should yield infrared bands of type A contour with $P-R$ separations

[4] F. A. Miller and B. L. Crawford, Jr., J. Chem. Phys. 14, 282 (1946).

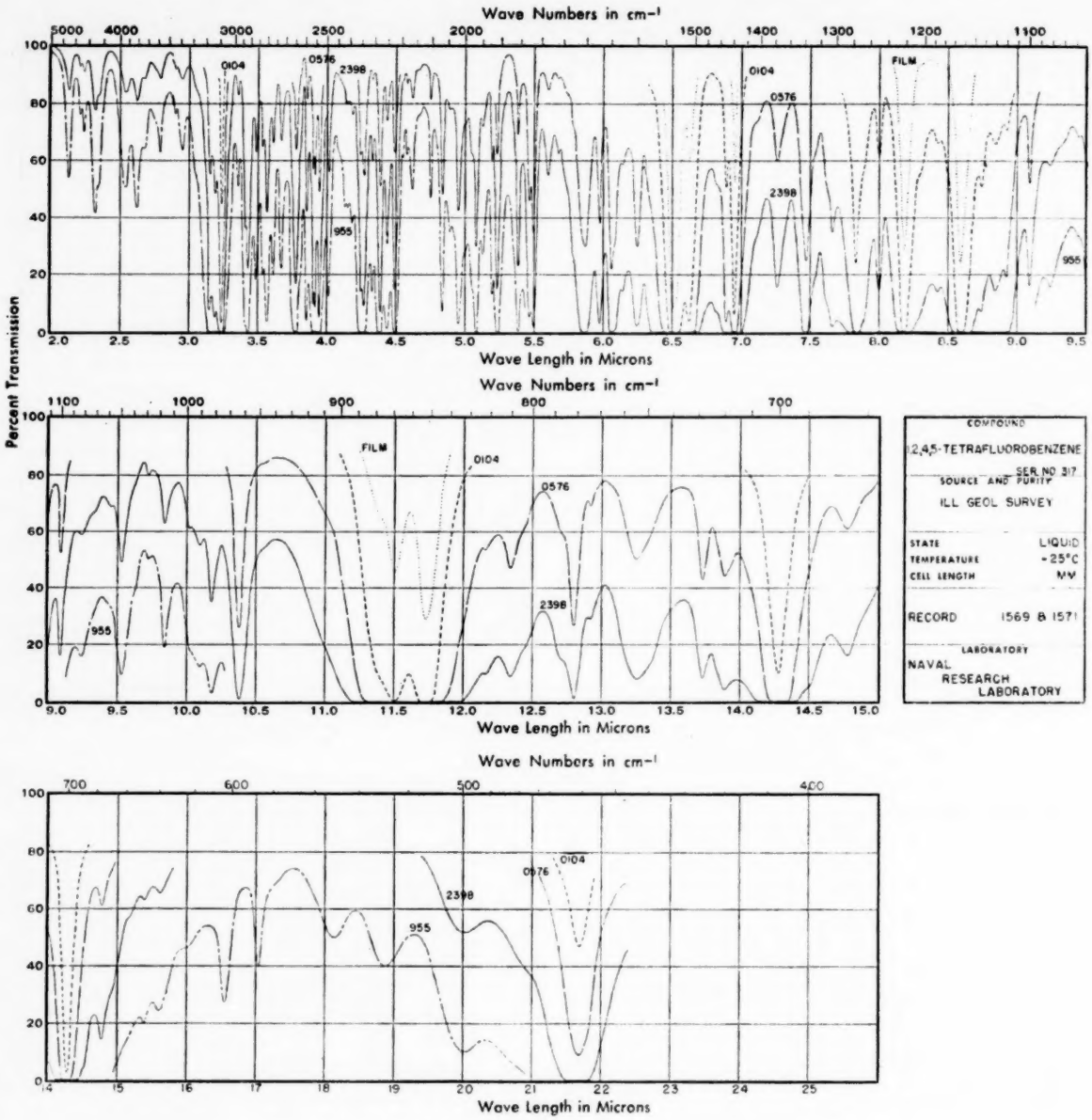

FIG. 2. Infrared spectrum of liquid 1,2,4,5-tetrafluorobenzene.

of approximately 8.5 cm^{-1}. The very strong bands at 853 and 1164 cm^{-1}, each having a measured $P-R$ separation of 8 cm^{-1}, are readily assigned as b_{3u} fundamentals. The strong band at 1277 cm^{-1} appears to have either type A or type C contour and, since it lies too high for a nonplanar vibration of species b_{2u}, it is assigned as a b_{3u} fundamental. The contour of the very strong band at 1534 cm^{-1} is not well resolved but the band is interpreted as a b_{3u} fundamental, since all b_{1u} fundamentals in this spectral region have been accounted for. The remaining b_{3u} fundamental is identified with the strong infrared band at 755 cm^{-1} of uncertain contour.

RAMAN-ACTIVE FUNDAMENTALS

Species a_g

There are six totally symmetric fundamentals of species a_g. Four of these can be identified with great certainty with the very intense, polarized Raman bands at 3097, 1374, 748, and 487 cm^{-1}.

The medium intensity band at 1335 cm^{-1}, with a measured depolarization ratio of 0.5, has the slightly diffuse appearance which is characteristic of Raman bands involving C—F stretching and is assigned as an a_g fundamental. This assignment, which is somewhat uncertain since the band can also be interpreted as the overtone of the 669 cm^{-1} b_{3g} fundamental, necessitates the

interpretation of a somewhat stronger, polarized Raman band at 1402 cm^{-1} as the overtone of the very strong b_{1u} fundamental at 700 cm^{-1}. The medium intensity, polarized band at 832 cm^{-1} is assigned as the remaining a_g fundamental. Although this is the strongest band available for this assignment, it could also be interpreted as the overtone of the b_{1g} fundamental at 417 cm^{-1}. Its assignment is therefore somewhat uncertain.

Species b_{1g}

The single normal vibration of species b_{1g} is an out-of-plane wagging of the fluorine atoms, the hydrogen atoms remaining fixed with respect to the carbon ring. It is undoubtedly represented by the strong, depolarized Raman band observed at 417 cm^{-1}.

Species b_{3g}

The three nonplanar b_{3g} fundamentals may be characterized approximately as hydrogen-bending, fluorine-bending, and ring-bending motions. The lowest of these is identified with the intense, depolarized Raman band at 295 cm^{-1}. The calculated frequency for this lowest b_{3g} fundamental is 288 cm^{-1}. The only other reasonable possibility for this assignment would be the weak Raman band at 202 cm^{-1}. The evidence for the choice of the stronger band for the lowest b_{3g} fundamental is strengthened by the observation that the nonplanar ring-bending fundamental of species e'' in 1,3,5-trifluorobenzene gives rise to a much stronger Raman band than any of the planar ring-bending modes.[1]

The medium intensity Raman band at 669 cm^{-1} is interpreted as the intermediate b_{3g} fundamental. The calculated frequency in this case is 645 cm^{-1}. The highest b_{3g} fundamental is identified with the very weak Raman band observed at 871 cm^{-1}. It has previously been observed that nonplanar hydrogen-bending modes give rise to weak Raman bands in both 1,3,5-trifluorobenzene,[2] and 1,4-difluorobenzene.[3] The calculated frequency in this case is 895 cm^{-1}.

Species b_{2g}

The strong depolarized Raman band at 1643 cm^{-1} can be interpreted as a b_{2g} fundamental with considerable certainty. The weak Raman band at 1196 cm^{-1} is also

TABLE I. Infrared absorption spectrum of 1,2,4,5-tetrafluorobenzene.

Gas Wave number	Gas Description	Liquid Wave number	Liquid Description	Interpretation
459	s	461	s	b_{2u} fundamental
~464				
		~499	w	[748−240=508 B_{2u}]
		~530	w	[295+240=535 B_{1u}]
		~551	w	[417+140=557 B_{1u}]
		587	w	1,2,4-Trifluorobenzene impurity
		604	w	1,2,4 impurity
		640	vw	[871−240=631 B_{1u}]; 853−202=651 B_{1u}
		650	vw	[417+240=657 B_{3u}]
		677	vw	963−295=668 B_{2u}
697	vs	700	vs	b_{1u} fundamental
704	vs			
		720	vw	[487+240=727 B_{2u}]
		728	vw	1,2,4 impurity
744	w			
751	w	755	m	b_{3u} fundamental
		774	vw	[635+140=775 B_{2u}]
~790	vw	781	m	1,2,4 impurity
		810	w	1,2,4 impurity
		822	vw	
850				
854	vvs	853	vvs	b_{3u} fundamental
858				
867	vvs	869	vvs	b_{2u} fundamental
873	vvs			
957	w			
963	w	963	m	b_{1u} fundamental
		982	w	[748+240=988 B_{2u}]
		990	vw	
		998	vw	700+295=995 B_{2u}
~1008	vvw			
		1016	w	[871+140=1011 B_{3u}]
		1029	vw	
~1049	vvw	1049	w	853+202=1055 B_{1u}
		1058	vw	1,2,4-impurity
		1082	vw	[832+240=1072 B_{2u}]
		1100	w	1,2,4-impurity
1125	w	1121	s	[871+240=1111 B_{1u}]
1133	w	1131	s	669+461=1130 B_{1u}
		1144	w	1,2,4 impurity
1163				
1167	vvs	1164	vvs	b_{3u} fundamental
1171				
		1188	w	487+700=1187 B_{1u}
1225	vvs	1222	vvs	b_{1u} fundamental
1233	vvs			
		1250	w	963+295=1258 B_{2u}
1271	vvs			
1277	vvs	1277	s	b_{3u} fundamental
1290				
1305	w	1305	w	832+461=1293 B_{2u}
1311	w			
~1342	w	1339	w	700+635=1335 B_{3u}; 853+487=1340 B_{3u}
		1377	w	700+699=1369 B_{2u}
1439	vvs	1439	vvs	b_{1u} fundamental
1445	vvs			
		1451	w	700+748=1448 B_{1u} 963+487=1450 B_{1u}
1513	vvs	1511	s	1222+295=1517 B_{2u}
1517	vvs			
1543	vvs	1534	vvs	b_{3u} fundamental
1599	w	1601	m	853+748=1601 B_{3u}
1603	w			
1622	w			
1628	w	1629	w	963+669=1632 B_{2u}
1650	w	1650	s	1164+487=1651 B_{3u}

TABLE I—*Continued.*

Gas Wave number	Gas Description	Liquid Wave number	Liquid Description	Interpretation
1673	w			
1677	w	1674	m	853+832=1685 B_{3u}
1682	w			
1701	m	~1704	s	1222+487=1709 B_{1u}
1707	m			
		1761	vw	1277+487=1764 B_{3u}
		1785	w	963+832=1795 B_{1u}
		1819	m	1130+700=1830 B_{3u}
1832		1830	w	1374+461=1835 B_{2u}
1837	w			
1841				
~1863	vw	1857	m	1222+635=1857 B_{3u}
		1911	m	
1919	vw	1925	w	1439+487=1926 B_{1u}
		1950	m	1534+417=1951 B_{2u}
~1978	vw	1969	vw	1222+748=1970 B_{1u}
~2017	vw	2020	m	1277+748=2025 B_{3u}
		2046	w	1222+832=2054 B_{1u}
~2073	vw	2069	m	1374+700=2074 B_{1u}
~2079	vw			
		2105	w	832+1277=2109 B_{3u}; 669+1439=2108 B_{2u}
		2165	w	1534+635=2169 B_{1u}
		2182	vw	1335+853=2188 B_{3u}
		2197	w	1439+748=2187 B_{1u}
~2232	vw	2226	m	1374+853=2227 B_{3u}
2256	vw	2254	m	1374+869=2243 B_{2u}
2288	w	2279	m	1439+832=2271 B_{1u}
		2310	m	963+1335=2298 B_{1u}
		2340	w	1374+963=2337 B_{1u}; 1643+700=2343 B_{3u}
2360	w	2353	m	1534+832=2366 B_{3u}
		2389	w	1643+755=2398 B_{1u}
		2407	vw	1130+1277=2407 B_{1u}
		2419	vw	1196+1222=2418 B_{3u}
2491	vvw	2490	w	1643+853=2496 B_{1u}; 1335+1164=2499 B_{3u}
		2534	m	1374+1164=2538 B_{3u}
2543	w			
		2554	m	1222+1335=2557 B_{1u}
2571	w	2564	m	1439+1130=2569 B_{3u}
2604	vw	2594	m	1222+1374=2596 B_{1u}
2648	vw	2649	m	1277+1374=2651 B_{3u}
		2726	m	1196+1534=2730 B_{1u}
		2771	m	1439+1335=2774 B_{1u}
2809	vw	2804	m	1164+1643=2807 B_{1u}
		2828	m	1439+1374=2813 B_{1u}
2877	vw	2869	m	1335+1534=2869 B_{3u} 1222+1643=2865 B_{3u}
2924	vw	2918	m	1534+1374=2908 B_{3u}
		2933	w	1643+1277=2920 B_{1u}
		2981	w	
3089	m	3088	s	b_{1u} fundamental; 1643+1439=3082 B_{3u}
3094	vw			
3138	vw	3137	w	
3185	vw	3176	w	1643+1534=3177 B_{1u}
		3390	w	295+3088=3383 B_{2u}
		3445	vw	
		3580	w	487+3088=3575 B_{1u}
		3730	vw	635+3088=3723 B_{3u}
		3820	w	3088+748=3836 B_{1u}
		~3940	w	853+3097=3950 B_{3u}
		4310	w	1222+3097=4319 B_{1u}
		4460	vw	1374+3088=4462 B_{1u}
		4520	vw	1439+3097=4536 B_{1u}
		4690	w	3088+1643=4731 B_{3u}

assumed to be a b_{2g} fundamental involving largely C—F stretching. Its value seems a little low, and it is possible that one of the weaker bands at 1255 or 1272 cm^{-1} should be assigned as this fundamental and that the 1196 cm^{-1} band should be interpreted as a binary sum band, 963+240=1203 B_{3g}. The medium intensity doublet observed at 1121 and 1130 cm^{-1} is interpreted to be a b_{2g} fundamental in resonance with 487+635 =1122 B_{2g}. The 1130 cm^{-1} band is slightly more intense and probably lies closer to the fundamental frequency.

The strong band at 635 cm^{-1} is assigned as a b_{2g} fundamental. This band and the band at 669 cm^{-1} assigned as a b_{3g} fundamental, may be reversed as to species assignment. The greatest uncertainty lies in the assignment of the lowest fundamental of this species which has been identified with the weak Raman band at 202 cm^{-1}. This seems to be a rather low value, and it is possible that the slightly more intense Raman band at 280 cm^{-1} should be assigned as this fundamental. However, the band at 280 cm^{-1} can be interpreted as the overtone of the lowest a_u fundamental whereas an alternative assignment for the 202 cm^{-1} band has not been found. The low measured depolarization ratio of 0.6 for this band is attributed to the experimental uncertainty introduced by its low intensity and proximity to the exciting line.

Species a_u

The two inactive a_u fundamental frequencies have been calculated, although with considerable uncertainty since the valence force constants for ring bending occur in unknown combinations. This situation is discussed in more detail in the paper on 1,4-difluorobenzene.[2] The calculated frequencies are 120 and 575 cm^{-1}. The frequency 140 cm^{-1} has been adopted for the low a_u fundamental, since the weak Raman band at 280 cm^{-1} can be interpreted as the overtone, while three infrared bands can be interpreted as binary sum bands involving 140 cm^{-1}, but not otherwise.

No good evidence has been found for assigning the highest a_u fundamental. It is possible that one of the weak infrared bands at 551, 640, 650, or 677 cm^{-1} may represent this fundamental, the selection rules being relaxed in the liquid state.

TABLE II. Raman spectrum of 1,2,4,5-tetrafluorobenzene (liquid).

Wave number	Relative intensity	Depolarization	Exciting Hg lines	Interpretation
202 cm^{-1}	w	0.6	e	b_{2g} fundamental
280	w		±e	[2×140=280 A_g]
295	19	0.85	±e, f	b_{3g} fundamental
417	21	0.87	±e, f	b_{1g} fundamental
487	35	0.25	±e	a_g fundamental
~533	vvw		e	
591	vw		e	2×295=590 A_g
635	3.6	0.89	±e	b_{2g} fundamental
669	0.67	0.8	e	b_{3g} fundamental
748	140	0.15	±e, f, g, k, i	a_g fundamental
783	vvw		e	487+295=782 B_{3g}
832	0.33	0.5	e	a_g fundamental; 2×417=834 A_g; 635+202=837 A_g
871	vw		e	b_{3g} fundamental; 669+202=871 B_{1g}
920	vw	0	e	2×459=918 A_g
964	vvw		e	295+669=964 A_g; 2×487=974 A_g
1000	vvw		e	[869+140=1009 B_{2g}]; [755+240=995 B_{1g}]
1027	vvw		e	832+202=1034 B_{2g}
1121	0.60	0.82	e	487+635=1122 B_{2g}
1130	0.75	0.78	e	b_{2g} fundamental
1164	vvw		e	700+461=1161 B_{3g}; 669+487=1156 B_{3g}; 871+295=1166 A_g
1196	0.28	0.6	e	b_{2g} fundamental
1255	vvw		e	832+417=1249 B_{1g}
1272	vvw		e	2×635=1270 A_g
1335	0.47	0.5	e	a_g fundamental; 2×669=1338 A_g
1374	14	0.1	e, f, k	a_g fundamental
1402	0.64	0.04	e	2×700=1400 A_g
1521	vvw		e	2×755=1510 A_g
1574	vvw		e	1374+202=1576 B_{2g}; 869+700=1569 B_{3g}
1610	vw		e	853+755=1608 A_g; 1196+417=1613 B_{3g}
1643	1.6	0.92	e	b_{2g} fundamental
1677	vvw		e	1196+487=1683 B_{2g}; 1374+295=1669 B_{3g}
1734	vvw		e	2×869=1738 A_g; 1277+461=1738 B_{1g}
1782	vvw		e	1374+417=1791 B_{1g}
1834	vvw		e	963+869=1832 B_{3g}
1864	vvw		e	1164+700=1864 B_{2g}; 1374+487=1861 A_g
2316	vvw		e	1439+869=2308 B_{3g}; 2×1164=2328 A_g
2439	vvw		e	1164+1277=2441 A_g; 2×1222=2444 A_g
3097	18	0.4	e	a_g fundamental

DISCUSSION

The interpretation for the infrared spectrum is given in Table I, for the Raman spectrum in Table II. On the basis of the twenty-eight active fundamentals listed in Table III, it has been possible to interpret all but two of the thirty-eight observed Raman shifts and one of these is the very weak band at 280 cm^{-1} which may be interpreted as the low a_u fundamental overtone.

Comparison of spectra shows that eight of the one hundred-one infrared maxima observed in liquid 1,2,4,5-tetrafluorobenzene are due to a trace of 1,2,4-trifluorobenzene. Of the remaining ninety-three bands, all but ten have been explained, three as difference bands, the rest as binary sums. Three additional bands are interpreted if 140 cm^{-1} is adopted for the low a_u fundamental frequency. Except for a medium intensity band at 1911 cm^{-1}, the remaining seven bands are all quite weak.

The frequencies for the liquid state are used in interpreting the spectra, since all the Raman bands are observed for the liquid state and since the majority of the infrared maxima are observed only in the liquid state. The frequency difference for the assigned infrared-active fundamentals is less than 10 cm^{-1} for the gaseous and liquid state in every case observed.

The interpretations enclosed in brackets involve a fundamental frequency not directly observed, either the lowest b_{2u} or the lowest a_u fundamental.

TABLE III. Fundamental vibration frequencies for 1,2,4,5-tetrafluorobenzene (liquid).

	a_g	b_{1g}	b_{2g}	b_{3g}	a_u	b_{1u}	b_{2u}	b_{3u}
C–H stretching	3097					3088		
C–F stretching	1335		1196			1222		1277
C–C stretching	1374		1643			1439		1534
C–C breathing	748					963		853
C–F bending	832	417	635	669	(~600)	700	461	755
C–H bending			1130	871			869	1164
C–C–C bending	487		202	295	(140)		(240)	

The seven active nonplanar vibration frequencies are calculated with an average difference from the observed frequencies of three percent, using only two of these frequencies to determine force constants (both small interaction constants) and transferring the remaining constants from benzene and 1,3,5-trifluorobenzene. This seems to substantiate previous indications[2,3] that such force constant transferring is quite good for out-of-plane motions in fluorinated benzenes.

ACKNOWLEDGMENT

The writers wish to acknowledge their indebtedness to Dr. G. C. Finger for the gift of the sample.

Vibrational Spectra of Fluorinated Aromatics. V. 1,3-Difluorobenzene*

E. E. FERGUSON, R. L. COLLINS,† AND J. RUD NIELSEN
Department of Physics, University of Oklahoma, Norman, Oklahoma

AND

D. C. SMITH†
Naval Research Laboratory, Washington, D. C.

(Received March 20, 1953)

The infrared absorption spectrum of liquid 1,3-difluorobenzene has been obtained in the region 2–22μ with the aid of LiF, NaCl, and KBr prisms. The contours of the strong infrared bands of the gaseous phase have also been observed in the region 5–22μ. The Raman spectrum of the liquid has been photographed with a three-prism glass spectrograph of linear dispersion 15 A/mm at 4358A, and depolarization ratios have been measured for the stronger Raman bands. A complete assignment of fundamental vibration frequencies is given and the spectra are interpreted in detail.

INTRODUCTION

IN PREVIOUS papers of this series[1–4] the infrared and Raman spectra of 1,3,5-trifluorobenzene, 1,4-difluorobenzene, and 1,2,4,5-tetrafluorobenzene, have been reported. Raman data for 1,3-difluorobenzene and a partial assignment of fundamental vibration frequencies are given in Landolt-Börnstein.[5] In the present paper new spectral data, assignments of fundamentals, and detailed interpretations of the spectra, will be presented.

EXPERIMENTAL

The sample of 1,3-difluorobenzene was kindly supplied by Dr. G. C. Finger of the Illinois State Geological Survey. No information is available as to the purity of the sample. The infrared absorption spectrum of the liquid phase was measured from 2–22μ in the manner previously described.[1] The infrared absorption band contours in the gaseous state were observed with a Perkin-Elmer Model 12C spectrometer having a NaCl prism and also on another instrument having both NaCl and KBr prisms. Only the spectral regions immediately surrounding strong bands were scanned in order to determine contours and band types.

The Raman spectrum was obtained at room temperature, and quantitative polarization measurements were made in the manner previously described.[1]

RESULTS

The infrared absorption of liquid 1,3-difluorobenzene is shown in Fig. 1, and the contours of some of the bands observed in the gas are shown in Fig. 2. The wave numbers of the observed absorption maxima are listed in the first two columns of Table I. The relative intensities of the bands are indicated by means of the previously used abbreviations. The observed Raman data for liquid 1,3-difluorobenzene are given in the next three columns of Table I.

INTERPRETATION

The 1,3-difluorobenzene molecule undoubtedly has the symmetry C_{2v}. The thirty vibrational modes divide into symmetry species in the following manner: $11a_1+10b_1$ (planar) and $3a_2+6b_2$ (nonplanar). The species a_1 gives rise to polarized Raman bands, the remaining species to depolarized Raman bands. Fundamentals of species a_1 should give rise to type B infrared bands, fundamentals of species b_1 to type A and fundamentals of species b_2 to type C infrared bands. The vibrations of species a_2 are inactive in infrared absorption.

Species a_1

The eleven fundamentals of species a_1 have been assigned mainly on the basis of Raman polarization measurements. Three of these fundamentals involve largely C—H stretching. One of them must be identified with the strong polarized Raman band and the strong infrared band at 3087 cm^{-1}. Another high a_1 fundamental is assumed to overlap a b_1 fundamental at 3096 cm^{-1}. The remaining high a_1 fundamental is assumed to lie at 3049 cm^{-1} where a very weak infrared band occurs in the liquid. This latter assignment is somewhat uncertain, although it can be used in interpreting four of the ten infrared absorption maxima observed with wave numbers exceeding 3086 cm^{-1}.

Five of the remaining a_1 fundamentals can be assigned with considerable certainty. One of these is

* Parts of this work have been supported by the U. S. Atomic Energy Commission under Contract No. AT-(40-1)-1074 and by the Office of Naval Research under Contract N7onr-398, T.O.I.

† Present address: Phillips Petroleum Company, Bartlesville, Oklahoma.

[1] Nielsen, Liang, and Smith, Disc. Faraday Soc. **9**, 177 (1950).

[2] Eldon Ferguson, J. Chem. Phys. **21**, 886 (1953).

[3] Ferguson, Hudson, Nielsen, and Smith, J. Chem. Phys. **21**, 1457 (1953).

[4] Ferguson, Hudson, Nielsen, and Smith, J. Chem. Phys. **21**, 1464 (1953).

[5] Landolt-Börnstein, Zahlenwerte und Funktionen, (Springer Verlag, Berlin, 1951), 6th ed., Vol. I, Part II, pp. 316 and 323.

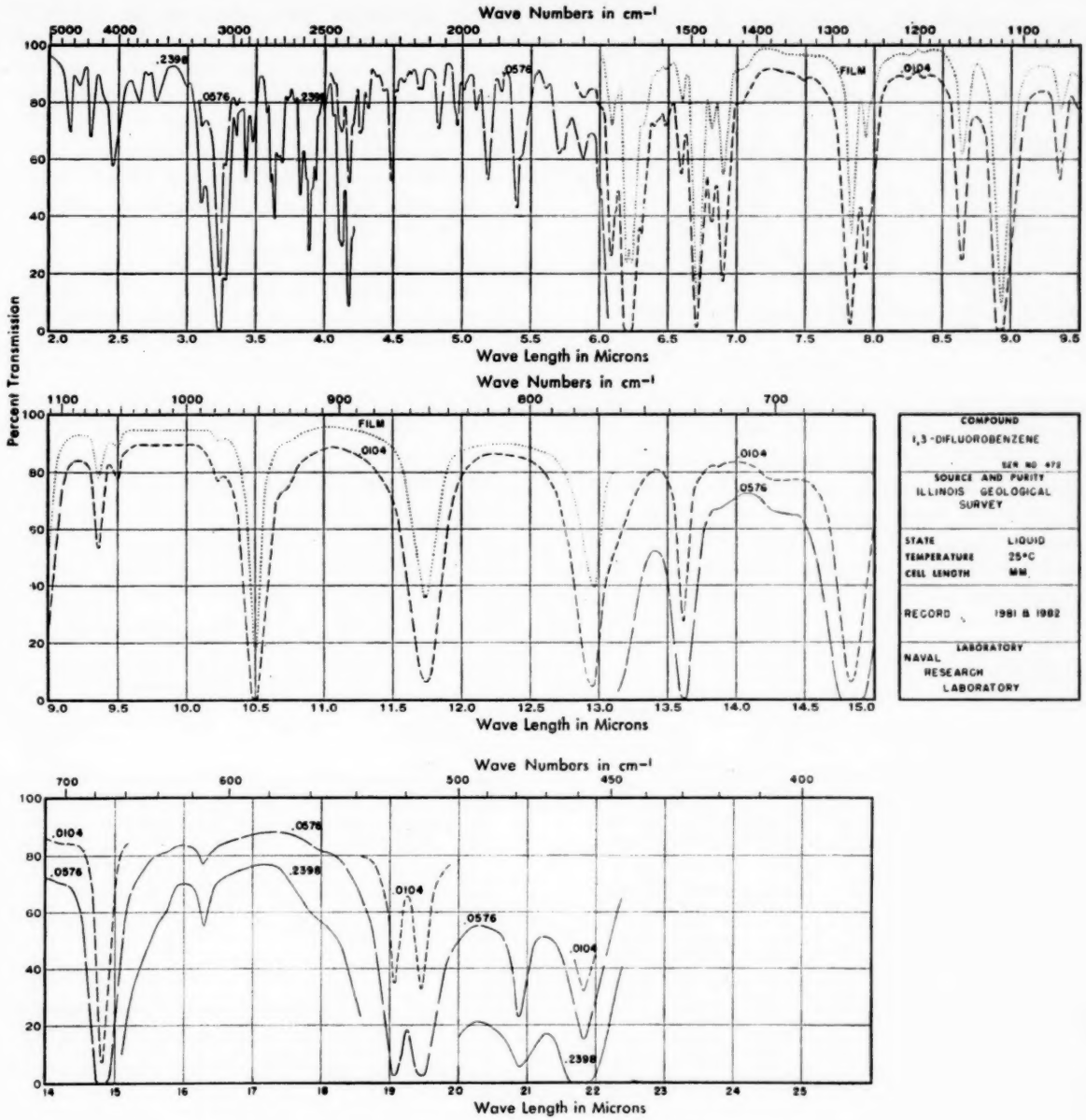

FIG. 1. Infrared spectrum of liquid 1,3-difluorobenzene.

represented by the strong polarized Raman band and very strong infrared band at 524 cm^{-1}. Another is revealed by the very strong polarized Raman band at 736 cm^{-1}. In this case the contour of the strong infrared band is definitely of type B with a P−R branch separation of 10 cm^{-1}, in accord with the predicted value. The very strong polarized Raman band at 1008 cm^{-1} and the medium intensity polarized Raman band at 1068 cm^{-1} undoubtedly also represent a_1 fundamentals. Corresponding to the latter there is a medium infrared absorption band with type B contour and a $P-R$ separation of 11 cm^{-1}. The strong polarized Raman band at 1279 cm^{-1} and the corresponding strong infrared band with $P-R$ separation of 8 cm^{-1} are also identified with an a_1 fundamental with considerable certainty. With somewhat less certainty, the weak polarized Raman band at 1256 cm^{-1} is assigned as an a_1 fundamental. There is a corresponding infrared band at 1259 cm^{-1} which is slightly less intense than the band at 1279 cm^{-1} and has a type B contour with measured $P-R$ separation 9 cm^{-1}. However, this band could also be explained as the combination $524+735=1259$ A_1, enhanced by Fermi resonance with the a_1 fundamental at 1279 cm^{-1}.

The remaining a_1 fundamental is identified with the medium infrared band at 1449 cm^{-1} having a type B contour with $P-R$ separation 11 cm^{-1}. The corresponding very weak Raman band appears to be polarized.

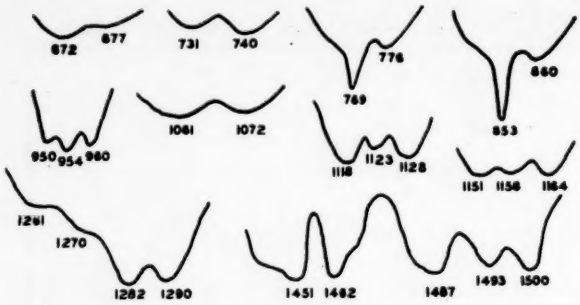

FIG. 2. Infrared contours of gaseous 1,3-difluorobenzene.

Species a_2

The three fundamentals of species a_2 are Raman-active but infrared-inactive. The medium Raman band at 599 cm^{-1} with measured depolarization ratio of 0.84 and the very weak Raman band at 879 cm^{-1} are readily assigned as a_2 fundamentals, corresponding approximately to fluorine bending and hydrogen bending, respectively. The low intensity of nonplanar hydrogen-bending modes is characteristic of fluorinated benzenes, having previously been observed in 1,3,5-trifluorobenzene,[2] 1,4-difluorobenzene,[3] and 1,2,4,5-tetrafluorobenzene.[4] The lowest a_2 fundamental, which involves largely a nonplanar ring bending, is assumed to be represented by the strong Raman band at 251 cm^{-1} with measured depolarization ratio 0.83. The only reasonable alternative is the strong Raman band at 235 cm^{-1} assigned here as a b_2 fundamental.

Species b_1

One of the ten b_1 fundamentals is a C−H stretching mode and is assigned as the medium intensity Raman band at 3096 cm^{-1}. The vibrations of species b_1 should yield infrared bands of type A contour with a $P-R$ separation of about 11 cm^{-1}. The strong infrared band at 1157 cm^{-1} and the very strong bands at 952 cm^{-1} and 1120 cm^{-1} are all assigned as b_1 fundamentals on this basis. They are all type A bands and have measured $P-R$ separations of 13 cm^{-1}, 10 cm^{-1}, and 10 cm^{-1}, respectively. The band at 952 cm^{-1} is not observed in the Raman spectrum. However, it lies exactly where the 1008-cm^{-1} shift from the 4347.5 A Hg line occurs, and

TABLE I. Infrared and Raman spectra of 1,3-difluorobenzene.

Infrared		Raman			
Gas	Liquid	Liquid	Depolarization	Interpretation
		235.3 s	0.84	b_2 fundamental
		251.0 s	0.83	a_2 fundamental
		331.4 w, sh	0.7	a_1 fundamental
	458 s	459 vw	dp	b_1 fundamental
	478 s	482 vw	dp	b_2 fundamental
	514 vs	513.7 s	0.85	b_1 fundamental
	524 vs	523.7 s, sh	0.35	a_1 fundamental
		599 m	0.84	a_2 fundamental
	613 w			862−251=611 B_1; 952−331=621 B_1
672 677	674 vs			b_2 fundamental
	723 vw	723.6 w, sh	p	478+235=713 A_1
731 740	734 s	736.1 vs, sh	0.09	a_1 fundamental
769 776	771 vs	774 w	0.85	b_2 fundamental
853 860	852 vs	849 vw, d	∼0.5	b_2 fundamental
		862 vvw, d		b_2 fundamental
		879 vw, d	dp	a_2 fundamental
950 954 960	952 vs			b_1 fundamental
	978 w			458+524=982 B_1; 458+514=972 A_1
		997.8 w, sh	p?	478+514=992 A_2; 235+772=1007 A_1
		1008.2 vs, sh	0.04	a_1 fundamental
	1053 w			2×524=1048 A_1; 458+599=1057 B_2
1061 1072	1068 m	1068 m, sh	0.28	a_1 fundamental
1118 1123 1128	1120 vs	1119 m	0.8	b_1 fundamental
1151 1158 1164	1157 s	1158 w, d	0.6	b_1 fundamental
	∼1196 vw	1197 w	p?	2×599=1198 A_1; 458+735=1193 B_1
	∼1212 vw			478+735=1213 B_2
		1227 w, d		458+772=1230 A_2
1261 1270	1259 m	1256.4 w, sh	0.20	a_1 fundamental; 524+735=1259 A_1
1282 1290	1277 s	1279 s, sh	0.08	a_1 fundamental
	1337 vw	1339 w, d		b_1 fundamental; 478+852=1330 A_1; 1008+331=1335 A_1
		1418 vvvw		478+952=1430 A_2
1451 1462	1449 m	1454 vw	p?	a_1 fundamental; 599+852=1451 B_1
	1466 w	1471 vw	p?	2×735=1470 A_1; 1008+458=1466 B_1
1487 1493 1500	1490 s	1496.6 w	∼0.9	b_1 fundamental; 1257+235=1492 B_2; 1157+331=1488 B_1; 478+1008=1486 B_2
	1515 w			514+1008=1522 B_2
	1543 vw	1545 vvvw		2×772=1544 A_1
	1555 vw			478+1068=1546 B_2
	1563 vw			599+952=1551 B_2
	1585 vw			514+1068=1582 B_1
1582 1608	1605 m	1604 w	∼0.6	b_1 fundamental; 331+1279=1610 A_1
1621	1613 m	1616 m	0.8	b_1 fundamental; 458+1157=1615 A_1
1628 1641	1642 w			524+1120=1644 B_1
	1701 w	1701 vvw		2×852=1702 A_1

TABLE I—*Continued.*

Infrared		Raman			
Gas	Liquid	Liquid		Depolarization	Interpretation
	1742 w				735+1008=1743 A_1; 458+1279=1737 B_1
	1751 w				599+1157=1756 B_2; 251+1496=1747 B_2
	1783 vw				524+1257=1781 A_1; 772+1008=1780 B_2
	1852 m				735+1120=1855 B_1; 852+1008=1860 B_2
	1890 vw				735+1157=1891 B_1
	1927 m	1932	vvw		331+1604=1935 B_1; 1068+862=1930 B_2
	1961 w				952+1008=1960 B_1
	1992 vw				735+1257=1992 A_1
	2012 m				2×1008=2016 A_1; 735+1279=2014 A_1
	2070 m				1008+1068=2076 A_1; 458+1604=2062 A_1
	2123 w				524+1604=2128 B_1; 514+1604=2118 A_1
	2132 w				2×1068=2136 A_1; 852+1279=2131 B_2
	2160 vw				1008+1157=2165 B_1
	2183 vw				1068+1120=2188 B_1
	2208 vw				952+1257=2209 B_1
	2227 m				735+1496=2231 B_1; 1068+1157=2225 B_1
	2257 vw				1008+1257=2265 A_1
	2283 vw				1008+1279=2287 A_1; 1120+1157=2277 A_1
	2315 w				2×1158=2316 A_1; 1453+862=2315 B_2
	2347 w				1068+1279=2347 A_1
	2392 m				1120+1279=2399 B_1
	2421 w	2419	vvw		1157+1257=2414 B_1
	2457 vw	2464	vw		1120+1339=2459 A_1; 852+1616=2468 A_2
	2500 vw				1008+1496=2504 B_1
	2538 vw				1257+1279=2536 A_1
	2571 m	2569	w	p	2×1279=2558 A_1; 1068+1496=2564 B_1
	2611 w				1120+1496=2616 A_1; 1008+1604=2612 B_1
	2646 vw				1157+1496=2635 A_1
	2667 vw				1068+1604=2672 B_1
	2681 vw				1068+1616=2684 B_1
	2710 vw				1257+1453=2710 A_1
	2732 vw				1279+1453=2732 A_1
	2747 m				1257+1496=2753 B_1
	2770 vw				1279+1496=2775 B_1; 1157+1616=2773 A_1
	2793 vw				1453+1339=2792 B_1
	2874 w				1257+1616=2873 B_1; 1279+1604=2883 B_1
	2915 m				2×1453=2906 A_1
		2957	w		1453+1496=2949 B_1; 1339+1616=2955 A_1
	2976 w				2×1496=2992 A_1
	3049 vw				a_1 fundamental
	3086 s	3087	s	0.3	a_1 fundamental
		3096	m		a_1 fundamental+ b_1 fundamental
	3215 w	3210	vw		2×1604=3208 A_1
		3230	vw		2×1616=3232 A_1
	3333 vw				3096+235=3331 B_2
	3597 w				3087+514=3601 B_1
	3690 vw				3096+599=3695 B_2
	3774 w				735+3049=3784 A_1
	4065 m				1008+3049=4057 A_1
	4348 m				1257+3087=4344 A_1
	4505 w				3049+1453=4502 A_1
	4651 m				1604+3049=4653 B_1

hence would be masked if of very low intensity. A medium intensity depolarized Raman band occurs at 1119 cm^{-1} and a weak diffuse Raman band at 1158 cm^{-1}. The latter band has a not very accurately measured depolarization ratio of 0.6, but the diffuse nature of the band indicates that it is depolarized.

The very weak depolarized Raman band at 459 cm^{-1}, and its strong infrared counterpart, are assigned as the lowest b_1 fundamental. It is possible that the very weak depolarized Raman band observed at 482 cm^{-1} and assigned as a b_2 fundamental should rather be assigned as a b_1 fundamental. However, the observation of a weak Raman band at 1227 cm^{-1} and a very weak Raman band at 1418 cm^{-1}, each having no infrared counterparts, strengthens the present assignment, since they can each be interpreted as a species A_2 combination band but could not be so interpreted if the species of the bands at 459 and 482 cm^{-1} were reversed. The weak depolarized Raman band at 1497 cm^{-1} with a corresponding strong infrared absorption and the medium Raman band at 1616 cm^{-1} with corresponding medium infrared absorption seem certainly to be b_1 fundamentals. The assignment of the weak Raman band at 1604 cm^{-1}, and the corresponding medium infrared band, as a b_1 fundamental is considerably less certain. The 1604 and 1616 cm^{-1} bands overlap in both infrared and Raman spectra. The band at 1616 cm^{-1} has a measured depolarization ratio of 0.8 and that at 1604 cm^{-1} has a measured depolarization ratio of 0.6 with a large uncertainty. Both bands have the diffuse appearance of depolarized bands. The infrared contours give no aid in interpreting the bands at 1497, 1604, and 1616 cm^{-1} because of the low resolution in this region, and because of overlapping with the water band at 6.28μ and mutual overlapping of the latter two bands. The strong Raman band and very strong infrared band at 514 cm^{-1} are assigned as a b_1 fundamental. The last b_1 fundamental is identified with the weak Raman band at 1339 cm^{-1} and the weak infrared counterpart. Since this band can also be interpreted in several ways as a binary sum band, its assignment is uncertain.

TABLE II. Fundamental vibration frequencies of 1,3-difluorobenzene (liquid).

Species a_1				Species b_1			
Raman		Infrared		Raman		Infrared	
Wave No.	Intensity	Wave No.	Intensity	Wave No.	Intensity	Wave No.	Intensity
331.4	w			459	vw	458	s
523.7	s	524	vs	513.7	s	514	vs
736.1	vs	734	s	?(overlapped)		952	vs
1008.2	vs	...		1119	m	1120	vs
1068	m	1068	m	1158	w	1157	s
1256.4	w	1259	m	1339	w	1337	vw
1279	s	1277	s	1496.6	w	1490	s
1454	vw	1449	m	1604	w	1605	m
...		3049	vw	1616	m	1613	m
3087	s	3086	s	3096	m	...	
3096	m	...					
Species a_2				Species b_2			
251.0	s	...		235.3	s		
599	m	...		482	vw	478	s
879	vw	...		...		674	vs
				774	w	771	vs
				849	vw	852	vs
				862	vvw	...	

Species b_2

The strong depolarized Raman band at 253 cm^{-1} is interpreted as the lowest of the six nonplanar fundamental vibrations of species b_2. The only uncertainty seems to be a possible interchange with the lowest a_2 fundamental discussed above. The next lowest b_2 fundamental is identified with the strong infrared band at 478 cm^{-1} and the very weak diffuse Raman band observed at 482 cm^{-1}. The possibility of an interchange of the assignment of species for 458 and 478 cm^{-1} has been discussed above.

The very strong infrared bands at 771 and 852 cm^{-1} have definitely type *C* contours and are therefore assigned as b_2 fundamentals. The Raman band observed at 774 cm^{-1} is weak and depolarized, and the Raman band at 849 cm^{-1} is very weak and diffuse, as is characteristic of nonplanar hydrogen-bending modes. The very strong infrared band at 674 cm^{-1} shows some evidence of having a type *C* contour and is also assigned as a b_2 fundamental.

The assignment of the remaining b_2 fundamental is rather uncertain. The very weak Raman band observed at 862 cm^{-1} is tentatively chosen, partly on the basis of an empirical sum rule suggested by Bernstein and Pullin.[6] It is found that the sum of the squares of the nonplanar fundamental frequencies for fluorobenzene, 1,4-difluorobenzene, 1,3,5-trifluorobenzene and 1,2,4,5-tetrafluorobenzene plotted against the number of fluorine atoms yield very nearly a straight line. If such a Bernstein and Pullin's rule is valid, the sum of the squares of the nonplanar frequencies of 1,3-difluorobenzene should equal that for 1,4-difluorobenzene. Actually, these sums differ only by about 1 percent when 862 cm^{-1} is taken as the last b_2 fundamental. The only other observed band that could be given this assignment is a weak infrared band at 613 cm^{-1}. Its adoption would lead to a difference of more than ten percent in the above sums. The frequency 862 cm^{-1} is not observed in the infrared spectrum but may be masked by the very intense broad band at 852 cm^{-1}.

The fundamental frequencies assigned are listed in Table II. The interpretation of the Raman and infrared spectra is included in Table I. All of the forty-one Raman bands and eighty-six infrared absorption maxima observed for the liquid state have been interpreted as either fundamentals or as binary combination or overtone bands. The only band interpreted as a difference band is the weak infrared band at 613 cm^{-1}. The corresponding sum band falls in a region of strong absorption.

ACKNOWLEDGMENT

The writers wish to acknowledge their indebtedness to Dr. G. C. Finger for the gift of the sample.

[6] H. J. Bernstein and A. D. E. Pullin, "An empirical sum rule for vibration frequencies in homologues," paper presented before the Symposium on Molecular Structure and Spectroscopy held at Ohio State University, June 10, 1952.

Vibrational Spectra of Fluorinated Aromatics. VI. Fluorobenzene*

D. C. SMITH†
Naval Research Laboratory, Washington, D. C.

AND

E. E. FERGUSON, R. L. HUDSON,‡ AND J. RUD NIELSEN
Department of Physics, University of Oklahoma, Norman, Oklahoma

(Received March 20, 1953)

The infrared absorption spectra of gaseous and liquid fluorobenzene have been obtained in the regions 2–22μ and 2–38μ, respectively, with the aid of LiF, NaCl, KBr, and KRS-5 prisms. The Raman spectrum of the liquid phase has been photographed with a three-prism glass spectrograph of linear dispersion 15 A/mm at 4358A. A complete assignment of fundamental vibration frequencies is given, and the spectra are interpreted in detail.

INTRODUCTION

IN previous papers of this series[1–5] the infrared and Raman spectra of 1,3,5-trifluorobenzene, 1,4-difluorobenzene, 1,2,4,5-tetrafluorobenzene, and 1,3-difluorobenzene have been reported. Raman data for liquid fluorobenzene, including polarization measurements, have been reported by Kohlrausch.[6] The infrared absorption spectrum of liquid fluorobenzene has been studied by Lecomte[7] and the ultraviolet absorption spectrum by Wollman.[8] Kohlrausch has assigned several of the fundamentals and Wollman has confirmed and modified some of these. Recently, Plyler[9] observed the infrared spectrum of liquid fluorobenzene from 15–38μ with the aid of a KRS-5 prism and assigned five fundamentals in this region. In the present paper more complete spectral data are presented, a complete assignment of fundamentals is given, and the spectra are interpreted in detail.

EXPERIMENTAL

The sample of fluorobenzene, believed to be of high purity, was kindly supplied by Dr. G. C. Finger of the Illinois State Geological Survey. The spectra do not indicate the presence of any of the related fluorinated benzenes studied or any other impurity. The spectral measurements were made with the same instruments and in the same manner as described in earlier papers.[10,11]

RESULTS

The infrared absorption of gaseous and liquid fluorobenzene from 2–22μ are shown in Figs. 1 and 2. The wave numbers of the observed absorption maxima are listed in Table I. The relative intensities of the bands are indicated by means of the previously used abbreviations. The observed Raman shifts for liquid fluorobenzene together with relative intensities and depolarization ratios for the stronger bands are also given in Table I.

INTERPRETATION

The fluorobenzene molecule undoubtedly has the symmetry C_{2v}, and the normal vibrations divide into symmetry species in the following manner: $11a_1+10b_1$ (planar) and $3a_2+6b_2$ (nonplanar). The species a_1 gives rise to polarized Raman bands, the remaining species to depolarized Raman bands. However, Ingold *et al.*[12] have shown that only one of the species a_2 fundamentals will be Raman-active. This effect arises because for none of the three a_2 fundamentals is there any motion of the fluorine atom which could be replaced by a hydrogen atom without affecting these vibrations. Hence the "effective symmetry" is D_{6h}, and the two a_2 fundamentals that correspond to the two e_{2u} fundamentals of benzene will be inactive, while the a_2 fundamental that corresponds to the e_{1g} fundamental in benzene will be Raman-active. The a_1, b_1, and b_2 vibrations give rise to infrared bands of types A, B, and C, respectively. Vibrations of species a_2 are infrared-inactive.

Species a_1

The polarized Raman bands at 519, 808, 1008, 1022, 1157, 1220, and 3067 cm^{-1} are assigned as a_1 fundamen-

* Part of this work has been supported by the U. S. Atomic Energy Commission under contract No. AT-(40-1)-1074 and by the Office of Naval Research under contract N7onr-398, T.O.I.

† Present address: Phillips Petroleum Company, Bartlesville, Oklahoma.

‡ Present address: Ethyl Corporation, Baton Rouge, Louisiana.

[1] Nielsen, Liang, and Smith, Disc. Faraday Soc. **9**, 177 (1950).

[2] Eldon Ferguson, J. Chem. Phys. **21**, 886 (1953).

[3] Ferguson, Hudson, Nielsen, and Smith, J. Chem. Phys. **21**, 1457 (1953).

[4] Ferguson, Hudson, Nielsen, and Smith, J. Chem. Phys. **21**, 1464 (1953).

[5] Ferguson, Collins, Nielsen, and Smith, J. Chem. Phys. **21**, 1470 (1953).

[6] K. W. F. Kohlrausch, *Ramanspektren* (Edwards Brothers, Inc., Ann Arbor, 1945), p. 380.

[7] J. Lecomte, J. de phys. et radium **8**, 489 (1937).

[8] S. H. Wollman, J. Chem. Phys. **14**, 123 (1946).

[9] E. K. Plyler, Disc. Faraday Soc. **9**, 100 (1950).

[10] Nielsen, Liang and Smith, J. Chem. Phys. **20**, 1090 (1952).

[11] Nielsen, Crawford, and Smith, J. Opt. Soc. Am. **37**, 296 (1947).

[12] Bailey, Gordon, Hale, Herzfeld, Ingold, and Poole, J. Chem. Soc. **149**, 304 (1946).

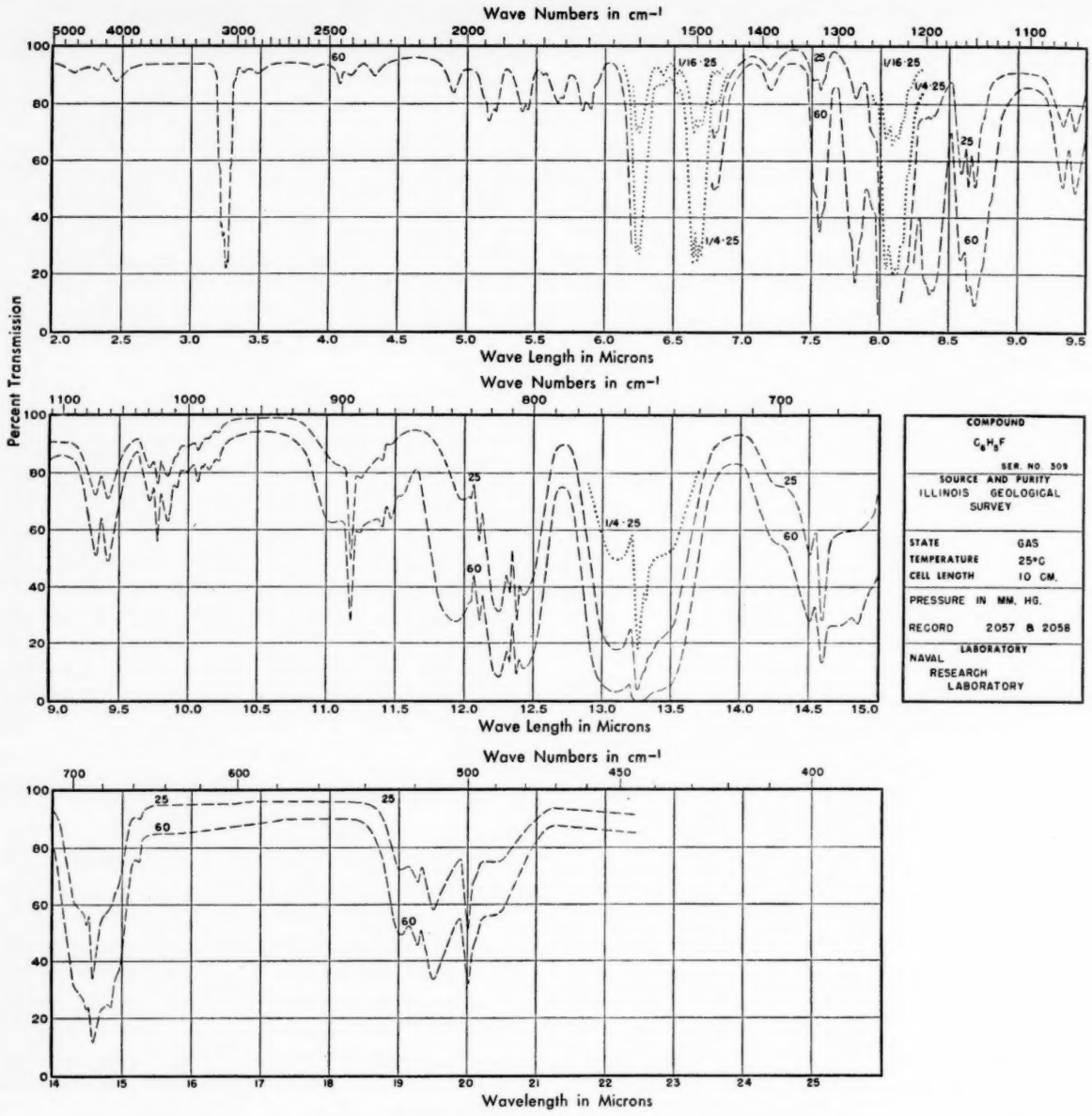

FIG. 1. Infrared spectrum of gaseous fluorobenzene.

tals with considerable certainty in agreement with Kohlrausch.[6] The infrared bands at 808, 1022, and 1157 cm^{-1} have type *A* contours while the infrared band at 519 cm^{-1} shows strong evidence for a type *A* contour. The medium intensity Raman band at 1600 cm^{-1} is assumed to be the superposition of an a_1 and a b_1 fundamental. Kohlrausch resolves two bands in the Raman spectrum at 1596 and 1603 cm^{-1}, measures their composite depolarization ratio to be 0.77, and assigns one of these bands as an a_1 fundamental. There is very strong infrared absorption at 1600 cm^{-1} but because of the low resolution in this region the two bands are not resolved in the liquid and their contours in the gas are of no aid in the interpretation. A very strong infrared band at 1499 cm^{-1}, which appears to have a type *A* contour, and its weak counterpart in the Raman spectrum, are assumed to represent an a_1 fundamental. The two remaining a_1 fundamentals involve C—H stretching and are identified with the strong infrared bands at 3044 and 3101 cm^{-1}. These bands are not resolved in the Raman spectrum from the very intense broad band at 3067 cm^{-1}. Also, a strong Hg line occurs where the 3044 cm^{-1} band would lie.

Species b_1

The assignment of the b_1 fundamentals is more difficult. The very strong infrared band observed in the liquid at 405 cm^{-1} is assumed to be a b_1 fundamental. Unfortunately, the spectrum of the gas did not extend into this region so that the contour is not known. This

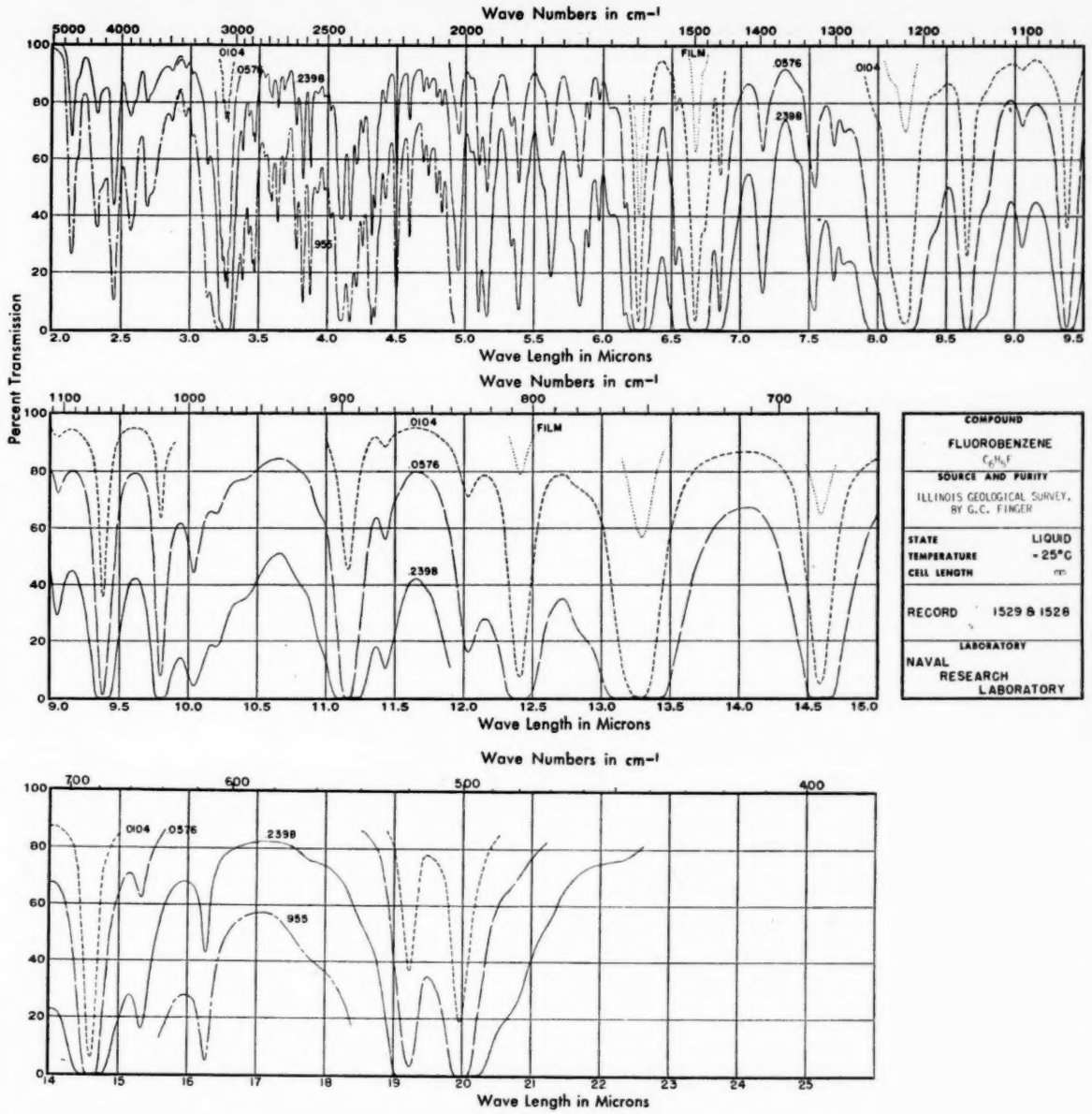

FIG. 2. Infrared spectrum of liquid fluorobenzene (KRS-5 region not shown).

assignment agrees with that of Plyler,[9] as does the assignment of the medium intensity depolarized Raman band at 613 cm^{-1} and the weak infrared band observed at about this wave number in the liquid. The medium intensity infrared band at 874 cm^{-1} and the strong band at 1066 cm^{-1} both have type *B* contours and are accordingly assigned as b_1 fundamentals. The very strong infrared band at 1236 cm^{-1} appears also to have a type *B* contour and is likewise assigned as a b_1 fundamental. The absorption at 1600 cm^{-1} is assumed to result from a superposition of a_1 and b_1 fundamentals as mentioned above. The two b_1 fundamentals involving largely C—H stretching are assumed to lie at 3058 and 3091 cm^{-1} where strong infrared absorptions occur. The assignment of the remaining two b_1 fundamentals is quite uncertain. The strong infrared band at 1460 cm^{-1} of uncertain contour seems likely to be a b_1 fundamental. A very weak Raman band is observed at 1457 cm^{-1}. The remaining b_1 fundamental is with even less certainty identified with the weak infrared band at 1323 cm^{-1}.

The frequencies assigned as b_1 fundamentals are either not observed or observed with low intensity in the Raman spectrum in every case except the medium bands at 614 and 1603 cm^{-1}.

Species b_2

The six nonplanar fundamental vibrations of species b_2 should give rise to depolarized Raman bands and type *C* infrared bands. The infrared bands observed at

TABLE I. Infrared and Raman spectra of fluorobenzene.

Infrared		Raman		
Gas cm^{-1}	Liquid cm^{-1}	Liquid cm^{-1}	Depolarization	Interpretation
		242 m	0.83	b_2 fundamental
	~270 w, b	277 vw, b		519 − 242 = 277 B_2
	405 vs, sh	407 vw	dp?	b_1 fundamental
~490				
~497				
500 s, sh	501 s, sh	499 w	dp?	b_2 fundamental
512				
519 s, sh	520 s, sh	519 m, sh	0.60	a_1 fundamental
~525	~540			
	~565?			(330 + 242 = 572 B_1)
	615 w, sh	613 m, sh	0.92	b_1 fundamental
656 m	653 m, sh			(2 × 330 = 660 A_1)
~668				
673				
~680				
685 s, sh	685 vs, sh	687 vw	dp	b_2 fundamental
689				
~702				
741				
749				
751				
754 vs, sh	752 vs	754 w, b	0.54	b_2 fundamental;
~763				242 + 500 = 742 A_1;
				242 + 519 = 761 B_2
	~780 w, b			
~805				
808 s, sh	806 vs	806 s, sh	0.12	a_1 fundamental
811 sh				
~816		818 vw		a_2 fundamental
826 s, sh	831 s	829 w, sh		b_2 fundamental
830				
~833				
~866				
872 m, sh	875 m			b_1 fundamental
876 m, sh				
889				
894 s, sh	896 s	896 vw		b_2 fundamental
~905	~915			
	~925			405 + 519 = 924 B_1;
				242 + 685 = 927 A_1
	~955			a_2 fundamental?;
				(330 + 614 = 944 B_2)
978	980 w			
985				
~989				
993 w, sh	996 m	997 m		2 × 500 = 1000 A_1
1001				
1008 w		1009 vs, sh	0.07	a_1 fundamental
1015				
1022 m, sh	1020 s, sh	1021 m, sh		a_1 fundamental
1029				
1062				
1072	1066 s, sh	1065 w	dp?	b_1 fundamental
	1105 w			
~1136				
~1143	~1140 w			242 + 894 = 1136 A_1
1151				
1157 s, sh	1156 s, sh	1156 m, sh	0.65	a_1 fundamental
1164				
1192				
1196 m	~1190 w			(330 + 874 = 1204 B_2)
~1202				
~1220				
~1224	1220 vs	1217 m	0.15	a_1 fundamental;
				2 × 614 = 1228 A_1
1230 vs				
1236 vs, sh	~1235			b_1 fundamental
1244 vs				
~1253				
~1262	~1255			242 + 1008 = 1250 B_2;
				500 + 754 = 1254 A_1
~1271				
1279 m, sh				405 + 874 = 1279 A_1
~1285	1290 w			
	1302 w			500 + 808 = 1308 B_2
~1316				
1323 m, sh	1326 m			b_1 fundamental
1330				500 + 826 = 1326 A_1;
				519 + 808 = 1327 A_1
	~1350 w	1369 w, sh		2 × 685 = 1370 A_1
~1389 w	1397 m, sh			500 + 894 = 1394 A_1
1464	1460 s, sh	1457 vw, sh		b_1 fundamental
1473 m				
	~1485			614 + 874 = 1488 A_1
1493				
1499 vs, sh	1499 vs, sh	1496 w		a_1 fundamental
1506				
1534 m	1531 m, sh			519 + 1008 = 1527 A_1
	~1540			519 + 1022 = 1541 A_1
1558 m				405 + 1157 = 1562 B_1
1600 vs, sh	1597 vs, sh	1602 m, b		b_1 fundamental + a_1
1605 vs, sh				fundamental
	1624 w, sh	1623 vw		405 + 1220 = 1625 B_1
	~1652 vw			2 × 826 = 1652 A_1
~1681	1676 vw, sh			519 + 1157 = 1676 A_1;
				808 + 874 = 1682 B_1
1695 w	1695 vw, sh	1693 vw		685 + 1008 = 1693 B_2;
				808 + 894 = 1702 B_2
1712 w	1714 w, sh			685 + 1022 = 1707 B_2
		1735 vw		500 + 1236 = 1736 A_2
1757 w				519 + 1236 = 1755 B_1
1767 w	1778 w, sh			754 + 1022 = 1776 B_2
~1799 vw		1789 vw		(330 + 1460 = 1790 B_2)
1842 w				685 + 1157 = 1842 B_2
1852 w	1855 w, sh			826 + 1022 = 1848 B_2
	1874 w, sh			808 + 1066 = 1874 B_1
1919 w		1915 vw		894 + 1022 = 1916 B_2
1938 w	1939			874 + 1066 = 1940 A_1
1960	1962 w, sh	1960 vw		808 + 1157 = 1965 A_1
	~1984 vw, sh			826 + 1157 = 1983 B_2
2041 w	2021 w, sh	2022 vw		2 × 808 = 1616 A_1;
				808 + 1220 = 2028 A_1
	2070 vw, sh			1008 + 1066 = 2074 B_1
	2085 vw, sh			1022 + 1066 = 2088 B_1
	2113 vw, sh	2117 vw		894 + 1220 = 2114 B_2
	2129 vw, sh			2 × 1066 = 2132 A_1
	2175 w, sh			1022 + 1157 = 2179 A_1
	2222 w, sh	2214 vw		1066 + 1157 = 2223 B_1
	2261 vw, sh			808 + 1460 = 2268 B_1
	2302 w, sh			1066 + 1236 = 2302 A_1;
				808 + 1499 = 2307 A_1
2309 vw	2313 w, sh	2313 vw		2 × 1157 = 2314 A_1
	2351 vw, sh	2359 vw		754 + 1596 = 2350 B_2
	2375 vw, sh			1157 + 1220 = 2377 A_1;
				874 + 1499 = 2373 B_1
~2404 vw	2400 w, sh			808 + 1602 = 2410 B_1
	~2434 w			826 + 1596 = 2422 B_2
2451 w	~2443 w	2443 vw		2 × 1220 = 2440 A_1
	2484 vw, sh	2491		2 × 1236 = 2472 A_1
	2503 vw, sh			1008 + 1499 = 2507 A_1
	2513 vw, sh			
~2564 vw	~2546 vw			1066 + 1499 = 2565 B_1
	2579 w, sh			
	2615 w, sh			1157 + 1460 = 2617 B_1
	2649 vw, sh			1157 + 1499 = 2656 A_1
	2713 vw, sh			1220 + 1499 = 2719 A_1
	2747 vw, sh	2745 vw		1157 + 1596 = 2753 A_1
	2781 vw			1460 + 1323 = 2781 A_1
	2821 vw, sh	2846 vw		1220 + 1603 = 2823 B_1;
				1236 + 1603 = 2839 A_1
2882 vw	2879 vw, sh	2869 vw		
	2882 vw, sh			
	2915 vw, sh			2 × 1460 = 2920 A_1
2959 vw	2955 w, sh	2948 vw		1460 + 1499 = 2959 B_1
		2979 vw		2 × 1499 = 2998 A_1
~3021 vw				
3044	~3040 s			a_1 fundamental
3058	3053 s, sh			b_1 fundamental
3067 vs, sh	3067 s	3072 s, sh	0.40	a_1 fundamental
~3078	~3078			1460 + 1603 = 3063 A_1
3091	3087			b_1 fundamental
3101 sh, sh	~3100 s			a_1 fundamental
~3115				1499 + 1603 = 3102 A_1
	3193 w	3184 w		2 × 1596 = 3192 A_1
	3317 vw			242 + 3067 = 3309 B_2
	3373 vw			(330 + 3058 = 3388 B_2)
	3480 vw			405 + 3067 = 3472 B_1
	3720 vw			685 + 3044 = 3729 B_2
	3890 w			808 + 3091 = 3899 B_1
~4065 w	4080 w			1022 + 3067 = 4089 A_1
4290 vw	4290 w			1220 + 3067 = 4287 A_1
4651 vw	4670 w			1603 + 3067 = 4670 B_1

TABLE II. Fundamental vibrational frequencies for fluorobenzene.

Species a_1	Species b_1	Species a_2	Species b_2
519 cm^{-1}	405	(330)	242
808	614	818	500
1008	874	(955)	685
1022	1066		754
1157	1236		826
1220	1323?		894
1499	~1460		
1596	1603		
3044	3058		
3067	3091		
3101			

500, 685, 754, and 894 cm^{-1} all have type *C* contours and are therefore assigned as b_2 fundamentals. The corresponding Raman band is weak in each case. The only one of these for which polarization measurements are available is the band at 754 cm^{-1} for which Kohlrausch gives a depolarization ratio of 0.54. This low value may be caused by the uncertainty in measuring depolarization ratios of weak Raman bands or it may be a result of overlapping with the combination band 242+500=742 A_1. The Raman band at 754 cm^{-1} is quite diffuse in appearance so that it undoubtedly has a depolarized component. The strong infrared band observed at 826 cm^{-1} also appears to have a type *C* contour and is assumed to represent a b_2 fundamental. The remaining fundamental of species b_2 is identified with the medium intensity depolarized Raman band at 242 cm^{-1}.

The assignment of the frequencies 685, 754, and 826 as b_2 fundamentals was previously made by Kohlrausch who assigned only these three b_2 fundamentals. The assignment of 754 cm^{-1} is also in accord with the interpretation of this frequency as an out-of-plane hydrogen-bending mode by Cole and Thompson.[13] The assignment of 242 and 500 cm^{-1} agrees with Plyler.[9]

[13] A. R. H. Cole and H. W. Thompson, Trans. Faraday Soc. **46**, 103 (1949).

Species a_2

The peculiarity of the selection rules for species a_2 has been discussed above. The single Raman-active a_2 fundamental is identified with the weak diffuse Raman band at 818 cm^{-1} with considerable certainty. This vibration is largely an out-of-plane hydrogen bending and corresponds to the e_{1g} fundamental at 850 cm^{-1} in benzene. The corresponding fundamental in 1,4-difluorobenzene[3] has a frequency 800 cm^{-1}. The remaining two a_2 fundamentals are inactive in both infrared absorption and the Raman effect. One of these corresponds fairly closely to a hydrogen-bending mode at 955 cm^{-1} in benzene. It may be represented by one of the extremely weak infrared bands observed in the liquid at 955 or 925 cm^{-1}. The other corresponds to an out-of-plane ring bending occurring at 404 cm^{-1} in benzene. It is assumed to lie around 330 cm^{-1} in fluorobenzene, since six observed frequencies can be interpreted as binary sum bands involving this frequency.

DISCUSSION

The interpretation of the infrared and Raman spectra is given in Table I. On the basis of the twenty-eight active fundamentals listed in Table II, it has been possible to interpret all but three of the forty-two observed Raman shifts as fundamentals or binary sum bands. These three bands are all very weak. One of them, the weak band around 277 cm^{-1} observed also in the infrared spectrum of the liquid, is satisfactorily interpreted as a difference band. The very weak band at 1789 cm^{-1} can be explained by invoking the value 330 cm^{-1} for the lowest a_2 fundamental. Of the ninety-six infrared absorption maxima observed for the liquid state, all but nine have been interpreted. The wave number 330 cm^{-1} has been utilized in the interpretation of six bands.

ACKNOWLEDGMENT

The writers wish to acknowledge their indebtedness to Dr. G. C. Finger for the gift of the sample.

Interactions of Randomly Disordered Molecules

MASAO ATOJI AND WILLIAM N. LIPSCOMB
School of Chemistry, University of Minnesota, Minneapolis 14, Minnesota
(Received February 23, 1953)

Some generalizations of previous theoretical expressions for the mean potential energy of interaction between two randomly disordered molecules have been derived and have been generalized to interactions in a molecular lattice. Values of the heats of vaporization of some tetrahedral molecules and halogens have been calculated, with results in reasonable agreement with experimental values. Application of the theory to the heat of sublimation of a disordered solid, hexachloroethane, is also discussed.

1. MEAN POTENTIAL ENERGY OF INTERACTION BETWEEN TWO ROTATING MOLECULES

IT is of interest to extend and apply the theory of interactions according to the general potential expression $V_n=C_m/R^n$ to unlike polyatomic nonpolar molecules. The simplifications for numerical comparison with experimental values are indicated for uncorrelated rotational motion. In some respects this is a generalization of an earlier theory of Lennard-Jones and Devonshire.[1]

In terms of the interatomic distance R and constants C_1, C_2, $\cdots$ the attractive potential between nonpolar molecules may be written as

$$V=-C_1/R^6-C_2/R^8-C_3/R^{10}-\cdots, \qquad (1)$$

where the terms, in order, represent dipole-dipole, dipole-quadrupole, quadrupole-quadrupole, $\cdots$ dispersion-type of interactions.[2] For the repulsive interactions we shall use, for purposes of convenience, the expression[3] $V_r=C_r/R^n$, where $9\leq n\leq 14$, depending upon the atoms involved.

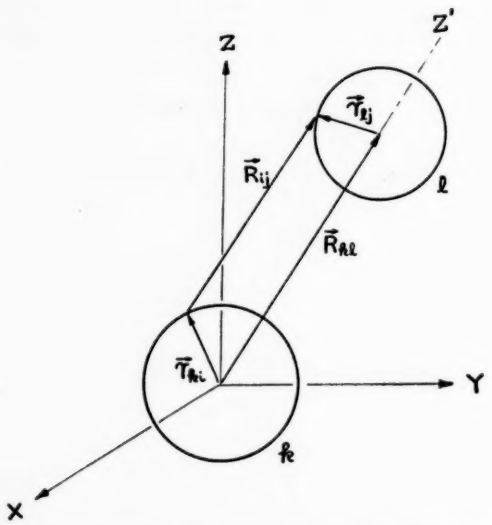

FIG. 1. Parameters for interaction between pairs of atoms.

We shall now express interactions between pairs of atoms in different molecules as indicated in Fig. 1. The distance between centers of rotating molecules k and l is R_{kl}, while the atom i is at a distance r_{ki} from the center of molecule k, and atom j is at a distance r_{lj} from the center of molecule l. The contribution to the potential energy of the term in R^{-n} is to be averaged over all possible orientations of all molecules, as indicated in the equation,*

$$\bar{V}_n=\left\langle\sum_{ij}\frac{C_m}{R_{ij}^n}\right\rangle_{Av}=C_m\sum_{ij}\left\langle\frac{1}{|\mathbf{R}_k+\mathbf{r}_{lj}-\mathbf{r}_{ki}|^n}\right\rangle_{Av}$$

$$=C_m\sum_{ij}\left\langle\frac{1}{|\mathbf{R}_{kl}-\mathbf{r}_{ij}|^n}\right\rangle_{Av}$$

$$=C_m\sum_{ij}\left\langle\frac{1}{(R_{kl}^2-2R_{kl}r_{ij}\cos\theta_{ij}+r_{ij}^2)^{n/2}}\right\rangle_{Av}$$

$$=\frac{C_m}{R_{kl}^n}\sum_{ij}\left\langle\frac{1}{\left\{1-2\dfrac{r_{ij}}{R_{kl}}\cos\theta_{ij}+\dfrac{(r_{ij})^2}{R_{kl}^2}\right\}^{n/2}}\right\rangle_{Av}, \qquad (2)$$

where $\mathbf{r}_{ij}=\mathbf{r}_{ki}-\mathbf{r}_{lj}$; $\cos\theta_{ij}=(r_{ki}\cos\theta_i-r_{lj}\cos\theta_j)/r_{ij}$, $R_{kl}=|\mathbf{R}_{kl}|$, $r_{ij}=|\mathbf{r}_{ij}|$, etc. The line joining the molecular centers is shown as the polar axis (Fig. 1). Now for the usual situation which is encountered we have $r_{ij}<R_{kl}$, so that binomial expansion of Eq. (2) leads to the result,

$$\bar{V}_n=\frac{C_m}{R_{kl}^n}\sum_{ij}\sum_{p=0}^{\infty}\frac{\frac{n}{2}\left(\frac{n}{2}+1\right)\left(\frac{n}{2}+2\right)\cdots\left(\frac{n}{2}+p-1\right)}{p!}\times\langle x^p\rangle_{Av} \qquad (3)$$

* For some applications Gegenbauer functions, $C_p^{n/2}(\cos\theta_{ij})$, are useful. [Some useful relations are given by W. Magnus and F. Oberhettinger, *Formulas and Theorems for the Special Functions of Mathematical Physics* (Chelsea Publishing Company, New York, 1949)]. Equation (2), before averaging, is then

$$V_n=\frac{C_m}{R_{kl}^n}\sum_{ij}\sum_{p=0}C_p^{n/2}(\cos\theta_{ij})\left(\frac{r_{ij}}{R}\right)^p.$$

The special case $n=1$, for which $C_p^{n/2}$ reduces to the Legendre polynomial, was discussed by Margenau (reference 2).

[1] J. E. Lennard-Jones and A. F. Devonshire, Proc. Roy. Soc. (London) **A163**, 53 (1937); **A165**, 1 (1938).
[2] H. Margenau, Revs. Modern Phys. **11**, 1 (1939).
[3] J. E. Lennard-Jones, Proc. Roy. Soc. (London) **A106**, 463 (1924).

TABLE I. The coefficients A_n^q.

q \ n	6	8	9	10	11	12
0	1	1	1	1	1	1
1	5	9.333	12	15	18.33	22
2	14	42	66	99	143	200.2
3	30	132	245.1	429	715	1144
4	55	333.7	715	1430	2701	4862
5	91	728	1768	3978	8398	1680×10
6	140	1428	3876	9690	2261×10	4974×10
7	204	2584	7752	2123×10	5448×10	1308×10^2
8	285	4389	1442×10	4326×10	1202×10^2	3125×10^2
9	385	7084	2530×10	8223×10	2467×10^2	6907×10^2
10	506	1096×10	4229×10	1480×10^2	4769×10^2	1431×10^3
11	650	1638×10	6786×10	2545×10^2	8765×10^2	2805×10^3
12	819	2375×10	1052×10^2	4207×10^2	1543×10^3	5245×10^3
13	1015	3356×10	1582×10^2	6725×10^2	2615×10^3	9414×10^3
14	1240	4638×10	2319×10^2	1043×10^3	4290×10^3	1630×10^4
15	1496	6283×10	3321×10^2	1578×10^3	6836×10^3	2734×10^4
16	1785	8366×10	4661×10^2	2330×10^3	1062×10^4	4459×10^4
17	2109	1097×10^2	6423×10^2	3372×10^3	1611×10^4	7089×10^4
18	2470	1418×10^2	8709×10^2	4790×10^3	2395×10^4	1120×10^5
19	2870	1810×10^2	1164×10^3	6691×10^3	3494×10^4	1677×10^5
20	3311	2284×10^2	1534×10^3	9204×10^3	5011×10^4	2505×10^5

with

$$\langle x^p\rangle_{Av}=\frac{1}{(4\pi)^2}\int_s\{r_{ij}(2\cos\theta_{ij}-r_{ij}/R_{kl})/R_{kl}\}^p ds, \quad (4)$$

where $ds=\sin\theta_i\sin\theta_j d\theta_i d\theta_j$ and $\cos\theta_{ij}=\cos\theta_i\cos\theta_j-\sin\theta_i\sin\theta_j\cos(\varphi_i-\varphi_j)$. The average value of x can be calculated with the help of the orthogonality of the trigonometric functions. The results are

$$\langle x\rangle_{Av}=-\frac{\alpha^2}{R_{kl}^2},\quad \langle x^2\rangle_{Av}=\frac{4\alpha^2}{3R_{kl}^2}+\frac{(\alpha^4+\beta^4/3)}{R_{kl}^4},$$

$$\langle x^3\rangle_{Av}=-\frac{4(\alpha^4+\beta^4/3)}{R_{kl}^4}-\frac{(\alpha^6+\alpha^2\beta^4)}{R_{kl}^6},$$

$$\langle x^4\rangle_{Av}=\frac{16(\alpha^4+\beta^4/3)}{5R_{kl}^4}+\frac{8(\alpha^6+\alpha^2\beta^4)}{R_{kl}^6}+\frac{(\alpha^8+2\alpha^4\beta^4+\beta^8/5)}{R_{kl}^8},$$

$$\langle x^5\rangle_{Av}=-\frac{16(\alpha^6+\alpha^2\beta^4)}{R_{kl}^6}-\frac{40(\alpha^8+2\alpha^4\beta^4+\beta^8/5)}{3R_{kl}^8}-0\left(\frac{1}{R_{kl}^{10}}\right)-\cdots, \quad (5)$$

$$\langle x^6\rangle_{Av}=\frac{64(\alpha^6+\alpha^2\beta^4)}{7R_{kl}^6}+\frac{48(\alpha^8+2\alpha^4\beta^4+\beta^8/5)}{R_{kl}^8}+0\left(\frac{1}{R_{kl}^{10}}\right)+\cdots,$$

$$\langle x^7\rangle_{Av}=-\frac{64(\alpha^8+2\alpha^4\beta^4+\beta^8/5)}{R_{kl}^8}-0\left(\frac{1}{R_{kl}^{10}}\right)-\cdots,$$

$$\langle x^8\rangle_{Av}=\frac{256(\alpha^8+2\alpha^4\beta^4+\beta^8/5)}{9R_{kl}^8}+0\left(\frac{1}{R_{kl}^{10}}\right)+\cdots,$$

where $\alpha^2=r_{ki}^2+r_{lj}^2$; $\beta^2=2r_{ki}r_{lj}$. When the calculations of $\langle x^p\rangle$ are continued and the proper substitutions are made, we obtain, by induction,

$$\bar{V}_n=\frac{C_m}{(n-2)R_{kl}^n}\sum_{q=0}^{\infty}\times\left\{\frac{(n-2)(n-1)n(n+1)(n+2)\cdots(n+2q-2)}{(2q+1)!}\right\}\times\frac{\Phi_q(r_{ki},r_{lj})}{R_{kl}^{2q}}$$

$$=\frac{C_m}{R_{kl}^n}\sum_{q=0}^{\infty}\frac{A_n^q\Phi_q(r_{ki},r_{lj})}{R_{kl}^{2q}}\quad\text{for}\quad r_{ki}\neq r_{lj} \quad (6)$$

$$=\frac{C_m}{R_{kl}^n}\sum_{q=0}^{\infty}\frac{B_n^q r^{2q}}{R_{kl}^{2q}}\quad\text{for}\quad r_{ki}=r_{lj}=r, \quad (7)$$

where

$$\Phi_q(r_{ki},r_{lj})=\frac{(2q+1)}{4\pi^2}\int_s(r_{ki}\cos\theta_i-r_{lj}\cos\theta_j)^{2q}ds. \quad (8)$$

For the special case of either $r_{ki}=0$ or $r_{lj}=0$, the expression becomes identical with that derived by Lennard-Jones and Devonshire[1] in their cell theory of liquids,

$$\bar{V}_n=\frac{C_m}{R_{kl}^n}\sum_{q=0}^{\infty}\frac{A_n^q r^{2q}}{R_{kl}^{2q}}=\frac{C_m}{2(n-2)rR_{kl}^{n-1}}\times\left\{\left(1-\frac{r}{R_{kl}}\right)^{-n+2}-\left(1+\frac{r}{R_{kl}}\right)^{-n+2}\right\}. \quad (9)$$

Numerical evaluations of the coefficients A_n^q and B_n^q are shown in Tables I and II. Table III shows the functions $\Phi_q(r_{ki},r_{lj})$.

TABLE II. The coefficients B_n^q.

q \ n	6	8	9	10	11	12
0	1	1	1	1	1	1
1	10	18.67	24	30	36.67	44
2	74.67	224	352	528	762.7	1068
3	480	2112	3922	6864	1144×10	1830×10
4	2816	1708×10	3661×10	7322×10	1383×10^2	2489×10^2
5	1553×10	1242×10^2	3017×10^2	6789×10^2	1433×10^3	2867×10^3
6	8192×10	8356×10^2	2268×10^3	5670×10^3	1323×10^4	2911×10^4
7	4178×10^2	5292×10^3	1588×10^4	4366×10^4	1116×10^5	2678×10^5
8	2075×10^3	3196×10^4	1050×10^5	3150×10^5	8751×10^5	2275×10^6
9	1009×10^4	1857×10^5	6632×10^5	2155×10^6	6466×10^6	1811×10^7
10	4823×10^4	1045×10^6	4031×10^6	1411×10^7	4546×10^7	1364×10^8
11	2272×10^5	5725×10^6	2372×10^7	8894×10^7	3064×10^8	9804×10^8
12	1057×10^6	3065×10^7	1357×10^8	5430×10^8	1991×10^9	6769×10^9
13	4865×10^6	1609×10^8	7584×10^8	3223×10^8	1254×10^{10}	4513×10^{10}
14	2219×10^7	8299×10^8	4150×10^9	1867×10^{10}	7677×10^{10}	2917×10^{11}
15	1004×10^8	4217×10^9	2229×10^{10}	1059×10^{11}	4588×10^{11}	1835×10^{12}
16	4510×10^8	2114×10^{10}	1178×10^{11}	5888×10^{11}	2682×10^{12}	1127×10^{13}
17	2013×10^9	1047×10^{11}	6131×10^{11}	3219×10^{12}	1538×10^{13}	6766×10^{13}
18	8934×10^9	5128×10^{11}	3150×10^{12}	1732×10^{13}	8662×10^{13}	3985×10^{14}
19	3944×10^{10}	2488×10^{12}	1599×10^{13}	9195×10^{13}	4802×10^{14}	2305×10^{15}
20	1734×10^{11}	1196×10^{13}	8031×10^{13}	4819×10^{14}	2642×10^{15}	1312×10^{16}

The condition that $r_{ij}<R_{kl}$, gives more rapid convergence the lower the density of the medium, but convergence is not unsatisfactory even for disordered solids and for liquids near the melting point.

We now assume that the interaction energy between pairs of atoms is given by a Lennard-Jones 6:12 potential function,

$$V=\nu/R^{12}-\mu/R^6=\epsilon[(r^*/R)^{12}-2(r^*/R)^6], \quad (10)$$

where ϵ and r^* are the equilibrium values of the potential energy and interatomic distance, respectively. We also assume that the mean potential energy of interaction of two uncorrelated spherically disordered molecules can then be obtained by averaging the interactions between all pairs of atoms in different molecules over all orientations. The result for molecules k and l is readily shown from Eqs. (6), (7), and (9) to be

$$\bar{V}=\sum_{ij}\sum_{q=0}^{\infty}\frac{\Phi_q(r_{ki},r_{lj})}{R^{2q+6}}\left[\frac{\nu_{ij}A_{12}^q}{R^6}-\mu_{ij}A_6^q\right](r_{ki}\neq r_{lj}), \quad (11)$$

$$\bar{V}=\sum_{ij}\sum_{q=0}^{\infty}\frac{r^{2q}}{R^{2q+6}}\left[\frac{\nu_{ij}B_{12}^q}{R^6}-\mu_{ij}B_6^q\right](r_{ki}=r_{lj}=r), \quad (12)$$

$$\bar{V}=\sum_{ij}\sum_{q=0}^{\infty}\frac{r^{2q}}{R^{2q+6}}\left[\frac{\nu_{ij}A_{12}^q}{R^6}-\mu_{ij}A_6^q\right](r_{ki}=0 \text{ or } r_{lj}=0). \quad (13)$$

Then by superposition of these averaged interatomic potentials using the constants in Tables I, II, and III and interatomic force constants selected appropriately, one can obtain the intermolecular potential curve from which values for ϵ and r^* are then easily obtained.† These values of ϵ and r^* may then be compared with corresponding values from the second virial coefficient, from viscosity data, or, less reliably, from critical data or boiling points.

Rowlinson[4] has previously calculated the intermolecular interaction energies and distances in a somewhat similar manner in CF_4 and SF_6. For the F−F interactions he employed potential constants, $\mu=0.224\times10^{-10}$ erg A^6 and $\nu=284.1\times10^{-10}$ erg A^{12}, obtained from viscosity data for F_2 gas.[5] For the C and S atoms whose contributions are less important, Rowlinson used the same parameters as those for the F atom. We have started with these same assumptions, but because of our use of a different method of obtaining the average interaction, we have obtained somewhat better agreement with experiment,[6] as summarized in Table IV. It is interesting that our results agree so well with those of Rowlinson for after our initial assumption of no correlation between the relative orientations of the interacting molecules we have made no mathematical approximations.

The intermolecular potential constants of CCl_4 were also evaluated. Values of $\nu=1.515\times10^{-10}$ erg A^6, $\mu=1620\times10^{-10}$ erg A^{12} for Cl were taken from the measurements of the virial coefficient of chlorine gas by Morino and Miyagawa.[7] For the less important C−Cl

† For example, the F−F and C−F interactions in CF_4 are calculated from Eqs. (12) and (13), respectively. The special case of the single C−C interaction, for which $r_{ki}=r_{lj}=0$, can be shown from Eq. (7) to be $\bar{V}=\nu/R_{kl}^{12}-\mu/R_{kl}^6$ for a 6:12 potential function. Numerical evaluation of all of these average potentials is greatly facilitated by use of tables of A_n^q/R^{2q} and B_n^q/R^{2q}. The magnitudes of successive terms in the series employed for some of the interactions in CF_4, SF_6, and CCl_4 at first increase, then decrease, perhaps resembling a Poisson distribution, but it was found that the inclusion of about twenty terms or less was sufficient to insure perfectly satisfactory convergence for all interactions discussed here.

[4] J. C. Rowlinson, J. Chem. Phys. **20**, 337 (1952).

[5] E. Kanda, Bull. J. Chem. Soc. Japan **12**, 463 (1937).

[6] K. E. MacCormack and W. G. Schneider, J. Chem. Phys. **19**, 849 (1951).

[7] Y. Morino and I. Miyagawa, J. Chem. Soc. Japan **68**, 62 (1947). Also private communication from Professor Y. Morino. Katayama, Shimanouchi, Morino, and Mizushima, J. Chem. Phys. **18**, 506 (1950). The virial data yield the interaction constants between Cl_2 molecules. The interatomic Cl−Cl interaction was then obtained by Corner's method. [J. Corner, Proc. Roy. Soc. (London) **A192**, 275 (1948)].

interaction, the value $r^*=3.34$A was taken as the arithmetic mean of the values of r^* for Ne−Ne interaction[8] and Cl−Cl interaction, and the value $\epsilon=13.16\times10^{-15}$ erg was taken as the geometric mean of the values of ϵ for these same interactions.[9] The much smaller C−C interaction energy was assumed to be equal to the interaction energy of Ne−Ne. The agreement with experiment,[10] as shown in Table IV, is considered to be satisfactory in view of the assumptions of the treatment.

In all of these calculations, the interatomic distances, C−F=1.36A, S−F=1.58A, and Cl−C=1.76A, were assumed.[11]

2. INTERACTIONS IN MOLECULAR LATTICES AND APPLICATIONS TO HEATS OF VAPORIZATION

Quasi-solid models for liquids have provided, with some success,[1,12,13] some understanding of many properties of liquids not too near their critical temperatures. Such treatments are usually based upon some law of interaction, and it is therefore of interest to apply the results of the previous section to a discussion of such properties as the heats of vaporization of liquids and the lattice energies of highly disordered solids.

The usual type of disperion forces are assumed. The interaction energies are here evaluated by means of the second-order perturbation theory of London[14] and Margenau[15] rather than Slater and Kirkwood's variation theory,[16] which seems to give slightly less satisfactory results for molecular crystals.[17] As in the previous section, we express the total energy of interaction as the sum of interactions between atoms in different molecules and then calculate the average for uncorrelated spherical rotation about the molecular centers. The result is [2,15,18]

$$\bar{V}=\sum_{i,j}\sum_{k,l}\Big\{-\frac{3}{4}Nh\frac{\alpha_{ki}\alpha_{lj}f_{ki}f_{lj}}{f_{ki}+f_{lj}}\sum_{q=0}^{\infty}\frac{A_6{}^q\Phi_q(r_{ki},r_{lj})}{R_{kl}{}^{6+2q}}$$
$$-\frac{45}{16}Nh^2\frac{\alpha_{ki}\alpha_{lj}f_{ki}f_{lj}}{e^2}\left(\frac{\alpha_{ki}f_{ki}}{2f_{ki}+f_{lj}}+\frac{\alpha_{lj}f_{lj}}{f_{ki}+2f_{lj}}\right)$$
$$\times\sum_{q=0}^{\infty}\frac{A_8{}^q\Phi_q(r_{ki},r_{lj})}{R_{kl}{}^{8+2q}}-\frac{315}{32}Nh^3\frac{\alpha_{ki}{}^2\alpha_{lj}{}^2f_{ki}{}^2f_{lj}{}^2}{e^4(f_{ki}+f_{lj})}$$
$$\times\sum_{q=0}^{\infty}\frac{A_{10}{}^q\Phi_q(r_{ki},r_{lj})}{R_{kl}{}^{10+2q}}. \quad (14)$$

The sum over k, l is over the molecular lattice, N is Avogadro's number, the α's are the polarizabilities, the f's are the principal specific frequencies and may be obtained from the dispersion equation or the ionization energy of the atom in question. The three terms of Eq. (14) represent, respectively, the dipole-dipole, dipole-quadrupole, and quadrupole-quadrupole energies. This equation applies to the interactions among unlike molecules, where in general $r_{ki}\neq r_{lj}$, and may easily be simplified for special cases such as the interactions between like molecules.

The summation over the lattice for the face-centered cubic and body-centered cubic arrangements[19] of mole-

TABLE III. $\Phi_q(r_{ki}, r_{lj})$ functions.

q \ n	$\Phi_q(r_{ki}, r_{lj})$: $[\alpha^2=r_{ki}{}^2+r_{lj}{}^2,\ \beta^2=2r_{ki}r_{lj}]$.
0	1
1	α^2
2	$\alpha^4+\beta^4/3$
3	$\alpha^6+\alpha^2\beta^4$
4	$\alpha^8+2\alpha^4\beta^4+\beta^8/5$
5	$\alpha^{10}+10\alpha^6\beta^4/3+\alpha^2\beta^8$
6	$\alpha^{12}+5\alpha^8\beta^4+3\alpha^4\beta^8+\beta^{12}/7$
7	$\alpha^{14}+7\alpha^{10}\beta^4+7\alpha^6\beta^8+\alpha^2\beta^{12}$
8	$\alpha^{16}+28\alpha^{12}\beta^4/3+14\alpha^8\beta^8+4\alpha^4\beta^{12}+\beta^{16}/9$
9	$\alpha^{18}+12\alpha^{14}\beta^4+126\alpha^{10}\beta^8/5+12\alpha^6\beta^{12}+\alpha^2\beta^{16}$
10	$\alpha^{20}+15\alpha^{16}\beta^4+42\alpha^{12}\beta^8+30\alpha^8\beta^{12}+5\alpha^4\beta^{16}+\beta^{20}/11$
11	$\alpha^{22}+55\alpha^{18}\beta^4/3+66\alpha^{14}\beta^8+66\alpha^{10}\beta^{12}+55\alpha^6\beta^{16}/3+\alpha^2\beta^{20}$
12	$\alpha^{24}+22\alpha^{20}\beta^4+99\alpha^{16}\beta^8+132\alpha^{12}\beta^{12}+55\alpha^8\beta^{16}+6\alpha^4\beta^{20}+\beta^{24}/13$
13	$\alpha^{26}+26\alpha^{22}\beta^4+143\alpha^{18}\beta^8+1716\alpha^{14}\beta^{12}/7+143\alpha^{10}\beta^{16}+26\alpha^6\beta^{20}+\alpha^2\beta^{24}$
14	$\alpha^{28}+91\alpha^{24}\beta^4/3+1001\alpha^{20}\beta^8/5+429\alpha^{16}\beta^{12}+1001\alpha^{12}\beta^{16}/3+91\alpha^8\beta^{20}+7\alpha^4\beta^{24}+\beta^{28}/15$
15	$\alpha^{30}+35\alpha^{26}\beta^4+273\alpha^{22}\beta^8+715\alpha^{18}\beta^{12}+715\alpha^{14}\beta^{16}+273\alpha^{10}\beta^{20}+35\alpha^6\beta^{24}+\alpha^2\beta^{28}$

[8] See R. H. Fowler and E. A. Guggenheim, *Statistical Thermodynamics* (Columbia University Press, New York, 1939), p. 285.
[9] Reference 8, p. 300.
[10] Hirschfelder, Bird, and Spotz, Trans. Am. Soc. Mech. Engrs. **71**, 921 (1941).
[11] P. W. Allen and L. E. Sutton, Acta Cryst. **3**, 46 (1950).
[12] H. Eyring, J. Chem. Phys. **4**, 283 (1936). J. F. Kincaid and H. Eyring, J. Chem. Phys. **6**, 620 (1938). R. H. Ewell and H. Eyring, J. Chem. Phys. **5**, 726 (1937).
[13] See also C. N. Wall, Phys. Rev. **54**, 1062 (1938).
[14] F. London, Z. Physik **63**, 245 (1930). Z. physik. Chem. **113**, 222 (1930).
[15] H. Margenau, Phys. Rev. **38**, 747 (1931). J. Chem. Phys. **6**, 896 (1938).
[16] J. Slater and J. G. Kirkwood, Phys. Rev. **37**, 682 (1931).
[17] Y. Sasada and M. Atoji, J. Chem. Phys. **21**, 145 (1953).
[18] For dispersion forces between unlike molecules or atoms, see J. F. Honig and J. O. Hirschfelder, J. Chem. Phys. **20**, 1812 (1952).
[19] J. E. Lennard-Jones and A. E. Ingham, Proc. Roy. Soc. (London), **A107**, 636 (1952).

TABLE IV. Intermolecular energies in CF_4, SF_6, and CCl_4.[a]

Molecule	r^*(A) Obs	Calc	Calc (Rowlinson)[a]	ϵ/k(°K) Obs	Calc	Calc (Rowlinson)[a]
CF_4	5.28[b]	5.47	5.53	153[b]	165	178
SF_6	6.19[b]	5.92	6.05	201[b]	237	269
CCl_4	6.60[c]	6.24		327[c]	528	
	6.08[d]			487[e]		
				435[d]		

[a] See reference 4.
[b] See reference 6.
[c] Values obtained from viscosity data (reference 10).
[d] Values obtained from critical volumes (reference 10).
[e] Values obtained from boiling points (reference 10).

cules can be written as

$$\sum R_{kl}^{-n} = \Gamma' a^{-n} \text{ for face-centered cubic, and}$$
$$= \Gamma a^{-n} \text{ for body-centered cubic structures,} \quad (15)$$

where a is the closest distance between molecular centers. The values of Γ and Γ' were estimated analytically for $6 \leq n \leq 30$ by Lennard-Jones and Ingham,[19] and a few further values have been calculated by us‡ by the same method.

The repulsive energies can probably be best treated by use of the exponential form proposed by Born and Mayer,[20] but partly for convenience and partly for easier comparison with experimental results,[21] we have used the form of Eq. (2), where, again for convenience, we have taken $n=12$, a value which may be a bit high. The repulsive energies then can be shown to be

$$\bar{V}_r = \sum_{i,j} \sum_{k,l} \sum_{q=0}^{\infty} \frac{N}{2} \frac{A_{12}{}^q \Phi_q(r_{ki}, r_{lj})}{R_{kl}{}^{12+2q}}. \quad (16)$$

If we make the usual assumptions[22] of spherical molecules, separable degrees of freedom, and constancy of internal modes of vibration during vaporization, and if we neglect relatively small corrections[23] (on the order of $\frac{1}{2}RT$) to the potential energy, we may assume that the enthalpy of vaporization is the mean value of the potential energy of intermolecular interactions in the liquid.

Values of the atomic polarizabilities employed in the calculations are listed in Table V. Except for methane[24] interatomic distances were taken from the review by Allen and Sutton.[11] The closest distances between molecular centers in liquids were estimated from the densities,[25] and the constants related to the dispersion forces were obtained from the first ionization potentials of the corresponding atoms.[26]

Values of the heats of vaporization of CCl_4, $SiCl_4$, $SnCl_4$, CH_4, Cl_2, Br_2, and I_2 are shown in Tables VI, VII, and VIII, where the various contributions to the mean potential energies at various temperatures are listed. As should be expected the higher-pole attractive energies and the repulsive energies are comparatively sensitive to the densities at the various temperatures. Agreement of the 6.25A in CCl_4 at its boiling point with the 6.24A distance in Table IV suggests that correlation of rotational motion is not of great significance and that the assumptions of the present treatment are not completely unreasonable. Correlation may, however, be expected to be important at lower temperatures.[27] If the repulsive energies could be estimated separately from such considerations as we have presented here, some information relating to restricted or correlated motions[28] of molecules may be obtainable in condensed phases.

Unfortunately, the discussion for the halogens is not so simple. Comparison of the intermolecular distance of

TABLE V. Atomic polarizabilities.

	H	C	Si	Sn	Cl	Br	I
$\alpha \times 10^{24}$ cm^3	0.4240[a]	0.9437[b]	1.904[c]	5.973[d]	2.299[b]	3.37[d]	5.406[d]

[a] F. Eisenlohr, Z. physik Chem. **75**, 585 (1910); **79**, 129 (1912).
[b] See reference 17.
[c] The polarizability of silicon atom was estimated from the polarizability of $SiCl_4$ which is 11.10×10^{-24} cm^3. See J. H. Hildebrand, J. Chem. Phys. **15**, 727 (1947).
[d] See reference 29.

‡ For values of $n>30$, $\Gamma'=12.000$, while values of Γ are listed as follows:

n	Γ	n	Γ	n	Γ
31	8.0694	36	8.0338	50	8.0045
32	8.0601	37	8.0293	55	8.0022
33	8.0521	38	8.0254	60	8.0011
34	8.0451	40	8.0190	70	8.0003
35	8.0391	45	8.0093	∞	8.0000

TABLE VI. Heat of vaporization (kcal/mole) of carbon tetrachloride.

Molecular dimension;[a] C−Cl = 1.76A				
Temperatures (in °K)	293	313	333	349.9 (bp)
Densities[b] (in g/cm^3)	1.594	1.555	1.515	1.482
Dipole-dipole interactions	7.66	7.13	6.68	6.31
Dipole-quadrupole interactions	4.60	4.10	3.62	3.39
Quadrupole-quadrupole interactions	1.93	1.65	1.44	1.27
Total attraction energies	14.19	12.88	11.74	10.97
Repulsive energies	6.57	5.38	4.53	3.86
Total energies	7.62	7.50	7.21	7.11
Observed values	7.88[c]	7.67[c]	7.46[c]	7.29[c]
	7.74[d]	7.53[d]	7.32[d]	7.14[d]

[a] See reference 11.
[b] See reference 25.
[c] K. K. Kelley, "Contribution to the Data on Theoretical Metallurgy, III. The Free Energy of Vaporization and Vapor Pressure of Inorganic Substances," Bureau of Mines, U. S. Department of Interior, Bulletin 383 (1935), p. 37. $\Delta H_v = 10\,960 - 10.5\,T$ (cal/mole).
[d] Derived from $\Delta H_v = 10\,815 - 10.5\,T$ (cal/mole) referring to data in N. A. Lange's *Handbook of Chemistry* (Handbook Publishers, Sandusky, 1946), 6th ed.

[20] M. Born and J. E. Mayer, Z. Physik **75**, 1 (1932).
[21] See reference 8, p. 285ff.
[22] S. W. Benson, J. Chem. Phys. **15**, 367 (1947).
[23] A. Harashima, Proc. Phys.-Math. Soc. Japan **23**, 977 (1941).
[24] Dickinson, Dillion, and Rassetti, Phys. Rev. **34**, 582 (1929).
[25] *International Critical Tables* (McGraw-Hill Book Company, Inc., New York, 1933).
[26] Landolt Bornstein, *Zahlenwerte und Funktionen* (Verlag Julius Springer, Berlin, 1950), Vol. 1, Part I.
[27] See A. Peterlin, Physik. Z. **37**, 413 (1936).
[28] See R. S. Halford, J. Chem. Phys. **8**, 496 (1940).

4.74A at the boiling point with the value of 4.81A in Table IV does indeed suggest that only dispersion interactions of freely rotating molecules constitutes a satisfactory model. Moreover, the comparison of only the dipole-dipole interaction with the heats of vaporization in Table VIII also suggests that near the boiling points the higher-order attractions tend to balance the repulsive interactions,[17,29] but the physical significance is doubtful.[30] However, anomalous intermolecular interactions involving some covalency certainly exist[31] in the solids, I_2, Br_2, and Cl_2 and it is perhaps surprising that these forces are not more apparent near the boiling point, but they may well have been overcome by the onset of free or nearly free rotation.

Cubic hexachloroethane[32] is a soft, "plastic"[33] crystal near its melting point of 458°K. From 344.6°K to 458°K the structure[34,35] consists of molecules in the body-centered cubic arrangement in site symmetry O_h, and the Laue-Bragg reflections are compatible with spherically disordered molecules in these positions. We have applied the theory of disorder interactions to this crystal, with the results listed in Table IX. The observed value, the heat of sublimation, includes the heat of fusion of 2.33 kcal/mole, with the corresponding attendant volume change and increase in disorder over the obviously correlated[34] disorder in the solid phase. When this correction is added the agreement with the present treatment is good, but it seems unwise to attempt an estimate of the correlation energy because the value ultimately depends on the differences between large terms.

TABLE VII. Heat of vaporization (kcal/mole) of silicon tetrachloride[a] at boiling point, 330°K.[b]

Dipole-dipole interactions	Dipole-quadrupole interaction	Quadrupole-quadrupole interaction	Total attraction energy	Repulsive energy	Total energy	Observed value
6.00	3.50	1.43	10.93	5.10[c]	5.83	6.13[d]

[a] Molecular dimension; Si−Cl=2.02A. See reference 11.
[b] Density at boiling point is 1.400 g/cm³. See reference 25.
[c] Calculated from Eq. (16) by the same methods as those discussed in Part I.
[d] Cited from *Physical Constants of the Principal Hydrocarbons* (The Texas Company, New York, 1943), 4th ed.

Finally some additional general criticisms of the model seem in order. The assumption of the isotropic three-dimensional oscillator on which Eq. (4) is based[2] is highly idealized; but the present treatment moderates the errors due to this assumption, by introducing different oscillators with their different frequencies. Of course, the assumption that these frequencies are constant is in error. Moreover, the repulsive term is probably incorrect both as to mathematical form and value of the exponent. Finally, the neglect of higher pole interactions, especially the dipole-octopole terms which are probably less than the quadrupole-quadrupole terms, may represent a further significant error.

TABLE VIII. Heat of vaporization (kcal/mole) of tin tetrachloride methane, chlorine, bromine, and iodine at boiling points.

Substances	Molecular dimensions[a] (in A)	Densities (in g/cm³) at bp[b]	Boiling points (in °K)	Dipole-dipole interactions (kcal/mole)	Observed values[c] (in kcal/mole)
$SnCl_4$	Sn−Cl=2.30	1.978	387	9.10	8.31
CH_4	C−H=1.08	0.415	109	2.01	2.04
Cl_2	Cl−Cl=2.00	1.559	239	4.65	4.42
Br_2	Br−Br=2.28	2.984	332	7.05	7.41
I_2	I−I=2.67	3.706	458	11.12	10.38

[a] See reference 11, except for methane for which see reference 24.
[b] See reference 25.
[c] See reference c in Table VI.

Treatment of the atomic centers as force centers in a complex molecule may be in error as was pointed out by Rowlinson for the case of CH_4. Harashima,[23] in a treatment of the whole molecule with central force at the molecular center, obtains the expression‡

$$\Delta H_v=\frac{N}{2}\epsilon\left[28.9\left(\frac{r^*}{a}\right)^6-12.1\left(\frac{r^*}{a}\right)^{12}\right], \qquad (18)$$

from which the rather larger value of 8.80 kcal/mole for CCl_4 is obtained at the boiling point if our values listed above for ϵ and r^* are used. Thus the sensitivity of the repulsive energies to the assumptions concerning the average shape of the molecule is again apparent. However, Harashima's equation does give good agreement for smaller molecules and monatomics, such as He, H_2, Ne, N_2, etc.[23] In a sense, then, our method of introducing individual parameters r_{ki}, r_{lj}, etc., and calculating mean interaction energies over various orientations is thereby partly justified. Again, the atomic approximation to a molecule may fail and is probably most serious when the bond polarizability is

TABLE IX. Lattice energy (kcal/mole) of cubic hexachlorethane[a] at melting point, 458°K.[b]

Dipole-dipole interaction	Dipole-quadrupole interaction	Quadrupole-quadrupole interaction	Total attraction energy	Repulsive energy	Total energy	Observed value
11.27	6.93	3.26	22.0[c]	12.54[d]	9.5	12.1[e]

[a] Molecular dimensions: C−C=1.54A, C−Cl=1.76A. Molecular center to chlorines is 2.14A. See reference 11.
[b] The lattice constant, $a=7.70$A at the melting point was obtained by extrapolation, using the linear expansion coefficient of about 3.4×10^{-4} which was obtained from the observed values of $a=7.44$A (353°K), $a=7.51$A (378°K) and $a=7.60$A (418°K). See references 34 and 35.
[c] For this term interactions of higher order than quadrupole-quadrupole interactions have been included. A detailed discussion of this calculation will appear elsewhere.
[d] Calculated by Eq. (16) using the same parameters as those used in the calculation of the intermolecular potential of carbon tetrachloride.
[e] See reference 36.

‡ This equation can be easily obtained from (6), (15), and (16) as a special case, namely, $r_{ki}=r_{lj}=0$.

[29] I. Nitta and S. Seki, J. Chem. Soc. Japan **64**, 475(1943).
[30] V. Deitz, J. Franklin Inst. **219**, 459 (1935).
[31] C. H. Townes and B. P. Dailey, J. Chem. Phys. **20**, 35 (1952).
[32] S. Seki and M. Momatani, Bull. Chem. Soc. Japan **23**, 30 (1950).
[33] J. Timmermans, J. chim. phys. **35**, 331 (1938).
[34] Atoji, Oda, and Watanabe (to be published).
[35] C. D. West, Z. Krist. **A88**, 195 (1934).

proportionally large, as in CH_4. Of course, the centers of polarizability need not then be chosen at the nuclear centers. For example, if the "polarizability center" for CH bonds is chosen at 0.694A (the "center of gravity" of polarizability)[36] from the carbon atom, and the bond polarizability[37] 0.6592×10^{-24} cm^3 and ionization potential[38] of 14.5 ev are assumed, we obtain 1.90 kcal/mole as the heat of vaporization at the boiling point in reasonable agreement with the observed value of 2.05 kcal/mole.

Support of this work by the U. S. Office of Naval Research is gratefully acknowledged.

[36] See I. Nitta and S. Seki, J. Chem. Soc. Japan **62**, 581 (1941).
[37] K. Fajans and C. A. Knorr, Ber. Deutsch. Chem. Ges. **59**, 256 (1926).
[38] *Handbook of Chemistry and Physics* (Chemical Rubber Publishing Company, Cleveland, 1951), 33rd ed.

THE JOURNAL OF CHEMICAL PHYSICS VOLUME 21, NUMBER 9 SEPTEMBER, 1953

Influence of Irradiation on Discharge Current in an Ozonizer

S. Deb, A. K. Saha, and M. Ghosh
Institute of Radio Physics and Electronics, University of Calcutta, Calcutta, India
(Received January 6, 1953)

The paper outlines the principal characteristics of the effects of irradiation on the discharge current in an ozonizer. The "electronic surface charge theory" of the effect developed by Deb and Ghosh, on a suggestion of Mitra, is explained and is further extended by taking into account the role played by the negative ions formed in the discharge space. It is assumed that the effect of irradiation is to decrease the charges deposited on the surface and to increase those in the volume. The former reduces the discharge current due to the neutralization of the surface charges and the latter increases the main discharge current due to the applied voltage. The net effect is generally a decrease if conditions are favorable for the capture of the electrons in the volume by neutral gas molecules, leading to the formation of negative ions. In all other conditions the effect is generally an increase. It is shown that the theory, in its extended form, is able to account for the origin and the characteristics of both the positive and the negative effects. Numerical calculations of the various rate processes involved in the proposed mechanism are also made. It is shown that the relative magnitudes of these processes are such as to support strongly the "electronic surface charge theory" of the effect.

I. INTRODUCTION

THE instantaneous decrease (or, under special conditions, increase) of the discharge current through an ozonizer tube when it is flooded with light, and its associated phenomena, have been the subject of numerous studies, especially in India where the effect was first observed.[1,2] A number of theories have also been proposed to explain the various observed effects. Unfortunately, none of the theories proposed so far gives a satisfactory and complete explanation of the various aspects of the effect. Of the various theories proposed the "electronic surface charge theory" proposed by Deb and Ghosh[3,4] appears to offer the most plausible explanation of the phenomena. However, this theory does not account for the "positive" effect—increase of discharge current on irradiation; this effect is obtained under special conditions. It is the purpose of the present paper to examine critically the various proposed theories including that of "electronic surface charge" which will be discussed in greater detail. It will be shown that this theory, suitably extended, is able to explain both the "negative" and the "positive" effects, as also the other associated phenomena.

[1] S. S. Joshi, Nature **154**, 147 (1944).
[2] S. S. Joshi and P. G. Deo, Nature **153**, 434 (1944).
[3] S. Deb and N. Ghosh, Science and Culture (India) **12**, 17 (1946–47).
[4] S. Deb and N. Ghosh, J. Indian Chem. Soc. **25**, 449 (1948).

II. A RESUME OF THE EFFECTS OBSERVED

The ozonizer discharge apparatus with which the phenomenon is most conveniently observed is shown diagrammatically in Fig. 1. Examination of the discharge current with a cathode-ray oscilloscope shows that a part of the current consists of numerous short duration discharge pulses (the so-called "high-frequency component") between the glass surfaces enclosing the discharge space (Fig. 2a). It is further found that it is this "high-frequency" component which is mainly affected by irradiation of the discharge tube. The effects which have been observed and which the proposed theory must explain may be summarized as follows:

(1) The main effect consists in the reduction $(-\Delta i)$ of the discharge current (i) when the discharge tube is flooded with light. This is the so-called "negative light effect." (The reduction in the optimum case may be about 90 percent. The relative reduction is conveniently expressed as *percentage reduction*, i.e., $|\Delta i|/i\times100$).

(2 Under special conditions, with low applied voltage and high pressure, there is an increase $(+\Delta i)$ in-

stead of the more commonly observed decrease ($-\Delta i$). This may be called the "positive light effect." $-\Delta i$ is of more frequent occurrence in gases of simple diatomic molecules. In polyatomic gases, $+\Delta i$ is more prominent. $+\Delta i$ is maximum at (and prior to) striking potential V_m and inverts to $-\Delta i$ by a small increase of the voltage. $+\Delta i$ sometimes occurs at very large values of applied voltage.[5]

(3) The negative effect depends markedly on the nature of the gas used. The maximum effect is observed in chlorine. Next in order comes bromine, iodine, oxygen, air, nitrogen, and hydrogen which are in the decreasing order of electron affinity.[5,6]

(4) The effect is pressure-dependent. Depending upon the applied voltage and the geometry of the tube, there is a pressure at which the effect is maximum.[2]

(5) The percentage value of the effect ($\Delta i/i_{\text{dark}} \times 100$) is maximum at a voltage slightly above the threshold voltage V_m of the discharge. It then diminishes slowly with further increase of voltage.[7]

(6) The effect depends markedly on the intensity of the incident radiation, the relative variation being more pronounced at lower values of the intensity.[8]

(7) The effect is much larger when the ozonizer tube is illuminated from the side than axially.[9]

(8) The effect decreases with increase of frequency of the applied (ac) voltage and ultimately vanishes at radio-frequencies.[10]

(9) The reduction in the discharge current on irradiation occurs in all parts of the spectrum—from extreme red to x-rays.[7] It occurs both within and outside the selective absorption bands characteristic of the enclosed gas.[11]

(10) The effect depends markedly on the condition of the wall of the discharge vessel. Thus, it depends on ageing and previous heat treatment.[1] Also, the percentage effect changes when the walls of the discharge tube are coated with different substances.[8,12]

III. THE ELECTRONIC SURFACE CHARGE THEORY

A number of theories have been proposed to explain the observed effects. These may be broadly classified under two heads. According to one, importance is given to the electrons and negative ions in the discharge space, it being assumed that the formation of the latter is promoted by the incidence of light on the contained gas.[13,14] According to the other, it is the deposit of the charges on the walls of the discharge space that is ultimately responsible for the effect.[3,4,15,16] It is, however, to be noted that, except for only a few, none of the theories takes account of the fact that it is the high-frequency component of the discharge current which is mainly affected.

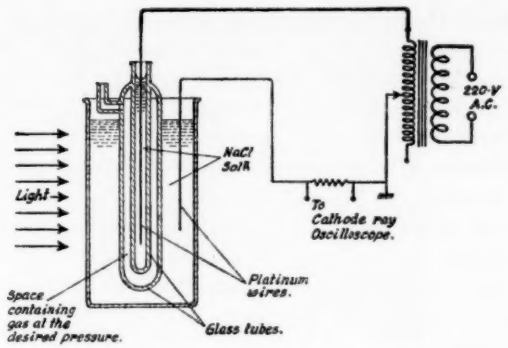

FIG. 1. The ozonizer discharge apparatus.

The starting point of the "electronic surface charge theory" of Deb and Ghosh[3,4] (developed on a suggestion by Mitra[17]), is the mechanism of the production of the high-frequency part of the discharge (first hinted at by Klemenc *et al.*[18]). This theory explains satisfactorily the commoner negative light effect. It, however, leaves unexplained the rarer positive effect. In what follows the theory of Deb and Ghosh will be extended, leaving unaltered their basic assumptions, to include an explanation of the positive effect also.

A. The Discharge Mechanism

The first step in the ozonizer discharge phenomena is the initiation of the discharge in the usual manner by the applied field. (See in Fig. 1 the space containing the gas.) This is followed by a separation of the electrons and positive ions under the influence of the field. This is because the electrons, on account of their lighter mass, are greatly accelerated by the field towards the positive wall and are deposited on the wall. (It is to be noted that the electronic surface charge is formed not directly on the glass wall but on an adsorbed layer of the gas molecules on the surface.) The positive ions, on the other hand, because of their heavier mass, hardly move within this time and remain as volume charge. The applied field within the discharge space of the ozonizer thus becomes neutralized by the field due to the separated charges—electronic surface charge and positive ion volume charge—and the discharge stops.

It is also to be noted that some of the electrons may be left free as space charge, especially in front of the

[5] S. S. Joshi, Current Sci. (India) **16**, 19 (1946).
[6] G. S. Deshmukh, J. Indian Chem. Soc. **24**, 211 (1947).
[7] S. S. Joshi and P. G. Deo, Current Sci. (India) **12**, 306 (1943).
[8] S. S. Joshi, Current Sci. (India) **14**, 35 (1945).
[9] N. R. Tawde and K. Gopalkrishnan, Proc. Indian Acad. Sci. **29A**, 171 (1949).
[10] S. N. Tewari and B. Prasad, Current Sci. (India) **14**, 229 (1945).
[11] S. S. Joshi, Current Sci. (India) **13**, 278 (1944).
[12] S. S. Joshi, Current Sci. (India) **13**, 253 (1944).
[13] S. S. Joshi, Current Sci. (India) **14**, 175 (1945).
[14] S. S. Joshi, Current Sci. (India) **14**, 317 (1945).
[15] W. L. Harries and A. von Engel, Proc. Phys. Soc. (London) **B64**, 916 (1951).
[16] W. L. Harries and A. von Engel, J. Chem. Phys. **19**, 514 (1951).
[17] S. K. Mitra, *Active Nitrogen—A New Theory* (The Indian Association for the Cultivation of Science, Jadavpur, Calcutta, 1945), p. 58.
[18] Klemenc, Hintenberger, and Hoffer, Z. Electrochem. **43**, 708 (1937).

negatively charged surface, and some of them may also attach themselves to the neutral molecules to form negative ions, the formation being facilitated by the comparatively high gas pressure, the gas molecules providing the "third body." The proportions in which the electrons will form surface charge, will form negative ions, or will be left free, depend on a number of factors, e.g., the gas pressure, the relative surface area, the temperature, and the previous history of the glass wall.

If now the applied field is switched off, the field due to the separated charges takes hold of the discharge phenomena. From the nature of the distribution of the charges as explained above, it follows that the volume charge of positive and negative ions will be more or less at constant potential and there will be a large fall of potential within a small distance close to negatively charged surface. Hence, positive ions drawn from the volume charge will be accelerated by the intense field in front of the negatively charged surface and will arrive in torrents on the same to recombine with the electrons, the recombination being facilitated by the surface molecules acting as the "third body." Further, if there are free electrons within the region of the fall of potential mentioned above, these will be accelerated towards the positive volume charge to recombine with positive ions or to attach themselves to neutral molecules to form negative ions. The currents due, firstly, to the torrent of positive ions on to the negative surface charge and secondly, to the motions of electrons towards the positive volume charge constitute the observed high-frequency neutralizing discharge current. The former provides the major part of the current, because, the neutralizing negative surface charge had been quickly and copiously formed during the part of the discharge when the applied field was on. It is to be remembered that the positive ions, coming as they are from different distances, do not all arrive at the same instant on the neutralizing wall. Hence, the neutralization is not instantaneous.

The existence of the high-frequency "pulse discharge," in a direction opposite to that of the initial discharge, has been verified experimentally by Klemenc *et al.*[18] by suddenly switching off the applied steady field and also by Deb and Ghosh[19] by using for the external field short-duration voltage pulses.

In the above, we have considered the case when a steady field is applied and when the same is removed. A little consideration shows that if, instead of steady field, we have a field increasing with time (as during one half-cycle of an alternating field) the starting and stopping of the discharge will occur a number of times but the phenomenon will essentially be the same as described above (Fig. 3a). (The case is fully discussed with photographic illustrations of the discharge current in the paper of Deb and Ghosh cited above.)

B. Effects of Irradiation

Next, let the experiment be performed when the discharge tube is flooded with light (say, visible white light). Since the electron affinity of the glass walls (i.e., of the layer of adsorbed molecules) is quite small, there will be photodetachment of electrons from the surface. The negative charge density on the surface will, therefore, be less when the light is acting, the detached electrons forming space charge in front of the cathode. The internal field, opposing the external field and stopping the discharge, will thus be that due to the positive volume charge (as before) separated from the electronic charges residing partly in the volume close to cathode surface and partly on the surface itself. Depending upon the pressure in the discharge tube, a proportion of the electrons will also attach themselves to the neutral gas molecules producing negative ions.

We can now make the two following postulates regarding the immediate effects of flooding the ozonizer with light on the neutralizing high-frequency "pulse" discharge currents when the applied field is removed:

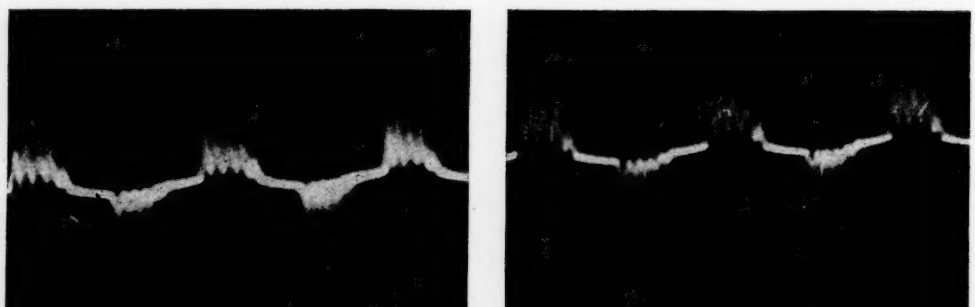

(a) (b)

FIG. 2. Oscillographic pictures of discharge current; (a) in darkness, (b) in light. The discharge current consists of a series of low-frequency pulses and a larger number of high-frequency pulses (for interpretation see Sec. III). The effect of irradiation is to reduce the high-frequency pulse component of the discharge current.

[19] S. Deb and N. Ghosh, Science and Culture, India **14**, 39 (1948–49).

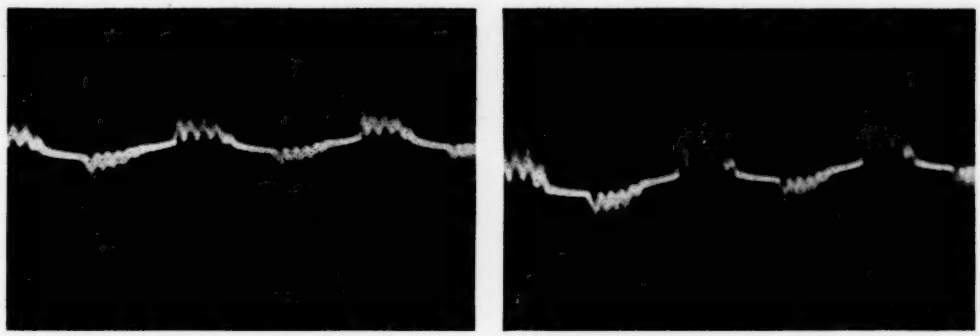

(a) (b)

FIG. 3. Oscillographic pictures of discharge current, with the high-frequency components by-passed through a 0.0003-μf condenser, showing pulses due to the alternate starting and stopping of discharge under the combined influence of the externally applied field and the field due to the surface charges; (a) in darkness, (b) in light. The stopping of the discharge current is not complete when the ozonizer is flooded with light. Further, the height of the pulses is increased. This is because a large number of electrons are now available for the initiation of the discharge, increasing thereby the stability of the discharge.

(1) Because of the decrease in the density of the negative surface charge, the part of the high-frequency current due to the torrent of positive ions neutralizing on the negative surface charge will decrease (Fig. 2b). (This we shall call effect No. 1.)

(2) Because of the increase in the concentration of electrons in the volume in front of the cathode surface (see above), the part of the high-frequency current resulting from the electrons being accelerated away from the cathode (due to the cathode fall of potential) will increase. The discharge current will also increase as more electrons are now available for the initiation and the stability of the discharge (Fig. 3b). (These we shall call effect No. 2.)

Let us now see how these postulates can explain the observed "light effects" and the associated phenomena.

(a) When the pressure is low—so low that the probability of negative ion formation is comparatively small—the electrons detached by the incidence of light will mostly remain free. Hence, the decrease in the high-frequency discharge current due to effect No. 1 will be amply compensated by the increase due to effect No. 2. In other words, there will be little or no effect of light on the discharge current.

When the pressure is higher, the electrons released from the surface (by the incidence of light) have higher probability of forming negative ions. As the ions have low mobility, effect No. 2 will be of less importance and effect No. 1 only will be mainly operative. Hence, there will be a sharp decrease in the neutralizing high-frequency discharge current. The commonly observed negative light effect is thus explained. (It is to be noted that the light will also release electrons from negative ions in the volume. But the proportionate number made free is much less at higher pressure on account of the enhanced probability of negative ion formation at such pressures.)

(b) Next, let the gas pressure be relatively high—so high that for the applied voltage, the discharge passes with difficulty. The electrons, produced by the intermittent discharge, are now prevented, by frequent collisions, from reaching the positive wall and hence the density of the electronic surface charge will be small. Under such conditions the few electrons that are released by irradiation help to increase the discharge current and hence stabilize the discharge. In such cases effect No. 1 is more than compensated by effect No. 2. There is thus a net increase in the discharge current. This is the less commonly observed positive light effect prominent when the applied field is just below that required for establishing a stable discharge.

(c) It is obvious that, other conditions remaining the same, the effect will be more pronounced in gases having high electronic affinity. This is because in such gases the electronic surface charge will be more copiously formed (it being recalled that the electrons are deposited not directly on the glass surface but on a layer of adsorbed molecules of the enclosed gas on the same) and the number of free electrons (as are detached from the surface) will be decreased due to the quick formation of negative ions. Effect No. 1 will thus increase and, at the same time, effect No. 2 will decrease.

(d) The magnitude and nature of the "light effect" will depend on the pressure of the gas in the discharge space as explained under (a) and (b).

(e) An increase in the applied voltage beyond the striking value will result in an increase in the direct discharge current, that is, in increased production of ions and electrons. The surface density of the electronic charge will not, however, increase proportionately because of the tendency for it to attain saturation value. The volume density of the ions, on the other hand, will go on increasing with the applied voltage. Hence, while effect No. 2 will go on increasing, effect No. 1 will not do so proportionately. The magnitude of the negative "light effect" will, therefore, increase less

relatively to the increase of the applied voltage. It will tend to a steady value and then decrease with the increase of the applied voltage.

(f) If the intensity of the light be increased, effect No. 1 will increase. But there will be proportionately more increase in effect No. 2, so that there is a net reduction in the magnitude of the negative "light effect."

(g) If the discharge tube is illuminated axially, avoiding the walls, then there will, obviously, be no negative "light effect" because effect No. 1 is absent.

(h) If the interval between the switchings on and off of the applied field be smaller than the time required for the electrons to travel up to the positive wall and form the surface charge, then the "light effect" will diminish. This, in other words, means that with the increase in the frequency of the exciting ac voltage the "light effect" will decrease.

(i) Radiations of all wavelengths, the energy of which is sufficient to detach electrons from the surface charge and from the negative ions, will be able to produce the "light effect." The effect will be the highest for wavelengths whose energy is only slightly greater than the detachment energy. Obviously, the wavelength of the radiation has no relation with the wavelength of the selective absorption bands of gas under discharge.

IV. NUMERICAL ESTIMATES OF THE VARIOUS RATE PROCESSES

In the preceding section we had to introduce, in connection with the development of the "electronic surface charge theory," various electronic processes and their rates, e.g., deposit of electrons on the glass walls, detachment of electrons from the same, negative ion formation, detachment of electrons from negative ions, etc. It is desirable that some quantitative estimates—even if they be very rough ones—be made of the rates of these processes, to check that there is no contradiction in the sequence of the various stages that have been proposed in the theory to explain the positive and the negative effects.

A. Rate of Formation of the Neutralizing Surface Charge

We first make estimate of the density of the electronic surface charge that would be necessary to stop the discharge. It is reasonable to assume that the saturation density of the surface charge is reached when one electron is deposited per one surface atom. This will correspond to about 10^{14} electrons per unit area of the wall. For the typical case of an ozonizer, whose inner and outer electrodes have diameters of the order of 1 cm and 3 cm, respectively, the capacity per unit length is about 1 $\mu\mu$f. Hence the potential developed by the surface charge of this density is

$$v=(10^{14}\times 1.6\times 10^{-19})/10^{-12}=10^{7} \text{ volts.}$$

This is many orders higher than the externally applied voltage. It follows, therefore, that the opposing field due to the surface charges will be able to stop the discharge even when a very small fraction of the surface atoms hold one electron each.

Now, under usual conditions of operation, the extinction potential for the discharge system is of the order of a few hundred volts only. In order that the surface charge is able to build up an opposing potential to reduce the net potential difference to this amount, the surface density of charge should be of the order

$$\frac{10^{14}}{10^{7}}\times(10^{3} \text{ to } 10^{4})=10^{10} \text{ to } 10^{11} \text{ electrons cm}^{-2}.$$

This may be taken as the maximum value of the surface charge built up in course of discharge in the system under consideration.

For estimating the rate of formation of the surface charge, we assume that the discharge current is almost wholly due to electrons derived from the discharge—the positive ions contributing only a negligible fraction. Since the discharge current in an ozonizer tube ranges from one-hundredth to one milliampere, we take the average value of the discharge current as 0.1 ma. The average rate of deposition of electrons on the wall surface is, therefore,

$$\frac{\text{current}}{\text{electronic charge}}=\frac{10^{-4}}{1.6\times 10^{-19}}\simeq 10^{15} \text{ sec}^{-1}.$$

Or, if the length of the ozonizer tube is taken as 10 cm, the rate is 10^{13} cm^{-2} sec^{-1}. Thus, the time required to build up a surface charge density of 10^{10} to 10^{11} electrons per sq cm is 10^{-4} to 10^{-3} sec. This is the interval between the starting and the stopping of discharge giving the low-frequency pulses (Fig. 3).

B. Rate of Photodetachment of Electrons

For estimating the rate of photodetachment of electrons from the charged wall surface, we require a knowledge of its photosensitivity. Unfortunately, no experimental data on photoemissions from a composite surface consisting of electrons held by adsorbed gas molecules on glass is known. We may, however, try to make a rough estimate by examining the results obtained for composite layers on metals, such as silver-sodium oxide-sodium, etc. Under properly treated conditions these surfaces may have a sensitivity of 50 μa per lumen. For the surface under consideration a reasonable value may, therefore, be taken as about 10 μa per lumen.

The "light effect" is generally observed by flooding the ozonizer tube by means of light from electric bulbs of power, say, 100 to 500 watts (backed by suitable reflector) and placed some 50 cm away from the discharge tube. The efficiency of a 200-watt bulb may be taken

as 15 lumens per watt. Taking into account the inverse square fall of intensity, the luminous flux at a point 50 cm away from the bulb would be about 1 lumen. But, considering the presence of the reflector a more reasonable estimate would be 10 lumens. The rate of photodetachment comes out to be of the order

$$\frac{10\times10^{-6}\times10}{1.6\times10^{-19}}=10^{15}\text{ electrons cm}^{-2}\text{ sec}^{-1}.$$

This is of the same order as that of the rate of deposition of electrons.

C. Rate of Formation of Negative Ions

If ν be the collisional frequency of electrons with gas molecules and n the fraction of collisions which results in the formation of negative ions, then the rate of formation of negative ions $=N_e n\nu$, where N_e is the number density of electrons in the discharge space.

At a pressure of 10 cm of mercury, which is typical of the pressure at which the "light effect" is observed,

$$\nu=10^{11}\text{ sec}^{-1}.$$

According to experimental results of Cravath,[20]

$$\text{for chlorine } n>10^{-3},$$
$$\text{for oxygen } n\simeq10^{-5}.$$

Therefore, the rate of formation of negative chlorine ions $\simeq10^{8}N_e$ sec^{-1}, and the rate of formation of negative oxygen ions $\simeq10^{6}N_e$ sec^{-1}. If the discharge current be 0.1 ma and the field 100 v/cm then, $N_e=10^{7}$ cm^{-3}. Hence, for this value of electron concentration, the rate of formation of negative chlorine ions $\simeq10^{15}$ cm^{-3} sec^{-1}, and the rate of formation of negative oxygen ions $\simeq10^{13}$ cm^{-3} sec^{-1}. These are of the same order as the rate of electron detachment from the surface.

D. Rate of Removal of Negative Ions: Electron Detachment and Mutual Neutralization

Electrons from the negative ions may be removed by several processes, namely, photodetachment, detachment by collisions with neutral gas molecules, and removal by mutual neutralization of negative and positive ions. Now for chlorine, electron affinity is such that ordinary visible radiation will be unable to effect any appreciable detachment. Further, if the pressure is high and the field strength low, then the charged particles will not be able to acquire sufficient energy within the distance of the mean free path and, hence, collisional detachment will remain small. However, for moderate pressure and high-field strength this process is likely to play a dominant role. The rate of removal by collisional detachment is given by

$$\alpha N^{-}N,$$

where $\alpha=$ the coefficient of collisional detachment[21] $=10^{-16}$, $N^{-}=$ number density of negative ions, and $N=$ number density of neutral molecules.

Supposing that the formation of negative ions proceeds for a time 10^{-4} sec which is the duration of discharge for each initiation, the maximum concentration that the negative ions can attain is, from Sec. IV, C above, $10^{15}\times10^{-4}=10^{11}$ cm^{-3}. A more reasonable value may be 10^{9} cm^{-3}. Hence, since the value of N at a pressure of 10 cm of Hg is of the order of 10^{19}, the rate of collisional detachment is 10^{12} sec^{-1} cm^{-3}.

At 10-cm pressure and ordinary field strength, negative ions will be removed largely through mutual neutralization of positive and negative ions. The rate at which negative ions disappear through this process is given by

$$\beta[N^{-}]^{2},$$

where β, the coefficient of mutual neutralization, is of the order 10^{-8}.[22] With $N^{-}=10^{9}$, the initial rate of removal through mutual neutralization $=10^{10}$ cm^{-3} sec^{-1}.

Comparing the above with the results obtained in Sec. IV C, we find that ordinarily—when collisional detachment is unimportant—the rate of removal of negative ions will be very small compared to the rate of formation. If, however, the pressure is reduced, or the field strength is increased keeping the pressure high, so that collisional detachment becomes operative, the rate of removal of negative ions may be comparable to the rate of formation. According to Cravath[20] collisional detachment comes into play if

$$N/p\geq100,$$

where N is the field across the discharge space in volts/cm and p is the pressure in mm. Thus at a pressure of 10 cm, collisional detachment will be appreciable if the field across the discharge space is increased beyond 10^{4} volts cm^{-1}.

V. DISCUSSION AND CONCLUDING REMARKS

Let us now discuss the bearings of the results of the numerical estimates made in the last section on the theory of the electronic surface charge developed in Sec. III.

We have found that the electronic surface charge necessary for producing the requisite opposing field to stop the discharge is many orders less than the maximum capacity of the surface to hold the electrons. Further, what is more important, the time required for building up the surface charge is of the order 10^{-4} to 10^{-3} sec which is small compared to the period (1/50 sec) of the ac voltage applied for observing the effect. The phenomenon of starting and stopping of discharge (the low-frequency pulses) will, therefore, occur, a number of times in course of one half-cycle. This agrees with

[20] A. M. Cravath, Phys. Rev. **33**, 603 (1929).

[21] A. P. Mitra, J. Geophys. Research **56**, 373 (1951).

[22] D. R. Bates and H. S. W. Massey, Proc. Roy. Soc. (London) **A189**, 261 (1946).

observation. Also, in conformity with this, the duration of the low-frequency pulses as observed experimentally is of the order 10^{-4} sec. It also at once follows that if the frequency of the applied ac field is raised to the order of 10 kilocycles sec^{-1}, the effect would disappear. This again agrees with observation.

The calculations also show that under average working condition the rate of photodetachment of electrons from the surface (10^{15} cm^{-2} sec^{-1}) is about as rapid as the rate of deposition of electrons. Because of this, the process of photodetachment becomes fully effective in a fraction of the interval between the starting and the stopping of the discharge. The instantaneous character of the effect of light is thus explained.

The rate of capture of electrons to form negative ions has been found to be as rapid as the rate of detachment from the surface due to irradiation. This shows why the negative effect is ordinarily the more dominant one.

The theory demands that for the wavelength and for the intensities of illumination usually employed, the rate of photodetachment of electrons from the negative ions should be much less than both the photodetachment from the surface and the rate of formation of negative ions by attachment. The calculated results show that this is actually the case.

It has been found that the detachment of negative ions by mutual collisions may become quite high if the field strength is high. This possibly explains why the negative effect changes over to a positive effect when the applied potential is increased to a sufficiently high value. For example, for pressure of about 10 cm of Hg a transition from negative to positive effect will occur when the voltage is raised to the order 10^4 volts. This is in reasonably good agreement with what is actually observed.

According to the theory, the positive effect is expected to occur under conditions which favor a low rate of formation of negative ions and a high rate of detachment of electrons from the same. Both these conditions are satisfied if the electron affinity of the gas used is small, the frequency of the light used is high, and the applied field strength is large. This is also in complete agreement with experimental results.

Again, according to the theory, if by means of an external field the electrons are deflected from their straight and shortest paths towards the electrode surface, two opposing effects will be expected to occur. On the one hand, there will be a diminution of the discharge current due to the restriction in the formation of the surface charge and, on the other, there will be an increase in the same due to greater chance of ionization resulting from the longer paths traversed by the electrons. Experiments performed by Bhiday, Bhide, and Asolkar[23] confirm these predictions. These authors placed the ozonizer tube in a magnetic field and found, that depending upon the pressure and the magnetic field, the strength of the discharge current sometimes showed an increase and sometimes a decrease.

From the discussion given above one is justified in concluding that the "electronic surface charge theory" as developed in Sec. III is able to account for all the principal features of the effect, both positive and negative. The two effects are always present and are controlled, firstly, by the electronic surface charge formation and the liberation of the electrons from the same by the incident light, and, secondly by the liberated electrons being captured by the neutral molecules in the volume. If the capture rate is high, we have the negative effect. If the capture rate is low, we have the positive effect. It is to be noted that, as mentioned in Sec. III A, the possibility of the formation of negative ions had also been suggested by Joshi. But the role played by these has not been interpreted correctly. The interpretation suggested earlier by Deb and Ghosh and developed further in this paper clarify the many puzzling and apparently conflicting experimental observations. The numerical calculations carried out in Sec. IV are, no doubt, based on many uncertain factors. Nevertheless, the degree of qualitative agreement obtained is quite satisfactory.

ACKNOWLEDGMENT

It is a pleasure to thank Professor S. K. Mitra for suggesting the work to us, and for his constant guidance and help in the course of preparation of the paper.

[23] Bhiday, Bhide, Asolkar, Nature **168**, 1006 (1951).

Hot Atom Recoils from $C^{12}(\gamma,n)C^{11}$*

FRANK S. ROWLAND† AND W. F. LIBBY
Institute for Nuclear Studies and Department of Chemistry, University of Chicago, Chicago, Illinois
(Received April 6, 1953)

Simple carbon systems have been irradiated with the University of Chicago betatron, producing C^{11} atoms by the reaction $C^{12}(\gamma,n)C^{11}$. The distribution of the radioactive atoms between CO and CO_2 for samples irradiated in the liquid phase was found to be 95–100 percent CO, and for samples irradiated in the solid phase about 50 percent of each oxide. A mechanism for these results is proposed.

IN contrast to the considerable amount of work done on the chemical effects following (n,γ) recoil, the effects following (γ,n) recoil have been investigated only briefly and qualitatively. The recoil energy from (γ,n) reactions is much larger than the recoil energy from (n,γ) reactions because particle emission is involved. Formulas[1] for the recoil from particle emission following gamma-ray excitation show that the average recoil energy for C^{11} atoms formed by 48-Mev betatron radiation on C^{12} should be in excess of 10^5 electron volts. With recoil energies of this magnitude the velocity of the nucleus will be sufficient to insure ionization of the recoiling atom. However, neutralization will occur rather early along the track, so little difference in the hot atom behavior between the lower-energy (n,γ) recoil studies will be expected because of this ionization directly. The intensity of the betatron gamma beam is so great, however, that a large amount of free radical formation may be expected, so considerable quantities of radiation decomposition products are likely. In the systems we have studied, however, the likely radiation decomposition products would not be particularly effective at attacking those molecules likely to result from the hot atom reactions, and we expect therefore that our results are not seriously in error because of any effect of the gamma radiation.

Several simple carbon systems have been irradiated with the University of Chicago betatron, producing C^{11} atoms by the reaction $C^{12}(\gamma,n)C^{11}$. The distribution of the radioactive atoms between CO and CO_2 then has been determined.

EXPERIMENTAL

Chemicals

The solid CO_2 samples were commercial dry ice, while the liquid CO_2 samples were commercial capsules containing about 5 grams of liquid CO_2 under 1000-lb/in.^{2} pressure. The carbonate salts were standard chemicals and were not further purified.

Irradiations

The University of Chicago betatron, operated with a maximum energy of 48 Mev during this research. The materials were irradiated at a distance of 120 cm from the radiation source, at an intensity of about 200 roentgens/minute.

Separation and Measuring Activity

The carbon dioxide from the irradiated samples was expanded into a comparable volume of carbon monoxide carrier. The entire volume was then passed through a liquid nitrogen trap to remove the carbon dioxide. The remaining gas was passed over hot copper oxide and the carbon monoxide fraction was condensed as the dioxide with another liquid nitrogen trap. Both samples were treated with hot $CaCl_2$ solution, filtered, and mounted as solid $CaCO_3$. They were counted with a glass-walled silver cathode counter from cylindrical geometry. An empirical calibration curve was used to correct for different weights of precipitate.

In the experiments with solid CO_2, a small non-volatile residue remained, containing less than 1 percent of the total activity.

RESULTS AND DISCUSSION

The carbon dioxide-carbon monoxide distributions from the $C^{12}(\gamma,n)$ reaction are shown in Table I. The results of these experiments may be split into two groups: those which were irradiated in the liquid phase and which gave 95–100 percent carbon monoxide,

TABLE I. Distribution of radioactivity between CO and CO_2 from $C^{12}(\gamma,n)C^{11}$.

Target material	Percent radioactivity CO_2	CO
Solid CO_2, −78°C	51±3	49±3
Solid CO_2	43±3	57±3
Solid CO_2	48±3	52±3
Liquid CO_2, 25°C	<5	>95
Liquid CO_2	2±2	98±2
Liquid CO_2	3±2	97±2
Powdered $NaHCO_3$, 25°C	52±3	48±3
Powdered $NaHCO_3$	47±3	53±3
$NaHCO_3$ in water, 25°C pH 8	0±1	100
Na_2CO_3 in water, 25°C	0±1	100

* This research was supported under Contract No. AT(11-1)-86 with the U. S. Atomic Energy Commission for the 36-in. cyclotron, and Contract No. N6ori20, Task Order XXII with the Office of Naval Research for the betatron.
† Now at Department of Chemistry, Princeton University.
[1] W. F. Libby, J. Am. Chem. Soc. 69, 2523 (1947).

and those which were irradiated in the solid phase and gave about 50 percent of each oxide. There appear to be no results for other (γ,n) reactions with which these results may be directly compared, but the two reactions $N^{14}(n,p)C^{14}$ and $B^{10}(d,n)C^{11}$ also give energetic carbon recoil atoms which are a basis for indirect comparison. The best data available are those of Norris and Snell, who found 56 percent CO and 44 percent CO_2 with less than 2 percent other products from neutron irradiation of NH_4NO_3 solution.[2] Mixtures of CO and CO_2 have been reported from deuteron bombardments of severals forms of boron targets[3–6] and from neutron irradiation of NH_4NO_3 crystals.[7] More complex nitrogenous crystals gave radioactive HCN, CH_4, CH_3OH, HCOOH, as well as the oxides of carbon, upon neutron irradiation.[7,8]

One observes that in the solid state roughly equal yields of CO and CO_2 occur, whereas in the liquid nearly all the radiocarbon forms CO. This striking result probably is due to the confinement of the free radicals generated along the recoiling C^{11} track in close proximity with one another in the solid phase, for a length of time sufficient for them to recombine; whereas in the liquid phase diffusion away from the track occurs to such an extent that the C^{11} atom has an excellent opportunity of getting away and reacting with the general medium. In other words, it is expected from ordinary thermodynamic data that a thermal carbon atom reacting either with CO_2 or water will give CO. In fact, the reactions (1) and (2) involving graphitic carbon are known to occur

$$C+CO_2=CO+CO, \tag{1}$$

$$C+H_2O=CO+H_2, \tag{2}$$

and since the heat of sublimation of carbon is so large it is very certain that atomic carbon will have sufficient energy to form CO from the general medium in all of the samples we have irradiated. The problem, therefore, is to explain why CO_2 is formed in the solid phase. The only free radicals which can be generated in the case of solid CO_2 are atomic oxygen and atomic carbon. Therefore the only stable carbon-containing molecules are CO and CO_2. The generation of CO_2 obviously requires a high concentration of atomic oxygen or the formation of an extremely excited CO molecule which will be capable of reacting according to Eq. (3)

$$C^*O+CO_2=CO+C^*O_2, \tag{3}$$

in which the asterisk indicates a radioactive carbon atom. The activation energy for reaction (3) probably is considerable. Both the reaction of atomic carbon to form CO and of CO with atomic oxygen to form CO_2 and reaction (3) will be strongly favored for reaction sites near the track of the recoiling carbon. Confinement of the free radicals in the vicinity of this track in the solid state might very well be expected to favor this type of hot or epithermal reaction.[9]

[2] L. Norris and A. Snell, Nucleonics **5**, No. 3, 18 (1948).
[3] D. Yost, L. Ridenour, and K. Shinohara, J. Chem. Phys. **3**, 133 (1938).
[4] Ruben, Hassid, and Kamen, J. Am. Chem. Soc. **61**, 661 (1939).
[5] Ruben, Kamen, and Hassid, J. Am. Chem. Soc. **62**, 3443 (1940).
[6] S. Ruben and M. Kamen, Phys. Rev. **57**, 549 (1949).
[7] Yankwich, Rollefson, and Norris, J. Chem. Phys. **14**, 131 (1946).
[8] P. Yankwich, J. Chem. Phys. **15**, 374 (1947).
[9] M. S. Fox and W. F. Libby, J. Chem. Phys. **20**, 487 (1952).

Hot Atom Chemistry of the Alkyl Bromides; Absence of Effects Due to High Radiation Density; Isotope Separation in Solids*

FRANK S. ROWLAND† AND W. F. LIBBY
Institute for Nuclear Studies and Department of Chemistry, University of Chicago, Chicago, Illinois
(Received April 6, 1953)

A 30-curie polonium-beryllium neutron source which gives less than 0.1 roentgen per hour in close contact was used to study the hot atom chemistry of a selection of alkyl bromides. Comparison of the results with those obtained with ordinary neutron sources containing gamma rays in abundance up to 700 roentgen/hour equivalent strongly indicates that the essential phenomena reported are free of effects due to the gamma-radiation density.

The separation of the bromine isotopes in crystalline alkyl bromides has been observed in several additional cases. No isotope effect is shown with CBr_4, however, nor with frozen glasses. The possible theoretical significance of these results is discussed.

I. INTRODUCTION

THE entire history of hot atom chemistry has been beclouded by the possibility that the phenomena observed were not due to the recoil or the electron excitation energy of the hot atoms produced by nuclear reactions, but rather to reaction of these atoms with a general crowd of free radicals and ions generated by the radiation density of the source being used. The reality of this effect for irradiations in the atomic piles[1] is recognized, though recent evidence[2–5] has indicated that it may not be as serious an effect as formerly feared. In order to elucidate this point further we have obtained a pure neutron source consisting of 30 curies of Po^{210} mixed with beryllium powder, which gives essentially pure neutron radiation, and performed standard experiments for comparison with the results normally obtained with ordinary sources. This source was obtained from the U. S. Atomic Energy Commission.

The separation of the bromine isotopes in crystalline isopropyl bromide observed previously[6] obviously needed further investigation, and additional data are reported below. The occurrence of the separation has been substantiated in additional cases and evidence against its occurring in frozen glasses accumulated. No separation has been found in the liquid state.

II. PROCEDURE

Chemicals

The alkyl bromides were purified by ozonization, successive washes with concentrated sulfuric acid, aqueous sodium bicarbonate, and water, drying over anhydrous sodium sulfate, and distillation, discarding the first and last tenths. The boiling points of the purified materials were in excellent agreement with the literature values.

The CBr_4 was purified by aqueous precipitation from an alcohol solution. It then was filtered and stored in a desiccator. A lauryl bromide sample was obtained from Dow Chemical Company and was not purified further.

Neutron Sources

The two chief neutron sources were the University of Chicago 36-in. cyclotron, utilizing a beryllium target, and the 30-curie polonium-beryllium source. In each case the neutrons were moderated in cubical paraffin blocks about 12 inches on a side. The thermal neutron flux from the cyclotron was about 10^7 neutrons/cm^2/sec, while that from the pollonium-beryllium source was much less since the total neutron yield was only about 4×10^7sec. A reasonable estimate for the flux from the Po-Be source might be 10^5 thermal neutrons/cm^2/sec. The gamma radiation flux from the cyclotron had been measured previously[6] and found to be about 700 roentgen/hour at the irradiation site. The gamma flux from the Po-Be source was measured both by inverse square extrapolation from Geiger counter survey meter measurements and from exposure of DuPont 552 x-ray film with the samples. These measured values were 0.2 and 0.1 roentgen/hour, respectively, and are only upper limits because of the uncertainty of the neutron contribution to the total effect. However, it is clear that the gamma radiation from the Po-Be source was entirely negligible, and we are free to take the source as being one essentially of pure neutrons.

Alkyl Bromide Glasses

These glasses were prepared by rapid immersion of the alkyl bromides in liquid nitrogen. A similar glass can be made with 3:1 hydrocarbon mixtures of isopentane and methyl cyclohexane containing up to 10 or 12 percent by volume of alkyl bromide. The glasses were colorless and transparent, in distinct contrast to the

* This research was supported under Contract No. AT(11-1)-86 with the U. S. Atomic Energy Commission for the 36-in. cyclotron.
† Now at Department of Chemistry, Princeton University.
[1] G. E. Boyd, J. W. Cobble, and S. Wexler, J. Am. Chem. Soc. 74, 237 (1952).
[2] Shaw and Collie, J. Chem. Soc. **1949**, 1221.
[3] Hornig, Levey, and Willard, J. Chem. Phys. **20**, 1556 (1952).
[4] S. Levey and J. Willard, J. Am. Chem. Soc. **74**, 6161 (1952).
[5] Hamill and Williams, Paper 99, p. 41T. Abstracts of the March, 1953 Meeting of the American Chemical Society.
[6] M. S. Fox and W. F. Libby, J. Chem. Phys. **20**, 487 (1952).

TABLE I. Retention of *n*-propyl bromide from three neutron sources at 25°C (4.4-hr Br^{80m}).

Neutron source	Percent retention	Gamma-ray flux roentgens/hour
Cyclotron	33.6±0.6	700
Radium-Beryllium	34.4±0.7	...
Polonium-Beryllium	34.0±0.9	0.1

white crystalline solids, and maintained this transparency unchanged during irradiation. Upon warming, the glasses usually crystallized and then melted. This was one of our principal proofs that the glass actually had existed during the irradiation.

Separation and Measurement of Activities

The samples were irradiated for varying lengths of time, normally about 15 minutes with the cyclotron and 1 hour with the Po-Be source. They were contained in quartz tubes immersed in liquid nitrogen, for low temperature runs, or in soft glass brown bottles for room temperature runs. About 5 minutes after the end of the irradiation the organic and inorganic fractions were separated by the established procedure of shaking with an aqueous $Br^- - SO_3^=$ solution. Because of the necessity for accuracy in the counting measurements involved in the isotope separation studies, it was thought best to avoid the correction factors necessary for differing densities. This was done by using identical counting solutions for both the organic and inorganic radioactivities. These solutions were usually a 3:7 mixture by volume of the alkyl bromide and of ethyl alcohol containing traces of dissolved LiBr. The inorganic solution was made by using the lithium salts in the original extracting solution, evaporating to dryness and dissolving in alcohol. Inactive alkyl bromide was then added in the proper proportions. The solution containing the organic combined activities was made by diluting with alcohol and traces of LiBr. Tests show that no radioactivity concentrated on the walls of the counting vessels from these solutions.

The solutions to be counted were placed in annular glass vessels of about 7-cc capacity and were measured with silver cathode glass-wall Geiger counters. A 1500 mg/cm² lead shield for the beta radiation of the Br^{80}, which also served as radiator for the Br^{82} gamma radiation, could be interposed between the solution and the counter. This allowed measurements of the Br^{82} activity to be made intermittently with measurements of the Br^{80m} 4.4-hour activity. When the PoBe source was used for isotope separation measurements a solution counter of about 18-cc volume was used instead, and the decay curves were resolved. The Br^{80m} activity actually was measured, of course, by the radiations of the Br^{80} daughter in equilibrium with it, care having been taken, as mentioned above, to insure that the daughter Br^{80} atoms were not segregated on the wall of the counting vessel.

TABLE II. Retention *vs* bromine concentration for Br_2 in *n*-propyl bromide at 25°C (18-min Br^{80}).

Mole fraction Br_2	Percent retention
0	34.0
4×10^{-3}	29.8
1×10^{-2}	27.5
2×10^{-2}	26.2
4×10^{-2}	23.5
8×10^{-2}	22.0

III. DATA ON THE ABSENCE OF THE RADIATION EFFECT

Three samples of normal propyl bromide, the material which had been so carefully studied earlier,[6] were irradiated on the same day with three different neutron sources, the two described above and an ordinary 500 mc Ra-Be source. The data are given in Table I, in which the fraction of the radiobromine retained in organic form, reported as the retention, is found to be the same within the experimental error for all three sources. The 4.4-hour Br^{80m} isotope was used for this work.

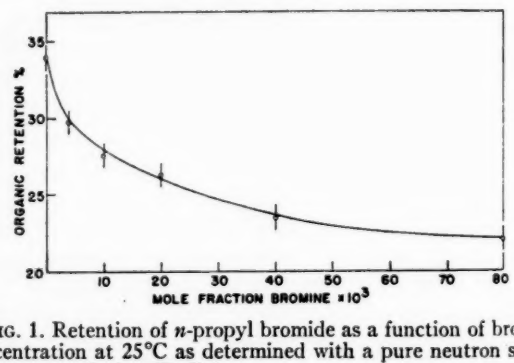

FIG. 1. Retention of *n*-propyl bromide as a function of bromine concentration at 25°C as determined with a pure neutron source of gamma radiation (Pr-Be).

It is fairly clear that any serious radiation chemical effect should be quenched by such agents as molecular bromine with which free radicals will have a voracious tendency to react, and it seemed therefore that a study of the retention of an alkyl bromide for various concentrations of added bromine might reveal radiation chemical effects. The data obtained in such a study on normal propyl bromide are given in Table II, and are reproduced in Fig. 1. The 18-min Br^{80} activity was used in this case.

The results are completely similar to those obtained for ethyl bromide and several alkyl iodides by Goldhaber, Chiang, and Willard[7,8] and therefore, like those on retentions in the pure alkyl bromides (Table I), show no evidence of radiation interference in the hot atom phenomena.

In addition, some of the data quoted later on the isotope separation were taken with the Po-Be source

[7] S. Levey and J. Willard, J. Am. Chem. Soc. **74**, 6161 (1952).
[8] S. Goldhaber and J. Willard, J. Am. Chem. Soc. **74**, 318 (1952).

rather than the cyclotron, and in so far as they agree with the others offer further substantiatory evidence. The general conclusion we draw from these results is that the sources ordinarily used in hot atom studies do not have sufficiently high-radiation densities to seriously obviate the conclusions about the principles and facts of hot atom chemistry, which we might define as the chemistry of the excited atoms formed by nuclear reactions in an otherwise undisturbed medium.

IV. ISOTOPE SEPARATION

The first experiments on isotope separation[6] revealed that in the crystalline state isopropyl bromide showed retentions of 81.6±2.0, 79.9±1.0, and 93.8±0.5 for the isotopes Br^{80} (18-minute), Br^{80m} (4.4-hour), and Br^{82} (36-hour), respectively. From the theory[6] which led to the experiment it was expected that the phenomena would be general, the separation varying somewhat with the ratio of the mass of the average atom to that of bromine, the hot atom, in such a manner that in the cases of nearly equal mass such as CBr_4, we would not expect to find isotope separation. This point will be discussed below. It obviously was imperative and a matter of considerable interest to obtain further information, in particular on the point as to whether the solid crystal was a necessary condition or whether the solid glassy state would suffice.

Capron and Crevecoeur[9] recently have reported different retentions for the two isomers of Br^{80} in bromobenzene at room temperature. Their results were 50±6 percent for the 18-min Br^{80} and 65±3 percent for the 4.4-hrs Br^{80m}. On the other hand, no difference beyond error of about 2 percent was found in isopropyl bromide and we note that we have obtained similar results for normal propyl bromide on comparing Tables I and II in obtaining the data for which the different isomers were employed. The results are rather definitely in disagreement though the errors are rather uncomfortably large in the bromobenzene case. Possibly the use of relatively unpurified reagents could account for the difference in that the longer lived Br^{80m} of 4.4-hr half-life would have more opportunity to react with impurities to form organic molecules and raise the retention than would the shorter lived, 18-minute Br^{80}.

The retention values and the values of a special function used for the determination of the relative retentions for the two isotopes Br^{80m} and Br^{82} for both crystalline and glassy solid alkyl bromides are listed in Tables III and IV. The 18-minute isotope Br^{80} was not studied in this research since the earlier result on isopropyl bromide[2] had shown no separation between it and the 4.4-hour Br^{80m}. The special function is defined as

$$F=\frac{(\text{organic activity of } Br^{80m})\,(\text{inorganic activity of } Br^{82})}{(\text{inorganic activity of } Br^{80m})\,(\text{organic activity of } Br^{82})}.$$

[9] P. Capron and E. Crevecoeur, J. chim. phys. **49**, 29 (1952).

TABLE III. Retention and F values for crystalline alkyl bromides at −196°C.

Compound	Percent Br^{82}	Retention Br^{80m}	F
n-propyl bromide	86.3	78.3	0.573
n-propyl bromide	85.6	77.6	0.583
n-propyl bromide	87.2	78.4	0.532
n-propyl bromide	87.5	78.2	0.523
Average	86.7	78.2	0.55
Isopropyl bromide	92.9	82.4	0.361
Isopropyl bromide	92.8	84.2	0.415
Isopropyl bromide	93.4	81.4	0.312
Average	93.0	82.9	0.36
n-butyl bromide[a]	92.1	83.9	0.451
n-amyl bromide	79.5	77.0	0.865
n-amyl bromide	82.3	80.5	0.885
Average	80.9	78.8	0.88
Lauryl bromide	79.2	68.5	0.572
Carbon tetrabromide	86.8	86.9	1.011
Carbon tetrabromide	86.7	87.2	1.048
Carbon tetrabromide[b]	90.0	91.4	1.167
Carbon tetrabromide[b]	82.2	88.5	1.229

[a] This run was performed with the polonium-beryllium source; all others with the cyclotron.
[b] These two runs were not dried as rigorously before irradiation as the first two listed.

This function is very sensitive to any separation of the isotopes between the two phases. A 5 percent range between 0.95 and 1.05 is indicative that there has been no separation between the two isotopes.

It seems clear from these results that the glassy state like the liquid state does not show isotope separation.

The data of Table III show that isotope separation is a fairly general phenomenon for the crystalline alkyl bromides. The CBr_4 showed no separation as was expected. The differences in magnitude of the results of the separations for the various compounds is best shown by the values of the function F.

V. DISCUSSION

Absence of Radiation Interference

The question of whether one should expect radiation interference with hot atom phenomena at the radiation

TABLE IV. Retention and F values for alkyl bromide glasses at −196°C.

Compound	Percent Br^{82}	Retention Br^{80m}	F
n-butyl bromide	66.8	66.4	0.981
n-amyl bromide	71.5	72.1	1.033
n-amyl bromide	70.6	70.2	0.981
n-amyl bromide	77.9	78.3	1.030
Average	73	73	1.01
Isoamyl bromide[a]	...	...	1.010
Isoamyl bromide	82.5	83.4	1.067
1-Br-2-Me-butane	83.5	82.8	0.950
1-Br-2-Me-butane	81.6	80.4	0.923
1-Br-2-Me-butane[b]	81.8	81.9	1.01
1-Br-2-Me-butane[b]	82.5	82.9	1.03
Average	82.4	82.0	0.97

[a] The retention values could not be calculated because of a spill.
[b] These runs were performed with the polonium-beryllium source. All others were cyclotron irradiated.

levels normally encountered with Ra-Be and cyclotron sources turns principally on two points. The first is the lifetime of the radioactive atom as a free agent before its fate is settled by combination with some free radical or by exchange with some inorganic species present in large abundance. The second point is the life time of free radicals in general that may be generated by the gamma radiation. If the time elapsed before the fate of the radioactive atom is settled is sufficiently short, the radiation density necessary to insure a sufficiently high concentration of free radicals in the steady state to insure a finite chance of reaction for the radioactive atom with such an extraneous radical will be enormous. According to the present notions, the likelihood of the radioactive atom's moving through more than a dozen or so solvent cages before suffering a de isive reaction is remote. The time involved in such a career can hardly exceed 10^{-8} second. We therefore must expect that in every 100 molecules or so there will be at least one free radical produced by the general gamma radiation every 10^{-8} second. This corresponds, however, to the high radiation flux of about 1 million roentgens per second, unattainable except in atomic explosions. In calculating this approximate flux corresponding to the free radical production density of 1 in every 100 molecules every 10^{-8} second, we have assumed a minimum of 4 ev to be necessary for the production of each pair of free radicals and taken a standard roentgen unit as 100 ergs per cc of condensed alkyl halide.

Of course it may be that the fate of the radioactive atoms is not settled so quickly, and slower processes will allow interference by lower gamma-ray fluxes. However, it is clear from this type of calculation that the assumption of times unreasonably long will be necessary to predict radiation chemical interference at densities below 1000 roentgen/hour.

A much more likely mechanism for radiation interference is that the molecular forms into which the radioactive atom normally settles after its life as a hot atom are susceptible of attack by products of the radiation decomposition of the general medium. It is quite possible that some of the observed effects in the atomic reactors are due to this type of interference. The alkyl bromides ought to be particularly free of this kind of attack, and we might well expect that these systems would be useful in atomic reactors of the highest fluxes for the preparation of radiobromine of high specific activity, not by the utilization of the aqueous soluble fraction which will be diluted by radiation decomposition but by the fractional distillation of a particular organic bromide different from that irradiated, e.g., *n*-propyl bromide from irradiated isopropyl bromide might be obtained at extreme specific activities and in good yield—some 30 percent[6] if the irradiation were conducted in the solid state.

For these reasons we do not find the experimental results in this research surprising. It is rather that radiation interference in the alkyl halide systems is extremely unlikely. This does not mean, however, that systems susceptible of reaction between the radiation decomposition products of the medium as a whole and the likely hot atom products will not show serious effects with some of the ordinary neutron sources.

Isotope Separation

Why should isotope separation be expected only in the crystalline solid? If one envisages that the recoiling bromine atoms possess a certain range, the solid will be melted along the track, the volume melted being larger at the beginning of the track and tapering down towards the end because the rate of liberation of energy will be larger the higher the kinetic energy of the hot atom, providing the mechanism is purely collisional.[6,9] For reasons elaborated earlier[6] we expect that the nature of the reactions occurring at the end of the range will be different from those occurring along the track—the former being in the "epithermal" class where collisions between the recoiling atoms and the solvent molecules as a whole become possible because the chemical bond energies no longer are negligible as compared to the hot atom energy, and the latter being in the "hot" range where chemical bond energies are taken as being negligible. The epithermal products will involve hydrogen substitution and polymer formation because carbon-hydrogen bond rupture is relatively likely in the epithermal type of process. It has been observed[6] that solidification of the propyl bromides greatly enhances certain types of hot atom products falling into this classification, the enhancement occurring mainly with the epithermal products which we have hypothesized are formed at the end of the hot atom's track. In other words, the yield of the epithermal products is increased by several fold in passing from the liquid to the solid phase, while the "hot" products are enhanced relatively less. The enhancement appears to be discontinuous at the melting point, and the retentions in the two phases appear to be quite independent of temperature for the propyl bromides.

On the basis of these notions, what would one expect the relative retentions for two bromine isotopes of different ranges being produced in the solid phase to be? It is quite clear that the enhancement of the epithermal products is probably due to the confinement of the rather dense free radical cloud formed at the end of the track so that fruitful recombination of the radioactive bromine atom is more likely. If this be so, the longer the track itself, i.e., the higher the recoil energy of the isotope, the less the chance of the bromine atom's living through all the collisions to reach the epithermal range, and therefore the less the phase enhancement of its overall retention. In particular, also, the less will be the enhancement of those hydrogen substitution and polymeric products characteristic of the epithermal

reaction so suceptible of phase enhancement. We predict and expect, therefore, that the bromine isotopes with the larger recoil energies will show the lower retentions in the solid phase despite the fact that they appear to show nearly the same retentions in the liquid and that the effect will be largest for the epithermal products. This latter point has not been tested.

The explanation can be stated in other words: The energy liberated by the recoiling atom melts a drop in the crystal. If the hot radioactive atom makes a head on collision and passes its momentum on to another nonradioactive bromine atom, the heating process and the physical tracing out of the track continues except that the radioactive bromine atom is now left behind in the center of the molten drop, so that it is physically surrounded by an assemblage of molecules and radicals not too dissimilar from that characteristic of its situation in the liquid state. On this basis we expect relatively little effect of change in phase on those products formed in the hot range and therefore no isotope separation in this range. At the end of the track, however, the smaller diameter molten drop is filled with a high density of free radicals which are better contained because the drop is smaller itself and more nearly surrounded by a solid crystalline wall. The yields of epithermal products are therefore high in the solid. For bromine atoms having different recoil energies, the ones with the lower energy should have the better chance of reaching the end of the range and showing a higher over-all retention and particularly high yields for the epithermal products.

The glassy state will be different from the crystalline in that the melting process will involve relatively little change in volume and therefore a much smaller heat of fusion. In other words the molecules are in essentially the same positions physically as they would have been in the liquid state. All that is needed is that energy be supplied them so that their amplitudes of vibration can be increased. It follows, therefore, that the size of the molten drop produced by the recoiling hot atom in the frozen glass will be much greater than that in the crystal and we should therefore expect relatively lower enhancement in retention and in particular a smaller isotope separation. The data of Tables III and IV are comparable for *n*-butyl bromide and *n*-amyl bromide. In these two cases, the retention in the glassy state is less than in the crystalline.

THE JOURNAL OF CHEMICAL PHYSICS VOLUME 21, NUMBER 9 SEPTEMBER, 1953

The Existence of Multiply Charged Molecular Ions of HBr, HCl, and DCl

W. H. JOHNSTON
Department of Chemistry, Purdue University, Lafayette, Indiana*
AND
J. R. ARNOLD
Institute for Nuclear Studies and Department of Chemistry, University of Chicago, Chicago, Illinois
(Received March 3, 1953)

Experimental evidence is presented for the DCl^{+1}, HCl^{+1}, DCl^{+2}, and HBr^{+2} molecular ions, using a modified Consolidated-Nier mass spectrometer. Although Cl^{+3}, Br^{+3}, and A^{+3} were observed, no evidence was obtained for $H^{1,2}Cl^{+Z}$, or HBr^{+Z} above $Z=2$. This result contradicts the recent calculations of Magee and Gurnee[2] that HBr^{+3} and HBr^{+4} would be stable toward dissociation. Finally a crude calculation is done assuming hydrogen 1*s* atomic orbitals which agrees amusingly with the experiments.

INTRODUCTION

RECENTLY Hamill and Young[1] stated that only a fraction of HBr^{80}_{gas} and DBr^{80}_{gas} bonds are ruptured following isomeric transition. In an effort to understand this mechanism, Magee and Gurnee[2] have calculated approximate potential energy curves for various molecular ions HBr^{+Z}. Their calculations show that these ions are stable with respect to the dissociation process for Z equal to 1, 2, 3, and 4.

$$HBr^{+Z} \rightarrow H^{+} + Br^{+(Z-1)}. \quad (1)$$

The theoretical existence of attractive states for the HBr^{+Z} molecules is used in support of Hamill and Young's mechanism.[1]

This paper describes an experimental search for the HBr^{+Z}, HCl^{+Z}, and DCl^{+Z} molecular ions using a mass spectrometer. If electrons of sufficient energy are used to produce the molecular ions and if these ions are stable, they should appear at the appropriate points on the mass spectrum.

EXPERIMENTAL

Hydrogen bromide was obtained from the Matheson Company. The deuterium chloride and hydrogen chloride which were analyzed together were prepared by hydrolysis of silicon tetrachloride or benzoyl chloride

* This work was supported in part by the U. S. Atomic Energy Commission under Contract No. At(11-1)-166 with Purdue University.
[1] W. H. Hamill and J. A. Young, J. Chem. Phys. **20**, 888–894 (1952).
[2] J. L. Magee and E. F. Gurnee, J. Chem. Phys. **20**, 894–898 (1952).

with water and deuterium oxide from the Stewart Oxygen Company.

The measurements were made with a modified Consolidated-Nier isotope ratio mass spectrometer, Model 21–201. The inlet system had been modified previously[3] by the addition of a second manifold utilizing a mercury diffusion pump, liquid nitrogen trap, and low-pressure inlet which avoided the usual fine copper capillary.

The voltage of the ionizing electron beam was made variable by the insertion of a battery supply in the gun circuit. Voltages from 83 to 153 could be achieved in steps of 3 volts.

Using various magnetic counter settings the relevant peaks were focused on one of the collectors (number 2) of the mass spectrometer. The voltages in millivolts developed across the collector resistance (4×10^{10} ohms) at each mass peak or fractional mass peak were recorded.

The hydrogen halides tended to desorb gas from the walls of the sampling manifold and analyzing tube resulting in a "dirty" spectrum. The air and water peaks were especially strong.

Molecular Ions of HCl and DCl

The search for HCl^{+2} ions was complicated by the water peaks. For this reason a mixture of DCl and HCl was analyzed, since water did not mask the half-integral peaks. On first introducing a sample of DCl, only the HCl spectrum could be seen—the apparatus had to be "deuterated" for some hours before equilibrium was reached.

The data on HCl and DCl are shown in Table I for various ionizing voltages and magnetic counter settings. In the last column are given the principal ions of the spectrum.

TABLE I. Search for HCl^{+z} and DCl^{+z}.

Accel. voltage	Mass peak	Peak size in millivolts: Sample 1 83 v	Sample 2 83 v	Sample 3 129 v	Sample 4 153 v	Principal ions
A. Magnetic counter setting of 1200 and ionizing voltages of 83, 129, and 153						
552	40	53				$(A^{40})^+$
567	39	6550	4440	4300	3250	$(DCl^{37})^+$
581	38	7350	4900	7600	4550	$(HCl^{37})^+$
595	37	24 100	16 400	16 000	12 000	$(DCl^{35})^+$, $(Cl^{37})^+$
613	36	25 200	16 900	26 300	15 600	$(HCl^{35})^+$
630	35	4800	3800	3800	2580	$(Cl^{35})^+$
688	32	460	460	1950	820	$(O_2^{16})^+$
781	28	3300	3100	12 200	5600	$(N_2^{14})^+$
1124	19.5	87	75	68	36	$(DCl^{37})^{+2}$
1149	19.0	1850	1630	2320	640	$(HDO^{16})^+$, $(HCl^{37})^{+2}$
1183	18.5	810	720	745	380	$(DCl^{35})^{+2}$, $(Cl^{37})^{+2}$
1212	18.0	1550	1370	1980	580	$(H_2O)^+$, $(DO)^+$, $(HCl^{35})^{+2}$
1251	17.5	1680	1520	1680	860	$(Cl^{37})^{+2}$
1281	17.0	340	296	455	125	$(HO)^+$
1553	14.0		260	1020	440	$(N_2^{14})^{+2}$, $(N^{14})^+$
1628	13.33		0	1.5	0.5	$(A^{40})^{+3}$
1666	13.0		13	12	4.5	$(HC)^+$, $(26)^{+2}$ [b]
1700–1709	12.67		0	0[a]	0[a]	$(HCl^{37})^{+3}$
1747	12.33		0	4.5	3.5	$(Cl^{37})^{+3}$
1798	12.0		27	33	13	$(C^{12})^+$
1847	11.67		0	15	13	$(Cl^{35})^{+3}$
B. Magnetic counter setting of 875 and ionizing voltage of 153						
605	20				350	$(D_2O)^+(A^{40})^{+2}$
622	19.5				23	$(DCl^{37})^{+2}$
637	19.0				450	$(HDO)^+$, $(HCl^{37})^{+2}$
654	18.5				242	$(DCl^{35})^{+2}$, $(Cl^{37})^{+2}$
672	18.0				400	$(H_2O)^+$, $(DO)^+$, $(HCl^{35})^{+2}$
693	17.5				510	$(Cl^{35})^{+2}$
709	17.0				87	$(HO)^+$
753	16.0				95	$(O_2)^{+2}$, $(O)^+$
859	14.0				410	$(N_2^{14})^{+2}$, $(N^{14})^+$
900	13.33				0.5	$(A^{40})^{+3}$
921	13.0				2.5	$(CH)^+$,$(26)^{+2}$
940–955	12.67				0[a]	$(HCl^{37})^{+3}$
971	12.33				2.5	$(Cl^{37})^{+3}$
1010	12.0				8	$(C^{12})^+$
1041	11.67				8	$(Cl^{35})^{+3}$
1220–1390	9.75–8.75				0[a]	$(H^{1,2}Cl^{35,37})^{+4}(Cl^{35,37})^{+4}$
1500	8.0				1.5	$(O^{16})^{+2}$
1520–1680	7.8–7.2				0[a]	$(H^{1,2}Cl^{35,37})^{+5}(Cl^{35,37})^{+5}$
1700	7.0				2.5	$(N^{14})^{+2}$

[a] Less than 0.1 mv.
[b] Less than 0.1 mv. Suggestion of trace of "decompositions" on both sides of indicated peak.

[3] W. H. Johnston and Robert E. Martin, J. Chem. Phys. **20**, 534 (1952).

The data of Table I show clearly the presence of HCl^{+1}, DCl^{+1}, and DCl^{+2}. The ion, HCl^{+2}, undoubtedly occurs also; however, it is masked by the water peaks. There is no evidence for the +3, +4, or +5 molecular ions. This is particularly interesting since the trivalent ions of Cl^{35}, Cl^{37}, and A^{40} were formed with ionizing voltages of 129 or 153 volts.

The normal abundance of about 24.6 percent Cl^{37} in chlorine provides a check of the peak assignments given in Table I. Thus the peak fractions 38 to (38+36) are 0.226, 0.225, 0.224, and 0.226 for samples 1, 2, 3, and 4, respectively. Likewise the peak fractions of 12.33 to (12.33+11.67) are 0.23 and 0.27 for samples 3 and 4 where the ionizing potentials were sufficient to produce Cl^{+3}. Furthermore a check can be made on the amount of $(DCl^{35})^{+2}$ in mass peak 18.5 by using the above experimental value of 0.225 and the $(Cl^{35})^{+2}$ peak (17.5) to obtain the contribution from $(Cl^{37})^{+2}$. When these values are subtracted from peak 18.5, the $(DCl^{35})^{+2}$ values are 323, 279, 258, and 130 for samples 1, 2, 3, and 4 in Table I. Compared with the $(DCl^{37})^{+2}$ values of peak 19.5, the isotope fractions of Cl^{37} are 0.21, 0.21, 0.21, and 0.22, respectively. The difference between these ratios and the known isotope fractions checks with the expected fractionation of our leak system.

Molecular Ions of HBr

The data of the search for molecular ions of HBr are shown in Table II. Three magnetic counter settings and two ionizing potentials were used. It is clear that HBr^{+1} and HBr^{+2} were detected. No evidence, however, was obtained for HBr^{+3} or HBr^{+4}, although the corresponding atomic ions of bromine were observed.

As in the case of chlorine, the ratio of the isotopes of bromine provides a check of the peak assignments in Table II. In the case of Br^{+3}, which appeared with an ionizing potential of 153 volts, the ratio of $(Br^{81})^{+3}$ to $(Br^{79})^{+3}$ is normal if correction is made for

TABLE II. Search for HBr^{+Z}.

Accel. voltage	Mass peak	Peak in millivolts Sample 1 83 v	Sample 2 83 v	Sample 3 83 v	Sample 4 153 v	Principal ions
		A. Magnetic counter setting of 7000 and ionizing voltage of 83				
730	82	5300	5900			$(HBr^{81})^{+1}$
738	81	2350	2700			$(Br^{81})^{+1}$
746	80	5600	6400			$(HBr^{79})^{+1}$
754	79	2400	3000			$(Br^{79})^{+1}$
1444	41.0	280	440			$(HBr^{81})^{+2}$
1462	40.5	275	570			$(Br^{81})^{+2}$
1480	40.0	700	620			$(HBr^{79})^{+2}$, $(A^{40})^{+1}$
1498	39.5	265	600			$(Br^{79})^{+2}$
1836	32	5450	2750			$(O_2^{16})^{+1}$
		B. Magnetic counter setting of 3500 and ionizing voltages of 83 and 153				
1224	41.0		460	960	1200	$(HBr^{81})^{+2}$
1239	40.5		560	1260	2280	$(Br^{81})^{+2}$
1253	40.0		610	1210	1480	$(HBr^{79})^{+2}$, $(A^{40})^{+1}$
1272	39.5		620	1300	2380	$(Br^{79})^{+2}$
1556	32.0		1500	3400	3400	$(O_2^{16})^{+1}$
1768	28.0		3950	18 300	18 200	$(N_2^{14})^{+1}$
1816	27.33		0[a]	0[a]	0[b]	$(HBr^{81})^{+3}$
1833	27.0		78	102	340	$(Br^{81})^{+3}(27)^{+1}$
1850–1860	26.67		0[a]	0[a]	0[b]	$(HBr^{79})^{+3}$
1874	26.33		0[a]	0[a]	245	$(Br^{79})^{+3}$
1896	26.0		24	50	45	$(26)^{+1}$
		C. Magnetic counter setting of 2000 and ionizing voltage of 153				
927	41.0				1050	$(HBr^{81})^{+2}$
937	40.5				1920	$(Br^{81})^{+2}$
948	40.0				1270	$(HBr^{79})^{+2}$, $(A^{40})^{+1}$
960	39.5				2000	$(Br^{79})^{+2}$
970	39.0				36	$(DCl^{37})^{+1}$ [c]
1354	28.0				14 100	$(N_2^{14})^{+1}$
1375–1385	27.33				0[b]	$(HBr^{81})^{+3}$
1405	27.0				295	$(Br^{81})^{+3}$, $(27)^{+1}$
1421	26.67				0[b]	$(HBr^{79})^{+3}$
1439	26.33				213	$(Br^{79})^{+3}$
1456	26.0				36[a]	$(26)^{+1}$
1800–1850	20.5				0[b]	$(HBr^{81})^{+4}$
1858	20.25				1.5	$(Br^{81})^{+4}$
1877	20.0				84	$(A^{40})^{+2}$
1898	19.75				2	$(Br^{79})^{+4}$
1970	19.0				112	$(HDO)^{+1}$

[a] Less than 0.1 mv.
[b] Less than 0.1 mv. Suggestion of trace of "decompositions" on both sides of indicated peak.
[c] Small amount of DCl present from adsorption in previous runs.

TABLE III. Theoretical binding energies for HBr^{+z}. (Expressed in atomic units.)

Species	Binding energy	Conclusion
HBr^{+4}	+0.062124	Unstable
HBr^{+3}	+0.028939	Unstable
HBr^{+2}	−0.004246	Stable
HBr^{+1}	−0.037431	Stable
HBr^{+0}	−0.070615	Stable[a]

[a] Note the comparison for Z = 0 with the experimental value of 0.138 au.

the 27.0 background (sample 3) which was observed at 83 volts ionizing potential.

DISCUSSION

In these experiments the molecular ions of charge +3 or greater were not observed, although the tri-positive atomic ions were observed in good yield. It is clear, however, that sufficient ionization energy was used to produce the tri-positive molecular ions. The transit time in the mass spectrometer is of the order of 30 microseconds, and any species formed by ionization, with a lifetime of this magnitude or greater, should appear.

We conclude that the ions HCl^{+3}, DCl^{+3}, and HBr^{+3}, and the corresponding +4 and +5 ions, are unstable, or metastable with lifetimes shorter than 30 microseconds.

It is physically extremely plausible that molecular ions should become more unstable as the charge is increased, and that a "crossover" should occur beyond which even metastability becomes impossible, due to increased Coulomb repulsion. The calculation of Gurnee and Magee does not show such an effect, but in view of the little progress made thus far in calculating bond energies in molecules, the failure of their Heitler-London type calculation is not astonishing.

It is interesting to attempt a much simpler quantum mechanical approximation. We will assume 1*s* hydrogen atomic orbitals and use a two electron model for HBr^{z}. The electronic energy is

$$E=-\frac{1}{1+I_{00}}\{Z'(G_0+z)+z^2I_{00}^2 +2I_{00}J_0(Z'-z)-z^2-K_{00,00}-L_{00,00}\}, \quad (1)$$

where Z' is the sum of the nuclear charges (equal to the ion charge +2), z is the exponential charge taken as 1, and the integrals are taken from Hirschfelder and Linnett,[4] and Roothaan.[5]

We shall employ the usual expression for the binding energy,

$$\text{B.E.}=E+(Z_AZ_B/R)-z^2+zZ', \quad (2)$$

where E is the electronic energy [Eq. (1)], Z_AZ_B is the product of the nuclear charges (equal to $Z'-1$), z is again the exponential charge equal to 1, and R is the internuclear distance, fixed at 2.50 Bohr radii, the value for HBr.

This equation was evaluated for the hydrogen bromide ions, +1, +2, +3, +4, and the neutral molecule. As shown in Table III the crossover from stability to instability occurs between HBr^{+2} and HBr^{+3}, in agreement with experiment, while the binding energy of HBr is within a factor of 2 of the experimental value.

Although this calculation is more amusing than significant because of its crudity, the comparison with Magee and Gurnee's calculation and with our experimental measurements serves to emphasize the dangers inherent in the interpretation of any quantum treatment which has been greatly simplified.

ACKNOWLEDGMENTS

The authors wish to thank Dr. C. R. Mueller of Purdue University for suggesting the form of the quantum-mechanical calculation and Mr. John Walton[6] for assisting with the modification of the ionizing potential of the mass spectrometer.

[4] J. O. Hirschfelder and J. W. Linnett, J. Chem. Phys. **18**, 130-142 (1950).

[5] C. C. J. Roothaan, J. Chem. Phys. **19**, 1445-58 (1951).

[6] U. S. Atomic Energy Commission research assistant at Purdue University.

Rotational Line-Width Measurements on NO, HCl, and HBr*

D. WEBER AND S. S. PENNER†
Jet Propulsion Laboratory, California Institute of Technology, Pasadena, California
(Received April 6, 1953)

Quantitative measurements of apparent rotational line half-widths are described for NO, HCl, and HBr. Theoretical relations, which apply to vibration-rotation bands with spectral lines of uniform half-width and Lorentz contour, have been used to obtain apparent rotational half-widths from experimental data for CO and for NO.

I. INTRODUCTION

APPARENT line-width measurements on diatomic gases are of interest in connection with attempts to calculate emissivities from spectroscopic data. They also enter into the interpretation of spectroscopic studies of combustion flames whenever concentration or temperature analyses are involved. The present paper contains new experimental measurements on NO, HCl, and HBr. Rotational half-widths‡ are calculated from the experimental data on the assumption that the rotational lines are described by the Lorentz collision formula and are of uniform half-width for a given vibration-rotation band. For CO and NO it has been found that the experimental data can be fitted to the assumed line shape. Some of the measured transmission values for HCl and HBr, however, cannot be correlated quantitatively. The results of the present investigations are summarized in Table I.

TABLE I. Rotational half-width estimates for CO and NO.

Infrared-active gas	Added gas	Apparent half-width of fundamental (cm^{-1} $atmos^{-1}$)	Apparent half-width of first overtone (cm^{-1} $atmos^{-1}$)
CO	H_2	0.064	0.065
	He	0.026	···
	A	0.031	···
	···	0.061	0.076[a]
NO	He	0.031	···
	···	0.043	0.025

[a] The value $b=0.076$ cm^{-1} $atmos^{-1}$ for the first overtone of CO is based on an extrapolation to zero slit width using measurements of b as a function of experimental slit width. W. S. Benedict and S. Silverman have studied the first overtone of CO with greatly improved resolution and have reported $b=0.095$ cm^{-1} $atmos^{-1}$ for self-broadening (paper presented at the Symposium on Molecular Structure and Spectroscopy, Columbus, June, 1952). Treatment of experimental data involves the assumption that the apparent integrated transmission can be used in place of the true integrated transmission. In this connection reference should be made to the exhaustive work of Nielsen, Thornton, and Dale, Revs. Modern Phys. **16**, 307 (1944). It was found experimentally that the apparent rotational half-width decreased somewhat as the experimental slit width was increased.

* This paper presents the results of one phase of research carried out at the Jet Propulsion Laboratory, California Institute of Technology, under Contract No. DA-04-495-Ord 18, sponsored by the U. S. Army Ordnance Department.

† Present address: Guggenheim Jet Propulsion Center, California Institute of Technology, Pasadena, California.

‡ The term rotational half-width is used in the present paper to denote one-half of the wave-number range for which the spectral absorption coefficient exceeds one-half of the maximum value for a given rotational transition.

II. BASIC RELATIONS

A simple method for the determination of rotational half-widths b of collision-broadened rotational lines, which do not overlap, has been described in previous publications.[1] The method involves the use of transmission measurements and is based on the assumption that the rotational half-widths are uniform across a given vibration-rotation band. The numerical calculations needed to determine half-width data are obviated by using a simple approximate evaluation, which will generally lead to half-widths which are somewhat too small.[2] However, by choosing the optical density X in the experimental studies in such a way that $S_{j\to j'}^{0\to n}X/2\pi b$ (here $S_{j\to j'}^{0\to n}$ represents the integrated absorption for the rotational transition $j\to j'$ and the vibrational transition $0\to n$) is greater than about three for the more intense rotational lines, line-width data which are correct to better than 10 percent can be obtained as long as the basic assumptions remain satisfied.

The useful relations[2] are obtained from the expression,

$$\int_{\Delta\omega}(R_{a\omega}/R_{s\omega})d\omega = (\alpha bX)^{\frac{1}{2}}(\gamma u)^{-\frac{1}{2}}[4.1(2)+6.1(0)\beta\lambda(\gamma u)^{\frac{1}{2}}], \quad (1)$$

where $R_{a\omega}$ and $R_{s\omega}$ denote, respectively, the spectral intensities absorbed by the uniformly distributed gases and emitted by the light source; $\Delta\omega$ (in cm^{-1}) is the effective width of the vibration-rotation band under study; α is the integrated absorption; b is the rotational half-width; $\gamma\equiv B_e/\omega_e$ represents a well-known spectro-

TABLE II. Spectroscopic constants for CO, NO, HCl, and HBr.[a]

Molecule	$\gamma\times10^3$	ω^*, cm^{-1}	u at 300°K	$(\gamma u)^{-\frac{1}{2}}[4.1(2)+6.1(0)(\gamma u)^{\frac{1}{2}}]$
CO	0.9011	2143.1	10.28	13.3
NO[b]	0.895	1876	8.995	14.7
HCl	3.542	2885.7	13.84	8.76
HBr	3.200	2559.3	12.27	9.50

[a] The spectroscopic constants for CO were calculated from the data given by Plyler, Benedict, and Silverman, J. Chem. Phys. **20**, 175 (1952).
[b] Average values were used for the $^2\Pi_{\frac{1}{2}}$ and $^2\Pi_{\frac{3}{2}}$ electronic levels of NO; $\beta=\frac{1}{2}$.

[1] S. S. Penner and D. Weber, J. Chem. Phys. **19**, 1351, 1361 (1951).
[2] S. S. Penner and H. S. Tsien, J. Chem. Phys. **20**, 827 (1952).

TABLE III. Integrated intensities and numerical values of k for CO, NO, HCl, and HBr.

Molecule	Fundamental αp (cm^{-2} atmos^{-1})	Fundamental k (cm^{-1} atmos$^{-\frac{1}{2}}$)	First overtone α_0 (cm^{-2} atmos^{-1})	First overtone k (cm^{-1} atmos$^{-\frac{1}{2}}$)
CO	237	205	1.64	17.0
NO	63	117[a]	2.1	21.3[a]
HCl	150	107	3.68	16.8
HBr	55	70.5	0.70	7.95

[a] Calculated on the assumption that $\beta=\frac{1}{2}$.

scopic constant;[3] $uT=hc\omega^*/k$ is the characteristic temperature corresponding to the $j=0\rightarrow j=0$ rotational and $n=0\rightarrow n=1$ vibrational transition; T is the absolute temperature, which must be close to room temperature; β is an empirically determined parameter which is less than or equal to unity; λ equals the component of electronic angular momentum about the internuclear axis. Useful spectroscopic data for CO, NO, HCl, and HBr are summarized in Table II. In agreement with the notation used in previous publications,[1] the integral appearing on the left-hand side of Eq. (1) will be represented by the symbol $A'\Delta\omega$.

In practice it is possible to evaluate b by utilizing two different types of experimental data. For self-broadening data

$$b\simeq b^0 p_T, \quad X=p_T l,$$

whence

$$d(A'\Delta\omega)/dp_T = (\alpha b^0 l)^{\frac{1}{2}}(\gamma u)^{-\frac{1}{2}}[4.1(2)+6.1(0)\beta\lambda(\gamma u)^{\frac{1}{2}}], \quad (2)$$

where p_T is the total pressure, l equals the optical path length, and b^0 is the rotational half-width at atmospheric pressure.

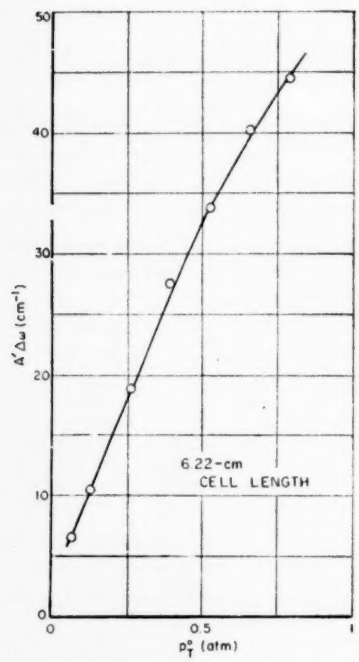

Fig. 1. Dependence of $A'\Delta\omega$ on p_T^0 for the fundamental of NO (self-broadening).

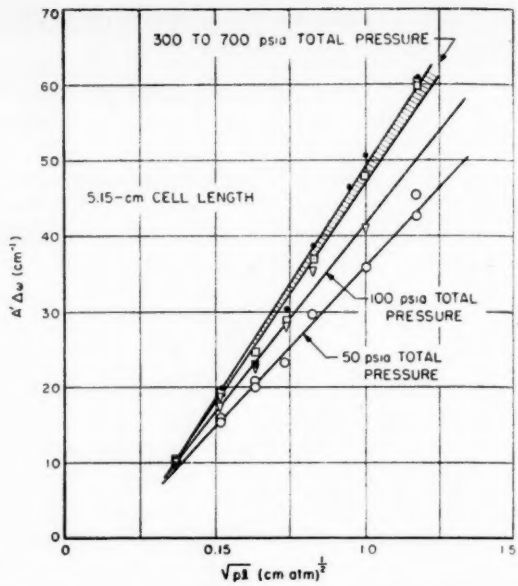

FIG. 2. Dependence of $A'\Delta\omega$ on $(pl)^{\frac{1}{2}}$ for the fundamental of NO pressurized with He.

For experiments at constant total pressure, in which broadening is achieved by an infrared-inactive gas M,

$$b\simeq (b^0)_M p_T, \quad X=pl,$$

whence

$$d(A'\Delta\omega)/d(pl)^{\frac{1}{2}} = [(b^0)_M p_T\alpha]^{\frac{1}{2}}(\gamma u)^{-\frac{1}{2}}[4.1(2)+6.1(0)\beta\lambda(\gamma u)^{\frac{1}{2}}], \quad (3)$$

or

$$d(A'\Delta\omega)/d(p_T)^{\frac{1}{2}} = [(b^0)_M p\alpha l]^{\frac{1}{2}}(\gamma u)^{-\frac{1}{2}}[4.1(2)+6.1(0)\beta\lambda(\gamma u)^{\frac{1}{2}}]. \quad (4)$$

The use of the preceding relations for the determination of line widths of CO, NO, HCl, and HBr is described in Secs. III to VI, respectively. The line-width estimates obtained in Sec. III are not new but are included in order to illustrate the use of Eqs. (2) to (4) for a case in which an accurate numerical evaluation of line widths is available. The equations used for calculating line widths in Secs. III to VI are

$$d(A'\Delta\omega)/dp_T=k(b^0l)^{\frac{1}{2}}, \quad (2a)$$

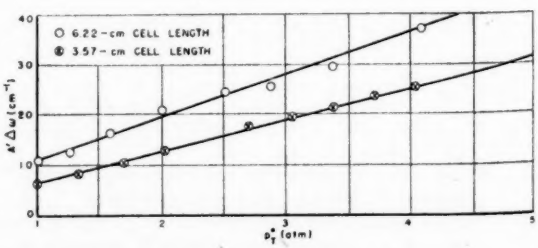

FIG. 3. Dependence of $A'\Delta\omega$ on p_T^0 for the first overtone of NO (self-broadening).

[3] G. Herzberg, *Spectra of Diatomic Molecules* (D. Van Nostrand Company, New York, 1950).

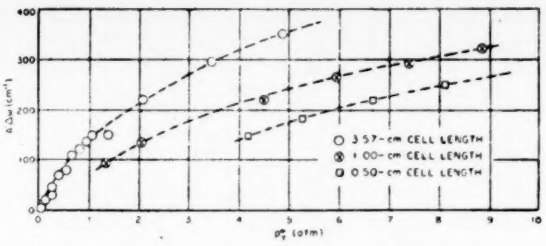

FIG. 4. Dependence of $A'\Delta\omega$ on p_T^0 for the fundamental of HCl (self-broadening).

for self-broadening, and

$$d(A'\Delta\omega)/d(pl)^{\frac{1}{2}}=k[(b^0)_M p_T]^{\frac{1}{2}}, \tag{3a}$$

or

$$d(A'\Delta\omega)/d(p_T)^{\frac{1}{2}}=k[(b^0)_M pl]^{\frac{1}{2}}, \tag{4a}$$

for broadening by infrared-inactive gas M. Here k is a numerical constant for a given vibration-rotation band. It is defined by the relation $k=(\alpha)^{\frac{1}{2}}(\gamma u)^{-\frac{1}{2}}[4.1(2)+6.1(0)\beta\lambda(\gamma u)^{\frac{1}{2}}]$. Numerical values of k for the fundamental and first overtone for each of the gases studied are listed in Table III together with the corresponding values of integrated absorption.[4,5]

III. LINE-WIDTH ESTIMATES FOR CO

From appropriate experimental data[1] and Eqs. (2a) to (4a), the half-widths summarized in Table I are obtained. Comparison with the results of numerical calculations (see reference 1) shows that the approximate line widths calculated by the use of Eqs. (2a) to (4a) are not in error by more than 10 percent.

IV. LINE-WIDTH ESTIMATES FOR NO

In order to compensate partially for extensive overlapping between the rotational lines of the Q branch of NO, it was assumed that $\beta=\frac{1}{4}$. The experimental data§ on NO which were used for the determination of rotational half-widths are plotted in Figs. 1 to 3. Estimated values of the rotational half-width are summarized in Table I.

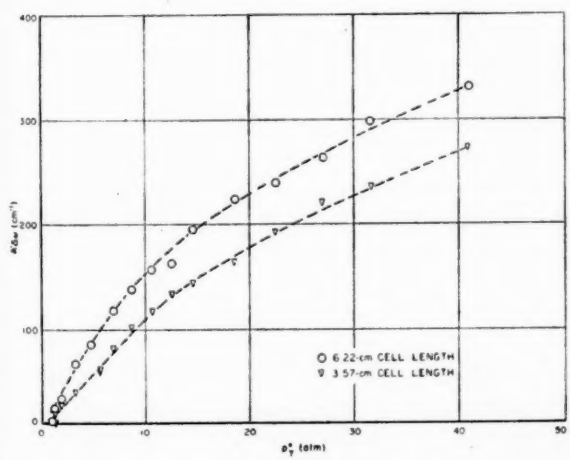

FIG. 5. Dependence of $A'\Delta\omega$ on p_T^0 for the first overtone of HCl (self-broadening).

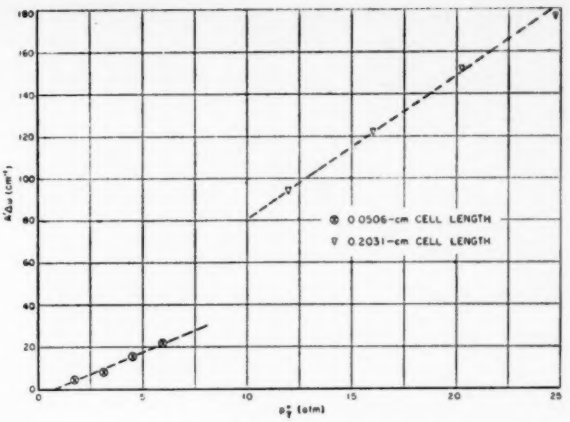

FIG. 6. Dependence of $A'\Delta\omega$ on p_T^0 for the fundamental of HBr (self-broadening).

V. LINE-WIDTH ESTIMATES FOR HCl

The experimental data on HCl are plotted in Figs. 4 and 5. It is evident by reference to Figs. 4 and 5 that the experimental data obtained for HCl are not correlated quantitatively by the Lorentz dispersion formula. This observation is in agreement with the findings of other investigators.[6,7]

VI. LINE-WIDTH ESTIMATES FOR HBr

Representative experimental data on HBr are plotted in Fig. 6. Reference to Fig. 6 shows that the transmission for HBr is not a linear function of the total pressure for self-broadening, i.e., the experimental data are not correlated by the Lorentz collision formula.

TABLE IV. Relation between optical and kinetic theory collision diameters.

Infrared-active gas	Added gas	Optical collision diameter[a] ρ(A)	Kinetic-theory collision diameter[b] σ(A)
CO	...	4.7	3.590
	H_2	2.9	3.279
	He	2.1	3.145
	A	3.4	3.504
NO	...	4.2	3.470
	He	2.5	3.085

[a] Calculated from half-width measurements on the fundamental vibration-rotation band.
[b] Obtained from the data given by Hirschfelder, Bird, and Spotz, Trans. Am. Soc. Mech. Engrs. 71, 921 (1949).

§ The symbol p_T^0 in any of the figures identifies the equivalent total pressure of ideal gas (see reference 5).

[4] S. S. Penner and D. Weber, J. Chem. Phys. **19**, 807, 817, 974 (1951).
[5] S. S. Penner and D. Weber, J. Chem. Phys. **21**, 649 (1953).
[6] E. Lindholm, dissertation, Upsala, 1942.
[7] G. Becker, Z. Physik **34**, 255 (1925).

VII. OPTICAL COLLISION DIAMETERS FOR CO AND NO

The line-width measurements on the fundamentals summarized in Secs. III and IV have been used to estimate optical collision diameters in the usual way. When independent measurements of the half-width were available, average values were used. The calculated optical collision diameters ρ are contrasted in Table IV with the collision diameters σ obtained from transport properties. In accord with the approximations implicit in the treatment of experimental data, the Lorentz equation

$$2b=\rho^2\bar{v}n_1, \tag{5}$$

was used for the calculation of optical collision diameters. Here $\bar{v}$ represents the mean molecular velocity, and n_1 is the number of molecules per unit volume. Reference to the data given in Table IV shows that the optical and transport collision diameters agree reasonably well in some cases.

THE JOURNAL OF CHEMICAL PHYSICS VOLUME 21, NUMBER 9 SEPTEMBER, 1953

Electron Impact Studies of the Vinyl Ion and Radical

F. H. FIELD
Technical and Research Divisions, Humble Oil and Refining Company, Baytown, Texas, and Department of Chemistry, University of Texas, Austin, Texas*

(Received December 11, 1952)

The appearance potentials of the vinyl ion as produced by electron impact from eight different compounds have been measured. The corresponding values of the heat of formation of the vinyl ion vary from 274 to 292 kcal/mole, with an average value of 281.$_5$ kcal/mole. It is pointed out that no definitive explanation for the variation can be given.

The heat of formation of the vinyl radical is found to be 82.$_3$ kcal/mole, which leads to a value of 122 kcal/mole for the first C–H bond dissociation energy in ethylene. The ionization potential of the vinyl radical is 200.$_5$ kcal/mole = 8.6$_9$ ev.

UTILIZING electron impact appearance potential values which have been published in the literature, one can calculate values for the heat of formation of a given ion as formed from several different compounds,[1] as for example, the heat of formation of the methyl ion as produced by electron impact from methane, ethane, methyl radical, etc. One thus finds that from some compounds the values of the heat formation of the given ion are essentially the same (to within 2–3 kcal/mole), while from others the values vary appreciably (as much as 10–20 kcal/mole).

The constancy that can be observed in many cases in the ionic heats of formation is of considerable interest in that the conditions under which the ions are produced in a mass spectrometer hardly appear, at least at first glance, to be conducive to such a result. Furthermore, one does not find these essentially constant values restricted to ions formed by relatively simple dissociation processes such as the fission of one bond. For example, the heat of formation of the $C_3H_3^+$ ions (presumably with the $CH_2=C=C^+H$ structure) formed from allene, propylene, propane, cyclopropane, and *i*-butene are 285, 280, 287, 286, and 290 kcal/mole, respectively.[1] It seems safe to say that agreement of this sort is not to be expected on the basis of the elementary theory of ionization and dissociation under electron impact, according to which the energy values obtained from appearance potentials must always be considered as upper limits to the true values because of the possibility of so-called excess energy in the fragments formed in the dissociation. However, the essential equality of the heats of formation of the $C_3H_3^+$ ion quoted above would thus mean that the amounts of excess energy in several dissociation processes are essentially the same, which would be surprising in view of the fact that the processes differ amongst themselves to a marked extent; or, alternatively, that essentially no excess energy is present.

Measurement of electron-impact appearance potentials provides the only method of determining the energies of gaseous radical-ions and some molecule-ions, and it seems to be an excellent method for the determination of bond dissociation energies and the energies of free radicals. Thus, it is of considerable practical, as well as theoretical, importance that the limitations of the method be correctly assessed, particularly with respect to the problem of excess energy. On the basis of available evidence, there appears to be a real possibility that the role of excess energy has been overestimated in the dissociation of polyatomic molecules. To say this does not, of course, deny the existence of excess energy,

* Present address.

[1] For calculations on several ions see F. H. Field, J. Chem. Phys. **20**, 1734 (1952). A paper giving a comprehensive listing of the heats of formation for all ions for which data is available is in preparation.

for it has been demonstrated experimentally[2] that in certain cases ions are formed with kinetic energy.

It is indeed possible that the discrepancies which are observed in the heats of formation of a given ion [the spread which exists in the values of $\Delta H_f(C_3H_3^+)$ given above is fairly typical] might be the result of excess energy. On the other hand, it is also quite possible that at least some of the discrepancies are the result of experimental error, for the data which may be used to calculate the values for a particular ion have been obtained by a number of different workers using different instruments and techniques. In general, appearance potential measurements are somewhat uncertain in that many of the conditions in the ion source of the measuring instrument are not under the direct control of the operator, and it is not at all inconceivable that variations in these conditions might sometimes occur between one instrument and measuring technique and another to such an extent as to produce the observed variations in the ionic heats of formation. Thus it is of considerable interest to determine the heat of formation of a single species of ion as produced from several different compounds using one mass spectrometer and one technique of measurement. The vinyl ion was chosen for the study reported here because heats of formation of this ion calculated from literature appearance potentials have a very wide spread, ranging from 278 to 310 kcal/mole. In the course of the investigation the heat of formation of the vinyl radical was also determined.

EXPERIMENTAL

The appearance potentials were determined with Westinghouse Type LV mass spectrometers using the vanishing current method. All measurements for the vinyl ion heats of formation were made with the University of Texas instrument; whereas, measurements for the vinyl radical heats of formation were made both with the University of Texas instrument and the Humble instrument. It is gratifying that in spite of the fact that certain of the operating characteristics of the instruments differed, in the cases where measurements on a compound were made with both instruments, the appearance potentials obtained were the same to within the precision of the method.

The procedure used in obtaining the appearance potentials was as follows. The gas yielding the ion under investigation was introduced into the instrument along with the gas used to calibrate the electron voltage scale (Xe for measurements on 3,3-dimethyl-1-butene; Kr for all others), such quantities being used as to yield equal peak heights of the two ions at an electron accelerating voltage of 75 v. With the instrument focusing either of the two ions of interest and starting at an electron accelerating voltage well above the vanishing-current voltage, the electron accelerating voltage was decreased in small steps, noting at each step the deflection of the ion-current galvanometer as the ions were alternately focused and defocused. Three to five deflection measurements were made at each value of the electron voltage. The process was continued until the deflections due to the ions could not be distinguished from random motions of the galvanometer (usually about ± 1 mm). Then without changing any of the conditions in the ion source, the other ion of interest was focused and the process repeated. Large scale plots of the deflections of the ion current galvanometer *vs* the electron accelerating voltage were made and extrapolated through the short distance corresponding to the amplifier "noise" to the electron voltage axis. These intercepts were taken as the vanishing current voltages, and the appearance potential was obtained by combining the difference between the vanishing current voltages with the ionization potential of the calibrating gas (using the value 14.01 ev for Kr and 12.15 ev for Xe). The instrument and method were checked periodically during the course of the measurements by redetermining known ionization potentials. Satisfactory agreement with values quoted in the literature was obtained in all cases.

The instrument conditions which obtained during the measurements were: minimum ion current detectable (1-mm galvanometer deflection above amplifier noise level) $= 1\times10^{-15}$ amp (Humble instrument), 2×10^{-15} (University of Texas instrument); ion pusher (drawout) voltage = 2 v (Humble), 3 v (University of Texas), electron collector voltage = 135 v, electron drawing out potentials (Plates 3 and 4) = 10 and 30 v, respectively; ion accelerating voltage and magnetic field strength adjusted as needed to focus ions; ion source temperature = 75°C (Humble), 215°C (University of Texas).

At least two determinations of each appearance potential were made. For all ions except $C_2H_5^+$ from 1-butene the differences between values obtained from replicate determinations were appreciably less than 0.1 ev, but in view of the somewhat subjective manner in which the vanishing current voltages are determined, the uncertainties are here quoted as ± 0.1 ev. In the case of $C_2H_5^+$ from 1-butene the uncertainty quoted is at least as large as the average deviation of the replicate determinations from the average.

The ethyl chloride and vinyl chloride were obtained from the Matheson Company; the 3,3-dimethyl-1-butene was an A.P.I. Standard sample; and all other compounds were Phillips research grade. No purification of compounds was attempted.

Heats of formation (all at 298°K) needed in this work were taken from the N.B.S. compilation,[3] and the papers of Roberts and Skinner,[4] and Szwarc.[5]

[2] See C. A. McDowell and J. W. Warren, Disc. Faraday Soc. **10**, 53 (1951) and subsequent papers as an example of some quite recent work.

[3] American Petroleum Institute Research Project 44 at the National Bureau of Standards. Selected values of properties of hydrocarbons.

[4] J. S. Roberts and H. A. Skinner, Trans. Faraday Soc. **45**, 339 (1949).

[5] M. Szwarc, Chem. Rev. **47**, 75 (1950).

TABLE I. Appearance potentials and heats of formation of $C_2H_3^+$.

Compound	Number of determinations	Appearance potentials (ev) This work	Literature[a,b]	$\Delta H_f(C_2H_3^+)$ (kcal/mole)	Ionization mechanism[c]
Propylene	3	$13.8_2 \pm 0.1$	14.6 ± 0.3[d]	292	$C_3H_6 \rightarrow C_2H_3^+ + CH_3\cdot$
Ethylene	2	$14.0_4 \pm 0.1$	14.2 ± 0.1[e]	284	$C_2H_4 \rightarrow C_2H_3^+ + H\cdot$
n-butane	3	$14.6_1 \pm 0.1$	14.2 ± 0.3[f]	282[g]	$n-C_4H_{10} \rightarrow C_2H_3^+ + C_2H_5\cdot + H_2$
1-butene	2	$14.9_6 \pm 0.1$	13.6 ± 0.3[h]	281	$1-C_4H_8 \rightarrow C_2H_3^+ + C_2H_4 + H\cdot$
Ethane	2	$15.3_4 \pm 0.1$	15.2 ± 0.2[f]	281	$C_2H_6 \rightarrow C_2H_3^+ + H_2 + H\cdot$
i-butane	2	$14.5_3 \pm 0.1$	14.7 ± 0.3[f]	279[g]	$i-C_4H_{10} \rightarrow C_2H_3^+ + C_2H_5\cdot + H_2$
Ethyl chloride	2	$14.3_5 \pm 0.1$		277	$C_2H_5Cl \rightarrow C_2H_3^+ + H_2 + Cl\cdot$
				276	$C_2H_5Cl \rightarrow C_2H_3^+ + HCl + H\cdot$
Vinyl chloride	3	$12.8_1 \pm 0.1$		274	$C_2H_3Cl \rightarrow C_2H_3^+ + Cl\cdot$
				Av 281.5	

[a] Corrected where necessary for change in ev—kcal/mole conversion factor.
[b] The appearance potentials of the vinyl ions from several of these compounds have been measured by Mitchell and Colemen [J. Chem. Phys. 17, 44 (1949)] and Koffel and Lad [J. Chem. Phys. 16, 420 (1948)]. However, the measurements were made using methods other than the vanishing current method, and thus the results are not comparable with those found in this work.
[c] For simplicity electrons not represented.
[d] J. Delfosse and W. Bleakney, Phys. Rev. 56, 256 (1939).
[e] Kusch, Hustrulid, and Tate, Phys. Rev. 52, 843 (1937).
[f] D. P. Stevenson and J. A. Hipple, J. Am. Chem. Soc. 64, 1588 (1942).
[g] The choice of these two values is somewhat arbitrary in view of the possibility of other mechanisms which give not unreasonable values, i.e.,

$$n-C_4H_{10} \rightarrow C_2H_3^+ + CH_3 + CH_4, \quad \Delta H_f(C_2H_3^+) = 293$$
$$n-C_4H_{10} \rightarrow C_2H_3^+ + C_2H_6 + H, \quad \Delta H_f(C_2H_3^+) = 275$$
$$i-C_4H_{10} \rightarrow C_2H_3^+ + CH_3 + CH_4, \quad \Delta H_f(C_2H_3^+) = 290$$
$$i-C_4H_{10} \rightarrow C_2H_3^+ + C_2H_6 + H, \quad \Delta H_f(C_2H_3^+) = 272$$

[h] D. P. Stevenson, J. Am. Chem. Soc. 65, 209 (1943).

DISCUSSION

The results of the studies on the vinyl ion are summarized in Table I. The only large significant disagreement of the values of the appearance potentials obtained in this study with those obtained by other workers lies in the case of 1-butene, for which Stevenson[6] found a value of 13.6 ev, 1.4 ev lower than ours. Stevenson's appearance potential corresponds nicely to the ionization reaction $1-C_4H_8 \rightarrow C_2H_3^+ + C_2H_5$, $\Delta H_f(C_2H_3^+) = 289$ kcal/mole, and thus is certainly not unreasonable. However, the experiment and data giving rise to the present value have been examined carefully in the light of the discrepancy, and they are simply not compatible with a value as low as 13.6 ev.

It is obvious from an examination of the vinyl ion heats of formation listed in Table I that a variation in the values does exist, and to an extent greater than can be explained comfortably on the basis of experimental error. However, the pattern of variation of the values is of considerable interest in that it is not readily understandable in terms of current theories of molecular dissociation under electron impact. It would appear from this, as well as previously reported work, that the heats of formation of a given ion when formed from most compounds cluster quite closely around an average value, but occasionally sport values occur in a random and unexplainable manner.

The peculiarity of the vinyl ion pattern of variation centers around the fact that the largest variation occurs with the ions formed by single-bond fission (propylene, ethylene, and vinyl chloride), whereas, quite surprisingly, the heats of formation of ions formed by more than single-bond fission (ethane, ethyl chloride, 1-butene, and the butanes) are neither particularly variable nor particularly high.

We adopt the point of view of Eyring and co-workers[7] that ionization and fragmentation of a molecule under electron impact occurs through the initial formation of the molecule-ion, which in turn breaks into fragments after a time relatively long as compared to the periods of molecular vibrations. Further decomposition of the fragments may also occur. In the decompositions of ethane and ethyl chloride, hydrogen molecules (possibly HCl in the latter case) are formed along with the ions, and consequently somewhere in the course of the decompositions processes akin to four-center reactions must occur. If one makes an analogy with the reactions of unionized substances one might expect an appreciable activation energy for such a process,[8] but since the activation energy would contribute to the appearance potential and heat of formation of the ion formed, it must be concluded from Table I that the activation energy of the four-center reaction is not larger than that of a simple-bond fission and might well be essentially zero.

Now let us consider the relatively large variation in the heats of formation of the ions formed by single-bond fission, concentrating attention for the moment on possible explanations for the high value found with propylene. Propylene obviously differs from ethylene and vinyl chloride in that the dissociation with which we are concerned yields a radical as a neutral fragment instead of a single atom. Thus it can be argued that the

[6] D. P. Stevenson, J. Am. Chem. Soc. 65, 209 (1943).

[7] Rosenstock, Wahrhaftig, and Eyring, *The Mass Spectra of Large Molecules. II. The Application of Absolute Rate Theory.* Technical Report Number II, University of Utah, Institute for Study of Rate Processes, Salt Lake City.

[8] The analogy must be made with some caution because of the polarization of the activated state of the ion by the formal charge,

propylene heat of formation is high either because the appearance potential corresponds to the formation of the methyl radical in a tetrahedral configuration, or because it includes any energy of activation involved in the breaking off of the methyl group or possibly both. However, such an argument should be quite generally applicable, and if it is to be accepted in this particular case, one should find uniformly high values of heats of formation when radicals or fragment ions are formed from molecules by electron impact. That this is not so is shown by the fact that bond dissociation energies obtained by electron impact are in excellent agreement with those obtained by other methods, and perhaps even more conclusively, by the fact that heats of formation of methyl and ethyl ions produced by the dissociation of organic molecules are in excellent agreement with the values obtained by the direct ionization of free methyl and ethyl radicals.

The activation energy part of the argument may be objected to on other grounds. Except for a polarization effect, the recombination of a vinyl ion and methyl radical to form the propylene molecule-ion is probably not appreciably different in character from free radical recombination reactions, which according to Steacie[9] occur with "small" (presumably essentially zero) activation energies. Indeed, the absence of activation energies in electron impact reactions such as that by which vinyl ion is produced from ethane makes it difficult for one seriously to entertain the possibility of appreciable activation energies in the propylene decomposition reaction. It is also of interest that the absence of reorganizational activation energy of the unionized fragment does not in itself insure agreement of ionic heats of formation, as can be seen from the vinyl ion values from ethylene and vinyl chloride.

Making use of Eyring's concept of the decomposition of molecules under electron impact, it is easy to rationalize the fact that in general appearance potentials do not correspond to the formation of fragments in strained, nonequilibrium configurations. If the decomposition of the molecule-ion formed initially by the impact of the bombarding electron is delayed for an appreciable time, as has been proposed, there exists ample opportunity for changes in the atomic configuration of the molecule-ion and for the transfer of energy between its parts. Qualitatively, the propylene molecule-ion dissociation of interest here might be looked upon as occuring through a mode of vibration wherein the dissociative elongation of the methyl carbon-vinyl carbon bond is accompanied by a simultaneous, synchronized movement of the methyl hydrogens into a plane containing the methyl carbon, plus an analogous reorganization of the vinyl ion.

It appears, therefore, that the divergent values of ionic heats of formation must be the result of characteristics which are more or less specific to the molecules for which the divergent values occur. It is possible to speculate that displacements of the minima in the potential energy hypersurfaces of molecule and molecule-ion might be enough different in different molecules somehow to give rise to the observed variations; that is, the sensitivity of mass spectrometers is not sufficient for appearance potentials to correspond in all cases to the energy of the vertical transition between the ground state of the molecule and the dissociation asymptote of the molecule-ion. It is, of course, well known that in those cases where molecular ionization potentials have been measured by both spectroscopic and electron impact methods, the electron impact values are invariably the higher and to an extent which varies in an irregular way from molecule to molecule. However, the differences are often quite small and are hardly ever greater than 0.2 ev; thus to attribute the 0.8-ev difference between the vinyl chloride and propylene vinyl ion heats of formation solely to this source tends to strain one's credulity.

The low heat of formation found with vinyl chloride and, to a lesser extent, with ethyl chloride poses a special problem. One can at least conceive of theoretical reasons why electron impact experiments might give high energetic values, but low values leave one completely at a loss.[10] Experimental error is, of course, an ever-present possibility in spite of the care exercised in making the measurements and the very good agreement of replicate determinations (appearance potential values of 12.80, 12.85, and 12.78 ev with vinyl chloride; 14.35 and 14.34 ev with ethyl chloride). On the other hand, it is possible that the 274-kcal/mole

TABLE II. Heats of formation of $C_2H_3\cdot$.

Compound	Ion detected	Number of determinations	Appearance potentials (ev)	$\Delta H_f(C_2H_3\cdot)$ (kcal/mole)	Ionization mechanism
Propylene	CH_3^+	4	$14.9_0\pm0.1$	84	$C_3H_6\rightarrow C_2H_3\cdot+CH_3^+$
1-butene	$C_2H_5^+$	5	$13.3_0\pm0.2$	82	$1\text{-}C_4H_8\rightarrow C_2H_3\cdot+C_2H_5^+$
3,3-dimethyl-1-butene	$t-C_4H_9^+$	2	$11.3_0\pm0.1$	81	$(CH_3)_3CCH=CH_2\rightarrow C_2H_3\cdot+t-C_4H_9^+$
				Av 82.3	

the result of which is a lowering of the activation energy. For a theoretical treatment of an ionic reaction see Glasstone, Laidler, and Eyring, *The Theory of Rate Processes* (McGraw-Hill Book Company, Inc., New York, 1941), pp. 220 ff.

[9] E. W. R. Steacie, *Atomic and Free Radical Reactions* (Reinhold Publishing Corporation, New York, 1946), pp. 519 ff.

[10] One of the referees of this paper suggests that possibly the low values obtained with the two chlorides result from the formation of Cl^- ions in an excited state.

value of the vinyl ion heat of formation found with vinyl chloride is the correct one (or most nearly correct one), and that for one reason or another the other values are all high. We are inclined to doubt this, however, because of the rather impressive concentration of values around 281–282 kcal/mole, particularly in view of the diverse nature of the ionization processes involved.

The results of the study of the vinyl radical are summarized in Table II. The ionic heats of formation used in the calculation of the vinyl radical heat of formation were: methyl, 264 kcal/mole;[11a] ethyl, 225 kcal/mole;[11b] and *t*-butyl, 166 kcal/mole.[11c]

The value of 82 kcal/mole obtained for the vinyl radical leads to the following typical bond dissociation energies (in kcal/mole): $D(C_2H_3-H)=122$; $D(C_2H_3-CH_3)=109$; $D(C_2H_3-C_2H_5)=107$; $D(C_2H_3-Cl)=104$; $D(C_2H_3-C_2H_3)=138$. The only previously published value for the C–H bond strength in ethylene is that of Stevenson,[6] $D(C_2H_3-H)=91.1$ kcal/mole, $\Delta H_f(C_2H_3\cdot)=51.6$ kcal/mole, which results from his value of 11.97 ev for the appearance potential of ethyl ion from 1-butene. Support for this value is found in Dibeler's[12] work on the 2-butenes, for which ethyl ion appearance potentials of 12.2 ev (*cis*) and 12.4 ev (*trans*) were found. Using the ionization process $2-C_4H_8\rightarrow C_2H_5^+ + C_2H_3\cdot$, the corresponding vinyl ion heat of formation is $\Delta H_f(C_2H_3\cdot)=57$ kcal/mole and $D(C_2H_3-H)=96$ kcal/mole. On the other hand, it has been found in this laboratory that the appearance potential of the ethyl ion from methyl cyclopropane is 13.3_8 ev, which corresponds to $\Delta H_f(C_2H_3\cdot)=90$ kcal/mole.

On the basis of the relative values of overlap integrals and stretching force constants, it is thought[13] that the strengths of bonds involving carbon atoms in different states of hydridization should be in the order $sp^3<sp^2<sp$. It is perhaps not unreasonable to think that the bond dissociation energies will fall in the same order, although it must be realized that in making such a prediction the reorganizational energy of the fragments is not taken into account. Our value of $D(C_2H_3-H)$ fits into the predicted order properly to the extent that it is greater than the established value for $D(CH_3-H)$ (101 kcal/mole). However, values of 111[14] and 115[15] kcal/mole have recently been obtained for $D(H-CN)$, and if a value in this range may be considered as typical for C–H bonds involving sp carbon atoms, it is clear that the value found for $D(C_2H_3-H)$ is appreciably higher than is to be expected on the basis of the theory. In spite of this, the fact that the value is the result of concordant measurements on three different compounds using two different mass spectrometers leads us to feel that it is correct.

The ionization potential of the vinyl radical is of course the difference between the heats of formation of the vinyl ion and radical. However, because of the spread of values for the ionic heats of formation (and, to a lesser extent, for the radical heats of formation), a question arises as to which values should be used. Quite arbitrarily we shall use average values, with the the consequence that the exact significance of the resulting ionization potential will be somewhat in doubt. The average value of the ionic heats of formation measured in this work is $281._5$ kcal/mole, omitting the values from the butanes because of inability to decide upon unambiguous ionization mechanisms. If one includes in the average values from the literature which seem to be reliable (from *i*-butene,[16] ethyl alcohol,[17] and cyclopropane[1] $\Delta H_f(C_2H_3^+)=282$, 286, and 288 kcal/mole, respectively), the average becomes 282.8 kcal/mole. Using this value the ionization potential of the vinyl radical is $I(C_2H_3\cdot)=282._8-82._3=200._5$ kcal/mole $=8.6_9$ ev.

It is of interest to point out that since the ionization potential of the vinyl radical is appreciably less than that of the methyl radical (10.07 ev), the dissociation of propylene to form methyl ion and vinyl radical constitutes an exception to Stevenson's rule[11c] that the dissociation of the molecule R_1R_2 into the entities R_1^+ and R_2 in their ground states occurs only if the ionization potential of R_1 is less than that of R_2. Similar exceptions seem to exist in the dissociations of methyl fluoroform[18] and methyl cyclopropane.[19]

The author wishes to acknowledge the financial support given to part of this work by the University of Texas Research Institute and the help of Mr. L. Battist of the University of Texas and Mr. R. K. Saunders of the Humble Oil and Refining Company in making the experimental measurements.

[11] Average values calculated from data obtained by several workers including:

(a) D. P. Stevenson and J. A. Hipple, Phys. Rev. **63**, 121 (1943); L. G. Smith, Phys. Rev. **51**, 263 (1937); C. A. McDowell and J. W. Warren, Disc. Faraday Soc. **10**, 53 (1951); J. Geerk and H. Neuert, Z. Naturforsch. **5A**, 502 (1950).

(b) D. P. Stevenson and J. A. Hipple, Phys. Rev. **63**, 121 (1943); D. P. Stevenson and J. A. Hipple, J. Am. Chem. Soc. **64**, 1588 and 2769 (1942).

(c) D. P. Stevenson, Disc. Faraday Soc. **10**, 35 (1951).

[12] V. H. Dibeler, J. Research Natl. Bur. Standards **38**, 329 (1947).

[13] C. A. Coulson, *Valence* (Oxford University Press, London, 1952), pp. 198–201.

[14] D. P. Stevenson, J. Chem. Phys. **18**, 1347 (1950).

[15] C. A. McDowell and J. W. Warren, Trans. Faraday Soc. **48**, 1084 (1952).

[16] D. P. Stevenson and J. A. Hipple, J. Am. Chem. Soc. **64**, 2769 (1942).

[17] C. S. Cummings and W. Bleakney, Phys. Rev. **58**, 787 (1940).

[18] Dibeler, Reese, and Mohler, J. Chem. Phys. **20**, 761 (1952).

[19] Unpublished work in this laboratory.

The Interpretation of Infrared Dichroism in Fibrous Protein Structures

R. D. B. FRASER
Biochemistry Unit, Wool Textile Research Laboratory, Commonwealth Scientific and Industrial Research Organisation, Melbourne, Australia

(Received April 22, 1953)

The increasing use of infrared dichroism measurements in studying the molecular structure of fibrous proteins necessitates a critical examination of its interpretation. Relationships between transition moment direction and dichroic ratio are derived for perfectly and imperfectly oriented fibers, and the effects of reflection losses, form dichroism, and convergence are considered. Uncertainties in the assignment of the transition moment directions associated with the principal vibrations of the $-CO\cdot NH-$ group are discussed.

INTRODUCTION

OBSERVATIONS of infrared dichroism in fibrous proteins and synthetic polypeptides have, until recently, been interpreted as indicating that a particular bond was preferentially oriented either parallel or perpendicular to the fiber axis or direction of shear. Such observations are of the greatest value in identifying α, β, or collagen configurations in oriented specimens and as qualitative support for models of their molecular structure.[1–3]

Detailed atomic coordinates of most of the models proposed for these configurations have now been published,[4–6] and the angles of inclination of the various bonds to the molecular axis may readily be calculated. Although these angles have been related directly to the observed infrared dichroisms,[2,7] the results can not be considered as having more than semiquantitative significance.

In this communication an attempt is made to place the interpretation of infrared dichroism on a more quantitative basis. It is only by continuous improvement in this direction that the precise orientation of the peptide group in the various configurations observed in fibrous proteins may be determined experimentally from dichroism measurements.

DICHROIC RATIO

In general the axes of the polypeptide chains in an oriented protein fiber have a preferred direction parallel to the fiber axis but no general order at right angles to this direction. Where crystallites occur they are randomly oriented about the fiber axis and the x-ray diagram closely resembles a crystal rotation pattern. The fiber therefore behaves optically as a uniaxial system with the optic axis parallel to the fiber axis. The absorption characteristics at any frequency are completely determined by the measurement of two extinction coefficients with plane polarized radiation incident normally to the fiber axis, the first, $\epsilon_\pi(\nu)$ obtained with the electric vector vibrating parallel to the axis and the second, $\epsilon_\sigma(\nu)$ perpendicular to this direction.

The dichroic ratio R of a particular absorption band is defined by the expression

$$R=\frac{\int_0^\infty \epsilon_\pi(\nu)\cdot d\nu}{\int_0^\infty \epsilon_\sigma(\nu)\cdot d\nu}, \tag{1}$$

where ν is the frequency and the integration applies only to absorption arising from the vibration under consideration. Before attempting to relate R to transition moment direction in the fiber it is necessary to consider the relationship between R and the experimentally determined dichroic ratio R' defined by

$$R'=D_\pi(\nu_0)/D_\sigma(\nu_0), \tag{2}$$

where D_π = the optical density with the electric vector vibrating parallel to the fiber axis; D_σ = vibrating perpendicular to the fiber axis; and ν_0 = the frequency of the absorption maximum. It has been shown[8] that, if the absorption band may be represented by a Lorentz type equation,

$$\epsilon(\nu)=\frac{a^2}{(\nu-\nu_0)^2+b^2}, \tag{3}$$

the integrals in expression (1) may be evaluated and the expression for R becomes

$$R=\epsilon_\pi(\nu_0)/\epsilon_\sigma(\nu_0). \tag{4}$$

The measurement of optical density at the absorption maximum is therefore justified, assuming that Eq. (3) is valid, and we shall in future write ϵ_π for $\epsilon_\pi(\nu_0)$ and ϵ_σ for $\epsilon_\sigma(\nu_0)$.

The ratio R' differs from the dichroic ratio R mainly due to the overlapping of neighboring absorption bands,

[1] Ambrose, Elliott, and Temple, Nature **163**, 859 (1949).
[2] E. J. Ambrose and A. Elliott, Proc. Roy. Soc. (London) **A206**, 206 (1951).
[3] R. D. B. Fraser, Disc. Faraday Soc. **9**, 398 (1950).
[4] Bragg, Kendrew, and Perutz, Proc. Roy. Soc. (London) **A203**, 321 (1950).
[5] L. Pauling and R. B. Corey, Proc. Natl. Acad. Sci. **37**, 235 (1951).
[6] L. Pauling and R. B. Corey, Proc. Natl. Acad. Sci. **37**, 729 (1951).
[7] C. Robinson and E. J. Ambrose, Trans. Faraday Soc. **48**, 854 (1952).
[8] A. Vallance-Jones, Ph.D. thesis, Cambridge, 1949.

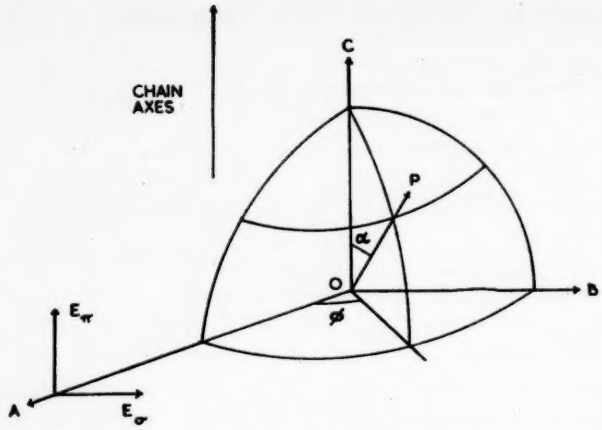

FIG. 1.

scattering and reflection losses, form dichroism, and the use of finite spectral slit widths. The extensive overlap of the α and β components of the CO·NH group absorptions *ca* 1540 and 1650 cm^{-1} in specimens containing both phases is particularly troublesome, and no satisfactory procedure is known at present for separating them. A further difficulty is encountered due to the small but significant contribution of side chains containing C=O, NH, and NH_2 groups.

Form dichroism and selective reflection due to surface texture may be detected and measured by observing the difference in optical density in a region free from absorption e.g. *ca* 2000 cm^{-1} in the case of the 1540 and 1650 cm^{-1} bands. The procedure generally adopted is to subtract the optical density at this frequency for each direction of the electric vector from the respective spectra. This also compensates for scattering losses, but involves the assumption that the effects are constant in the frequency range over which the correction is applied. It is important therefore to choose the absorption-free frequency as close as possible to the region under investigation.

The reflection coefficient attains an extremely high value in the neighborhood of an intense absorption band, and no simple procedure can be used to correct for the radiation losses involved. This effect is of great interest, and reflection spectra have recently been studied in considerable detail by Robinson.[9] Reflection losses as well as scattering, surface texture effects, and form dichroism are considerably reduced if the specimen is immersed in a transparent medium of similar refractive index. Liquid paraffin (Nujol), perfluorokerosine, hexachlorobutadiene, and carbon tetrachloride are among the liquids which are suitable for this purpose.

In the following sections it is assumed that the necessary corrections to R' have been made and the relation between R and transition moment inclination α will be derived.

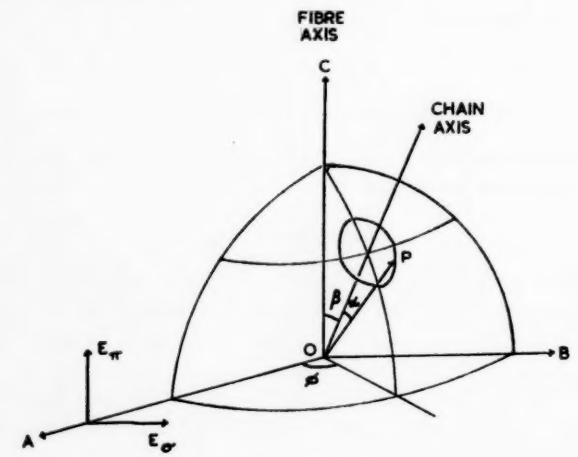

FIG. 2.

$R(\alpha)$ WITH PERFECT AXIAL ORDER

The relation between R and transition moment direction has been given for doubly oriented polymers[10] and crystals.[11] The relation for a uniaxial fiber has only been given in a comparatively inaccessible publication[12] and will be repeated.

Consider a right-handed system of coordinates *Oabc*, as in Fig. 1, within the specimen. Plane polarized radiation is incident along *aO* with components E_π parallel to *Oc* or E_σ parallel to *Ob*. The direction of the chain axes is parallel to *Oc* which is therefore also the optic axis. The direction of the oscillating dipole moment associated with vibration of a particular group is represented by a vector P inclined at an angle α to the molecular axis. The vectors P will lie on a cone of semi-angle α with *Oc* as axis. The absorption will be proportional to the squared scalar product of the electric vector and P, so that

$$R=\frac{\epsilon_\pi}{\epsilon_\sigma}=\frac{\frac{1}{2\pi}\int_0^{2\pi}\cos^2\alpha\cdot d\phi}{\frac{1}{2\pi}\int_0^{2\pi}\sin^2\alpha\cdot\sin^2\phi\cdot d\phi} \qquad (5)$$

$$R(\alpha)=2\cot^2\alpha.$$

As α varies from 0 to $\pi/2$ we note that R varies from ∞ to 0 and that no dichroism is observed ($R=1$) for $\alpha=54°\,44'$.

$R(\alpha)$ WITH PARTIAL ORDER

In practice the orientation of the polypeptide chains in a fibrous protein is never perfect and we may conveniently consider the specimen as containing a certain fraction f of perfectly oriented material and $(1-f)$

[9] T. S. Robinson, Ph.D. thesis, London, 1953.
[10] Ambrose, Elliott, and Temple, Proc. Roy. Soc. (London) **A199**, 183 (1949).
[11] Ambrose, Elliott, and Temple, Proc. Roy. Soc. (London) **A206**, 192 (1951).
[12] R. D. B. Fraser, Ph.D. thesis, London, 1951.

perfectly random. Expression (5) then becomes

$$R(\alpha, f)=\frac{f\cos^2\alpha+\frac{1}{3}(1-f)}{\frac{1}{2}f\sin^2\alpha+\frac{1}{3}(1-f)}. \tag{6}$$

Alternatively, we may regard all the molecular chains as displaced by the same angle β from parallelism with the optic axis. It follows from Fig. 2 that the expression for R becomes

$$R(\alpha,\beta)=\frac{\frac{1}{2\pi}\int_0^{2\pi}[\cos^2\alpha\cdot\cos^2\beta+\frac{1}{2}\sin^2\alpha\cdot\sin^2\beta]d\phi}{\frac{1}{2\pi}\int_0^{2\pi}[\cos^2\alpha\cdot\sin^2\beta\cdot\sin^2\phi+\frac{1}{2}\sin^2\alpha(\cos\phi+\sin\phi\cdot\cos\beta)^2]d\phi} \tag{7}$$

$$R(\alpha,\beta)=\frac{2\cot^2\alpha\cdot\cos^2\beta+\sin^2\beta}{\cot^2\alpha\cdot\sin^2\beta+(1+\cos^2\beta)/2}.$$

THE EFFECT OF CONVERGENCE

Most observations of infrared dichroism are made with convergent radiation on account of the experimental difficulties involved in using parallel radiation. So long as large specimens are used the semi-angle of the incident radiation cones can be limited to a few degrees and no sensible errors are involved. The increasing use of magnifying arrangements, in particular high numerical aperture reflecting microscopes,[13] involves the use of highly convergent cones and a significant component of the electric vector vibrates along the axis of the cone. The relation between the direction of transition moment and dichroism is derived as follows.

Consider a right-handed system of axes $Oxyz$, as in Fig. 3, within the specimen. Oz is the axis of the microscope and the chain axes are parallel to Ox. BO is an oblique ray passing through an elementary area δs of the microfocus at the origin. At a point B in the wave front the electric vector vibrates tangentially to the wave front and parallel to the plane xOz with the polarizer in the π position. Let $ABCO$ be a semigreat circle such that AC is parallel to E_π. The components of E_π will be

$$\left.\begin{aligned}E_x&=E_\pi\sin\psi\\E_y&=0\\E_z&=E_\pi\cos\psi\end{aligned}\right\}. \tag{8}$$

In the spherical triangle ZBC we have

$$\cos\pi/2=\cos\theta\cos\psi+\sin\theta\sin\psi\cos(\pi-\phi). \tag{9}$$

So that (8) becomes, after simplification

$$\left.\begin{aligned}E_x&=E_\pi/(1+\tan^2\theta\cos^2\phi)^{\frac{1}{2}}\\E_y&=0\\E_z&=E_\pi\tan\theta\cos\phi/(1+\tan^2\theta\cdot\cos^2\phi)^{\frac{1}{2}}\end{aligned}\right\}. \tag{10}$$

The components of E_σ are obtained by substituting $(\frac{1}{2}\pi-\phi)$ for ϕ, and writing x for y in Eq. (10)

$$\left.\begin{aligned}E_x&=0\\E_y&=E_\sigma/(1+\tan^2\theta\sin^2\phi)^{\frac{1}{2}}\\E_z&=E_\sigma\tan\theta\sin\phi/(1+\tan^2\theta\cdot\sin^2\phi)^{\frac{1}{2}}\end{aligned}\right\}. \tag{11}$$

[13] R. D. B. Fraser, Disc. Faraday Soc. **9**, 378 (1950).

If we consider that the specimen consists of a film of thickness t with plane surfaces parallel to xOy, the path length within the specimen will be $t/\cos\theta$. The ratio of the transmitted to incident intensity for the direction BO will be, from (10) and (11),

$$\frac{I}{I_0}=\frac{e^{-\epsilon_\pi t/\cos\theta}+e^{-\epsilon_\sigma t/\cos\theta}\cdot\tan^2\theta\cdot\cos^2\phi}{1+\tan^2\theta\cdot\cos^2\phi}, \tag{12}$$

for the π position, and

$$I/I_0=e^{-\epsilon_\sigma t/\cos\theta}, \tag{13}$$

for the σ position.

Now the incident flux dF_0 associated with the direction BO will be

$$dF_0=I_0\sin\theta\cdot d\theta\cdot d\phi, \tag{14}$$

and the intensity I_0 for polarized radiation,

$$I_0=\tfrac{1}{2}n^2B\cdot\delta s\cos\theta, \tag{15}$$

where n is refractive index and B brightness. The total incident radiant flux F_0 is obtained by integrating dF_0 over the wave front

$$F_0=\tfrac{1}{2}n^2B\cdot\delta s\cdot\int_0^{2\pi}\int_{\theta_1}^{\theta_2}\sin\theta\cdot\cos\theta\cdot d\theta\cdot d\phi, \tag{16}$$

where θ_1, θ_2 are the semi-angles of the cones including the incident radiation. The transmitted flux in the π position is

$$F_\pi=\tfrac{1}{2}n^2B\cdot\delta s\cdot\left\{e^{-\epsilon_\sigma t}\int_0^{2\pi}\int_{\theta_1}^{\theta_2}\sin\theta\cdot\cos\theta\cdot d\theta\cdot d\phi+(e^{-\epsilon_\pi t}-e^{-\epsilon_\sigma t})\int_0^{2\pi}\int_{\theta_1}^{\theta_2}\frac{\sin\theta\cdot\cos\theta\cdot d\theta\cdot d\phi}{1+\tan^2\theta\cdot\cos^2\phi}\right\}, \tag{17}$$

and in the σ position

$$F_\sigma=\tfrac{1}{2}n^2B\cdot\delta s\cdot e^{-\epsilon_\sigma t}\int_0^{2\pi}\int_{\theta_1}^{\theta_2}\sin\theta\cdot\cos\theta\cdot d\theta\cdot d\phi, \tag{18}$$

where the increased path length $t[(1/\cos\theta)-1]$ has been neglected. The error involved in neglecting this will be of the second order. The corresponding transmittances $T_\pi = F_\pi/F_0$ and $T_\sigma = F_\sigma/F_0$ are,

$$T_\pi = e^{-\epsilon_\sigma t} + \frac{e^{-\epsilon_\pi t} - e^{-\epsilon_\sigma t}}{\pi(\sin^2\theta_2 - \sin^2\theta_1)} \int_0^{2\pi}\int_{\theta_1}^{\theta_2} \frac{\sin\theta\cdot\cos\theta\cdot d\theta\cdot d\phi}{1+\tan^2\theta\cdot\cos^2\phi}, \quad (19)$$

and

$$T_\sigma = e^{-\epsilon_\sigma t}. \quad (20)$$

Evaluation of the integral in expression (19) yields

$$T_\pi = e^{-\epsilon_\sigma t} + \tfrac{2}{3}(e^{-\epsilon_\pi t} - e^{-\epsilon_\sigma t}) \times \left[\frac{\cos^2\theta_1+\cos^2\theta_2+\cos\theta_1\cos\theta_2}{\cos\theta_1+\cos\theta_2}\right]. \quad (21)$$

Writing

$$m = \tfrac{2}{3}(\cos^2\theta_1+\cos^2\theta_2+\cos\theta_1\cdot\cos\theta_2)/\cos\theta_1+\cos\theta_2, \quad (22)$$

we have

$$T_\pi = e^{-\epsilon_\sigma t} + m[e^{-\epsilon_\pi t} - e^{-\epsilon_\sigma t}], \quad (23)$$

$$T_\sigma = e^{-\epsilon_\sigma t}, \quad (24)$$

and the dichroic ratio R is

$$R = \frac{\epsilon_\pi}{\epsilon_\sigma} = \frac{\ln\left[T_\pi + \left(\frac{1}{m}-1\right)(T_\pi - T_\sigma)\right]}{\ln T_\sigma}, \quad (25)$$

or

$$R = \frac{\log[T_\pi + M(T_\sigma - T_\pi)]}{\log T_\sigma}, \quad (26)$$

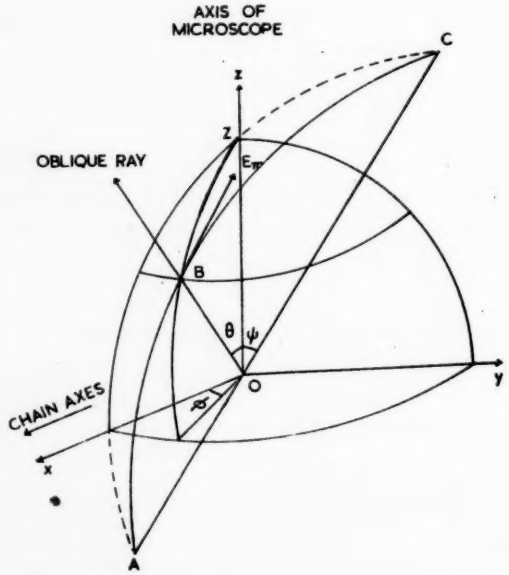

FIG. 3.

where

$$M = 1 - \tfrac{3}{2}(\cos\theta_1+\cos\theta_2)/\cos^2\theta_1+\cos^2\theta_2+\cos\theta_1\cos\theta_2. \quad (27)$$

This may be compared with the expression for parallel radiation, see Eq. (2),

$$R = \log T_\pi/\log T_\sigma. \quad (28)$$

With a reflecting microscope, the values of θ_1 and θ_2 in the parameter M of Eq. (26) are obtained from the numerical apertures (in air) of the objective $(N.A.)_1$ and central obstruction $(N.A.)_2$ by the expressions

$$\left.\begin{aligned}\sin\theta_1 &= (N.A.)_1/n,\\ \sin\theta_2 &= (N.A.)_2/n.\end{aligned}\right\} \quad (29)$$

The effect of convergence is not as great as might at first be expected for the semi-angle of the radiation cone is considerably reduced within the specimen as will be seen from Eq. (29). For example, using a high numerical aperture reflecting microscope in which $(N.A.)_1 = 0.81$ and $(N.A.)_2 = 0.28$,[13] we obtain $\theta_1 = 32.7°$ and $\theta_2 = 10.7°$ in a specimen with $n = 1.5$. With $T_\pi = 0.44$ and $T_\sigma = 0.67$, the value of $R = 2.04$, uncorrected, and 2.16 after correcting for convergence. The corresponding values of the transition moment inclinations from expression (5) are 45° and 44°, respectively.

TRANSITION MOMENT DIRECTION

In the previous sections the relation between transition moment direction and infrared dichroism has been discussed. It remains to consider the transition moment directions associated with the principal absorption bands observed in the spectra of fibrous proteins, so that the results of such measurements may be correlated with models of their molecular structure.

The absorption bands *ca* 3300, 1650, and 1540 cm^{-1}, in which dichroism is usually measured arise from vibrational modes of the *N*-substituted amide group $-CO\cdot NH-$. This group is considered by Pauling, Corey, and Branson[14] to be planar on account of the resonance between structures I and II of Fig. 4. The three absorption bands, in view of their frequencies, must correspond to in-plane modes of vibration, that is to say the atomic motions will be confined to the plane of the amide group. A further important structural feature proposed by Pauling *et al.*, is that the angle between the NH and NO vectors in the $>C=O\cdots H-N<$ hydrogen bond between neighboring amide groups is small.

It is generally accepted that the 3300 cm^{-1} absorption is the N−H stretching vibration reduced in frequency by hydrogen bonding. The vibration will be practically confined to an oscillation of the hydrogen atom in the bond direction and the associated transition moment direction will be almost parallel to it. It has been

[14] Pauling, Corey, and Branson, Proc. Natl. Acad. Sci. **37**, 205 (1951).

pointed out by Ambrose and Elliott[15] that the transition moment direction associated with this vibration might be considerably displaced towards the direction of the hydrogen bond in cases where the angle between the vectors NH and NO is large, but recent evidence[16] indicates that this configuration is not as stable as that proposed by Pauling *et al.* We may be reasonably certain therefore that the transition moment direction associated with the 3300 cm^{-1} band is nearly that of the N−H direction.

The interpretation of the absorptions *ca* 1650 and 1540 cm^{-1} is much less certain. An excellent summary of various assignments that have been suggested has been given by Sutherland[17] who concludes that the question is still open. The 1650 cm^{-1} absorption is generally attributed to the C=O stretching vibration, and the 1540 cm^{-1} absorption to N−H bending or C−N stretching modes, none of these however explain the spectral changes that occur when simple *N*-substituted amides are *N* deuterated.[18] Recently, Fraser and Price[19] have suggested that these absorptions are due to non-localized vibrations, as the natural frequencies of the C=O and C−N stretching and N−H bending vibrations are sufficiently close for considerable mechanical interaction to occur. This is a direct result of the increased CO and reduced CN bond lengths associated with the resonance in the amide group.[14] An approximate treatment of the normal modes of vibration leads to the prediction of these absorptions together with a third *ca* 1300 cm^{-1}. A particularly pleasing feature of these calculations[20] is that the vibrational frequencies predicted for the −CO·ND− grouping agree well with the observed values, including the absorption band *ca* 1480 cm^{-1} for which no explanation has previously been given.

From the extent of the mechanical interaction Fraser and Price estimated that the transition moment direction is displaced *ca* 5° from the CO bond direction towards the direction NC in the 1650 cm^{-1} vibration. A more important effect however in this case is due to the changes in the proportions of the resonating structures I and II of Fig. 4 that take place during the vibration. This leads to an additional oscillating dipole moment in the direction NO. The resulting displacement of transition moment direction was estimated to be *ca* 15° in the same direction as that due to mechanical interaction.

FIG. 4.

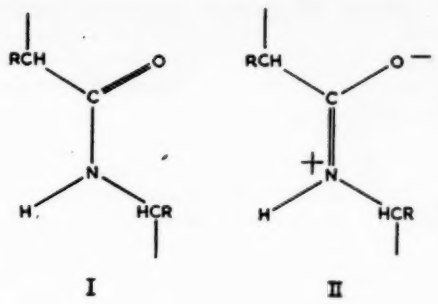

I II

Assuming a total displacement of 20° for the 1650 cm^{-1} absorption and zero for that at 3300 cm^{-1} it was shown that the dichroic ratio measured by Ambrose and Elliott[15] at these frequencies for poly-γ-benzyl-*L*-glutamate in the folded configuration were in good agreement with those predicted from the 3.7 residue helix proposed by Pauling *et al.*

In the past it has been assumed that the transition moment direction associated with overtone and combination bands was either perpendicular or parallel to the bond direction depending upon the type of vibration.[2,21] In view of the effects of mechanical interaction and orbital-following mentioned above, these assumptions can not be accepted except perhaps in the case of the first overtone of the N−H stretching vibration. The establishment of the relation between transition moment direction and bond direction for these absorptions must await an exact treatment of the normal modes of vibration and detailed calculations of the contribution of orbital-following.

ACKNOWLEDGMENTS

I should like to record my gratitude to Professor J. T. Randall F.R.S. and Dr. F. G. Lennox, in whose laboratories this work was undertaken, and to Dr. W. C. Price for his guidance and many helpful suggestions. Some of the calculations were presented in a thesis for the degree of Ph.D. in the University of London, and part of the work done during the tenure of a Nuffield Foundation Research Fellowship.

[15] E. J. Ambrose and A. Elliott, Proc. Roy. Soc. (London) **A205**, 47 (1951).
[16] J. Donohue, J. Phys. Chem. **56**, 502 (1952).
[17] G. B. B. M. Sutherland, Advances in Protein Chemistry **7**, 291 (1952).
[18] H. Lenormant, Ann. Chim. **5**, 459 (1950).
[19] R. D. B. Fraser and W. C. Price, Nature **170**, 490 (1952).
[20] Fraser, Price, and Seeds (to be published).
[21] J. D. Bath and J. W. Ellis, J. Phys. Chem. **45**, 204 (1941).

Bond Moments and Derivatives in CF_4, SiF_4, and SF_6 from Infrared Intensities*

P. N. SCHATZ AND D. F. HORNIG
Metcalf Chemical Laboratories, Brown University, Providence, Rhode Island

(Received March 9, 1953)

The absolute intensities of the fundamental infrared absorption bands of SiF_4, CF_4, and SF_6 were measured utilizing the pressure broadening technique. The effective bond moments, μ_0, and bond moment derivatives, $\partial u/\partial r$, are calculated as a function of the most general potential constants. Based on a valence force field plus repulsion between nonbonded atoms, the most probable values (first column) and the alternatives (second column) are as follows:

SiF_4	$\mu_0=2.3\ d$ $\partial u/\partial r=-7.49\ d/A$	$3.3\ d$ $3.66\ d/A$
CF_4	$\mu_0=1.12\ d$ $\partial u/\partial r=4.88\ d/A$	$2.36\ d$ $3.35\ d/A$
SF_6	$\mu_0=2.65\ d$ $\partial u/\partial r=3.85\ d/A$	$0.65d$ $-6.58\ d/A$

The results are discussed.

INTRODUCTION

THIS paper reports the absolute infrared intensities of the fundamental vibrations of three fluorine-containing molecules and some properties of bonds to fluorine inferred from these measurements. In particular, the bond moment and its derivative with respect to interatomic distance have been calculated for the compounds investigated.

A considerable amount of work has been done in the past several years on the measurement and interpretation of the absolute intensities of infrared bands. The results have usually been interpreted on the basis of molecules composed of noninteracting bond dipole moments, with the assumption that the change in moment during stretching is directed along the bond and that during bending, perpendicular to it. The fact that the same bond moment calculated from different modes of vibration sometimes has significantly different values (e.g., in ethylene[1]) indicates that this simple model is not always satisfactory. Nevertheless, such a model has given valuable information about the charge distributions in molecules and was employed in this present work.

One of the effects which can cause the preceding assumptions to break down is the polarization of one bond by another. In this respect fluorine compounds constitute relatively favorable cases. The polarizability of a bond is measured by its refraction, which is generally small in bonds to fluorine, being about the same as the C−H and C−C bonds but considerably smaller than multiple bonds or other halogen bonds. (For example, C−H, 1.7; C−C, 1.2; C−F, 1.6; S−F, 2.0; but C=C, 4.2; C−Cl, 6.6[2].)

Consequently, it is hoped that the polarization interactions among the various bonds were kept to a minimum. Of course, hybridization changes during a vibration may still cause large interaction effects.

BASIC THEORY

The experimentally observed absolute intensity, A, is related to the absorption coefficient α_ν by

$$A=\int_{\text{Band}}\alpha_\nu d\nu=\frac{1}{pl}\int \ln\frac{I_0}{I}d\nu, \tag{1}$$

where p is the partial pressure of absorbing gas, l is the path length of the cell, I_0 is the incident intensity of radiation of frequency ν, and I is the transmitted intensity. It has been shown[3] that

$$A_{i}^{i'}=\left(\frac{8\pi^3\nu_i^{i'}}{3hc}\right)\left(\frac{N_i}{g_i}\right)\left[1-\exp\left(-\frac{h\nu_i^{i'}}{kT}\right)\right]S_i^{i'}, \tag{2}$$

where $\nu_i^{i'}$ is the frequency corresponding to the transition between the energy levels i and i', N_i is the population of the energy level i, and g_i is its multiplicity. Here $S_i^{i'}$ is known as the line strength and is defined by

$$S_i^{i'}=\sum_{a_i,\ a_{i'}}|(i|p|i')|^2, \tag{3}$$

the summation being carried out over all the individual degenerate states a_i and $a_{i'}$. p is the vector dipole moment in a space-fixed coordinate system, and $(i|p|i')$ is the matrix element of the electric moment between the states i and i'. The integrated intensity of a vibration-rotation band is the sum of expressions (2) over all transitions. Such a summation has been carried out for diatomic molecules[3] (a closely similar

* Based on a thesis presented by P. N. Schatz in partial fulfillment of the requirements for the degree of Doctor of Philosophy, Brown University, 1952. This work was supported by U. S. Office of Naval Research.

[1] Thorndike, Wells, and Wilson, J. Chem. Phys. **15**, 157 (1947).

[2] C. P. Smyth, Phil. Mag. **50**, 361 (1925).

[3] B. L. Crawford, Jr., and H. L. Dinsmore, J. Chem. Phys. **18**, 983, 1682 (1950).

treatment applies to linear molecules)[4] and is readily extended to spherical top molecules. Assuming as a first approximation that the rotational and vibrational wave functions are separable, and that the electronic wave function remains constant for transitions giving rise to absorption in the infrared region, the line strength $S_i^{i'}$ may be expressed as a product of rotational and vibrational line strengths;[3]

$$S_i^{i'}=S_r^{r'}S_v^{v'}. \tag{4}$$

To this degree of approximation, the vibrational wave function can be expressed as a product of independent harmonic oscillator wave functions, one corresponding to each normal mode of vibration. The energy levels corresponding to any particular mode of vibration are given by

$$E_v=(v+\tfrac{1}{2})h\nu_0, \tag{5}$$

where v is an integer and ν_0 is the classical frequency of vibration. The eigenvalues and eigenfunctions of the symmetric top (of which the spherical top is a special case) are well known.[5] The rotational energy levels of a spherical top are given by

$$E_j=(h^2/8\pi^2A)j(j+1), \tag{6}$$

where A is the principal moment of inertia and j is an integer. There is a $(2j+1)^2$-fold degeneracy corresponding to any given value of j, since every level has a $(2j+1)$-fold degeneracy because j may have $(2j+1)$ orientations with respect to a fixed direction in the molecule (quantum number k) in addition to the usual $(2j+1)$-fold space degeneracy (quantum number m).

The expression for the total intensity corresponding to any given vibrational transition, $A_v^{v'}$, is obtained by summing the expression for $A_i^{i'}$ over all transitions occurring in the band. Making use of Boltzmann statistics and Eq. (4)

$$A_v^{v'}=\frac{8\pi^3N_v}{3hcZ}S_v^{v'}\sum_{r,\,r'}\nu_{vj}^{v'j'}\times\left[1-\exp\left(\frac{h\nu_{vj}^{v'j'}}{kT}\right)\right]e^{-E_j/kT}S_r^{r'}, \tag{7}$$

where the symbol $\sum_{r,r'}$ indicates a summation over all allowed rotational transitions. N_v is the total molecular concentration in the lower vibrational level, and Z is the rotational partition function defined by

$$Z=\sum_{j=0}^{\infty}(2j+1)^2e^{-E_j/kT}. \tag{8}$$

The selection rules for the vibration-rotation transitions of a symmetric top are different depending on whether the transition moment is parallel or perpendicular to the figure axis. However, in the case of a spherical top, any axis fixed in the molecule may be considered as the figure axis.[6] For convenience, then, let the figure axis be chosen so that the transition moment is parallel to it. Then the selection rules are[7]

$$\begin{aligned}&\Delta k=0,\quad \Delta j=0,\pm1,\quad \text{if } k\neq0.\\&\Delta k=0,\quad \Delta j=\pm1,\quad \text{if } k=0.\end{aligned} \tag{9}$$

The symbol $\sum_{r,r'}$ appearing in Eq. (7) is actually a triple sum, since in summing over any j value the two previously mentioned degeneracies must be considered. Hence Eq. (7) may be written

$$A_v^{v'}=\frac{8\pi^3N_v}{3hcZ}S_v^{v'}\sum_{j,j'}\left[\nu_{vj}^{v'j'}\exp(-E_j/kT)-\exp\left(\frac{-h\nu_v^{v'}}{kT}\right)\nu_{vj}^{v'j'}\exp(-E_{j'}/kT)\right]\times\sum_{k,k'}\sum_{m,m'}S_r^{r'}. \tag{10}$$

The summation $\sum_{m,m'}S_r^{r'}$ has been carried out by Rademacher and Reiche[8] with the result

$$\sum_{m,\,m'}S_r^{r'}=S_{jk}^{j'k'}=\frac{k^2(2j+1)}{j(j+1)}\delta_{j,\,j'}+\frac{(j+k)(j-k)}{j}\delta_{j',\,j-1}+\frac{(j+1+k)(j+1-k)}{(j+1)}\delta_{j',\,j+1}. \tag{11}$$

It is now necessary to evaluate the sum, $\sum_{k,\,k'}S_{jk}^{j'k'}$. Since $k'=k$ (Eq. (9)), it will merely be necessary to sum the terms corresponding to the $(2j+1)$ possible orientations allowed for k. This may easily be done if it is noted that

$$\sum_{k=-j}^{k=+j}k^2=\frac{1}{3}j(j+1)(2j+1). \tag{12}$$

Thus,

$$S_j^{j'}=\sum_{k=-j}^{k=j}S_{jk}^{j'k'}=\frac{1}{3}(2j+1)^2\delta_{j,\,j'}+\left(\frac{4}{3}j^2-\frac{1}{3}\right)\delta_{j',\,j-1}+\left(\frac{4}{3}j^2+\frac{8}{3}j+1\right)\delta_{j',\,j+1}. \tag{13}$$

Hence Eq. (10) becomes

$$A_v^{v'}=\frac{8\pi^3N_v}{3hcZ}S_v^{v'}\left[\sum_{j,j'}(\nu_{vj}^{v'j'}e^{-E_j/kT}S_j^{j'})-\exp\cdot\left(-\frac{h\nu_v^{v'}}{kT}\right)\sum_{j,j'}\nu_{vj}^{v'j'}e^{-E_{j'}/kT}S_j^{j'}\right]. \tag{14}$$

[4] D. F. Eggers, Jr., and B. L. Crawford, Jr., J. Chem. Phys. **19**, 1554 (1951).

[5] F. Reiche and R. Rademacher, Z. Physik **39**, 444 (1926).

[6] G. Herzberg, *Infrared and Raman Spectra of Polyatomic Molecules* (D. Van Nostrand Company, Inc., New York, 1945), p. 38.

[7] See reference 6, p. 414.

[8] R. Rademacher and F. Reiche, Z. Physik **41**, 453 (1927).

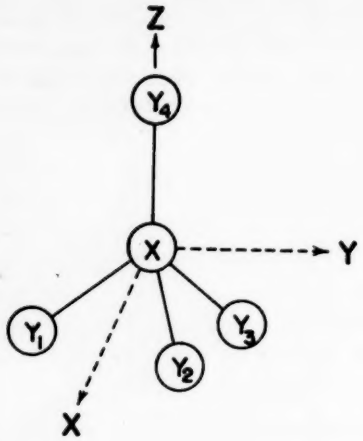

FIG. 1. Tetrahedral XY_4 molecule.

Summing finally over j' and j yields

$$A_v^{v'}=\frac{8\pi^3 N_v}{3hc}S_v^{v'}\left\{\nu_v^{v'}\left[1-\exp\left(-\frac{h\nu_v^{v'}}{kT}\right)\right]+2B\left[1+\exp\left(-\frac{h\nu_v^{v'}}{kT}\right)\right]\right\}. \quad (15)$$

In order to obtain the total intensity of the band, $A^{(n)}$, $A_v^{v'}$ must be summed over all values of v, and it must be noted that the infrared active vibrations of tetrahedral and octahedral molecules are triply degenerate. That is,

$$A^{(n)}=3\sum_{v=0}^{\infty}A_v^{v+n}. \quad (16)$$

This summation has been carried out by Crawford and Dinsmore[3] with the result that

$$A^{(n)}=\frac{8\pi^3 N}{hc}S_0^n\left\{\nu_0^n\left[1-\exp\left(-\frac{nh\nu_0}{kT}\right)\right]+2B\left[1+\exp\left(-\frac{nh\nu_0}{kT}\right)\right]\right\}Q^n, \quad (17)$$

where Q is the vibrational partition function and N is the total molecular concentration. For fundamental vibrations n is equal to unity, and for all of the molecules studied in this work the quantity $2B/\nu_0^1$ is extremely small. Therefore,

$$A^{(1)}\equiv A=\frac{8\pi^3 N\nu_0}{hc}S_0^1. \quad (18)$$

It is interesting to note that for fundamental vibrations the effect of induced emission is exactly offset by the sum of the vibrational transitions 1–2, 2–3, 3–4$\cdots$, provided $2B/\nu_0^1\ll 1$.

If the vector dipole moment is expanded in a Taylor's series as a function of the normal coordinates and terms higher than linear are neglected, the quantity S_0^1 is easily shown to be[1]

$$S_0^1=\frac{h}{8\pi^2\nu_0}\left(\frac{\partial\mu}{\partial Q_i}\right)^2, \quad (19)$$

where Q_i is the normal coordinate for the particular vibration under consideration, and μ is the vector dipole moment of the molecule (coordinates fixed in the molecule). With this result, Eq. (18) becomes

$$A_i=\frac{N\pi}{c}\left(\frac{\partial\mu}{\partial Q_i}\right)^2, \quad A_i'=\frac{N\pi}{c^2}\left(\frac{\partial\mu}{\partial Q_i}\right)^2, \quad (20)$$

where A_i is the absolute intensity of the ith rotation-vibration band in cycles/cm atmos sec, and A_i' is the same quantity expressed in cm^{-1}/cm atmos, if N is the molecular concentration at one atmosphere pressure.

Since, as Crawford and Dinsmore[3] have shown, higher order effects such as electrical and mechanical anharmonicity produce negligible changes in the intensity of fundamental vibrations, they have been ignored.

BOND MOMENTS AND DERIVATIVES

In order to obtain information about the individual bonds of a molecule the relationship between the normal coordinates and internal coordinates must be utilized. If the molecule possesses any symmetry the latter are most conveniently taken as symmetry coordinates which factor the secular determinant. In the three molecules discussed here only one symmetry species (F_2 of T_d, F_{1u} of O_h) can be infrared active; it contains two normal coordinates, Q_1 and Q_2, each a normalized linear combination of two symmetry coordinates, R_1 and R_2. In Wilson's notation,[9] the desired relationship is

$$\frac{\partial\mu}{\partial R_k}=L_{1k}^{-1}\left(\frac{\partial\mu}{\partial Q_1}\right)+L_{2k}^{-1}\left(\frac{\partial\mu}{\partial Q_2}\right) \quad k=1, 2, \quad (21)$$

where L^{-1} is the matrix of the transformation $Q=L^{-1}R$. The elements of L^{-1} are given explicitly in terms of Wilson's F (potential energy) and G (kinetic energy) matrices by the expressions

$$\frac{L_{i1}^{-1}}{L_{i2}^{-1}}=-\frac{(GF)_{2i}-\lambda_2\delta_{2i}}{(GF)_{1i}-\lambda_1\delta_{1i}}=n_i \quad i=1, 2 \quad (22)$$

and

$$(L_{i2}^{-1})^{-2}=G_{22}+2n_iG_{12}+n_i^2G_{11} \quad i=1, 2, \quad (23)$$

where δ is the Kronecker symbol and $\lambda_i=4\pi^2\nu_i^2$, if ν_i is the frequency of the ith normal vibration.

Unfortunately, the force constants, F_{ij}, can only be ascertained by fitting the roots of the secular equation, which for the infrared active species of the molecules studied here is[6]

$$\left[\begin{vmatrix}F_{11} & F_{12}\\ F_{12} & F_{22}\end{vmatrix}\begin{vmatrix}G_{11} & G_{12}\\ G_{12} & G_{22}\end{vmatrix}-\begin{vmatrix}\lambda & 0\\ 0 & \lambda\end{vmatrix}\right]=0. \quad (24)$$

[9] E. B. Wilson, Jr., J. Chem. Phys. 7, 1047 (1939); 9, 76 (1941).

Since there are three force constants and but two frequencies, the problem is indeterminate and the best that can be done in the general case, in the absence of precise measurements on isotopic molecules, is to obtain a relation between the three force constants.

A definite solution can, however, be obtained through the use of a physical model which reduces the number of independent constants which must be determined empirically. In the case of a large number of tetrahedral molecules a model based on the Urey-Bradley field, a simple valence potential plus central forces between nonbonded atoms, has been used successfully by both Heath and Linnett[10] (3 constants) and Simanouti[11] (4 constants). Heath and Linnett have also considered an orbital valency force field plus central forces between nonbonded atoms (3 constants) with even greater success. They also applied both of the preceding models to SF_6, SeF_6, and TeF_6 but the results were not as good, particularly for the lowest frequency bending mode.[12]

These models probably fix the force constants fairly adequately, but because of the uncertainty it is important that the moments and derivatives be calculated not only for the values derived from the models but for adjacent values, so that the sensitivity to the potential function can be taken into account in arriving at conclusions. We have done this.

(a) Tetrahedral Molecules, XY_4.

We have used the following symmetry coordinates:

$$R_{1z}=\frac{1}{\sqrt{6}}(\Delta r_1+\Delta r_2-2\Delta r_3),$$

$$R_{2z}=\frac{r_0}{\sqrt{12}}(-2\Delta\alpha_{12}+\Delta\alpha_{23}+\Delta\alpha_{13}-\Delta\alpha_{14}-\Delta\alpha_{24}+2\Delta\alpha_{34}),$$

$$R_{1y}=\frac{1}{\sqrt{2}}(\Delta r_2-\Delta r_1),$$

$$R_{2y}=\frac{r_0}{2}(-\Delta\alpha_{23}+\Delta\alpha_{13}+\Delta\alpha_{14}-\Delta\alpha_{24}),$$

$$R_{1z}=\frac{1}{\sqrt{12}}(3\Delta r_4-\Delta r_1-\Delta r_2-\Delta r_3),$$

$$R_{2z}=\frac{r_0}{\sqrt{6}}(-\Delta\alpha_{14}-\Delta\alpha_{24}-\Delta\alpha_{34}+\Delta\alpha_{12}+\Delta\alpha_{23}+\Delta\alpha_{13}),$$

where the r's and α's are the bond lengths and angles of Fig. 1, and r_0 is the equilibrium X–Y distance. These coordinates are all chosen so that the direction of motion of the Y atoms is in the positive x, y, or z direction when R is positive.

[10] J. W. Linnett and D. F. Heath, Trans. Faraday Soc. **44**, 561, 878, 884 (1948); J. Chem. Phys. **19**, 801 (1951).
[11] T. Simanouti, J. Chem. Phys. **17**, 245, 734, 848 (1949).
[12] D. F. Heath and J. W. Linnett, Trans. Faraday Soc. **45**, 264 (1949).

If it is *assumed* that stretching produces a change in moment along the bond direction and that bending produces a moment perpendicular to the bond, it is readily shown from the geometry of Fig. 1 that

$$\frac{\partial\mu}{\partial r}=\frac{\sqrt{3}}{2}\frac{\partial\mu}{\partial R_{1x(y\text{ or }z)}},$$

and (25)

$$\mu_0=\frac{r_0\sqrt{3}}{2}\frac{\partial\mu}{\partial R_{2x(y\text{ or }z)}}.$$

These equations are most easily obtained from R_{1z} and R_{2z}. The positive sense of all moments is taken from X to Y.

In the calculations $G_{11}=\mu_y+4\mu_x/3$, $G_{12}=8\mu_x/3$ and $G_{22}=2\mu_y+16\mu_x/3$, where the μ_x and μ_y are the reciprocals of the masses of atoms X and Y, respectively.[9,11]

(b) Octahedral Molecules, XY_6.

A convenient set of symmetry coordinates is

$$R_{1x}=1/\sqrt{2}(\Delta r_1-\Delta r_4),$$

$$R_{2x}=\frac{r_0}{\sqrt{8}}(\Delta\alpha_{46}+\Delta\alpha_{34}+\Delta\alpha_{45}+\Delta\alpha_{24}-\Delta\alpha_{12}-\Delta\alpha_{15}-\Delta\alpha_{13}-\Delta\alpha_{16}),$$

$$R_{1y}=\frac{1}{\sqrt{2}}(\Delta r_3-\Delta r_6),$$

$$R_{2y}=\frac{r_0}{\sqrt{8}}(\Delta\alpha_{56}+\Delta\alpha_{26}+\Delta\alpha_{46}+\Delta\alpha_{16}-\Delta\alpha_{23}-\Delta\alpha_{35}-\Delta\alpha_{34}-\Delta\alpha_{13}),$$

$$R_{1z}=\frac{1}{\sqrt{2}}(\Delta r_2-\Delta r_5),$$

$$R_{2z}=\frac{r_0}{\sqrt{8}}(\Delta\alpha_{15}+\Delta\alpha_{35}+\Delta\alpha_{45}+\Delta\alpha_{56}-\Delta\alpha_{12}-\Delta\alpha_{23}-\Delta\alpha_{24}-\Delta\alpha_{26}),$$

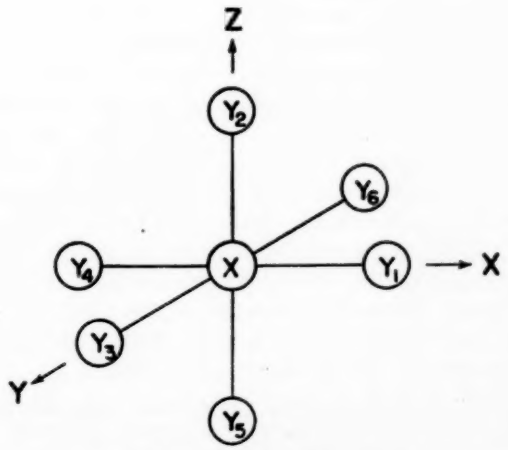

FIG. 2. Octahedral XY_6 molecule.

where the same conventions are used as before. (See Fig. 2.)

In this case

$$G_{11}=2\mu_x+\mu_y, \quad G_{12}=4\mu_x, \quad G_{22}=8\mu_x+2\mu_y.$$

The equations utilizing these matrix elements are consistent with those of Eucken and Sauter,[13] and Heath and Linnett,[12] but do not agree with those of Wilson, quoted by Yost, Steffens, and Gross,[14] which appear to be in error. It should be noted in comparing Linnett's force constants (f) with ours that

$$F_{11}=f_{11}; \quad F_{12}=\frac{-f_{12}}{\sqrt{2}}, \quad F_{22}=\frac{f_{22}}{2}.$$

Assuming again that stretching moments are developed along bonds and bending moments perpendicular to them, the geometry of Fig. 2 shows that

$$\frac{\partial\mu}{\partial r}=\frac{1}{\sqrt{2}}\frac{\partial\mu}{\partial R_{1x(y \text{ or } z)}}, \qquad \mu_0=\frac{r_0}{\sqrt{2}}\frac{\partial\mu}{\partial R_{2x(y \text{ or } z)}}. \tag{26}$$

Aside from the potential constants, another problem lies in the ambiguity of signs, both of the $\partial\mu/\partial Q$'s obtained from Eq. (20) and of the coefficients of L^{-1} from Eq. (23). These ambiguities reflect the indeterminacy in the positive direction of μ with respect to Q, and of Q with respect to Cartesian axes fixed in the molecule. When they are all taken into account, Eq. (21) yields four solutions but only two different results for the absolute values of $\partial\mu/\partial R_k$. One or the other value is obtained depending on the sign of the ratio $(\partial\mu/\partial Q_1)/(\partial\mu/\partial Q_2)$; the sign ambiguity in L^{-1} merely interchanges the four results. Since there is no loss of generality in doing so, we have chosen the sign of the L^{-1} elements so that each Q has the same sign as the predominant symmetry coordinate in that motion.

It seems worth pointing out that as a consequence of Eq. (22) an unambiguous value for the ratio $(\partial\mu/\partial R_1)/(\partial\mu/\partial R_2)$ can be found corresponding to each choice of the sign of $(\partial\mu/\partial Q_1)/(\partial\mu/\partial Q_2)$. This has the important consequence that if one of the coordinates (e.g. R_1) is a stretching coordinate and the other (e.g. R_2), a bending coordinate, the sign of the ratio of the bond moment to the bond moment derivative, $\partial\mu/\partial r$, is determinate; i.e., if the absolute sign of one is known from any other arguments, the sign of the other may be found from the intensities. Similarly, if they are both bends, the relative direction of the bond moments can be determined; and if they are both stretches, the relative signs of the $\partial\mu/\partial r$'s can be found.[15]

[13] A. Eucken and F. Sauter, Z. physik. Chem. **26B**, 463 (1934).

[14] Yost, Steffens, and Gross, J. Chem. Phys. **2**, 313 (1934).

[15] These statements are readily generalized. If there are g vibrations in a given symmetry class, there are 2^{g-1} independent solutions for each $\partial\mu/\partial R_k$, but to each of these solutions corresponds a determinate value for the ratios $(\partial\mu/\partial R_1):(\partial\mu/\partial R_2):\cdots:(\partial\mu/\partial R_g)$. However it is doubtful whether this can prove useful in the more general case.

EXPERIMENTAL

The Wilson-Wells extrapolation technique[16] was used to obtain the integrated absorption intensity over a complete vibration-rotation band (Eq. 1). Wilson and Wells showed that the intensity as defined by this equation cannot be measured directly with an ordinary spectrometer, but can be obtained from either of the two experimental quantities

$$B=\frac{1}{pl}\int \ln\frac{T_0}{T}d\nu,$$

$$C=\frac{1}{pl}\int \frac{T_0-T}{T_0}d\nu,$$

where T_0 and T are the measured intensities of incident and transmitted radiation. Briefly, one measures the integrated apparent absorption intensity for unit pressure (B or C) at a series of values of the equivalent path length, and the limiting value, determined as the equivalent path length approaches zero, is the absolute intensity. (As an alternative, the limiting slope of the integrated apparent absorption, Bpl or Cpl, as a function of pl may be determined.) Atmospheric absorption is kept to a minimum in the region of the band in order that I_0 be constant over the slit width, and a sufficiently high pressure of broadening gas is used that the rotational fine structure is eliminated.

The general procedure used in any given run was to measure the absorption at about five different partial pressures of absorbing gas, maintaining the total pressure approximately constant at 800 millimeters with nitrogen. The pressures used were such that the absorption usually varied roughly (peak value) from 35 percent to 8 percent. The adequacy of 800 millimeters total broadening pressure was confirmed by noting in all cases that if a sample of pure gas sufficient to cause about twenty percent absorption was scanned after successive 200 millimeter increments of nitrogen were added, the area of the band had stopped increasing by the time the total pressure was 800 millimeters.

The very low partial pressures required were obtained by successive dilutions of the pure gas with nitrogen. In order to insure complete mixing of the gases, the mixing bulb was equipped with a manual stirrer which was used after each dilution. In addition, the bulb was always permitted to stand unused for at least twenty-four hours after every dilution.

The spectrometer used throughout this work was essentially identical with one that has been described in detail in the literature.[17]

[16] E. B. Wilson, Jr., and A. J. Wells, J. Chem. Phys. **14**, 578 (1946).

[17] Hornig, Hyde, and Adcock, J. Opt. Soc. Am. **40**, 497 (1950).

Briefly, it consisted of a double beam optical system used with a Perkin-Elmer Model 83 Monochromator. The instrument gave a continuous recording of the ratio of light intensity transmitted by sample and blank cells. The instrument had an automatic slit control which maintained the energy received by the detector from the blank path constant.

In all cases "absorption areas" (C), determined directly from the recorder chart, were used. The area of each band was measured at least twice with a compensating polar planimeter. It was possible to use the areas directly as recorded because the change in dispersion across the bands was small. (In the case of the 632 cm^{-1} CF_4 band and the 615 cm^{-1} SF_6 band it was necessary to divide the bands in halves and treat each half separately to insure that the change in dispersion across these bands would not cause appreciable errors.) Since the absorption area is independent of the resolving power,[18] fairly wide slits were used to obtain a low noise level.

Both the limiting value of C and the limiting slope of $C'(\equiv Cpl)$ were determined for each band. The latter is shown in Figs. 3a–8a, the former in Figs. 3b–8b. In addition, the limiting slope of C' was obtained by plotting each individual run separately. These individual runs may be distinguished by the variously shaded circles although the individual C' curves are not shown. The final intensity reported for each band is an average of the following three quantities: (1) the limiting value of C, (2) the limiting slope of C', (3) the average of the limiting slopes of C' obtained from the individual runs. The intensities and $\partial\mu/\partial Q$'s obtained are summarized in Table I.

A correction for stray light was always made before extrapolation to zero equivalent path length. Only in the case of the 391 cm^{-1} band of SiF_4 (KRS-5 region) was the amount of stray light ever greater than 10 percent (approx. 11 percent).

A consideration of the errors involved in measuring the intensity of absorption shows that the combined errors in the measurement of C probably do not exceed 5 percent. The uncertainty introduced by the extrapolations is estimated to be no greater than 5 percent. Hence the absolute intensities reported should be accurate to ± 10 percent or better.

SILICON TETRAFLUORIDE

The SiF_4 used was prepared by heating pure barium fluosilicate. The gas formed was passed through a dry-ice and acetone bath to remove nonvolatile impurities. It was then condensed in a vacuum system with liquid nitrogen, and any noncondensable gases present were pumped off. The SiF_4 thus prepared was thought to be almost 100 percent pure.

A thallium bromide-iodide (KRS-5) prism was used for the 391 cm^{-1} band. When a potassium bromide scattering filter was used, and the glass mirror before the entrance slit was replaced with one of polished stainless steel, the stray light was reduced to about 11 percent. Since there are atmospheric water bands in this region of the spectrum, the optical path was thoroughly dried. No band was scanned unless the presence of water vapor was indetectable when the spectrometer was operated as a single beam instrument. The average resolution was very roughly estimated to have been 20 to 25 cm^{-1}. The approximate peak-to-peak noise level on the records was 1 to 1.5 percent.

A rock salt prism was used for the 1031 cm^{-1} band, and the average resolution was about 16 cm^{-1}. The peak-to-peak noise level on the records was about 0.5 percent.

TABLE I. Absolute intensities (cm^{-1}/cm atmos) and $\partial\mu/\partial Q$ values (esu) for SiF_4, CF_4 and SF_6.

SiF_4	CF_4	SF_6
$A(\nu_3)\cdots 2635(Q_1)$	$A(\nu_3)\cdots 4540(Q_1)$	$A(\nu_5)\cdots 4800(Q_1)$
$A(\nu_4)\cdots\ 507(Q_2)$	$A(\nu_4)\cdots\ 41.7(Q_2)$	$A(\nu_6)\cdots\ 280(Q_2)$
$\frac{\partial\mu}{\partial Q_1}\cdots\pm 167.4$	$\frac{\partial\mu}{\partial Q_1}\cdots\pm 219.8$	$\frac{\partial\mu}{\partial Q_1}\cdots\pm 226.1$
$\frac{\partial\mu}{\partial Q_2}\cdots\pm 73.45$	$\frac{\partial\mu}{\partial Q_2}\cdots\pm 21.07$	$\frac{\partial\mu}{\partial Q_2}\cdots\pm 54.62$

The results obtained are plotted in Figs. 3a, 3b, 4a, and 4b. μ_0, $\partial\mu/\partial r$ and the values of the coefficients of L^{-1} in the equations $Q=L^{-1}R$, are plotted as functions of the potential constants obtained from the general solution over a wide range of values in Fig. 9. The frequencies used in these calculations are listed in Table II, and the Si—F distance was taken as 1.54A.[19]

As mentioned before, the relative signs of μ_0 and $\partial\mu/\partial r$ are correct, but the absolute signs are indeterminate. The value given by the Simanouti model[11] for F_{11} is indicated by the dashed line, and it does not seem likely that the true potential constant differs by more than a few percent from this result. Consequently we can conclude either that

$$\mu_0=2.3\,d \qquad \partial\mu/\partial r=-7.49\,d/A$$

or that

$$\mu_0=3.3\,d \qquad \partial\mu/\partial r=3.66\,d/A.$$

CARBON TETRAFLUORIDE

The CF_4 used was obtained from the Minnesota Mining and Manufacturing Company. It contained

TABLE II. Fundamental frequencies of SiF_4, CF_4, and SF_6 (cm^{-1}).

SiF_4[a]	CF_4	SF_6
$\nu_1(A_1)$ (liq.) = 800	$\nu_1(A_1)=904$[b]	$\nu_1(A_{1g})=775$[d]
$\nu_2(E)$ (liq.) = 268	$\nu_2(E)$ (liq.) = 437[b]	$\nu_2(E_g)$ (liq.) = 644[d]
$\nu_3(F_2)=1031\,(Q_1)$	$\nu_3(F_2)=1267\,(Q_1)$[c]	$\nu_3(F_{2g})$ (liq.) = 524[d]
$\nu_4(F_2)=391\,(Q_2)$	$\nu_4(F_2)=632.5\,(Q_2)$[c]	$\nu_4(F_{2u})=363$[d]
		$\nu_5(F_{1u})=947\,(Q_1)$[e]
		$\nu_6(F_{1u})=615\,(Q_2)$[e]

[a] Jones, Kirby-Smith, Woltz, and Nielsen J. Chem. Phys. 19, 242 (1951).
[b] Yost, Lassetre, and Gross, J. Chem. Phys. 4, 325 (1936).
[c] Nielsen, Richards, and McMurry, J. Chem. Phys. 16, 67 (1948).
[d] R. T. Lagemann and E. A. Jones, J. Chem. Phys. 19, 534 (1951).
[e] D. Edelson and K. B. McAfee, J. Chem. Phys. 19, 1311 (1951).

[18] D. M. Dennison, Phys. Rev. 31, 503 (1928).

[19] L. O. Brockway, Revs. Modern Phys. 8, 231 (1936).

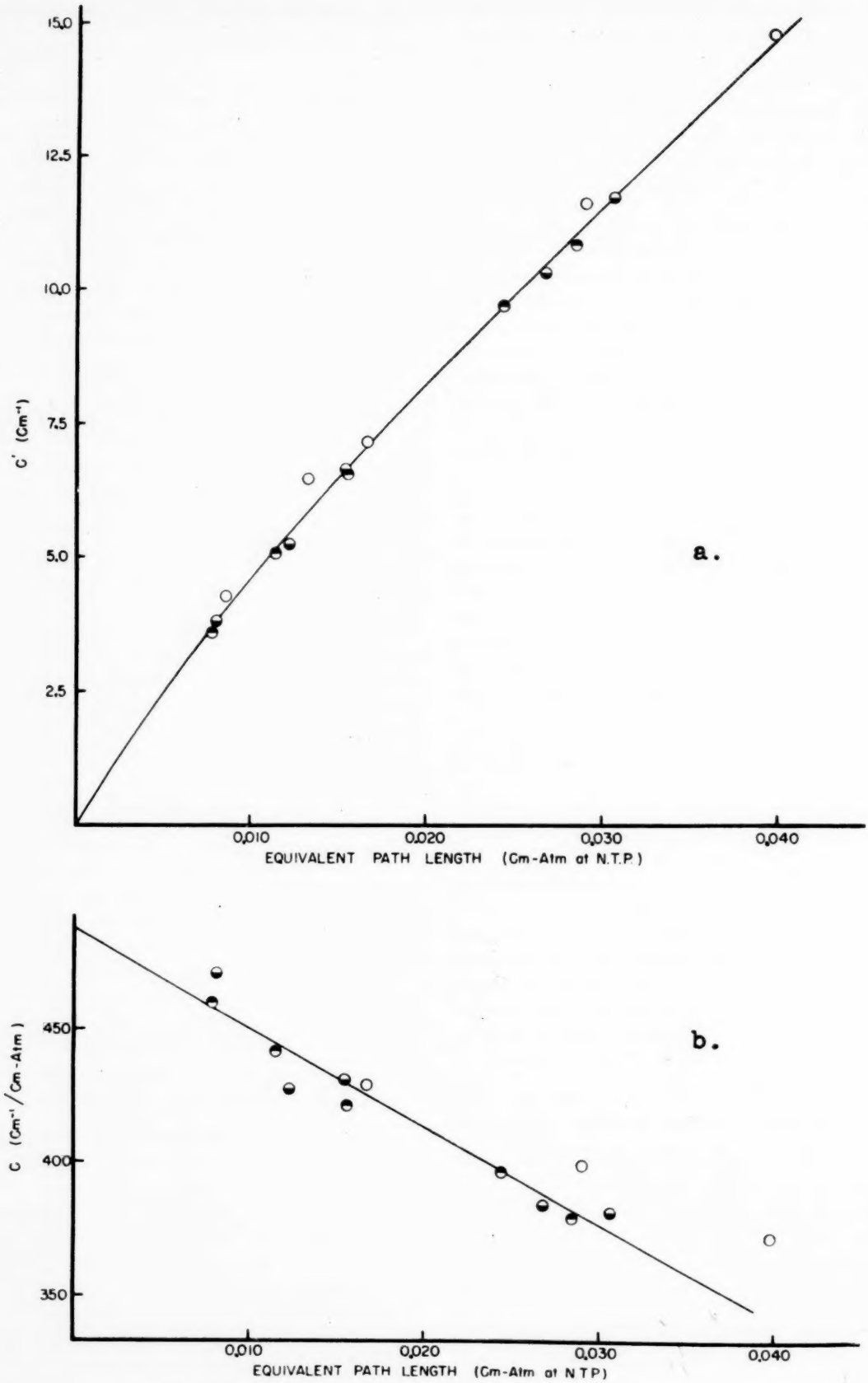

FIG. 3. Integrated absorption intensity of the 391 cm^{-1} band of SiF_4.

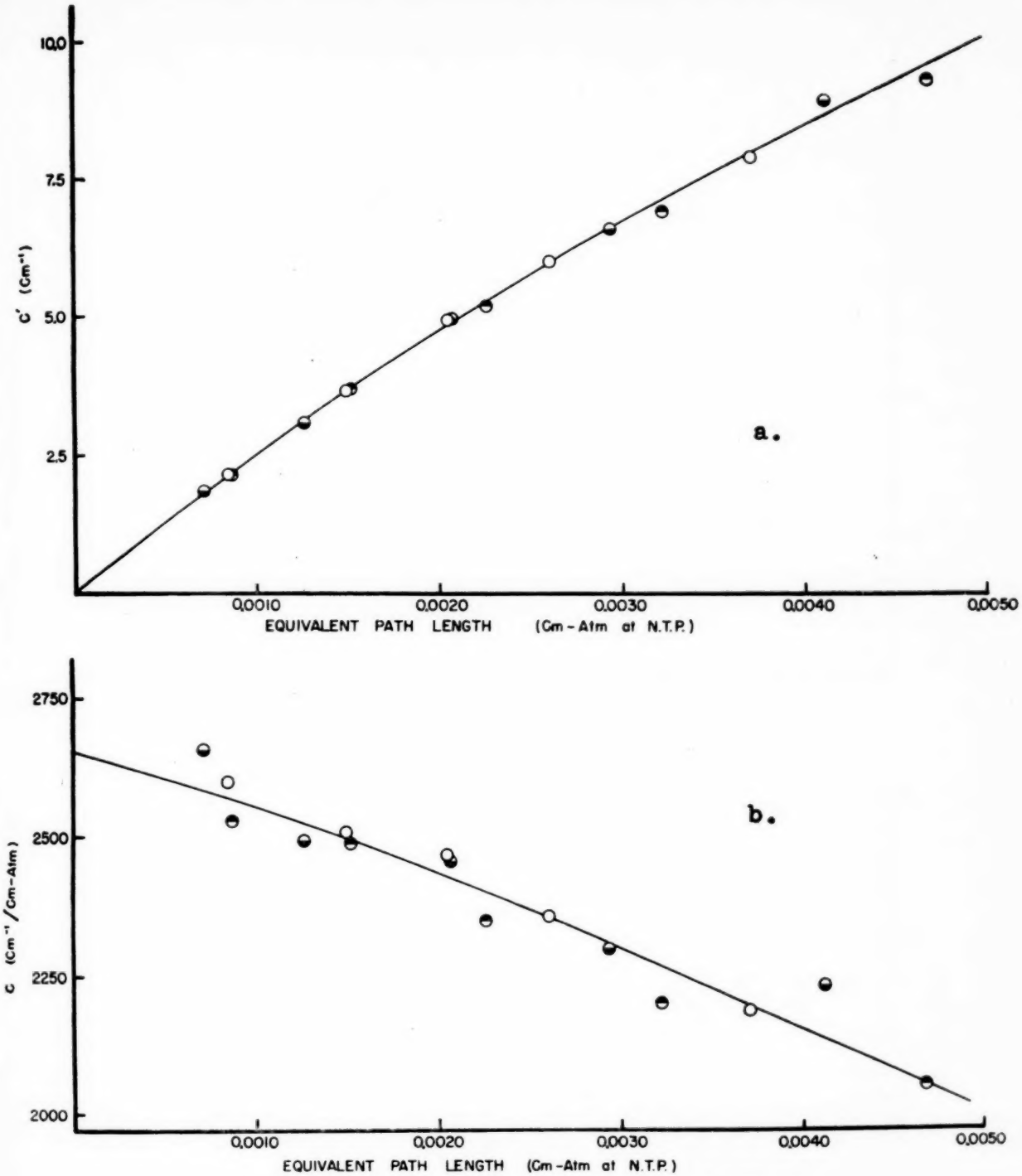

FIG. 4. Integrated absorption intensity of the 1031 cm^{-1} band of SiF_4.

about 5 percent fluoroform and traces of carbon dioxide, hexafluoroethane, and an unidentified material. The gas was fractionally distilled twice, and it was estimated from the decrease in peak value of the most intense CF_3H fundamental (1152 cm^{-1}) that about 90 percent of the CF_3H originally present was removed. Hence the CF_4 used was of greater than 99 percent purity.

The intensity of the 632 cm^{-1} band was determined using a potassium bromide prism. This band was sufficiently close to the 15 micron carbon dioxide band that it was necessary to exclude atmospheric carbon dioxide. No band was scanned until the strong Q branch of the carbon dioxide fundamental was indetectable on single beam operation. The average resolution used was about 14 to 15 cm^{-1}. A rocksalt prism was

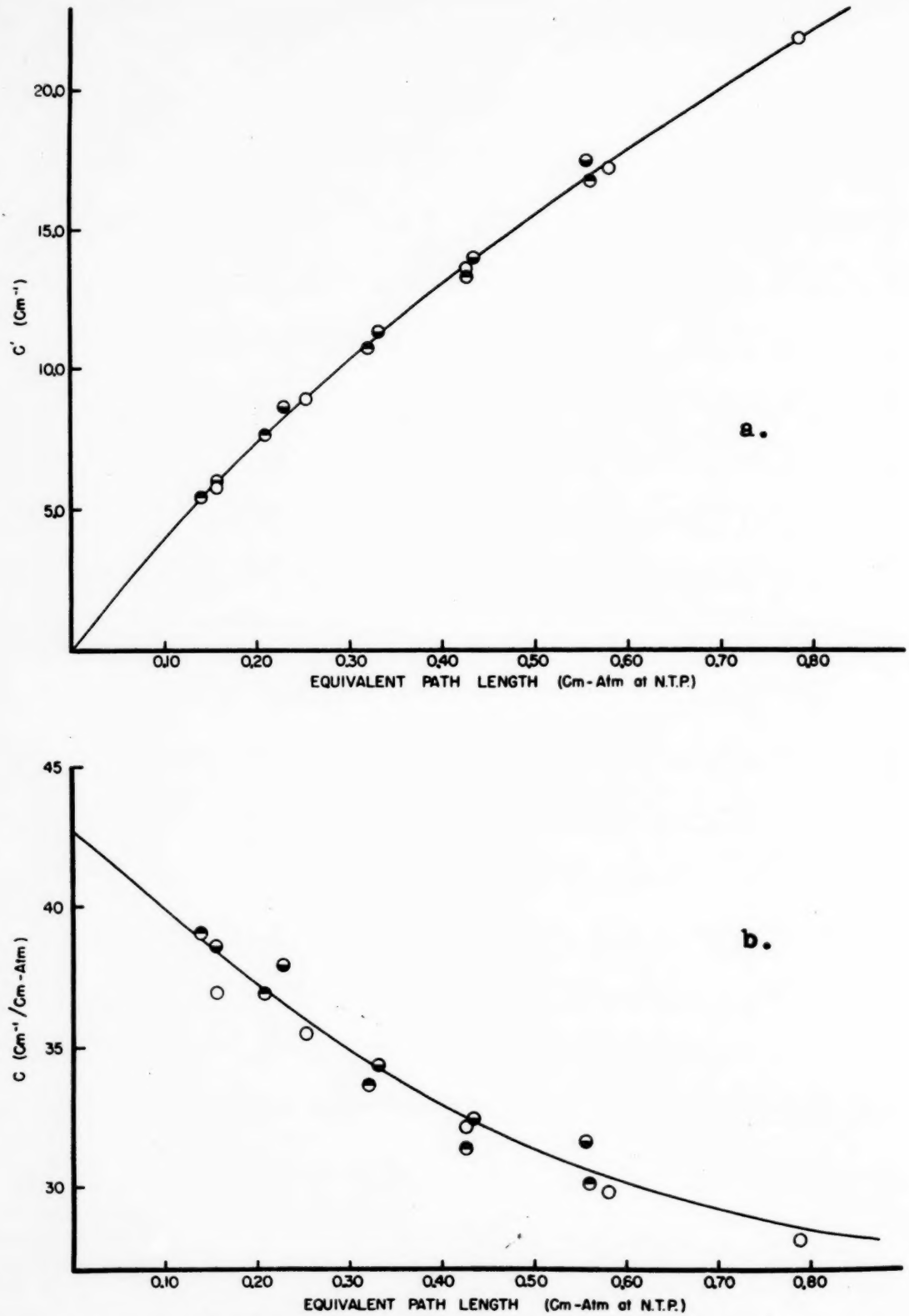

FIG. 5. Integrated absorption intensity of the 632 cm^{-1} band of CF_4.

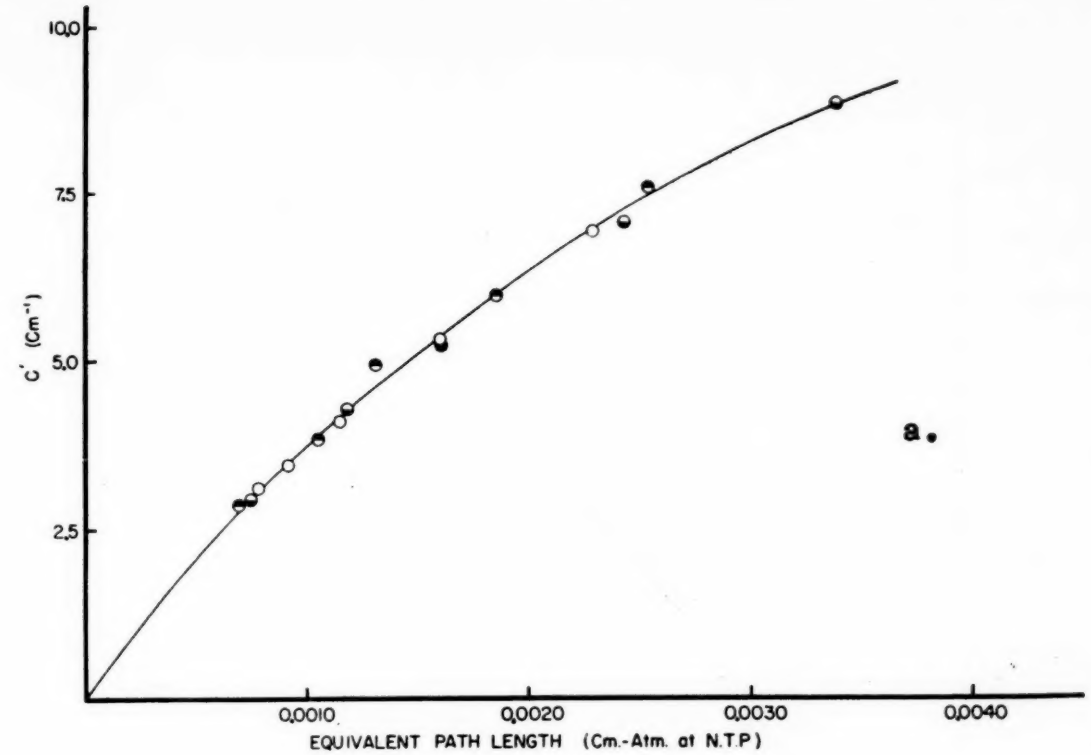

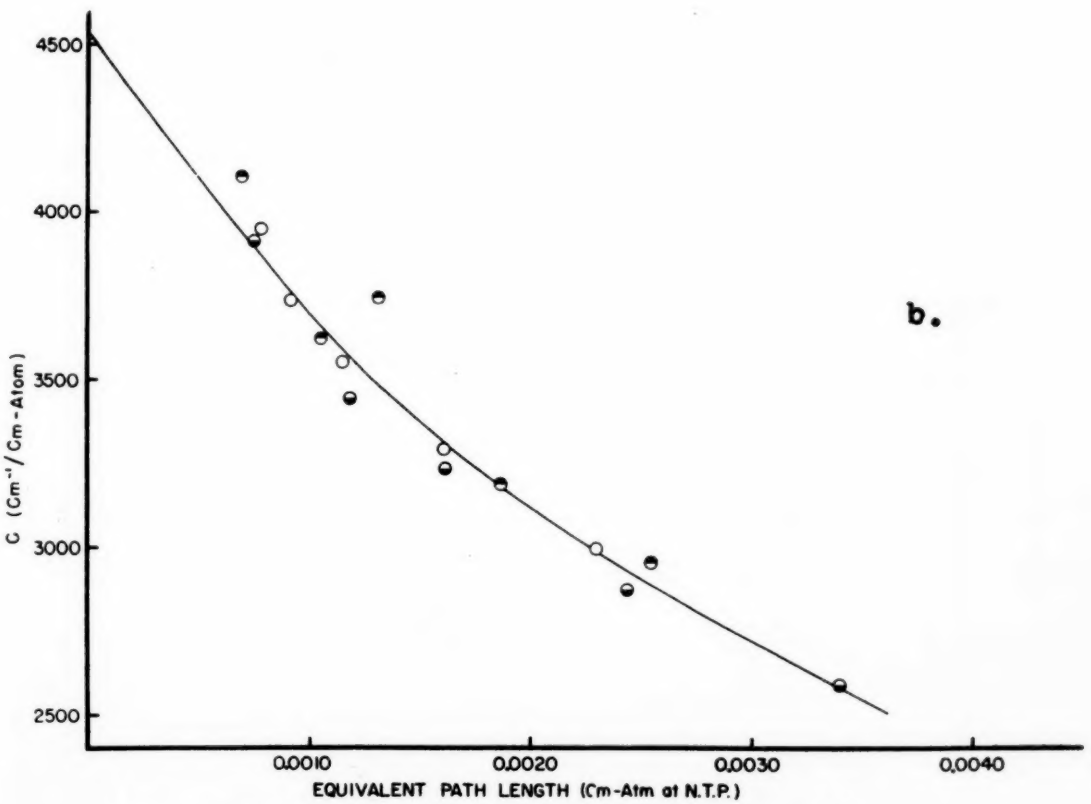

FIG. 6. Integrated absorption intensity of the 1267 cm^{-1} band of CF_4.

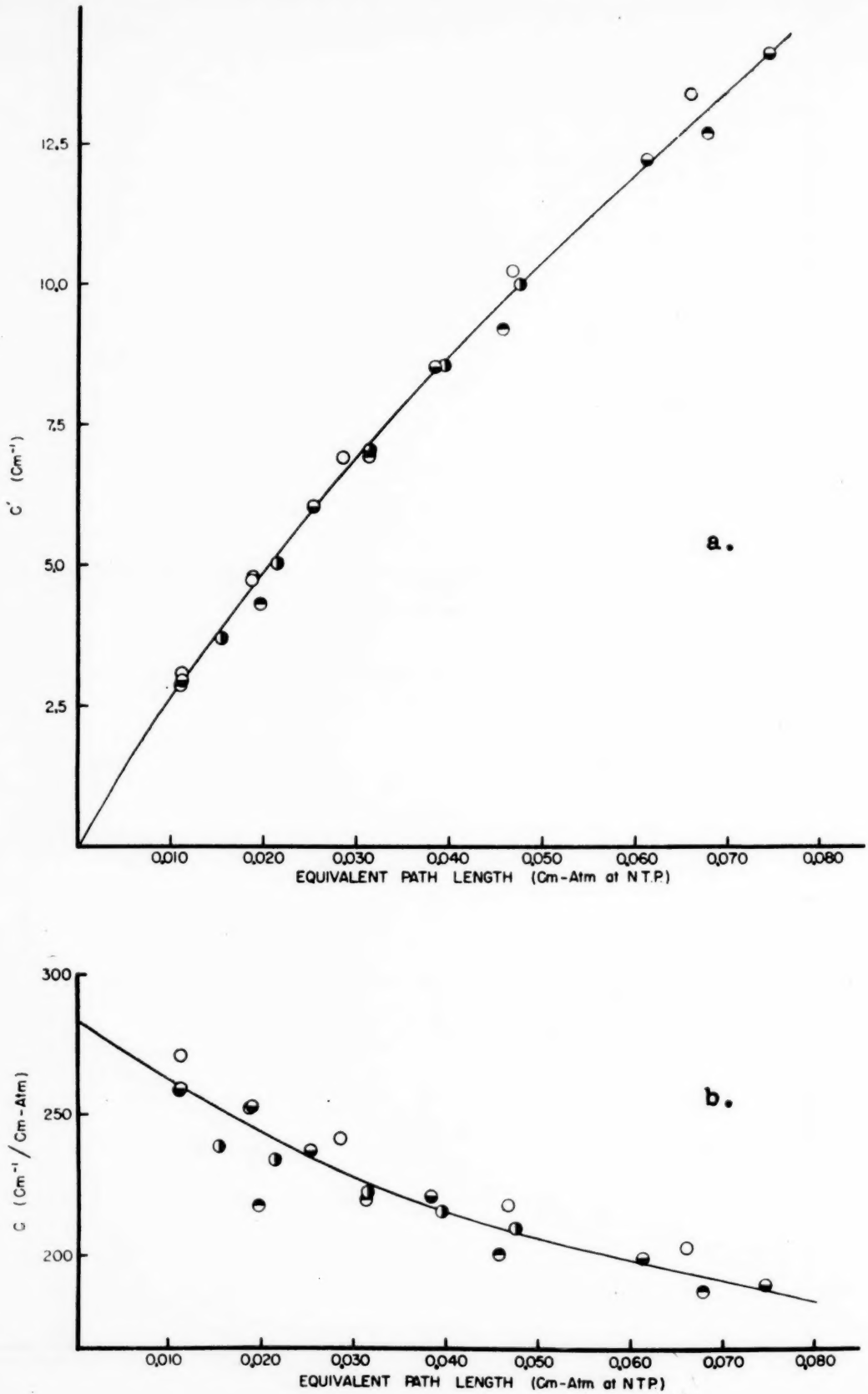

FIG. 7. Integrated absorption intensity of the 615 cm^{-1} band of SF_6.

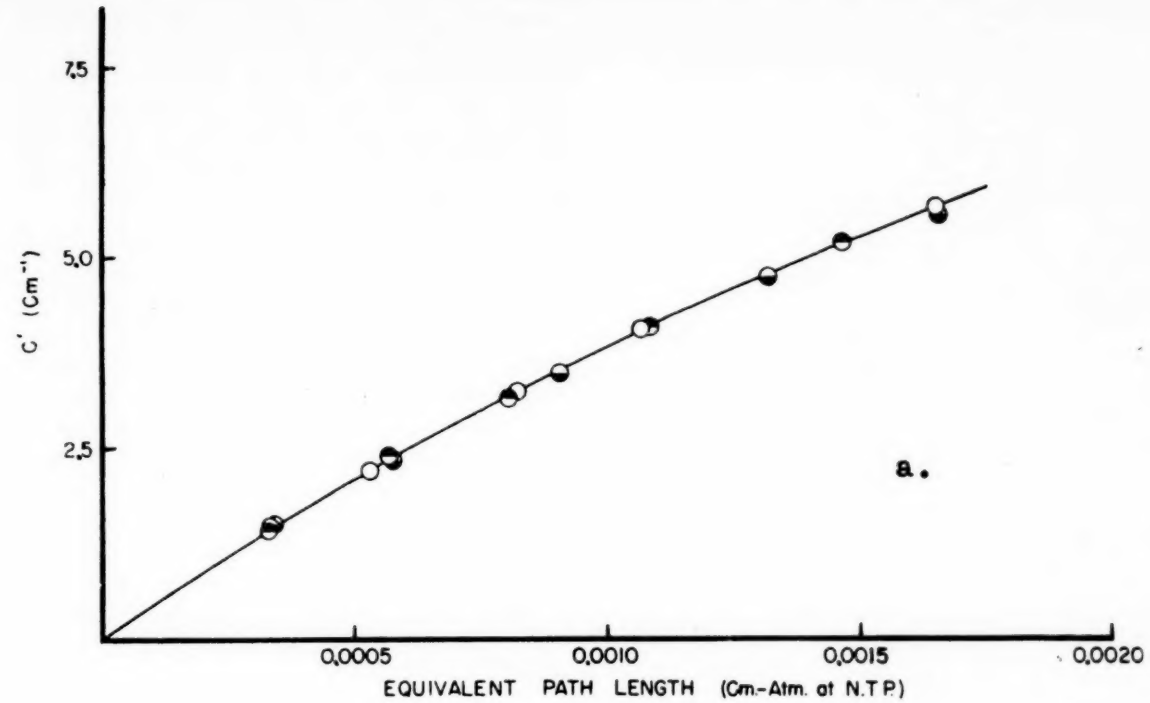

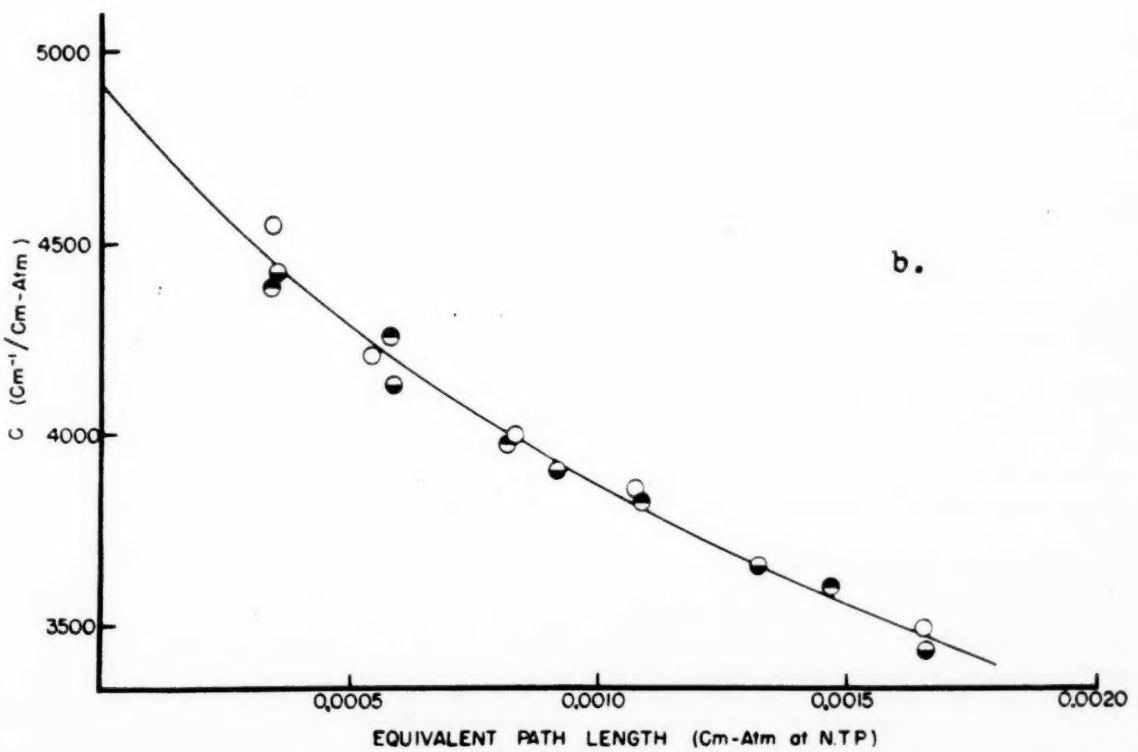

FIG. 8. Integrated absorption intensity of the 947 cm^{-1} band of SF_6.

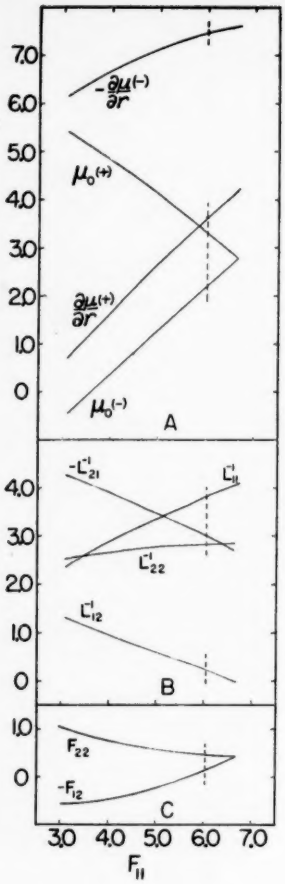

FIG. 9. SiF_4 (A) Bond moments (d) and bond moment derivatives (d/A). (B) Coefficients in normal coordinate transformation ($\times 10^{12}$). (C) Force constants ($\times 10^{-5}$); all as functions of the Si−F stretching force constant, $F_{11}(\times 10^{-5})$. Dashed line indicates most probable value of F_{11}.

used for the 1267 cm^{-1} band, and the resolution was roughly 20 cm^{-1}. The peak-to-peak noise level on the records was less than 1.5 percent in both cases.

The experimental results are plotted in Figs. 5a, 5b, 6a, and 6b; μ_0, $\partial\mu/\partial r$ and L^{-1} elements as functions of the potential constants appear in Fig. 10 in the same way as for SiF_4. The frequencies used in the calculation are listed in Table II; and 1.36A was used for the C−F distance.[19] Subsequent to the completion of the calculation, a newer investigation[20] has assigned ν_3 to a frequency of 1283 cm^{-1}, a change of slightly more than one percent which would not significantly alter the results.

As before, the potential constants of Simanouti lead to the alternate results

$$\mu_0=1.12\,d \quad \partial\mu/\partial r=4.88\,d/A, \quad \text{or} \quad \mu_0=2.36\,d \quad \partial\mu/\partial r=3.35\,d/A.$$

SULFUR HEXAFLUORIDE

The SF_6 used was obtained from the Matheson Company. The only appreciable impurity reported by them was two percent of noncondensable gases (as air) by volume. This was removed by pumping on the condensed gas so that essentially 100 percent pure SF_6 was employed.

A potassium bromide prism was used for the 615 cm^{-1} band, and a rocksalt prism, for the 947 cm^{-1} band. The average resolution was about 11 to 12 cm^{-1}, and the peak-to-peak noise on the records was less than 1.5 percent in both cases.

The results are plotted in Figs. 7a, 7b, 8a, and 8b and in Fig. 11 as in the previous cases. The frequencies used in the calculations are listed in Table II. The S−F distance was taken to be 1.57A.[19]

The most probable values in Fig. 11 are indicated by dashed lines. Although the Heath and Linnett solution does not fit the lowest bending frequency $\nu(F_{2u})$ very well (4 percent error), the constant F_{11} is determined only by the two strong Raman active modes, $\nu(A_{1g})$ and $\nu(E_g)$, so we have chosen to determine F_{11} in this way. It is also possible to establish an independent upper limit for F_{11} as follows. Employing the Wilson F and G matrices the following results are obtained, where a complete quadratic potential function has been used:

for the A_{1g} species,

$$A+4B+L=\lambda(A_{1g})m_y=6.723\times 10^5 \text{ dynes/cm}; \quad (27)$$

for the E_g species,

$$A-2B+L=\lambda(E_g)m_y=4.642\times 10^5 \text{ dynes/cm}. \quad (28)$$

The definitions of the force constants used are those of Decius[21] $A\equiv f^2_{rr}$, $B\equiv f^1_{rr}$ (right angles), $L\equiv f^i_{rr}$ (linear). From the above equations it follows that $A+L=5.336\times 10^5$ dynes/cm. L is the bond stretching interaction force constant between two bonds lying along a straight line. This constant would be expected to be positive either on the basis of resonance arguments or by considering that there are repulsion forces acting between the F atoms. That is, one would expect the one S−F bond length to decrease if the other S−F bond were stretched. This conclusion is strengthened by the fact that B (the bond stretching interaction force constant for bonds at right angles) is $+0.347\times 10^5$ dynes/cm [obtained from Eqs. (27) and (28)]. Consequently, if it is assumed that L cannot be less than zero, then F_{11} cannot be greater than 5.336×10^5 dynes/cm.

Therefore, the most probable results are

$$\mu_0=2.65\,d \quad \partial\mu/\partial r=3.85\,d/A \quad \text{or} \quad \mu_0=0.65\,d \quad \partial\mu/\partial r=-6.58\,d/A.$$

CONCLUSIONS

The problem of distinguishing between the alternative solutions is a difficult one, except for SF_6. One

[20] P. J. H. Woltz and A. H. Nielsen, J. Chem. Phys. **20**, 307 (1952).

[21] J. C. Decius, J. Chem. Phys. **16**, 1025 (1948).

would expect a value of approximately 2.2 d for the Si−F moment on the basis of electronegativities.[22]

On the other hand, the dipole moment of SiH_3F has been accurately determined from the microwave spectrum as 1.27 d.[23] This implies either a lower Si−F moment or an Si−H moment of the order of 1 d (H^--Si^+). However, both arguments lead to the choice $\mu_0=2.3\,d$, and it seems that the error does not exceed $\pm 0.3\,d$.

The difficulty with this conclusion is that the corresponding value of $\partial\mu/\partial r$, $-7.5\,d/A$, is much larger than in the other two molecules as well as of opposite sign; i.e. the moment decreases when the bond is stretched, whereas in CF_4 and SF_6 it increases. Consequently, some caution is advisable, particularly since the identification of μ_0 with the static moment of the bond is open to question.

For CF_4, electronegativities suggest a value of roughly 1.5 d for the C−F moment,[22] intermediate between the two possibilities. The dipole moment of CF_3H is reported to be 1.59 d[24] and this leads to C−F moments of 1.19 d or 1.99 d, depending on the polarity of the C−H dipole which we assume has a magnitude of 0.4 d.

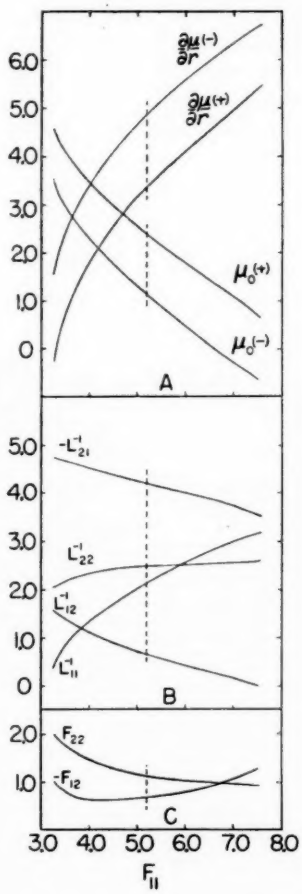

FIG. 10 CF_4 (A) Bond moments (d) and bond moment derivatives (d/A). (B) Coefficients in normal coordinate transformation ($\times 10^{12}$). (C) Force constants ($\times 10^{-5}$); all as functions of the C−F stretching force constant, F_{11} ($\times 10^{-5}$). Dashed line indicates most probable value of F_{11}.

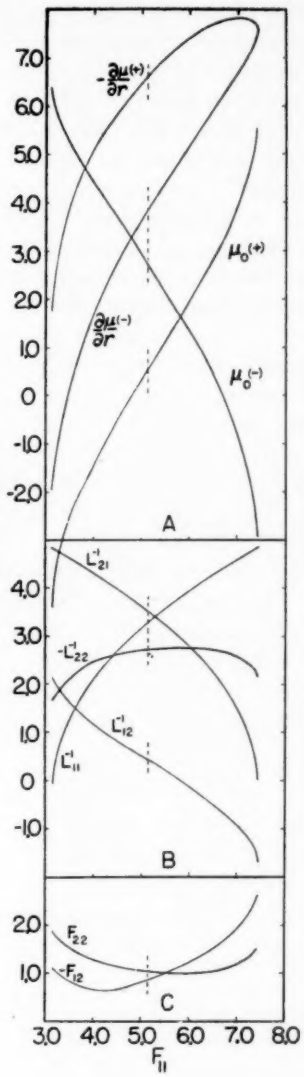

FIG. 11. SF_6 (A) Bond moments (d) and bond moment derivatives (d/A). (B) Coefficients in normal coordinate transformation ($\times 10^{12}$). (C) Force constants ($\times 10^{-5}$); all as functions of the S−F stretch-force constant, F_{11}($\times 10^{-5}$). Dashed line indicates most probable value of F_{11}.

If the conventional polarity, C^--H^+, is correct, we conclude that we must choose $\mu_0=1.12\,d$ and $\partial\mu/\partial r=4.9\,d/A$. However, there are strong theoretical arguments,[25,26] for the polarity C^+-H^-, and in this case the other choice, 2.36 d, becomes the better. Moreover, if the true value of F_{11} is 5.6×10^5 dynes/cm rather than 5.2×10^5 dynes/cm, the moment corresponding to positive $(\partial\mu/\partial Q_1)/(\partial\mu/\partial Q_2)$ would be reduced to 2.0 d. Consequently, a clear choice on this basis seems impossible at present.

However, Barrow and McKean[27] found that in CH_3F $\partial\mu/\partial r=4.70\,d/A$ for the C−F bond (the less reasonable alternative was 4.50 d/A), a value close to that associated with the lower dipole moment. Therefore it seems

[22] L. Pauling, *Nature of the Chemical Bond* (Cornell University Press, Ithaca, 1948), p. 64 ff.
[23] Sharbaugh, Thomas, and Pritchard, Phys. Rev. **78**, 64 (1950).
[24] K. L. Ramaswamy, Proc. Indian Acad. Sci. **2A**, 364 (1935).
[25] C. A. Coulson, Trans. Faraday Soc. **38**, 433 (1942).
[26] W. L. G. Gent, Quart. Revs. (London) **2**, 383 (1948).
[27] G. M. Barrow and D. C. McKean, Proc. Roy. Soc. (London) **A213**, 27 (1952).

most likely that $\partial\mu/\partial r = 4.88\, d/A$. The magnitude of the moment increases as the bond is stretched (this last conclusion is valid in either case). We must also conclude then that in CF_3H the polarity is $C^- - H^+$.

The choice is a little easier for SF_6. An electronegativity based on di- or tetravalent sulfur (sp hybridization[22]) predicts an S—F moment of about 1.5 d but in hexacovalent sulfur (spd hybridization) the moment might be expected to be greater. It seems reasonable that the hexavalent S—F moment should be greater than that of Si—F. Since one of the choices is only 0.65 d, it seems quite likely that $\mu_0 = 2.65\, d$ is correct, in which case $\partial\mu/\partial r = 3.85\, d/A$ and the moment increases as the bond stretches. The only reservation that must be made is that if F_{11} is actually as great as 6×10^5 dynes/cm, the other choice of ratio also leads to a sufficiently large μ_0. However since, as was pointed out before, this would require a large negative stretch-stretch interaction term in the potential function, it seems safe to discount the possibility.

The most striking feature of the results for all three molecules is the large value obtained for $\partial\mu/\partial r$. Except in CH_3F such large values have been obtained previously only for highly resonating molecules such as CO, N_2O, CO_2, and COS. The fact that the moment in CF_4 and SF_6 increases as the bond is stretched implies that, if F is at the negative end of the dipole at equilibrium, the negative ion resonance form becomes more pronounced as the bond is stretched, in good agreement with the usual resonance argument. However, if our earlier conclusions are correct, the magnitude of $\partial\mu/\partial r$ is even greater in SiF_4 than in CF_4 or SF_6, and the moment decreases when the bond is stretched. For this we have no present explanation, although one can formally include a no-bond resonance form to produce this result. Nevertheless, this would still not explain the great difference between SiF_4 and the other two. The fact that the value of $\partial\mu/\partial r$ obtained for the C—F bond in CF_4 is so nearly the same as in CH_3F where there cannot be much resonance, implies that the large values may be associated with bonds to fluorine rather than resonance in the molecules.

Finally, the sensitivity of our results to the choice of potential function leads us to conclude that no bond moment or derivative calculated from the infrared intensities of a polyatomic molecule can be regarded as reliable unless the general potential function has been determined accurately or the sensitivity of the results to reasonable variations in the potential function has been calculated.

THE JOURNAL OF CHEMICAL PHYSICS VOLUME 21, NUMBER 9 SEPTEMBER, 1953

Effects of Electronic Charge Transfer between Adsorbate and Solid on Chemisorption and Catalysis

P. B. WEISZ
Socony-Vacuum Laboratories, Division of Socony-Vacuum Oil, Inc., Research and Development Department, Paulsboro, New Jersey
(Received September 25, 1952)

When chemisorption on a semiconductive solid is accompanied by electronic charge transfer between adsorbate and solid, an electronic boundary layer analogous to that in rectifying junctions may develop and polarization of charges in the solid may result. These phenomena may limit or control the chemisorption characteristics. The boundary layer theory developed for electrical contacts and elementary considerations concerning the effect of the polarization potential are applied to derive the form of relationships for the extent, heats, and rates of chemisorption and some consequences with respect to catalysis. An attempt is made to illustrate the detailed physical processes in order to examine the meaning of "heterogeneity" and "active centers" in cases of this type of chemisorption.

A. INTRODUCTION

THE application of knowledge concerning the electronic structure of solids to their behavior in chemisorption and catalysis is a logical extension of the fact that the chemical behavior of molecules is determined by the number and energy scheme characterizing their electronic orbitals. At this laboratory we have pursued the study of such relationships using concepts similar to those outlined by Dowden.[1] Boudart[2] has outlined a qualitative picture involving changes of Fermi level of the surface, which he considers as a quasi-isolated entity, with chemisorbed species equivalent to added impurities and applying analogies with behavior of bulk Fermi level in semiconductors.

When the interaction between adsorbate molecules (atoms) and a solid surface involves transfer of charge, electronic boundary phenomena can be expected to arise analogous to those encountered in the study of electrical contacts between solids and considerations concerning surface states.[3] It appears promising to extend existing theory regarding such contacts to determine the consequences and limitations upon chemisorption of electronic charge transfer processes. This will be attempted in this paper in regard to nonmetallic conductors.

B. GENERAL CONCEPTS

Upon contact of two different solids the initial difference in the free energy of the electrons in the two solids (Fermi levels) results in a flow of electrons across the contact boundary. The potential energy associated with the resulting accumulation of excess charge effectively raises the energy of the acceptor system towards that of the donor system until they are equal, in equilibrium. The number of charges transferred to attain equilibrium will depend on the initial difference in energy levels and on the amount of potential energy associated with the resulting progressive charge accumulation. When chemisorption of molecules is associated with the transfer of charge (e.g., one electronic charge per chemisorbed molecule), such process involving molecules A on a solid B may be likened to a contact of materials A and B; and the amount of chemisorption may be related to the electronic properties of materials A and B.

In analogy to the surface process upon contact of a metal and semiconductor to form a rectifying contact, Fig. 1 demonstrates by a customary energy diagram the processes involved in the chemical adsorption of gas molecules. Referring to Fig. 1(a), the P-type semiconductor in the upper portion of the figure is characterized by a work function Φ, and a density of acceptor levels n_D, located above the filled band by an amount $2Q$ with the Fermi level E_F half-way between. The adsorbable molecules have an ionization potential I. Transfer of a number N electrons to the solid (from N accordingly "chemisorbed" molecules) creates the space charges indicated by $(-)$ and is associated with the addition of potential energy to the solid shifting the total energy of the surface relative to the bulk solid by E, as indicated in Fig. 1(b). Exothermic donation will continue until the resulting charge transfer has raised the Fermi level of the solid to coincide with that in the adsorbate, i.e. by an amount $E_0=\Phi-I$. At this time therefore, a maximum number N_0 of chemisorbed molecules is reached [Fig. 1(c)]. A corresponding picture, Fig. 2, can be drawn for the interpretation of an N-type semiconductor and adsorbate molecules having an electron affinity α, with resulting donation to the adsorbate and depletion of impurity electrons and positive space charge in the boundary layer of the solid, until $E_0=\alpha-\Phi$.

The theory of the electronic boundary layer has had among its objects the calculation of the variation of the electrical potential with depth into the solid, $E(x)$, enabling subsequently the description of the characteristics of current flow across this potential barrier, and through the contact. In Sec. C following, analogous inquiries will be made into problems involving the chemisorbed layer to obtain information on the amount of charge transfer allowed in equilibrium, and into rate problems of the sorption processes by examining limit-

[1] D. A. Dowden, J. Chem. Soc. **1950**, 242.
[2] M. Boudart, J. Am. Chem. Soc. **74**, 1531 (1952).
[3] J. Bardeen, Phys. Rev. **71**, 717 (1947).

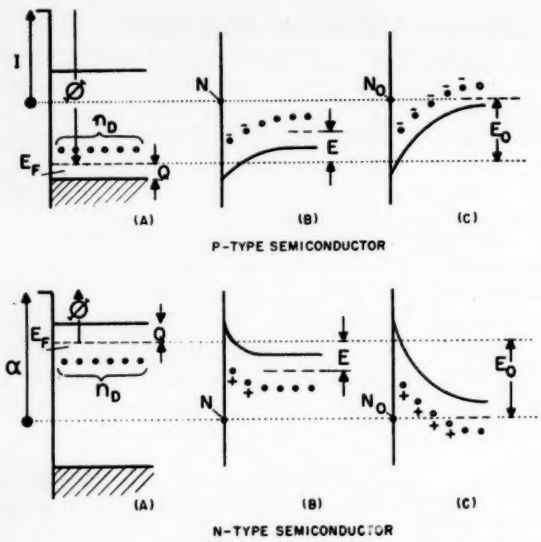

FIG. 1. Energy diagrams of semiconductors (a) before (b) after partial, and (c) after equilibrium chemisorption on surface. The abscissa represents depth (x) into the semiconductor.

ing electron transfer rates analogous to certain current flow problems.

The simple theory of the electronic boundary layer is based on the calculation of the electrical potential resulting from the accumulation of charges within the semiconductor. In the treatment of the boundary layer the effect of the remaining opposite surface charge finds expression only in the process of assigning the potential $E_0=\Phi-I$ (or $\alpha-\Phi$) as a boundary condition at $x=0$. The Coulomb field associated with this surface charge itself can modify the relationships of the simple boundary theory, and such "polarization effects" may themselves determine the nature of chemisorption phenomena. This will be discussed in Sec. D.

The incorporation of both effects into a general theory presents mathematical difficulties. However as in the case of study of electrical contacts, within the large realm of possible physical conditions which may be encountered, many will be dominated by one or the other mechanism. Furthermore it will be seen that both lead to similar consequences as regards certain chemisorption phenomena.

C. APPLICATION OF THE BOUNDARY LAYER THEORY

1. Amount of Chemisorption

The theory of the boundary layer[4,5] develops the form of the potential $E(x)$ in the boundary layer by applying

(a) Poisson's equation:

$$\frac{d^2E}{dx^2}=\pm\frac{4\pi}{\epsilon}\rho(x), \tag{1}$$

where $\rho(x)$ is the charge density at x, ϵ the dielectric constant.

(b) Considerations of local chemical equilibrium between all charge carriers (electrons and holes) and their donors and acceptors, which define a function

$$\rho(x)=en_hf(p);\quad p=\frac{n(x)}{n_h}, \tag{2}$$

where n_h is the density of mobile current carriers in the bulk semiconductor, $n(x)$ their density at x, and where $f(p)$ is determined by electronic constants of the solid.

(c) The relationship resulting from equating the opposing forces on the carriers from diffusive concentration gradients and electrical field, resulting in

$$\frac{dE}{dx}=\mp\frac{kT}{e}\frac{1}{p}\frac{dp}{dx}. \tag{3}$$

(The upper sign in Eqs. (1) and (3) is applicable to electron, the lower to hole conduction.)

These considerations determine the potential energy function in the boundary layer. If the surface density of chemisorbed molecules is set to correspond to the total excess charge found in the boundary layer—divided by the unit electronic charge—we have

$$N_0=-\frac{1}{e}\int_0^\infty\rho dx=\frac{\epsilon}{4\pi e}\int_0^\infty\frac{d^2E}{dx^2}dx, \tag{4a}$$

$$\frac{d^2E}{dx^2}=\pm\frac{4\pi}{\epsilon}n_hf(p), \tag{4b}$$

$$p=\exp(-eE/kT). \tag{4c}$$

As boundary conditions we expect that: $E=E_0$ at $x=0$ and, measuring the potential with respect to that of the bulk of the semiconductor, $E=0$ at $x=\infty$. In general, $f(p)$ is a complicated function of the existence, volume densities, and energy levels of electron donor and acceptor levels, of traps, and activation energy for intrinsic conductivity. However, a few cases can be discussed with relative ease and are expected to embrace a large number of cases of interest.

If the semiconductors have no appreciable density of traps or appreciable intrinsic semiconductivity, the Schottky theory yields for the remaining cases

$$f(p)=\frac{1}{p+A}-\frac{P}{1+A}, \tag{5}$$

where $A=K/n_h$ is an expression of the amount of semiconductivity in the bulk semiconductor, with K representing the equilibrium constant for the thermal production of mobile charge carriers,

$$K=\left(\frac{2\pi mkT}{h^2}\right)^{\frac{3}{2}}\exp(-2eQ/kT)$$
$$10^{19}\exp(2eQ/kT)\ \text{cm}^{-3}, \tag{6}$$

[4] W. Schottky and E. Spenke, Wiss. Veröffentl. Siemens-Werken **18**, 1 (1939).
[5] N. F. Mott, Proc. Roy. Soc. (London) **A171**, 27 (1939); Proc. Cambridge Phil. Soc. **34**, 568 (1938).

and n_h given by[6]

$$n_h=\frac{K}{2}\left[1+\left(1+4\frac{n_D}{K}\right)^{\frac{1}{2}}\right], \tag{7a}$$

which for the case of a small degree of ionization to mobile carriers ($K<n_D$; or $A<1$) simplifies to

$$n_h=(Kn_D)^{\frac{1}{2}}. \tag{7b}$$

Three types of possible conditions can be classified.

Case a

$$E_0\gg Q,\quad Q\sim kT/e\quad\text{or}\quad Q>kT/e.$$

Whenever, as is here the case, $E\gg kT/e$, we find $p\ll 1$ over most of the boundary region [in view of (4c)]. Furthermore, in this case one can show with Eqs. (6), (7), and (4c) that $p\ll A$, and therefore Eq. (5) is approximated by $f(p)=1/A$, and (4b) becomes simply

$$\frac{d^2E}{dx^2}\approx\pm\frac{4\pi}{\epsilon}n_D. \tag{8}$$

Since the "tail" of the potential barrier is thus neglected, finite boundary conditions can be used to solve Eq. (8): $E=E_0$ at $x=0$, $dE/dx=0$ at $x=D$, implying an essentially finite depth D over which the space charge density is constant and equal to the density of donors (or acceptors) n_D.

For such a saturated space charge layer Eq. (8) the number of molecules chemisorbable (4a) becomes

$$N_0=\left(\frac{\epsilon}{2\pi e}E_0n_D\right)^{\frac{1}{2}}=10^3(\epsilon E_0'n_D)^{\frac{1}{2}}, \tag{9}$$

where E_0 is in practical ev units. The boundary layer involves a thickness of solid

$$D=10^3(\epsilon E_0'/n_D)^{\frac{1}{2}} \tag{9a}$$

of the semiconductor.*

It is instructive to express the maximum possible amount of molecules chemisorbable by an electron transfer process in terms of the fraction of surface sites thus covered, θ_M, and the relative concentration of active donors (or acceptors) to total atomic sites, B, in the semiconductor. If we assume 4.6A^2 for a typical magnitude of a surface "site," and $B\approx n_D/10^{23}$,

$$\theta_M=0.15(\epsilon E_0'B)^{\frac{1}{2}}. \tag{9b}$$

It will be noted that for a reasonable order of magnitude of E_0' of unity (ev), and a favorably high $\epsilon=10$, even the absurdly high assumption of $B=1$ does not allow complete surface coverage in chemisorption. Consequently, the mechanism leads to a small fraction of surface sites capable of involvement in chemisorption, as if only a very small number of special "active centers" were capable of chemisorption. For example, for a "promoter" concentration of $B=10^{-4}=0.01$ percent, a dielectric constant $\epsilon=5$, and $E_0=1$ ev, one obtains $\theta_M\approx 0.4$ percent.

It is to be noted that this model does not contain any temperature dependence of chemisorption.

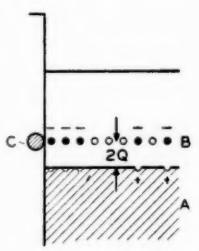

FIG. 2. Semiconductor with acceptor levels ionized thermally in the bulk and by electronic chemisorption near the surface.

Case b

$$E_0\ll Q,\quad Q>kT/e.$$

In this case Eq. (5) simplifies to

$$f(p)=(1/p)-p, \tag{10}$$

and formulas (4a, b, c) are integrable to give the chemisorbable quantity

$$N_0=2\left(\frac{\epsilon}{4\pi e}n_h\frac{kT}{e}\right)^{\frac{1}{2}}\left[\cosh\left(\frac{eE_0}{kT}\right)-1\right]^{\frac{1}{2}}, \tag{11}$$

with Eqs. (6) and (7b)

$$n_h\approx 3\times 10^9 n_D^{\frac{1}{2}}\exp(-eQ/kT). \tag{12}$$

It is instructive to compare chemisorption under this condition with that which would occur in the case of "saturation," formula (9). For this purpose we will call the number of chemisorbable molecules under that condition $N_{0\text{ISAT}}$. With obvious approximations we obtain from Eq. (11)

for $E_0\approx kT/e$:

$$N_0\approx N_{0\text{ISAT}}\times(n_h/n_D)^{\frac{1}{2}}. \tag{13}$$

for $E_0\gg kT/e$:

$$N_0\approx N_{0\text{ISAT}}\times(n_h/n_D)^{\frac{1}{2}}\exp(eE_0/kT). \tag{14}$$

Since $n_h<n_D$, and by definition of this case ($E_0\ll Q$), both cases imply that there is less chemisorption in this case than in the case of "saturation" in the boundary layer. This case of chemisorption is clearly temperature dependent and, for a given temperature, is dependent on the activation energy for the production of mobile carriers (by way of n_h).

[6] N. F. Mott and R. W. Gurney, *Electronic Processes in Ionic Crystals* (Oxford University Press, New York, 1950), p. 158.

* Since the author's first paper [P. B. Weisz, J. Chem. Phys. **20**, 1483 (1952)] went to press and during preparation of this manuscript, a journal was received containing the papers: P. Aigrand and C. Dugas, Z. Electrochem. **56**, 363 (1952); K. Hauffe and H. J. Eugell, *ibid.* **56**, 366 (1952). These authors also derive and discuss the relation Eq. (9).

Case c

$$E_0 \approx Q, \quad Q \approx kT/e \quad \text{or} \quad Q > kT/e.$$

For low ionization in the semiconductor ($Q > kT/e$), $A < 1$, but neither p nor A may be neglected relative to each other, and Eq. (5) becomes

$$f(p) = 1/(p+A), \tag{15}$$

while for high ionization ($Q \approx kT/e$) the second term must also be included

$$f(p) = (1/p+A) - p. \tag{16}$$

The Eqs. (4a, b, c) are not directly soluble with Eqs. (15) or (16). However it is clear that the terms Q/kT (from A) and E_0/kT (from p) will appear in the solution of these cases, implying that chemisorption will be temperature dependent, or at a given temperature will depend on the activation energy for the production of mobile carriers in the semiconductor.

2. Temperature Dependence of Amount Chemisorbable

With the exception of one case (Case a), in which the energy levels involved lead to a "saturated" boundary layer, the amount chemisorbable proves to be temperature dependent on the basis of this model of formation of an electric boundary layer. The dependence is in most cases of the form $N_0 \approx \exp(-U/kT)$.

A temperature dependence may also arise when the semiconductor is of such structure that its Fermi level, and therefore E_0, move appreciably with temperature. This will be the case for $Q \approx kT/e$ in which case the Fermi level may move appreciably from its position between impurity level and the nearest band edge to the center of the forbidden region. This will lower E_0 with increasing temperature and in Case a above, when $Q \approx kT/e$, the appropriate choice of E_0 would be affected by this consideration.

3. The Heat of Chemisorption

On the basis of the above electronic picture the first electron transferred between adsorbate and solid will be associated with a heat of adsorption equal to E_0, $(\Phi - I)$ or $(\alpha - \Phi)$. The transfer will result in a rise of potential energy of the surface as already illustrated in Sec. 1 above. Subsequent electron transfer will be subject to ever decreasing net energy release. The heat of adsorption will decrease with coverage.

In the solutions of Eqs. (4a, b) above, E_0 enters as a boundary condition of the potential at $x=0$, for the equilibrium condition. It can be considered to be the potential E_{0f} when only N_{0f} entities have been adsorbed. In the simplest case of the semiconductor developing a "saturated" boundary layer, we have from Eq. (9),

$$E_{0f}' = \frac{N_{0f}^2}{\epsilon n_D} 10^{-6}, \tag{17}$$

where E_{0f}' is E_{0f} in practical ev units. With this the energy drop, equal to the incremental heat of adsorption is

$$|\Delta H_f| = E_0' - \frac{N_{0f}^2}{\epsilon n_D} 10^{-6}, \tag{18}$$

or

$$|\Delta H_f| = E_0'(1 - (\theta/\theta_M)^2), \tag{19}$$

where θ and θ_M are the instantaneous and maximum fractions of surface covered, respectively. This is illustrated by curve (A) in Fig. 3.

The topic of the variation of heat of chemisorption with coverage has been subject to speculation concerning questions of heterogeneity of the surface, and interaction among adsorbed species as alternative causes. The electronic model of solid-adsorbate interaction leads to the required type of variation due to a cause which does not fall strictly into either category. The model requires no heterogeneity on the surface. "Interaction" is a term more nearly applicable to this case, although it follows mainly as a matter of semantics in that the presence of an adsorbed molecule will cause the next to experience a new environment. The solid surface acquires potential energy due to the electronic charge transfer accompanying chemisorption, and the effect can be visualized as being "felt" by the surface as a whole through the agency of the mobile carriers responsible for electrical conductivity of the solid. The phenomenon is closely associated, therefore, with the ability of the solid to be an electrical conductor. In Sec. D it will be seen that a type of direct electrostatic interaction must also take place, particularly in the initial stage of chemisorption; the intent here is to point out that the declining heats of chemisorption result from a model involving the creation of an electronic boundary layer alone.

4. Nature of the Active Center

Some of the physical implications concerning the mechanistic nature of the processes involved in electronic interaction as treated in this paper are of interest.

Figure 2 shows the energy diagram of a P-type semiconductor having a chemisorption layer. It will serve as

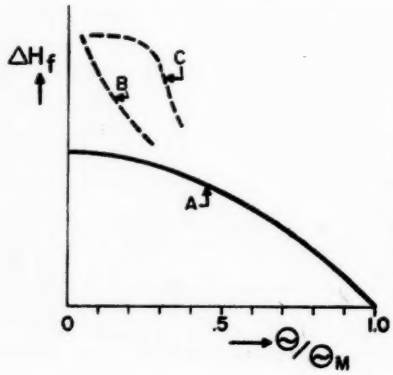

FIG. 3. Heat of chemisorption *vs* fraction of total possible coverage: *A* barrier layer theory, *B* modification by polarization, *C* modifications by two-dimensional treatment of Coulomb forces.

a guide for discussion. The variation of electrical potential in the boundary has been omitted. The valence band of a *P*-type semiconductor is pictured (*A*), with acceptor levels (*B*) located energetically above the filled band, by the energy difference $2Q$, and chemisorbed molecules on the external surface (*C*). In the interior, semiconductivity is due to a number of electrons having been raised to and combined with acceptor levels, rendering these negative in charge but leaving an equal number of positive and mobile holes in the valence band. In the boundary layer however, electron donation from chemisorbed species has resulted in "stopping up" holes which may at any one time have occurred due to thermal activation (dotted indication of would-be holes). Excess negative charge exists in this layer.

There are at the surface proper a number of "impurity" or acceptor levels. When chemisorbable molecules first contact the solid, it is logical to assume that they are available for "bond" formation. A number of chemisorbed species may be expected to result, at most equal to the number of such surface acceptors and locatable at the geometrical sites of the latter. At this point geometrically identifiable "active sites" may be said to exist.

The present picture of electronic interaction provides that if the energy relationships so allow, further interaction and chemisorption is possible, involving the acceptance of electronic charge due to acceptor sites deeper within the solid. While such acceptance is associated with the existence of sites which are geometrically identifiable in the volume of the solid, there are no longer specific sites on the surface which will be the "active" centers of sorption. Moreover, the acceptor sites within the solid can be "blurred out" over a considerable depth, and in a portion of the barrier region (where $E \sim kT$) the accepted electrons continually "change places."

Another aspect of the model is important for the illustration of rate processes. Once the surface acceptors have been involved, a chemisorption candidate will "know" about the existence of additional acceptors only by virtue of mobile holes appearing at the surface. If the interior of the solid were an insulator (or a semiconductor at zero absolute temperature), no further chemisorption could take place. The rate of appearance of holes at the surface would be governed by the temperature, the activation energy Q, and any electric field already set up in the boundary by previous chemisorptive processes. The hole being a migrating valence-electron deficiency of the solid would not be preferentially locatable on any portion of the surface. (This does not imply, of course, that there may not exist secondary factors, e.g., steric considerations with respect to surface structure, which might lead to preferences.)

5. Rate Problems

When the mobile carriers of electrical current existing in the solid are the agents by which the mechanism proceeds, the velocity with which such chemisorptive processes can proceed will be determined or *at least limited* by the rate of appearance of such mobile carriers at the reaction site, i.e., at the surface ($x=0$ in the boundary layer).

a. Rate of Sorption

It is of interest to see the conditions which determine the magnitude of the initial rate of chemisorption, i.e., rate of transfer of chemisorption electrons between solid and adsorbate. The condition of having a finite and large amount of chemisorption *possible* in equilibrium is not sufficient for observing it, if the rate of establishment is too long in terms of a practicable time scale in the laboratory.

At the start of chemisorption, no potential barrier exists. Mobile electrons (or holes) from the interior of the semiconductor need not overcome a potential rise to reach the surface. The situation is analogous to having at the surface a certain vapor pressure of electrons (holes) which can react with adsorbate molecules there. We can deduce the flux of electrons (holes) $\mathfrak{N}_i$ striking a unit area of surface:

$$\mathfrak{N}_i = \tfrac{1}{4} n_h \bar{v}, \quad \bar{v} = (3kT/m)^{\frac{1}{2}}, \tag{20}$$

where m and $\bar{v}$ are the velocity and the mass of the electrons (holes), respectively. The velocity $\bar{v}$, at 300°K, has the magnitude of 10^7 cm/sec. With this, and with Eq. (12), we find for the initial rate of arrival of charge carriers

$$\mathfrak{N}_i \approx 10^{16} n_D \exp(-eQ/kT). \tag{21}$$

As an example we may inquire into the maximum activation energy Q characterizing the semiconductor which will allow the chemisorbed layer in the example of Sec. C.1, Case a, ($\sim 10^{13}$ molecules per cm^2) to be formed in one second. The result is given in Table I for different concentrations of donor (acceptor) levels, and for $T \approx 700$°K. This should be viewed properly as based upon the *initial* rate of chemisorption. As chemisorption proceeds the potential barrier built up will reduce the incidence of charge carriers at the surface. Referring for the sake of familiarity to the case of electrons in the case of the *N*-type semiconductor, after some chemisorption has proceeded (Fig. 1(b), bottom), electrons must now overcome the potential E in order to arrive at the surface.

This rate of incidence of charge carriers is calculable as the number of electrons (holes) striking the surface due to the presence of a concentration $n_{x=0}$, having a mobility b, and being under the influence of the field $(dE/dx)_{x=0}$, as

$$\mathfrak{N} = n_{x=0} b \left(\frac{dE}{dx}\right)_{x=0}, \tag{22}$$

where $n_{x=0}$ is obtainable from (4c), and $(dE/dx)_{x=0}$ from the solution of Eq. (4b) appropriate for the particular solid and condition. For example, in the simplest case

TABLE I. Maximum activation energy Q in semiconductor, allowing initial chemisorption rate of 10^{13} molecules/sec/cm².

n_D (cm^{-3})	Q (ev)
10^{20}	1.9
10^{18}	1.7
10^{16}	1.55

of the saturated type barrier, we obtain

$$\mathfrak{N}=3\times10^{9}b\left(\frac{2\pi e}{\epsilon}E_{0f}n_D\right)^{\frac{1}{2}}n_h\exp(-eE_{0f}/kT). \quad (23)$$

Since the potential E_{0f} at any time is a function of the amount of chemisorption coverage θ at that time, this relation placed into Eq. (23) will result in a relation of the rate of chemisorption *vs* the amount chemisorbed. Again, for the simplest case, we have $E_{0f}=\text{const}\,(\theta/\theta_M)^2$ (from Eq. (17)), and therefore Eq. (23) takes the form

$$\mathfrak{N}=C_1\cdot\exp\left[-e\left(Q+C_2\left(\frac{\theta}{\theta_M}\right)^2\right)\Big/kT\right], \quad (23a)$$

with C_1 being a relatively insensitive function of θ, and the term Q being negligible if $E_0\gg Q$. In this manner therefore, relationships result between adsorption rate and coverage, containing θ in the exponential term, a phenomenon encountered in experiments.

b. *Rate of desorption*

Of interest is the limit to the rate of desorption from the equilibrium chemisorbed layer based on electronic limitations. Since, in equilibrium, this rate will equal the adsorption rate with $E=E_0$, we can employ Eq. (23) and obtain

$$\mathfrak{N}_d\approx10^{7}n_D\exp(-eE_0/kT)\exp(-eQ/kT) \quad (24)$$

by assuming the order of magnitudes $\epsilon\approx1$, $E_0\approx1$ ev, $b\approx10$ cm/sec (v/cm)$^{-1}$ to obtain the relatively insensitive frequency factor.

Table I gives the desorption rates for various concentrations of donor (acceptor) levels n_D, and for various values of $(Q+E_0)$ in ev, for $kT/e=0.065$ ev ($T=700$°K).

The desorption rates vary within a relatively narrow range of the electronic properties of both solid and adsorbate $(Q+E_0)$ from measurable magnitudes of desorption to essentially "permanent" chemisorption. In the latter case elevation of temperature (equivalent to an inversely proportional decrease in $(Q+E_0)$) can result in measurable rates of removal.

The total number adsorbed, as seen in Sec. C.1 would increase with E_0, but invariably this would be accompanied by a higher activation energy for desorption (E_0+Q) as seen in Eq. (24).

Measurable laboratory rates of desorption correspond to a magnitude $>10^{11}$ sec^{-1} cm^{-2}, and Table II indicates such to occur only for $(Q+E_0)<2$ ev, i.e., smaller than about 45 kcal/mole.

6. Catalysis

The presence of a solid catalyst may create a new chemical reaction path by formation of a chemisorbed species whose electronic and therefore chemical properties differ from that of the normal molecule. In such cases electronic phenomena regarding chemisorption will carry along definite consequences concerning catalytic behavior.

a. Poisoning

If we assume that some chemical change can proceed involving N_a chemisorbed species, any agency which will reduce the number N_a may be expected to act as a catalytic poison. This amount of chemisorption has been shown to depend on the electronic energies making up E_0 and on the number of impurity levels in the semiconductor n_D capable of creating charge carriers. Impurities can be added to a semiconductor which are of the opposite type to those initially producing semiconductivity. This effectively reduces n_D and consequently the addition can act as a catalytic poison. As a constituent of the solid catalyst, it would become a "permanent" poison.

Aside from this, molecules in the gas phase may have favorable electronic energy levels to compete with the reactant for chemisorption as demonstrated in Sec. C.1. In equilibrium the relative concentration of adsorbed species a and b should depend on the free energy change involved in their respective chemisorption reactions

$$\frac{N_a}{N_b}=\exp\left[-\frac{e(E_b-E_a)}{kT}\right]. \quad (25)$$

Formula (25), incidentally, shows the tendency of reduced poisoning effects at higher temperatures often observed in that in the limit $N_a/N_b\to1$, as $T\to\infty$.

Such chemisorption "poisons" are expected to be reversible in principle, although rates of desorption may become impracticably small, as demonstrated by the discussion in Sec. C.5.b and Table II. In such cases elevation of temperature to again achieve a reasonable exponent $-e(Q+E_0)/kT$ for the rate of desorption Eq. (24) may result in successful desorption.

b. Selectivity

The rapid change of desorption rates with the magnitude of the exponent $-e(Q+E_0)/kT$ indicates a mechanism by which selectivity with respect to desorption of certain products (I entering into E_0) from certain solid catalysts (Φ entering into E_0; and Q) may be achieved.

The critical dependence of maximum possible desorption and adsorption rates on $(Q+E_0)$ and Q, respectively, indicates a mechanism by which selectivity of specific solids with respect to certain catalytic reactions

TABLE II. Maximum desorption rates *vs* energy $(Q+E_0)$ for various semiconductor impurity concentrations n_D.

n_D (cm^{-3})	Rate of desorption $\mathfrak{N}_d$ (sec^{-1} cm^{-2}) $(Q+E_0)$ (ev)			
	1.2	1.8	2.4	3.0
10^{20}	10^{19}	10^{15}	10^{11}	10^{7}
10^{18}	10^{17}	10^{13}	10^{9}	10^{5}
10^{16}	10^{15}	10^{11}	10^{7}	10^{3}
10^{14}	10^{13}	10^{9}	10^{5}	10^{1}

can result. In order to attain a usefully large over-all reaction rate, both adsorption rates and desorption rates must be sufficiently large. If we assume—for simplicity—that reactant and product molecules have similar electronic energy levels (i.e., same E_0), then the criteria for obtaining useful rates, $Q<2.0$ (from Table I, Adsorption) and $(Q+E_0)<2.4$ (from Table II, Desorption) when combined, require that $E_0<0.5$ ev; $Q<2.0$ ev, in order to obtain a successful over-all rate of reaction.

c. Kinetic Constants

In deriving the kinetics of the "rate of conversion" in a catalytic reaction, the individual rates of adsorption, desorption, and conversion of all species must be considered. It was shown in Sec. C.5.a that the rates of adsorption due to the above electronic mechanism will be of the form $A\exp-(eE/kT)$, where E is the potential set up by the boundary layer for the steady-state solution of the specific reaction scheme. Since E itself is a function of the total number of molecules ΣN_i chemisorbed, any change made in the reaction system affecting the numbers N_i will be reflected in an exponential term also, or conversely, any change resulting in altering an exponential (activation energy) will result in a change in the coefficients made up of ΣN_i. Interdependence of "frequency factors" and "activation energies" will result, with increasing frequency factors accompanying increases in activation energy.

D. CHEMISORPTION AND POLARIZATION ENERGY

In the absence of an appreciable electronic boundary layer "polarization" of the solid may cause and control chemisorption effects. This applies to the initial chemisorption events in the process of building up a boundary layer, or to cases where no such layer of appreciable thickness can develop.

Polarization refers to the phenomenon of redistribution of electrical changes within the solid conductor due to the attractive Coulomb potential of a charged molecule adsorbed on its surface. The only gain of potential energy arising from such redistribution may cause the over-all energetics of chemisorption with charge transfer to be favorable.

Figure 4 illustrates the first chemisorption event in such a process involving the polarization energy. The energy cycle consists of (a) removal of an electron from molecule M to infinity (A), requiring ionization energy I; (b) inserting this electron (at infinity, A') into the solid, returning the energy of the work function Φ. (c) The positively charged molecule M at the surface attracts mobile electrons in the solid due to the Coulomb potential "P," fitted at infinity to the Fermi potential of the solid. The Coulomb potential is given by

$$P=e/2\epsilon x. \tag{26}$$

Relocation of an electron from the bulk semiconductor (B) to a position close to the surface results in an energy gain which at x_L is of sufficient magnitude to make the process exothermic for any final location $x<x_L$. Thus chemisorption may occur involving the acceptor levels within x_L from the surface. Figure 4 demonstrates the energy returnable due to polarization to be P_1, P_2, P_3 for progressively deeper lying acceptor levels.

1. Amount of Chemisorption

We may assume that the density of charge donors (or acceptors) n_D is the same for any depth. The number of molecules adsorbed (per cm^2 of surface) will be N_0, the thickness of involvement x_L,

$$N_0=x_L n_D \tag{27}$$

for the total amount adsorbable, where x_L is given by

$$I-\Phi-\frac{e}{2\epsilon x_L}=0. \tag{28}$$

The total amount adsorbable is, therefore,

$$N_0=\frac{en_D}{2\epsilon(I-\Phi)}. \tag{29}$$

It will be noted that Eqs., (28) and (29) will yield $x_L\to\infty$ and $N_0\to\infty$ for $I-\Phi\to 0$; however this treatment on the basis of polarization alone will not apply for such cases of extended depth of involvement, as pointed out initially.

2. Heat of Chemisorption

The total energy of chemisorption involving a site at x will be given as $\Delta H=e(I-\Phi-P_x)$. As a function of amount adsorbed, N,

$$\Delta H=e\left(I-\Phi-\frac{en_D}{2\epsilon N}\right), \tag{30}$$

or in terms of fraction of the total chemisorbable amount θ/θ_M,

$$\Delta H=e(I-\Phi)\left(1-\frac{\theta_M}{\theta}\right). \tag{31}$$

3. Rate Considerations

The adsorption process must involve mobile carriers (holes in the P-type solid of Fig. 4) as charge transfer

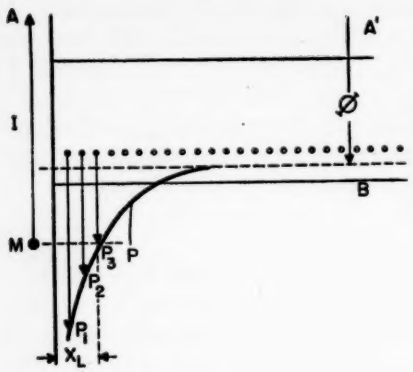

FIG. 4. Energy relationships in chemisorption involving electronic polarization.

agents. Therefore, the rate is limited by the rate of appearance of carriers at the surface, following the considerations of Sec. C.5.a for the case of no potential barrier.

The desorption process will require an activation energy at least equal to ΔH, and the desorption rate will depend on coverage, with an activation energy given by Eq. (31).

4. Apparent Heterogeneity

The above picture indicates exothermic processes, with energies dependent on geometric depth of the acceptor site. The physical process can be described also as a process of ionization in which the ionized species loses its charge to a finite distance. Instead of the normally defined ionization potential I, a small ionization potential $I'=I-P=I-e/2\epsilon x$ is operative. The contribution of P could be thought of as being associated with the solid in the sense of an effective work function $\Phi'=\Phi+P=\Phi+e/2\epsilon x$. Operationally this could lead to an interpretation of chemisorption phenomena as indicating sites of heterogeneous sorptive energies; e.g., electron acceptor levels may in chemical language appear to have different "acidities," caused by the variation of polarization energies with depth of location.

E. POLARIZATION AND BOUNDARY LAYER—CONCLUSION

In practical units the Coulomb potential (26) is

$$P_{(ev)}=\frac{7.2}{\epsilon x_{(A)}}. \tag{32}$$

An estimate of the range over which it will be "felt" in the solid can be had as the distance x_P at which this potential will "drown" in thermal diffusion potentials, i.e., $P\approx kT/e$,

$$x_P\approx 300/\epsilon \text{ A units.} \tag{33}$$

Comparison of this magnitude with the depth D of a calculated electronic boundary layer will indicate to what extent the polarization effect or the boundary layer phenomenon will prevail and in what cases both may have to be considered.

Polarization effects will modify the relationships developed from barrier layer theory[7] when the thickness of the layer D becomes smaller than the magnitude x_P. In addition to normal exothermic donation, polarization can add additional electrons only at locations beyond D.

In the process of formation of the chemisorbed layer the *initial* lay-down processes are expected to be influenced by polarization. The relationship of heat of adsorption *vs* coverage (Fig. 3) will need to be modified in the vicinity of $\theta=0$ in the direction of the hyperbolic law Eq. (31), as indicated by curve B, Fig. 3.

The effective range of the Coulomb force must also be considered in determining how the change of the potential energy resulting from formation of a given adsorption site will be "felt" on other parts of the two-dimensional surface. The presentation of a heat of adsorption *vs* coverage curve (Fig. 3) assumed that the potential energy of the entire surface rises uniformly with progress of chemisorption (one-dimensional model). Formula (33) indicates that for $\epsilon=5$ applicable to the semiconductor example in Sec. C.1, the effective radius of a potential hill created by an initial adsorption site will be 60A. This is to be compared with an average distance between acceptor levels of 210A in that example. In the initial stages of chemisorption subsequent adsorption events do not "know" about each other and modify Fig. 3 as indicated by curve C.

Two possible physical phenomena have been discussed independently with a view on their possible role in chemisorption: The development of an electronic barrier layer within the solid surface and the effect of polarization of the electronic defects. In any specific case one mechanism may predominate or both may be operative. There are many limitations to the applicability of the simple quantitative treatments given above. For example, in developing the barrier theory the applicability of the "diode" *vs* the "diffusion" theory to express the rate processes must be examined; in some cases the concentration of defects in the semiconductor may itself not remain constant in time or space.[8] In considerations of polarization involving relatively short-distance Coulomb interaction, the limitations of classical laws when electronic wave functions begin to overlap must be remembered. Quantitative treatments of the cases in which both polarization and barrier layer phenomena are essential are subject to many possible choices for conditions and approximations, leading to various laborious treatments. Such efforts would appear to become more timely after the simpler considerations have served as initial guides for experimental orientation in this field.

In conclusion, the author wishes to thank his colleagues M. L. Deutsch and C. D. Prater for discussions which have contributed to this work.

[7] The effect of such modification on the potential energy barrier was discussed by H. A. Bethe, Bib. Sci. Ind. Rept. **1**, 290b (1946) for metal semiconductor rectifying junction.

[8] Carl Wagner (private communication).

Heat Capacity and Thermal Diffusivity of Silver Bromide*

T. E. POCHAPSKY
Institute for the Study of Metals, The University of Chicago, Chicago, Illinois
(Received May 20, 1953)

Rapid heat capacity measurements are reported for silver bromide at temperatures in the range from room temperature to 411°C. Thermal diffusivities and conductivities are derived for the same temperature range from an analysis of the cooling of a platinum wire embedded in the bromide. The results show that vacancy equilibrium is established in less than about 10^{-4} second above 350°C.

IT is commonly agreed that there is more than a percent fraction of defect sites in a silver bromide lattice near the melting temperature and that the energy required to produce this number of imperfections is manifest in an abnormally high heat capacity at elevated temperatures.[1] If these defects are of the Schottky type, so that vacancies are produced by a diffusion of ions to sinks, it is reasonable to suppose that there will be a delay before thermal equilibrium can be established in silver bromide that is heated suddenly. Some of the defects might also be expected to migrate in a temperature gradient to produce an anomalous thermal conductivity.

Exploratory measurements were made to investigate both of these possibilities. Rapid heat capacity measurements were made by coating a layer of silver bromide on a 5-mil platinum wire and determining the heating effect of current pulses relative to that obtained for an uncoated wire. Details of the apparatus will be published elsewhere. For the present, it is sufficient to say that two equal and opposite current pulses, separated by desired times, were used; crudely, the first pulse might be considered as functioning to heat the wire and the second pulse to measure the increase in resistance caused by the rise in temperature. Resistance measurements throughout the tests gave no indication of any attack of the platinum wire by the silver bromide. Specimens were heated in a vacuum furnace and test temperatures were picked at random rather than in an increasing sequence. Thermal diffusivities were determined from the cooling characteristics of a fine platinum wire along the axis of a 3-mm diameter rod of cast silver bromide.

The heat capacity determinations compare favorably with the results of Kanzaki,[2] as shown in Fig. 1. Higher values were obtained at the higher temperatures by Christy and Lawson.[3]

Values for the thermal diffusivity, shown in curve A of Fig. 2, are calculated on the basis of Tranter's[4] solution for the cooling of a perfectly conducting wire in an infinite medium subject to the condition that there is no thermal resistance at the interface of the wire and medium. Curve B in Fig. 2 shows the diffusivity obtained if no correction is made for the relative specific heat capacities of the platinum and silver bromide.

Thermal conductivities, derived from the diffusivities at the different temperatures, are shown in Fig. 3 along with a curve representing a $1/T$ dependence on temperature T. Kanzaki's[2] determinations for the specific heat and Strelkow's[5] results for the change in density with temperature are used in the derivation.

Considering that the diffusivity calculations are based on an idealized model, the agreement with published values in the range 0°C–100°C is good. Nevertheless, the increase near the melting temperature is questionable. Outside this small region, the conductivity has a normal inverse temperature dependence.

The time needed to heat a silver bromide film of the thickness used is somewhat less than 0.1 second, so that agreement with Kanzaki shows that vacancy equilibrium is established faster than this. A much shorter time can be deduced from the thermal diffusion

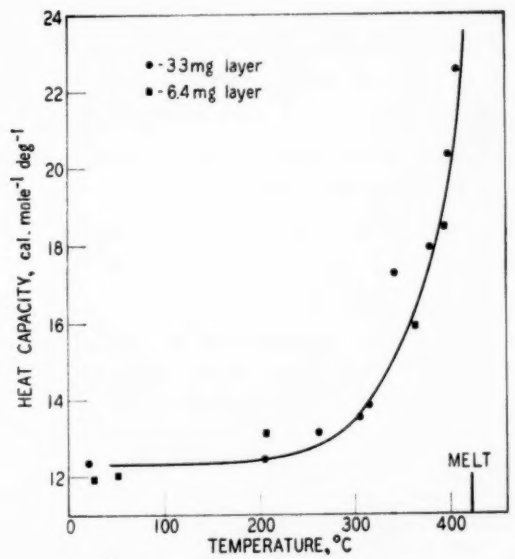

FIG. 1. Heat capacity of silver bromide.

* This work was supported in part by the U. S. Army Ordnance Department.

[1] A summary of these properties is given by S. W. Kurnick, J. Chem. Phys. **20**, 218 (1952).
[2] H. Kanzaki, Phys. Rev. **81**, 884 (1951).
[3] R. W. Christy and A. W. Lawson, J. Chem. Phys. **19**, 517 (1951).
[4] C. J. Tranter, Phil. Mag. **38**, 131 (1947).
[5] P. G. Strelkow, Physik. Z. Sowjetunion **12**, 77 (1937).

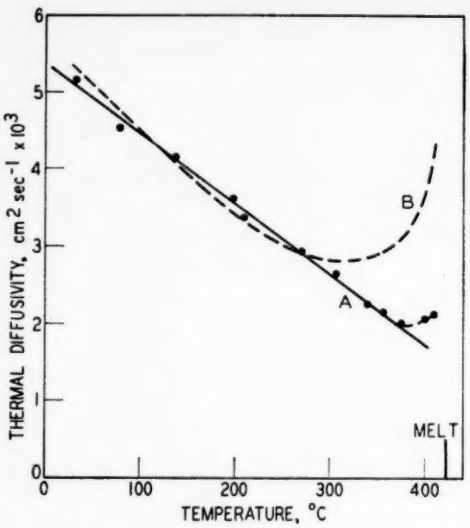

FIG. 2. Thermal diffusivity of silver bromide. Curve B represents results that are uncorrected for changes in heat capacity.

experiments. This faster estimate is based on the fact that the cooling curves can be simply transformed so that they all coincide. Such would not be the case if the heat capacity varied with time during the high temperature runs, as is apparent from the shape of curve B in Fig. 2. Furthermore, the platinum wire lost almost half of the heat supplied to it by a millisecond pulse before the pulse terminated. If the heat capacity did not reach an equilibrium value in a time of about 10^{-4} second at temperatures above 350°C, it would have been apparent in an abnormal initial cooling rate.

As shown by Kurnick,[1] there is strong evidence to believe that the defects in the silver bromide lattice are predominantly of the Schottky type above 300°C. If so, the time to establish thermal equilibrium is such that bromide vacancies can only come from sources that are not farther apart than the dimensions of mosaic blocks, i.e., 10^3-10^4 atomic distances. This conforms with the mechanism proposed by Seitz[6] who suggests that, on cooling, vacancies condense to form dislocation-like clusters or to join existing dislocations.

Summarizing, the results of the pulsed heat capacity measurements agree with those published by Kanzaki

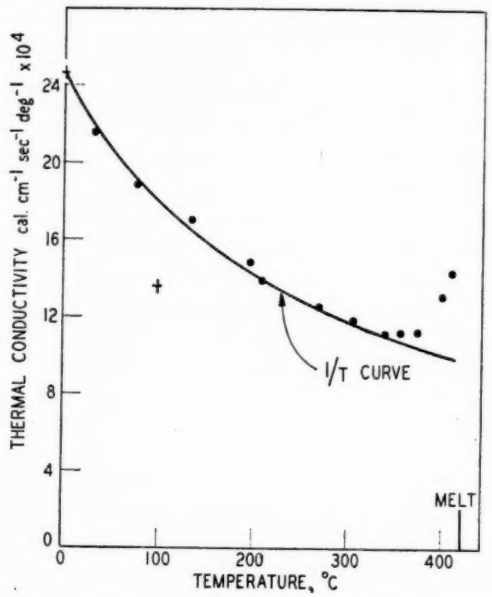

FIG. 3. Thermal conductivity of silver bromide. + values from *International Critical Tables*.

and show that the imperfections in silver bromide achieve temperature equilibrium in less than about 10^{-4} sec above 350°C. These imperfections have a small effect, if any, on the thermal conductivity at temperatures up to a few degrees of the melting point.

[6] F. Seitz, Revs. Modern Phys. **23**, 328 (1951).

Hindered Rotation Involving Two Asymmetric Groups

DONALD G. BURKHARD
University of Colorado, Boulder, Colorado
(Received April 27, 1953)

The wave equation is derived for two partially asymmetric tops rotating about a common axis and subject to an arbitrary hindering potential. Matrix elements of the Hamiltonian are evaluated using the hindered-rotation wave functions derived by Koehler and Dennison on the basis of a simplified model.

Evaluation of matrix elements involving the Eulerian polar angle is carried out by obtaining and making use of the factorizations of the symmetric-top wave equation.

THE structure of methyl alcohol has been investigated by Burkhard and Dennison[1] using a model which consists of a rigid hydroxyl group undergoing restricted rotation with respect to a rigid methyl group. This model has been extremely fruitful in identifying the complex microwave spectrum of methyl alcohol. The theory for methyl alcohol, however, only applies to a symmetric and an asymmetric group undergoing rotation about a common axis. In the present paper we will not attempt to generalize the problem to two completely asymmetric tops undergoing hindered rotation about a common axis but will simply examine the effect of replacing the symmetric methyl group in methyl alcohol by a partially asymmetric group. The remainder of the molecule will be left unchanged. The simplest kind of molecule to which the theory is applicable is shown in Fig. 1 where we regard the *STT* group as a rigid unit rotating with respect to the rigid *VW* group about the symmetry axis of the *STT* group. Some molecules which may fall into this category are hydroxyl amine and the 1, 1 disubstituted ethylenes. The derivation of an expression for the kinetic energy of the configuration shown in Fig. 1 proceeds in the same manner as for methyl alcohol. We repeat the argument here for convenience. Consider two vectors $\boldsymbol{\varrho}_1$ and $\boldsymbol{\varrho}_2$ drawn from the center of gravity of the molecule (which for simplicity is assumed to be stationary) to the respective centers of gravity of the *VW* and *STT* groups. Let $\mathbf{r}_i$ be a vector drawn from the center of gravity of the *VW* group to the mass m_i of that group. Let $\mathbf{R}_i$ be the corresponding vector from the center of gravity of the *STT* to the mass M_i. Let x, y, z and X, Y, Z be two sets of axes moving rigidly with the *VW* and *STT* groups, respectively, and with origins at the center of gravities of those groups. The Z axis is taken to be the symmetry axis of the *STT* group and small z is chosen to be parallel to Z. The *VW* atoms are assumed to lie in the yz plane.

The angular velocities of the *VW* and *STT* groups will be denoted by the vectors $\boldsymbol{\omega}$ and $\boldsymbol{\Omega}$, respectively, and their components along the moving axes will be $\omega_x, \omega_y, \omega_z$ and $\Omega_X, \Omega_Y, \Omega_Z$.

With these definitions the vector velocities of the individual particles in each group are, respectively,

$$\mathbf{v}_i=\frac{d\boldsymbol{\varrho}_1}{dt}+\boldsymbol{\omega}\times\mathbf{r}_i,$$

$$\mathbf{V}_i=\frac{d\boldsymbol{\varrho}_2}{dt}+\boldsymbol{\Omega}\times\mathbf{R}_i.$$

Since, from their definitions $\Sigma m_i\mathbf{r}_i=\Sigma M_i\mathbf{R}_i=0$, twice the kinetic energy becomes

$$2T=\Sigma m_i\left(\frac{d\boldsymbol{\varrho}_1}{dt}\right)^2+\Sigma M_i\left(\frac{d\boldsymbol{\varrho}_2}{dt}\right)^2 +\Sigma m_i(\boldsymbol{\omega}\times\mathbf{r}_i)^2+\Sigma M_i(\boldsymbol{\Omega}\times\mathbf{R}_i)^2.$$

The vector $\boldsymbol{\varrho}_1$ has a constant length and lies in the yz plane. The angle which it makes with the *VW* line is a constant. Thus $\boldsymbol{\varrho}_1$ moves as though it were rigidly connected to the *VW* group. The velocity of the entire molecule as seen from the moving x, y, z coordinate system is $(\boldsymbol{\omega}\times\boldsymbol{\varrho}_1)$. This is, however, the negative of the velocity of the x, y, z origin as viewed from the center of gravity of the molecule. Therefore,

$$d\boldsymbol{\varrho}_1/dt=-(\boldsymbol{\omega}\times\boldsymbol{\varrho}_1).$$

From the definition of $\boldsymbol{\varrho}_1$ and $\boldsymbol{\varrho}_2$ one has

$$\Sigma m_i\boldsymbol{\varrho}_1+\Sigma M_i\boldsymbol{\varrho}_2=0$$

and a substitution yields

$$2T=\Sigma m_i(\boldsymbol{\omega}\times\boldsymbol{\varrho}_1)^2+\Sigma M_i(\boldsymbol{\omega}\times\boldsymbol{\varrho}_2)^2 +\Sigma m_1(\boldsymbol{\omega}\times\mathbf{r}_i)^2+\Sigma M_i(\boldsymbol{\Omega}\times\mathbf{R}_i)^2.$$

Expanding the above expression one obtains

$$2T=A_1\omega_x^2+B_1\omega_y^2+C_1\omega_z^2-2D_1\omega_y\omega_z +A_2\Omega_X^2+B_2\Omega_Y^2+C_2\Omega_Z^2. \quad (1)$$

In general Eq. (1) gives the form of the kinetic energy for any two tops whose asymmetry is such that a principal axis of inertia of one (*STT* group) lies along the axis of mutual rotation of the two groups and the momental ellipsoid of the other (*VW* group) with one axis along the axis of mutual rotation, contains a single product of inertia in addition to moments of inertia about axes parallel and perpendicular to the axis of mutual rotation.

The moments of inertia appearing in Eq. (1) may be defined in a general way as follows: Let a coordinate

[1] D. G. Burkhard and D. M. Dennison, Phys. Rev. 84, 408 (1951).

system ξ, η, ζ be introduced whose origin is at the center of gravity of the entire molecule and whose axes are parallel to the axes xyz. The following moments of inertia may then be defined

$$A=\Sigma\mu_i(\eta_i^2+\zeta_i^2),$$
$$B=\Sigma\mu_i(\xi_i^2+\zeta_i^2),$$
$$C=\Sigma\mu_i(\xi_i^2+\eta_i^2),$$
$$D=\Sigma\mu_i\eta_i\zeta_i,$$

where μ_i is the mass of an atom at ξ_i, η_i, ζ_i, and the summation is over all the atoms in the molecule. The moments of inertia A_2, B_2, C_2 arise from an evaluation of the term $\Sigma M_i(\boldsymbol{\Omega}\times\mathbf{R}_i)$ in the kinetic energy. They are moments of inertia of the *STT* group about its center of gravity. A_2 is the moment of inertia of the *STT* group about an axis perpendicular to the *STT* plane. B_2 is the moment of inertia about an axis in the *STT* plane perpendicular to the axis of rotation. C_2 is the moment of inertia of the *STT* group about an axis parallel to the axis of rotation. In general, the term $\Sigma M_i(\boldsymbol{\Omega}\times\mathbf{R}_i)$ will take the same form for any group one of whose principal axes of inertia is parallel to the axis of mutual rotation.

With these definitions, A_1, B_1, C_1, and D_1 in Eq. (1) are then defined by the equations

$$A_1=A-A_2,$$
$$B_1=B-B_2,$$
$$C_1=C-C_2,$$
$$D_1=D.$$

To obtain the Hamiltonian we now add to T the potential energy V. For a simple sinusoidal n-fold potential V may be written in the form

$$V=(H/2)[1-\cos n(\varphi_1-\varphi_2)].$$

For Fig. 1, n would be 2. To obtain the wave equation we proceed exactly as in the case of methyl alcohol.

The orientation of the x, y, z axes which determine the position of the VW group may be specified by means of the Eulerian angles θ, φ_1, ψ and as usual one obtains

$$\omega_x=\dot\theta\cos\varphi_1+\dot\psi\sin\theta\sin\varphi_1,$$
$$\omega_y=-\dot\theta\cos\varphi_1+\dot\psi\sin\theta\cos\varphi_1,$$
$$\omega_z=\dot\varphi_1+\dot\psi\cos\theta.$$

The Eulerian angles which fix the orientation of the *STT* group are θ, φ_2, ψ and since the z and Z axes are always parallel, only differ from the preceding ones in the angle φ_2 which measures the rotation of the *STT* group about its symmetry axis. Expressions for Ω_x, Ω_y, Ω_z are obtained from ω_x, ω_y, ω_z by replacing φ_1 by φ_2. A substitution into Eq. (1) then yields the kinetic energy as a function of θ, ψ, φ_1, φ_2 and their time derivatives. When this is done the wave equation may be obtained in the usual manner by expressing the Laplacian in curvilinear coordinates for which the metric is given by $2T$. The metric in this case has the value

$$\{(A_1+A_2)C_2[(B_1+B_2)C_1-D_1^2]+[(A_1-B_1)C_1+D_1^2](A_2-B_2)C_2\sin^2x\}\sin^2\theta.$$

After writing out the Laplacian, making the substitutions,

$$\varphi=\frac{C_1}{C}\varphi_1+\frac{C_2}{C}\varphi_2,$$

$$x=\varphi_1-\varphi_2,$$

and the abbreviation

$$\delta=\frac{[(A_1-B_1)C_1+D_1^2](A_2-B_2)}{(A_1+A_2)[(B_1+B_2)C_1-D_1^2]}$$

and inserting the hindering potential, the wave equation takes the following form:

$$\mathrm{I}\quad\Bigg\{-\left[\frac{1}{A_1+A_2}+\frac{(A_1+A_2-B_1-B_2)C_1+D_1^2}{2(A_1+A_2)[(B_1+B_2)C_1-D_1^2]}\right]\left[\frac{1}{\sin\theta}\frac{\partial}{\partial\theta}\left(\sin\theta\frac{\partial u}{\partial\theta}\right)+\cot^2\theta\frac{\partial^2u}{\partial\varphi^2}-\frac{2\cot\theta}{\sin\theta}\frac{\partial^2u}{\partial\varphi\partial\psi}+\frac{1}{\sin^2\theta}\frac{\partial^2u}{\partial\psi^2}\right]$$
$$-\frac{1}{C}\frac{\partial^2u}{\partial\varphi^2}-\frac{C}{C_1C_2}\frac{\partial^2u}{\partial x^2}+\frac{2}{\hbar^2}\left[\frac{H}{2}(1-\cos nx)-E\right][1+\delta\sin^2x],$$

$$\mathrm{II}\quad\Bigg\{-\left[\frac{D_1^2}{C_1[(B_1+B_2)C_1-D_1^2}+\frac{(A_1-B_1)(A_2-B_2)\sin^2x}{(A_1+A_2)[(B_1+B_2)C_1-D_1^2]}\right]\left[\frac{C_1^2}{C^2}\frac{\partial^2u}{\partial\varphi^2}+\frac{2C_1}{C}\frac{\partial^2u}{\partial\varphi\partial x}+\frac{\partial^2u}{\partial x^2}\right]$$
$$-\left[\frac{[(A_1-B_1)C_1+D_1^2](A_2-B_2)}{C_2(A_1+A_2)[(B_1+B_2)C_1-D_1^2}\right]\left[\sin^2x\left(\frac{C_2^2}{C^2}\frac{\partial^2u}{\partial\varphi^2}-\frac{2C_2}{C}\frac{\partial^2u}{\partial\varphi\partial x}+\frac{\partial^2u}{\partial x^2}\right)-\tfrac{1}{2}\sin2x\left(\frac{C_2}{C}\frac{\partial u}{\partial\varphi}-\frac{\partial u}{\partial x}\right)\right]$$
$$+\frac{1}{2(A_1+A_2)[(B_1+B_2)C_1-D_1^2]}\left[\left((A_1+A_2)(B_1+B_2)+\frac{(A_1-B_1)(A_2-B_2)}{2}\right)\frac{\delta\sin2x}{1+\delta\sin^2x}\right.$$
$$\left.-\frac{(A_1-B_1)(A_2-B_2)}{4}\frac{\delta\sin4x}{1+\delta\sin^2x}-2(A_1-B_1)(A_2-B_2)\sin2x\right]\left[\frac{C_1}{C}\frac{\partial u}{\partial\varphi}+\frac{\partial u}{\partial x}\right],$$

$$\text{IIIa}\left\{+\frac{2D_1}{(B_1+B_2)C_1-D_1^2}\left[-\cos\left(\varphi+\frac{C_2}{C}x\right)\left(\frac{1}{\sin\theta}\frac{\partial}{\partial\psi}-\cot\theta\frac{\partial}{\partial\varphi}\right)+\sin\left(\varphi+\frac{C_2}{C}x\right)\frac{\partial}{\partial\theta}\right]\left(\frac{C_1}{C}\frac{\partial u}{\partial\varphi}+\frac{\partial u}{\partial x}\right),\right.$$

$$\text{IIIb}\left\{+\frac{D_1}{(B_1+B_2)C_1-D_1^2}\left[\sin\left(\varphi+\frac{C_2}{C}x\right)\left(\frac{1}{\sin\theta}\frac{\partial u}{\partial\psi}-\cot\theta\frac{\partial u}{\partial\varphi}\right)+\cos\left(\varphi+\frac{C_2}{C}x\right)\frac{\partial u}{\partial\theta}\right],\right.$$

$$\text{IIIc}\left\{-\frac{2(A_2-B_2)D_1\sin x}{(A_1+A_2)[(B_1+B_2)C_1-D_1^2]}\left[\sin\left(\varphi-\frac{C_1}{C}x\right)\left(\frac{1}{\sin\theta}\frac{\partial}{\partial\psi}-\cot\theta\frac{\partial}{\partial\varphi}\right)+\cos\left(\varphi-\frac{C_1}{C}x\right)\frac{\partial}{\partial\theta}\right]\left(\frac{C_1}{C}\frac{\partial u}{\partial\varphi}+\frac{\partial u}{\partial x}\right),\right.$$

$$\text{IIId}\left\{-\frac{(A_2-B_2)D_1\cos x}{(A_1+A_2)[(B_1+B_2)C_1-D_1^2]}\left[\sin\left(\varphi-\frac{C_1}{C}x\right)\left(\frac{1}{\sin\theta}\frac{\partial u}{\partial\psi}-\cot\theta\frac{\partial u}{\partial\varphi}\right)+\cos\left(\varphi-\frac{C_1}{C}x\right)\frac{\partial u}{\partial\theta}\right],\right.$$

$$\text{IIIe}\left\{+\frac{(A_2-B_2)D_1}{(A_1+A_2)[(B_1+B_2)C_1-D_1^2]}\left(\frac{\delta\sin^2x\cos x}{1+\delta\sin^2x}\right)\left[\sin\left(\varphi-\frac{C_1}{C}x\right)\left(\frac{1}{\sin\theta}\frac{\partial u}{\partial\psi}-\cot\theta\frac{\partial u}{\partial\varphi}\right)+\cos\left(\varphi-\frac{C_1}{C}x\right)\frac{\partial u}{\partial\theta}\right].\right.$$

$$\text{IIIf}\left\{+\frac{D_1}{(B_1+B_2)C_1-D_1^2}\frac{\delta\sin x\cos x}{1+\delta\sin^2x}\left[-\left(\frac{1}{\sin\theta}\frac{\partial u}{\partial\psi}-\cos\theta\frac{\partial u}{\partial\varphi}\right)\cos\left(\varphi+\frac{C_2}{C}x\right)+\frac{\partial u}{\partial\theta}\sin\left(\varphi+\frac{C_2}{C}x\right)\right],\right.$$

$$\text{IVa}\left\{-\frac{(A_1-B_1)C_1+D_1^2}{2(A_1+A_2)[(B_1+B_2)C_1-D_1^2]}\left[\left(\frac{1}{\sin^2\theta}\frac{\partial^2u}{\partial\psi^2}-\frac{\partial^2u}{\partial\theta^2}+\cot^2\theta\frac{\partial^2u}{\partial\varphi^2}-\frac{2\cot\theta}{\sin\theta}\frac{\partial^2u}{\partial\varphi\partial\psi}+\cot\theta\frac{\partial u}{\partial\theta}\right)\cos2\left(\varphi+\frac{C_2}{C}x\right)\right.\right.\right.$$
$$\left.\left.\left.+\left(2\cot\theta\frac{\partial^2u}{\partial\theta\partial\varphi}-\frac{2}{\sin\theta}\frac{\partial^2u}{\partial\theta\partial\psi}+\frac{2\cot\theta}{\sin\theta}\frac{\partial u}{\partial\psi}-(1+2\cot^2\theta)\frac{\partial u}{\partial\varphi}\right)\sin2\left(\varphi+\frac{C_2}{C}x\right)\right],\right.$$

$$\text{IVb}\left\{-\frac{(A_2-B_2)C_1}{2(A_1+A_2)[(B_1+B_2)C_1-D_1^2]}\left[\left(\frac{1}{\sin^2\theta}\frac{\partial^2u}{\partial\psi^2}-\frac{\partial^2u}{\partial\theta^2}+\cot^2\theta\frac{\partial_2u}{\partial\varphi^2}-\frac{2\cot\theta}{\sin\theta}\frac{\partial^2u}{\partial\varphi\partial\psi}+\cot\theta\frac{\partial u}{\partial\theta}\right)\cos2\left(\varphi-\frac{C_1}{C}x\right)\right.\right.\right.$$
$$\left.\left.\left.+\left(2\cot\theta\frac{\partial^2u}{\partial\theta\partial\varphi}-\frac{2}{\sin\theta}\frac{\partial^2u}{\partial\theta\partial\psi}+\frac{2\cot\theta}{\sin\theta}\frac{\partial u}{\partial\psi}-(1+2\cot^2\theta)\frac{\partial u}{\partial\varphi}\right)\sin2\left(\varphi-\frac{C_1}{C}x\right)\right].\right.$$

The boundary conditions governing the solutions of the wave equation are the same as those which were applicable to the simpler model studied by Koehler and Dennison[2] and are that the functions must remain finite at the poles $\theta=0$ or π and that they must be periodic with period 2π in the angles ψ, φ_1, and φ_2. The wave equation has been divided into four groups of terms.

We note that the equation has the following form:

$$[\text{group I}]+[\text{groups II to IV}]+\frac{2}{\hbar^2}[V-E][1+\delta\sin^2x]u=0$$

or

$$\frac{[\text{group I}]}{1+\delta\sin^2x}+\frac{[\text{groups II to IV}]}{1+\delta\sin^2x}+\frac{2}{\hbar^2}[V-E]u=0$$

which may be written

$$[\text{Group I}]+\frac{2}{\hbar^2}[V-E]-\frac{\delta\sin^2x[\text{group I}]}{1+\delta\sin^2x}+\frac{[\text{groups II to V}]}{1+\delta\sin^2x}=0.$$

Note that $[\text{group I}]+2/\hbar^2[V-E]$ (we shall hereafter refer to these terms as group I′) when set equal to zero is identical with the wave equation discussed by Koehler and Dennison provided that the reciprocal of their moment of inertia $1/A$ is replaced by

$$\frac{1}{A_1+A_2}+\frac{(A_1+A_2-B_1-B_2)C_1+D_1^2}{2(A_1+A_2)[(B_1+B_2)C_1-D_1^2]}.$$

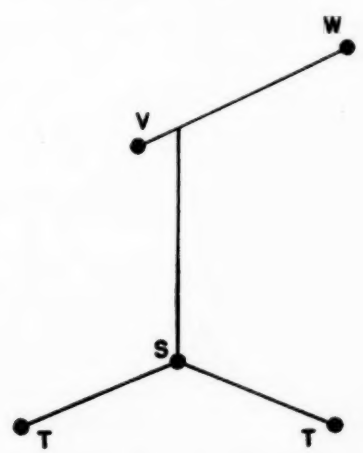

FIG. 1.

[2] J. S. Koehler and D. M. Dennison, Phys. Rev. **57**, 1006 (1940).

Its solutions, subject to the boundary conditions, may be written,

$$u=\frac{1}{2\pi}e^{iK\varphi}\exp(iM\psi\Theta_{JKM})\exp(-iC_1Kx/C)P(x)^{K\tau n}.$$

The quantity $e^{iK\varphi}\exp(iM\psi)\Theta_{JKM}$ is the usual symmetric-top wave function.

$$M(x)=\exp(-iC_1Kx/C)P(x)^{K\tau n}$$

for a potential of periodicity n satisfies the equation

$$d^2M/dx^2+(R+S\cos nx)M=0,$$

where

$$R=(2C_1C_2/C\hbar^2)(E^{K\tau n}-H/2),\quad S=C_1C_2H/C\hbar^2.$$

The n in the function $P(x)^{K\tau n}$ is not related to the periodicity of the barrier but is a quantum number classifying the internal rotational states. In the limit of an infinitely high barrier (parabolic potential) n goes over to the simple harmonic oscillator vibrational quantum number. The total energy is equal to the sum of $E^{K\tau n}$ and E^{JK} where the latter is the symmetrical top energy. The $E^{K\tau n}$ arise from the internal motion and are the eigenvalues of the equation in $M(x)$.

$$E^{JK}=\frac{\hbar^2}{2}\left[\frac{1}{A_1+A_2}+\frac{(A_1+A_2-B_1-B_2)C_1+D_1^2}{2(A_1+A_2)[(B_1+B_2)C_1-D_1^2]}\right]\times[J^2+J-K]+\frac{\hbar^2K^2}{2(C_1+C_2)}.$$

The boundary conditions require $P(x)^{K\tau n}$ to be periodic in x with period 2π, and it is customary to express it as

$$P(x)^{K\tau n}=\sum_{-\infty}^{+\infty}a_me^{imx}.$$

The matrix elements of the Hamiltonian corresponding to the complete wave equation may now be evaluated using the wave functions for the group I′ terms. The results of the evaluation of these matrix elements will be given below. The details of the evaluation are left for the appendix.

Group I′ terms yield elements of the Hamiltonian which are diagonal in all four quantum numbers. Terms of group II do not contain θ nor φ and are therefore diagonal in J and K. Some of the integrals in x in group II will vanish for certain symmetries. When evaluating the matrix elements of all of the groups (except group I′), one must remember that each term is divided by the quantity $1+\delta\sin^2x$. Each term of groups IIIa and IIIb contains either the sine or cosine of $[\varphi+(C_2x/C)]$ and will therefore connect states where $K\rightarrow K\pm1$. It will be noted that this group as well as the first term in group II are of the same form in θ, φ, and ψ as the corresponding terms in methyl alcohol and arise from the existence of a product of inertia D. Groups IIIc to IIIf also connect states where $K\rightarrow K\pm1$. They arise, however, from the fact that $A_2\neq B_2$; that is, they arise from the asymmetry of the STT group of Fig. 1. Group IIIc is the same function of θ, φ, and ψ and their derivatives as group IIIa and will therefore be the same function of J and K as group IIIa. Likewise groups IIId, IIIe, and IIIf are similar to groups IIIb. When the sine and cosine functions of $[\varphi+C_2x/C]$ in these groups are replaced by exponentials, the remaining terms in θ, φ, ψ and their derivatives, connecting $K\rightarrow K\pm1$ in groups IIIb, IIId, IIIc, and IIIf have exactly the same form. Note that in groups IIIc to IIIf additional integrals in x occur.

The matrix elements of groups IIIa and IIIb have been previously evaluated.[1] Their evaluation is discussed in detail and carried out in a different manner in the appendix of the present paper.

Groups IVa and IVb connect $K\rightarrow K\pm2$. The value of the matrix elements in θ for these terms are well known since they occur in the rigid asymmetric-top problem.[3] They are also discussed in the appendix.

Since one will be interested in the Stark effect, it will be convenient to add terms of that type to the Hamiltonian. For a geometry such as Fig. 1 they are

$$\mu_{\parallel}\mathcal{E}\cos\theta+\mu_{\perp}\mathcal{E}\sin\theta\cos\phi_1.$$

$\mathcal{E}$ is the electric field intensity and $\mu_{\parallel}$ and $\mu_{\perp}$ are the respective components of the electric moment of the molecule, parallel and perpendicular to the symmetry axis of the STT group.

Assembling the results of collecting the matrix elements one obtains

$$\begin{aligned}H_{JK\tau'n'^{JK\tau n}}=\frac{\hbar^2}{2}\Bigg\{&\left[\left(\frac{1}{A_1+A_2}+\frac{(A_1+A_2-B_1-B_2)C_1+D_1^2}{2(A_1+A_2)[(B_1+B_2)C_1-D_1^2]}\right)(J^2+J-K^2)+\frac{K^2}{2(C_1+C_2)}\right]\\
&\times\left(\int_0^{2\pi}(P^{K\tau n})^*P^{K\tau'n'}dx-\delta\int_0^{2\pi}\frac{\sin^2x(P^{K\tau n})^*P^{K\tau'n'}}{1+\delta\sin^2x}dx\right)-\frac{D_1^2}{C_1[(B_1+B_2)C_1-D_1^2]}\\
&\times\int_0^{2\pi}\frac{(P^{K\tau n})^*}{1+\delta\sin^2x}\frac{d^2}{dx^2}P^{K\tau'n'}dx-\frac{(A_1-B_1)(A_2-B_2)}{(A_1+A_2)[(B_1+B_2)C_1-D_1^2]}\left(\int_0^{2\pi}\frac{\sin^2x(P^{K\tau n})^*}{1+\delta\sin^2x}\frac{d^2}{dx^2}P^{K\tau'n'}dx\right.\\
&\left.+\int_0^{2\pi}\frac{\sin2x(P^{K\tau n})^*}{1+\delta\sin^2x}\frac{d}{dx}P^{K\tau'n'}dx\right)+\frac{[(A_1-B_1)C_1+D_1^2](A_2-B_2)}{(A_1+A_2)[(B_1+B_2)C_1-D_1^2]C_2}\left(K^2\int_0^{2\pi}\frac{\sin^2x(P^{K\tau n})^*P^{K\tau'n'}}{1+\delta\sin^2x}dx\right.\end{aligned}$$

[3] S. C. Wang, Phys. Rev. **34**, 243 (1929).

$$+2iK\int_0^{2\pi}\frac{\sin^2x(P^{K\tau n})^*}{1+\delta\sin^2x}\frac{d}{dx}P^{K\tau'n'}dx-\int_0^{2\pi}\frac{\sin^2x(P^{K\tau n})^*}{1+\delta\sin^2x}\frac{d^2}{dx^2}P^{K\tau'n'}dx$$

$$+\frac{iK}{2}\int_0^{2\pi}\frac{\sin2x(P^{K\tau n})^*P^{K\tau'n'}}{1+\delta\sin^2x}dx-\tfrac{1}{2}\int_0^{2\pi}\frac{\sin2x(P^{K\tau n})^*}{1+\delta\sin^2x}\frac{d}{dx}P^{K\tau'n'}dx\Big)$$

$$+\frac{[2(A_1+A_2)(B_1+B_2)+(A_1-B_1)(A_2-B_2)]\delta}{4(A_1+A_2)[(B_1+B_2)C_1-D_1^2]}\int_0^{2\pi}\frac{\sin2x}{(1+\delta\sin^2x)^2}(P^{K\tau n})^*\frac{d}{dx}P^{K\tau'n'}dx$$

$$-\frac{(A_1-B_1)(A_2-B_2)\delta}{8(A_1+A_2)[(B_1+B_2)C_1-D_1^2]}\int_0^{2\pi}\frac{\sin4x}{(1+\delta\sin^2x)^2}(P^{K\tau n})^*\frac{d}{dx}P^{K\tau'n'}dx\Big\}$$

$$+\Big[E^{K\tau n}+\frac{\mu_{11}\mathcal{E}KM}{J^2+J}\Big]\int_0^{2\pi}(P^{K\tau n})^*P^{K\tau'n'}dx,$$

$$H_{JK+1\tau'n'}{}^{JK\tau n}=\frac{h^2}{2}\Big[\frac{D_1}{(B_1+B_2)C_1-D_1^2}\int_0^{2\pi}\Big(\frac{1}{2}\frac{e^{-ix}(P^{K\tau n})^*P^{K+1\tau'n'}}{1+\delta\sin^2x}-e^{-ix}\frac{(P^{K\tau n})^*}{i(1+\delta\sin^2x)}\frac{d}{dx}P^{K+1\tau'n'}\Big)dx$$

$$+\frac{(A_2-B_2)D_1}{(A_1+A_2)[(B_1+B_2)C_1-D_1^2]}\int_0^{2\pi}\Big(\frac{1}{2}\frac{\delta\sin x\cos x}{(1+\delta\sin^2x)^2}(P^{K\tau n})^*P^{K+1\tau'n'}-\frac{\sin x(P^{K\tau n})^*}{(1+\delta\sin^2x)}\frac{d}{dx}P^{K+1\tau'n'}$$

$$-\frac{1}{2}\frac{\cos x(P^{K\tau n})^*P^{K+1\tau'n'}}{(1+\delta\sin^2x)}\Big)dx-\frac{D_1\delta}{4[(B_1+B_2)C_1-D_1^2]}\int_0^{2\pi}\frac{i\sin2x}{(1+\delta\sin^2x)^2}e^{-ix}(P^{K\tau n})^*P^{K+1\tau'n'}dx$$

$$+\frac{\mu_\perp\mathcal{E}M}{J^2+J}\int_0^{2\pi}(P^{K\tau n})^*e^{-ix}P^{K+1\tau'n'}dx\Big]\Big[(J+K+1)(J-K)\Big]^{\frac{1}{2}},$$

$$H_{JK+2\tau'n'}{}^{JK\tau n}=\frac{h^2}{8}\Big[\frac{(A_1-B_1)C_1+D_1^2}{(A_1+A_2)[(B_1+B_2)C_1-D_1^2]}\int_0^{2\pi}\frac{(P^{K\tau n})^*e^{-i2x}P^{K+2\tau'n'}}{1+\delta\sin^2x}dx$$

$$+\frac{(A_2-B_2)C_1}{(A_1+A_2)[(B_1+B_2)C_1-D_1^2]}\int_0^{2\pi}\frac{(P^{K\tau n})^*P^{K+2\tau'n'}}{1+\delta\sin^2x}dx\Big]\Big[(J-K)(J-K-1)(J+K+1)(J+K+2)\Big]^{\frac{1}{2}},$$

$$H_{J+1K\tau n}{}^{JK\tau n}=\frac{\mu_{11}\mathcal{E}\big[(J+K+1)(J-K+1)(J+M+1)(J-M+1)\big]^{\frac{1}{2}}}{(J+1)\big[(2J+1)(2J+3)\big]^{\frac{1}{2}}},$$

$$H_{J-1\tau Kn}{}^{JK\tau n}=\frac{\mu_{11}\mathcal{E}\big[(J^2-K^2)(J^2-M^2)\big]^{\frac{1}{2}}}{J\big[4J^2-1\big]^{\frac{1}{2}}},$$

$$H_{J+1K\pm1\tau'n'}{}^{JK\tau n}=\pm\frac{\mu_\perp\mathcal{E}\big[(J\pm K+1)(J\pm K+2)(J+M+1)(J-M+1)\big]^{\frac{1}{2}}}{(J+1)\big[(2J+1)(2J+3)\big]^{\frac{1}{2}}}\int_0^{2\pi}(P^{K\tau n})^*e^{\mp ix}P^{K\pm1\tau'n'}dx,$$

$$H_{J-1K\pm1\tau'n'}{}^{JK\tau n}=\frac{\mp\mu_\perp\mathcal{E}\big[(J\pm K)(J\pm K-1)(J^2-M^2)\big]^{\frac{1}{2}}}{2J\big[4J^2-1\big]^{\frac{1}{2}}}\int_0^{2\pi}(P^{K\tau n})^*e^{\mp ix}P^{K\pm1\tau'n'}dx.$$

APPENDIX. EVALUATION OF MATRIX ELEMENTS

We discuss first the groups IIIa to IIIf. All of these form K to $K\pm1$ connections. When these terms are divided by $1+\delta\sin^2x$ and the simple integrals in ψ and φ are evaluated, one is left with the following integrals in x:

Group IIIa	$-\frac{1}{2}\int_0^{2\pi}\frac{(P^{K\tau n})^*e^{-ix}}{i(1+\delta\sin^2x)}\frac{dP^{K+1\tau'n'}}{dx}dx,$
Group IIIb	$\frac{1}{2}\int_0^{2\pi}\frac{(P^{K\tau n})^*e^{-ix}P^{K+1\tau'n'}}{1+\delta\sin^2x}dx,$

Group IIIc $$\frac{1}{2}\int_0^{2\pi}\frac{\sin x(P^{K\tau n})^*}{1+\delta\sin^2 x}\frac{dP^{K+1\tau' n'}}{dx}dx,$$

Group IIId $$\frac{1}{2}\int_0^{2\pi}\frac{\cos x(P^{K\tau n})^*P^{K+1\tau' n'}}{1+\delta\sin^2 x}dx,$$

Group IIIe $$\frac{\delta}{2}\int_0^{2\pi}\frac{\sin^2 x\cos x(P^{K\tau n})^*P^{K+1\tau' n'}}{(1+\delta\sin^2 x)^2}dx,$$

Group IIIf $$\frac{i\delta}{2}\int_0^{2\pi}\frac{\sin x\cos x e^{-ix}(P^{K\tau n})^*P^{K+1\tau' n'}}{(1+\delta\sin^2 x)^2}dx.$$

Groups IIIa to IIIf all have the same integral in θ. The θ integral is

$$\int_0^{2\pi}\Theta_{JKM}\left[\frac{-M}{\sin\theta}+(K+1)\cot\theta+\frac{d}{d\theta}\right]\Theta_{J'K+1M}\sin\theta d\theta. \tag{1}$$

After carrying out the φ and ψ integration in the K to $K+2$ matrix element, one is left with the following integrals in x:

Group IVa $$-\frac{1}{2}\int_0^{2\pi}\frac{(P^{K\tau n})^*e^{-i2x}\rho^{K+2\tau' n'}}{1+\delta\sin^2 x}dx,$$

Group IVb $$-\frac{1}{2}\int_0^{2\pi}\frac{(P^{K\tau n})^*P^{K+2\tau' n'}}{1+\delta\sin^2 x}dx.$$

Both of these have in common the same integral in θ. It is

$$\int_0^{2\pi}\Theta_{JKM}\left[\frac{M^2}{\sin^2\theta}+\frac{d^2}{d\theta^2}+K^2\cot^2\theta+2K\cot^2\theta\right.$$
$$-2KM\frac{\cot\theta}{\sin\theta}-2M\frac{\cot\theta}{\sin\theta}+2K\cot\theta\frac{d}{d\theta}$$
$$\left.+3\cot\theta\frac{d}{d\theta}-\frac{2M}{\sin\theta}\frac{d}{d\theta}-(K+2)\right]\Theta_{J'K+2M}\sin\theta d\theta. \tag{2}$$

This integral occurs in the rigid asymmetric top[3] and has the value

$$\frac{[(J-K)(J-K-1)(J+K+1)(J+K+2)]^{\frac{1}{2}}}{2}.$$

The matrix elements of the stark contribution $\mu_{\parallel}\mathcal{E}\cos\theta+\mu_{\perp}\mathcal{E}\sin\theta\cos\varphi$ involve, respectively, the following integrals in θ:

$$\int_0^{2\pi}\Theta_{JKM}\cos\theta\Theta_{J'KM}\sin\theta d\theta$$

and

$$\int_0^{2\pi}\Theta_{JKM}\sin\theta\Theta_{J'K+1M}\sin\theta d\theta.$$

The second integral has a factor

$$\int_0^{2\pi}(P^{K\tau n})^*e^{-ix}P^{K+1\tau' n'}dx.$$

These integrals are well known.[4,5] They will be evaluated here, however, by making use of the factorization of the symmetric-top equation. We now evaluate integral (1) by factoring[6] the differential equation in K. The symmetric-top wave equation in θ is

$$\frac{d}{d\theta}\left(\sin\theta\frac{\Theta}{d\theta}\right)-\frac{(M-K\cos\theta)^2}{\sin^2\theta}\Theta+\left(\alpha W-\frac{AK^2}{c}\right)\sin\theta\Theta=0,$$

where

$$\alpha=\frac{8\pi^2 A}{h^2}.$$

Following Infeld and Hull this may be put in the standard form

$$\frac{d^2Y}{d\theta^2}-\left[\frac{(K-\frac{1}{2})(K+\frac{1}{2})+M^2-2MK\cos\theta}{\sin^2\theta}\right]Y+\left[\alpha W+\left(1-\frac{A}{C}\right)K^2+\frac{1}{4}\right]Y=0,$$

where $Y=\sin^{\frac{1}{2}}\theta\Theta$. The above equation is "Type A." The factorization is

$$k(\theta, M)=(K-\tfrac{1}{2})\cot\theta-M/\sin\theta$$

and

$$L(M)=(K-\tfrac{1}{2})^2.$$

The solutions are therefore

$$Y_{JJM}=\left[\frac{\Gamma(2J+2)}{\Gamma(J-M+1)\Gamma(J+M+1)}\right]^{\frac{1}{2}}\times\sin^{J-M+\frac{1}{2}}\frac{\theta}{2}\cos^{J+M+\frac{1}{2}}\frac{\theta}{2}.$$

Corresponding to the eigenvalues

$$\lambda'=(J+1-\tfrac{1}{2})^2=(J+\tfrac{1}{2})^2,$$

where

$$\lambda'=\left(1-\frac{A}{C}\right)K^2+\frac{1}{4}.$$

Thus

$$W=\frac{h^2}{8\pi^2}\left[\frac{1}{A}(J^2+J)+\left(\frac{1}{C}-\frac{1}{A}\right)K^2\right].$$

[4] H. Rademacher and F. Reiche, Z. Physik **41**, 453 (1927).
[5] Cross, Hainer, and King, J. Chem. Phys. **12**, 210 (1944).
[6] L. Infeld and T. E. Hull, Revs. Modern Phys. **23**, 1, 21 (1951).

For other normalized solutions we have

$$Y_{JK-1M}=\frac{\left[(K-\tfrac{1}{2})\cot\theta-\frac{M}{\sin\theta}+\frac{d}{d\theta}\right]}{[(J-K)(J-K+1)]^{\frac{1}{2}}}Y_{JKM},$$

$$Y_{JK+1M}=\frac{\left[(K+\tfrac{1}{2})\cot\theta-\frac{M}{\sin\theta}-\frac{d}{d\theta}\right]}{[(J-K)(J+K+1)]^{\frac{1}{2}}}Y_{JKM}.$$

Expressing the above in terms of θ and changing K to $K+1$, one has

$$\sin^{\frac{1}{2}}\theta\Theta_{JKM}=\frac{\sin^{\frac{1}{2}}\theta\left[(K+1)\cot\theta-\frac{M}{\sin\theta}+\frac{d}{d\theta}\right]\Theta_{JK+1M}}{[(J-K)(J+K+1)]^{\frac{1}{2}}}, \quad (3)$$

$$\sin^{\frac{1}{2}}\theta\Theta_{JK+2M}=\frac{\sin^{\frac{1}{2}}\theta\left[(K+1)\cot\theta-\frac{M}{\sin\theta}-\frac{d}{d\theta}\right]\Theta_{JK+1M}}{[(J+K+2)(J-K-1)]^{\frac{1}{2}}}. \quad (4)$$

If we multiply (3) by $\sin^{\frac{1}{2}}\theta\Theta_{JKM}$ and integrate over θ, we see that the right-hand side is just the integral (1) divided by $[(J-K)(J+K+1)]^{\frac{1}{2}}$. Thus integral (1) has the value $[(J-K)(J+K+1)]^{\frac{1}{2}}$. It is apparent that integral (1) has no J connections since the Θ functions are orthogonal in J, when K and M are constant. Thus $J'=J$. To evaluate integral (2) we write Eq. (3) as follows:

$$\Theta_{JK+1M}=\frac{\left[(K+2)\cot\theta-\frac{M}{\sin\theta}+\frac{d}{d\theta}\right]\Theta_{JK+2M}}{[J-K-1)(J+K+2)]^{\frac{1}{2}}}.$$

Substituting this expression for Θ_{JK+1M} in (3) we have

$$[(J-K)(J-K-1)(J+K+1)(J+K+2)]^{\frac{1}{2}}\Theta_{JKM}=\left[(K+1)\cot\theta-\frac{M}{\sin\theta}+\frac{d}{d\theta}\right]\times\left[(K+2)\cot\theta-\frac{M}{\sin\theta}+\frac{d}{d\theta}\right]\Theta_{JK+2M}.$$

Carrying out the multiplication of the right-hand side of this equation we observe that the operator is the same as that in Eq. (2). Thus the integral in (2) has the value*

$[(J-K)(J-K-1)(J+K+1)(J+K+2)]^{\frac{1}{2}}$ and $J'=J$.

* One can deduce also the value of integrals (1) and (2) by recognizing that in the matrix treatment of Klein [O. Klein, Z. Physik **58**, 730 (1929)], Dennison [D. M. Dennison, Revs. Modern Phys. **3**, 2, 280 (1931)], and King, Hainer and Cross [King, Hainer, and Cross, J. Chem. Phys. **11**, 27 (1943)] the following matrix representations satisfy the commutation relations obeyed by the total angular momentum:

$$(K|P_x|K+1)=\frac{i\hbar}{2}[(J-K)(J+K+1)]^{\frac{1}{2}},$$

$$(K|P_y|K+1)=\frac{\hbar}{2}[(J-K)(J+K+1)]^{\frac{1}{2}}.$$

From which

$$(K|P_x^2|K+2)=\frac{\hbar^2}{4}[(J-K)(J-K-1)(J+K+1)(J+K+2)]^{\frac{1}{2}}.$$

This particular representation is the one used by King, Hainer, and Cross. One may verify that the analytical expression in θ for $(2/\hbar)P_x$ and $(4/\hbar^2)P_x^2$ after the integrals in ψ and φ and x are evaluated correspond respectively to integrals (1) and (2) with a reversal of sign in the case of integral (1). Thus making use of the above equations one can conclude that integral (1) has the value $[(J-K)(J+K+1)]^{\frac{1}{2}}$ and integral (2) the value

$$[(J-K)(J-K-1)(J+K+1)(J+K+2)]^{\frac{1}{2}}.$$

The representation implicit in the present paper differs from that of both Dennison and King, Hainer, and Cross. Our representation can be made equivalent to that of the latter by substituting $(-1)^K\Theta_{JKM}$ for our Θ_{JKM}. Thus all our K to $K+1$ matrix elements $[(K|P_x|K+1), (K|\sin\theta|K+1)]$ will differ in sign from those given in reference 5. Also it should be mentioned that the wave function in the present paper differs from that used in reference 1 by the phase factor, $(-1)^K$.

The factorization method can be used to advantage in determining the matrix elements of $(K|\sin\theta|K+1)$ and $(K|\cos\theta|K)$ which enter the expressions for the dipole moments.[4,5] Its usefulness here is somewhat lessened because in the course of the application a normalization integral must be evaluated. However, after one integration all of the relevant matrix elements of $\sin\theta$ and $\cos\theta$ may be obtained by making use of the recurrence relations associated with the factorizations in J and in K. To examine matrix elements which connect different J values (as do $\sin\theta$ and $\cos\theta$) we must factor the symmetric top equation in J. We first write the differential equation in θ in the form

$$\frac{d}{d\theta}\left(\sin\theta\frac{d}{d\theta}\right)\Theta+\left[J(J+1)\sin\theta+2MK\cot\theta-\frac{M^2+K^2}{\sin\theta}\right]\Theta=0 \quad (5)$$

and recall that the normalization condition is

$$(JKMJ'KM)=\int_0^\pi \sin\theta\Theta_{JKM}\Theta_{J'KM}d\theta=\delta_{JJ'}. \quad (6)$$

Equation (5) may be put into the form of a class E factorization type by introducing the new independent variable $x=\ln\tan\theta/2$ and putting $\lambda=-(M^2+K^2)$. Equation (5) then becomes

$$\frac{d^2\Theta}{dx^2}+\left[\frac{J(J+1)}{\cosh^2x}-2MK\tanh x\right]\Theta+\lambda\Theta=0.$$

This is a class E type with

$$k_J(x)=J\tanh x+(MK/J)$$

and

$$L(J)=-\left(J^2+\frac{M^2K^2}{J^2}\right).$$

The shift operators

$$^{\pm}H_J=k_J\pm\frac{d}{dx}$$

may be used to raise and lower J values for fixed K, M, but the standard normalizing condition which would normalize according to

$$\int_0^{\pi}|\Theta_{JKM}|^2dx=\int_0^{\pi}|\Theta_{JKM}|^2\frac{d\theta}{\sin\theta}$$

cannot be used.[6] Instead we must normalize according to (6). It is convenient to express everything in terms of the original independent variable θ. The shift operators become

$$^{\pm}H_J=\frac{MK}{J}-J\cos\theta\pm\sin\theta\frac{d}{d\theta},$$

$^{+}H_J$ and $^{-}H_J$ are no longer mutually adjoint.† In fact, since $(d/d\theta)^{\dagger}=-(1/\sin\theta)(d/d\theta)\sin\theta$, we have

$$^{+}H_J\dagger=\frac{MK}{J}-J\cos\theta+\left(\frac{d}{d\theta}\right)^{\dagger}\sin\theta$$

$$^{+}H_J\dagger=^{-}H_J-2\cos\theta$$

and

$$^{-}H_J\dagger=^{+}H_J+2\cos\theta.$$

If Θ_{JKM} is normalized according to (6) we may obtain other normalized $\Theta_{J+1,KM}$ by means of

$$\Theta_{J+1,KM}=N^{+}{}_{JKM}{}^{-}H_{J+1}\Theta_{JKM}$$

and

$$\Theta_{J-1,KM}=N^{-}{}_{JKM}{}^{+}H_J\Theta_{JKM},$$

where $N^{\pm}{}_{JKM}$ are normalization constants. The shift operators satisfy the relations

$$^{+}H_{J+1}{}^{-}H_{J+1}\Theta_{JKM}=P^2{}_{J+1KM}\Theta_{JKM}$$

and

$$^{-}H_J{}^{+}H_J\Theta_{JKM}=P^2{}_{JKM}\Theta_{JKM},$$

where

$$P^2{}_{JKM}=J^2+\frac{M^2K^2}{J^2}-(M^2+K^2).$$

$N^{+}{}_{JKM}$ is determined from

$$\begin{aligned}1&=(J+1,KM|J+1KM)\\&=(N^{+}{}_{JKM})^2(^{-}H_{J+1}\Theta_{JKM}|^{-}H_{J+1}\Theta_{JKM})\\&=(N^{+}{}_{JKM})^2(\Theta_{JKM}|^{-}H^{\dagger}{}_{J+1}{}^{-}H_{J+1}\Theta_{JKM})\\&=(N^{+}{}_{JKM})^2(\Theta_{JKM}|(^{+}H_{J+1}+2\cos\theta)^{-}H_{J+1}\Theta_{JKM})\\&=(N^{+}{}_{JKM})^2(\Theta_{JKM}|^{+}H_{J+1}{}^{-}H_{J+1}\Theta_{JKM})\\&\quad+2N^{+}{}_J(\Theta_{JKM}|\cos\theta N^{+}{}_J{}^{-}H_{J+1}\Theta_{JKM}).\end{aligned}$$

† The adjoint of an operator A is the operator $A^{\dagger}$ satisfying $(A\varphi|\psi)=(\varphi|A^{\dagger}\psi)$.

Finally,

$$1=(N^{+}{}_{JKM})^2P^2{}_{J+1KM}+2N^{+}{}_{JKM}+(JKM|\cos\theta|J+1,KM).$$

Similarly,

$$1=(N^{-}{}_{JKM})^2P^2{}_{JKM}-2N^{-}{}_{JKM}(JKM|\cos\theta|J-1,KM).$$

Let

$$Q_{JKM}\equiv(JKM|\cos\theta|J-1KM),$$

then the two preceding equations become, when solved for $N^{+}{}_{JKM}$, and $N^{-}{}_{JKM}$,

$$N^{+}{}_{JKM}=-\frac{1}{P^2{}_{J+1}}[Q_{J+1KM}+(Q^2{}_{J+1KM}+\rho^2{}_{J+1KM})^{\frac{1}{2}}]$$

$$N^{-}{}_{JKM}=\frac{1}{P^2{}_{JKM}}[Q_{JKM}-(Q^2{}_{JKM}+P^2{}_{JKM})^{\frac{1}{2}}].$$

$Q_{J+1,KM}$ has the value

$$\frac{1}{J+1}\left[\frac{[(J+1)^2-M^2][(J+1)^2-K^2]}{(2J+1)(2J+3)}\right]^{\frac{1}{2}}.$$

$N^{\pm}{}_{JKM}$ are then

$$N^{+}{}_{JKM}=-\frac{J+1}{2J+1}\left[\frac{(2J+1)(2J+3)}{[(J+1)^2-M^2][(J+1)^2-K^2]}\right]^{\frac{1}{2}},$$

$$N^{-}{}_{JKM}=-\frac{J}{2J+1}\left[\frac{(2J-1)(2J+1)}{(J^2-M^2)(J^2-K^2)}\right]^{\frac{1}{2}}.$$

The final result for the factorization may be written

$$\Theta_{J+1KM}=N^{+}{}_{JKM}\times\left[\frac{MK}{J+1}-(J+1)\cos\theta-\sin\theta\frac{d}{d\theta}\right]\Theta_{JKM},\quad(7)$$

$$\Theta_{J-1KM}=N^{-}{}_{JKM}\left[\frac{MK}{J}-J\cos\theta+\sin\theta\frac{d}{d\theta}\right]\Theta_{JKM}.\quad(8)$$

We may add (7) and (8) as follows

$$\frac{\Theta_{J+1KM}}{N^{+}{}_{JKM}}+\frac{\Theta_{J-1KM}}{N^{-}{}_{JKM}}=MK\left(\frac{1}{J+1}+\frac{1}{J}\right)\Theta_{JKM}-(2J+1)\cos\theta\Theta_{JKM}.$$

Thus

$$\cos\theta\Theta_{JKM}=\frac{MK}{J(J+1)}\Theta_{JKM}-\frac{\Theta_{J+1,KM}}{(2J+1)N^{+}{}_{JKM}}-\frac{\Theta_{J-1,KM}}{(2J+1)N^{-}{}_{JKM}}.\quad(9)$$

This recurrence relation is sufficient for calculation of the matrix elements of $\cos\theta$. Thus

$$(JKM|\cos\theta|JKM)=\frac{MK}{J^2+J},$$

$$(JKM|\cos\theta|J+1KM)=\frac{1}{(2J+3)N^-_{J+1KM}}=\frac{[(J+1)^2-M^2)(J+1)^2-K^2)]^{\frac{1}{2}}}{(J+1)[(2J+1)(2J+3)]^{\frac{1}{2}}}.$$

$$(JKM|\cos\theta|J-1KM)=\frac{1}{(2J-1)N^+_{J-1KM}}=\frac{[(J^2-M^2)(J^2-K^2)]^{\frac{1}{2}}}{J[(2J-1)(2J+1)]^{\frac{1}{2}}}.$$

We now evaluate $(JKM|\sin\theta|J'K+1M)$. From (4) we have

$$[(J-K)(J+K+1)]^{\frac{1}{2}}\sin\theta\Theta_{JK+1M}=\left[K\cos\theta-M-\sin\theta\frac{d}{d\theta}\right]\Theta_{JKM}. \quad (10)$$

We can obtain an expression for $\sin\theta(d/d\theta)\Theta_{JKM}$ by subtracting (7) from (8).

$$\sin\theta\frac{d}{d\theta}\Theta_{JKM}=\frac{\Theta_{J-1KM}}{2N^-_{JKM}}-\frac{\Theta_{J+1KM}}{2N^+_{JKM}}-\frac{MK\Theta_{JKM}}{2J(J+1)}-\frac{\cos\theta\Theta_{JKM}}{2}. \quad (11)$$

If we put (11) into (10) and then use Eq. (9) for $\cos\theta\Theta_{JKM}$ we obtain

$$\sin\theta\Theta_{JK+1M}=-\frac{M[(J-K)(J+K+1)]^{\frac{1}{2}}}{J^2+J}\Theta_{JKM}-\frac{[(J-K)(J-K+1)(J+1-M)(J+1+M)]^{\frac{1}{2}}}{(J+1)[(2J+1)(2J+3)]^{\frac{1}{2}}}\Theta_{J+1KM}+\frac{[(J+K)(J+K+1)(J-M)(J+M)]^{\frac{1}{2}}}{J[(2J-1)(2J+1)]^{\frac{1}{2}}}\Theta_{J-1KM},$$

which immediately yields

$$(JKM|\sin\theta|J,K+1,M)=-\frac{M[(J-K)(J+K+1)]^{\frac{1}{2}}}{J^2+J},$$

$$(JKM|\sin\theta|J+1,K+1,M)=\frac{[(J+K+1)(J+K+2)(J-M+1)(J+M+1)]^{\frac{1}{2}}}{(J+1)[(2J+1)(2J+3)]^{\frac{1}{2}}}$$

$$(JKM|\sin\theta|J-1,K+1,M)=-\frac{[(J-K)(J-K-1)(J-M)(J+M)]^{\frac{1}{2}}}{J[(2J-1)(2J+1)]^{\frac{1}{2}}}.$$

We proceed in a similar manner for the matrix elements of $\sin\theta$ when $K\rightarrow K-1$. In this case we start with Eq. (3)

$$[(J-K+1)(J+K)]^{\frac{1}{2}}\sin\theta\Theta_{JK-1M}=\left[K\cos\theta-M+\sin\theta\frac{d}{d\theta}\right]\Theta_{JKM}. \quad (12)$$

Putting (11) into (12) and then using (9) for $\cos\theta\Theta_{JKM}$, we have

$$\sin\theta\Theta_{JK-1M}=-\frac{M[(J-K+1)(J+K)]^{\frac{1}{2}}}{J^2+J}\Theta_{JKM}+\frac{[(J+K)(J+K+1)(J+1-M)(J+1+M)]^{\frac{1}{2}}}{(J+1)[(2J+1)(2J+3)]^{\frac{1}{2}}}\Theta_{J+1KM}-\frac{[(J-K)(J-K+1)(J-M)(J+M)]^{\frac{1}{2}}}{J[(2J-1)(2J+1)]^{\frac{1}{2}}}\Theta_{J-1KM},$$

which immediately yields

$$(JKM|\sin\theta|JK-1M)=-\frac{M[J-K+1)(J+K)]^{\frac{1}{2}}}{J^2+J},$$

$$(JKM|\sin\theta|J+1K-1M)=-\frac{[(J-K+2)(J-K+1)(J-M+1)(J+M+1)]^{\frac{1}{2}}}{(J+1)[(2J+1)(2J+3)]^{\frac{1}{2}}},$$

$$(JKM|\sin\theta|J-1K-1M)=\frac{[(J+K-1)(J+K)(J-M)(J+M)]^{\frac{1}{2}}}{J[(2J-1)(2J+1)]^{\frac{1}{2}}}.$$

A Note on Work Functions and Chemical Potentials

PIERRE VAN RYSSELBERGHE
Department of Chemistry, University of Oregon, Eugene, Oregon
(Received January 26, 1953)

It is shown that the work of extraction (equal to the product of work function by molar charge) cannot be considered as equal to the chemical potential. In particular the electron work function of a metal does not correspond to the chemical potential of the electron in the metal and cannot be used in attempts at obtaining absolute metal-solution potential differences. The exact relationships involving these quantities are derived and linked with Galvani and Volta potential differences.

IN view of the frequent use by electrochemists of the electron work function of metals in attempts to reach absolute electrical potential differences at metal-solution contacts, and in view of the fact that several detailed discussions[1-3] of this important problem do not appear to have been sufficiently taken into account, it seems advisable to insist on the fact that the work of extraction of one mole of electrons from a metal (i.e., the electron work function in volts multiplied by the molar charge in coulombs if the joule is used as energy unit) is not equal to the molar chemical potential of the electrons inside the metal. It is this latter quantity which is required in the tentative calculation of absolute electrical potential differences at metal-solution contacts. The purpose of the present brief article is to clarify this point in a more direct manner than in previous analyses and to warn electrochemists against the misleading results obtained through the implicit identification of these two quantities.

Let us consider an electrode α and a solution β in contact with each other. It is understood that the areas of the surfaces of contact between phases (metal and gas or vacuum; metal and solution) must be regarded as being finite. A potential-determining reaction

$$X+e^-=X^-, \tag{1}$$

occurs at the contact between the two phases. The symbols X and X^- represent, respectively, the oxidized and reduced forms of the couple (X, X^-); they correspond to single species (for instance: $X=\frac{1}{2}$ Zn^{++}, $X^-=\frac{1}{2}$ Zn) or to several (for instance: $X=\frac{1}{4}O_2+H^+$, $X^-=\frac{1}{2}H_2O$; $X=\frac{1}{2}Hg_2Cl_2$, $X^-=Hg+Cl^-$). The symbol e^- represents the electron present only in the metallic phase α. If reaction (1) has come to electrochemical equilibrium, the absolute electrical potential difference from metal to solution is

$$\varphi^\alpha-\varphi^\beta=1/F(\mu_X+\mu_{e^-}{}^\alpha-\mu_{X^-}), \tag{2}$$

in which the φ's are the internal electrical potentials of the phases, the μ's are the chemical potentials (or sums of chemical potentials) of the species involved in the electrode reaction, and F is the faraday.

Formula (2) is equivalent to the statement that

$$\mu_X'+\mu_{e^-}{}'^\alpha-\mu_{X^-}'=0, \tag{3}$$

in which the μ''s are the electrochemical potentials.

The quantity $1/F(\mu_X-\mu_{X^-})$ is often called the "potential" of the couple (X, X^-), but it actually is the electromotive force of the cell corresponding to the reaction

$$X+\tfrac{1}{2}H_2(p_{H_2}=1 \text{ atmos})=X^-+H^+(a_{H^+}=1), \tag{4}$$

the standard "potential" of the couple $(H^+, \frac{1}{2}H_2)$ being arbitrarily taken equal to zero. Let us assume, however, that, by means of suitable assumptions concerning the free energy of solvation of gaseous ions such as those advanced by several authors and which we shall not discuss here, the true absolute value of $1/F(\mu_X-\mu_{X^-})$ has been obtained. The addition of $\mu_{e^-}{}^\alpha$ would then give the absolute electrical potential difference defined by formula (2). It is here that the electron work function of the physicist is brought in but incorrectly used.

Let us consider the extraction process from metal to vacuum of ions i carrying the charge z_iF per mole. For electrons $z_i=-1$ and the extraction process is that corresponding to thermionic emission or to the photoelectric effect. In the general case ions are transferred from the bulk of the metal, where the electrical potential is φ^α, to points immediately beyond the practical radius of action of the image forces, i.e., to distances of the order of 10^{-4} cm beyond the geometrical boundary of the metal. The electrical potential at these distances is ψ^α and the contribution of image forces to the work of extraction at such distances is of the order of 10 calories per mole for a univalent ion or for the electron. When the area of the surface of separation between metal and vacuum is finite the electrical potential decays from the value ψ^α at 10^{-4} cm to the value zero at infinite distance. The work function corresponds to the extraction from potential φ^α to potential ψ^α. The problem before us is to examine whether this work of extraction is equal or not to the chemical potential $\mu_i{}^\alpha$ inside the metal. Between the internal electrical

[1] W. G. Burgers, Chem. Weekblad **39**, No. 16-17, pp. 1-12 (1942).
[2] R. Piontelli, Proceedings of 2d Meeting of International Committee of Electrochemical Thermodynamics and Kinetics. Milan, Tamburini, 1951. See pp. 344-369.
[3] H. Strehlow, Z. Elektrochem. **56**, 119 (1952).

potential φ^α and the external one ψ^α we have the relation of Lange[4]

$$\varphi^\alpha=\psi^\alpha+\chi^\alpha, \tag{5}$$

in which χ^α is the surface electrical potential difference due to the presence of a heterogeneous charge distribution, for instance that resulting from a layer of oriented dipoles. The ions or electrons, as extracted in the process corresponding to the work function, are in a state equivalent to that defined by Schottky[5] as follows: the particles of constituent i are immobilized, i.e. deprived of all translational kinetic energy, at distances from one another sufficient to make all interionic forces negligible, the internal degrees of freedom of the ions contributing the full energy corresponding to the statistical distribution at the temperature being considered.

The work of extraction per mole of ion or electron includes the electrical term

$$w_{ie}{}^\alpha=z_iF(\psi^\alpha-\varphi^\alpha)=-z_iF\chi^\alpha, \tag{6}$$

and the chemical term

$$w_{ic}{}^\alpha=\mu_{iS}-\mu_i{}^\alpha, \tag{7}$$

in which μ_{iS} represents the chemical potential of the species i in the Schottky state. This value may be taken as the zero of chemical potential, in which case we simply have

$$w_{ic}{}^\alpha=-\mu_i{}^\alpha. \tag{8}$$

Since

$$\mu_i{}'^\alpha=\mu_i+z_iF\varphi^\alpha \tag{9}$$

we find that the work of extraction can be written under the following forms:

$$w_i{}^\alpha=w_{ie}{}^\alpha+w_{ic}{}^\alpha=z_iF\psi^\alpha-\mu_i{}'^\alpha=-z_iF\chi^\alpha-\mu_i{}^\alpha. \tag{10}$$

In the case of the electron we have

$$w_{e^-}{}^\alpha=-F\psi^\alpha-\mu_{e^-}{}'^\alpha=F\chi^\alpha-\mu_{e^-}{}^\alpha \tag{11}$$

in exact agreement with the definition of the true work function given by Herring and Nichols.[6]

The work of extraction $w_i{}^\alpha$ is thus not equal to $-\mu_i{}^\alpha$ as has been implicitly assumed by several authors, nor is it to be regarded as corresponding exclusively to the electrical work $-z_iF\chi^\alpha$. The ratio $w_i{}^\alpha/F$ taken in absolute value is the physicist's work function. The ratio $w_i{}^\alpha/z_iF$ taken in absolute value could be considered as the extraction voltage of the species i from the phase α. It is readily seen that the work of extraction cannot be used in place of $\mu_{e^-}{}^\alpha$ in Eq. (2). The experimental values of $w_{e^-}{}^\alpha$ cannot be decomposed into their electrical and chemical terms but it is interesting to note that as conservative an estimate as ± 0.1 v for χ^α, making $F\chi^\alpha=\pm 2.3$ kilocalories in the case of the work function of mercury, would introduce an uncertainty of ± 20 percent in the estimation of the absolute electrical potential difference of the calomel half-cell suggested by Latimer, Pitzer, and Slansky,[7] with the unavoidable conclusion that no argument can thereby be adduced in favor of regarding the electrocapillary maximum as a state of zero electrical potential difference.

Another point which can readily be clarified on the basis of the foregoing reasoning is the difference between Volta and Galvani electrical potential differences at the contact between two metals, α and β. When electrochemical equilibrium with respect to electron transfer has established itself at the contact we have

$$\mu_{e^-}{}'^\alpha=\mu_{e^-}{}'^\beta, \tag{12}$$

or, on the basis of (9),

$$\varphi^\alpha-\varphi^\beta=1/F(\mu_{e^-}{}^\alpha-\mu_{e^-}{}^\beta). \tag{13}$$

This is the Galvani potential difference. On the basis of (5) and (11) we find

$$\begin{aligned}\psi^\alpha-\psi^\beta&=-(\chi^\alpha-\chi^\beta)+1/F(\mu_{e^-}{}^\alpha-\mu_{e^-}{}^\beta)\\&=1/F(w_{e^-}{}^\beta-w_{e^-}{}^\alpha).\end{aligned} \tag{14}$$

This is the Volta potential difference.[8]

[4] E. Lange, *Handbuch der Experimentalphysik*, (Akademische Verlagsgesellschaft, Leipzig, 1933), Vol. 12; also E. Lange, Proceedings of 2d Meeting of International Committee of Electrochemical Thermodynamics and Kinetics. Milan, Tamburini, Italy, 1951. See pp. 317–343.

[5] W. Schottky, *Handbuch der Experimentalphysik* (Akademische Verlagsgesellschaft, (Leipzig, 1928). Vol. 13.

[6] C. Herring and M. H. Nichols, Revs. Modern Phys. **21**, 185 (1949).

[7] Latimer, Pitzer, and Slansky, J. Chem. Phys. **7**, 108 (1939). W. Latimer, *The Oxidation States of the Elements and their Potentials in Aqueous Solutions* (Prentice-Hall, Inc., New York, 1952), second edition, pp. 22–23.

[8] The present note is in agreement with recommendations on electrochemical nomenclature and definitions contained in reports prepared by a sub-committee of the International Committee of Electrochemical Thermodynamics and Kinetics (CITCE). See P. Van Rysselberghe, Proc. 3d Meeting CITCE. Milan, Manfredi, 1952, pp. 409–415. Also Proc. 4th Meeting CITCE, in print. Besides the present author, the following persons have collaborated in the preparation of these reports: J. O'M. Bockris (London), R. Defay (Brussels), E. Lange (Erlangen), R. Piontelli (Milan), and G. Valensi (Poitiers).

Equilibria Involving the CF(g) and $CF_2(g)$ Radicals at High Temperatures

JOHN L. MARGRAVE* AND KARL WIELAND†
Departments of Chemistry and Physics, University of California, Berkeley
(Received March 25, 1953)

The absorption spectrum of carbon tetrafluoride (CF_4) gas thermally decomposed under equilibrium conditions in a graphite tube furnace shows the bands of CF_2 at a temperature $T \approx 1900°K$ and also the bands of CF at a temperature $T \approx 2400°K$. These results are in approximate agreement with thermodynamic calculations made by Potocki and Mann when the high value of 170 kcal/mole for the heat of sublimation of graphite and when f values of about 10^{-3} for both the CF_2 and the CF bands are assumed.

THERE is at present considerable interest in the carbon-fluorine bond and also in the stabilites of various free radicals, like CF and CF_2, which appear to be important intermediates in many reactions. Several experimenters have obtained data indicating the probable importance of CF_2 radicals in the photolysis of $CF_4(g)$ and in the CF_3I+Na reaction as evidenced by considerable formation of C_2F_4 and polymers of this C/F ratio.[1] Steunenberg and Cady[2] have pyrolyzed various fluorocarbons and found both $CF_4(g)$ and polymers of the formula $(CF_2)_n$ among the products. They also suggest CF_2 radicals as likely intermediates.

Mass spectrometer studies of the fragments formed by electron bombardment of fluorocarbons have shown that appreciable amounts of CF_3^+, CF_2^+, and CF^+ ions are among the products,[3] and the appearance potentials of the CF_3^+, CF_2^+, and CF^+ ions have been determined.[4] Energetically, CF_3, CF_2, and CF are indicated to be important species in the decomposition products of fluorocarbons.

There are no spectroscopic data on CF_3. The spectra of the molecules CF and CF_2 are known from high frequency discharges through $CF_4(g)$. Venkateswarlu[5] has reported and partially analyzed emission bands of the CF_2 molecule, and the same spectrum has been observed in absorption in a discharge through CF_4 by Laird, Andrews, and Barrow.[6] Andrews and Barrow[7] have also detected emission bands of the CF molecule in a similar discharge. In no case was equilibrium attained, but the CF_2 spectrum is of special interest since it is one of the few spectra of polyatomic radicals yet observed. NH_2 has been detected in flames and by photolysis of NH_3. A band system at 4050A possibly due to the C_3 molecule has been detected in electric discharges, in flash photolysis, and in special flames. All attempts to detect the important CH_2 spectrum have been in vain.[8]

EXPERIMENTAL WORK

On the basis of the above mentioned indications for the existence of CF and CF_2 radicals of relatively stable character and with their spectra at least partially known, it was reasonable to attempt a study of substances which might yield these radicals by thermal dissociation, ideally of course, under equilibrium conditions. A close approach to equilibrium conditions over a wide range of temperatures (800–2900°K) can be obtained by heating either pure fluorine or a fluorocarbon in the graphite tube furnace used by Brewer, Gilles, and Jenkins[9] in previous equilibrium studies of the C_2 molecule.

The use of pure fluorine in the apparatus available was not practical without considerable modification. The gas CF_4 is a convenient material with which to work and was used for most of the experiments. In some experiments the solid polymer, Teflon (polytetrafluoroethylene) was used. Teflon, apparently, first vaporizes as a heavy polymer molecule which then breaks up into C_2F_4 units and finally at high temperatures into CF_2. Pure C_2F_4 gas was also used in some experiments.

The spectra were obtained with a small Hilger Quartz spectrograph on Ilford Q2 plates, and included visible and ultraviolet wavelengths longer than 1900A,

TABLE I. Calculated pressures of CF(g) and $CF_2(g)$

	High heat of sublimation (170 kcal)		Low heat of sublimation (136 kcal)	
$T°K$	P_{CF} (atmos)	P_{CF_2} (atmos)	P_{CF} (atmos)	P_{CF_2} (atmos)
1500°	8×10^{-13}	3×10^{-10}	7×10^{-8}	9×10^{-8}
2000°	4×10^{-8}	1×10^{-6}	2×10^{-4}	7×10^{-5}
2500°	3×10^{-5}	1×10^{-4}	3×10^{-2}	3×10^{-3}

* U. S. Atomic Energy Commission, Post-doctoral Fellow in Chemistry 1951–1952. Present address: Department of Chemistry, University of Wisconsin, Madison.

† Fellow of the Swiss Foundation "Stiftung fuer Stipendien auf dem Gebiete der Chemie."

[1] J. Dacey and J. Hodgins, Can. J. Research **28B**, 90, 173 (1950); J. Hodgins and R. Haines, Can. J. Chem. **30**, 473, (1952); J. Dacey, Trans. Faraday Soc. (to be published).

[2] R. Steunenberg and G. Cady, J. Am. Chem. Soc. **74**, 4165 (1952).

[3] Dibeler, Mohler, and Reese, Bull. Am. Phys. Soc. **27(3)**, 37 (1952).

[4] Mohler, Dibeler, and Reese, J. Research Natl. Bur. Standards **49**, 343 (1952); J. W. Warren and J. D. Craggs, *Mass Spectrometry* (Institute of Petroleum, London, 1950), pp. 36–46.

[5] P. Venkateswarlu, Phys. Rev. **77**, 676 (1950).

[6] Laird, Andrews, and Barrow, Trans. Faraday Soc. **46**, 803 (1950).

[7] E. Andrews and R. Barrow, Proc. Phys. Soc. (London) **64A**, 481 (1951).

[8] For references see K. Wieland, Z. Physik **133**, 229 (1952).

[9] Brewer, Gilles, and Jenkins, J. Chem. Phys. **16**, 797 (1948).

TABLE II. Band heads of CS_2 (observed as an impurity in absorption). λ values from this work (M−W) are given in A units and refer to the short-wave edge of a band; wave numbers, σ, are given in K units[a]; intensities, I, are on a relative scale 1–10.

I	λ(M−W)	σ(M−W)	σ(P−S)[15]	σ(H)[16]	I	λ(M−W)	σ(M−W)	σ(P−S)[15]	σ(H)[16]
			46370		7	2028.4	49284	49290	49318
					5	2025.0	49367		49382
1	2136.7	46786	46790						
2	2135.5	46813			8	2011.3	49703	49710	49740
					7	2008.0	49785		49833
3	2118.7	47184	47200						
2	2116.5	47233			8	1997.8	50039		50010
					8	1995.8	50089	50110M	50138
3	2101.7	47565							
4	2099.9	47606	47610						
2	2097.8	47654			9	1980.4	50478	50480	
					8	1978.0	50540		50536
3	2083.3	47985	48020M						50651
5	2079.5	48073		48112					
					10	1965.6	50858		50868
6	2063.5	48446	48440M		9	1964.3	50892	50900	50929
5	2062.5	48469							51047
3	2060.5	48515		48519					51130
					10	1949.4	51281	51280	51304
7	2045.3	48877	48870		9	1947.4	51334		
6	2042.8	48937		48941					51470
								51720	·
				49100				52140	·
									59199

[a] The Joint Commission for Spectroscopy recommends σ instead of ν as the designation for wave number, and K (Kayser) instead of cm^{-1}.

the limit set by the absorption of atmospheric O_2. In a given experiment the gas or solid to be studied was placed in the furnace, heated to the desired temperature, and then an exposure of 1–4 minutes duration was made through the heated gas using a hydrogen lamp as a source of ultraviolet continuum. The temperature was determined with an optical pyrometer to ±20°C.

RESULTS

The band spectra of CF, (λλ2240–2025), and CF_2, (λλ2580–2399), molecules were obtained on a number of plates in absorption from heating either CF_4 or Teflon in the graphite tube. Other experiments in which either CF_4, C_2F_4, or Teflon were heated in both clean and soot-coated quartz tubes over the temperature range 300–1500°K failed to give any of these spectra.

Compilations of thermodynamic functions for the molecules CF, CF_2, CF_3, CF_4, and C_2F_2 are now available,[10] but these data contain many uncertainties due to the use of estimates. It is possible, however, to calculate the approximate equilibrium amounts of the various molecules formed when CF_4 is heated in the presence of excess graphite. The main uncertainties in the calculated values result from (1) the wide choice of values for the heat of sublimation of graphite (136–170 kcal/mole) and (2) the lack of data on the heats of formation and/or dissociation energies of fluorocarbon molecules into gaseous atoms. Recent data[9,11–13] have favored both high and low values for the heat of sublimation of graphite. In Table I are listed the calculated pressures of CF(g) and CF_2(g) in equilibrium with CF_4(g) under a total pressure of 0.1 atmos obtained using "intermediate" values for the heats of formation of the various molecules[10] and the extremes (170 and 136 kcal/mole) for the heat of sublimation of graphite.

Experimentally it was found possible to detect in absorption the CF(g) spectrum at 2400±100°K and the CF_2(g) spectrum at 1900±100°K. If the transition probabilities for the various electronic transitions involved were known, one could make a decision as to which of the calculated values in Table I were most nearly correct. They are, however, not known.

One can show by considering various diatomic molecules (OH, C_2, etc.) for which measurements are available that a molecule may be detected spectroscopically in absorption under ideal conditions when the product $flp \approx 10^{-8}$ cm-atmos where f is related to the transition probability for the transition observed, l is the path length of absorbing gas in cm, and p is the gas pressure in atmos. In our experiments the path length was of the order of 10 cm so that $fp \approx 10^{-9}$ atmos.

Assuming f values near 10^{-3} one might expect to detect CF(g) and CF_2(g) when they are present in a system with a pressure of 10^{-6} atmos or more. Inspection of the calculations in Table I shows that the use of the high value for the heat of sublimation of graphite indicates a CF_2(g) pressure of 10^{-6} atmos present at about 2000°K. and a CF(g) pressure of 10^{-6} atmos present at about 2400°K. Calculations made on the

[10] L. Haar and C. Beckett, Natl. Bur. Standards Report 1164 (October 1, 1951); R. Potocki and D. Mann, Natl. Bur. Standards Report 1439 (February 15, 1952).

[11] M. Farber and A. Darwell, J. Am. Chem. Soc. **74**, 3941 (1951).

[12] Doehaerd, Goldfinger, and Waelbroek, J. Chem. Phys. **20**, 757 (1952).

[13] W. A. Chupka and M. G. Inghram, J. Chem. Phys. **21**, 371 (1953).

basis of the low value for the heat of sublimation of graphite indicate that both $CF(g)$ and $CF_2(g)$ would be present with a pressure of 10^{-6} atmos at about the same temperature, 1700°K. It appears that the experimental data favor slightly the high value for the heat of sublimation of graphite, particularly since $CF(g)$ has only been detected at temperatures near 2400°K.

In addition to the two band systems due to CF and CF_2, some strong bands in the wavelength region λλ2140–1950A were often observed. These bands appeared only when fluorocarbons were heated in the graphite tube furnace to temperatures greater than about 1600°K. Once formed, however, they persisted even at room temperature for some time. These bands are not listed in the compilation of Pearse and Gaydon.[14] It was at first thought that they might be the result of the fluorine analog of acetylene, C_2F_2, which would be stable under these conditions according to the tables of Potocki and Mann.[10] These bands are now known to be the very strong absorption bands of CS_2 previously observed by Price and Simpson[15] and also by Hauptman.[16] The wave-number data of both these authors, particularly those of Hauptman, are not very accurate and do not agree too well with the present measurements. Therefore, in Table II are listed the CS_2 bands as observed and also the data of Price and Simpson and Hauptman for comparison.

The authors gratefully acknowledge many helpful discussions with Professors Leo Brewer and F. A. Jenkins.

[14] R. W. B. Pearse and A. G. Gaydon, *The Identification of Molecular Spectra* (Chapman and Hall, London, 1950), second edition.

[15] W. C. Price and D. M. Simpson, Proc. Roy. Soc. (London) **A165**, 272 (1938).

[16] E. Hauptman, Acta Phys. Polon. **7**, 86 (1938).

Studies of Bond Rupture in the Decay of RaD as Tetramethyl Lead*

R. R. EDWARDS, J. M. DAY, AND R. F. OVERMAN
Department of Chemistry, University of Arkansas, Fayetteville, Arkansas
(Received April 17, 1953)

Studies of bond rupture in tetramethyl lead caused by the beta decay of Pb^{210}(RaD) have been made in solution and in vapor phase. The apparent bond rupture did not show the simple concentration dependence predicted for condensed systems by the cage hypothesis. Vapor phase results were consistent with those from solution in indicating failure of bond rupture in the primary beta and internal conversion processes. Indications are that bond rupture results from secondary processes involving neighboring atoms following the decay process.

I. INTRODUCTION

THE fate of a molecule when one of its constituent atoms undergoes a nuclear transition has been the object of much speculation and considerable experimental interest.[1,2] In many cases the energy necessary for disruption is available but the process may be obscured by the tendency for the fragments to recombine to form a molecule similar to or identical with that resulting when no disruption occurs. Libby[3] has shown that this can be explained on the basis of the Franck-Rabinowitch[4] "cage hypothesis." In the primary cage effect, the disruption products may be retained in a "cage" of solvent molecules, lose energy by collision and then recombine to form a stable molecule. In the secondary cage effect, the excited atom is not retained in its initial cage but may collide with a bound atom of about the same mass, transferring much or all of its energy. If the energy of the recoil atom is sufficient to break bonds, it may be immobilized in the vicinity of reactive free radicals or ions. In a liquid medium the probability is high that reaction will occur. As the concentration of atoms of like mass decreases, the probability of recombination decreases so that in a simple case the true fraction of bonds ruptured can be obtained by extrapolating to infinite dilution a curve of concentration *vs* apparent efficiency of rupture.

The present study was concerned with bond rupture in Pb^{210}-labeled tetramethyl lead resulting from the beta decay to Bi^{210}. A preliminary study of this system has been made by Mortensen and Leighton.[5] This system had much to recommend it for a hot-atom study. The 22-year half-life of Pb^{210} allowed the preparation and storage of tetramethyl lead. The 5-day half-life of the daughter Bi^{210} was long enough to permit isolation of the products yet short enough to allow growth of reasonable daughter activity over a short period of time. The parent activity is available in a volatile form [$Pb(CH_3)_4$] and the nonrupture product may be expected to be volatile while the rupture products should be nonvolatile. It is further possible to absorb the soft beta particles from Pb^{210} and count only the hard beta particles from Bi^{210}. This study was an extension of an earlier vapor phase study.[6]

There are two obvious processes available for bond rupture accompanying nuclear transitions, *viz.*, recoil and ionization. For Pb^{210}, whose maximum beta energy has recently been reported as 15.2 kev,[7] the maximum recoil energy is calculated[1] to be 0.040 ev which is barely above thermal energies. The most prominent (46.7-kev) gamma ray leads to only 0.006-ev recoil which is far less than thermal energies. Conversion of the gamma rays in the L, M, and N shells leads to 0.084 ev, 0.116 ev, and 0.12 ev, respectively, for recoil energies. On this basis no bond rupture would be expected from recoil processes.

Recent discussions of excitation and ionization accompanying the beta-decay process[8–10] predict a negligible probability of multiple ionization in the beta decay itself.

As shown by DeVault and Libby,[11] a high degree of ionization of the daughter atom will result from conversion of the gamma rays and the accompanying Auger processes. If the decaying atom is bound in a molecule, this charge will probably be distributed among the various atoms, producing electrostatic forces sufficient to rupture bonds. It has been shown[12–14] that *L* conversion of the 46.7-kev γ ray occurs in about 63 percent of Pb^{210} disintegrations. The fluorescence yield has been estimated[15] to be 0.475 for the *L* conversions.

* This work was supported in part by the U. S. Atomic Energy Commission.

[1] R. R. Edwards and T. H. Davies, Nucleonics **2**, No. 6, 44 (1948).
[2] W. F. Libby, J. Am. Chem. Soc. **69**, 2523 (1947).
[3] W. F. Libby, J. Am. Chem. Soc. **62**, 1930 (1940).
[4] J. Franck and E. Rabinowitch, Trans. Faraday Soc. **30**, 125 (1934).
[5] R. A. Mortensen and P. A. Leighton, J. Am. Chem. Soc. **56**, 2397 (1934).
[6] R. R. Edwards and C. D. Coryell, AECU-50 (1948), BNL-C-7 (1948).
[7] A. A. Jaffe and S. G. Cohen, Phys. Rev. **89**, 454 (1953).
[8] H. M. Schwartz and R. R. Edwards, J. Chem. Phys. **19**, 385 (1951).
[9] R. Serber and H. S. Snyder, Phys. Rev. **87**, 152 (1952).
[10] H. M. Schwartz, J. Chem. Phys. **21**, 45 (1953).
[11] D. DeVault and W. F. Libby, J. Am. Chem. Soc. **63**, 3216 (1941).
[12] L. Cranberg, Phys. Rev. **77**, 155 (1950).
[13] D. K. Butt and W. D. Brodie, Proc. Phys. Soc. (London) **A64**, 791 (1951).
[14] P. E. Damon and R. R. Edwards, Phys. Rev. **89**, 280 (1953).
[15] B. B. Kinsey, Can. J. Research **A26**, 421 (1948).

Thus one estimates 0.33' Auger event per Pb^{210} disintegration.

II. EXPERIMENTAL

A. Preparation of Materials

The tetramethyl lead was prepared by the method of Calingaert.[16] Lead chloride containing RaD (El Dorado Mining and Refining, Ltd.) was prepared by precipitation, filtered and washed thoroughly, and dried at 130° for 8 to 24 hours. Methyl magnesium chloride was made by bubbling dried methyl chloride into absolute ether containing magnesium turnings; the methyl chloride was refluxed to the mixture with a cold finger containing dry ice and acetone. The excess methyl chloride was driven off and lead chloride was added slowly. After refluxing two hours, the excess Grignard reagent was decomposed with ice and the ether solution separated, dried over drierite, and distilled through a six-inch refluxing column. The product was distilled at its boiling point, 110°.

The solvents used in the solution study were taken from freshly opened bottles and boiled before using to drive off any dissolved oxygen. The inert gases used in the vapor phase study were of the highest purity obtainable (Matheson).

B. Bond Rupture Studies in Solution

1. Apparatus and Procedure

The tetramethyl lead and the solvent were introduced into individual tubes attached to a vacuum system. After freezing the solutions, the system was evacuated and flushed with the inert gas to be used in the experiment. The solutions were allowed to stand in an inert atmosphere (argon or nitrogen at one atmosphere pressure) for 5 to 7 days. The solutions were then again frozen and the system evacuated. The solutions were then warmed and condensed in another tube with liquid nitrogen. Each tube was then analyzed for its Bi^{210} activity.

The nonvolatile bismuth was put into solution by adding 4 ml of 10 *N* nitric acid and 1-ml standardized bismuth nitrate solution and digesting at 100° for 3 hours. The solution was then diluted to 40 ml in a 50-ml centrifuge tube and bismuth phosphate precipitated by addition of a neutral solution of dibasic sodium phosphate. The precipitate was transferred quantitatively to an aluminum planchette, weighed, and counted.

The distillate was transferred to a 50-ml centrifuge tube and carbon tetrachloride, 5-ml 1 M nitric acid and 1-ml standardized bismuth nitrate solution were added. Bromine was added to decompose the tetramethyl lead and trimethyl bismuth. The bismuth was precipitated as the phosphate, transferred, weighed, and counted.

The radiations were counted through an aluminum absorber (22 mg/cm^2) which absorbed the Po^{210} alpha particles and the weak beta particles from Pb^{210}. Absolute geometry and counting efficiency were not determined since relative values were desired.

2. Results

The results are shown in Fig. 1. Down to mole fraction 0.05 the general shape predicted by the cage hypothesis[4] is followed. Below this value a sharp drop in the amount of apparent bond rupture appears. Extrapolation of the higher concentration portion of the curve to infinite dilution would predict a total bond rupture of 92 percent. Observations show that the bond rupture falls off and approaches a value somewhat less than 10 percent at extreme dilutions.

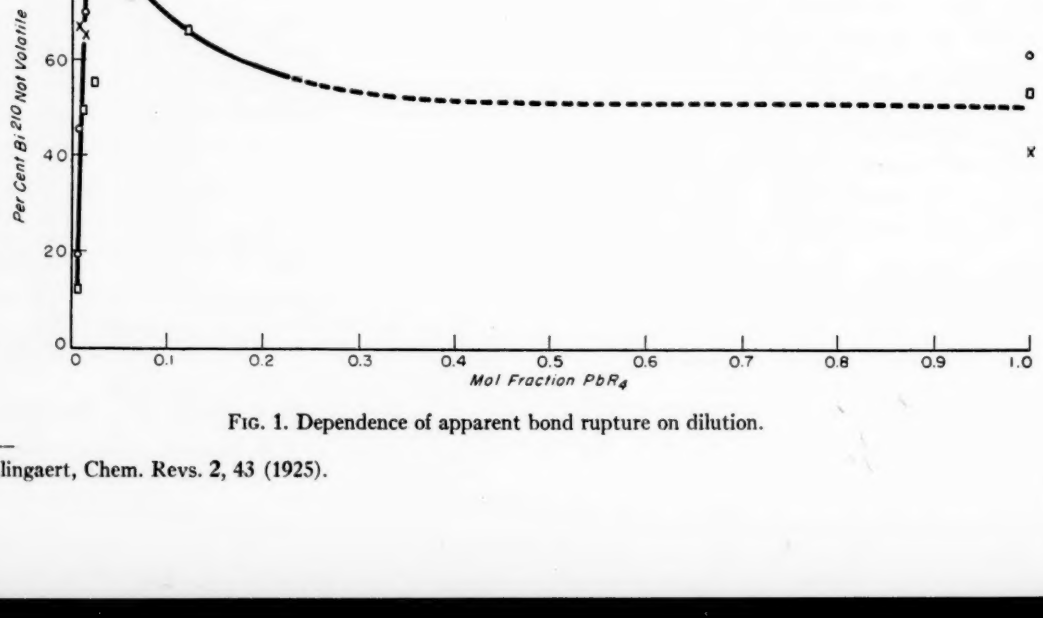

FIG. 1. Dependence of apparent bond rupture on dilution.

[16] G. Calingaert, Chem. Revs. 2, 43 (1925).

C. Bond Rupture Studies in Vapor Phase

1. Apparatus and Procedure

The apparatus, besides a vacuum manifold, consisted of a series of Pyrex vessels of the shape of cylindrical annuli 35-mm o.d., 25-mm i.d., and 125 mm long, with a side arm extending out from one end. The inner wall was drawn as thin and uniform as possible. A thin-walled beta counter was mounted concentrically for counting. The two thin walls absorbed out the Po^{210} alphas and the Pb^{210} betas.

Seven sample vessels were connected by the side arms to the vacuum manifold and evacuated. Tetramethyl lead was introduced to a pressure of from 8 to 10-mm Hg in all the vessels. Then each vessel was filled with the appropriate diluent gas at the desired pressure. The tubes were then sealed off after freezing out the tetramethyl lead with liquid nitrogen.

The tubes were allowed to stand from 20 to 30 days, during which time a growth curve of Bi^{210} into the tetramethyl lead was obtained. Then the volatile portion was frozen out into the side arm (liquid nitrogen bath) after counting total activity. The activity of the nonvolatile fraction was then observed and taken as a measure of apparent bond rupture. In some cases the side arms were sealed off with the gas inside and decay of the nonvolatile activity was followed; in others the volatile material was allowed to diffuse back into the vessels and later measurements taken. Reproducible results were obtained if the material was immediately revolatilized and recondensed. At least 2000 total counts were obtained in each measurement, and at least three measurements were made in each case. Backgrounds were about 40 counts per minute.

One series of experiments was designed to determine the influence of mass of inert gas diluent atoms on the extent of bond rupture. The five inert gases from helium to xenon were used as diluents at pressures close to atmospheric. The results are shown in Table I. Earlier data had shown considerably higher rupture values with the light gases; this was shown to be attributable to a "vapor block" to diffusion of the active molecules, since the diluent gas itself did not condense. The extent of rupture is seen to be small, and no orderly dependence on mass of the diluent atoms is observed.

A second series of experiments was designed to measure the effect of pressure of diluent gas on the extent of rupture. Krypton was used in these runs to avoid any condensation difficulties. Pressures varied from zero to 722-mm Hg. Results are shown in Table II. Again the extent of rupture was small and there was no significant variation of bond rupture with pressure.

In a single case, a similar study of rupture with argon as the diluent gas was made in a tube with a center wire carrying 1000 volts, and silvered walls. Here about 8 percent of the product appeared as nonvolatile species.

TABLE I. Effect of mass of collision partner on bond rupture in "hot" $Pb(CH_3)_4$.

Diluent gas	Pressure (mm Hg)	PbR_4 (mm Hg)	Growth period (days)	Total activity (c/m)	Non-volatile (c/m)	Percent non-volatile
Helium	696	10	28	1143	31.5	2.8
	696	10	93	1135	80.3	7.1
Neon	660	10	29	1544	75	4.8
	660	10	93	1579	71.4	4.5
Argon	685	10	68	1283	96.1	7.5
	685	10	91	1282	47.3	3.7
Krypton	695	10	65	1335	112	8.4
	695	10	88	1328	94.9	7.1
Xenon	695	10	40	977.5	105.3	10.8
	695	10	68	941	100	10.6
	695	10	89	979	97.7	10.0
None	...	10	22	780	150	19.3
	...	10	23	774	166	21.4
	...	10	49	766	81.8	10.7
	...	10	69	815	74.5	9.1
	...	10	89	735	75.0	10.2

III. DISCUSSION

The most striking feature of the results is the apparent failure of bond rupture in the gas phase and in solution at high dilution, where cage-recombination effects should be minimized. Provided the decay of Pb^{210} proceeds via β emission and prompt de-excitation of the 46.7-kev state with a high conversion probability, as seems well established, these data represent the first clear-cut evidence of molecular survival in a process involving internal conversion.

The experiments of Wexler and Davies[17] indicate that ionization in the primary beta process is not extensive, in agreement with predictions by Schwartz.[10] However, their finding that isomeric transition with internal conversion in Br^{80} leads to electronic charges of 8 to 13 is in accord with earlier studies showing extensive molecular disruption in this process.

The maximum extent of bond rupture observed in the

TABLE II. Effect of pressure on bond rupture in "hot" $Pb(CH_3)_4$.

Series	Pressure of Kr (mm Hg)	Total activity (c/m)	Nonvolatile (c/m)	Percent nonvolatile
A	704	716.8	61.0	8.51
	417.5	1225.9	81.5	6.65
	167	674.5	41.7	6.18
	68	1200.2	55.5	4.62
	30.5	820.1	40.7	4.96
	0	917.4	33.7	3.67
B	722	1123.4	72.2	6.43
	300.5	798.2	69.2	8.67
	122.5	649.8	40.1	6.17
	50.5	941.5	93.5	9.93
	23	1045.3	67.6	6.47
	13	564.7	47.5	8.41
	0	727.5	39.8	5.47

[17] S. Wexler and T. H. Davies, Phys. Rev. 88, 1203 (1952).

solution studies is 82 percent, which is near the value expected for disruption accompanying each conversion process.[12] The role of the solvent molecules in this process is not at all clear. Perhaps they supply a cage, preventing a molecular breakup for a period of time sufficiently long to permit the charge to become distributed over the molecule in such a way as to yield a more extensive decomposition. Conversely, in the gas phase, the hot molecule may stabilize itself by dropping off a single charged radical or several protons without delay. The solution data indicate that carbon tetrachloride is more effective at high dilution than are hydrocarbon solvents in contributing to the disruption process. Further studies will perhaps show whether this effect is attributable to the greater mass and/or ionization potential of the solvent molecules. With hydrocarbon diluents, the extent of rupture decreases at mole fractions less than about 0.04, indicating that the presence of a $Pb(CH_3)_4$ molecule or so in the vicinity of the decay (acting perhaps as a heavy reaction partner) is a necessary condition for efficient disruption of the hot molecule.

The results of the gas phase studies are consistent with those from solution at high dilution in indicating a failure of extensive molecular disruption as an immediate consequence of the decay process. Failure of the rupture to occur even in heavy gas media at pressures near atmospheric indicates that the disruptive process is not simply a collision phenomenon, since collisions will be abundant in such circumstances.

It is hoped that further studies of the decay process and of the molecular disruption under other conditions will make possible a more complete explanation of these observations.

The Vibrational Spectra and Structure of Nitrogen Tetrasulfide

ELLIS R. LIPPINCOTT, *Department of Chemistry, Kansas State College, Manhattan, Kansas*

AND

MARVIN C. TOBIN,* *Department of Chemistry, University of Connecticut, Storrs, Connecticut*

(Received December 31, 1952)

The infrared and Raman spectra of nitrogen tetrasulfide (N_4S_4) are presented along with the infrared spectrum of nitrogen hydrogen sulfide ($N_4S_4H_4$). These data have been considered in terms of the several proposed structures for nitrogen tetrasulfide and have been found to be consistent with a cage structure of D_{2d} symmetry. With the aid of a normal coordinate analysis of the nondegenerate symmetry species, a complete assignment of frequencies to their normal modes of vibration has been made for nitrogen tetrasulphide. A tentative assignment of frequencies is also given for nitrogen hydrogen sulfide.

INTRODUCTION

THE structure of nitrogen tetrasulfide, N_4S_4, is one of the unsolved problems of inorganic chemistry. This is not a result of neglect for a considerable amount of study by both chemical and physical means has been spent on it, but rather of the fact that the results of the chemical studies have not lent themselves to conclusive interpretations, and the physical studies have been, for the most part, either incomplete, or have given ambiguous results.

Arnold, Hugill, and Hutson,[1] Lu and Donahue,[2] and Goehring,[3] give quite detailed reviews of the chemistry of nitrogen tetrasulfide, and of the possible structures which have been suggested for this compound on the basis of chemical studies. Suffice it to say that few workers support the same structure although the most recent workers support a cyclic structure containing resonating partial—double N—S bonds, and no N—N bonds. This last is based on the fact that no compounds containing N—N bonds have ever been detected in the degradation products of nitrogen tetrasulfide.

Lu and Donahue,[2] on the basis of electron diffraction results support a cyclic eight-membered ring structure of D_{2d} symmetry (Fig. 1), herein referred to as the ring structure. This structure is supported by x-ray diffraction measurements made by Clark,[4] but Hassel and Viervoll,[5] on the basis of other x-ray diffraction measurements, support a structure which also has D_{2d} symmetry, but which now has the nitrogen atoms in its eight-membered ring bonded in pairs, so that the structure is now a tetracyclic cage (Fig. 2). This structure is herein referred to as the cage structure.

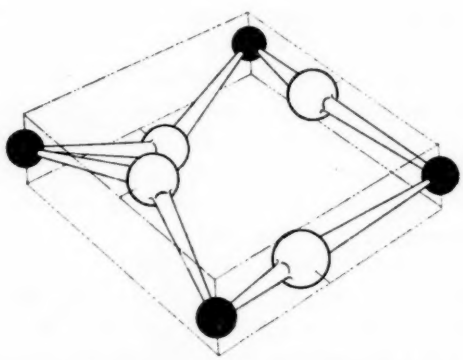

FIG. 1. Ring model of nitrogen tetrasulfide. Nitrogen atoms—black. Sulfur atoms—white.

EXPERIMENTAL

A. Samples

Nitrogen tetrasulfide was prepared by the action of dry ammonia gas on S_2Cl_2 in chloroform, the method of Arnold, Hugill, and Hutson.[1] The crystals were acicular, and golden-orange in color at room temperature.[6] They were not explosive with ordinary handling, but could be exploded by percussion.

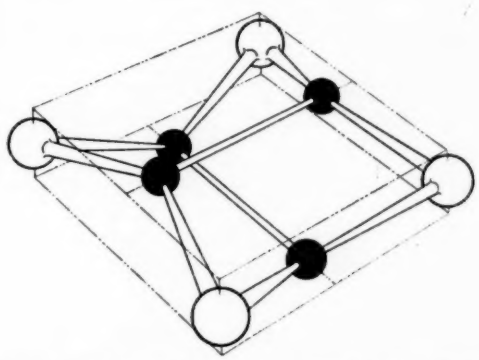

FIG. 2. Cage model of nitrogen tetrasulfide. Nitrogen atoms—black. Sulfur atoms—white.

* Based on a Ph.D. thesis presented by Marvin C. Tobin to the Graduate School of the University of Connecticut, Storrs, Connecticut, 1952. Presented as a paper before the symposium on Spectroscopy and Molecular Structure, Ohio State University, Columbus, Ohio, June, 1952. Present address, Arthur D. Little, Inc., Cambridge, Massachusetts.

[1] Arnold, Hugill, and Hutson, J. Chem. Soc. **1936**, 1645.

[2] C. Lu and J. Donahue, J. Am. Chem. Soc. **66**, 818 (1944).

[3] M. Goehring, Ber. deut. chem. Ges. **80**, 110 (1947).

[4] D. Clark, J. Chem. Soc. **1952**, 1615.

[5] O. Hassel and H. M. Viervoll, Tidsskr. Kjemi Bergvesen Met. **3**, No. 2, 7 (1943).

[6] It was observed in the course of this work that nitrogen tetrasulfide is blood-red at 100°C and canary-yellow at the boiling point of liquid ammonia.

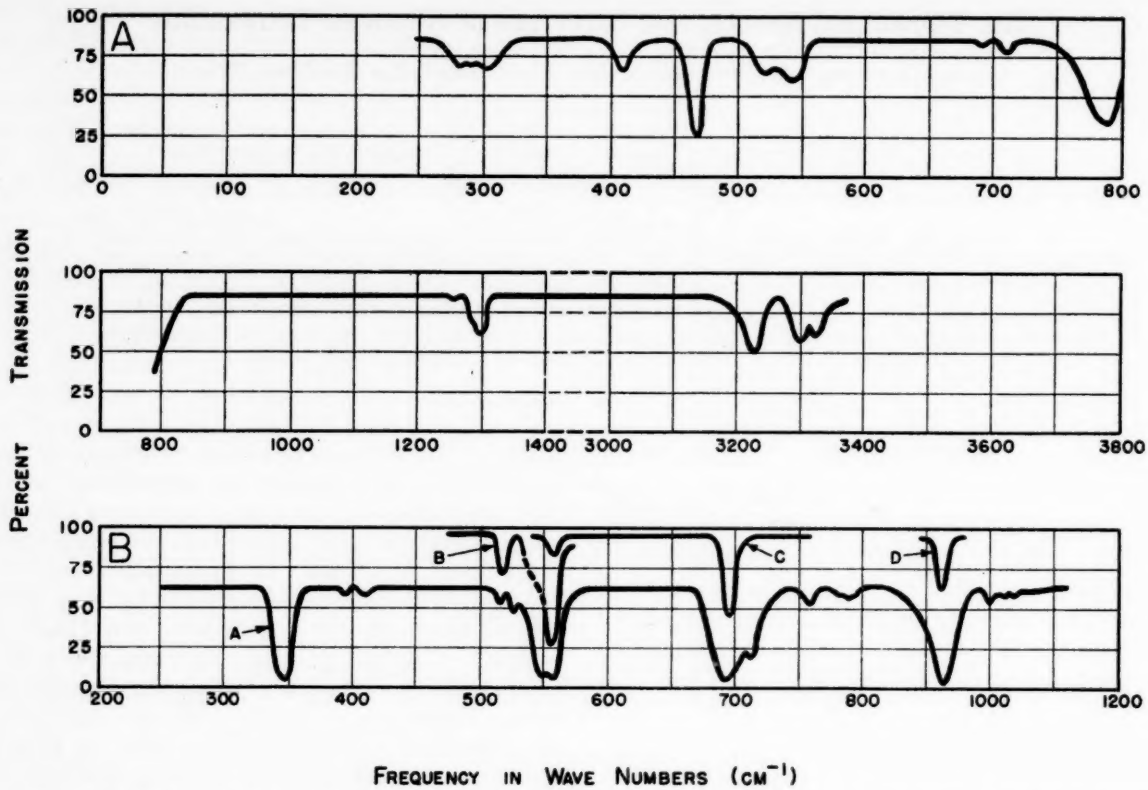

FIG. 3. A (upper case)—Infrared spectrum of nitrogen hydrogen sulfide in Nujol mull. B (lower case)—Infrared spectrum of nitrogen tetrasulfide. A (lower case)—in Nujol mull, B (lower case)—in benzene, C (lower case)—in cyclohexane, D (lower case)—in dioxane.

Nitrogen hydrogen sulfide was prepared as a white crystalline powder, by a modification of the method of Meuwesen,[7] by reducing nitrogen tetrasulfide with $SnCl_2$ in an alcohol-benzene solvent. The product was washed with a mixture of equal parts of one normal HCl and pyridine, then with dilute aqueous HCl and pyridine, then with dilute aqueous HCl, after which it was dried.

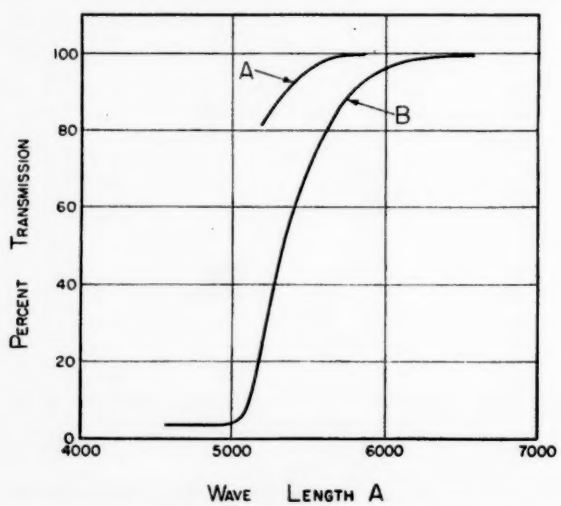

FIG. 4. Absorption spectrum of nitrogen tetrasulfide. 1-cm cell length. A—saturated $CHCl_3$. B—saturated CS_2.

[7] A. Meuwesen, Ber. deut. chem. Ges. **62**, 1959 (1929).

B. Solvents

Since nitrogen tetrasulfide decomposes violently near its melting point, obtaining spectra of the melt was out of the question. It was not considered feasible to attempt to obtain Raman spectra of the crystals or vapor. It was therefore necessary to find a suitable solvent.

A search of the literature disclosed that the common solvents, benzene, alcohol, and carbon disulfide, dissolve nitrogen tetrasulfide only to the extent of about 0.005 mole/liter. It was found to be almost, or completely insoluble in nitromethane, acetonitrile, nitrobenzene, liquid ammonia, and *n*-pentane.

It was somewhat soluble in pyridine and thiophene, but reacted with the former to give a gray gum, and with the latter to give a red oil, apparently the same oil formed as a by-product in the synthesis of nitrogen tetrasulfide. The most satisfactory solvent turned out to be dioxane purified by the method of Hess and Frahm.[8] The solubilities were 0.018-mole N_4S_4 per mole of dioxine at 25°C, and 0.020-mole N_4S_4 per mole of dioxane at 60°C. Nitrogen tetrasulfide seemed quite inert toward dioxane, from which it could be recrystallized unchanged.

[8] K. Hess and M. Frahm, Ber. deut. chem. Ges. **71**, 2627 (1938).

C. Preparation of Solutions

In view of the dilute solutions used, it was necessary to obtain optically blank samples of nitrogen tetrasulfide solution for Raman spectra. This was accomplished by making sure that all operations after preparation of the original sample and purification of the dioxane involved use of carefully cleaned glass apparatus only. All apparatus was scrubbed with Vel detergent, rinsed in tap water, steamed, and oven dried. The nitrogen tetrasulfide was twice recrystallized from benzene which was distilled from sodium in a cleaned, all-glass still (no sealing grease was used in the standard taper joints) directly into the beaker containing the nitrogen tetrasulfide. After recrystallization, the sample was drained on a cleaned sintered-glass filter and air dried.

A special all-glass loading apparatus was constructed so that the solution could be drawn directly into the Raman tube through a Corning 33900 GVYKU ultrafine sintered-glass bacteriological filter. The solution was prepared using as solvent the middle fraction of a charge of pure dioxane distilled from sodium in a cleaned, all-glass still. This technique has since given excellent results with aqueous solutions of inorganic complex ions.[9,10]

D. Raman Spectra

The Raman spectra were taken on a Hilger E612 glass Raman spectrograph. The camera had an aperture of $f/5.7$, and the excitation unit was fitted with MgO reflectors.[11]

The absorption spectrum of N_4S_4 in the visible region showed almost complete cutoff below 5000A, with about 70 percent transmission at 5450A (Fig. 3). It was decided to use the Hg line at 5461A for excitation, with a $NdCl_3$ filter to cut down the intensity of the Hg 5770–5790A doublet. Optimum exposure time on Kodak 103aE plates was found to be 70 min, about 20 times the exposure necessary to obtain spectra of similar intensity when the sample is a pure colorless liquid.

E. Infrared Spectra

Infrared spectra of nitrogen tetrasulfide and nitrogen hydrogen sulfide were taken in Nujol mulls in the region 250–3500 cm^{-1}, using KSR-5, KBr, and NaCl prisms in the appropriate regions. The strong bands of nitrogen tetrasulfide in the KBr and NaCl regions were re-ex-

TABLE I. Observed spectra and assignment of frequencies for nitrogen tetrasulfide and nitrogen hydrogen sulfide.

Nitrogen tetrasulfide					Nitrogen hydrogen sulfide		
Raman (in cm^{-1}) in dioxane	Infrared (in cm^{-1}) crystal in Nujol mull	Infrared (in cm^{-1}) in solution[b]	Assignment		Infrared (in cm^{-1}) in Nujol mull	Assignment	
	173[a]		A_2				
177 (10)			A_1, B_2		(177)[c]	A_1, B_2, A_2	angle
213 (10)			B_1, E	angle	(213)	B_1, E, B_2	bending
347 (2)	347 s		E	bending	280–302 m	E, (A_1 ?)	and
	397 w		177+213		407 m	177+213	torsion
	412 w		2×213				
	460[a]		A_2		462 s	A_2	
519 (4)	519 m	524	B_2		516 m	B_2	
	531		347+177				
561 (4)	552 s	538[d]					
	557 s	554 s	E		541 m	E	N–S
615 (3)			A_1	N–S stretching	(615)	A_1	stretching
655 ?							
692 ?[e]	696 s	700 s	E		693 w	E	
720 (4)	719 s				705 w		
	762 w		934−177				
785 (0)	792 vw		B_1		780 s	B_1	
888 (2)		in dioxane	A_1	N–N			
934 (2)	925 s	920 m	B_2	stretching			
	1000 w		785+213				
	1025 w						
	1040 w		2×519				
					1262 w		N–H
					1296 w		bending
					1302 m		
					3220 s		N–H
					3285 s		stretching
					3320 m		

[a] Calculated.
[b] Benzene or cyclohexane.
[c] ( ) indicate estimated value.
[d] Masked by benzene band.
[e] Masked by Hg line.

[9] Lippincott, Psellos, and Tobin, J. Chem. Phys. **20**, 536 (1952).
[10] Julius L. Silver, Ph.D. thesis, University of Connecticut, 1953.
[11] A. Menzies and J. Skinner, Rev. Sci. Instr. **26**, 299 (1949).

amined with the NaCl dissolved in cyclohexane, benzene, or dioxane. (Fig. 4).

Attempts were made to obtain a spectrum of the vapor in a 1½-meter cell, but these failed because of the low vapor pressure of nitrogen tetrasulfide.

The instruments used were a Perkin-Elmer recording infrared spectrometer at the Spectroscopy Laboratory of the Massachusetts Institute of Technology (KSR-5 and KBr regions), and a Beckman IR-2 recording infrared spectrometer at the University of Connecticut (NaCl region).

THE STRUCTURE OF NITROGEN TETRASULFIDE

Strictly speaking, selection rules based on a molecular symmetry group apply rigorously only to spectra of vapors. Experience has shown, however, that perturbations resulting from liquid forces usually exert only a minor influence on the gross features of vibrational spectra. The spectra in solution will therefore be interpreted on the basis of the molecular symmetry selection rules, with proper allowance being made for crystal forces in interpretation of the spectra taken of Nujol mulls.

The observed spectra are given in Table I. Considering the solution spectra, it is seen that some, but not all, Raman lines are infrared active while all strong infrared bands are Raman active. These features eliminate all models having a center of symmetry, as well as the C_{3v} model suggested as a possibility by Arnold, Hugill, and Hutson[1,2] and the S_4 tub model.[2]

The sharp infrared band at 555 cm^{-1} in cyclohexane solution is split into two bands at 552 and 557 cm^{-1} in the crystal spectrum. We interpret this as splitting of a degenerate mode of vibration, rather than splitting under the factor group, due to interaction of like modes of vibration of adjacent molecules. The reasoning behind this interpretation is based on the fact that nitrogen tetrasulfide has the space group C_{2h}^5, with only C_i available as a site symmetry.[12,13] The nitrogen tetrasulfide molecules, however, cannot lie on these sites since C_i has a center of symmetry, and the nitrogen tetrasulfide molecule, as already shown, has none. The molecules, then, must lie on sites of symmetry C_1. All degeneracies should then be removed in the crystal spectrum, and all frequencies should become active, although the effects may not be detectable in all cases. The magnitude of the splitting of the 555 cm^{-1} band makes it probable that this split is the result of a split degeneracy rather than of splitting under the factor group. This latter type of splitting has been observed so far only at very low temperatures.

TABLE II. D_{2d} selection rules.

Type	Infrared	Raman	Fundamentals
A_1	ia[a]	a[b]	3
A_2	ia	ia	2
B_1	ia	a	2
B_2	a	a	3
E	a	a	4

[a] ia = inactive.
[b] a = active.

[12] M. Buerger, Am. Mineralogist **21**, 575 (1936).
[13] R. Halford, J. Chem. Phys. **14**, 8 (1946).

The idea of nitrogen tetrasulfide having degenerate vibrational modes is supported by the low number of vibrational bands observed.

We are thus led to eliminate all models having low symmetry. Molecules having a dipole moment (such as the C_{4v} crown model) may be eliminated because of the small dipole moment of nitrogen tetrasulfide[14] and the large N—S bond moment.[15] The symmetry that best fits the gross features of the spectra is the D_{2d} symmetry. A model based on this symmetry would have degenerate vibrational modes, no dipole moment, and no symmetry center. The activities, and numbers of predicted and observed strong infrared and Raman-active lines are roughly the same (Tables I, II). A check of the observed and predicted numbers of polarized Raman lines would have been desirable, but no polarization measurements could be made, because of the weakness of the spectra.

Two models having D_{2d} symmetry have been suggested for nitrogen tetrasulfide, the ring and the cage. An examination of the detailed features of the spectra, along with the infrared spectrum of nitrogen hydrogen sulfide, allows us to eliminate the ring model. The skeletal frequencies of nitrogen hydrogen sulfide represent the vibrations of a singly bonded N—S ring,[16] while the vibrations around 1300 and 3200 cm^{-1} are N—H vibrations. A comparison of the infrared spectra of the two compounds shows several coincidences (Table I). This leads us to believe that they contain similar types of bonds, namely, N—S single bonds. This favors the cage model over the ring model, which would have resonating N—S bonds with partial double-bond character.

An examination of the selection rules and symmetry coordinates (Tables II, III) for the cage model shows that there should be one A_1 and one B_2 N—N stretching frequency. These are nicely fitted by the Raman line at 888 cm^{-1} (hydrazine has its N—N stretching frequency at 893 cm^{-1}) and the Raman and infrared bands at 934 cm^{-1}. The latter infrared band disappears on reduction of nitrogen tetrasulfide, as is to be expected. Further examination of the selection rules shows that the ring model should have seven low and five high frequencies ("high" and "low" corresponding to bond stretching and angle bending and torsion vibrations, respectively), and the cage model seven high and five low frequencies. The small number of observed low frequencies thus favors the cage model.

[14] N. Phalnikar and B. Bhide, Current Sci. India **8**, 473 (1939).
[15] J. Moede and C. Curran, J. Am. Chem. Soc. **71**, 852 (1949).
[16] E. R. Lippincott and M. C. Tobin, J. Am. Chem. Soc. **73**, 4990 (1951). The bands at 705 and 780 cm^{-1} are incorrectly given in this note as lying at 712 and 828 cm^{-1}.

TABLE III. Symmetry coordinates for nondegenerate vibrations of cage model.

$$A_1 \quad R_1=\Delta(r_1+r_2+r_3+r_4+r_5+r_6+r_7+r_8)/(8)^{\frac{1}{2}}$$
$$R_2=\Delta(D_1+D_2)/(2)^{\frac{1}{2}}$$
$$R_3=\Delta(\theta_1+\theta_2+\theta_3+\theta_4+\theta_5+\theta_6+\theta_7+\theta_8)/(8)^{\frac{1}{2}}$$

$$A_2 \quad R_4=\Delta(r_1-r_2+r_3-r_4+r_5-r_6+r_7-r_8)/(8)^{\frac{1}{2}}$$
$$R_5=\Delta(\theta_1-\theta_2+\theta_3-\theta_4+\theta_5-\theta_6+\theta_7-\theta_8)/(8)^{\frac{1}{2}}$$

$$B_1 \quad R_6=\Delta(r_1+r_2-r_3-r_4+r_5+r_6-r_7-r_8)/(8)^{\frac{1}{2}}$$
$$R_7=\Delta(\theta_1+\theta_2-\theta_3-\theta_4+\theta_5+\theta_6-\theta_7-\theta_8)/(8)^{\frac{1}{2}}$$

$$B_2 \quad R_8=\Delta(r_1-r_2-r_3+r_4+r_5-r_6-r_7+r_8)/(8)^{\frac{1}{2}}$$
$$R_9=\Delta(D_1-D_2)/(2)^{\frac{1}{2}}$$
$$R_{10}=\Delta(\theta_1-\theta_2-\theta_3+\theta_4+\theta_5-\theta_6-\theta_7+\theta_8)/(8)^{\frac{1}{2}}$$

F Matrices for cage model

$$A_1 \quad \begin{pmatrix} f_r+7f_{rr} & 4f_{Dr} & 8df_{r\theta} \\ 4f_{Dr} & f_D+f_{DD} & 4df_{D\theta} \\ 8df_{r\theta} & 4df_D & d^2f_\theta+7d^2f_{\theta\theta} \end{pmatrix}$$

$$A_2 \quad \begin{pmatrix} f_r-f_{rr} & 0 \\ 0 & d^2f_\theta-d^2f_{\theta\theta} \end{pmatrix}$$

$$B_1 \quad \begin{pmatrix} f_r-f_{rr} & 0 \\ 0 & d^2f_\theta-d^2f_{\theta\theta} \end{pmatrix}$$

$$B_2 \quad \begin{pmatrix} f_r-f_{rr} & 0 & 0 \\ 0 & f_D-f_{DD} & 0 \\ 0 & 0 & d^2f_\theta-d^2f_{\theta\theta} \end{pmatrix}$$

Evaluated *G* matrices for nitrogen tetrasulfide cage model

$$A_1 \quad \begin{pmatrix} 4.47\times10^{22} & -2.9\times10^{22} & 1.5\times10^{30} \\ -2.9\times10^{22} & 8.56\times10^{22} & -4.5\times10^{30} \\ 1.5\times10^{30} & -4.5\times10^{30} & 5.6\times10^{38} \end{pmatrix}$$

$$A_2 \quad \begin{pmatrix} 5.2\times10^{22} & 0.5\times10^{30} \\ 0.5\times10^{30} & 5.6\times10^{38} \end{pmatrix}$$

$$B_1 \quad \begin{pmatrix} 7.19\times10^{22} & -8.9\times10^{30} \\ -8.9\times10^{30} & 17.9\times10^{38} \end{pmatrix}$$

$$B_2 \quad \begin{pmatrix} 5.1\times10^{22} & 2.9\times10^{22} & -0.9\times10^{30} \\ 2.9\times10^{22} & 8.56\times10^{22} & -4.5\times10^{30} \\ -0.9\times10^{30} & -4.5\times10^{30} & 5.4\times10^{38} \end{pmatrix}$$

We are now in a position to see why the reduction products of nitrogen tetrasulfide never contain N−N bonds. The fact that the infrared spectrum of nitrogen hydrogen sulfide very closely resembles that of nitrogen tetrasulfide in the region 250–1000 cm^{-1} makes it appear probable that the skeleton is intact and that the N−N bonds of nitrogen tetrasulfide were broken to form N−H bonds. In other words, the N−N bonds were attacked more readily than the N−S bonds.

FORCE CONSTANT CALCULATIONS

To add support to the proof of structure just given and to facilitate an assignment of frequencies, a normal coordinate analysis was thought desirable. The secular equations were set up by the *F G* matrix method of Wilson,[17] using the N−S bond stretchings, the N−N bond stretchings, and the N−N−S angle bendings as internal coordinates. These formed symmetry coordinates containing no redundancies, by fortunate choice. The most general simple—harmonic potential function was used.

[17] E. B. Wilson, J. Chem. Phys. **7**, 1047 (1939); **9**, 76 (1941).

The bond lengths were taken as the sums of the normal covalent atomic radii, in the absence of more reliable information. These were 1.40A for the N−N bond and 1.74A for the N−S bond. The N−S−N angle was assigned the value 100° from the S−S−S angle in S_8, and the S−N−S angle the value 108° from the C−N−C bond angle in dimethylamine.[18] Calculation for the N−N−S angle gave 109°, so that the cage model is essentially unstrained.

The symmetry coordinates, *F* matrices, and *G* matrices are given in Table III. In the actual calculations, the coefficients in the expressions for the *S* vectors were evaluated before combination into *G* matrix elements, due to the complicated form of the *S* vectors.

Since the assignment of no one vibrational species was known in advance, and no value for the N−S force constant was available, it was necessary to resort to an artifice to get a starting point. The A_1 and B_1 species are infrared inactive for D_{2d}, while the B_2 and *E* species are infrared active (Table II); but lacking polarization data, the selection rules give us no further help in assigning the frequencies.

The symmetry coordinates indicate that the B_1 species should contain one N−S bond stretching and one angle bending frequency. The possible B_1 wave numbers were 785, 615, 213, and 177 cm^{-1}. It was found that combination of the two higher frequencies gave imaginary force constants when inserted into the B_1 secular equation. Clearly then, 177 or 213 cm^{-1} is the B_1 bending frequency, while 785 or 615 cm^{-1} could be the stretching frequency. Combination of either of the two higher frequencies with 347 cm^{-1} also gave imaginary force constants, so no B_1 frequency could be coincident with another frequency at this position.

It is seen from Table III that off-diagonal elements of the B_1 and B_2 *F* matrices are zero, and that the diagonal elements are identical, except for the factor involving the N−N stretching force constant. Using the well-known relationship

$$|F||G|=\prod_i^n \lambda_i,$$

where n is the number of vibrations in a symmetry species, we have

$$\frac{|F||G|(B_1)}{|F||G|(B_2)}=\frac{\lambda_1\lambda_2(B_1)}{\lambda_1\lambda_2\lambda_3(B_2)}.$$

Using the calculated values for the *G* matrices, the known B_2 frequency 934 cm^{-1} (λ_3), and an approximate N−N stretching force constant of 3.8×10^5 dyne/cm (calculated from hydrazine, considering it as a diatomic molecule), we find

$$\lambda_1\lambda_2(B_1)\simeq 4\lambda_1\lambda_2(B_2).$$

[18] L. Pauling, *Nature of the Chemical Bond* (Cornell University Press, Ithaca, 1948), first edition, p. 80.

TABLE IV. Force constants and calculated frequencies for nitrogen tetrasulfide.

N−S bond stretching	(f_r)	2.67×10^5 dyne/cm
N−N bond stretching	(f_D)	3.08×10^5 dyne/cm
N−N−S angle bending	(f)	0.0975×10^5 dyne/cm
N−N bond—N−N bond	(f_{DD})	0.00×10^5 dyne/cm
N−S bond—N−S bond	(f_{rr})	0.19×10^5 dyne/cm
N−N−S angle—N−N−S angle	(f)	0.00264×10^5 dyne/cm

	Observed	Calculated	% Error
A_1	888	980	10
	615	570	7.3
	177	177	0
A_2		460	
		173	
B_1	785[a]	785	0
	213[a]	213	0
B_2	934[a]	934	0
	519	510	2
	177	160	9.6

[a] Used to obtain major force constants.

From a table of $\lambda_1\lambda_2(B_1)$ and $4\lambda_1\lambda_2(B_2)$, it was found that the best fit was given by 785 and 213 cm^{-1} for B_1, and 519 and 177 cm^{-1} for B_2. The B_1 frequencies were used with the secular equation to get the B_1 F matrix elements. These were substituted into the B_2 equation with the known B_2 frequency to get the B_2 F matrix element corresponding to N−N stretching.

Use of these matrix elements in the A_1 secular equation, ignoring off-diagonal F matrix elements, gave predicted A_1 frequencies of 164, 470, and 920 cm^{-1}. This seemed to favor 177, 615, and 888 cm^{-1} for the A_1 frequencies, this last frequency being already known.

Adjustment of the diagonal F matrix elements to give the closest possible fit to these[19] gave 980, 570, and 177 cm^{-1} as the predicted A_1 frequencies.

The combined B_2 and A_1 F matrix elements were used to get the force constants given in Table IV. It is seen that these are all of the right order of magnitude except for the N−S bond stretching interaction constant. When it is considered, however, that each N−S bond is bound to two others in a tightly closed cage, this large interaction becomes reasonable.

Several other combinations of possible A_1 frequencies were examined but these either gave a much poorer match between predicted and observed frequencies, or demanded unreasonably large interaction constants for a fit.

It is seen in Table IV that all calculated frequencies match the observed frequencies to within 10 percent. This is a quite satisfactory result, since only five force constants were used to calculate eight frequencies.

[19] This process corresponds to allowing for N−S bond-bond interaction and N−N−S angle-angle interaction. N−N bond-bond interaction is not possible, since the N−N bonds share no atoms in common, so that the N−N F matrix element was held at the value it had in the B_2 matrix.

ASSIGNMENT OF FREQUENCIES

We are now in a position to give a complete assignment of frequencies for nitrogen tetrasulfide. On the basis of the force constant calculations and the selection rules, we assign 177, 615, and 888 cm^{-1} to A_1, the calculated frequencies 173 and 460 cm^{-1} to A_2, 213 and 785 cm^{-1} to B_1, and 177, 519, and 934 cm^{-1} to B_2. In view of the lack of off-diagonal interaction force constants, and the fact that the E secular equation is of the fourth degree, it was decided to assign the E frequencies on the basis of the selection rules, the other frequencies having been already assigned. The infrared and Raman active frequencies 347 and 561 cm^{-1} are certainly E frequencies. The second E bending frequency cannot lie far from 213 cm^{-1} and may be assumed to be coincident with the B_2 frequency at this position.

The last E stretching frequency may be assigned at 720 cm^{-1}, if it is assumed that the strong Raman line at 720 cm^{-1} and the strong infrared band at 700 cm^{-1} are the same. The lines at 696 and 719 cm^{-1} in the Nujol mull may then be interpreted as a split degeneracy. Although the discrepancy is rather large, it could very well be the result of the experimental error in this case, since the Raman line is diffuse. Unfortunately, the position at 692 cm^{-1} in the Raman spectrum is blocked by a mercury line.

The other observed bands are assigned as overtones or combination tones, with the exception of the very weak infrared band at 792 cm^{-1} in the Nujol mull. This is

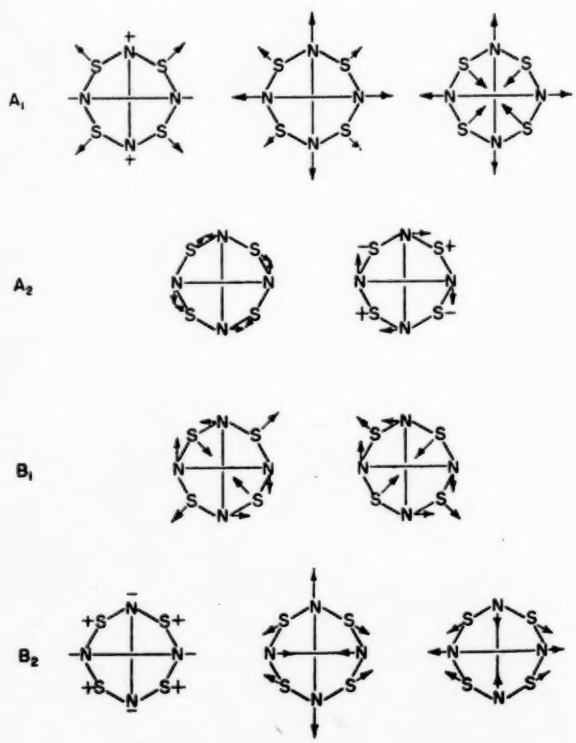

FIG. 5. Schematic nondegenerate vibrational modes of nitrogen tetrasulfide.

interpreted as the forbidden B_1 frequency, activated by crystal forces under the site group.

The complete assignment is given in Table I. Schematic representations of the nondegenerate vibrations of nitrogen tetrasulfide are given in Fig. 5.

THE STRUCTURE OF NITROGEN HYDROGEN SULFIDE

The close resemblance between the infrared spectra of nitrogen tetrasulfide and nitrogen hydrogen sulfide points to the conclusion that the two molecules are analogous in structure, except that in nitrogen hydrogen sulfide, the two N—N bonds of nitrogen tetrasulfide have been broken to form N—H bonds.

On the basis of a D_{2d} symmetry we may give an assignment, admittedly tentative, of the observed frequencies of nitrogen hydrogen sulfide. The types of vibration will be unchanged, except that the A_1 and B_2 N—N stretching frequencies of nitrogen tetrasulfide will be replaced by N—S—N—S torsions in nitrogen hydrogen sulfide.

The 780 cm^{-1} band may be assigned to a B_1 vibration activated by crystal forces; the 541 cm^{-1}, and the 693–705 cm^{-1} doublet may be assigned to E; the 516 cm^{-1} may be assigned to B_2; and the 462 cm^{-1} may be assigned to an A_2 frequency activated by crystal forces, in view of the predicted A_2 frequency at 460 cm^{-1} in nitrogen tetrasulfide. The 280–302 cm^{-1} complex may be expected to contain the E angle bending, and the A_1 or B_2 torsions.

We may hazard a guess as to where the remaining frequencies might appear were the Raman spectrum available. The A_1 N—S stretching frequency should appear at about 615 cm^{-1}. Two or more bands may be expected in the 150–215 cm^{-1} region, these representing one torsional and five angle bending modes. This assignment is tabulated in Table II.

We are indebted to a grant-in-aid from the Research Corporation which enabled this work to be undertaken. The authors wish to thank Professor Richard C. Lord for the use of infrared equipment at the Massachusetts Institute of Technology. They also wish to express their thanks to Mr. James H. Orr of Arthur D. Little, Inc., for preparing the drawings of this paper.

THE JOURNAL OF CHEMICAL PHYSICS VOLUME 21, NUMBER 9 SEPTEMBER, 1953

Free-Electron Network Model for Conjugated Systems. I. Theory*

KLAUS RUEDENBERG AND CHARLES W. SCHERR
Laboratory of Molecular Structure and Spectra, Physics Department, University of Chicago, Chicago 37, Illinois

(Received December 30, 1952)

The free-electron model for conjugated systems is consistently developed as the limiting case of a three-dimensional quantum-mechanical treatment of the π electrons in such systems. Joint conditions (for branching points) and boundary conditions (for free end points) are derived and the hermiticity of the Hamiltonian is shown. A matrix formulation of the theory is established which makes the application to large systems feasible, and at the same time leads to a close analogy with the LCAO model (LCAO MO treatment considering only nearest neighbor interactions). Quantities analogous to the quantities q (the charge in an atomic orbital) and p (the bond order) are defined, and special attention is given to alternant conjugated systems for which a population theorem, analogous to the one in LCAO theory, is valid.

INTRODUCTION

SYSTEMS of conjugated double bonds in organic molecules are, in a first approximation, described by assuming that the σ electrons form bonds which maintain the molecular frame and that the π electrons move in the potential of this frame. Interesting properties of the molecules depend, in a first approximation, on the π electrons, e.g., the relative bond lengths, certain types of chemical reactivity, ultraviolet spectra, and (to a lesser degree) dipole moments; it is therefore of interest to investigate the motion of the π electrons by itself. A basic characteristic of this motion is the high mobility or delocalization, i.e., the fact that the different electrons are not bound to definite bonds, but move rather freely over the whole conjugated structure. The description by molecular orbitals (MO's) seems therefore particularly suited for this case.

The classical method of constructing MO's consists of forming them as LCAO MO's (linear combination of atomic orbitals). The rigorous application of this method leads to an extremely large number of difficult integrals, and only benzene has been successfully treated in this way.[1] In order to achieve a more general method, applicable to larger classes of molecules, one generally makes the assumption that

* This work was assisted in part by the U. S. Office of Naval Research under Task Order IX of Contract N6ori-20 with The University of Chicago.

[1] M. Goeppert-Mayer and A. L. Sklar, J. Chem. Phys. **6**, 645 (1938); C. C. J. Roothaan and R. G. Parr, J. Chem. Phys. **17**, 1001 (1949); Parr, Craig, and Ross, J. Chem. Phys. **18**, 1561 (1950); and C. C. J. Roothaan, Revs. Modern Phys. **23**, 69 (1951).

only nearest neighbors interact and considers the remaining integrals as parameters in the final result. This simplified method[2] has been rather successful, and in the following we always mean this *simplified LCAO theory* whenever we mention the *LCAO model* without further specification.

On the other hand, the existence of the core potential suggests the possibility of expressing this potential in terms of coordinates which are fitted to the particular frame of the molecule, e.g., cylindrical coordinates in the case of benzene. As a consequence, the molecular orbitals would be expressed in terms of the same coordinates. Again, this approach can be carried through for benzene,[3] but it becomes very complicated for larger molecules. Here too, however, there exists a simplified formulation, applicable to any conjugated system: the one-dimensional free-electron model.

This model is not new,[4] but it has mostly been regarded as a pictorial but rough description. It is the purpose of the present paper to show that the free-electron model deserves the same recognition and standing as the simplified LCAO model. A close analogy will be derived between the mathematics of the two models,[4c] and in the second paper of the present series, a close agreement will be established between the numerical results obtained by the two models.[5] Thus, from an empirical point of view, the free-electron model seems to serve as well to describe conjugated systems as the simplified LCAO model.

But also from the theoretical point of view, the free-electron model offers several attractive properties: (1) Once the free-electron model is chosen, the quantum-mechanical problem is rigorously solved. One makes no further approximations of virtually uncontrolled implications, as e.g., the assumption of only considering nearest neighbor interactions in the LCAO model. (2) The free-electron model (as developed here) has only one parameter, the neighbor distance D, as compared to the two parameters β, S of the LCAO model.[6] (3) The meaning of the parameter D in terms of *measurable* quantities is more precisely defined than the meaning of the parameters occurring in the LCAO model. Therefore there is but little "leeway" to "adjust" D, and the free-electron model comes closer to being an "absolute theory" (no adjustable parameters). (4) The free electron wave functions are easy to visualize; a fact which is demonstrated by the model of Platt explained in the third paper of this series.[7] Of course the LCAO model has the advantage that it is in a position to describe simultaneously *all* electrons, not only the π electrons, in a molecule.

The present paper is restricted in scope to the case that all atoms in a conjugated structure are mathematically equivalent, i.e., practically to the case of hydrocarbons. A method to include the effect of heteroatoms is in preparation.

1. GENERAL CONCEPTS

The Model

The organic molecules to which the present theory applies are characterized by the fact that each of them contains a so-called conjugated system of bonds, i.e., a system of alternating single and double bonds. Each atom within a conjugated system contributes two σ electrons and one π electron for the chemical binding of the conjugated structure. In the approximation considered here, the σ electrons form σ bonds which maintain the geometrical arrangement; and the molecular framework, stripped of the π electrons, forms a "skeleton" or "core" which, owing to its positive charge, creates a potential under whose influence *all* π electrons move throughout the *entire* conjugated structure. Thus, if formula I of Fig. 1 describes for example the naphthalene molecule, the formula II in the same figure would be an appropriate description of the corresponding molecular skeleton. Indeed, this formula gives even a correct *geometrical* picture of the physical skeleton,

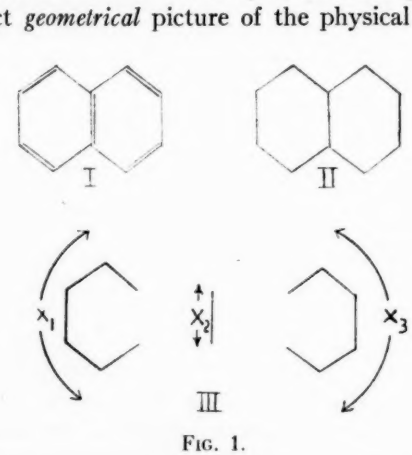

FIG. 1.

[2] See, e.g., Coulson and Longuet-Higgins, Proc. Roy. Soc. (London) **A191**, 39 (1947); see also reference 8.

[3] See K. Ruedenberg and R. G. Parr, J. Chem. Phys. **19**, 1268 (1951).

[4a] L. Pauling, J. Chem. Phys. **4**, 673 (1936); O. Schmidt, Ber. deut. chem. Ges. **73A**, 97 (1940); J. R. Platt, J. Chem. Phys. **17**, 484 (1949); H. Kuhn, Helv. Chim. Acta **31**, 1441 (1948), **31**, 1780 (1948); J. Chem. Phys. **16**, 840 (1948), **17**, 1198 (1949); Helv. Chim. Acta **32**, 2247 (1949); Z. Elektrochem. **53**, 165 (1949); Helv. Chim. Acta **34**, 1308 (1951), **34**, 2371 (1951); and Z. Elektrochem. **55**, 220 (1951); S. Nikitine, J. chim. phys. **47**, 614 (1950); T. Nakajima and H. Kon, J. Chem. Phys. **20**, 750 (1952); M. V. Volkenshtein and L. A. Borovinskii, Doklady Akad. Nauk. (S.S.S.R.) **85**, 737 (1952).

[4b] N. S. Bayliss, J. Chem. Phys. **16**, 287 (1948), **17**, 1853 (1949); Australian J. Sci. Research **A3**, 109 (1950); N. S. Bayliss and J. C. Riviere, *ibid.* **A4**, 344 (1951); W. T. Simpson, J. Chem. Phys. **16**, 1124 (1948).

[4c] An analogy between the LCAO model and the FE model in the simplest cases (no branch points) was already noticed by W. T. Simpson, J. Chem. Phys. **17**, 1218 (1949) and H. H. Jaffe, J. Chem. Phys. **20**, 1646 (1952).

[5] C. W. Scherr, J. Chem. Phys. **21**, 1582 (1953).

[6] For a fair comparison it should be noted that the correlation of the LCAO model with experimental data can be obtained by assigning a fixed value to S and treating β as the only empirical parameter.—The LCAO model actually contains a third parameter α, which, however, serves only to calibrate the zero point of the energy.

[7] J. R. Platt, J. Chem. Phys. **21**, 1597 (1953).

since it is well known that all atoms belonging to a conjugated system lie in one plane.

The starting point of the theory to be developed here is the assumption that the core potential is infinitely high everywhere except on the bond lines of the skeleton structure II, where it is finite. Obviously such a potential has to be considered as the limiting case of a potential which is infinitely high everywhere except within a thin tube extending along the bond lines. Furthermore, the interelectronic interaction is, in a first approximation, neglected between the π electrons so that the latter move independent of each other under the influence of the core potential.

Linear Bond Paths

In order to determine the implications of the assumptions just made, let us, as a first example, consider the motion of an electron in a long thin box of length l and with a square cross section of sidelength $\epsilon \ll l$ (see Fig. 2). This model corresponds to the π-electronic

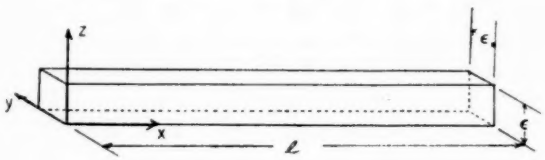

FIG. 2.

motion in a polyene, e.g., butadiene. The eigenfunctions

$$\Phi_{nmm'}(x, y, z) = (2/l)^{\frac{1}{2}}(2/\epsilon)\sin(\pi nx/l) \times \sin(\pi my/\epsilon)\sin(\pi m'z/\epsilon) \quad (1.1)$$

must be antisymmetric with respect to the plane $z=\epsilon/2$, which we take to be the nodal plane of the π electrons so that the quantum numbers assume the values

$$n=1, 2, 3, \cdots;\ m=1, 2, 3, \cdots;\ m'=2, 4, 6, \cdots. \quad (1.2)$$

From the expression for the eigenvalues

$$E_{nmm'} = (h^2/8m)[(n/l)^2+(m/\epsilon)^2+(m'/\epsilon)^2], \quad (1.3)$$

it follows that, because of $\epsilon \ll l$, the motions in the y and z directions remain in their ground state ($m=1$, $m'=2$) while the x motion is excited to its lower levels, so that

$$E = E_{n12} = (h^2/8m)[(n/l)^2+(5/\epsilon^2)] = E_n + \text{const}, \quad (1.4)$$

$$E_n = (h^2/8ml^2)n^2, \quad (1.5)$$

and the wave functions have a single nodal plane perpendicular to the z axis in agreement with the nodal properties of $2p\pi$ atomic orbitals. Hence the y and z motion may be neglected for low excitations, and it is sufficient to work with the energies (1.5) and the wave functions

$$\phi_n(x) = (2/l)^{\frac{1}{2}}\sin(\pi nx/l), \quad (1.6)$$

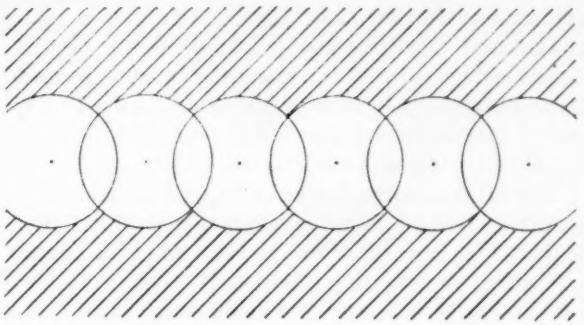

FIG. 3.

which may be defined by the equations

$$\phi_n^2(x) = \int_0^\epsilon dz \int_0^\epsilon dy \Phi_{n12}^2(x, y, z) = \int_Q dQ \Phi_{n12}^2, \quad (1.7)$$

$$\text{sign of } \phi_n(x) = \text{sign of } \Phi_{n12}\ (x, y=\epsilon, z=\tfrac{1}{4}\epsilon), \quad (1.7')$$

where Q denotes a cross section of the tube and $dQ=dzdy$, a cross-section element. The functions (1.6) are the normalized eigenfunctions of the *one-dimensional* eigenvalue problem considered by the free-electron model and the energies E_n (1.5) are the corresponding energy eigenvalues.

The limiting process $\epsilon \to 0$ leaves $\phi_n(x)$ and E_n unaffected and therefore meaningful, whereas Φ_{n12} and E_{n12} become infinite. The latter circumstance means that the y and z excitation energies become *infinitely* high so that $\phi_n(x)$ and E_n give (for $\epsilon=0$) a correct description of the system for *all finite* excitations of the x motion, i.e., for all finite quantum numbers n.

Since high excitations effect, however, structural changes in organic molecules, they do not have to be considered; and the assumption $\epsilon \ll l$ is actually sufficient to justify the use of the one-dimensional description given by (1.5) and (1.6), i.e., the physical assumption is only that the π electrons form a cloud whose length is large compared to its width. The passage to the limit $\epsilon \to 0$ is only a matter of mathematical convenience and does not imply that the π-electron cloud is actually infinitely thin.

Comparison with the LCAO Model

The present theory is thus, physically, a three-dimensional theory and the electron cloud of a π electron is its MO. These MO's are not entirely different in nature from the MO's formed as linear combinations of atomic orbitals (LCAO MO's), *if all matrix elements between nonneighboring atoms are neglected*—the assumption adopted in the LCAO MO model.[8] Indeed, such an assumption implies that the radii of the (finite) atomic

[8] An introduction to the LCAO MO treatment and further literature may be found in B. Pullman and A. Pullmann, *Les theories electroniques de la chimie organique* (Masson and Company, Paris, 1952), Chap. IV, p. 2.

orbitals are smaller than one bond length in straight chains and smaller than $\frac{1}{2}\sqrt{3}=0.87$ bond lengths in benzene rings, so that the molecular orbitals formed by them obtain also a tubular shape as shown in Fig. 3, where the circles indicate the atomic orbitals and the shaded area is inaccessible to the π electrons.

The MO's constructed as LCAO MO's correspond to a potential which is not constant within the accessible region. This generalization can be readily introduced in our model by assuming a potential $V=V(x)$ inside the box of Fig. 2. Thereby the eigenvalues (1.5) and the eigengunctions (1.6) will be changed, but they will remain finite so that all arguments presented above remain unaltered.

There is no need to introduce a potential which depends also on y and z, since, because of $\epsilon \ll l$, the motions in the y and z directions will in any case stay in the ground state so that the (y, z) dependence remains irrelevant. The LCAO MO model (with neglect of nonneighbor interaction) also considers essentially only "longitudinal excitations," since one can see from Fig. 3 that the "transversal profile," i.e., the (y, z) dependence, of the LCAO MO is much less changed by varying the coefficients of the different atomic orbitals than the "longitudinal profile."

The purpose of the foregoing remarks is not to justify the free-electron model by vague analogies with the LCAO MO model—but to give a plausible reason for the agreement which exists, as we hope to show, between the two methods.

Nonlinear Bond Paths

Let us take benzene as an example of the case that the bond path is no longer a straight line and let us for the moment assume that the π electrons move in a thin circular tube (torus of radius R) rather than in a hexagonal tube. Let us further replace the annular well potential representing the torus by the analytic potential

$$V(r, \varphi, z)=U(2\alpha)^{-2}\{(z/R)^2+[(r/R)-(R/r)]^2\}, \quad (1.8)$$

$$U=\hbar^2/2mR^2, \quad (1.9)$$

where the cylindrical coordinates z, r, and φ (z perpendicular to the molecular plane) are used and α is a dimensionless constant $\ll 1$. It is sensible to define

$$\epsilon=\alpha R \quad (1.10)$$

as the diameter of the corresponding tube, whereas $l=2\pi R$ is its length, so that indeed $\epsilon/l=\alpha/2\pi \ll 1$.

It has been shown[3] that the potential (1.8) leads to energy levels

$$E_{n_\varphi, n_r, n_z}=E_{n_\varphi}+E_{n_r}+E_{n_z}, \quad (1.11)$$

where E_{n_φ} corresponds to angular excitations, E_{n_r} corresponds to radial excitations and E_{n_z} corresponds to out-of-plane excitations. The energy levels E_{n_φ} of the "longitudinal motion" are given by

$$E_{n_\varphi}=Un_\varphi^2 f(\alpha^2 n_\varphi^2); \quad n_\varphi=0, \pm 1, \pm 2, \cdots; \quad (1.12)$$

$$f(x)=[(1+4x)^{\frac{1}{2}}-1]/2x=1-x+\cdots; \quad (1.13)$$

and for the two transversal motions the excitation energies are

$$\Delta E_{n_r}=\Delta E_{n_z}=2U/\alpha \gg \Delta E_{n_\varphi}. \quad (1.14)$$

It is therefore again true that the excitations of the transversal motions can be neglected and that the energy levels of the longitudinal motion approximate the limiting levels

$$\lim_{\epsilon \to 0} E_{n_\varphi}=Un_\varphi^2. \quad (1.15)$$

These are, however, identical with the levels obtained by considering the one-dimensional motion of a particle along the line which is the limit of the tube as $\epsilon \to 0$.

These conclusions can be expected to be independent of the particular example chosen, i.e., to hold not only for a circular tube, but for a tube along *any* arbitrary bond path, e.g., for the hexagonal tube of benzene. This expectation will be justified at the end of the next subsection. We have then the general result that the assumption of a potential, infinite everywhere except on the bond skeleton is equivalent to describing the electronic motion by an one-dimensional MO, $\phi(x)$, depending on the "bond path coordinate" x, and assuming for $\phi(x)$ the Schrödinger equation

$$\{(d/dx)^2+(2m/\hbar^2)[E-V(x)]\}\phi(x)=0, \quad (1.16)$$

where $V(x)$ is an *appropriate* potential along the bond skeleton. The complete description of the electron is then furnished by a three-dimensional molecular orbital which can approximately be written as

$$\Phi(x, y, z) \approx \phi(x)(2/\epsilon)\sin(\pi y/\epsilon)\sin(2\pi z/\epsilon), \quad (1.17)$$

with

$$0 \leqslant y \leqslant \epsilon, \quad -\tfrac{1}{2}\epsilon \leqslant z \leqslant \tfrac{1}{2}\epsilon, \quad \epsilon \ll l. \quad (1.17')$$

Here the x coordinate is tangential to the bond paths, y is perpendicular to x in the molecular plane, and z is perpendicular to the molecular plane, which is chosen to be the plane $z=0$. The orbital $\Phi(x, y, z)$ is antisymmetric with respect to this plane. The rigorous form for $\Phi(x, y, z)$ is obtained by solving the thin tube problem corresponding to the bond skeleton; between such a $\Phi(x, y, z)$ and the one-dimensional orbital $\phi(x)$ one has, in analogy with (1.7) and (1.7'), the relation

$$\phi^2(x)=\lim_{\epsilon \to 0}\int_{Q(x)} dQ\Phi^2(x, y, z), \quad (1.18)$$

$$\text{sign of } \phi(x)=\text{sign of } \Phi(x, y=\tfrac{1}{2}\epsilon, z=\tfrac{1}{4}\epsilon), \quad (1.19)$$

where ϵ is the diameter of the tube and $Q(x)$ its cross section at the point x.

Branching Points (Joints)

Those points in a conjugated structure where three branches meet (we call them branching points or joints) present the one-dimensional formulation with a particular problem. Let us split the skeleton of Fig. 1(II) up into three branches and define on each branch an independent arbitrary coordinate system as shown by Fig. 1(III). Let $\phi_B(x_B)$ be the part of the wave function $\phi(x)$ which lies on the branch $B(=1, 2, 3)$; more precisely, let $\phi_B(x)$ be defined by

$$\left.\begin{aligned} &\phi_B(x)=\phi(x), \quad \text{if } x=x_B, \text{ i.e., on branch } B,\\ &\phi_B(x)\equiv 0, \quad \text{if } x\neq x_B, \\ &\qquad \text{i.e., on all other branches,}\end{aligned}\right\} \tag{1.20}$$

so that

$$\phi(x)=\sum_B \phi_B(x). \tag{1.21}$$

Then Eq. (1.16) holds for each branch function $\phi_B(x_B)$, and the question arises, how does one fit together those $\phi_B(x_B)$ which meet in one joint.

A first condition is quite clearly the "continuity condition": The three branch functions $\phi_1(x_1)$, $\phi_2(x_2)$, $\phi_3(x_3)$ must assume the same value at their meeting point, i.e.,

$$\phi_1(x_{1J})=\phi_2(x_{2J})=\phi_3(x_{3J}), \tag{1.22}$$

where x_{BJ} is the coordinate of the joint on branch B.

However, since Eq. (1.16) is a second-order differential equation, we must also derive a condition involving the first derivatives of the functions $\phi_B(x_B)$. For this purpose we consider again the system of thin tubes corresponding to a bond skeleton. Let Fig. 4(a) illustrate the part of this system in the neighborhood of a joint. As before, let $\Phi(x, y, z)$ be the solution of the three-dimensional Schrödinger equation inside the tubes, fulfilling the boundary condition $\Phi(x, y, z)=0$ at the walls. From

$$\operatorname{div}(\Phi \operatorname{grad}\Phi)=\operatorname{grad}^2\Phi+\Phi\Delta\Phi \tag{1.23}$$

we obtain, by virtue of Gauss' theorem,

$$\int_V dV(\operatorname{grad}^2\Phi+\Phi\Delta\Phi)=\int_S dS\Phi(\partial/\partial n)\Phi$$
$$=\tfrac{1}{2}\int_S dS(\partial/\partial n)\Phi^2, \tag{1.24}$$

where S is the surface of the volume V, and $(\partial/\partial n)$ is the derivative in the direction of the outer normal on S. For the volume V we choose the volume indicated by the shaded area in Fig. 4(b). Since Φ vanishes on the walls and Q_1, Q_2, Q_3 are planar cross sections, Eq. (1.24) simplifies to

$$\sum_B (\partial/\partial x_B)\int_{Q_B} dQ\Phi^2=2J, \tag{1.25}$$

$$J=\int_V dV(\operatorname{grad}^2\Phi+\Phi\Delta\Phi), \tag{1.25'}$$

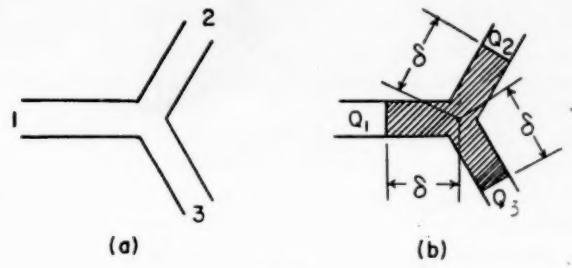

FIG. 4.

where the coordinate x_B is tangential to the tube branch B, and pointing away from the joint. Now consider *first* the limit $\epsilon\to 0$ (ϵ= tube diameter). By virtue of Eqs. (1.18) and (1.20) the left-hand side of Eq. (1.25) goes into

$$\sum_B [(\partial/\partial x_B)\phi^2(x)]_{Q_B}$$
$$=\sum_B [(\partial/\partial x_B)\phi_B{}^2(x_B)]_{x_B=x_{BJ}+\delta}=\text{finite}; \tag{1.26}$$

hence it follows that also

$$\lim_{\epsilon\to 0} J=\text{finite},$$

and therefore the integrand of J becomes infinite of the order ϵ^{-2} as $\epsilon\to 0$. *Secondly*, consider the limit {lim$\epsilon\to 0$ *and* lim$\delta\to 0$}, where δ is the distance of each of the three surfaces Q_B from the joint midpoint [see Fig. 4(b)]. Since the surfaces Q_B are purely fictitious and Φ does not fulfill any boundary conditions on them, the limit $\delta\to 0$ (in distinction from the limit $\epsilon\to 0$) does in no way cause Φ to become infinite. Hence, in the limit {$\epsilon\to 0$, $\delta\to 0$}, the integrand of J, once again, goes to infinity as ϵ^{-2} and hence

$$\lim_{\epsilon\to 0,\delta\to 0} J=0.$$

Therefore, the expression (1.26) must vanish for $x_B\to x_{BJ}$, and we find the new boundary condition

$$\sum_B (\partial/\partial x_B)\phi^2(x_B)$$
$$=\sum_B \phi_B(x_B)(\partial/\partial x_B)\phi_B(x_B)=0,$$
$$\text{at the joint } x_B=x_{BJ}, \tag{1.27}$$

which by virtue of the continuity condition (1.22) is equivalent to

$$[\sum_B (\partial/\partial x_B)\phi_B(x_B)]_{\text{Joint}}=0. \tag{1.28}$$

Since Eq. (1.28) may be derived also in the case of complex wave functions, it is clear that Eq. (1.28) expresses the conservation of the quantum-mechanical current density:

$$(i\hbar/2m)[\phi(d\phi^*/dx)-\phi^*(d\phi/dx)]. \tag{1.29}$$

However, since all wave functions $\phi(x)$ which occur as solutions of our problems are (with a few exceptions)

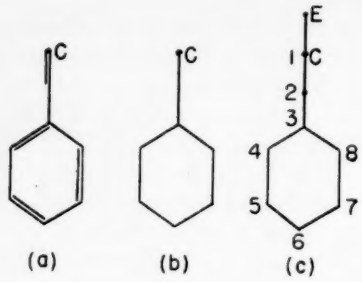

FIG. 5.

real, their current density vanishes everywhere so that the current conservation becomes trivial. We shall call Eq. (1.28) the "conservation condition."

The derivation of the conservation condition is independent of the number of branches meeting at one joint. Although for our purposes only the case of three branches per joint is useful, it is still of interest to note that also in the general case the conditions (1.22) and (1.28) suffice precisely to determine the solution of the eigenvalue problem, if the wave function is required to have a unique value everywhere. In order to recognize this, consider a system containing

a_3 joints collecting 3 branches,
a_4 joints collecting 4 branches,
.....
a_j joints collecting j branches,
and b "free end points."

If $B_{\max}$ is the total number of branches, then

$$2B_{\max}=3a_3+4a_4+\cdots+ja_j+b. \tag{1.30}$$

Since Eq. (1.16) is a second-order differential equation, the left-hand side of Eq. (1.30) gives the number of constants in the total wave function $\phi(x)$; the right-hand side of Eq. (1.30), on the other hand, gives the total number of joint and end-point conditions. Since there is one more parameter (the eigenvalue) and one more condition (the normalization of the wave function) in the problem, the number of unknowns to be determined equals the number of equations to be fulfilled, so that the eigenvalue problem (1.16) has a discrete eigenvalue spectrum.

Furthermore, it is easily seen that, in the case of one closed branch, as in benzene, the joint conditions are equivalent to the condition: that the wave function have a period that is an integral fraction of the branch length.

On the basis of the joint conditions (1.22), and (1.28) it is possible to give a more rigorous justification for the statements leading up to Eq. (1.16), namely, that there is no difference in the treatment of linear and nonlinear band paths. Consider any nonbranching point on a bond path as a joint with two branches; the conditions (1.22) and (1.28) then are applicable and yield the result that both $\phi(x)$ *and* $(d\phi/dx)$ are continuous at any such point. This, however, entails the validity of Eq. (1.16) throughout the entire bond path containing such points only. Consider in particular a "corner" in the bond path, e.g., in naphthalene [see Fig. 1(II)]: On the two straight portions of the bond path, meeting at the corner, Eq. (1.16) is valid; at the corner ϕ and $(d\phi/dx)$ have to be continuous and, if $V(x)$ is continuous, Eq. (1.16) yields that the left limit of $(d/dx)^2\phi$ equals the right limit of $(d/dx)^2\phi$. It follows that $(d/dx)^2\phi$ *exists at* the corner and equals the common limit so that Eq. (1.16) is valid *at* the corner. Hence, corners in a bond path have no implications, if the π-electronic potential is continuous.

The conditions (1.22) and (1.28) were first used by Hans Kuhn.[9] As yet no proof or discussion of the conservation condition (1.28) seems to have been given.

Formulation of the General Mathematical Problem

It may be useful to collect at this point the equations which determine the one dimensional free-electron molecular orbital (FEMO). They are as follows:

(1) the Schrödinger equation on the branches,

$$\mathcal{H}\phi(x)=\{(-h^2/2m)(d/dx)^2+V(x)\}\phi(x)=E\phi(x), \tag{1.31}$$

(2) the joint conditions,

$$[\phi_1(x_1)=\phi_2(x_2)=\phi_3(x_3)]_{\text{at joint}} \quad \text{(continuity condition)}, \tag{1.32}$$

$$\sum_B (\partial\phi_B/\partial x_B)_{\text{Joint}}=0 \quad \text{(conservation condition)}, \tag{1.33}$$

(3) the boundary conditions for free end points,

$$\phi(x)=0 \quad \text{at free end point.} \tag{1.34}$$

Concerning the branches having free end points there is still a question that remains to be settled, namely, where should the end point be located. For reasons which will become clear later (see Sec. 2 and Appendix) we adopt the following postulate: *The free-electron path terminates one bond length beyond the last atom.* Thus, for the styrene molecule of Fig. 5(a), whose bond skeleton is given by Fig. 5(b); the free-electron path is pictured in Fig. 5(c): It extends up to the point E, whereas the last atom is situated at the point C.

The definition initially given for the free-electron model should therefore be modified to read: The potential for the π-electronic motion is assumed to be infinite everywhere except on the *free-electron path*, where it is finite; the free-electron path is identical with the bond skeleton except that it exceeds the latter at its free end points by one bond length. Some authors[4b] have used different conventions concerning the free end points in order to fit certain experimental data; our choice is based on theoretical grounds, as will be shown in the Appendix.

[9] H. Kuhn, Helv. Chim. Acta **32**, 2247 (1949).

Hermiticity, Orthogonality, Normalization

The problem just formulated is an eigenvalue problem in an one-dimensional, but multiconnected configuration space. Let [see Eqs. (1.20) and (1.21)]

$$f(x)=\sum_B f_B(x_B) \tag{1.35}$$

be a function in this space satisfying the joint and endpoint conditions [(1.32), (1.33), and (1.34)], but otherwise arbitrary. The integral over the configuration space is then defined as

$$\int_l dx f(x)=\sum_B \int_{l_B} dx_B f_B(x_B), \tag{1.36}$$

where l indicates the total length of the free-electron paths and l_B indicates the length of branch number B. In connection with such integrals the following generalization of Green's theorem is important.

Consider the integration over the one dimensional space indicated in Fig. 6, where the coordinates x_B runs from 0 (at the joint) to a_B (at the endpoints). Let $f(x)$ and $g(x)$ be two functions of the type (1.35) which, however, do not vanish at the points a_B, since Fig. 8 is assumed to be part of a larger bond skeleton. Then the following theorem holds:

$$\sum_{B=1}^{3}\int_0^{a_B} dx_B[f_B(d/dx_B)^2 g_B-g_B(d/dx_B)^2 f_B]$$
$$=\sum_{B=1}^{3}[f_B(d/dx_B)g_B-g_B(d/dx_B)f_B]_{x_B=a_B}. \tag{1.37}$$

Indeed, Greens' theorem yields

$$\int_0^{a_B} dx_B[f_B(d/dx_B)^2 g_B-g_B(d/dx_B)^2 f_B]$$
$$=[f_B(d/dx_B)g_B-g_B(d/dx_B)f_B]_0^{a_B} \tag{1.38}$$

for each branch. If one now sums over the three branches, those terms on the right-hand side of (1.38) which are taken at the joint ($x_B=0$) vanish by virtue of the joint conditions [(1.32), (1.33), and (1.34)]:

$$\sum_B [f_B(d/dx_B)g_B-g_B(d/dx_B)f_B]_{x_B=0}$$
$$=f(0)\sum_B (dg_B/dx_B)_0-g(0)\sum_B (df_B/dx_B)_0=0,$$

and hence Eq. (1.37) results.

If one now decomposes the total free-electron path of a bond skeleton into parts of the form of Fig. 6 and applies (1.37) to each part, then all right-hand side contributions of Eq. (1.37) cancel each other or vanish at the free end points, where $f=g=0$. Hence

$$\int_l dx f(x)(d/dx)^2 g(x)=\int_l dx g(x)(d/dx)^2 f(x), \tag{1.39}$$

where the integration extends over the total bond skeleton, i.e., $(d/dx)^2$ is a Hermitian operator with respect to our multiconnected configuration space, and so is the Hamiltonian $\mathcal{H}$ of the Schrödinger Equation (1.31). As a consequence, the eigenvalues of that equation are real and eigenfunctions belonging to different eigenvalues are mutually orthogonal. (Eigenfunctions belonging to the same eigenvalue can, of course, be chosen so as to be mutually orthogonal.) *The validity of these properties depends essentially on both joint conditions* [(1.32) and (1.33)].

The eigenfunctions are required to be normalized:

$$\int_l dx\phi^2(x)=\sum_B \int_{l_B} dx_B \phi_B^2(x_B)=1. \tag{1.40}$$

There can be little doubt that they form a complete set.

2. CASE OF CONSTANT POTENTIAL

General Form of the Solution

If the potential $V(x)$ is constant throughout the entire free-electron path, it can be assumed to vanish identically and the Schrödinger Equation (1.31) is readily solved. The eigenfunction of the energy level E_n has the form

$$\phi_n(x)=\sum_B \phi_{Bn}(x), \tag{2.1}$$

$$\phi_{Bn}(x_B)=a_{Bn}\cos(k_n x_B+\delta_{Bn}), \tag{2.2}$$

with

$$E_n=(h^2/2m)k_n^2. \tag{2.3}$$

In the following we shall omit the subscript n wherever it is not needed. The conditions which determine the parameters k, a_B, δ_B ($B=1, 2, 3, \cdots$) become very simple.

The continuity conditions (1.32),

$$a_1\cos(kx_{1J}+\delta_1)=a_2\cos(kx_{2J}+\delta_2)$$
$$=a_3\cos(kx_{3J}+\delta_3); \tag{2.4}$$

the conservation conditions (1.33),

$$a_1\sin(kx_{1J}+\delta_1)+a_2\sin(kx_{2J}+\delta_2)$$
$$+a_3\sin(k_{3J}+\delta_3)=0, \tag{2.5}$$

or, by virtue of (2.4),

$$\tan(kx_{1J}+\delta_1)+\tan(kx_{2J}+\delta_2)$$
$$+\tan(kx_{3J}+\delta_3)=0. \tag{2.6}$$

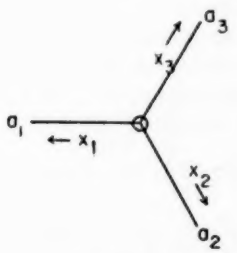

FIG. 6.

In these equations, x_{BJ} denotes the coordinate of the joint on the branch B. The normalization condition becomes (for $k \neq 0$)

$$\tfrac{1}{2}\sum_B a_B^2 l_B = \int_l dx\phi^2(x) = 1, \tag{2.7}$$

where l_B denotes, as usual, the length of the Bth branch. Equation (2.7) is established in the following way. On branch B one obtains

$$\int_0^{l_B} dx_B a_B^2 \cos^2(kx_B+\delta_B)$$
$$= \tfrac{1}{2}a_B^2 \int_0^{l_B} dx_B[1+\cos 2(kx_B+\delta_B)],$$
$$= \tfrac{1}{2}a_B^2\{l_B + k^{-1}[\sin(kx_B+\delta_B)\cos(kx_B+\delta_B)]_0^{l_B}\},$$

i.e.,

$$\int_0^{l_B} dx_B\phi_B^2(x_B) = \tfrac{1}{2}a_B^2 l_B + \tfrac{1}{2}k^{-2}\{[\phi_B(d\phi_B/dn)]_0 + [\phi_B(d\phi_B/dn)]_{l_B}\}, \tag{2.8}$$

where (d/dn) denotes the derivative at a joint (or end point in *that* direction on the branch which points *away* from the joint (or end point). By virtue of the normalization, the left-hand side of (2.8) will become unity after summation over all branches; hence

$$k^2\{2-\sum_B a_B^2 l_B\} = \sum_B \{[\phi_B(d\phi_B/dn)]_0 + [\phi_B(d\phi_B/dn)]_{l_B}\}. \tag{2.9}$$

Here each branch enters on the right-hand side only by its first and last point. These are either joints or free end points. The latter do not contribute anything since $\phi=0$ at a free end point. The terms arising from joints, on the other hand, may be ordered according to joints, so that the right-hand side of (2.9) may be written

$$\sum_J \{\sum_{b=1}^{3} \phi_b(d\phi_b/dn)\}_{\text{on joint } J}, \tag{2.10}$$

where $b=1, 2, 3$ denotes the three branches merging in joint J and $\sum_J$ denotes the sum over all joints of the bond skeleton. By virtue of Eqs. (1.32) and (1.33), each term in the summation over J vanishes separately, and thus Eq. (2.7) is proved. This equation may be considered a generalization of the familiar result obtained in the case of a single branch, namely, that the mean value of $\cos^2 t$ between 0 and π is $\frac{1}{2}$.

It is useful to introduce, at this point, a few conventions. First of all we note that

$$a_B\cos(kx_B+\delta_B) = a_B'\cos(kx_B+\delta_B'),$$

with

$$a_B' = -a_B, \quad \delta_B' = \delta_B \pm \pi.$$

In order to eliminate any ambiguity we shall always choose the phase δ_B such that

$$-\tfrac{1}{2}\pi < \delta_B \leqslant \tfrac{1}{2}\pi, \tag{2.11}$$

thereby simultaneously fixing the relative signs of the amplitudes a_B of the different branches. At the same time this establishes a one to one correspondence between δ_B and $\tan\delta_B$.

There is, of course, still a factor $e^{i\gamma}$ (γ = real) which is arbitrary in the normalized functions (2.1). However, we require the wave function to be real and thus only a factor (-1) remains arbitrary in the total function $\phi(x)$ of Eq. (2.1).

In the second place, it is seen that the sign of k and δ_B may be simultaneously reversed without affecting the wave function (2.2) or the eigenvalue (2.3). We adopt the convention always to choose

$$k \geqslant 0, \tag{2.12}$$

which entails in each case a definite sign for δ_B. The de Broglie wavelength λ_ϕ of the motion described by the molecular orbital (2.1) is then given by

$$\lambda_\phi = 2\pi/k. \tag{2.13}$$

Since a *constant* potential $V(x)$ treats all atoms as equals, it is natural to consider the distance D between neighboring atoms as a constant throughout the conjugated structure. We adopt this assumption and define the dimensionless constant

$$\kappa = kD, \tag{2.14}$$

which will prove to be convenient. Equation (2.3) can then be written

$$(E_n/E_H) = (a/D)^2\kappa_n^2, \tag{2.14'}$$

where $a=\hbar^2/e^2m$ is the Bohr radius and $E_H=e^2/2a$ is the ionization potential of the hydrogen atom. It will soon become clear that for our purposes, κ lies always in the range

$$0 \leqslant \kappa \leqslant \pi, \tag{2.15}$$

so that a one to one correspondence exists between κ, $\sin\kappa$, and $\cos\kappa$.

Eigenvectors of a Free-Electron Eigenfunction

Let

$$\phi(1), \phi(2), \cdots \phi(N), \tag{2.16}$$

denote the values which the eigenfunction $\phi(x)$ [Eq. (2.1)] assumes at the N atoms of the conjugated structure. We define the N dimensional column vector

$$\boldsymbol{\phi} = \begin{bmatrix} \phi(1) \\ \phi(2) \\ \cdots \\ \cdots \\ \phi(N) \end{bmatrix}. \tag{2.17}$$

and call it the free-electron eigenvector corresponding to the eigenfunction $\phi(x)$, Eq. (2.1). This vector is

uniquely determined by the function $\phi(x)$; however, inversely $\phi(x)$ is also uniquely determined by the eigenvector $\boldsymbol{\phi}$ in conjunction with its eigenvalue (2.3). Indeed, each branch B contains at least two atoms, say P and Q, so that the constants a_B and δ_B can, by virtue of (2.2), be expressed in terms of $\phi(P)$, $\phi(Q)$, and $k=(E2m/\hbar^2)^{\frac{1}{2}}$. In order to obtain explicit expressions for a_B and δ_B it is convenient to employ the relation

$$\phi_B(x_B+\xi)=\cos(k\xi)\phi_B(x_B) +k^{-1}\sin(k\xi)(d\phi_B/dx_B)_{x_B}, \quad (2.18)$$

where ξ is arbitrary. Equation (2.18), which will also prove to be useful later, follows from (2.2) by virtue of the addition theorem for the cosine or else by means of the Taylor expansion

$$\phi_B(x_B+\xi)=\sum_{n=0}^{\infty}(\xi^n/n!)\partial^n\phi_B(x_B)=e^{\xi\partial}\phi_B(x_B),$$
$$\phi_B(x_B+\xi)=[\cos i\xi\partial - i\sin i\xi\partial]\phi_B(x_B), \quad (2.19)$$

where $\partial=(d/dx)$. The equivalence of (2.18) and (2.19) follows from the Schrödinger equation

$$(\partial^2+k^2)\phi(x)=0. \quad (2.20)$$

This derivation of Eq. (2.18) can be generalized to the case $V(x)\neq$const.

In practice one chooses the origin of the coordinate on a branch always such as to have it coincide with an atom or with the midpoint of a bond. Consider therefore first the case that $x_B=0$ coincides with an atom P so that

$$\phi_B(P)=a_B\cos\delta_B, \quad (2.21)$$

and let Q denote the atom next to P at $x_B=D$, so that by virtue of (2.18) and (2.14)

$$\phi_B(Q)=\phi_B(P)[\cos\kappa-\sin\kappa\tan\delta_B]. \quad (2.22)$$

From (2.21) and (2.22) one obtains the relations

$$\tan\delta_B=[\cos\kappa-\phi_B(Q)/\phi_B(P)]/\sin\kappa, \quad (2.23)$$

$$a_B^2=\phi_B^2(P)/\cos^2\delta_B=(1+\tan^2\delta_B)\phi_B^2(P), \quad (2.24)$$

for the calculation of $\tan\delta_B$ and a_B^2. The sign of a_B must be the same as the sign of $\phi_B(P)$, since in Eq. (2.21) one has $\cos\delta_B>0$ because of the convention (2.11). On the other hand, if $x_B=0$ coincides with the midpoint of the bond between the atoms P and Q, then application of (2.18) for $x_B=0$, $\xi_P=-\frac{1}{2}D$, and $\xi_Q=\frac{1}{2}D$ yields

$$\phi_B(P)=a_B[\cos\tfrac{1}{2}\kappa\cos\delta_B+\sin\tfrac{1}{2}\kappa\sin\delta_B], \quad (2.25)$$

$$\phi_B(Q)=a_B[\cos\tfrac{1}{2}\kappa\cos\delta_B-\sin\tfrac{1}{2}\kappa\sin\delta_B], \quad (2.26)$$

or

$$\phi_B(P)+\phi_B(Q)=2a_B\cos\tfrac{1}{2}\kappa\cos\delta_B, \quad (2.27)$$

$$\phi_B(P)-\phi_B(Q)=2a_B\sin\tfrac{1}{2}\kappa\sin\delta_B, \quad (2.28)$$

hence one obtains for $\tan\delta_B$ and a_B^2

$$\tan\delta_B=\frac{1+\cos\kappa}{\sin\kappa}\frac{\phi_B(P)-\phi_B(Q)}{\phi_B(P)+\phi_B(Q)}, \quad (2.29)$$

$$a_B^2=[\phi_B^2(P)+\phi_B^2(Q) -2\cos\kappa\phi_B(P)\phi_B(Q)]/\sin^2\kappa. \quad (2.30)$$

Since $\cos\delta_B>0$, the sign of a_B is the same as the sign of $[\phi_B(P)+\phi_B(Q)]$, see Eq. (2.27).

It is useful to define another N dimensional column vector, namely,

$$\hat{\boldsymbol{\varphi}}=\begin{bmatrix}\varphi_1\\ \varphi_2\\ \cdots\\ \varphi_N\end{bmatrix}, \quad (2.31)$$

whose elements φ_1, $\varphi_2\cdots\varphi_N$ have subscripts corresponding again to the N atoms of the system and are defined in the following manner (see 2.16)

$$\left.\begin{aligned}&\varphi_P=D^{\frac{1}{2}}\phi(P),\\ &\quad\text{if } P \text{ is not a joint ("ordinary atoms"),}\\ &\varphi_Q=(\tfrac{3}{2}D)^{\frac{1}{2}}\phi(Q), \quad \text{if } Q \text{ is a joint.}\end{aligned}\right\} \quad (2.32)$$

The vector $\hat{\boldsymbol{\varphi}}$ has, as we shall show, the property

$$\hat{\boldsymbol{\varphi}}^*\hat{\boldsymbol{\varphi}}=\sum_{P=1}^{N}\varphi_P^2=\sum_B\tfrac{1}{2}a_B^2l_B$$
$$=\int_l dx\phi^2(x)=\sum_B\int_{l_B}dx_B\phi_B^2(x_B), \quad (2.33)$$

where $\hat{\boldsymbol{\varphi}}^*$ denotes the Hermitian conjugate matrix of $\hat{\boldsymbol{\varphi}}$, which here is identical with the transposed matrix. Since $\phi(x)$ is assumed to be a normalized eigenfunction (see 1.40), we obtain

$$\hat{\boldsymbol{\varphi}}^*\hat{\boldsymbol{\varphi}}=\sum_{P=1}^{N}\varphi_P^2=1, \quad (2.34)$$

and therefore call $\hat{\boldsymbol{\varphi}}$ the normalized free-electron eigenvector.

In order to establish (2.33) consider first the n atoms $Q_1, Q_2, Q_3, \cdots Q_n$ on one branch B. If x_F is the coordinate of the first atom $Q_1=F_B$ and $x_E=x_F+(n-1)D$ is the coordinate of the last atom $Q_n=E_B$, then let us denote the argument of the cosines in (2.2) by (see 2.14)

$$\left.\begin{aligned}&f=kx_F+\delta_B \quad &&\text{(first atom: } F_B),\\ &e=kx_E+\delta_B=f+(n-1)\kappa \quad &&\text{(last atom: } E_B).\end{aligned}\right\} \quad (2.35)$$

For the sum

$$S_B=\sum_{\nu=1}^{n}\phi_B^2(Q_\nu), \quad (2.36)$$

one obtains

$$S_B=a_B^2\sum_{\nu=0}^{n-1}\cos^2(\kappa\nu+f)$$

$$=\tfrac{1}{4}a_B^2\sum_{\nu=0}^{n-1}\{2+e^{i2(\kappa\nu+f)}+e^{-i2(\kappa\nu+f)}\},$$

$$=\tfrac{1}{4}a_B^2\left\{2n+\frac{e^{i2f}(e^{i2n\kappa}-1)}{(e^{i2\kappa}-1)}+\frac{e^{-i2f}(e^{-i2n\kappa}-1)}{(e^{-i2\kappa}-1)}\right\},$$

and by virtue of (2.35)

$$S_B=\tfrac{1}{4}a_B^2\{2n+(e^{i(f+e)}+e^{-i(f+e)})\times(e^{i(e-f+\kappa)}-e^{-i(e-f+\kappa)})/(e^{i\kappa}-e^{-i\kappa})\},$$

$$S_B=\tfrac{1}{2}a_B^2\{n+\tfrac{1}{2}[\sin(2e+\kappa)-\sin(2f-\kappa)]/\sin\kappa\},$$

$$S_B=\tfrac{1}{2}a_B^2\{(n-1)+\cot\kappa(\sin e\cos e-\sin f\cos f)+\cos^2 e+\cos^2 f\}. \quad (2.37)$$

Giving l_B the same meaning as in Eq. (2.7) and giving (d/dn) the same meaning as in Eq. (2.8) one can, in the case of a branch between two joints, write (2.37) as

$$DS_B=\tfrac{1}{2}a_B^2l_B+\tfrac{1}{2}D[\phi_B^2(F_B)+\phi_B^2(E_B)]+(D/2k)\cot\kappa\{[\phi_B(d\phi_B/dn)]_{F_B}+[\phi_B(d\phi_B/dn)]_{E_B}\}. \quad (2.38)$$

If a branch B contains a free end point and Q_n is the last atom, then the free end point with the boundary condition $\phi=0$ is located one bond length beyond Q_n, i.e., at the site of a fictitious atom Q_{n+1}. Since $\phi(Q_{n+1})=0$, one has in this case

$$S_B(n)=\sum_{\nu=1}^{n}\phi_\nu^2(Q_n)=\sum_{\nu=1}^{n+1}\phi_\nu^2(Q_n)=S_B(n+1);$$

and we obtain Eq. (2.38) again; but all terms coming from the free end vanish.

Let us now sum Eq. (2.38) over all branches of a conjugated structure and write the result in the form

$$D\sum_B\{S_B-\tfrac{1}{2}\phi_B^2(F_B)-\tfrac{1}{2}\phi_B^2(E_B)\}=\sum_B\tfrac{1}{2}a_B^2l_B+(D/2k)\cot\kappa\sum_B\times\{[\phi_B(d\phi_B/dn)]_{F_B}+[\phi_B(d\phi_B/dn)]_{E_B}\}. \quad (2.39)$$

Taking into consideration that all contributions from free end points vanish, one recognizes that, by virtue of (2.36) and (2.32), the left-hand side of (2.39) is identical with

$$\sum_{P=1}^{N}\varphi_P^2=\mathfrak{\phi}^*\mathfrak{\phi},$$

where the sum over P includes all atoms of the conjugated system. Furthermore the second term on the right-hand side of (2.39) is of the same nature as the right-hand side of (2.9) and vanishes for the reasons given there. Thus Eq. (2.39) becomes identical with Eq. (2.33) and the proof is completed.

FIG. 7.

The normalization theorem is not limited to the eigenvector $\mathfrak{\phi}$ (2.31). Choose, on the free-electron path, any set of L *equidistant* points R_1, R_2, $\cdots R_L$, whose neighbor distance, d, is adjusted in such a manner that *all joints and end points are contained in the set*, and define the L dimensional column vector

$$\mathfrak{\phi}'=\begin{pmatrix}\varphi_1'\\ \varphi_2'\\ \cdots\\ \varphi_L'\end{pmatrix}, \quad (2.40)$$

with

$$\left.\begin{aligned}\varphi_R'&=d^{\frac{1}{2}}\phi(R), && \text{if } R \text{ is not a joint,}\\ \varphi_R'&=(\tfrac{3}{2}d)^{\frac{1}{2}}\phi(R), && \text{if } R \text{ is a joint.}\end{aligned}\right\} \quad (2.41)$$

From the preceding derivation it is apparent that the normalization theorem [(2.33) and (2.34)] holds equally for $\mathfrak{\phi}$.

For example, one may choose $d=\frac{1}{2}D$, and then the points R_1, R_2, $\cdots R_L$ are: all atoms *plus* all bond midpoints. One obtains

$$\varphi_R'^2=\tfrac{1}{2}\varphi_R^2, \quad \text{at atoms} \quad R=P,$$

$$\varphi_R'^2=\tfrac{1}{2}D\phi^2(R), \quad \text{at bond midpoints } R=M;$$

hence

$$\sum_R\varphi_R'^2=\tfrac{1}{2}\sum_P\varphi_P^2+\tfrac{1}{2}D\sum_M\phi^2(M). \quad (2.42)$$

By virtue of the normalization theorem the left-hand side of (2.42) is unity and the first term on the right-hand side is $\frac{1}{2}$; hence one finds

$$D\sum_M\phi^2(M)=1, \quad (2.43)$$

where the sum extends over all bond midpoints. Equation (2.43), which may be called the normalization theorem for the bond midpoint serves as a convenient numerical check in any computation involving the $\phi^2(M)$.

A different example is provided by the stilbene molecule (see Fig. 7). There it is possible to choose a four-dimensional normalized column vector $\mathfrak{\phi}'$, corresponding to the four atoms A, B, C, D with the neighbor distance $d=3D$.

Matrix Form of the Eigenvalue Problem

Consider three consecutive points P_{-1}, P_0, P_{+1} on a branch with coordinates (x_B-D), x_B, (x_B+D), respectively. Applying the relation (2.18) for $\phi_B(P_{-1})$ and $\phi_B(P_{+1})$, one obtains

$$\phi_B(P_{-1})-2\cos\kappa\phi_B(P_0)+\phi_B(P_{+1})=0. \quad (2.44)$$

If P_0 is the last atom at a free end, then $\phi(P_{-1})=0$ and hence

$$-2\cos\kappa\phi_B(P_0)+\phi_B(P_{+1})=0 \tag{2.45}$$

in that case. Consider furthermore a joint J and its three neighboring atoms P_1, P_2, P_3. Applying Eq. (2.18) for (P_1), (P_2), (P_3) and adding all three relations, one obtains

$$\sum_{B=1}^{3}\phi_B(P_B)=3\cos\kappa\phi(J)+k^{-1}\sin\kappa\sum_{B=1}^{3}(d\phi_B/dx_B)_J.$$

Because of the conservation condition (1.33) the second term on the right-hand side vanishes and the result is

$$\phi(P_1)+\phi(P_2)+\phi(P_3)-3\cos\kappa\phi(J)=0. \tag{2.46}$$

Since for each atom one has one relation of the type (2.44, 2.45, 2.46) one finds exactly as many equations as there are atoms. Hence one has a system of N homogeneous linear equations for N quantities $\phi(P_1)$, $\phi(P_2)$, $\cdots\phi(P_N)$. This may be written

$$\mathbf{F}\boldsymbol{\phi}=0, \tag{2.47}$$

where $\boldsymbol{\phi}$ is the eigenvector defined in Eq. (2.17) and $\mathbf{F}$ is a matrix whose structure is most easily explained by writing it down in a special case, say styrene. If the atoms are numbered in the way indicated in the free electron path of Fig. 5(c), then the matrix assumes the form

$$\mathbf{F}=\begin{array}{c|cccccccc} & 1 & 2 & 3 & 4 & 5 & 6 & 7 & 8 \\ \hline 1 & -F & 1 & & & & & & \\ 2 & 1 & -F & 1 & & & & & \\ 3 & & 1 & -\tfrac{3}{2}F & 1 & & & & 1 \\ 4 & & & 1 & -F & 1 & & & \\ 5 & & & & 1 & -F & 1 & & \\ 6 & & & & & 1 & -F & 1 & \\ 7 & & & & & & 1 & -F & 1 \\ 8 & & & 1 & & & & 1 & -F \end{array}, \tag{2.48}$$

where all elements which are omitted vanish and

$$F=2\cos\kappa. \tag{2.49}$$

Let $\mathbf{T}$ be the diagonal matrix defined by

$$\left.\begin{aligned} T_{PQ}&=T_P\delta_{PQ},\\ T_P&=\begin{cases}1, & \text{if } P \text{ is not a joint,}\\ (\tfrac{2}{3})^{\frac{1}{2}}, & \text{if } P \text{ is a joint,}\end{cases}\end{aligned}\right\} \tag{2.50}$$

so that the normalized eigenvector [(2.31) and (2.32)] is given by

$$\hat{\boldsymbol{\phi}}=D^{\frac{1}{2}}\mathbf{T}^{-1}\boldsymbol{\phi}. \tag{2.51}$$

Then Eq. (2.47) can be rewritten as the eigenvalue equation

$$\mathfrak{F}\hat{\boldsymbol{\phi}}=F\hat{\boldsymbol{\phi}}, \tag{2.52}$$

where $\mathfrak{F}$ is the matrix

$$\mathfrak{F}=\mathbf{TFT}+F\mathbf{I}, \tag{2.53}$$

($\mathbf{I}$ = unit matrix). In the case of styrene,

$$\mathfrak{F}=\begin{array}{c|cccccccc} & 1 & 2 & 3 & 4 & 5 & 6 & 7 & 8 \\ \hline 1 & 0 & 1 & & & & & & \\ 2 & 1 & 0 & (\tfrac{2}{3})^{\frac{1}{2}} & & & & & \\ 3 & & (\tfrac{2}{3})^{\frac{1}{2}} & 0 & (\tfrac{2}{3})^{\frac{1}{2}} & & & & (\tfrac{2}{3})^{\frac{1}{2}} \\ 4 & & & (\tfrac{2}{3})^{\frac{1}{2}} & 0 & 1 & & & \\ 5 & & & & 1 & 0 & 1 & & \\ 6 & & & & & 1 & 0 & 1 & \\ 7 & & & & & & 1 & 0 & 1 \\ 8 & & & (\tfrac{2}{3})^{\frac{1}{2}} & & & & 1 & 0 \end{array}. \tag{2.53'}$$

Since $\mathfrak{F}$ is a symmetric matrix it follows that the eigenvalues F are real (by virtue of (2.49) they are $\leqslant 2$) and that the eigenvectors belonging to different eigenvalues are mutually orthogonal. From (2.34) we know that the eigenvectors are normalized. Different eigenvectors of one degenerate level can of course be orthogonalized. Hence the eigenvectors $\hat{\boldsymbol{\phi}}_1$, $\hat{\boldsymbol{\phi}}_2$, $\cdots\hat{\boldsymbol{\phi}}_n$ of (2.52), corresponding to the eigenfunctions $\phi_1(x)$, $\phi_2(x)$, $\cdots\phi_n(x)$, satisfy the relations

$$\hat{\boldsymbol{\phi}}_n^*\hat{\boldsymbol{\phi}}_m=\sum_{P=1}^{N}\varphi_{nP}\varphi_{mP}=\delta_{mn}, \tag{2.54}$$

in analogy with

$$\int_l dx\phi_n(x)\phi_m(x)=\delta_{mn}. \tag{2.55}$$

The eigenvalues F_n are found as solutions of the secular equation corresponding to (2.52) or (2.47):

$$|\mathfrak{F}-F\mathbf{I}|=0 \tag{2.56}$$

or

$$|\mathbf{F}|=0. \tag{2.57}$$

From the eigenvalues F_n one finds the energy levels E_n by means of (2.49) and (2.14′).

When the eigenvalues are found, the eigenvectors $\hat{\boldsymbol{\phi}}_n$ can be determined as solutions of the system of Eqs. (2.52), or the eigenvectors $\boldsymbol{\phi}_n$ can be determined as solutions of (2.47). Finally, the free-electron wave functions $\phi_n(x)$ can be calculated from the eigenvectors by the method outlined in Eqs. (2.21)–(2.30).

In this way, energy levels and eigenfunctions of the free-electron problem with constant potential can be determined without explicit use of the boundary condition (1.34) and the joint conditions [(2.4), (2.5), and (2.6)]; and application of the model to larger molecules is made possible. Whereas the determination of the eigen-*values* must always be done by means of the secular equations (2.56) and (2.57) (except in the very simplest cases), it is sometimes more convenient to determine the free-electron wave functions directly than to calculate the eigenvectors. This is the case when the phases of the wave function are immediately given by the symmetry of the system (for example, in naphthalene); once the eigenvalue and all phases δ_B of a wave function are known, it is easy to determine its amplitudes a_B by use of Eqs. (2.4) and (2.7).

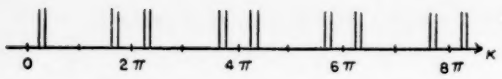

FIG. 8.

It should be noted that the matrix form of the eigenvalue problem can equally well be developed for eigenvectors of the type discussed in Eq. (2.40). A nice application of this fact to the stilbene molecule of Fig. 7 will be discussed later. Another consequence is that the orthonormality relations (2.54) hold also for the eigenvectors $\mathfrak{k}_n'$ (2.40). Incidentally it may be mentioned that the orthogonality of eigenvectors belonging to different eigenvalues can also be derived directly by the method employed in the proof of the normalization theorem (2.34).

Discussion, Applications

The N values which are obtained for $F=2\cos\kappa$ give rise to infinitely many values of κ. There are N values $\kappa_n (n=1, 2\cdots N)$ in the range $0\leqslant\kappa_n\leqslant\pi$ and each of these N values κ_n gives rise to an infinite set of κ values, namely,

$$\kappa_{n\nu}{}^{\pm}=\pm\kappa_n+\nu 2\pi, \quad \nu=1, 2, 3\cdots. \tag{2.58}$$

A possible situation in the case $N=2$ is shown in Fig. 8. We note that by definition $\kappa\geqslant 0$ [see (2.12)]. To each value $\kappa_{n\nu}{}^{s}(s=\pm)$ belongs, by means of (2.14′), one eigenvalue $E_{n\nu}{}^{s}$ and, by means of Eqs. [(2.21)–(2.30)], one wave function $\phi_{n\nu}{}^{s}(x)$.

Thus each eigenvector $\mathfrak{k}_n$ gives rise to an infinite set of eigenfunctions $\phi_{n\nu}{}^{s}(x)$. For the N lowest energy levels, i.e., those in the range $(0\leqslant\kappa\leqslant\pi)$, the de Broglie wavelength λ_ϕ (2.13) is

$$\lambda_\phi\geqslant 2D; \tag{2.59}$$

hence there can be no more than one node from each wave function between two neighboring atoms. For the wave functions corresponding to $\kappa>\pi$, on the other hand, there always exists pairs of neighboring atoms between which are at least two nodes.

The eigenvalue $\kappa_n=0$ (corresponding to $F_n=2$) implies $\lambda_\phi=\infty$, i.e., a constant wave function. Hence it does *not* occur if the electron path has a free end point, since a constant wave function would have to vanish identically. This eigenvalue *always* occurs, however, if the electron path has no free end points.

Since the molecule contains N π electrons, the one-half N lowest levels are doubly occupied in the ground state. If N is odd, then the highest level is only singly occupied in the ground state. Later, it will be shown that for alternant hydrocarbons all ground-state levels have

$$\kappa\leqslant\tfrac{1}{2}\pi; \tag{2.60}$$

but also for those nonalternant hydrocarbons which were investigated by one of us,[5] the condition (2.60) was always found to be valid for the ground-state levels.

The excitations of the highest electrons to the next higher levels correspond to the π-electron spectra of the conjugated molecule. The transition energy $\Delta E=E_m-E_n$ between two levels E_m, E_n is given by

$$\Delta E=E_D\Delta(\kappa^2), \tag{2.61}$$

with

$$E_D=E_{\mathrm{H}}(a/D)^2; \tag{2.62}$$

the corresponding wave number, $(1/\lambda)=hc\Delta E$, by

$$(1/\lambda)=(1/\lambda_D)\Delta(\kappa^2), \tag{2.63}$$

or

$$(1/\lambda)=\tfrac{1}{2}\lambda_c\Delta(1/\lambda_\phi{}^2), \tag{2.64}$$

with

$$(1/\lambda_D)=\lambda_c/8\pi^2D^2. \tag{2.65}$$

Here the symbol Δx always has the meaning x_m-x_n; λ_ϕ is the de Broglie wavelength (2.13) of a free-electron orbital; $a=0.529151$A is the Bohr radius; $E_{\mathrm{H}}=13.6035$ ev is the atomic ionization potential of hydrogen; $\lambda_c=0.0242607$A is the Compton wavelength. For $D=D_c=1.40000$A (the subscript c stands for "conjugated," the value 1.40000 being a mean value for the bond distance in conjugated systems) one obtains the numerical values[9a]

$$E_c=1.9432 \text{ ev}=44.827 \text{ kcal/mole}, \tag{2.66}$$

$$(1/\lambda_c)=15\,677 \text{ cm}^{-1}. \tag{2.66′}$$

For other values of D one finds E_D and λ_D by means of the relation

$$(E_D/E_c)=(\lambda_c/\lambda_D)=(D_c/D)^2. \tag{2.67}$$

Because of Eq. (2.60) it follows then that the lowest π-electronic excitation energies are of the order of magnitude given in Eqs. (2.66) and (2.66′), or rather a little larger. This result is in agreement with experiment. In contrast, the excitation of an electron from a ground-state level to a level with $\kappa\geqslant\pi$ needs an energy $\Delta E\geqslant(\pi^2-\frac{1}{4}\pi^2)E_D=14.3$ ev. Since the ionization energy for benzene is 9.24 ev, such a level cannot have a physical meaning, i.e., the approximations of the free-electron model, which do not allow for ionization, become insufficient for excitations of this magnitude.

The lowest N levels of the free-electron model correspond to the N levels found in LCAO theory. The similarity between the form of the matrix $\mathfrak{F}$ (2.53) and the matrix which determines the eigenstates in LCAO theory is striking; indeed, the only difference is that each joint introduces a factor $(\frac{2}{3})^{\frac{1}{2}}$ into the matrix $\mathfrak{F}$, whereas it does not do so in the LCAO matrix. The set of linear Eqs. [(2.44), (2.45), (2.46)] is of the same nature as the corresponding system in LCAO theory, and the simplifications on the basis of the molecular symmetry can therefore be achieved by exactly the same methods which are used in LCAO theory.[10] It

[9a] 1 Thermochemical calorie $=4.1840\times10^7$ ergs. See E. A. Guggenheim, *Thermodynamics* (North-Holland Publishing Company, Amsterdam, 1950), p. 85.

[10] See, e.g., reference 8, page 196.

should be noted that each free-electron eigenfunction belongs to a definite representation of the *three-dimensional* symmetry group of its molecule. In order to find this representation one has to take into account that the total three-dimensional free-electron wave function (see Eq. (1.17) *ff*) is antisymmetric with respect to the molecular plane. It follows that a one to one correspondence exists between the free-electron states and the LCAO states according to their group theoretical classification. However, the *order* of the energies is not always the same; an example is given by the fourth and fifth levels in perylene (see references 5 and 8): The LCAO model furnishes $E_{A_u} > E_{B_{1u}}$, the free-electron theory, $E_{B_{1u}} > E_{A_u}$. Also the free-electron method may yield accidental degeneracies not shown by the LCAO model and vice versa. (For example, the sixth to ninth levels inclusive in perylene are degenerate in the LCAO model, but not in the free-electron model.)

Let M_- and M_+ be the two bond midpoints on both sides of a nonjoint atom P, and let P and Q be the two atoms on both sides of a bond midpoint M. Then it is sensible to define an *atom population* a' on P and a *bond population* b' on the bond PQ by the equations

$$a'(P)=\sum_n g_n \int_{M-}^{M+} dx\phi_n^2(x), \quad (2.68)$$

$$b'(M)=b'(PQ)=\sum_n g_n \int_P^Q dx\phi_n^2(x), \quad (2.68')$$

where $g_n=0$, 1, 2 denotes the number of electrons occupying the orbital $\phi_n(x)$. The sum extends only over the filled orbitals since $g_n=0$ for the other cases. For an atom P_J at a joint the atom population has to be defined by

$$a'(P_J)=\sum_n g_n \sum_{B=1}^{3} \int_{P_J}^{M_B} dx_B\phi_{Bn}^2(x_B), \quad (2.68'')$$

where M_1, M_2, M_3 are the three bond midpoints between P_J and its three neighbor atoms.

Instead of using the quantities a' and b', it is simpler to work with the quantities a and b, defined by [see Eq. (2.32)]

$$a(P)=\sum_n g_n\varphi_{nP}^2=T_P^{-2}D\omega(P), \quad (2.69)$$

$$b(PQ)=b(M)=D\omega(M), \quad (2.69')$$

where

$$\omega(x)=\sum_n g_n\phi_n^2(x) \quad (2.70)$$

denotes the total, π-electronic, linear density at the point x, and T_P is defined in Eq. (2.50). One would have $a=a'$ and $b=b'$ if $\phi(P)$, $\phi(M)$, $\phi(P_J)$ would represent the mean value of the function $\phi^2(x)$ in the integrals (2.68), (2.68'), (2.68''), respectively. Although this is, in general, not true for a single atom or bond, it can be considered to hold *on the average*, in the sense of the following argument. According to Eqs. (2.33) and (2.43) the total π-electronic population of the molecule can be expressed as

$$N=\sum_n g_n \int_l dx\phi_n^2(x)=\sum_P a(P)=\sum_M b(M), \quad (2.71)$$

whence

$$\sum_P a'(P)=\sum_P a(P)=N, \quad (2.71')$$

$$\sum_M b'(M)=\sum_M b(M)=N, \quad (2.71'')$$

where the summation over P contains all atoms and the summation over M contains all bond midpoints (N is the number of electrons). Hence, *on the average*, $a(P)$ may be considered as the contribution of atom P to the total population, and $b(PQ)$ may be considered as the contribution of the bond PQ to the total population. In the following, we shall apply the term atom population and bond population to a and b, respectively.

The quantities a, b have a similar physical meaning as the analogous quantities q(=the number of electrons on an atom) and p(=bond order between two atoms) of the LCAO model.[2] It follows then that the reactivities of the different atoms and the total π-electronic dipole moment of the molecule are connected with the a's in the same way as they are connected with the q's and the application can directly be taken over from LCAO theory. It should be noted, however, that at the joints there is a difference between the electron density and the electron population (this difference is unknown in LCAO theory) and one may raise the question whether the former or the latter decides the chemical reactivity. The quantities b, on the other hand, are related to the bond lengths and the so-called free valences of the atoms in the same way as the LCAO quantities, p.

On this basis the free-electron wave functions may be correlated with experimental facts. The numerical comparison shows that the free-electron results are in no way inferior to the results obtained from the LCAO model.

Alternant Conjugated Systems

We conclude the present paper by showing that the free-electron theory describes the particular character of the alternant conjugated systems with an even number of atoms in the very same way as the LCAO model does.[11] This important group of molecules, which includes all conjugated structures composed of even membered rings, is defined by the following properties: The conjugated structure contains an even number of atoms, and *it must be possible to divide all atoms into*

[11] Alternant systems with an odd number of atoms present no difficulties and will be dealt with in a subsequent paper.

two classes, e.g., "starred ones" and "unstarred ones," in such a fashion that no two neighbors belong to the same class.

The theoretical characteristics of these molecules have their origin in the "pairing theorem," which we shall now establish. Let $\mathbf{J}$ be the matrix

$$\mathbf{J}=\begin{pmatrix} 1 & & & & & \\ & -1 & & 0 & & \\ & & 1 & & & \\ & & & -1 & & \\ & 0 & & & \cdot & \\ & & & & & \cdot \end{pmatrix}, \tag{2.72}$$

i.e., $\mathbf{J}$ is a diagonal matrix in which all elements corresponding to the *starred* atoms are 1 and all elements corresponding to the *unstarred* atoms are -1. Then

$$\mathbf{J}^2=\mathbf{I}, \tag{2.73}$$

where $\mathbf{I}$ denotes the unit matrix, and obviously,

$$\mathbf{J}\mathfrak{F}\mathbf{J}=-\mathfrak{F}, \tag{2.74}$$

where $\mathfrak{F}$ is the matrix (2.53). Hence it follows from (2.52) that

$$\mathfrak{F}\mathfrak{k}'=F'\mathfrak{k}', \tag{2.75}$$

with

$$\mathfrak{k}'=\mathbf{J}\mathfrak{k}, \tag{2.76}$$

$$F'=-F. \tag{2.77}$$

That is, if $\mathfrak{k}$ is an eigenvector with the eigenvalue F, then $\mathfrak{k}'$ is an eigenvector with the eigenvalue $F'=-F$. Hence, if κ_n is an eigenvalue of κ [see Eq. (2.49)], then

$$\kappa_n'=\pi-\kappa_n \tag{2.78}$$

is also an eigenvalue. Combined with Eq. (2.58) this leads to the result that with $\kappa_n(\leqslant\frac{1}{2}\pi)$ one has simultaneously the eigenvalues

$$\left.\begin{aligned}\kappa_{n\nu}&=\kappa_n+\nu\pi\\ \kappa_{n\nu}'&=(\pi-\kappa_n)+\nu\pi\end{aligned}\right\}\nu=0,\ 1,\ 2,\ 3\cdots. \tag{2.79}$$

Figure 9 shows all the eigenvalues generated by one κ_n, which must appear together in an alternant system.

Let κ_n be the smaller one and let κ_n' be the larger one of the two paired eigenvalues $\leqslant\pi$, i.e.,

$$0\leqslant\kappa_n\leqslant\tfrac{1}{2}\pi, \tag{2.80}$$

$$\tfrac{1}{2}\pi\leqslant\kappa_n'\leqslant\pi. \tag{2.81}$$

Then it follows for the two paired eigenfunctions $\phi_n(x)$ and $\phi_n'(x)$ that

$$\lambda_{\phi_n}\geqslant 4D, \tag{2.82}$$

$$4D\geqslant\lambda_{\phi_n'}\geqslant 2D, \tag{2.83}$$

i.e., for $\phi_n(x)$ two nodes are at least two bond lengths apart, and for $\phi_n'(x)$ the distance of two nodes lies between one and two bond lengths. Moreover, one sees from Eq. (2.76) that

$$\left.\begin{aligned}\phi_n(P)&=\phi_n'(P), &&\text{at each starred atom,}\\ \phi_n(P)&=-\phi_n'(P), &&\text{at each unstarred atom,}\end{aligned}\right\} \tag{2.84}$$

or vice versa, depending on the choice of the arbitrary signs in the wave functions.

The explicit form of the wave function $\phi_n'(x)$ becomes simple on a branch where the point $x_B=0$ coincides with an atom: If $\phi_n(x)$ is given by Eq. (2.2) then $\phi_n'(x)$ is given by

$$\phi_{Bn}'(x)=a_{Bn}\cos[(D^{-1}\pi-k_n)x_B-\delta_{Bn}], \tag{2.85}$$

as may be verified by taking account of Eqs. (2.78) and (2.84) in Eqs. (2.23) and (2.24) which determine k_n, δ_{Bn}, k_n', δ_{Bn}'. From (2.85) follows indeed that

$$\phi_{Bn}'(\nu D)=(-1)^\nu\phi_{Bn}(\nu D),\quad \nu=1,\ 2,\ 3\cdots, \tag{2.86}$$

which is identical with (2.84), if one chooses the point $x_B=0$ to be a starred atom. On the other hand, on a branch where $x_B=0$ coincides with a bond midpoint one finds, by virtue of (2.29) and (2.30) and (2.78) and (2.84), that

$$\phi_{Bn}'(x)=a_{Bn}\cos[(D^{-1}\pi-k_n)x_B+(\tfrac{1}{2}\pi-\delta_{Bn})], \tag{2.87}$$

whence

$$\phi_{Bn}'[(\nu-\tfrac{1}{2})D]=(-1)^\nu\phi_{Bn}[(\nu-\tfrac{1}{2})D],\qquad \nu=1,\ 2,\ 3\cdots, \tag{2.88}$$

which agrees with (2.84) if $x_B=-\frac{1}{2}D$ is chosen as a starred atom.

An immediate consequence of the pairing theorem is the *population theorem*, which states that *the total π-electronic population at each atom is unity in the ground state of an alternant conjugated system.* This theorem, which excludes, for example, the existance of a π-electronic dipole moment for alternant systems, is established in the following way: By virtue of the pairing theorem, in particular Eq. (2.84) the π-electronic atom population (2.70) in the ground state can be written

$$a(P)=\sum_{n=1}^{\frac{1}{2}N}2\varphi_{nP}^2=\sum_{n=1}^{N}\varphi_{nP}^2. \tag{2.89}$$

Now Eq. (2.54) states that the quantities φ_{nP}, taken for $n=1,\ 2,\ \cdots N$, form an orthogonal matrix, and hence

$$a(P)=1. \tag{2.90}$$

This population theorem is the counterpart of the identical theorem in the LCAO model.

Since the secular equation simultaneously has the eigenvalues F and $-F$, it is possible to write it as two systems of $\frac{1}{2}N$ equations containing only F^2. Such a

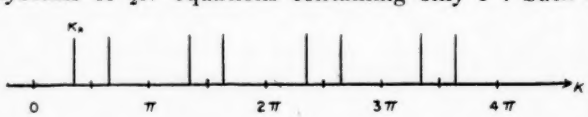

FIG. 9.

system can be obtained in the following manner: The matrix $\mathfrak{F}^2$ commutes with $\mathbf{J}$ (2.72):

$$\mathfrak{F}^2\mathbf{J}=\mathbf{J}^2\mathfrak{F}\mathbf{J}^2\mathfrak{F}\mathbf{J}=\mathbf{J}(-\mathfrak{F})(-\mathfrak{F})=\mathbf{J}\mathfrak{F}^2, \quad (2.91)$$

and hence has no elements (different from zero) connecting starred and unstarred atoms. Hence the vector transformation described by $\mathfrak{F}$ leaves both the "starred subspace" and the "unstarred subspace" invariant, and hence the eigenvectors of $\mathfrak{F}$ can be assumed to have only starred components or only unstarred components. The eigenvalue of $\mathfrak{F}^2$ is of course F^2. Indeed: from (2.52) and (2.75), (2.76), and (2.77) it follows that

$$\mathfrak{F}^2\mathfrak{\hat{p}}=F^2\mathfrak{\hat{p}}, \quad (2.92)$$

$$\mathfrak{F}^2\mathbf{J}\mathfrak{\hat{p}}=F^2\mathbf{J}\mathfrak{\hat{p}}, \quad (2.92')$$

whence

$$\mathfrak{F}^2\mathfrak{\hat{p}}_+=F^2\mathfrak{\hat{p}}_+, \quad (2.93)$$

$$\mathfrak{F}^2\mathfrak{\hat{p}}_-=F^2\mathfrak{\hat{p}}_-, \quad (2.93')$$

with

$$\mathfrak{\hat{p}}_\pm=\tfrac{1}{2}(\mathbf{I}\pm\mathbf{J})\mathfrak{\hat{p}}. \quad (2.94)$$

Since

$$\tfrac{1}{2}(\mathbf{I}+\mathbf{J})=\begin{bmatrix}1&&&&\\&0&&0&\\&&1&&\\&&&0&\\&0&&&\\&&&&.\end{bmatrix},\quad \tfrac{1}{2}(\mathbf{I}-\mathbf{J})=\begin{bmatrix}0&&&&\\&1&&0&\\&&0&&\\&&&1&\\&0&&&\\&&&&.\end{bmatrix}, \quad (2.95)$$

one may write Eqs. (2.93) and (2.93′) as

$$(\mathfrak{F}^2)_\star\mathfrak{\hat{p}}_\star=F^2\mathfrak{\hat{p}}_\star, \quad (2.96)$$

$$(\mathfrak{F}^2)_0\mathfrak{\hat{p}}_0=F^2\mathfrak{\hat{p}}_0, \quad (2.96')$$

where $\mathfrak{\hat{p}}_\star$ is the $\frac{1}{2}N$ dimensional vector obtained from $\mathfrak{\hat{p}}_+$ by omitting all unstarred components, and $\mathfrak{\hat{p}}_0$ is the $\frac{1}{2}N$ dimensional vector obtained from $\mathfrak{\hat{p}}_-$ by omitting all starred components. Similarly, $(\mathfrak{F}^2)_\star$ and $(\mathfrak{F}^2)_0$ are obtained from $\mathfrak{F}^2$ by omitting all unstarred or all starred elements, respectively. The eigenvalues F^2 are therefore solutions of the two equations

$$|(\mathfrak{F}^2)_\star-F^2\mathbf{I}|=0, \quad (2.97)$$

$$|(\mathfrak{F}^2)_0-F^2\mathbf{I}|=0. \quad (2.97')$$

The eigenvectors $\mathfrak{\hat{p}}_\star$, $\mathfrak{\hat{p}}_0$ of (2.96) and (2.96′), corresponding to the same eigenvalue F^2, furnish the two eigenvectors $\mathfrak{\hat{p}}_+$ and $\mathfrak{\hat{p}}_-$ of $\mathfrak{F}^2$. From these, one obtains the two eigenvectors

$$\mathfrak{\hat{p}}=\mathfrak{\hat{p}}_++\mathfrak{\hat{p}}_-, \quad (2.98)$$

$$\mathfrak{\hat{p}}'=\mathbf{J}\mathfrak{\hat{p}}=\mathfrak{\hat{p}}_+-\mathfrak{\hat{p}}_-, \quad (2.98')$$

of $\mathfrak{F}$, corresponding to the two eigenvalues $+F$ and $-F$. Which eigenvalue belongs to which eigenvector is decided by checking the relation (2.44), i.e., *one* of the equations of the set (2.52), between three neighboring points.

As an illustration let us finally consider the problem of finding the eigenvalues of the stilbene molecule, whose free-electron path has already been shown in Fig. 7. In the first place, we note that one may set up a secular equation for the four points A, B, C, D, which have the neighbor distance $3D$. Since they form an alternant system the four eigenvalues, F_n', of *this* problem form two pairs, and since there are no free end points, one pair must be $F_1'=2$, $F_4'=-2$, corresponding to $\kappa_1'=0$, $\kappa_4'=\pi$, where $\kappa'=3Dk$. Hence there actually remains one eigenvalue to be determined. The matrix (2.53) becomes, for these four points,

$$\mathfrak{F}=\begin{array}{c|cccc} & A & B & C & D\\ \hline A & 0 & 2(\frac{2}{3})^{\frac{1}{2}} & 0 & 0\\ B & 2(\frac{2}{3})^{\frac{1}{2}} & 0 & \frac{2}{3} & 0\\ C & 0 & \frac{2}{3} & 0 & 2(\frac{2}{3})^{\frac{1}{2}}\\ D & 0 & 0 & 2(\frac{2}{3})^{\frac{1}{2}} & 0 \end{array}, \quad (2.99)$$

whence

$$\mathfrak{F}'^2=\begin{bmatrix}(8/3)&0&(4/3)(\frac{2}{3})^{\frac{1}{2}}&0\\0&(28/9)&0&(4/3)(\frac{2}{3})^{\frac{1}{2}}\\(4/3)(\frac{2}{3})^{\frac{1}{2}}&0&(28/9)&0\\0&(4/3)(\frac{2}{3})^{\frac{1}{2}}&0&(8/3)\end{bmatrix}, \quad (2.100)$$

and

$$(\mathfrak{F}'^2)_0=(\mathfrak{F}'^2)_\star=\begin{pmatrix}(28/9)&(4/3)(\frac{2}{3})^{\frac{1}{2}}\\(4/3)(\frac{2}{3})^{\frac{1}{2}}&(8/3)\end{pmatrix}. \quad (2.101)$$

The secular equation (2.97) becomes

$$(3F')^4-52(3F')^2+576=0, \quad (2.102)$$

and since $(3F')^2=36$ (corresponding to $F'=\pm2$) must be one root, it follows that $(3F')^2=52-36=16$ is the second root. Thus, we find for $\frac{1}{2}F'=\cos\kappa'$, and for κ', the four eigenvalues

$\cos\kappa'$	1	$\frac{2}{3}$	$-\frac{2}{3}$	-1
κ'	0	0.268π	0.732π	π

in the range $(0\leqslant\kappa'\leqslant\pi)$. These eigenvalues plus those

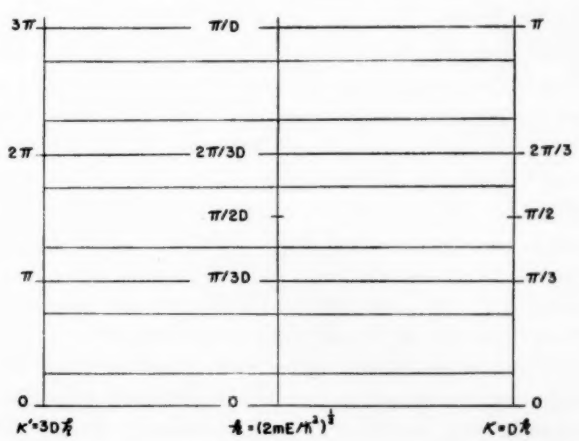

FIG. 10.

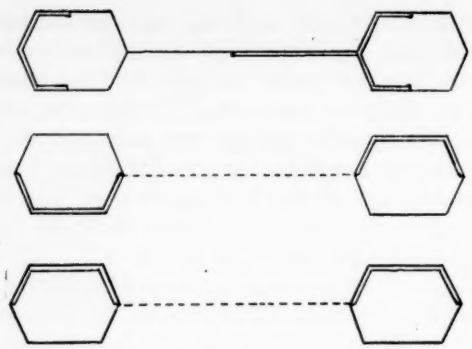

FIG. 11.

generated in the range between π and 3π are drawn in Fig. 10 on horizontal lines. The first vertical scale shows the values of κ' and the second (middle) vertical scale shows the corresponding values of $k=\kappa'/3D$.

Since the eigenvalues of k depend only on the free electron path and not on the manner in which one assumes equidistant points on the path, no other eigenvalues, k, can be found by solving the 14 dimensional secular equation corresponding to the 14 atoms of the molecule. However, in this problem one works with the quantities $\kappa=Dk=\frac{1}{3}\kappa'$. The 14 states with $0\leqslant\kappa\leqslant\pi$ correspond to the 14 LCAO states of the molecules. Now the third (right) scale in Fig. 10 shows the values of κ for the eigenvalues which were found; one recognizes that there exists only 10 levels in this range; hence some of these must be degenerate. Indeed, the levels $k_n=\frac{1}{3}\pi$ and $\kappa_n=\frac{2}{3}\pi$ are both triply degenerate, thus providing the extra four levels. This degeneracy is easily recognized: The eigenfunctions for $\kappa_n=\frac{1}{3}\pi$ have $\lambda_\phi=6D$ and one sees that one can construct three mutually orthogonal wave functions with this wavelength; they are shown in Fig. 11 where a

full line is drawn, wherever the wave function is positive,
hollow line is drawn, wherever the wave function is negative
dotted line is drawn wherever the wave function is identically zero.

Since there are three independent wave functions for $\kappa=\pi/3$, the same must be true for $\kappa=2\pi/3$ by virtue of the pairing theorem. In order to find all wave functions one solves the system of two linear equations obtained from (2.96) by substituting $(\mathfrak{F}'^2)_\star$ of (2.101) for $(\mathfrak{F}^2)_\star$; by the method described after (2.97), one then obtains the eigenvectors of $\mathfrak{F}'$ (2.99) and hence by the usual methods [see Eqs. (2.21)–(2.30)] the wave functions for the 14 lowest states. Finally one can determine the symmetries of the different wave functions.

Of course it would have been possible from the beginning to separate out the eigenvalue equations corresponding to the different symmetry types; this procedure would be advantageous in dealing with a molecule of sufficiently high symmetry. Since this method operates in precisely the same way as in the LCAO model,[10] we do not have to go into details at this point, and refer the reader to the following paper[5] for an illustrative example.

APPENDIX: JUSTIFICATION OF THE BOUNDARY CONDITION FOR FREE END POINTS

The assumption that the wave function $\phi(x)$ goes to zero one bond length D beyond the last atom at a free end [see comments after Eq. (1.34)] has been essential in deriving the normalization of the eigenvectors [see after Eq. (2.38)] and in deriving the matrix formulation of the eigenvalue problem [see Eq. (2.45)]. Hence, also the orthogonality of the eigenvectors, and thereby the pairing theorem, depend on the present choice of the boundary conditions [see comments after (2.53′)].

It will now be shown that this boundary condition is the *only* one which guarantees the normalization of the eigenvectors as well as the existence of the pairing theorem for alternant systems.

Consider the proof starting after Eq. (2.34). Let us assume that the branch B considered there has a free end point; let the "first atom F_B" [definition: between Eqs. (2.34) and (2.35)] be the one nearest to the free end point; and let the end point of the electron path be located at a distance ξD beyond the atom F_B. Then the branch length becomes

$$l_B=D(n-1+\xi). \tag{A.1}$$

We choose the path end point to be the origin $x_B=0$ of the coordinate x_B, which increases in the direction away from the end point. Hence, the wave function vanishes for $x_B=0$, and has therefore the form

$$\phi_B(x_B)=a_B\cos(kx_B-\tfrac{1}{2}\pi), \tag{A.2}$$

so that the argument of the cosine becomes, for the first atom F_B,

$$f=\xi\kappa-\tfrac{1}{2}\pi, \tag{A.3}$$

[see Eq. (2.35)].

The course of the proof subsequent to Eq. (2.37) shows that under the present circumstances [note

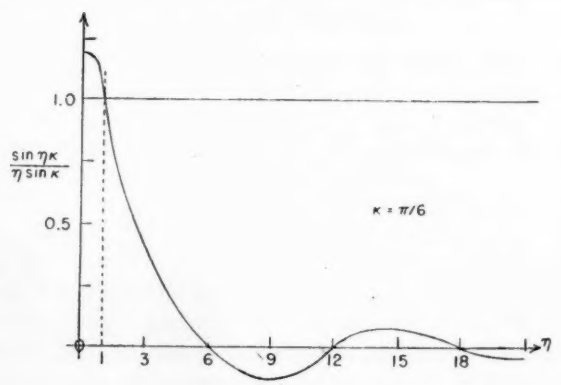

FIG. 12.

Eq. (A.1)] the Eq. (2.33) results from Eq. (2.37) only if the relation

$$-\cot\kappa \sin f \cos f+\cos^2 f=\xi \qquad \text{(A.4)}$$

is fulfilled.[12] Hence,

$$-\frac{\sin(2f-\kappa)}{\sin\kappa}=(2\xi-1), \qquad \text{(A.4')}$$

and by virtue of (A.3),

$$\frac{\sin\eta\kappa}{\eta \sin\kappa}=g(\eta)=1, \qquad \text{(A.5)}$$

with

$$\eta=2\xi-1. \qquad \text{(A.6)}$$

Now there are always eigenfunctions with κ in the range $0<\kappa<\frac{1}{2}\pi$ (the eigenvalue $\kappa=0$ is excluded if there exists a free end point). For any such κ, the function $g(\eta)$ has the behavior schematically shown in Fig. 12 for the case $\kappa=\frac{1}{6}\pi$. At $\eta=0$, the function starts out with the first maximum $g(\eta)=\kappa/\sin\kappa>1$; it assumes the value $g(\eta)=1$ for $\eta=1$ and has its first zero at $\eta=\pi/\kappa>2$. Hence, all subsequent maxima are successively decreasing in magnitude. Now the second maximum obviously lies very close to the point $\eta=5\pi/2\kappa$, where

$$g(\eta)=2\kappa/5\pi \sin\kappa<1/5,$$

so that it is clear that $g(\eta)$ never again rises to the value 1. Since $g(\eta)$, furthermore, is symmetric in η we obtain the result that Eq. (A.5) is only fulfilled for $\eta=\pm 1$, which, by virtue of (A.6), is equivalent to $\xi=0$ and $\xi=1$. Since the path end point should certainly not coincide with the last atom, we are left with $\xi=1$.

However, Eq. (A.4') is also satisfied by the value $\xi=\frac{1}{2}(\eta=0)$. It is easily recognized that *this* boundary condition would lead to the relation

$$\phi_B(P_{+1})-(1+2\cos\kappa)\phi_B(P_0)=0 \qquad \text{(A.7)}$$

instead of to Eq. (2.45). Consequently, the matrix $\mathfrak{F}$ entering in the eigenvalue equation (2.51) would contain the *diagonal* element (-1) for each end atom; and hence, Eq. (2.74), the basis for the pairing theorem, would not hold.

Thus, the choice of the path end point adopted in this paper is the only one which yields the matrix formulation and at the same time establishes the parallelism between the LCAO model and the free-electron model.

[12] If there are several branches with free end points, then Eq. (A.4) must still hold for each branch separately in order that our results remain generally valid.

ACKNOWLEDGMENTS

The second part of the present investigation was suggested by Professor J. R. Platt, and owes a great deal of stimulation to him. The existence of a detailed analogy between the LCAO model and the free-electron model in general, and of the normalization theorem (2.34), and the population theorem (2.90) in particular, were his conjectures; also the pairing theorem in the form (2.85), and the Eqs. (2.44), (2.45), and (2.46) are due to him. The authors wish to express their gratitude for the many fruitful discussions with him. One of us (K. R.) wishes to acknowledge an interesting conversation with Professor H. Kuhn.

Free-Electron Network Model for Conjugated Systems. II. Numerical Calculations*

CHARLES W. SCHERR
Laboratory of Molecular Structure and Spectra, Department of Physics, The University of Chicago, Chicago 37, Illinois
(Received December 30, 1952)

Numerical calculations are carried out on a large number of aromatic and polyene type conjugated molecules by the methods of the first paper of this series. These calculations include all energy levels, the wavelengths of the first four electronic transitions, the complete π-electron wave functions, the bond densities and bond orders, free valence and reactivities, and dipole moments. A method of estimation of bond lengths with a root-mean-square error of 0.016A is presented. Wherever possible, comparisons are made with experiment and with the results of the LCAO molecular orbital theory in the approximation developed by Coulson and Longuet-Higgins. The results in general are at least as good as those of the LCAO calculations.

THE first paper of the present series[1] has presented a detailed consistent mathematical framework for the application of the free-electron model to conjugated π-electron systems. The present paper presents the results of a series of calculations designed to demonstrate the applicability and test the potentialities of the free-electron model.

Much of the previous theoretical calculations on conjugated hydrocarbons has been done by the LCAO (linear combination of atomic orbitals) molecular orbital theory in the approximation developed by Coulson and Longuet-Higgins.[2] It is emphasized that this method will be referred to throughout this paper as the LCAO method, and that this abbreviation will refer *only* to the Coulson-Longuet-Higgins approximation just mentioned. It has been pointed out in I that the LCAO three-dimensional, one-electron model actually closely approximates a one-dimensional model, such as the present theory, so it is not surprising that there exists a very close equivalence between the LCAO results and the results of the present paper. For this reason a detailed comparison of the two theories is presented at the end of this report.

The complete π-electron wave functions for each of the molecules considered here are presented. These wave functions will be useful to calculate the π-electron density at any point, to make perturbation treatments, and to calculate oscillator strengths of the electronic transitions.

In referring to particular atoms, the standard organic numbering, as indicated on Fig. 1, is followed; bonds are referred to by their terminal atoms. For example, the bond connecting the α and β positions in naphthalene is referred to as bond 1–2.

THE SECULAR EQUATION AND THE ENERGY LEVELS

No particular difficulty was encountered in solving the secular equations for the eigen*values*. The largest determinant after factorization according to symmetry species was 9×9 (ovalene). The first n energy levels (n is the number of π-electrons) and their symmetries are presented in Table I. The remaining levels and their symmetries are trivially found from these tabulated values. By the pairing theorem for energy levels of alternant molecules (see paper I), for every solution κ_i, where

$$\left.\begin{aligned} &\kappa_i = 2\pi D/\lambda_i, \\ &D = \text{the internuclear distance}, \\ \text{and}\quad &\\ &\lambda_i = \text{the wavelength of } \phi_i, \text{ the } i\text{th} \\ &\pi\text{-electron wave function}, \end{aligned}\right\} \tag{1}$$

there exist solutions $\kappa_{mn\pm i} = m\pi \pm \kappa_i$ where m may take any integral value, positive or negative, or zero, and with the restriction that $\kappa_{mn\pm i} > 0$. The ith level between $m\pi$ and $(m+1)\pi$ (altogether the $(mn+i)$th level) has the same symmetry as the ith level between zero and π; the energy relation being, as indicated above, $\kappa_{mn+i} = m\pi + \kappa_i$. The energy levels of nonalternant molecules are not mirrored at half-integral multiples of π; that is, for every κ_i there only exist solutions $\kappa_{mn+i} = m\pi + \kappa_i$, $m = 0, \pm 1, \pm 2 \cdots$.

Instead of κ_i, the value actually entered in Table I is $\cos\kappa_i$. The symmetries tabulated refer to the axes of Fig. 2 and are convenient for purposes of calculation. The group theory notation is also referred to these same axes.[3]

THE WAVE FUNCTIONS

The wave function of the ith orbital, ϕ_i, may be represented by

$$\phi_i = \sum_B \phi_{Bi}, \tag{2}$$

where ϕ_{Bi} is that part of ϕ_i located on branch B and is zero elsewhere. Each ϕ_{Bi}, then, is of the form

$$\phi_{Bi} = a_{Bi} \cos(\kappa_i x + \delta_{Bi}), \tag{2a}$$

* This work was assisted in part by the U. S. Office of Naval Research under Task Order IX of Contract N6ori-20 with The University of Chicago.

[1] K. Ruedenberg and C. W. Scherr, J. Chem. Phys. **21**, 1565 (1953), hereinafter referred to as I.

[2] C. A. Coulson and H. C. Longuet-Higgins, Proc. Roy. Soc. (London) **A191**, 39 (1947).

[3] The Z axis is always taken perpendicular to and out of the plane of the paper except for molecules with C_{2v} symmetry, where the Z axis is as indicated in Fig. 2 and the X axis is perpendicular to the plane of the paper. The orbitals are antisymmetric with respect to σ_h, designating reflection at the plane of the molecule.

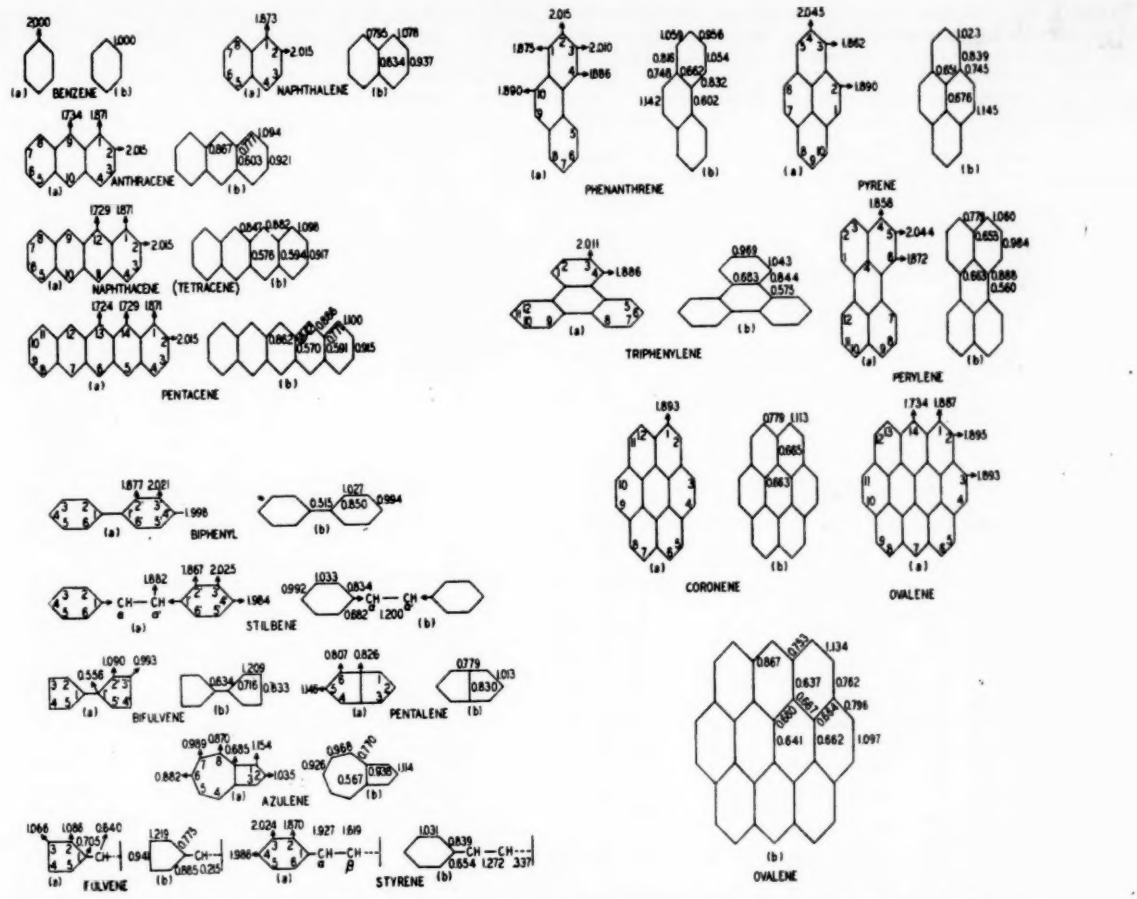

FIG. 1. Bond densities and bound valences. The members of each pair marked (a) present the bound valences of the atoms indicated. The members marked (b) present the total mobile bond densities. The bound valences for joint atoms of the alternant molecules are not presented; they are generally greater than 2.0, usually around 2.3.

where δ_{Bi} is the phase of ϕ_{Bi}, referred to an (arbitrary) coordinate axis located on branch B.

The complete π-electron wave functions of all molecules considered in this paper are presented in Tables I, II, and III. Table I lists $\cos\kappa_i$, Table II lists a_{Bi}^2 and Table III lists $\tan\delta_{Bi}$. Figure 2 depicts the numbering of the branches, and the origins of the x_B's. The bases of the arrows are the origins, and the heads indicate the direction of positive x_B. In no calculations, except those of the spectral lines, was it necessary to know κ_i or δ_{Bi} explicitly.[4] Wherever the phase is obvious by a symmetry consideration, no entry has been made in Table III.

There are two methods, described in the Appendix, which may be employed to find the wave functions. The first method consists of solving for a_{Bi}^2 and $\tan\delta_{Bi}$ directly from the joint conditions [I, Eqs. (1.32), (1.33), and (1.34)] and from Eq. (2.7) of I. The second method consists of finding the eigen*vectors* of the secular equations by the usual methods, [see I, particularly Eqs. (2.56), and (2.57)] as in LCAO calculations. The first method is generally most convenient if the molecule possesses symmetry. The second is generally more convenient if the molecule is large and/or possesses little or no symmetry. The only molecule for which the second method was used in the present calculations is ovalene.

The second method only gives the value of the wave function at the atoms. The π-electron density at the midpoint of a bond is found from:

$$\text{value of } \phi_i \text{ at bond } r-s,\ \phi_i(r-s)=\frac{\phi_i(r)+\phi_i(s)}{2\cos\frac{1}{2}\kappa_i}. \quad (3a)$$

The quantities of Tables II and III are then found from

$$\tan\delta_{Bi}=\frac{\phi_{Bi}^2(-\kappa_{i/2})-\phi_{Bi}^2(+\kappa_{i/2})}{2(\sin\kappa_i)\phi_{Bi}^2(0)} \quad (3b)$$

and

$$a_{Bi}^2=(1+\tan^2\delta_{Bi})\phi_{Bi}^2(0), \quad (3c)$$

where $\phi_i(r)$ is the value of the ith orbital at atom r, for example, and in 3*b* and 3*c*, $\phi_i(x)$ is its value in branch B at coordinate x.

[4] The phase angle is arbitrary by an additive factor $\pm m\pi$, m integral. One takes $\pi/2\geq\delta_{Bi}>-\pi/2$.

TABLE I. The π-electron wave functions: $\cos k_i$. The symmetries (SS, SA, etc.) and the group theory notation refer to the axes of Fig. 2. The symmetries indicate the behavior of the orbital upon reflection at the plane of the molecule, taken in the order X, Y. Hence, AS would mean antisymmetric upon reflection at the XZ plane, symmetric upon reflection at the YZ plane; S^3A^3, symmetric upon reflection at any of three equivalent XZ planes, antisymmetric at any of three equivalent YZ planes. A single letter (e.g., in molecules with C_{2v} symmetry) indicates the behavior upon reflection at the Z axis (at the XZ plane).

Benzene	D_{6h}
1. S^3S^3 A_{2u}	1.0
2. AS } E_{1g}	0.5
3. SA }	
4. AA } E_{2u}	−0.5
5. SS }	
6. A^3S^3 B_{2g}	−1.0
7. S^3A^3 B_{1g}	−1.0

Naphthalene	V_h
1. SS B_{1u}	1.0
2. SA B_{2g}	0.80902
3. AS B_{3g}	0.59023
4. SS B_{1u}	0.42356
5. AA A_u	0.30902
6. SA B_{2g}	−0.30902
7. AS B_{3g}	−0.42356
8. SS B_{1u}	−0.59023
9. AA A_u	−0.80902
10. AS B_{3g}	−1.0

Anthracene	V_h
1. SS B_{1u}	1.0
2. SA B_{2g}	0.90627
3. SS B_{1u}	0.65841
4. AS B_{3g}	0.62139
5. AA A_u	0.46685
6. SA B_{2g}	0.39392
7. AS B_{3g}	0.20369
8. SS B_{1u}	−0.20369
9. AA A_u	−0.39392
10. SA B_{2g}	−0.46685
11. SS A_{1u}	−0.62139
12. AS B_{3g}	−0.65841
13. AA A_u	−0.90627
14. AS B_{3g}	−1.0

Naphthacene	V_h
1. SS B_{1u}	1.0
2. SA B_{2g}	0.94490
3. SS B_{1u}	0.79002
4. AS B_{3g}	0.63640
5. SA B_{2g}	0.57008
6. AA A_u	0.53783
7. SS B_{1u}	0.37823
8. AS B_{3g}	0.36518
9. AA A_u	0.14382
10. SA B_{2g}	−0.14382
11. SS B_{1u}	−0.36518
12. AS B_{3g}	−0.37823
13. SA B_{2g}	−0.53783
14. AS B_{3g}	−0.57008
15. SS B_{1u}	−0.63640
16. AS B_{3g}	−0.79002
17. AA A_u	−0.94490
18. AS B_{3g}	−1.0

Pentacene	V_h
1. SS B_{1u}	1.0
2. SA B_{2g}	0.96385
3. SS B_{1u}	0.85968
4. SA B_{2g}	0.70083
5. AS B_{3g}	0.64491
6. AA A_u	0.57601
7. SS B_{1u}	0.51454
8. AS B_{3g}	0.45582
9. SA B_{2g}	0.36855
10. AA A_u	0.29056
11. AS B_{3g}	0.10681
12. SS B_{1u}	−0.10681
13. SA B_{2g}	−0.29056
14. AA A_u	−0.36855
15. SS B_{1u}	−0.45582
16. AS B_{3g}	−0.51454
17. SA B_{2g}	−0.57601
18. SS B_{1u}	−0.64491
19. AA A_u	−0.70083
20. AS B_{3g}	−0.85968
21. AA A_u	−0.96385
22. AS B_{3g}	−1.0

Diphenyl	V_h
1. SS B_{1u}	1.0
2. SA B_{2g}	0.92249
3. SS B_{1u}	0.57180
4. AA A_u	0.5
5. AS B_{3g}	0.5
6. SA B_{2g}	0.31597
7. SS B_{1u}	−0.31597
8. AA A_u	−0.5
9. AS B_{3g}	−0.5
10. SA B_{2g}	−0.57180
11. SS B_{1u}	−0.92249
12. SA B_{2g}	−1.0

Stilbene	V_h
1. SS B_{1u}	1.0
2. SA B_{2g}	0.96096
3. SS B_{1u}	0.72011
4. SA B_{2g}	0.5
5. AS B_{3g}	0.5
6. AA A_u	0.5
7. SS B_{1u}	0.24085
8. SA B_{2g}	−0.24085
9. AS B_{3g}	−0.5
10. AA A_u	−0.5
11. SS B_{1u}	−0.5
12. SA B_{2g}	−0.72011
13. SS B_{1u}	−0.96096
14. SA B_{2g}	−1.0

Styrene	C_{2v}
1. S B_2	0.97903
2. S B_2	0.66594
3. A A_2	0.5
4. S B_2	0.31308
5. S B_2	−0.31308
6. A A_2	−0.5
7. S B_2	−0.66594
8. S B_2	−0.97903

Difulvene	V_h
1. SS B_{1u}	1.0
2. SA B_{2g}	0.89830
3. SS B_{1u}	0.42356
4. AA A_u	0.30902
5. AS B_{3g}	0.30902
6. SA B_{2g}	0.11020
7. SS B_{1u}	−0.59023
8. AS B_{3g}	−0.80902
9. AA A_u	−0.80902
10. SA B_{2g}	−0.84183

Fulvene	C_{2v}
1. S B_2	0.96262
2. S B_2	0.44376
3. A A_2	0.30902
4. S B_2	−0.12480
5. S B_2	−0.78158
6. A A_2	−0.80902

Methylene-3 pentadiene 1,4	C_{2v}
1. S B_2	0.83041
2. A A_2	0.5
3. S B_2	0.24581
4. S B_2	−0.24581
5. A A_2	−0.5
6. S B_2	−0.83041

Pentalene	V_h
1. SS B_{1u}	1.0
2. SA B_{2g}	0.70711
3. AS B_{3g}	0.43426
4. SS B_{1u}	0.19371
5. AA A_u	0.0
6. SA B_{2g}	−0.70711
7. AS B_{3g}	−0.76759
8. SS B_{1g}	−0.86038

TABLE I.—(*Continued*).

Azulene		C_{2v}
1. S	B_2	1.0
2. S	B_2	0.81254
3. A	A_2	0.63253
4. S	B_2	0.39186
5. A	A_2	0.22398
6. S	B_2	−0.18536
7. A	A_2	−0.35032
8. S	B_2	−0.77636
9. A	A_2	−0.83952
10. S	B_2	−0.90934

Phenanthrene		C_{2v}
1. S	B_2	1.0
2. A	A_2	0.89689
3. S	B_2	0.72015
4. S	B_2	0.56250
5. A	A_2	0.5
6. A	A_2	0.33647
7. S	B_2	0.28404
8. A	A_2	−0.28404
9. S	B_2	−0.33647
10. S	B_2	−0.5
11. A	A_2	−0.56250
12. A	A_2	−0.72015
13. S	B_2	−0.89689
14. A	A_2	−1.0

Pyrene		V_h
1. SS	B_{1u}	1.0
2. AS	B_{3g}	0.87017
3. SA	B_{2g}	0.78868
4. SS	B_{1u}	0.64306
5. AA	A_u	0.5
6. SS	B_{1u}	0.41731
7. AS	B_{3g}	0.35687
8. SA	B_{2g}	0.21132
9. AA	A_u	−0.21132
10. SS	B_{1u}	−0.35687
11. AS	B_{3g}	−0.41731
12. SA	B_{2g}	−0.5
13. AS	B_{3g}	−0.64306
14. AA	A_u	−0.78868
15. SS	B_{1u}	−0.87017
16. AS	B_{3g}	−1.0

Perylene		V_h
1. SS	B_{1u}	1.0
2. AS	B_{3g}	0.92104
3. SA	B_{2g}	0.82261
4. AA	A_u	0.75120
5. SS	B_{1u}	0.64460
6. AS	B_{3g}	0.43524
7. SS	B_{1u}	0.42469
8. SA	B_{2g}	0.42178
9. AS	B_{3g}	0.37968
10. AA	A_u	0.15986
11. SA	B_{2g}	−0.15986
12. SS	B_{1u}	−0.37968
13. AA	A_u	−0.42178
14. AS	B_{3g}	−0.42469
15. SS	B_{1u}	−0.43524
16. AS	B_{3g}	−0.64460
17. SA	B_{2g}	−0.75120
18. AA	A_u	−0.82261
19. SS	B_{1u}	−0.92104
20. AS	B_{3g}	−1.0

Triphenylene		D_{3h}
1. S^3	A_2''	1.0
2. S	E''	0.89610
3. A		
4. S^3	A_2''	0.59023
5. S	E''	0.55400
6. A		
7. A^3	A_1''	0.42356
8. S	E''	0.29074
9. A		
10. A	E''	−0.29074
11. S		
12. S^3	A_2''	−0.42356
13. A	E''	−0.55400
14. S		
15. A^3	A_1''	−0.59023
16. A	E''	−0.89610
17. S		
18. A^3	A_1''	−1.0

Coronene		D_{6h}
1. S^3S^3	A_{2u}	1.0
2. AS	E_{1g}	0.89349
3. SA		
4. SS	E_{2u}	0.70998
5. AA		
6. S^3S^3	A_{2u}	0.61693
7. S^3A^3	B_{1g}	0.5
8. A^3S^3	B_{2g}	0.45026
9. AS	E_{1g}	0.38018
10. SA		
11. SS	E_{2u}	0.23036
12. AA		
13. SA	E_{1g}	−0.23036
14. AS		
15. AA	E_{2u}	−0.38018
16. SS		
17. S^3S^3	A_{2u}	−0.45026
18. A^3A^3	A_{1u}	−0.5
19. A^3S^3	B_{2g}	−0.61693
20. SA	E_{1g}	−0.70998
21. AS		
22. AA	E_{2u}	−0.89349
23. SS		
24. A^3S^3	B_{2g}	−1.0

Ovalene		V_h
1. SS	B_{1u}	1.0
2. SA	B_{2g}	0.93890
3. AS	B_{3g}	0.90269
4. AA	A_u	0.80139
5. SS	B_{1u}	0.79300
6. SS	B_{1u}	0.67428
7. SA	B_{2g}	0.63641
8. AS	B_{3g}	0.59895
9. SA	B_{2g}	0.52671
10. SS	B_{1u}	0.41907
11. AS	B_{3g}	0.41900

Ovalene		V_h
12. AA	A_u	0.41279
13. SS	B_{1u}	0.34698
14. AA	A_u	0.30085
15. SA	B_{2g}	0.24635
16. AS	B_{3g}	0.14602
17. SS	B_{1u}	−0.14602
18. AA	A_u	−0.24635
19. SA	B_{2g}	−0.30085
20. AS	B_{3g}	−0.34698
21. SA	B_{2g}	−0.41279
22. SS	B_{1u}	−0.41900

Ovalene		V_h
23. AS	B_{3g}	−0.41907
24. AA	A_u	−0.52671
25. SS	B_{1u}	−0.59895
26. AA	A_u	−0.63641
27. AS	B_{3g}	−0.67428
28. AS	B_{3g}	−0.79300
29. SA	B_{2g}	−0.80139
30. SS	B_{1u}	−0.90269
31. AA	A_u	−0.93890
32. AS	B_{3g}	−1.0

SPECTRA

The wavelengths of radiation for the four transitions between the two highest filled and the two lowest unfilled energy levels are presented in Table IV. The nomenclature and assignment is due to Platt and Klevens.[5] These wavelengths are compared with the center of gravity of the corresponding singlets and triplets.[6] Unfortunately, most of these triplet data are estimates. Where the estimates of the triplets were not available, only the singlets are listed. There will, of course, always be triplets, which generally lie in such a direction as to improve the agreement of the theoretical calculations. Some corresponding LCAO calculations[5] are also tabulated for comparison.

The free-electron model (and the LCAO model) gives agreement to within 10 000 cm^{-1}, usually better. Indeed the prediction of the longest wavelength transition is generally quite good. These results are the more remarkable when one considers that there is *only one* (quasi-) adjustable parameter in the free-electron model, D, the internuclear distance. Actually, no attempt at adjustment was made; D has been taken to be 1.39A

[5] H. B. Klevens and J. R. Platt, J. Chem. Phys. **17**, 470 (1949); J. R. Platt, J. Chem. Phys. **18**, 1168 (1950).

[6] K. Ruedenberg and J. R. Platt, private communication.

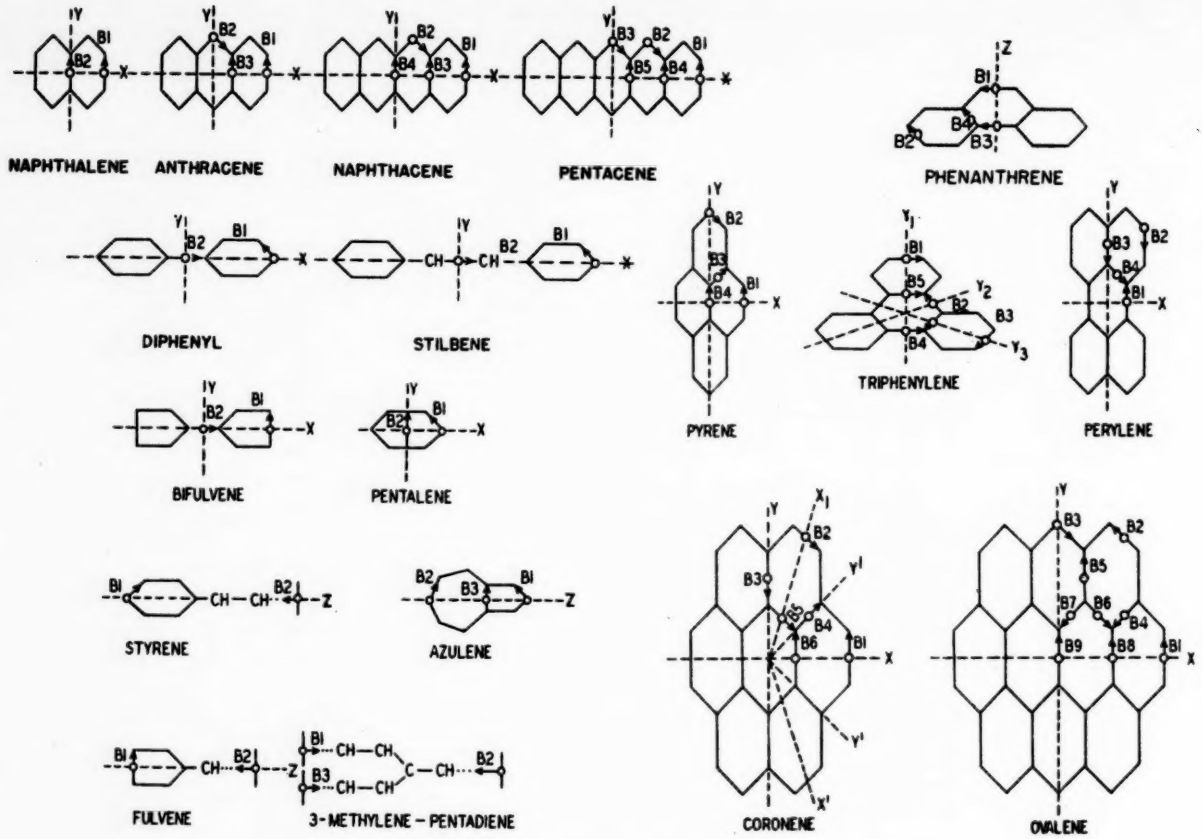

FIG. 2. The arbitrary coordinates.

(the benzene C—C distance) in the aromatic systems, and, 1.34A (the ethylene C—C distance) in the *n*-polyenes. When comparing the LCAO model predictions with the free-electron model predictions, it should be borne in mind that in the former there are two adjustable parameters, S and β; S is usually fixed at about 0.25 and β is varied to give a best fit.

BOND DENSITIES

The total mobile bond order, defined by Coulson and Longuet-Higgins[1] for their LCAO theory would be, in free-electron terms, as follows:

$$p_{rs}=2\sum_{j=1}^{n/2}\phi_j(r)\phi_j(s), \tag{4}$$

where p_{rs} is the total mobile bond order of bond $r-s$, j refers to the orbital, and $\phi_j(r)$ and $\phi_j(s)$ are the values of the jth orbital wave function at atoms r and s, respectively. This definition is an approximation to the electron density in the bond.

The total mobile bond density for the free-electron model is defined by

$$b_{(rs)}=2\sum_{j=1}^{n/2}\phi_j^2(r-s), \tag{5}$$

where $\phi_j(r-s)$ is the value of the jth orbital at the midpoint of bond $r-s$. This definition is also an approximation to the electron density in the bond which, however, is consistent with the definition of the electron density at the atoms. For comparison with Eq. (4), Eq. (5) may be written approximately as

$$b_{(rs)}\approx f[\tfrac{1}{2}+\sum_{j=1}^{n/2}\phi_j(r)\phi_j(s)], \tag{6}$$

where f is some constant, equivalent to a mean value of $1/\cos^2\frac{1}{2}\kappa_i$ and may be taken as ≈ 1.25. It would seem

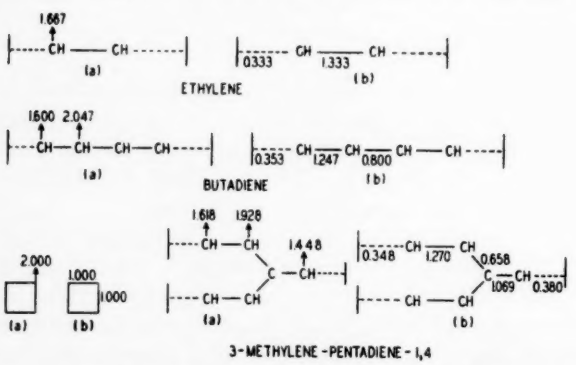

FIG. 3. Bond densities and bound valences for polyene-type molecules. The members of each pair marked (a) present the bound valences of the atoms indicated. The members marked (b) present the total mobile bond densities.

TABLE II. The π-electron wave functions: a_{Bi}^2.

Molecule	Orbital	Symmetry	$B1$	$B2$	$B3$	$B4$	$B5$
Benzene	1.	SS	0.16667				
	all others	—	0.33333				
Naphthalene	1.	SS	0.09091	0.09091			
	2.	SA	0.20000	0			
	3.	AS	0.16029	0.39709			
	4.	SS	0.17737	0.22629			
	5.	AA	0.20000	0			
Anthracene	1.	SS	0.06250	0.06250	0.06250		
	2.	SA	0.13145	0.15669	0.02938		
	3.	SS	0.15062	0.09786	0.05116		
	4.	AS	0.08829	0.13827	0.28202		
	5.	AA	0.16417	0.03631	0.10652		
	6.	SA	0.11615	0.13053	0.15822		
	7.	AS	0.11526	0.20137	0.02098		
Naphthacene	1.	SS	0.04762	0.04762	0.04762	0.04762	
	2.	SA	0.09818	0.11588	0.04560	0	
	3.	SS	0.10744	0.10172	0.00075	0.11041	
	4.	AS	0.05350	0.10216	0.19168	0.26441	
	5.	SA	0.12148	0.07672	0.08575	0	
	6.	AA	0.12154	0.05190	0.18469	0	
	7.	SS	0.08364	0.09986	0.11729	0.13022	
	8.	AS	0.12245	0.07548	0.00852	0.15466	
	9.	AA	0.07260	0.15206	0.02878	0	
Pentacene	1.	SS	0.03846	0.03846	0.03846	0.03846	0.03846
	2.	SA	0.07850	0.08976	0.09635	0.04878	0.00696
	3.	SS	0.08343	0.09394	0.07243	0.00468	0.05757
	4.	SA	0.09212	0.06625	0.09885	0.01759	0.05914
	5.	AS	0.03473	0.07385	0.09174	0.13253	0.21491
	6.	AA	0.08952	0.07172	0.01353	0.19585	0.04265
	7.	SS	0.10135	0.07257	0.04580	0.09537	0.01601
	8.	AS	0.10750	0.02507	0.10962	0.05930	0.08371
	9.	SA	0.06366	0.07884	0.08447	0.09071	0.10668
	10.	AA	0.09041	0.10248	0.03000	0.00059	0.07744
	11.	AS	0.04882	0.11040	0.14194	0.02679	0.00362
Diphenyl	1.	SS	0.07692	0.07692			
	2.	SA	0.12834	0.45990			
	3.	SS	0.15162	0.18062			
	4.	AA	0.16667	0			
	5.	AS	0.16667	0			
	6.	SA	0.14312	0.28256			
Stilbene	1.	SS	0.06667	0.06667			
	2.	SA	0.10000	0.26667			
	3.	SS	0.10000	0.26667			
	4.	SA	0.13333	0.13333			
	5.	AS	0.16667	0			
	6.	AA	0.16667	0			
	7.	SS	0.10000	0.26667			
Styrene	1.	S	0.16667	0.33333			
	2.	S	0.16667	0.33333			
	3.	A	0.33333	0			
	4.	S	0.16667	0.33333			
3-methylene-pentadiene 1,4	1.	S	0.24267	0.27200			
	2.	A	0.33333	0			
	3.	S	0.18590	0.44229			
n-polyenes	all	—	$a^2=(n+1)/2$				
Fulvene	1.	S	0.21263	0.46841			
	2.	S	0.25771	0.35574			
	3.	A	0.40000	0			
	4.	S	0.17011	0.57472			
	5.	S	0.28262	0.29344			
	6.	A	0.40000	0			
Difulvene	1.	SS	0.09091	0.09091			
	2.	SA	0.14847	0.51526			
	3.	SS	0.17737	0.22628			
	4.	AA	0.20000	0			
	5.	AS	0.20000	0			
	6.	SA	0.17074	0.29254			
	7.	SS	0.16026	0.39738			
	8.	AS	0.20000	0			
	9.	AA	0.20000	0			
	10.	SA	0.18078	0.19218			

TABLE II.—(*Continued*).

Molecule	Orbital	Symmetry	B_1	B_2	B_3	B_4	B_5	B_6
Azulene	1.	S	0.09091	0.09091	0.09091			
	2.	S	0.21251	0.17624	0.01997			
	3.	A	0.24759	0.05576	0.29139			
	4.	S	0.13757	0.25045	0.17278			
	5.	A	0.09852	0.31370	0.15409			
	6.	S	0.25032	0.08126	0.17303			
	7.	A	0.23673	0.12498	0.07972			
	8.	S	0.07224	0.35786	0.13512			
	9.	A	0.17010	0.19968	0.18068			
	10.	S	0.23644	0.04328	0.40821			
Pentalene	1.	SS	0.11111	0.11111				
	2.	SA	0.25000	0				
	3.	AS	0.19678	0.42575				
	4.	SS	0.21201	0.30392				
	5.	AA	0.25000	0				
	6.	SA	0.25000	0				
	7.	AS	0.21989	0.24088				
	8.	SS	0.17688	0.58498				
Phenanthrene	1.	S	0.06250	0.06250	0.06250	0.06250		
	2.	A	0.08388	0.13763	0.28522	0.04344		
	3.	S	0.26855	0.09889	0.00024	0.10258		
	4.	S	0.00604	0.14006	0.17369	0.20381		
	5.	A	0.10526	0.14035	0	0.14035		
	6.	A	0.06350	0.13652	0.23718	0.10354		
	7.	S	0.23379	0.11248	0.06470	0.05457		
Pyrene	1.	SS	0.05263	0.05263	0.05263	0.05263		
	2.	AS	0.07753	0.14284	0.05336	0.17865		
	3.	SA	0.17108	0.05423	0.13492	0		
	4.	SS	0.07788	0.17511	0.02558	0.02954		
	5.	AA	0.09091	0.12121	0.12121	0		
	6.	SS	0.14839	0.00677	0.19991	0.25581		
	7.	AS	0.07214	0.12265	0.09708	0.19766		
	8.	SA	0.12263	0.14507	0.02591	0		
Perylene	1.	SS	0.04167	0.04167	0.04167	0.04167		
	2.	AS	0.20944	0.07468	0.10377	0.04468		
	3.	SA	0.04289	0.08942	0	0.12089		
	4.	AA	0.05927	0.11336	0	0.01692		
	5.	SS	0.07808	0.07634	0.18266	0.06427		
	6.	AS	0.02954	0.10032	0.10148	0.03320		
	7.	SS	0.00091	0.09080	0.10994	0.08135		
	8.	SA	0.11647	0.08526	0	0.10071		
	9.	AS	0.14035	0.04476	0.17476	0.16339		
	10.	AA	0.08905	0.10427	0	0.03839		
Triphenylene	1.	S^3	0.04762	0.04762	0.04762	0.04762	0.04762	0.04762
	2.	S	0.18166	0.21504	0.04872	0.02054	0.03201	0.06096
	3.	A	0.00440	0.08538	0.13734	0.27988	0.07061	0.04166
	4.	S^3	0.10686	0.06618	0.10686	0.06618	0.06618	0.06618
	5.	S	0.04318	0.02800	0.11865	0.10658	0.03346	0.20079
	6.	A	0.14381	0.08038	0.06833	0.00180	0.25657	0.08924
	7.	A^3	0.11825	0.03771	0.11825	0.03771	0.03771	0.03771
	8.	S	0.10506	0.17010	0.08435	0.04660	0.16241	0.04098
	9.	A	0.07745	0.08777	0.09816	0.21127	0.00050	0.12194
Coronene	1.	S^3S^3	0.03333	0.03333	0.03333	0.03333	0.03333	0.03333
	2.	AS	0.04460	0.08193	0.10637	0.02659	0.04619	0.12266
	3.	SA	0.09438	0.05704	0	0.07978	0.09717	0.02070
	4.	SS	0.11648	0.07566	0.09186	0.02296	0.02834	0.00209
	5.	AA	0.06205	0.10288	0	0.06889	0.01084	0.03709
	6.	S^3S^3	0.03575	0.03575	0.13826	0.13826	0.08781	0.08781
	7.	S^3A^3	0.11111	0.11111	0	0	0	0
	8.	A^3S^3	0.07675	0.07675	0.07840	0.07840	0.02469	0.02469
	9.	AS	0.00083	0.04581	0.17363	0.04341	0.16545	0.13126
	10.	SA	0.06081	0.01583	0	0.13023	0.14265	0.17684
	11.	SS	0.10474	0.07754	0.08527	0.02132	0.04098	0.01065
	12.	AA	0.06847	0.09568	0	0.06395	0.02075	0.05107

TABLE II.—(*Continued*).

Molecule	Orbital	Symmetry	*B*1	*B*2	*B*3	*B*4	*B*5	*B*6	*B*7	*B*8	*B*9
Ovalene	1.	*SS*	0.02439	0.02439	0.02439	0.02439	0.02439	0.02439	0.02439	0.02439	0.02439
	2.	*SA*	0.06112	0.04629	0.05903	0.05548	0.00789	0.06620	0.06656	0.02859	0
	3.	*AS*	0.02949	0.05420	0.06282	0.01651	0.07766	0.03514	0.03086	0.08646	0.10773
	4.	*AA*	0.04515	0.08005	0.06200	0.04064	0.02387	0.00902	0.02514	0.06293	0
	5.	*SS*	0.10014	0.03944	0.03729	0.05989	0.02353	0.06586	0.03479	0.00140	0.03772
	6.	*SS*	0.00072	0.04866	0.04314	0.03813	0.12447	0.02594	0.08395	0.02681	0.09563
	7.	*SA*	0.11886	0.05881	0.05649	0.01869	0.03367	0.01529	0.02067	0.00099	0
	8.	*AS*	0.05110	0.07309	0.06700	0.06240	0.02424	0.02796	0.01109	0.00891	0.02771
	9.	*SA*	0.01407	0.04831	0.00031	0.11440	0.04433	0.08158	0.04029	0.10609	0
	10.	*SS*	0.13469	0.04634	0.06245	0.02628	0.01248	0.03294	0.00496	0.03652	0.00634
	11.	*AS*	0.01197	0.03162	0.02500	0.02764	0.09961	0.06727	0.08059	0.08798	0.17225
	12.	*AA*	0.05460	0.05478	0.06481	0.05847	0.05914	0.03791	0.03182	0.00320	0
	13.	*SS*	0.00433	0.03539	0.04882	0.06331	0.00714	0.06746	0.11828	0.08638	0.15663
	14.	*AA*	0.01726	0.05798	0.00078	0.04236	0.06208	0.07559	0.06561	0.10744	0
	15.	*SA*	0.05235	0.05089	0.09020	0.02158	0.05873	0.04567	0.02374	0.01991	0
	16.	*AS*	0.05059	0.05775	0.12909	0.03677	0.01737	0.01762	0.03238	0.00688	0.05678

that the most exact, but probably unnecessary, definition for the electron density would be an integrated density extending half a bond length to either side of the point in question.

The bond densities calculated from Eq. (5) are presented in Figs. 1 and 3.

BOUND VALENCE AND REACTIVITIES

Coulson and Longuet-Higgins[7] have defined a useful quantity, *the free valence*, which has been successfully correlated by many authors with chemical reactivity. It is a second-order effect which becomes of importance in alternant hydrocarbons because the "electron density" at the atoms (the first-order effect) is the same (but v.i.). The free valence is the potential bond forming power a particular atom in a molecule has. The free valence is obtained by forming the sum of the bond orders of the bonds terminating on the atom under consideration and then subtracting this sum from a certain number, $N_{\max}$. $N_{\max}$ is obtained in the following manner: If one were to have available calculations on all possible hydrocarbons, then he would be able to pick out the maximum possible value for the sum just mentioned above. This maximum value is taken to be $N_{\max}$. Analytically the

$$\text{free valence of atom } r = N_{\max} - \sum_{\substack{\text{all } s \text{ neighboring} \\ \text{to } r}} p_{rs} .$$

This concept may be taken over, *in toto*, into the free-electron picture. The present author has chosen to tabulate merely the sums of the bond densities, and in order to indicate the complementary nature of these sums to the free valence, has called them, following a suggestion of Ruedenberg's, *the bound valence*. Hence, the smaller the bound valence, the more reactive the atom (to electrophillic reagents). These *bound valences* are presented in Figs. 1 and 3. The base of the arrows indicates the corresponding atom.

In the first paragraph of this section it has been mentioned that the first-order effect for reactivities is the "electron *density*"; however, it should be noted that the LCAO model has tacitly implied that the first-order effect is due to the electron *population* (see paper I, since to the author's knowledge this distinction between density and population has never been made before). This point is being investigated further. In this paper, since D has been taken as the unit of length, there is no numerical difference between density and population for bond or for nonjoint atom densities. At the joints the population is 3/2 of the density. No *bound valences* are reported for joint atoms (they are generally greater than 2.0, usually around 2.3). In nonalternant molecules, it is the total electron density at the atoms which is reported rather than the *bound valence*.

Table V compares the (theoretically) most reactive atoms in each molecule with the known chemistry of the hydrocarbons. The only serious discrepancy with experiment is found in the phenanthrene molecule, where the 1,8 positions are indicated to be slightly more reactive than the 9,10 positions. If one attempts to explain this by noticing that there is an over-all very high concentration of π-electron density about the 9,10 positions (i.e., atoms 9 and 10 contiguous and connected by the very high density 9—10 bond) then a difficulty arises in explaining why the somewhat similar pyrene molecule is not reactive at the pyrene 1,2 positions. An exactly similar difficulty is encountered in the LCAO model.

DIPOLE MOMENTS

Of all the molecules considered here, only fulvene and azulene can (theoretically) have dipole moments, and indeed, this is an experimental fact, that alternant hydrocarbons have, at most, small dipole moments. The calculated moments are: fulvene 4.4 D (Debyes);

[7] C. A. Coulson and H. C. Longuet-Higgins, Rev. sci. 85, 929 (1947).

TABLE III. The π-electron wave functions: $\tan\delta_{Bi}$. The reference coordinates are shown in Fig. 2. Wherever the phase is obvious from symmetry considerations, no entry has been made.

Molecule	Orbital:	2	3	4	5	6	7	8	9	10	11	12	13	14	15	16
Naphthacene	Branch															
Pentacene	*B2*	−1.6333	1.0925	0.066212			15.631	0.63293								
Phenanthrene	*B2*	−0.092822	3.0250	0.28906	0.10148	−0.25623	−1.4330	5.9578	9.7850	0.25472	−0.23250					
	B1	−0.87844	0.41338	−1.2236	1.7321	−0.99169	1.5007									
	B4	−1.0895	−2.8417	1.9800	−1.7321	0.10223	0.13161									
Pyrene	*B3*			0.78433		1.2107	−0.02519									
Perylene	*B2*	0.46039			1.5269	−1.4366	−0.69744		−0.70262							
	B3	1.15656			17.292	0.81522	0.063547		−1.2338							
	B4	1.3300			−0.50211	28.402	1.3007		0.46804							
Triphenylene	*B2*	−6.3933	2.1311		−0.22518	0.075061		−3.6881	1.2294							
	B3	−0.26968	0.089892		3.1611	−1.0537		−1.4872	0.49572							
	B4	−2.5724	0.85747		−4.7962	1.5987		−0.096145	0.032048							
Coronene	*B2*	0.39688		1.2642					−0.067714		−1.4004					
	B3	1.0704		1.2523					−1.1245		0.32469					
	B4	−1.0704	−1.0704	−1.2523	−1.2523	2.7752		−0.87759	1.1245	1.1245	−0.32469	−0.32469				
	B5	1.4055		7.2845					0.49741		3.7931					
Ovalene	*B2*	0.75161	−0.45800	0.054668	9.7656	−0.38012	−0.69565	1.0065	−0.021495	0.38941	−0.57068	92.121	0.16745	−0.21940	1.4730	−0.35993
	B4	0.69905	1.0701	1.1320	1.9561	2.0230	4.2473	1.3591	−1.8669	0.82172	0.29987	1.1876	1.2520	−0.29737	0.049343	0.64402
	B5	0.16904	−1.1287	−0.66845	−0.27687	138.63	−0.52226	−0.39123	2.1416	−1.3251	2.6748	−0.27299	−1.7090	1.0954	−0.25094	3.2016
	B6	−1.7143	1.5406	0.27330	5.2209	−0.039311	1.2565	4.7215	−0.44961	−1.7400	0.35086	2.2731	−1.5176	0.15720	8.8338	3.3322
	B7	5.6332	1.3231	3.0116	−0.54088	−0.73290	2.1215	0.33171	1.7960	−1.2067	0.09435	1.5511	−1.3786	1.3640	1.2860	−0.18934

azulene 6.3 *D*. These may be compared with the (unrefined) LCAO values of 4.8 *D* and 6.9 *D*, respectively.[8] Experimentally, fulvene would be expected to have a dipole moment of about 1.2 *D* on the basis of the dipole moments of its derivatives, while that of azulene is of the order of unity.[8] There are many well-known reasons for these discrepancies among which the σ-electron contribution to the dipole moment and the effect of the true bond length should be mentioned.

BOND LENGTHS

Coulson[9] has successfully demonstrated that on the basis of the total π-electron density (Coulson's total mobile bond order) at the bonds, predictions of the bond lengths in these molecules can be made which agree fairly well with experiment; usually within the experimental error. The present author has found the following completely empirical equation to be satisfactory for use with the bond densities calculated on the basis of the free-electron model. It reproduces the known bond lengths with a root-mean-square deviation of 0.016A:

$$\text{length of bond } r-s(\text{A}) = 1.665 - 0.1398(1+b(rs)). \quad (7)$$

Equation (7) has been obtained from the curve of Fig. 4. Figure 4 is analogous to the well-known figure due to Coulson[9] constructed on the basis of the LCAO model results, and indeed, the present Fig. 4 is constructed to facilitate comparison. Experimental bond lengths are plotted against calculated bond densities. The solid line is a straight line which can be drawn through the points.[10] The dashed lines represent 0.020A deviations from the solid line, and correspond to the experimental error for most of the molecules considered. The present author has calculated the root-mean-square deviations on both Fig. 4 and the analogous plot of Coulson.[11] These deviations are, for the free-electron model, 0.016A; LCAO, 0.018A. Table VI presents a breakdown of these figures.[12] The predictions of

[8] LCAO data taken from B. Pullman and A. Pullman, *Les theories electroniques de la chimie organique* (Masson and Company, Paris, 1952), pp. 399 and 406.

[9] C. A. Coulson, Proc. Roy. Soc. (London) **A207, 91** (1951), and also in J. Phys. Chem. **56**, 311 (1952).

[10] A better fit to the experimental data could perhaps be obtained if one disregards the somewhat doubtful polyene points and the certainly dubious pyrene points. Because of this uncertainty of how to weight the experimental data, the best line has been estimated by an inspection.

[11] The bulk of the necessary data is taken from J. M. Robertson, Proc. Roy. Soc. (London) **A207**, 101 (1951). It has been necessary to make a few corrections to this data; see, for example, reference b of Table VI.

[12] The experimental lengths for butadiene, and in particular the 1−2 bond (1.46A), are somewhat dubious. [See, e.g., Coulson, Daudel, and Robertson, Proc. Roy. Soc. (London) **A207**, 311 (1951).) For a discussion of the polyene bond lengths from a free-electron point of view see H. Kuhn, J. Chem. Phys. **16**, 840 (1948); **17**, 1198 (1949). Also N. Bayliss, Austrian J. Sci. Research **A4**, 344 (1951) and earlier references given there; his treatment does not conform to that of the present paper. For these and other reasons the butadiene point was not included in this calculation. With this point in they become: free-electron 0.017A; LCAO unchanged.

TABLE IV. Spectral predictions. The LCAO model predictions (with $S=0.25$; $\beta(\text{ring})=23\,000\ \text{cm}^{-1}$; and $\beta(\text{polyene})=32\,000\ \text{cm}^{-1}$) and the experimental data have all been taken from references 5 and 6. The experimental data in parentheses are estimations.

Molecule	Transition	Predicted transition energy (cm^{-1}) FEMO	LCAO	Observed singlets	Observed triplets	Center of gravity of singlets and triplets	Correction FEMO	LCAO
Benzene	L_a, L_b, B_b, B_a (fourfold degen. in this approx.)	52 300	49 100	48 000 (c.g.) 38 200 54 000 54 000	29 300 (43 800) (40 000) (40 000)	(43 400)	−9000	−5500
Naphthalene	L_a	31 400	29 000	35 000	21 300	28 200	−3000	−1000
	L_b	36 100	35 000	32 200	(36 200)	33 200	−3000	−2000
	B_b	39 100	43 000	45 000	(35 000)	39 200	0	−4000
	B_a	43 700	49 000	59 000	(49 300)	54 500	+11 000	+5500
Anthracene	L_a	20 500	19 000	26 700	14 700	20 700	0	+1500
	L_b	28 500	29 000	(29 000)	(33 000)	31 000	+2500	+2000
	B_b	32 400	39 300	38 500	(30 000)	34 500	+2000	−5000
	B_a	40 500	49 000	53 700	(44 700)	49 200	+9000	0
Naphthacene	L_a	14 420	13 500	21 000	(9500)	15 500	+1000	+2000
	L_b	24 000	26 000	(25 500)	(29 500)	27 500	+3500	+1500
	B_b	27 800	37 000	36 700	(28 200)	32 500	+4500	−4500
	B_a	37 400	49 000	47 400	(39 000)	43 200	+6000	−6000
Pentacene	L_a	10 690	10 000	17 300	(6200)	11 800	+1000	+2000
	L_b	18 880	24 000	24 000(?)	(28 000)	26 000	+9000	+2000
	B_b	21 300	35 500	33 000	(24 300)	28 300	+7000	−7000
	B_a	29 500	49 000	(43 000)	(35 000)	39 000	+9500	−10 000
Phenanthrene	L_a	28 800		33 000	(22 000)	27 500	−1500	
	L_b	31 000		28 300	(33 700)	31 000	0	
	B_b	32 100		39 400	(29 700)	34 500	+2500	
	B_a	34 300		53 400	(44 400)	48 900	+14 500	
Triphenylene	L_a, L_b, B_b, B_a (fourfold degen. in this approx.)	29 500		34 000 (c.g.)	(29 800) (c.g.)	32 800	+3500	

Molecule	Transition	Predicted transition energy (cm^{-1}) FEMO	LCAO	Observed singlets	Correction for singlets only FEMO	LCAO
Diphenyl	^1L_a (?)	32 100	33 800	39 200	+7000	+5500
	^1L_b (?)	39 500	38 200	(41 000)	+1500	+3000
		44 900	44 400	48 000	+3000	+3500
		52 300	49 000	56 000	+2500	+7000
Fulvene	The three filled levels to the lowest unfilled	20 600	18 600	27 000	+6500	+7500
		26 300	24 700	35 500	+9000	+11 000
		44 800	38 000	54 000	+9000	+16 000
Styrene	^1L_a	31 800	31 300	34 000	+2000	+2500
	^1L_b	39 300	36 700	38 500	−1000	+1000
	^1B_b	44 800	43 800	46 500	+1500	+2500
	^1B_a	52 300	49 000	58 000	+5500	+9000
Azulene	^1L_b	20 300	20 000	14 400	−6000	−5500
	^1L_a	27 400	27 000	27 500	0	+ 500
	^1B_b	30 400	30 600	34 000	+3500	+3500
	^1B_a	37 500	37 500	48 000	+10 500	+10 500
Coronene	^1L_a, ^1L_b, ^1B_b, ^1B_a (fourfold degen. in this approx.)	23 200	25 200	29 000 (c.g.)	+6000	+4000
Ethylene	$N_1 \rightarrow V_1\ ^1B_b$	55 900	68 000	57 000	+1000	−11 000
Butadiene	$N_1 \rightarrow V_1\ ^1B_b$	33 800	40 500	43 000	+9000	+2500
Hexatriene	$N_1 \rightarrow V_1\ ^1B_b$	24 200	28 700	38 000	+14 000	+9500

bond lengths by the free-electron model are consistently better than the predictions by the LCAO model.

DISCUSSION OF SPECIAL POINTS

Detailed calculations on a series of n-polyenes has not been given. One may conveniently find the total mobile bond density from the following formula:

$$\underset{s=r+1}{b(rs)} = 1 - \frac{(-1)^r}{(n+1)\sin\{\pi(r+\tfrac{1}{2})/(n+1)\}}, \qquad (8)$$

where r in Eq. (8) is the systematic number of the rth

TABLE V. Bound valences and chemical reactivities. Under the heading "Theoretically most reactive atom(s)—bond," the atom position with the lowest bound valence or, respectively, the bond with the highest π-electron density is listed for each molecule. Positionally equivalent atoms are indicated by enclosure in parentheses.

Molecule	Theoretically most reactive atom(s)	bond	Positions attacked upon oxidation	halogenation	nitration	sulfonation
Naphthalene	(1,4,5,8)		1,4	1 1,5 1,4	1 1,5 1,8	1
Anthracene	(9,10) then (1,4,5,8)		9,10	9 9,10	9 9,10	1,5 1,8
Naphthacene	(9,10,11,12)		9,10	9,10		
Pentacene	(6,13)		6,13			
Diphenyl	(2,2′) then (4,4′)		all reactions at the 4 atom; (steric effects?)			
Stilbene	(2,2′)	$\alpha-\alpha'$	addition to the $\alpha-\alpha'$ bond			
Styrene	β	$\alpha-\beta$	addition to the $\alpha-\beta$ bond			
Phenanthrene	(1,8)	9—10	9,10	9 9,10	9	1 2 3 9
Pyrene	(3,5,8,10)		3,8 3,10	3,5,8		
				3,5,8,10		3,5,8,10
Perylene	(3,4,9,10)		3,9 3,10	3,9	3,10	3,9
				3,10	3,4,9,10	3,10
				3,4,9,10		

atom, and n is the number of atoms in the polyene chain. This equation clearly shows the "alternating single and double bonds" of polyene chains. It also shows that the strongest bond in any n-polyene is the 1—2 bond and its sister, the $(n-1)-n$ bond. The formula implies that very long chains would show only a slight conjugation effect.

In the cyclo-butadiene molecule there exists a filled level, $\kappa_2=\frac{1}{2}\pi$, degenerate with the lowest unfilled level, and, hence, cyclo-butadiene has a triplet ground state.[13] Properly speaking, that is, there are two half-filled orbitals in the ground state, and Eq. (5) must be used in its general form,

$$b(rs)=\sum_{j=1}^{\infty} n_j\phi_j^2(r-s), \qquad (5a)$$

where n_j is the number of π electrons in the jth orbital. Longuet-Higgins[14] has considered the following three hypothetical hydrocarbons from the LCAO approach which also have, on that model, a triplet ground state; $1,3-(CH_2)_2C_6H_4$, and $1,1-(CH_2)_2C=CH_2$, Clar's hydrocarbon,[15] none of which have a Kekulé structure, but all of which have unstrained σ bonds and an even number of π electrons. As might be expected, all three of these also have a triplet ground state on the basis of the free-electron model calculations.

The lowest *bound valence* in the cata-condensed ring systems considered here was found in pentacene, which agrees with the observation that the higher members of the polyacene series are not only highly unstable, but progressively more unstable.

A COMPARISON WITH THE LCAO MODEL

A general statement can be made concerning the comparison of the LCAO model of Coulson and Longuet-Higgins and the free-electron model on the basis of the calculations carried out here; namely, that the free-electron model predictions are equivalent to or slightly better than the LCAO results. The superiority is slight and may not be real.

The accuracy of the predictions of spectra seems to be about equal, particularly when the center of gravity of the singlet and triplet lines are considered. This equality actually is in favor of the free-electron model, since (in the present calculations) no parameter has been varied in order to give optimal fit, whereas in the LCAO calculations at least one of the available parameters has been freely adjusted to give optimal fit.

The *relative* bond densities in any series of related bonds are both qualitatively and quantitatively reproduced with amazing fidelity in the two theories, despite their divergent approaches. Figure 5 shows the LCAO bond orders[8] plotted against the free-electron bond densities, both to the same scale. The points closely align themselves, according to broad generalizations of bond type (terminating in two joints; terminating in

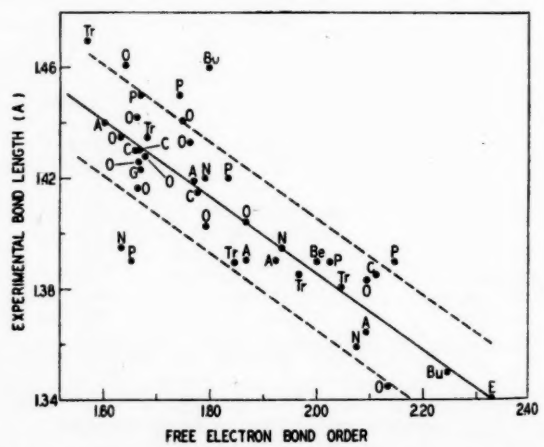

FIG. 4. This curve shows the relationship between the calculated total mobile bond density and the experimental data that is available. A, anthracene; Be, benzene; Bu, butadiene; C, coronene; G, graphite; N, naphthalene; O, ovalene; P, pyrene; Tr, triphenylene; and E, ethylene.

[13] See for example, C. A. Coulson and G. S. Rushbrooke, Proc. Cambridge Phil. Soc. **36**, 193 (1940), p. 198.

[14] H. C. Longuet-Higgins, J. Chem. Phys. **18**, 265 (1950).

[15] E. Clar, *Aromatische Kohlenwasserstoffe* (Verlag. Julius Springer, Berlin, 1941), p. 311. This hydrocarbon consists of six benzene rings, peri-condensed into an equilateral triangle.

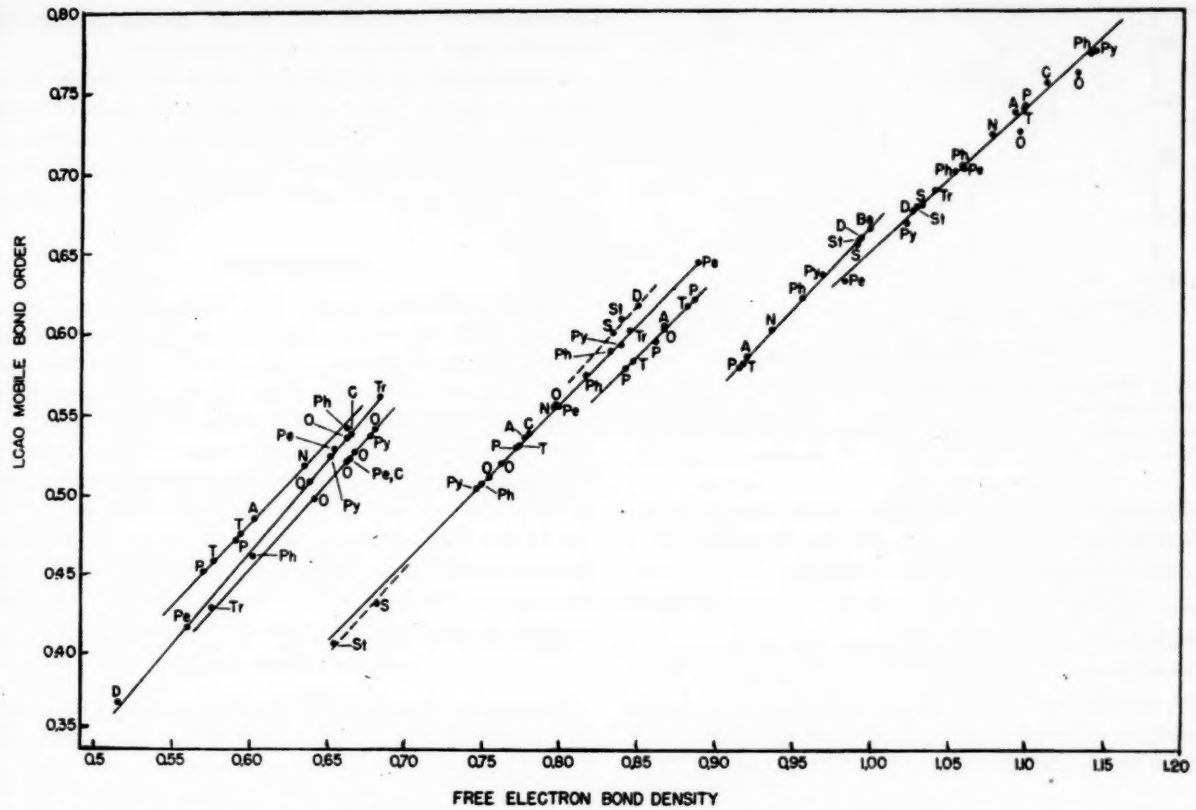

FIG. 5. These curves indicate the close correspondence of the free-electron model and the LCAO model calculated bond densities (orders) for alternant molecules; both coordinates to the same scale. A, anthracene; Be, benzene; C, coronene; D, diphenyl; N, naphthalene; O, ovalene; P, pentacene; Pe, perylene; Ph, phenanthrene; Py, pyrene; S, stilbene; St, styrene; T, tetracene; and Tr, triphenylene.

one joint, etc.), on lines whose slopes are very close to unity. The deviations of the points from these straight lines rarely exceeds 0.02 density unit, much too small to be decisive in comparisons with experiment. However, there do exist certain differences which can be subjected to experimental test; whenever a point on a left-lying line is higher than a point on a right-lying line (of Fig. 5), then the relative bond lengths of the bonds involved are reversed in the two theories. Such pairs of points will be particularly decisive when they include bonds from the *same* molecule. The present experimental data are not precise enough to differentiate and could only permit such comparisons to indicate a trend.

TABLE VI. A comparison of the predictions of bond lengths by the free-electron model and the LCAO model.

Molecule	Root mean square deviations (A) Free-electron model	LCAO model[a]
Benzene	0.004	0.004
Naphthalene	0.023	0.025[b]
Anthracene	0.008	0.013
Pyrene	0.025	0.025
Triphenylene[c]	0.015	0.020
Coronene	0.007	0.014
Ovalene	0.014	0.016
Graphite	0.009	0.010
Ethylene	0.000	0.000
Butadiene		
2—3 bond	0.004	0.000
1—2 bond	0.046	0.016
All molecules except polyenes	0.016	0.018
All molecules	0.017	0.018

[a] These numbers were calculated by the present author, mainly from the data of reference 11.
[b] It should be noted that the often quoted value of 0.018 for this molecule (see references 9, 11, and 16) refers, not to Coulson's plot (reference 9) but to a special, less general curve from reference 16, which has been heavily weighted in favor of this molecule and a few others.
[c] Klug, Acta Cryst. 3, 165 (1950).

Nevertheless, in predictions of bond lengths based on these electron densities the free-electron model is *consistently* superior. In the important case of the naphthalene molecule, important because of the high degree of precision claimed for the x-ray investigation, both models give unsatisfactory predictions. The root-mean-square deviations for this molecule are: free-electron model 0.023A; LCAO 0.025A. It has been pointed out in Table VI that the LCAO root-mean-square deviation of 0.018A claimed[9,11,16] for the LCAO predictions of the bond lengths in this molecule is obtained, not from Coulson's graph,[9] but from a special graph[16] which heavily weights the naphthalene, the anthracene, and the graphite predictions. These very poor root-mean-square deviations are directly attributable to their

[16] Coulson, Daudel, and Robertson, Proc. Roy. Soc. (London) **A207**, 306 (1951).

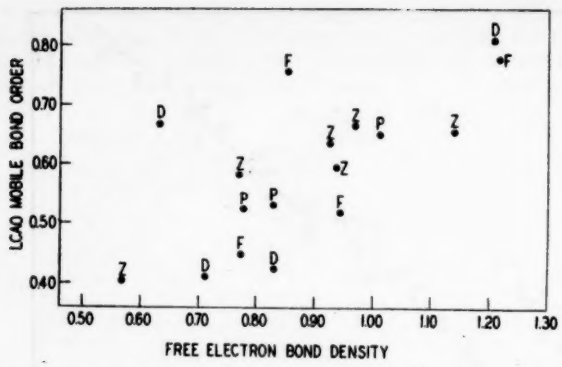

FIG. 6. This plot shows the lack of correspondence of the free-electron model and the LCAO model calculations of the bond densities (orders) for nonalternant molecules; both coordinates to the same scale. D, difulvene; F, fulvene; P, pentalene; Z, azulene.

(almost identically) poor prediction of the length of the cross-linked bond.[17] As has been discussed elsewhere[11,16] it is this particular bond which is subject to an experimental error about twice those of the other three bonds in naphthalene.

There is a possible fruitful field of comparison of bond length predictions. As can be clearly seen in Fig. 6, the predictions of bond lengths in the odd-membered ring systems by the two theories are widely divergent. Even comparatively rough bond length measurements on azulene would suffice for a discrimination.[18]

A comparison of the physical labor involved in solving molecular problems by the two methods is difficult to make. The time involved for a complete calculation on one molecule ran from one minute for the polyenes through four and a half hours for pentacene to six days for ovalene.

CONCLUSION

The free-electron model has been shown to be a versatile and respectable tool for use in the investigation of molecular structure. It is capable of extension to other systems of interest than those considered here and seems to be capable of extension to include electron interaction; it deserves more attention than has hitherto been given to it. It seems quite reasonable to expect that the theory may be refined to the same degree as the LCAO model theory. On the other hand, the free-electron model seems to have the same limitations and inaccuracies that the LCAO method has, and further its present treatment of polyenes is unsatisfactory.

ACKNOWLEDGMENT

The author would like to thank Professor J. R. Platt for suggesting this problem, and for his continued and helpful interest.

APPENDIX: ILLUSTRATION OF THE METHOD: NAPHTHACENE

Matrix Formulation

The naphthacene molecule has V_h symmetry; expressed in terms of Cartesian coordinates the symmetry species are SS, SA, AS, AA [where the letters refer to the behavior (symmetric or antisymmetric)] upon reflection at XY and YZ planes, respectively. See Fig. 2.

In the case of SS symmetry

$$\left.\begin{aligned}&\phi(1)=\phi(4)=\phi(5)=\phi(8),\\&\phi(2)=\phi(3)=\phi(6)=\phi(7),\\&\phi(9)=\phi(10)=\phi(11)=\phi(12),\\&\phi(1,12)=\phi(4,11)=\phi(5,10)=\phi(8,9),\\&\phi(9,12)=\phi(10,11),\end{aligned}\right\} \tag{A.1}$$

[where $\phi(r,s)$ designates the value of the wave function at the joint atom located between atoms r and s, and is to be distinguished from $\phi(r-t)$, the value of the wave function at bond $r-t$.] Hence, there are only five independent variables. If we write the secular equations [I, Eq. (2.44), (2.45), (2.46)], keeping the relations of (A.1) in mind, we arrive at

$$\left.\begin{aligned}(-3\cos\kappa+1)\phi(9,12)+\;2\phi(12)&=0\\\phi(9,12)-2\cos\kappa\phi(12)+\;\phi(1,12)&=0\\\phi(12)+(1-3\cos\kappa)\phi(1,12)+\;\phi(1)&=0\\\phi(1,12)-2\cos\kappa\phi(1)+&=0\\\phi(1)+(1-2\cos\kappa)\phi(2)&=0\end{aligned}\right\}. \tag{A.2}$$

[17] The value predicted by both models is about 1.437A, which value seems to be more reasonable, on the basis of a comparison with the similar bond in anthracene (1.440A) than the experimental value (1.395A) of reference 11.

[18] Dr. Heilbronner (E. T. H., Zurich) has kindly supplied the author with some advanced tentative results of electron diffraction measurements made on the azulene molecule, which indicate that the cross-linked bond in azulene is about 1.45A. Free-electron model prediction 1.446A; LCAO, from reference 9, greater than 1.49; LCAO from reference 16, about 1.45.

By similar considerations, we can write for *AS* symmetry

$$\left.\begin{aligned}
-(1+3\cos\kappa)\phi(9,12)+\quad 2\phi(12) &= 0\\
\phi(9,12)-2\cos\kappa\phi(12)+\quad \phi(1,12) &= 0\\
\phi(12)+(1-3\cos\kappa)\phi(1,12)+\quad \phi(1) &= 0\\
\phi(1,12)-2\cos\kappa\phi(1)+\quad \phi(2) &= 0\\
\phi(1)-(1+2\cos\kappa)\phi(2) &= 0
\end{aligned}\right\}. \tag{A.3}$$

For *SA* symmetry,

$$\left.\begin{aligned}
\phi(9,12)=\phi(10,11) &= 0\\
-2\cos\kappa\phi(12)+\quad \phi(1,12) &= 0\\
\phi(12)+(1-3\cos\kappa)\phi(1,12)+\quad \phi(1) &= 0\\
\phi(1,12)-2\cos\kappa\phi(1)+\quad \phi(2) &= 0\\
\phi(1)+(1-2\cos\kappa)\phi(2) &= 0
\end{aligned}\right\}. \tag{A.4}$$

For *AA* symmetry,

$$\left.\begin{aligned}
\phi(9,12)=\phi(10,11) &= 0\\
-2\cos\kappa\phi(12)+\quad \phi(1,12) &= 0\\
\phi(12)-(1+3\cos\kappa)\phi(1,12)+\quad \phi(1) &= 0\\
\phi(1,12)-2\cos\kappa\phi(1)+\quad \phi(2) &= 0\\
\phi(1)-(1+2\cos\kappa)\phi(2) &= 0
\end{aligned}\right\}. \tag{A.5}$$

The Eigenvalues

From this point on we will discuss only the symmetry *SS*. From (A.2) we obtain the following secular equation:

$$\left.\begin{vmatrix}
(1-3\cos\kappa) & 2 & & & & \\
1 & -2\cos\kappa & 1 & & & \\
 & 1 & (1-3\cos\kappa) & 1 & & \\
 & & 1 & -2\cos\kappa & 1 & \\
 & & & 1 & (1-2\cos\kappa) &
\end{vmatrix}=0\right\}, \tag{A.6}$$

giving

$$-72(\cos\kappa)^5+84(\cos\kappa)^4+34(\cos\kappa)^3-48(\cos\kappa)^2-3\cos\kappa+5=0$$

or

$$(\cos\kappa-1)[72(\cos\kappa)^4-12(\cos\kappa)^3-46(\cos\kappa)^2+2\cos\kappa+5]=0.$$

(In the absence of free end points, the solution $\cos\kappa=1$ can be anticipated for *SS* symmetry.) The solutions of (A.6) are given in Table I for the *SS* orbitals. The negatives of these roots are the roots of the *AS* symmetry secular equation.

Wave Function Obtained via the Eigenvectors

The secular equation (A.2) may now be solved, for each eigenvalue, to give the *relative* values of the eigenvectors. Application of the normalization condition [I, Eq. (2.34)] fixes their *absolute* values.

Thus

$$\left.\begin{aligned}
\phi(2)&=(-1+2\cos\kappa)^{-1}\phi(1),\\
\phi(1,12)&=[2\cos\kappa-(-1+2\cos\kappa)^{-1}]\phi(1),\\
\phi(12)&=\{(-1+3\cos\kappa)[2\cos\kappa\\
&\qquad -(-1+2\cos\kappa)^{-1}]-1\}\phi(1),\\
\phi(9,12)&=2\{(-1+3\cos\kappa)[2\cos\kappa-(-1\\
&\qquad +2\cos\kappa)^{-1}]-1\}(-1+3\cos\kappa)^{-1}\phi(1),
\end{aligned}\right\} \tag{A.7}$$

and

$$4\phi^2(1)+4\phi^2(2)+4\phi^2(12)+4(3/2)\phi^2(1,12)+2(3/2)\phi^2(9,12)=1. \tag{A.8}$$

For example, for the eigenvalue $\cos\kappa=1$

$$\phi(r)=\phi(1) \text{ for all } r,$$
$$\phi^2(1)=1/21=0.04762.$$

For the eigenvalue, $\cos\kappa=0.79002$,

$$\phi(1)=\phi(1),$$
$$\phi(2)=1.7240\phi(1),$$
$$\phi(1,12)=-0.1440\phi(1),$$
$$\phi(12)=-1.1973\phi(1),$$
$$\phi(9,12)=-1.7478\phi(1),$$

and from (A.8)

$$\phi^2(1)=0.03235, \quad \phi(1)=\pm 0.1799.$$

If we arbitrarily select $\phi(1)$ to be positive, all the other eigenvectors are uniquely determined. We may now find the value of the wave function at the midpoint of a bond from Eq. (3a). We can find a_B and δ_B from the considerations of I, Eq. (2.21)–(2.30) and the accompanying text; of a_B^2 and $\tan\delta_B$ (the quantities listed in Tables II and III) from Eq. (3b) and (3c), and a_B and δ_B from these. Since $\pi/2\geq\delta_B>-\pi/2$, we obtain, for

example, for $\cos\kappa = 0.79002$,

$$\left.\begin{aligned}\delta_1 &= 0,\\ \delta_2 &= 0.8296,\\ \delta_3 &= 0,\\ \delta_4 &= 0,\end{aligned}\right\} \qquad \text{(A.9a)}$$

in radians. Hence, $0.1799 = \phi(1) = a_1 \cos(3\kappa/2) = 0.5488$, etc., so that one finds

$$\left.\begin{aligned}a_1 &= 0.3278,\\ a_2 &= -0.3189,\\ a_3 &= -0.0274,\\ a_4 &= -0.3323.\end{aligned}\right\} \qquad \text{(A.9b)}$$

Wave Function Obtained via the Joint Conditions

This method works without excessive labor if the molecule is small and/or there is enough symmetry to supplement it. Consider the case in question (*SS* symmetry). Here $\delta_1 = \delta_3 = \delta_4 = 0$, since we have chosen our branch origins to lie on the symmetry axis. (If the axis had been an *A* axis, we would have $\delta_B = \pi/2$.) There remains δ_2 to be determined. We write, e.g., at the joint atom (9,12) the boundary conditions

$$-2\tan(-\kappa+\delta_2)+\tan(\kappa/2)=0, \qquad \text{(A.10a)}$$

$$a_2\cos(-\kappa+\delta_2)=a_4\cos(\kappa/2). \qquad \text{(A.10b)}$$

By use of

$$\tan(\kappa x_B+\delta_B) = (\tan\kappa x_B+\tan\delta_B)/(1-\tan\kappa x_B\tan\delta_B), \qquad \text{(A.11)}$$

Eq. (A.10a) is transformed from a *transcendental* equation in δ_2 into an *algebraic* equation in $\tan\delta_2$, which is readily solved to yield the value in (A.9a). By virtue of (A.11), the system of joint conditions is, in all cases, equivalent to a system of algebraic equation.

The values of the δ_B, when substituted into the equations of the type (A.10b), readily determine the *ratios* of the a_B's. The normalization condition I, Eq. (2.7) then gives the *absolute* values listed in (A.9b).

The value of the wave function at any point is now easily found, e.g.,

at atom 12: $\phi(12) = a_2\cos\delta_2$,

at atom 9,12: $\phi(9,12) = a_2\cos(-\kappa+\delta_2) = a_4\cos(\kappa/2)$,

at bond 9,12−12: $\phi(9,12-12) = a_2\cos(-\kappa/2+\delta_2)$.

Use of Tables I, II, and III for the Construction of the Wave Functions

The δ_B's may be obtained from the $\tan\delta_B$'s, listed in Table III. The signs of the δ_B's are the same as the signs of the $\tan\delta_B$'s [See I, Eq. (2.11)]. The magnitudes of the a_B's are the square roots of the a_B^2's listed in Table II. We arbitrarily choose one of the a_B (say a_1) to be positive. To find the sign, of a_2, we write the continuity condition I, Eq. (1.32) or (2.4), at atom (1,12):

$$a_1\cos 5\kappa/2 = a_2\cos(\kappa+\delta_2).$$

The *signs* of the cosines determine the sign of the a_2. We may then consider (A.10b) to find the sign of a_4, etc. . . .

Convenient checks on the calculations are provided by I, Eqs. (2.43), (2.89), and (2.90).

Free-Electron Network Model for Conjugated Systems. III. A Demonstration Model Showing Bond Order and "Free Valence" in Conjugated Hydrocarbons*

JOHN R. PLATT
Laboratory of Molecular Structure and Spectra, Department of Physics, University of Chicago, Chicago, Illinois
(Received December 30, 1952)

A mechanical model of a conjugated hydrocarbon has been constructed, based on the free-electron density theorems of Ruedenberg and Scherr. Stiff steel music wires strung on dowels above a baseboard follow the carbon skeleton. When the height of the wire above the board at each atomic position is fixed to constant theoretical values, and when simple boundary conditions are met at branch points and terminal atoms, then the height in the centers of bonds is a direct measure of electron density and bond order and "free valence." The measured heights may be used to predict bond lengths and positions of substitution, even for large or unsymmetrical molecules which are hard to handle theoretically. The model should be especially useful for demonstrations and for giving students a feeling for electronic behavior in conjugated systems.

RUEDENBERG and Scherr have shown that in the free-electron model of a conjugated hydrocarbon the electron densities at the carbon atoms are one electron per bond for each carbon atom with two carbon neighbors and two-thirds of an electron per bond for each carbon atom having three carbon neighbors.[1] The electron-density function is a smooth, continuous function with continuous first derivatives along the conjugated chain between any two branch points. Its maxima are approximately two bonds apart, and its minima approximately the same distance apart.

It is natural to think of representing this density function by a wire model which will pass through the values $\frac{2}{3}$ at the branch points, and 1 at the other points, and which will therefore show the same oscillating maxima and minima as is shown by the correct solutions of the free-electron model. A demonstration model has therefore been constructed for representing free-electron densities in conjugated systems as shown in the photograph of Fig. 1. The wire passes loosely through hooks in the tops of wooden dowels representing the carbon atoms. The dowels fit into holes in a board in the proper geometrical arrangement outlining the planar carbon skeleton. Wherever there is a joint carbon with three carbon neighbors, the wires are passed into small brass washers which hold the three wires meeting at a joint at angles of 120° apart and also hold the ends of the three wires in a plane. This mechanism imposes the proper "Kuhn condition" on the three derivatives of the density function at the joint as discussed by Ruedenberg and Scherr.

The dowels at the joints are adjusted up or down until the tops of the wires meeting at the joint would intersect at a point $66\frac{2}{3}$ mm above an arbitrary base line. The wires passing through the tops of the other dowels are adjusted to be 100 mm above the arbitrary base line. At the end of a polyene chain, or a ring-chain system, the wires are brought down to the arbitrary base line itself at a distance of 1 bond length beyond the terminal atom. They are made tangent to the base line at this point, to make the derivative zero as in the electron density function itself.

The horizontal bending of the wire to fit into ring hexagons or zigzag chains is in first approximation independent of the vertical bending as long as both bendings are comparatively small. The horizontal bending can therefore be ignored when measurements are being made on the vertical height.

It can be seen from Fig. 1 that this model gives a useful qualitative and even semiquantitative representation of the variation of electron densities from bond to bond in a conjugated system. The alternating maxima and minima of hexatriene in Fig. 1, for example, correspond exactly to the alternating single and double bonds of the traditional representation of this molecule. The correspondence extends to smaller details, such as the higher maxima in the end bonds than in the center bond, corresponding to higher electron densities in these bonds as given by Scherr,[2] and to the traditional expectation of more double-bond character in the end bonds.

In stilbene, the strength of the central bond is clearly represented by the wires, as well as the strength of the

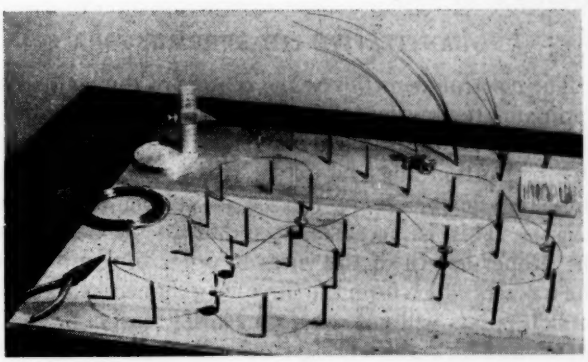

FIG. 1. Demonstration model showing naphthalene, stilbene, and hexatriene.

* This work was assisted in part by the Office of Ordnance Research under Project TB2-0001 (505) of Contract DA-11-022-ORD-1002 with The University of Chicago.

[1] K. Ruedenberg and C. W. Scherr, J. Chem. Phys. **21**, 1565 (1952).

[2] C. W. Scherr, J. Chem. Phys. **21**, 1582 (1953).

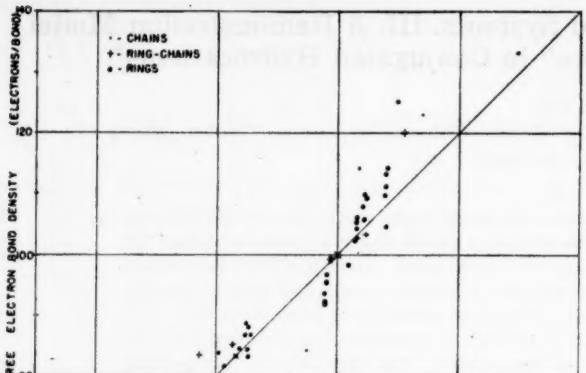

FIG. 2. Comparison of electron densities determined from the wire model with those given by the free-electron theory.

two side bonds in the ring which correspond to a quinone type of structure. The weakness of the bonds adjacent to the central bond is also seen. In the wire model as in the free-electron calculations, all bonds adjacent to a branch point will be weak, and bonds between two branch points will be especially weak. This is clearly seen in naphthalene, where the central bond has the lowest electron density. The corner bonds in naphthalene have the highest electron density corresponding to the highest bond order in the usual Pauling model of this molecule. The end bonds are slightly weaker than the corner bonds.

It is clear that this model is useful only for those molecules and for those conditions given by Ruedenberg and Scherr, that is to say, for alternant hydrocarbons (even-ring hydrocarbons) with a singlet ground-state. Whether it can be adapted in any way to the representation of heterocyclics or substitutional perturbations remains to be seen.

QUANTITATIVE MEASUREMENTS

The electron densities at the centers of the bonds are approximated by the heights of the wires at the centers. These can be measured by a vertical millimeter scale. One precaution must be taken. If the wire used is too thin and flexible there will be an ambiguity in the heights. This is because it is difficult to determine the proper length of the wires in order to assure that the washers which form the three-way connections at the branch points will not exert tangential tension or compression. Thick stiff spring steel wire must be used as described in Appendix I.

It is easy to set the heights of the wire at the dowels to the proper value within 0.2 mm, corresponding to 0.002 density unit on the model described here. The heights at the centers of the inner $(J-J)$ and outer $(O-O)$ bonds can then be measured with a mean deviation of ± 0.5 mm. The total spread of values in the same bonds on independent setups is never more than 2 mm for these bonds. The total spread for the meso $(J-O)$ bonds is up to 3 mm, because these bonds are especially sensitive to the slope and freedom from mechanical constraint of the connecting washers and to the shaping of the ends of the wires where they fit into these washers. Since the heights in bonds encountered in condensed ring systems lie between 55 mm and 111 mm above the base line, these variations are comparatively small, and useful measurements may be made of the heights in spite of them.

The agreement between the measured heights and the electron densities determined from the free-electron calculations of Scherr is shown in Fig. 2. The mean deviation between the measured and calculated values for ring systems is ± 0.04 density unit. There is a general tendency in the outer and meso bonds for the maxima and the minima of the wire to be less marked than the maxima and the minima in the free-electron calculations. The wires used here had some permanent curvature or "set," and consequently the maxima and minima in the short wires of the inner bonds tend to be more marked than given by theory. If wires are used which are free from permanent set, the heights of all bonds should approach the theory more closely. Alternatively, one might use longer wires which will exaggerate the maxima and the minima, especially in the outer bonds. The larger set of wire lengths suggested in Appendix I gives moderately good agreement with the free-electron model for the outer bonds and some improvement in the agreement for the meso and inner bonds. This increase in length introduces again a certain ambiguity in heights since they are now very sensitive to length as mentioned above.

One may also make empirical corrections to the observed values for a particular model. With the model of Figs. 1 and 2, if the measured deviations of the outer bonds from 1.000 and of the meso bonds from 0.833 are doubled systematically, the resulting "corrected" values agree with the free-electron theoretical values for ring systems with a mean deviation of ± 0.028 density unit.

The correlation between the uncorrected heights of the wires and the bond lengths as measured by Robertson's group by x-ray methods in ten molecules is shown in Fig. 3. It is obvious that the wire model is useful for predicting bond lengths in molecules such as benzperylene which are difficult to calculate by traditional molecular-orbital or valence-bond methods.

The fit with Robertson's data is about as good as the fit of Coulson's "mobile bond order"[3,4] with those data. There are three additional compounds included in Fig. 3 which were not included on Coulson's curve, and which increase the spread of the measurements

[3] C. A. Coulson, Proc. Roy. Soc. **A207**, 91 (1951).
[4] C. A. Coulson, J. Phys. Chem. **56**, 311 (1952).

especially on the inner bonds. They would increase the scatter on Coulson's plot in much the same way.

The accuracy of prediction in Fig. 3 and in Coulson's diagrams is limited by the estimated experimental error of the x-ray measurements, about ± 0.02A and not by the accuracy of the wire model or the theoretical calculations. In fact, the x-ray precision is so poor that it would be almost as good to take a single fixed value of the bond length for each bond type: 1.430A for the inner bonds; 1.411A for the meso bonds; and 1.382A for the outer bonds. This fits the data with a mean deviation of ± 0.015A, which is as good as the fit to Coulson's calculations, or to the wire heights. No really definitive test of the present method, or the free-electron model, or Coulson's calculations is possible without an improvement of about a factor of 10 in the precision of the x-ray measurements. If and when such precision is achieved, the present method may still be useful for quick predictions, especially for large or unsymmetrical molecules, perhaps with empirical corrections as described above.

The naphthalene bond length of 1.395 ± 0.01A is stated by Robertson to be one of the most accurately determined lengths. It is nevertheless almost 0.05A from the value predicted by the free-electron model, the LCAO MO model, or by the present wire model. Such a discrepancy in a simple molecule is disconcerting; perhaps a remeasurement of this crucial

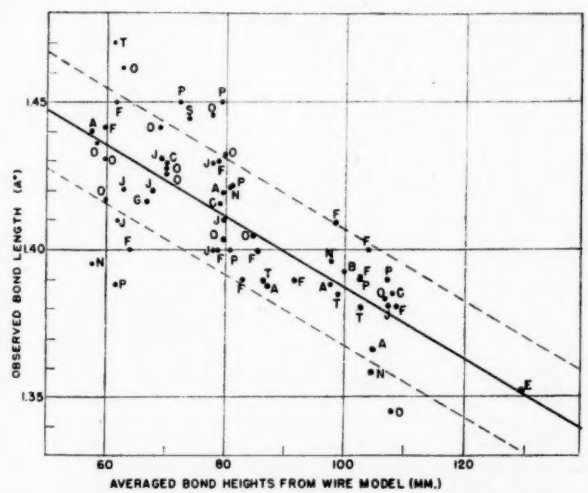

FIG. 3. Relation between densities obtained from wire model and observed bond lengths. *E*—Ethylene: Herzberg, *IR and Raman Spectra* (D. Van Nostrand Company, Inc., New York, 1945), p. 439 (accurate vapor). *G*—Graphite: *Handbook of Chemistry and Physics*, Chemical Rubber Publishing Company, Cleveland, Ohio, 30th ed. (accurate crystal). *B*—Benzene: J. Chem. Soc. **1939**, 1324 (electron diffraction). *S*—Stilbene: Proc. Roy. Soc. (London) **A162**, 568 (1937). *N*—Naphthalene: Acta Cryst. **2**, 238 (1949). *A*—Anthracene: Acta Cryst. **3**, 251 (1950). *T*—Triphenylene: Klug, Acta Cryst. **3**, 165 (1950). *F*—Dibenzanthracene: Acta Cryst. **1**, 101 (1948). *P*—Pyrene: Acta Cryst. **1**, 101 (1948). (Most uncertain: ± 0.03A.) *J*—Benzperylene: Acta Cryst. **1**, 101 (1948). J. Chem. Soc. **1948**, 1398. *C*—Coronene: J. Chem. Soc. **1948**, 1398. *O*—Ovalene: Proc. Roy. Soc. (London) **A207**, 101 (1951). (X-ray measurements by Robertson and coworkers estimated accuracy ± 0.02, except as noted.)

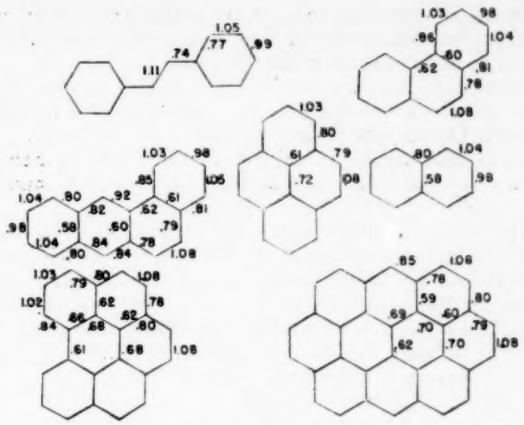

FIG. 4. Typical bond densities from wire model.

bond distance is indicated. If confirmed, this discrepancy would create considerable doubt as to the usefulness of any of these models for predicting bond lengths. They might still be useful for predicting electron densities, since Robertson has pointed out that observed densities agree better than observed bond lengths with the densities or bond orders predicted by theory. The reason for the lack of correlation between observed densities and observed bond lengths is not clear.

The sum of densities in the bonds adjacent to an atom has been called the "bound valence" by Scherr and has been shown to be about as useful for predicting chemical reactivities at different positions in a molecule as the "free valence" of Coulson and co-workers (which is the LCAO counterpart of this density sum, but with a negative sign). This sum can also be obtained from the wire model. In fact, the measured bound valence values have a mean deviation of only ± 0.018 density unit (± 1 percent) from Scherr's theoretical values. This is almost three times as accurate as the individual bond densities obtained from the wire model. Probably the improvement in the density sum comes about because a deviation of the wire height in one direction in one bond produces compensating deviations in the opposite direction in adjacent bonds. The wire model is evidently several times more accurate for predicting second derivatives of the density function than for predicting the first derivatives or the function itself.

Since a difference in bound valence of 0.02 or 0.03 density unit seems to produce an appreciable difference in chemical reactivity, the wire model could evidently be adapted to quantitative reactivity predictions, which would be especially valuable in large or unsymmetrical molecules.

I am indebted to Mr. Ralph Regalbuto for advice and help in constructing the model described here.

APPENDIX. CONSTRUCTION DETAILS OF THE WIRE MODEL

The principal features of construction of the wire model are shown in Fig. 1. The baseboard is a 1 in.×24 in.×40 in. board planed flat and varnished. One-eighth-inch holes are drilled

through this board in an accurate triangular network, with a distance between centers of three inches. A hexagonal network would be usable but less convenient.

The one-eighth-inch dowel rods are 3 in. long. Small hooks bent from fine wire are pushed into their ends to hold the density-wire in place. Dowels representing the joint carbons where three wires come together have a pin or fine wire pushed through them transversely near the middle to hold the brass connecting washers up (or down).

The brass connecting washers are $\frac{1}{8}$ in. thick and $\frac{3}{4}$ in. diameter with a $\frac{5}{16}$ in. hole in the center. In each, three radial holes, 0.043 in. in diameter, are drilled in the median plane at 121° intervals. These hold the three connecting wires which are supposed to meet in a plane at a joint carbon. The holes in the washers are made much larger than the dowels. This allows freedom of motion around the dowels and allows tilting of the washer up to about 45° which is occasionally required.

The wire used to represent the electron-density function is No. 18 steel music wire, 0.040 in. in diameter. ***Caution: Use safety goggles when handling music wire.*** It is convenient to cut a number of pieces of this wire in advance corresponding to various numbers of bonds which will be needed in the wire branches, thus: $2\frac{3}{4}$ in. for a one-bond branch; 6 in. for a two-bond branch; $9\frac{1}{4}$ in. for a three-bond branch; and so on in arithmetic progression. The extra length in the longer bonds makes up approximately for the curvature of the wires in the longer branches, so that these wires exert no tension or compression forces on the brass washers into which the ends are inserted. As mentioned in the text, a better approximation to the free-electron theoretical densities was given by the present wire model when the wires were made somewhat longer so that their maxima and minima are accentuated, thus: $2\frac{3}{4}$ in.; $6\frac{1}{4}$ in.; $9\frac{3}{4}$ in.; and so on. However, the measurements of Fig. 2 were made with the shorter wires.

Objectionable burrs on the ends of the wires which prevent them from slipping easily into the washers may be avoided if the ends are not cut through but are merely dented with wire cutters and then broken square across by being bent back and forth two or three times. Best results are obtained if the one-bond sections are carefully straightened before use; straightening other sections is less important, since the vertical curvatures important for the height measurements are approximately independent of the large horizontal curvatures to which the natural set principally contributes. The No. 18 wires used here are near the largest size that can be used for three-inch spacing between centers on the model and for the vertical scale adopted here of 1 mm = 0.01 electron-density unit. In fact, the two-bond sections were occasionally bent past their elastic limit and took on a permanent set. This of course decreased the agreement of the wire model with the theoretical calculations for bonds adjacent to these two-bond units. A smaller sized wire or a smaller height unit or a larger spacing on the board might be helpful.

For quantitative measurements, a millimeter scale is set vertically in a 4 in. diameter aluminum base as shown in Fig. 1. A slider can be fitted on which is useful for reaching around dowels and into inaccessible places. One edge of the slider must be kept accurately horizontal. The scale in Fig. 1 is about 10 cm high, but its working range is from about the 3 cm to the 7 cm mark.

To adjust the density wire height at non-branch carbons, the slider can be set 100 mm above an arbitrary base line (6 cm above the board is convenient for ring systems) and can be moved from one dowel to another in turn. The height of the density wire at the dowels may be set at the desired value by pushing the dowels up or down with the fingers or with a pair of long-nosed pliers

The heights of the wires at the branch carbons may be set to 66.7 mm above the base line in the same way. The setting is really made on the center of the top or bottom of the connecting washer, making allowance for the washer thickness.

For permanent displays it might be best to paint the wire and the baseboard or other background in contrasting colors. It might also be better to have the models mounted at approximately eye level so that the electron densities in different parts of the model are easily seen as a vertical coordinate.

The Diffusion of Iodine in Carbon Tetrachloride under Pressure

E. W. Haycock, B. J. Alder, and J. H. Hildebrand
Department of Chemistry and Chemical Engineering, University of California, Berkeley, California
(Received April 6, 1953)

The diffusion of iodine in carbon tetrachloride was studied over a temperature range from 10 to 55°C and a pressure range from 1 to 200 atmospheres by the capillary cell technique and by an optical comparison method. The results of the two methods agree well, and the data can be represented by an activation energy at constant pressure of 3300 cal/mole compared to an activation energy at constant volume of 1070 cal/mole.

INTRODUCTION

An understanding of the diffusion mechanism in liquids is fundamental to any comprehensive theory of transport processes occurring in the liquid state. The importance of the diffusion coefficient rests in the fact that it is directly related to the frictional forces which a molecule experiences when it undergoes molecular Brownian motion under the influence of its interacting neighbors. The other important irreversible properties, namely the viscosity and thermal conductivity, have already been related to this frictional force and other equilibrium properties of the liquid in the transport theory presented by Kirkwood.[1]

Any diffusion theory can be tested more critically if it takes full account of the pressure dependence of the diffusion coefficient. The behavior under pressure is particularly important in view of the predictions made on the Eyring[2] picture, where the volume available to the system of molecules plays a significant role. Thus, pressure experiments were undertaken to see how the diffusion coefficient would behave at constant total volume. With this same end in mind other investigators[3] have already studied viscosity and thermal conductivity as a function of pressure.

From a theoretical viewpoint the simplest system to study would be the self-diffusion in a liquid consisting of a condensed rare gas, because of their spherically symmetric force fields, but because of the short and inconveniently located temperature range of the monatomic liquids, carbon tetrachloride was chosen as conforming reasonably well to the monatomic model. Because of the lack of any quantitative data on diffusion under pressure, it was necessary to check upon the experimental techniques and accuracies, and thus the simpler system of iodine diffusing in CCl_4 was studied preliminary to a study of self-diffusion in CCl_4.

APPARATUS AND PROCEDURE 1

Of the various methods available for the study of diffusion in liquids the capillary cell technique, previously described by Anderson and Saddington,[4] was chosen for this investigation since this method could be readily adapted for use at moderately elevated pressures. In this procedure capillary cells containing the diffusate are submerged in a relatively large (assumed infinite) volume of the diffusent, and the total amount of diffusate transferred in a given time is measured. In all previous experiments of this type the diffusion process has been followed by means of tracer techniques. Throughout the course of this research however, the use of cells somewhat larger than those previously employed has enabled the concentration changes to be measured by chemical microanalytical methods.

The experiments at atmospheric pressure were carried out in an all-glass apparatus similar to that described by previous workers.[5] Accurately calibrated capillary cells, ranging in length from 6 to 7 cm and each having a capacity of approximately 0.25 cc, were supported in a liter reservoir of CP CCl_4, which was thermostated to ±0.02°C. With the tops of the capillary cells just above the surface of the liquid in the reservoir, the system was first allowed to reach temperature equilibrium. The cells were next filled with a 10 mg/cc solution of iodine in CCl_4, which was at the same temperature as the liquid in the reservoir, and then carefully lowered beneath the CCl_4 surface. Diffusion was allowed to proceed for approximately three days. The cells were then removed and their iodine concentration was determined, with an accuracy of 1 percent, by the standard microanalytical procedure described by Pregl.[6] A layer of granulated zinc at the bottom of the reservoir kept the concentration of iodine in the CCl_4 practically at zero, thus enabling it to be used for a large number of experiments.

Experiments were carried out at pressures up to 200 atmospheres in the apparatus shown schematically in Fig. 1. The capillary cells were held in a brass stand which was supported by means of metal spring clips in an iron pressure bomb of standard design. The bomb, which had an internal capacity of 430 cc, was mounted so that it could be held above or immersed below the surface of an oil bath which was thermostated to ±0.01°C. The pressure seal was made by compressing the Teflon ring (A) between the coverplate (B) and the

[1] J. G. Kirkwood, J. Chem. Phys. **14**, 180 (1946).
[2] Glasstone, Laidler, and Eyring, *Theory of Rate Processes* (McGraw-Hill Book Company, Inc., New York, 1941).
[3] (a). See A. Bondi, J. Chem. Phys. **14**, 591 (1946). (b) A. Uhlir, Jr., J Chem. Phys. **20**, 463 (1952).
[4] J. S. Anderson and K. Saddington, J. Chem. Soc. S 381 (1949).
[5] See reference 4 and also J. H. Wang, J. Am. Chem. Soc. **72**, 510 (1951).
[6] F. Pregl, *Quantitative Organic Microanalysis* (revised and edited by Grant) (The Blakiston Company, Philadelphia, 1946).

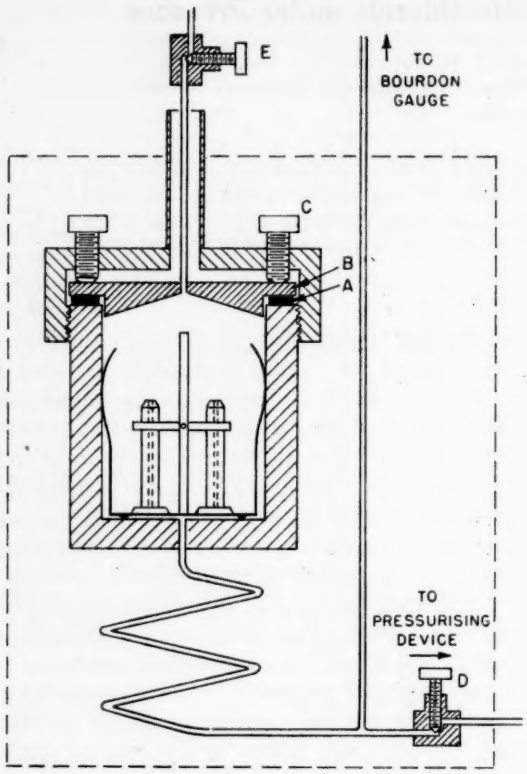

FIG. 1. Diagram of apparatus for the study of diffusion under pressure.

rim of the bomb by means of eight symmetrically placed steel bolts (*C*). Pressures up to 65 atmospheres were applied via the needle valve (*D*) by means of a compressing plunger (not shown), and pressures up to 200 atmospheres were obtained from a cylinder of compressed air which was connected to the system through a reservoir of CCl_4. Pressures were measured on an air thermostated "Heise Bourdon Laboratory Test Gauge," which was calibrated so that it could be read to ±1 psi. All connecting leads were of stainless steel capillary tubing. The system was such that it could be completely filled with CCl_4.

The procedure adopted to carry out an experiment was as follows: With the rim of the bomb held just above the level of the oil bath, the capillary cells were allowed to achieve temperature equilibrium as in the experiments at one atmosphere. The cells were then filled with iodine solution, which was at the same temperature as the thermostat, and lowered beneath the CCl_4 surface. The coverplate of the bomb, which had been previously heated to the temperature of the thermostat, was then placed in position and the pressure seal made. While this operation was being performed, the conical cavity in the coverplate and the capillary tube leading to the needle valve (*E*) were filled with CCl_4, which was introduced through valve (*D*) by slowly turning the pressurizing plunger. The needle valve (*E*) was then closed and the system pressurized, whereupon valve (*D*) was closed and the bomb carefully lowered into the oil bath. The loading operation took approximately ten minutes and complete temperature and pressure equilibrium was established within thirty minutes. Diffusion was allowed to proceed for approximately three days, whereupon the pressure was released and the iodine content of the cells determined as in the experiments at one atmosphere.

EXPERIMENTAL RESULTS

The integral diffusion coefficients were calculated using the relationship[7]

$$\frac{C_{Av}}{C_0}=\frac{8}{\pi^2}\sum_{n=0}^{\infty}\left[\frac{1}{(2n+1)^2}\exp\left[\frac{-(2n+1)^2\pi^2Dt}{4L^2}\right]\right], \quad (1)$$

where C_{Av} is the average concentration of iodine in the capillary cell after time t, C_0 is the initial concentration of iodine in the capillary at zero time, L is the length of the cell, and D is the integral diffusion coefficient. Five cells were used for each experiment and two experiments were carried out at each temperature; hence each reported diffusion coefficient is a mean of ten results.

The integral diffusion coefficient of iodine from a 10 mg/cc solution in CCl_4 into pure CCl_4 was studied over a temperature range of 10 to 55°C and over a pressure range of 1 to 200 atmospheres. The experimental results are given in Table I and are shown graphically in Fig. 2. The solid lines represent the curves obtained by plotting $\log D$ *vs* $1/T$ at 1, 65, and 200 atmospheres. These are linear over most of the range studied but there is some evidence of curvature in the higher density region as the solid phase is approached. The linear portions of these curves can be expressed by the following empirical equations:

$$1 \text{ atmos}, \quad D=338.2\exp(-1662/T)$$
$$65 \text{ atmos}, \quad D=311.7\exp(-1662/T)$$
$$200 \text{ atmos}, \quad D=277.5\exp(-1662/T),$$

where D has the units of cm^2/day. The broken lines il-

TABLE I. Values of the diffusion coefficient.

$P=1$ atmos T°C	$D^{(b)}$ cm^2/day	$P^a=65$ atmos T°C	$D^{(b)}$ cm^2/day	$P^a=200$ atmos T°C	$D^{(b)}$ cm^2/day
10.2	0.95	14.0	0.91	18.6	0.88
17.0	1.12	22.0	1.09	31.5	1.19
25.1	1.25	27.0	1.19	50.7	1.65
31.0	1.45	35.2	1.44		
37.8	1.59	42.6	1.64		
43.3	1.79	50.1	1.84		

[a] In the actual experiment the elevated pressures were not always exactly at the pressures given, and the values of D have been corrected to the pressure indicated by linear interpolation.

[b] The mean values of 5 determinations by two experiments had a maximum deviation of 2.5 percent, while in individual determinations the maximum deviation was as large as 5 percent from the mean.

[7] H. S. Carslaw and J. C. Jaeger, *Conductivity of Heat in Solids* (Oxford University Press, London, 1947), p. 79.

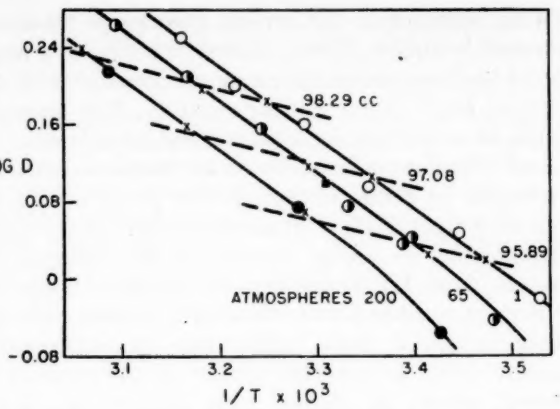

FIG. 2. Temperature dependence of the diffusion coefficient of iodine in carbon tetrachloride as a function of pressure.

lustrate the temperature coefficient of diffusion at the constant molar volumes of 95.89 cc, 97.08 cc, and 98.29 cc. These lines have been calculated assuming the compressibility of the iodine solution to be the same as that of pure CCl_4.[8] The experimental activation energy, E_v, determined from these constant volume lines is 1070 cal/mole compared to 3300 cal/mole for E_p, the activation energy at constant pressure. Both E_v and E_p were constant, within experimental errors, over the range studied.

The maximum deviation from the curves drawn is 3 percent. Such deviations arise from the fact that the iodine content of the cells after diffusion could not be estimated to better than 1 percent. In the experiments at elevated pressures the initial compression of the iodine solution in the capillary cells results in an increase in concentration of the iodine solution and a shortening of the diffusion path. In the case of the 200 atmos experiments, where these effects are greatest, the decrease in volume of the solutions in the cells is approximately 2 percent. The errors introduced by neglecting these effects when calculating the diffusion coefficients from Eq. (1) are, however, somewhat offset by errors of opposite sign, which are inherent in the experimental procedure. These include the turbulence effects occurring when the cells are lowered into the reservoir and the diffusion which takes place at one atmosphere between the time the cells are lowered and the time at which the system is pressurized. The estimated over-all errors incurred from these effects are smaller than the errors arising from the inaccuracy of the determination of the iodine concentration.

APPARATUS AND PROCEDURE 2

In order to check upon the accuracy of the experimental procedure used in the above determination, the depression of the diffusion coefficient by the application of 65 atmos pressure was also measured by a more direct optical comparison method. Two capillary tubes, approximately 40 cm in length and of equal internal diameter (0.2 cm), were sealed at one end and supported side by side in a water bath thermostated to 0.01°C. One tube was left open to the atmosphere and the other could be connected, by means of a metal to glass pressure seal,[9] to a pressurizing device similar to that used in the previous experiment. Pressures were again measured with a Heise Bourdon gauge. An interface was set up simultaneously in both tubes between an iodine solution at the bottom of the tubes and pure CCl_4 at the top. A sharp interface was achieved by lowering a glass hair capillary until its end was below the diffuse interface initially formed and slowly withdrawing liquid. Upon pressurizing the one capillary tube the two interfaces could be quickly adjusted such that they were at the same level on a centimeter scale which was supported between the two tubes. Diffusion was allowed to proceed for 7 to 10 days until diffusion gradients of approximately 20 cm in length were obtained. A screen with two adjustable vertical slits was mounted in front of the tubes, and the system was uniformly illuminated from behind. A series of photographs were then taken, and the density gradients obtained on the photographic negatives were analyzed using a Zeiss microdensitometer. Equal densities on the negatives correspond to equal concentrations in the capillary tubes. The depression of the diffusion coefficient could then be calculated using the expression

$$D_1/D_{65} = (h_1/h_{65})^2, \qquad (2)$$

where h_1 and h_{65} are the distances from the original interface at which equal densities are measured on the two negatives. Using a value of D_1 obtained at one atmosphere from the first experimental procedure,

TABLE II. Determination of the diffusion coefficient from the optical comparison method.

Density (arbitrary units)	h_1 (cm)	Temp. = 29.3°C h_{65} (cm)	$\frac{D_{65}}{D_1}$
3	6.78	6.36	0.88
7	5.28	4.98	0.89
10	3.78	3.59	0.90
14	2.59	2.51	0.94
			Av. 0.90

TABLE III. Variation of $D\eta/T$* with temperature and pressure.

Pressure 1 atmos		65 atmos		200 atmos		Molar volume cc
t°C	$10^5 \times \frac{D\eta}{T}$	t°C	$10^5 \times \frac{D\eta}{T}$	t°C	$10^5 \times \frac{D\eta}{T}$	
10	3.82	16.5	3.79	25.3	3.69	95.3
20	3.86	26.7	3.82	36.2	3.78	96.5
30	3.89	36.4	3.89	47.1	3.87	97.7
40	3.96	46.0	3.94	58.1	3.92	98.9

* $D\eta/T$ calculated with D in cm²/day and η in poises. Values of η were calculated from data quoted in reference 3a.

[8] R. E. Gibson and O. H. Loeffler, J. Am. Chem. Soc. 63, 898 (1941).

[9] Davis, Gore, and Kurata, Ind. Eng. Chem. 43, 1826 (1951).

D_{65} could then be calculated. The results of such an experiment at 29.3°C are given in Table II, and the average value of D_{65} obtained is shown in Fig. 2 as a black square. This can be seen to agree well with the results of the first experimental procedure.

DISCUSSION

This investigation was undertaken in the hope of testing the relative applicability of two models of diffusion: the one, in which a molecule moves into an adjacent hole; the other, in which two molecules have sufficient kinetic energy in opposite directions to exchange places, overcoming repulsive forces and pushing neighboring molecules aside. In the first model it is frequently assumed that the rate determining step of diffusion is the formation of the hole, and hence the activation energy for diffusion is determined by the energy necessary for this process. Furthermore, with this model, the diffusion depends predominantly upon the number of holes and hence at constant volume, when the number of holes presumably remains constant, the diffusion coefficient should be nearly independent of temperature. With the second model, the average kinetic energy of the molecules and therefore their ability to surmount the repulsive potential barrier increase with temperature. Also the greater fluctuation of nearest neighbors increases the probability of finding lower potential barriers to overcome. On this model one would expect an appreciable temperature coefficient of diffusion at constant volume. In the case we have investigated, $1/D(\partial D/\partial T)_P$ at one atmosphere and 25°C is 0.0185, and $1/D(\partial D/\partial T)_V$ is 0.0034, if taken from points on the experimental log$D$ *vs* $1/T$ curves obtained at 1 and 65 atmos, or 0.0053, if taken from the smoothed straight line isochore shown in Fig. 2. These may be compared with the temperature coefficient of the kinetic energy which is equal to 0.00335.

With reference to the general theories of transport processes in liquids, it is of interest to study, as a function of temperature and pressure, the constancy of the quantity $D\eta/T$, where η is the viscosity. This quantity should be a constant for a pure liquid, that is when D is a self diffusion coefficient,[2] and furthermore should be expressible in terms of equilibrium properties of the system.[1] Values of $D\eta/T$ at temperatures and pressures corresponding to several constant molar volumes are given in Table III. It will be seen that there is about a 10 percent variation over the range studied. The increase in $D\eta/T$ with temperature at atmospheric pressure would be expected in view of the decrease in internal energy of mixing with temperature which Hildebrand[10] has calculated for the solution of iodine in carbon tetrachloride. The decrease of $D\eta/T$ with pressure and the near constancy of $(D\eta/T)_V$ found at larger volumes are again in accord with our knowledge of the interaction of iodine with carbon tetrachloride obtained from thermodynamic data of solutions.[11] A more quantitative treatment of the diffusion process will be postponed until the experimental results for the self-diffusion of carbon tetrachloride are presented.

[Since this work was completed, Koeller and Drickamer[12] have reported measurements of the self-diffusion coefficient of carbon disulfide over a much larger pressure range. Although the absolute values of the diffusion coefficients reported by these authors may be in error due to difficulties in their experimental procedure, the general trends shown by their results are similar to those shown in the presently reported experiments.]

This work was supported in part by the U. S. Atomic Energy Commission.

[10] J. H. Hildebrand, J. Am. Chem. Soc. **59**, 2038 (1937).
[11] See J. H. Hildebrand and R. L. Scott, *Solubility of Nonelectrolytes* (Reinhold Publishing Corporation, New York, 1950), p. 272.
[12] R. C. Koeller and H. G. Drickamer, J. Chem. Phys. **21**, 267 (1953).

Letters to the Editor

THIS section will accept reports of new work, provided these are terse and contain few figures, and especially few half-tone cuts. The Editorial Board will not hold itself responsible for opinions expressed by the correspondents. Contributions to this section should not exceed 600 words in length and must reach the office of the Editor not later than the 15th of the second month preceding that of the issue in which the Letter is to appear. No proof will be sent to the authors. A publication charge of $10.00 per Letter is made which, when honored, will entitle the Institution to 100 free reprints.

Proton Relaxation Phenomena in Complex Ion Formation

J. R. ZIMMERMAN*
University of Colorado, Boulder, Colorado
(Received July 10, 1953)

THE study of complex ion formation and proton exchange rates[1] in aqueous solutions appears to be feasible in some instances by consideration of the classical nuclear relaxation times (T_1, T_2) of the water molecules.

It has been observed that the presence of some of the weak organic acids has a large influence on the relaxation times of the protons in aqueous solutions of V^{++++} prepared by the reduction of vanadium pentoxide with hydroxylamine hydrochloride. The relaxation ratio, T_1/T_2, for an aqueous solution of 0.01 M V^{++++}, where V^{++++} is the dominating relaxing agent, is of the order of two, in good agreement with earlier theoretical considerations.[2] As the weak acid concentration is increased, T_1 and T_2 are found to vary as shown in Fig. 1 (curves I and II, respectively) for the case of oxalic acid. The observation of these effects is enhanced by considering the ratio T_1/T_2 (see curve III). It is of particular interest that no appreciable change in either T_1 or T_2 occurs until the concentrations of the oxalic acid and vanadium ions are equal; i.e., 0.01 M. Another change in the relaxation ratio growth rate occurs when the concentration of oxalic acid is approximately 0.03 M and that of V^{++++} is 0.01 M; this result may be interpreted to be in agreement with the generally accepted coordination number 6 for the V^{++++} ion. For acid concentrations higher than 0.03 M, T_2 continues to be dependent upon concentration of oxalic acid such that T_2 varies approximately as $M^{-0.4}$, If one assumes proton exchange as the dominant relaxing factor for concentrations of oxalic acid in the neighborhood of 0.2 M, then $\lambda \sim 50$ sec^{-1}, where λ is the reciprocal of the life time of a proton with a given m state in a water molecule. More accurate data, which are quite easy to obtain for this range of relaxation times using spin-echo[3] techniques, would clearly define the slopes and regions of slope change in the curves.

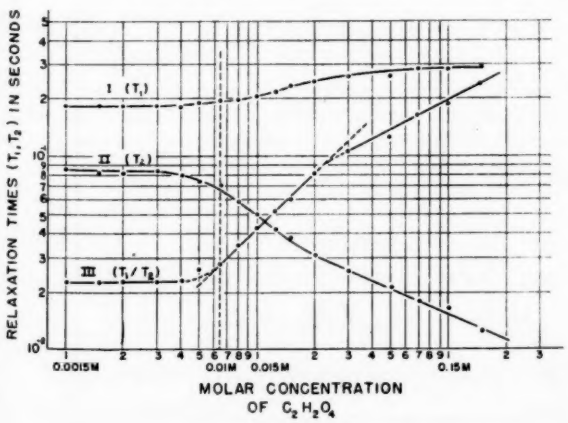

FIG. 1.

If magnetic moments of ions are to be inferred from nuclear relaxation measurements,[2] from the observed effects of oxalic acid on T_1 in the case of V^{++++}, it is apparent that judicious selection of the reducing agents in the preparation of paramagnetic ions in aqueous solutions is extremely important in some instances. For example, taking the magnetic moment of Cu^{++} ion as 2.00 magnetons, this author has found the magnetic moment of V^{++++} to be 1.76×0.04 magnetons. This value is to be compared with the calculated value of 1.73 and the corresponding experimental value of 1.7 obtained from magnetic susceptibility measurements.[4] On the other hand the V^{++++} ion in the presence of oxalic acid could give values as low as 1.4 for the magnetic moment.

Similar effects have been observed in other cases with different metallic ions. Malonic acid with V^{++++} gives comparable relaxation effects. This method of analysis should lend itself to the study of many chemical reactions where large variations in ion exchange rates in the solvent are involved. An analytical study of these phenomena is being continued.

* This experimental work was carried on at the Field Research Laboratories, Magnolia Petroleum Company, Dallas, Texas, where the author was on leave of absence from the University of Colorado from July, 1952 to January, 1953.
[1] E. L. Hahn and D. H. Maxwell, Phys. Rev. **88**, 1070 (1952) have recently been concerned with the damping of proton coupling in methyl alcohol due to small percentages of water present. The above study, however, is concerned with relaxation measurements of the protons of the water molecules, not of the organic acids.
[2] Bloembergen, Purcell, and Pound, Phys. Rev. **73**, 679 (1948).
[3] E. L. Hahn, Phys. Rev. **80**, 580 (1950).
[4] G. J. Gorter, *Paramagnetic Relaxation* (Elsevier Publishing Company, Inc., New York, 1947), p. 15.

Nuclear Magnetic Resonance Splittings in Weak Fields*

WARREN E. QUINN† AND RICHARD M. BROWN‡
The State College of Washington, Pullman, Washington
(Received July 14, 1943)

THE existence of fine structure in the nuclear magnetic resonances for nuclei contained in complex molecules has been observed and explained by several investigators.[1,2] One property of the phenomenon predicted by the theory and observed at high fields is that the structure splitting factors should be independent of the applied magnetic field. As a stringent check on this, the splittings for several compounds examined at higher fields by Gutowsky, *et al.*[2] were measured at magnetic field strengths near 200 gauss utilizing a radio frequency spectrometer previously described.[3] Table I shows the results of this work compared to the values given by Gutowsky *et al.*

With the exception of the singlet fluorine resonance in $F_2PO(OH)$ at 200 gauss, all splittings agree closely with those measured at the higher field strengths.

In other experiments, the absence of measurable structure arising either from the absence of nonequivalent nuclei of the

TABLE I.

Nucleus and compound	Ho	Measured splitting	Splitting at 6385 gauss[2]
F^{19} in:			
HPF_6	175 gauss	0.177 ±0.001 gauss	0.178 gauss
$FPO(OH)_2$	170	0.240 ±0.001	0.238
$F_2PO(OH)$	550	0.240 ±0.015	0.244
	200	Singlet	
P^{31} in:			
HPF_6	275	0.406 ±0.010	0.41
$HPO(OH)_2$	400	0.406 ±0.010	0.41
H^1 in:			
$HPO(OH)_2$	165	0.164 ±0.002	0.166
$H_2PO(OH)$	160	0.133 ±0.001	0.137

same species or from the "washing-out effect" of quadrupole interactions was confirmed for the F^{19} resonances in NH_4HF_2, HBF_4, and SbF_3. In these cases, a single narrow line was observed.

The behavior of the F^{19} resonance in $F_2PO(OH)$ is as yet unexplained. The doublet structure observed at an applied field of 550 gauss coalesced as the field was decreased until a single broad resonance ($\Delta H \approx 0.250$ gauss) was reached at approximately 237 gauss. Magnet current drift prevented even approximate evaluation of line widths or splittings in the intermediate region. It is clear, however, that in the vicinity of these field strengths some process enters to suppress the structure seen at higher fields. Further work on this is planned.

* Work assisted by the U. S. Atomic Energy Commission and by the Research Committee of the State College of Washington.
† Now at Harvard University, Cambridge, Massachusetts.
‡ Temporarily on leave at Control Systems Laboratory, University of Illinois, Urbana, Illinois.
[1] H. S. Gutowsky and C. J. Hoffman, J. Chem. Phys. **19**, 1259 (1951); Phys. Rev. **80**, 110 (1950); E. L. Hahn, Phys. Rev. **80**, 580 (1950).
[2] Gutowsky, McCall, and Slichter, J. Chem. Phys. **21**, 279 (1953).
[3] J. H. Burgess and R. M. Brown, Rev. Sci. Instr. **23**, 334 (1952).

New Infrared-Investigations in the *Cis-Trans* Isomerism of *Ortho*-Halogenphenols

G. Rossmy, W. Lüttke, and R. Mecke
Institute of Physical Chemistry of the University of Freiburg i. Br., Hebelstrafe 38, Germany
(Received June 26, 1953)

THE infrared spectrum of *o*-chlorophenol in CCl_4 solution in the region of the first overtone of the OH-vibration was first reported by O. R. Wulf and U. Liddel.[1] They observed two peaks, a small one at 7050 cm^{-1} having the same position as the monomer absorption of unsubstituted phenol and another one about ten times more intense shifted to lower frequencies at 6910 cm^{-1}. L. Pauling[2] gave the interpretation of this complexity by assuming *cis*- and *trans*-configurations of the phenolic hydroxyl group with respect to the adjacent *ortho*-substituent. From the ratio of the areas of the peaks he calculated a free energy difference of about 1.4 kcal/mole stabilizing the *cis*-orientation. He pointed out that this interpretation could be proved by studying the effect of temperature on the relative areas of the two peaks. In consequence the investigations were extended to the fundamental OH band, to higher overtones and to the analogous halogenphenols. The further works of C. R. Wulf and co-workers[3] gave strong support to the interpretation given by L. Pauling. Though Wulf did not investigate the predicted effect of temperature, it was reported by M. M. Davies[4] working in the fundamental region with solutions of *o*-chlorophenol in CCl_4 and by L. R. Zumwalt and R. M. Badger[5] for the gaseous state.

Several reasons lead us now to doubt at least the quantitative conclusions cited above:

1. The relation N_{cis}/N_{trans} derived from the relative intensities of the two peaks differed considerably in the results given by various authors determined in various harmonies.

2. No special efforts to remove the impurity, phenol, were reported in the publications cited. The presence of phenol seemed to us to be very probable considering the small differences in the boiling points of *o*-chlorophenol, *o*-bromophenol, and phenol itself. W. J. Wohlleben[6] found considerable amounts of phenol in purchased samples of *o*-chloro- and *o*-bromophenol.

3. The effect of temperature predicted by Pauling remained doubtful.

We were able to verify the presence of phenol in our samples of *o*-chlorophenol and *o*-bromophenol by running the spectrum in the region of 1–15.5μ. In the liquid state a peak at 14.56μ appeared to be caused by the impurity, phenol. The peak disappeared when the samples were purified by chromatographic adsorption. The OH-absorption of the *ortho*-halogenphenols, purified and examined in such manner, were investigated by us from the fundamental up to the third overtone ($v'=1-4$).

Many of the absorption peaks previously attributed to the transconfiguration have been very greatly reduced. Table I also shows very clearly the existence of combination-frequencies involving the OH_{cis} vibration. The values can in every case be checked with Raman data giving satisfactory agreement. The strong halogen dependence of the combination frequency suggests the presence of a carbon-halogen bending motion. This had already been proposed by Wulf and Deming[3c] who also observed such subsidiary peaks in the region of two overtones. We have also investigated the effect of temperature on the relative intensities I_{cis}/I_{trans} of *o*-iodophenol in the gaseous state. Plotting log K against $1/T$ we get a energy difference of 3.2 kcal/mole in favor of the *cis*-configuration, the difference of free energy being 2.8 kcal/mole. Both values agree within the limits of error. For the dilute solution in CCl_4 we observed a free energy difference of only 1.4 kcal/mole. The trans-configuration appears to be stabilized by about 1.4 kcal/mole with respect to the gaseous state by interaction with the solvent. For *o*-bromophenol in CCl_4 we determine ΔF to be about 2.1 kcal/mole, the values for the gaseous state and for *o*-chlorophenol being still greater. It must be stated therefore that all quantitative measurements of earlier investigators had been affected by the neglectance of combination

Table I.

	o-chlorophenol ν[cm^{-1}]	$\Delta\nu$ [cm^{-1}]	Ra. [cm^{-1}]	*o*-bromophenol ν[cm^{-1}]	$\Delta\nu$ [cm^{-1}]	Ra. [cm^{-1}]	*o*-jodophenol ν[cm^{-1}]	$\Delta\nu$ [cm^{-1}]	Ra. [cm^{-1}]	
νOH "*cis*"	3577			3557			3535			gas
νOH "*trans*"	~3650 (174°C ≤1:70)	83		108°C not observed 174°C ~3650	93		3650 125°C (1:36) 200°C (1:19)	115		gas
νOH "*cis*"	3545			3530			3509			solution in CCl_4
νOH "*trans*"	3600 (1:44)	55		3605 (1:37)	75		3601 (1:12)	92		solution in CCl_4
νOH + δ_{c-hal}	3801 (1:190)	256	266 (2*b*, *dp*)	3742 (~1:100)	212	210 (1*dp*)	3701 (~1:80)	192	~190	solution in CCl_4
2νOH "*cis*"	6920			6888			6835			solution in CCl_4
2νOH "*trans*"	not separated			7080–7095 (1:14)	192–207	210	7036 (1:6)	201	~190	solution in CCl_4
2νOH + δ_{c-hal}	7180 (1:50)	260	266							solution in CCl_4
3νOH "*cis*"	10 089			10 020			9912			solution in CCl_4
3νOH "*trans*"	10 323 (1:215)	234	266	~10 340 ? (*Sh*) (≤1:40)	320		10 296 (1:7, 5)	384		solution in CCl_4
3νOH + δ_{c-hal}				10 235 (1:15)	215	210	10 100 (1:8, 5)	188	~190	solution in CCl_4
4νOH "*cis*"	13 078			12 975			12 785			solution in CCl_4
4νOH "*trans*"	?			?			13 395 (~1:6)	610		solution in CCl_4
	13 180 ? (*Sh*)	102		13 085 (*Sh*)	110		~12 935 ? (*Sh*)	150		solution in CCl_4
	13 320 (~1:10)	242								solution in CCl_4
4νOH + δ_{c-hal}	13 340 (~1:16)	262	266	13 175 (~1:4) (*b*)	200	210	13 000 ? (*Sh*)	215	~190	solution in CCl_4

[a] The relative intensities with respect to the "*cis*-peaks" are given in parentheses.

tones and phenol absorptions. Our investigations and the discussion of results will be published in greater detail in Z. f. Elektrochemie. At this time we wish only to emphasize that the calculations based on simple electrostatic interactions[7] lose their good agreement with experimental data. Consequently, the conclusion regarding the predominantly simple electrostatic character of the hydrogen-bond drawn from these calculations is greatly diminished in force.

[1] O. R. Wulf and U. Liddel, J. Am. Chem. Soc. **57**, 1464 (1935).
[2] L. Pauling, J. Am. Chem. Soc. **58**, 94 (1936).
[3] (a) Wulf, Liddel, and Hendricks, J. Am. Chem. Soc. **58**, 2287 (1936). (b) O. R. Wulf and E. J. Jones, J. Chem. Phys. **8**,745 (1940); (c)O. R. Wulf and L. S. Deming, *ibid.*, 753.
[4] M. M. Davies, Trans. Faraday Soc. **34**, 1427 (1938).
[5] L. R. Zumwalt, and R. M. Badger, J. Am. Chem. Soc. **62**, 305 (1940).
[6] W. J. Wohlleben, Ber. deut. Chem. Ges. **42**, 4370 (1909).
[7] M. M. Davies, Trans. Faraday Soc. **36**, 333 (1940).

Erratum: On the Vibrational Spectra of Crystals

[J. Chem. Phys. **18**, 1056 (1950)]

WAYNE A. BOWERS AND HERBERT B. ROSENSTOCK
University of North Carolina, Chapel Hill, North Carolina

THE statement labeled "*b*" which begins eight lines from the end of this paper should read: "(*b*) the distribution is everywhere finite, although its slope has an infinity of inverse square root nature at $\tilde{\omega}^2=\frac{1}{3}$ and $\tilde{\omega}^2=\frac{2}{3}$." We are indebted to Dr. L. vanHove for pointing this out.

Vibrations of a Simple Cubic Lattice. I

HERBERT B. ROSENSTOCK, *Naval Research Laboratory, Washington, D. C.*
AND
GORDON F. NEWELL, *Institute for Fluid Dynamics and Applied Mathematics, University of Maryland, College Park, Maryland*

(Received July 2, 1953)

TO make an analytical calculation of the distribution of vibrational frequencies feasible for even the simplest three-dimensional lattice, simplifying assumptions concerning the nature of the interaction between particles must be made.[1,2] The purpose of this and the following letter[3] is to point out two more sets of such assumptions which make this possible.

Consider here a simple monatomic cubic lattice, with non-central forces between nearest neighbors only; i.e., assume that the interaction energy between two nearest neighbors is of the form,

$$V=\tfrac{1}{2}\alpha(\Delta u_{11})^2+\tfrac{1}{2}\beta(\Delta u_{\perp})^r,$$

in which Δu_{11} and $\Delta u_{\perp}$ are, respectively, the components of the relative displacements parallel and perpendicular to the line joining the two particles. The secular equation for this system has no off-diagonal terms and yields directly the frequencies,

$$\omega^2=(2\alpha/m)[1-C_1+\sigma(2-C_2-C_3)]\equiv\psi(x_1,x_2,x_3),$$

and two more expressions obtainable from Eq. (1) by rotating the indexes 1, 2, 3. Here $\sigma=\beta/\alpha$, $C_i=\cos X_i$ and (X_1, X_2, X_3) is the propagation vector. ω^2 runs from 0 to $\omega^2_{\max}=(4\alpha/m)(1+2\sigma)$. Each branch depends on all three X_i as long as $\sigma\neq 0$, in contrast to the essentially one-dimensional expressions obtained when $\sigma=0$ (central force approximation).

The distribution of $\tilde{\omega}^2=\omega^2/\omega^2_{\max}$, given by

$$g(\tilde{\omega}^2)=(\omega^2_{\max}/\pi^3)\int_0^{\pi}\int_0^{\pi}\int_0^{\pi}\times\delta[\omega^2-\psi(X_1,X_2,X_3)]dX_1dX_2dX_3; \quad (2)$$

yields,

$$g(\tilde{\omega}^2)=[(2+4\sigma)/\sigma\pi^3]\int_{-1}^{1}dC(1-C^2)^{-\frac{1}{2}}F(C,\lambda), \quad (3)$$
$$\lambda=(2+4\sigma)\tilde{\omega}^2/\sigma,$$

where $F(C,\lambda)$, the result of the first two integrations in Eq. (2), takes on the following values in the space (C,λ):

$$F(C,\lambda)=\begin{cases}0 & C<C^1\\ F_1(C,\lambda) & C^1<C<C^2\\ F_2(C,\lambda) & C^2<C<C^3\\ F_1(C,\lambda) & C^3<C<C^4\\ 0 & C^4<C\end{cases} \quad (4)$$

where

$$C^1=1-\lambda$$
$$C^2=3-\lambda$$
$$C^3=1+(2/\sigma)-\lambda$$
$$C^4=3+(2/\sigma)-\lambda$$

and the F_i are functions involving complete elliptic integrals of the first kind of arguments which are rational functions of C and λ. The argument approaches unity, giving rise to a logarithmic singularity in F, on the boundary between F_1 and F_2. It follows from Eqs. (3) and (4) that $g(\tilde{\omega}^2)$ can have singularities only at the points $\lambda=0$, λ_1, λ_2, λ_3, λ_4, $\lambda_{\max}$ where $\lambda_1=2$, $\lambda_2=4$, $\lambda_3=\lambda_{\max}-4$, $\lambda_4=\lambda_{\max}-2$ and expansion of Eq. (3) in the neighborhood of these points reveals that the behavior there is as given in Table I, in accordance with the general theorems of vanHove.[4] Behavior near the singular points not listed in Table I may be inferred from the symmetry of g about $\tilde{\omega}^2=\frac{1}{2}$. Since we have

$$0<\lambda_1<\lambda_2\leq\lambda_3<\lambda_4<\lambda_{\max} \quad \text{for} \quad \sigma\leq\tfrac{1}{2}$$

but

$$0<\lambda_1<\lambda_3\leq\lambda_2<\lambda_4<\lambda_{\max} \quad \text{for} \quad \sigma\geq\tfrac{1}{2}$$

it follows from Table I that the general features of the distribution are as sketched in Fig. 1. Note that for small σ, the distribution approaches the shape found for central forces with small next nearest-neighbor interaction, leading to the expected inverse square root singularity at both end points in the extreme case $\sigma=0$. In the other extreme, $\sigma=1$, the distribution is identical

TABLE I. Singularities in the frequency distribution.

λ	$g(\lambda-\epsilon)$	$g(\lambda+\epsilon)$
0		$\sim\epsilon^{\frac{1}{2}}$
λ_1	$\sim-\epsilon^{\frac{1}{2}}$	$\sim\epsilon$
λ_2	$\sim\epsilon$	$\sim-\epsilon^{\frac{1}{2}}$

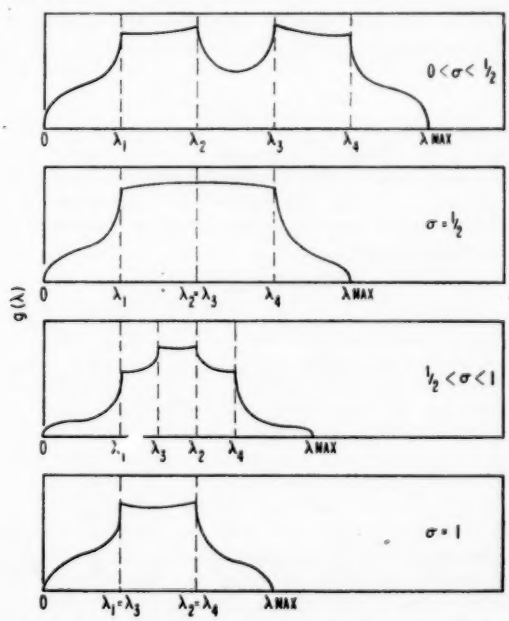

FIG. 1. Sketches (not to scale) of frequency distributions for various values of σ.

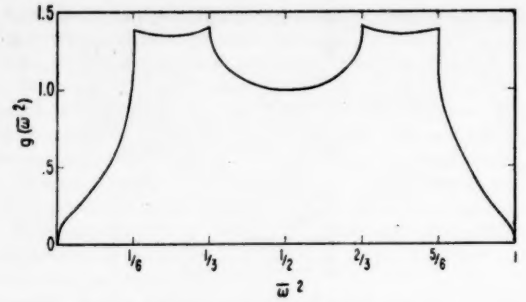

FIG. 2. Frequency distribution, $\sigma=\frac{1}{4}$.

with the one obtained for nearest neighbor interaction with vibrations in a "fourth dimension".[2]

Since the above discussion shows all the general features of the distribution, the actual calculation of g for any given value of σ requires numerical evaluation of Eq. (3) at only very few points. An example, $\sigma=\frac{1}{4}$, is shown in Fig. 2.

We wish to thank Mr. D. A. Patterson for checking certain calculations.

[1] G. F. Newell, J. Chem. Phys. (to be published).
[2] W. A. Bowers and H. B. Rosenstock, J. Chem. Phys. **18**, 1056 (1950).
[3] H. B. Rosenstock and H. M. Rosenstock, J. Chem. Phys. (following letter).
[4] L. vanHove, Phys. Rev. **89**, 1189 (1953).

Vibrations of a Simple Cubic Lattice. II

HERBERT B. ROSENSTOCK, *Naval Research Laboratory, Washington, D. C.*
AND
HILDA M. ROSENSTOCK, *Washington, D. C.*
(Received August 2, 1953)

As in the preceding letter,[1] consider a simple monatomic cubic lattice but assume that the forces are central and non-negligible down to third nearest neighbors, i.e., set

$$V=\Big[\tfrac{1}{2}\alpha\sum_{\substack{\text{nearest}\\\text{nbrs.}}}+\tfrac{1}{2}\beta\sum_{\substack{\text{2d nearest}\\\text{nbrs.}}}+\tfrac{1}{2}\gamma\sum_{\substack{\text{3d nearest}\\\text{nbrs.}}}\Big]d^2,$$

d being the distance between two atoms. By expanding about equilibrium positions keeping only the first nontrivial (i.e., quadratic) terms, we obtain, in the usual manner, the secular equation

$$\Delta(\omega^2;\sigma,\tau;c_1,c_2,c_3)=0, \tag{1}$$

which determines the frequencies ω^2. Explicitly, Δ is a 3×3 determinant with diagonal elements $f_{ii}=1-c_i+\sigma(2-c_ic_j-c_ic_k)+\tau(1-c_ic_jc_k)-m\omega^2/2\alpha$ and off-diagonal elements $f_{ij}=s_is_j(\sigma+\tau c_k)$. Here $\sigma=\beta/\alpha$, $\tau=4\gamma/3\alpha$, $s_i=(1-c_i^2)^{\frac{1}{2}}$ and c_i is defined in I. (1), begin a cubic in ω^2, may be solved for ω^2 by elementary algebra to give three solutions

$$\omega^2=\omega_1^2,\ \omega^2=\omega_2^2,\ \omega^2=\omega_3^2, \tag{2}$$

but the expressions $\omega_i^2=\omega_i^2(\sigma,\tau,c_1,c_2,c_3)$ are irrational and rather complicated and therefore of little use in finding the distribution of frequencies. One is therefore led to search for values of σ,τ such that one or more of the ω_i^2 become rational.

It is known that this happens in the mathematically simple and physically trivial case $\sigma=\tau=0$. We find that the only other case in which this happens is $\sigma=3/7$, $\tau=2/7$ (meaning $\beta/\alpha=6/14$, $\gamma/\alpha=3/14$). We then obtain

$$\omega_1^2=(2\alpha/7m)[21-\sum_i c_i-4\sum_{i>j}c_ic_j-6c_1c_2c_3] \tag{3}$$

but ω_2^2 and ω_3^2 remain irrational,

$$\omega_{2,3}^2=(2\alpha/7m)[12-3\sum_i c_i-\sum_{i>j}c_ic_j \pm\{\tfrac{1}{2}\sum_{j\neq i\neq k}(1-c_i)^2(c_j-c_k)^2\}^{\frac{1}{2}}]. \tag{4}$$

We are unable to compute the distribution of the ω_2^2 and ω_3^2 branches. The distribution of the ω_1^2 branch can, on the other hand, be obtained with the use of (3) in Eq. (2) of I. As in I, the first two integrations can be done in closed form, leading to elliptic integrals, and a study of the behavior of these in the $(c-\omega_1^2)$ plane enables one to locate the points of interest (i.e., the singularities) of the distribution function and to infer its behavior there. (The nature and location of the singularities may also be understood from the connectedness of the surfaces of constant ω_1^2 in (X_1,X_2,X_3) space as given by (3).) The calculation of the distribution may then be completed by numerical integration of the last remaining integral at a very few points. The distribution is exhibited in Fig. 1. The function is very small from 0 to 0.60; more than half of the frequencies seem to be concentrated in the region $0.60<\bar{\omega}_1^2<0.80$. It is continuous throughout its range and has square root behavior at each end point; in the neighborhood of each of the other four singular points, it shows square root behavior at one side and is linear on the other, in agreement with van Hove's[2] general results.

We wish to thank Dr. W. A. Bowers and Dr. G. F. Newell for helpful discussions.

[1] H. B. Rosenstock and G. F. Newell, J. Chem. Phys. **21**, 1607 (1953) (preceding letter), henceforth referred to as I.
[2] L. van Hove, Phys. Rev. **89**, 1189 (1953).

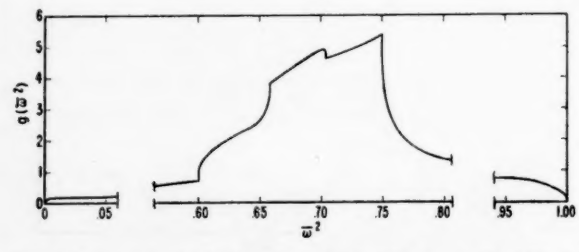

FIG. 1. Frequency distribution. The singularities are at $\bar{\omega}^2=6/10$, $2/3$, $(35+10^{\frac{1}{2}})/54$ and $3/4$. To save space, the regions $0.05<\bar{\omega}^2<0.55$ and $0.85<\bar{\omega}^2<0.95$, in which the function is smooth, are not shown.

Detection of the HO_2 Radical by Mass Spectrometry*

S. N. FONER AND R. L. HUDSON
Applied Physics Laboratory, The Johns Hopkins University, Silver Spring, Maryland
(Received June 29, 1953)

ALTHOUGH the HO_2 radical has been postulated as an intermediate in many chemical reactions, no direct experimental proof of the existence of this radical has been presented to date. This letter reports the mass spectrometric detection of the HO_2 radical in the gas phase reaction of hydrogen atoms with oxygen molecules.

The experimental arrangement which we have employed is shown in Fig. 1. Oxygen mixed with an inert gas, which serves both to stabilize the gas flow and to deactivate molecules, is in-

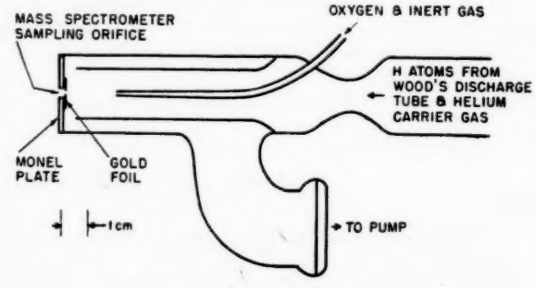

FIG. 1. Experimental arrangement.

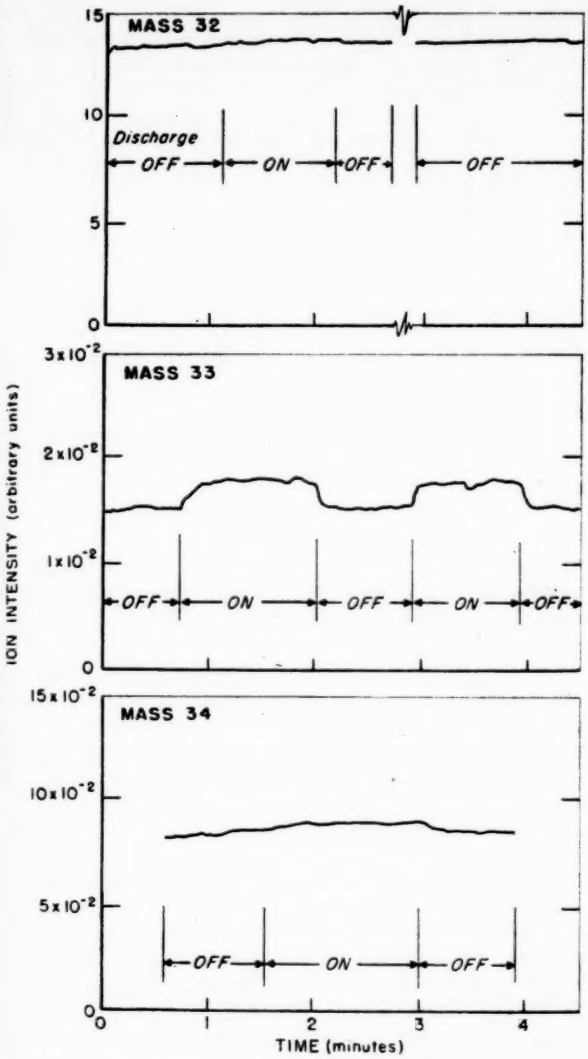

FIG. 2. Ion intensities of masses 32, 33, and 34 at 60 volts electron energy for the reaction of hydrogen atoms with oxygen molecules. The ordinate scale for mass 32 should be multiplied by 1.6. Measurements were made in the sequence: mass 32, mass 33, mass 34, followed by a check on mass 32 indicated by the break in the abscissa.

jected into the center of the atomic hydrogen stream. A constriction in the glass system prevents back diffusion of oxygen molecules into the discharge tube. The reaction products enter a special mass spectrometer, previously described,[1] which employs a molecular beam sampling system. The inlet orifice is a pinhole 0.010 cm diameter in a foil 0.0025 cm thick.

The ion intensities at the oxygen isotopic masses 32, 33, and 34 were observed to determine if any HO_2 was being produced. Measurement of mass 34 intensity is necessary to rule out isotopic diffusion effects and to monitor the production of H_2O_2 which yields some HO_2^+ as an ionization fragment. At pressures of a few cm of Hg. we have found that the intensity of the mass 33 peak increased abruptly when the discharge tube was turned on, while under the same conditions the ion intensities at masses 32 and 34 remained substantially constant. In Fig. 2 are shown tracings of the records for a run at a pressure of 3.7 cm of Hg when CO_2 was mixed with the oxygen. The gas velocity in the reaction region was about 500 cm/sec. Generation of hydrogen atoms in the discharge tube in clearly correlated with a stepwise rise in the mass 33 ion intensity well above the $O^{16}O^{17}$ isotopic level. In this experiment a slight rise in the 34 peak, which might be due to H_2O_2, was observed with the discharge on. The contribution of such a small amount of H_2O_2 to the mass 33 peak would, however, be less than the noise level. Increases in mass 33 intensity have similarly been observed with argon and helium serving as the inert gas mixed with the oxygen. In 16 out of 18 observations made under various experimental conditions no increase in the 34 peak was observed, while in all cases an increase, averaging 9.2±2.1 percent, in the 33 peak was obtained.

The ion intensity at mass 33 cannot come from any impurity in the system as turning off the oxygen supply completely removes the 33 peak. The presence of HO_2 when operating the system at a few cm pressure is in accord with the prediction that HO_2 is formed in intermolecular collisions:

$$H+O_2+M\rightarrow HO_2+M, \quad (1)$$

where the third body, M, removes excess energy.

Some rough values of ion intensities in one of the experiments are given in Table I. It will be observed that considerable amounts

TABLE I. Ion intensities at 60 volts electron energy. Total pressure = 3 cm, CO_2:O_2 ratio 2:1. The OH intensity has been corrected for the contribution from H_2O.

Component	Ion intensity (arbitrary units)
H	0.45×10^{-2}
H (O_2 off)	1.42×10^{-2}
H_2	18.2×10^{-2}
OH	3.0×10^{-2}
H_2O	9.2×10^{-2}
HO_2	0.14×10^{-2}
O_2	11.9
He	6.4

of OH and H_2O are produced in the reaction. The OH is formed presumably by the reaction,

$$HO_2+H_2\rightarrow OH+H_2O, \quad (2)$$

since the endothermic reaction,

$$H+O_2\rightarrow OH+H, \quad (3)$$

at room temperature has small probability of occurring in the $\sim10^{-2}$ sec residence time in the reaction zone. In the experiments described we estimate that roughly 1 percent of the hydrogen atoms end up in HO_2 at the sampling orifice.

Experiments on the HO_2 problem are in progress and a complete report on this research will be presented later.

* This research was supported by the Bureau of Ordnance, U. S. Navy.

[1] S. N. Foner and R. L. Hudson, J. Chem. Phys. **21**, 1374 (1953).

Extra Laue Reflections of Tetraphenylethylene Crystal

M. N. DUTT
Physics Department, Calcutta University, Calcutta, India
(Received June 25, 1953)

TETRAPHENYLETHYLENE was dissolved in alcohol which was heated till it dissolved completely, then benzene was added. The whole mixture was allowed to evaporate slowly; then the crystal of tetraphenylethylene was obtained. Morphological data indicates that it belongs to the holo axial monoclinic system with the axial ratio $a:b:c=1.213:1:1.078$, $\beta=68°20'$. The rotation photographs about the three crystallographic axes using Ni radiation show $a=11.36$ Aμ, $b=9.37$ Aμ, and $c=10.10$ Aμ. The density (ρ) was found to be 1.057. The number of molecules per unit cell was calculated to be one. A systematic study of x-ray reflections from a large number of planes, indicates that the space group of this crystal is P^2/m. The crystal was set with the needle axis (b-axis) vertical and x-ray (unfiltered Ni-radiation) falls normal to (001) face. Laue photographs were taken in this position at an interval of 5°.

The planes (312), (514), (200), (210), (400), (523), and (627) show diffuse spots. The diffuse spots appear on layer lines in the first photographs (Fig. 1) which vanish after 6° orientations.

FIG. 1. X-ray (unfiltered), Ni radiation passes through C axis, b axis vertical. The arrangements of diffuse spots on layer lines are to be noted.

This shows that extra Laue spots are of low intensity and of thermal origin, according to the Faxen Waller theory. When exposed to cobalt radiation, some of the extra spots are relatively displaced (Fig. 2), but the others remain practically, in the same

FIG. 2. The same position as the previous one. X-ray co-radiation passes, diffuse spots are displaced slightly to one side.

position. The author expresses his grateful thanks to Professor S. N. Bose, Head of the Department of Physics, for his valuable advice.

The Solubility Diagram and the Temperature-Composition Diagram at Atmospheric Pressure of the Liquid System Ozone-Oxygen*

HANS JOACHIM SCHUMACHER
Instituto de Investigaciones Facultad de Quimica Universidad Nacional de La Plata, Argentina
(Received May 15, 1953)

IT is well known that liquid oxygen and liquid ozone do not dissolve each other in all proportions.[1] If for example a gaseous mixture of oxygen with 20 percent of ozone is liquified at the temperature of liquid air two phases will appear: a light blue one, representing the solution of some percent of ozone in oxygen and a dark violet one of a much higher density, representing the solution of some percent of oxygen in ozone.

After Riesenfeld[2] the oxygen phase consists at liquid air temperature of approximately 70 percent of oxygen and 30 percent of ozone and the ozone phase of approximately 70 percent of ozone and 30 percent of oxygen. However, these figures represent only a very rough estimation because there exist no analytical determinations of the concentrations in question.

The critical temperature of solubility is said to be at −158°C; but there are many reasons to believe that this is a too high value. The experimental technic applied by Riesenfeld did not permit to determine the correct temperature. The temperature measured

TABLE I. The ozone concentrations of the "oxygen" and the "ozone" phase at different temperatures.

	Mole percent O_3	
T°C	O_2 phase	O_3 phase
−195	5.3	65
−188	10.0	58
−183	18.0	48
−182	...	44.5
−181	24.5	...

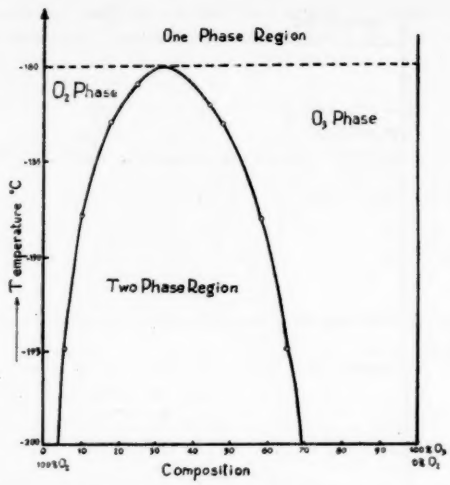

FIG. 1. The solubility diagram of the system ozone-oxygen.

by him corresponded to the temperature of a liquid considerably superheated. In fact the critical temperature derived from the complete solubility diagram is found to be at a much lower temperature, at -180 ± 0.2 C.

In order to be able to construct the entire solubility diagram of the system ozone-oxygen we determine the concentrations of the components of the two phases at different temperatures. As liquids of the thermostat we used for the measurements, we had liquid nitrogen, liquid oxygen, a mixture of liquid nitrogen and oxygen and liquid methane cooled down by liquid oxygen.

The experimental results are represented in Table I and Fig. 1.

The temperature-composition diagram of ozone-oxygen was not known until now. We measured it using a thermostat which kept the temperature in the range between the boiling points of oxygen and ozone for several hours within a tenth of a degree constant. The apparatus for measuring the ozone concentrations of the liquid and the gas phase at different temperatures and at the constant pressure of one atmosphere, was constructed in such a way that we could be certain that the two phases were always in perfect equilibrium.

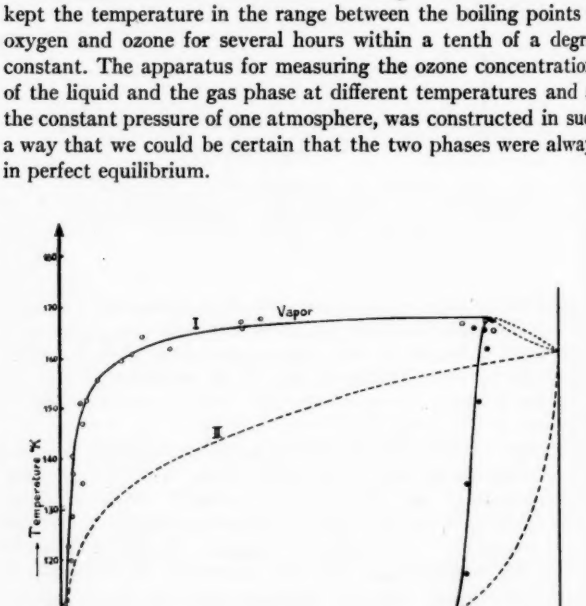

FIG. 2. The temperature-composition diagram of the system ozone-oxygen at atmospheric pressure. ——— experimental curve; - - - - - theoretical curve; O measured values of the gas phase; ● measured values of the liquid phase.

Curve I in Fig. 2 gives the experimental results. Curve II is the "theoretical" curve, assuming that Raoult's law will hold.

Curves I and II are quite different. The "experimental" curve I shows at 167, 8±1°K (−105.3±1°C) a small but distinct maximum. At this temperature and a pressure of 760 mm of mercury the gas and the liquid phase have the same composition.

It is interesting to mention and for certain kinds of experiments important to know that up to an ozone concentration in the liquid phase of more than 80 percent the gas phase contains only very little ozone. The condensation curve rises steeply and then rather suddenly flattens down continuing almost parallel to the x-axis forming at 167, 8°K the maximum mentioned above.

The large difference between the shapes of the curves I and II does not surprise, because the forces between the different types of molecules in the liquid phase (O_2, O_4, O_8) will be quite different.

* The complete work will be published in the *Anales de la Asociación Química Argentina.*

[1] E. H. Riesenfeld and G. M. Schwab, Ber. deut. Chem. Ges. **55**, 2088 (1922).

[2] E. H. Riesenfeld, Naturwiss. **15**, 780 (1927).

A Light Scattering Study of a Mixture of CCl_4 and CS_2†

JOSEPH POWERS AND RICHARD S. STEIN
Department of Chemistry, University of Massachusetts, Amherst, Massachusetts

(Received June 25, 1953)

THE depolarization of Rayleigh scattering is different for substances in the liquid and gaseous states.[1] The usual higher depolarization in the liquid state is ascribed to interaction between the scattering molecule and its neighbors. This would depend upon the environment of the molecule in solution, and upon the composition of a solution of the material in a solvent. In an effort to study this effect, the depolarization and intensity of the light scattered from a mixture of CCl_4 and CS_2 was studied as a function of composition. CS_2 was chosen because of its high anisotropy (and depolarization) and scattering power, while CCl_4 was chosen because of its symmetry and low scattering ability. Both substances are nonpolar.

Pure CCl_4 and CS_2‡ were redistilled* and mixtures were prepared. These were repurified by repeated distillation directly into dust-free rectangular light scattering cells. The composition of the distillate was determined after making the scattering measurement by measuring its refractive index.

The scattering power R for scattering at an angle of 90° from the incident beam was determined at room temperature for light of wavelength 5461A using a modification of an apparatus of a type originally described by Zimm[2] and Carr.[3] The apparatus was calibrated by measuring the scattering of pure benzene.[3] The depolarization for unpolarized incident light, ρ, was obtained from the ratio of measured scattering with horizontal and vertical orientation of a polaroid filter between the cell and the photometer. The method gave a depolarization of 0.64 for pure CS_2 which may be compared with a value of 0.64–0.68 reported by Stuart.[4]

The variation of R_{12} with the mole fraction of CS_2 in the mixture is given in Fig. 1. The scattering increases approximately linearly with composition. This type of variation is to be expected providing refractive index, compressibility and activity of the liquid mixture all vary linearly with composition.

The variation of the depolarization of the liquid mixture (Fig. 2) shows curvature, particularly at low carbon disulfide concentrations.

On the assumption that the contribution to the scattering per unit volume of solution of each of the two components is proportional to its volume fraction, and that the depolarization of the solvent (the carbon tetrachloride) is independent of the concentration of the solution, one may calculate ρ_2 the effected

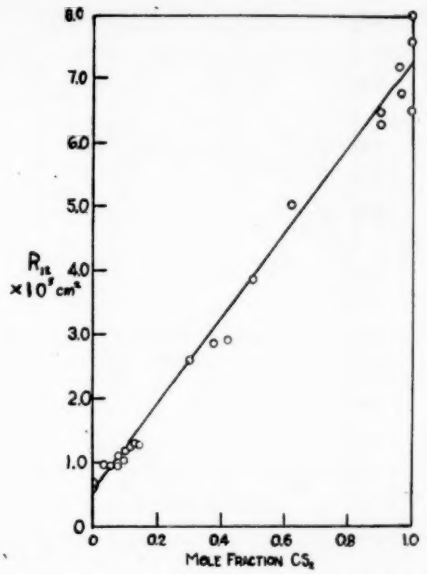

FIG. 1. The vibration of the scattering ratio at 90° R_{12}, of a solution of carbon disulfide and carbon tetrachloride with mole fraction of carbon disulfide.

depolarization of the carbon disulfide molecules in solution, using a modification of an equation proposed by Lotmar[5] and used by Doty and Kauffman.[6]

$$\rho_2=\frac{\rho_{12}R_{12}(1+\rho_{10})+\rho_{10}\phi_1R_{10}(1+\rho_{12})}{R_{12}(1+\rho_{10})-R_{10}(1+\rho_{12})}.$$

ρ_{12} is the measured depolarization of the solution for unpolarized incident light. $R_{12}=I_{12}r^2/I_0$, where I_{12} is the intensity of scattering from a unit volume of solution at a distance r from the solution and at an angle of 90° from the incident beam with unpolarized incident light of intensity I_0. ρ_{10} is the measured depolarization of pure carbon tetrachloride, R_{10} is the scattering power of pure carbon tetrachloride, and ϕ_1 is the volume fraction of carbon tetrachloride.

The values of ρ_2 which were calculated using this equation are plotted in Fig. 3. One observes that ρ_2 decreases with decreasing concentration of carbon disulfide, approaching a value of approximately 0.10 to 0.30 at infinite dilution. The precision of the extrapolation is poor because of the rapid variation of ρ_2 in this region and the low precision of measurement at the low concentrations.

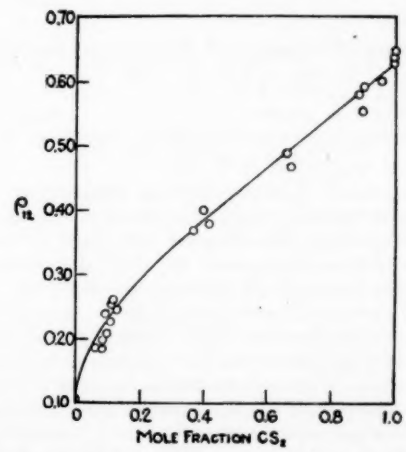

FIG. 2. The variation of the depolarization ρ_{12} (unpolarized incident light) of a solution of carbon disulfide and carbon tetrachloride with mole fraction of carbon disulfide.

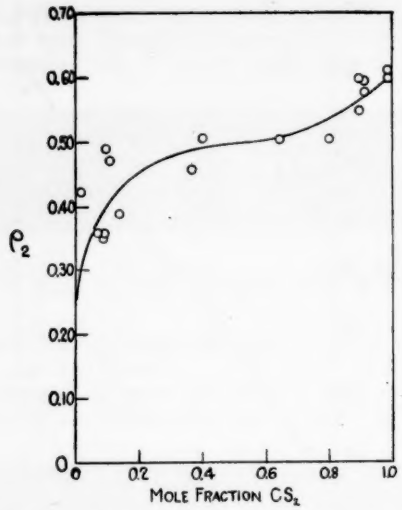

FIG. 3. The variation of the calculated depolarization of the carbon disulfide, ρ_2, in a solution with carbon tetrachloride with mole fraction of carbon disulfide.

The value of ρ_2 at infinite dilution corresponds to that for a carbon disulfide molecule completely surrounded by symmetrical carbon tetrachloride molecules. It is of interest to compare this value with $\rho=0.115$ for carbon disulfide in the gaseous state.[7] Any difference occurring between these two values would apparently result from the polarization field of the dipoles induced in the carbon tetrachloride, and is analogous to the difference between dipole moments measured in the gaseous phase and in solution at infinite dilution.[8]

† This work is part of a senior honors research problem conducted by Mr. Powers as partial fulfillment of the requirements for a degree of B.S. in Chemistry at the University of Massachusetts. The work was partially supported by a contract with the U. S. Office of Naval Research.

[1] S. Bhagavantam, *The Scattering of Light and the Raman Effect* (Chemical Publishing Company, New York, 1942), p. 99.

‡ The CCl_4 was Eastman Spectro Grade. The CS_2 was Mallinckrodt Analytical Reagent Grade.

* Further purification by filtering did not result in a greater reduction of turbidity.

[2] B. H. Zimm, J. Chem. Phys. **16**, 1099 (1948).

[3] C. I. Carr and B. H. Zimm, J. Chem. Phys. **18**, 1616 (1950).

[4] H. A. Stuart, *Die Struktur des Freien Molekules* (Julius Springer, Berlin, 1952), Vol. I, p. 356.

[5] W. Lotmar, Helv. Chim. Acta **21**, 792 (1938).

[6] P. M. Doty and H. S. Kauffman, J. Phys. Chem. **49**, 592 (1945).

[7] Reference 4, p. 354.

[8] C. P. Smyth, *Dipole Moment and Molecular Structure* (Chemical Catalog Company, New York, 1931), p. 32.

Experimental Evidence of Restricted Rotation in $CH_3-C\equiv C-CF_3$

BØRGE BAK, LISE HANSEN, AND JOHN RASTRUP-ANDERSEN
Chemical Laboratory, University of Copenhagen, Copenhagen, Denmark
(Received June 22, 1953)

THE problem of demonstrating the presence of potential barriers in molecules and, if possible, finding the barrier height has successfully been attacked by means of microwave technique[1–4] which has thus proved to be useful as a supplement to existing thermodynamic and spectroscopic methods.

So far, the microwave spectroscopists have concentrated their efforts on molecules like CF_3CH_3,[1–3] SiH_3CH_3,[4] and CH_3OH.[5,6] In all these cases the groups that are supposed to interact are at close distances to each other (1.50–2.00A). In order to enlarge the experimental background for the current theoretical discussion on the origin of potential barriers it seemed interesting to investigate molecules of the general type $CX_3-C\equiv C-CY_3$ in which the distance between the end groups is roughly 4–4.5A. $CH_3-C\equiv C-CH_3$ belongs to such molecules. Heat capacity measurements[7,8] have shown a practically complete absence of hinderence to the rotation of the methyl groups. Studies of the infrared spectrum under high resolution[9] seemed to show that the barrier must be very low if not zero. Recently, the temperature variation of the dipole moment of $CH_2Cl-C\equiv C-CH_2Cl$ *in solution*[10] was determined. The rotation was shown to be restricted but the result was not too conclusive because of the presence of the solvents. In a microwave experiment with some gas at a low pressure this difficulty is circumvented.

Because of lack of dipole moment $CH_3-C\equiv C-CH_3$ is unsuited for microwave investigation. It was decided to investigate $CH_3-C\equiv C-CF_3$ because none of its nuclei have spins differing from 0 or 1/2. Therefore, the complications which might arise from a spin hyperfine structure in the spectrum are avoided. If, furthermore, the potential barrier in $CH_3-C\equiv C-CH_3$ is small the introduction of three fluorine atoms instead of hydrogen probably means an amplification of the phenomenon to be studied.

The hitherto unknown molecule $CH_3-C\equiv CF_3A$ was prepared by mixing CF_3J(0.005 mole) and $CH_3-C\equiv CH$(0.01 mole) at room temperature in a sealed-off Pyrex tube (30 cc) which was afterwards irradiated by mercury light for ten days. A pure compound (I) (vp=39.5 mm Hg at 20.5°C) was isolated by careful, repeated destillations. Yield: 0.001 mole. Presumably the compound is $CH_3-CJ=CH(CF_3)$ since Haszeldine[11] prepared $CHJ=CH(CF_3)$ by a similar reaction. In the present case the compound $CH_3-C(CF_3)=CHJ$ (II) may also be formed. However, the pure compound next obtained (III) by refluxing (I) over dry KOH in a sealed-off tube at 150°C for 60 hours[12] consisted of symmetric top molecules as shown by the appearance of the microwave spectrum. Therefore, (II) has not been formed, or (II) and its reaction products have been discarded at one of destillations which finally resulted in (III). Yield: 0.0003 mole. The pure compound (III) had vp=12 mm Hg at −46.0°C. Under the influence of KOH (I) may split off HJ in two different ways forming either (*A*) or $CF_3-CH=C=CH_2$ (*B*). Since *B*-molecules are far from being symmetric tops we conclude that (III) is mainly the compound we want, $CH_3-C\equiv C-CF_3$.

If the possible barrier in $CH_3-C\equiv C-CF_3$ is high (2–3 kcal/mole) the microwave spectrum must be similar to e.g., that of CF_3CH_3,[1–3] i.e., it will consist of a few (3–5 or so) isolated lines spread over a 0–200 Mhz range. These lines correspond to molecules in torsionally excited levels.

If there is no barrier the *energy level diagram* certainly deviates from what it would be for a perfectly rigid rotor but due to the selection rules the spectra will be identical ($\Delta K_1=\Delta K_2=0$), i.e., the spectrum must consist of single lines separated by $2B$, where B is the rotational constant corresponding to rotation about an axis perpendicular to the axis of symmetry. For $CH_3-C\equiv C-CF_3$ this separation will be about 2600 Mhz.

The microwave spectrum, studied in the 21670–25830 Mhz region by means of Stark modulation technique, proved to represent an intermediate between the two possibilities sketched above. Two groups of lines, *the groups being of very similar structure*, were found. One group extended from 21900–22130 Mhz, the other from 24650–24890 Mhz. Both groups were observable at low field intensities (300 volts/cm) at 0.06 and 0.01 mm gas pressure and dry ice temperature. Both groups were flanked by numerous Stark components (unresolved). This indicates almost with certainty that symmetric top molecules are present. Furthermore, if we assume that $d_{C-F}=1.38$, $d_{C-H}=1.09$, $d_{C-C}=1.54$, and $d_{C\equiv C}=1.20$A and that the valence angles are tetrahedral (whether this is perfectly correct or not) we find that the $J=7\rightarrow 8$ transition of a perfectly rigid $CH_3-C\equiv C-CF_3$ molecule will cause microwave absorption at 20752 Mhz, the $J=8\rightarrow 9$ transition at 23346 Mhz. The ratio of these frequencies is $9/8=1.125$. The ratio of the frequencies corresponding to the centers of the two domains of microwave absorption, is $\frac{24770}{22015}=1.125$. Therefore, the two groups of lines found represent absorption due to $J=7\rightarrow 8$ and $J=8\rightarrow 9$ transitions, complicated by the presence of restricted rotation.

Both groups of lines consist of 6 subgroups, each subgroup extending over a 15–20 Mhz range. We interpret each subgroup as consisting of several unresolved lines since a microwave line width of 15–20 Mhz would be something very exceptional. Indeed, we doubt at present that it will be possible to resolve the spectrum using ordinary Stark technique because probably the "quadratic" Stark components of some lines coincide with unperturbed lines.

The presence of hindered rotation in $CX_3-C\equiv C-CY_3$ compounds is thus firmly established. The barrier height is certainly less than for e.g., CH_3SiH_3 where it is about 1200 cal/mole.[3] Further studies of the spectra of $CH_3-C\equiv C-CF_3$ are planned in order to try to fix the approximate magnitude of the potential barrier.

[1] W. F. Edgell and A. Roberts, J. Chem. Phys. **16**, 1002 (1948).
[2] Dailey, Minden, and Shulman, Phys. Rev. **75**, 1319 (1949).
[3] H. T. Minden and B. P. Dailey, Phys. Rev. **82**, 338 (1951).
[4] D. R. Lide and D. K. Coles, Phys. Rev. **80**, 911 (1950).
[5] D. G. Burkhard and D. M. Dennison, Phys. Rev. **84**, 408 (1951).
[6] Hughes, Good, and Coles, Phys. Rev. **84**, 418 (1951).
[7] G. B. Kistiakowsky and W. W. Rice, J. Chem. Phys. **8**, 618 (1940).
[8] Yost, Osborne, and Garnes, J. Am. Chem. Soc. **63**, 3492 (1941).
[9] Harald H. Nielsen (private communication).
[10] Morino, Miyagawa, and Wada, J. Chem. Phys. **20**, 1976 (1952).
[11] Haszeldine, J. Chem. Soc. 1950, 3037 (1950).
[12] Haszeldine, J. Chem. Soc. 1951, 588 (1951).

The Infrared Spectrum of Dimethyltriacetylene

ALFONS WEBER, SALVADOR M. FERIGLE, AND FORREST F. CLEVELAND
Spectroscopy Laboratory, Department of Physics, Illinois Institute of Technology, Chicago 16, Illinois

(Received July 7, 1953)

DIMETHYLTRIACETYLENE (octa-2,4,6,-triyne) has been synthesized by Jones[1,2] and co-workers,[3] who have described its chemical and physical properties. Cook *et al.*[4] have obtained the infrared absorption spectra of $CH_3-(C\equiv C)_n-CH_3$ ($n=2-6$) in CCl_4 solution with a Perkin-Elmer double-beam spectrometer with NaCl prisms and have reported the location of the $-C\equiv C-$ stretching band for this series of compounds.

Since there is considerable interest in the spectra of polyacetylenic compounds,[5,6] we are investigating the vibrational spectra of dimethyltriacetylene (DMTA). Table I shows the infrared bands of DMTA obtained in CS_2 and CCl_4 solution with a Perkin-Elmer Model 21 double-beam spectrometer with NaCl optics and a Beckman IR-2 spectrometer with KBr optics, in juxtaposition to the results communicated by Jones.[7] Except for three low wave number skeletal vibrations, all allowed infrared fundamentals have been identified. The remaining bands have not been assigned as yet pending an investigation of the Raman spectrum. Table II lists some of the more prominent infrared absorption bands of the series of molecules $CH_3-(C\equiv C)_n-CH_3$ for $n=2$ to $n=6$ as communicated by Jones.[7] An investigation of the Raman spectrum and work on the normal coordinate treatment is in progress. The sample of DMTA was supplied through the courtesy of Professor E. R. H. Jones. Thanks are due to Dr. R. B. Bernstein of the Chemistry Department for placing the Perkin-Elmer spectrometer at our disposal. The authors also appreciate the assistance of the Office of Ordnance Research, U. S. Army; the Research Corporation; and the American Academy of Arts and Sciences for partial support of this research.

TABLE I. Infrared spectral data for dimethyltriacetylene $(CH_3-C\equiv C-C\equiv C-C\equiv C-CH_3)$.[a]

PR	ν(cm⁻¹) I	J	Description	PR	ν(cm⁻¹) I	J	Description
443	w			1378	vs	1380	$-CH_3$
604	w			1428	s	1432	$-CH_3$
654	vvw			1466	w		
674	vvs		$\equiv C-C\equiv$	1807	w		
764	m			1956	w		
808	m			2036	m	2038	
853	vw			2221	vvs	2222	$-C\equiv C-$
932	m		$\equiv C-C\equiv$	2396	w		
1020, 1033	m	1019	$-CH_3$	2445	w		
				2724	w		
1067	vvw			2835	m	2837	
1118	w			2912	s	2913	$-C-H$
1177	w			2955	m	2960	$-C-H$
1247	vvw			3022	m		
1290	w			3064	vvw		
1326	vvw			3080	w		
1363	vvw			3283	vw		

[a] PR = Present Results; I = estimated relative intensity (v = very, w = weak, m = medium, s = strong); J = Jones, reference 7.

TABLE II. Infrared spectral data for some dimethylpolyacetylenes $[CH_3-(C\equiv C)_n-CH_3, n=2, 3, 4, 5, 6]$.[a]

$n=2$	$n=3$	$n=4$	$n=5$	$n=6$
2961	2960	2915	2932	
2915	2913			
2845	2837	2840	2855	
2725				
2216	2222	2237	2221	2207
2156				
2050	2038			
		1704		
1437	1432	1419	1466	
1370	1380	1374	1379	
		1280	1261	
			1092	
1025	1019	1019	1012	

[a] Private communication, reference 7. All values are in cm⁻¹. The spectra were obtained in CCl_4 solution with a Perkin-Elmer double-beam instrument with NaCl optics.

[1] E. R. H. Jones, J. Chem. Soc. **1950**, 754.
[2] Jones, Whiting, Armitage, Cook, and Entwistle, Nature **168**, 900 (1951).
[3] Armitage, Cook, Jones, and Whiting, J. Chem. Soc. **1952**, 2010.
[4] Cook, Jones, and Whiting, J. Chem. Soc. **1952**, 2883.
[5] Ferigle, Cleveland, and Meister, J. Chem. Phys. **20**, 1928 (1952), and references cited therein.
[6] S. M. Ferigle and A. Weber, J. Chem. Phys. **21**, 722 (1953), and references cited therein.
[7] E. R. H. Jones (private communication, June 21, 1952).

Raman Spectrum of Oxalyl Chloride

B. D. SAKSENA, *National Physical Laboratory of India, New Delhi, India*
R. E. KAGARISE, *Naval Research Laboratory, Washington, D. C.*
AND
D. H. RANK, *Physics Department, The Pennsylvania State College, State College, Pennsylvania*

(Received June 8, 1953)

RECENTLY a paper by Ziomek, Meister, Cleveland, and Decker[1] on the Raman and infrared spectrum of oxalyl chloride has appeared in which doubts are cast on some of the experimental results obtained by Saksena and Kagarise.[2]

The discrepancies in question are not large and undoubtedly can be explained, but not in the manner proposed by ZMCD. The criticisms advanced by ZMCD are based on the contention that the experimental methods used by SK were inadequate in three respects: (1) polarization method, (2) resolving power, and (3) filtering technique.

It is possible to see the detail referred to by SK by reference to their Fig. 1. However, the reproductions are too small and the quality of the paper is inadequate to show the excellence of the polarization technique and resolution of the instruments used. We should like the reader to compare Fig. 1 of a paper by Rank, Saksena, and Shull[3] with Fig. 2 of Cleveland's[4] paper describing his polarization method. As a test of our supposedly inadequate resolution, Figs. 1 and 2 of a paper by Kagarise and Rank[5] may be consulted. The results of SK were obtained by the same methods and instruments which produced the plates from which the figures referred to above were prepared.

The 15-ft grating spectrograph has resolved sharp Raman lines of less than 3-cm⁻¹ separation and has a linear dispersion of 3.5A/mm in contrast to ZMCD's dispersion of 33A/mm. Our prism spectrograph has a dispersion of 19A/mm and resolving power limited only by the grain size of the type 1 photographic

plates used. Neither the prism nor the grating instrument showed any sign of splitting in the so-called doublets at 240–277 and 346–367 or the triplet 450–471–488 cm^{-1}, respectively. Only single very broad bands were observed with our instruments. It can be pointed out that large dispersion and resolving power might conceivably make any slight changes of intensity across such broad diffuse lines and tend to be less obvious than on photographs taken at lower dispersion. In view of the total situation, it seems very doubtful that these slight intensity changes across a broad band (if they exist) will have a very profound physical meaning.

The polarization method of Cleveland[4] requires critical anlysis to display some of its shortcomings. The method of excitation is essentially that described by Wood and Rank.[6] However, if improperly used, large convergence errors are introduced (later corrected empirically by comparing results with good data obtained by better methods). Douglas and Rank[7] have discussed this type of illumination in the first paragraphs of the experimental part of their paper. When the arc and scattering tube are near the paraxial foci of the cylindrical lens, the convergence error is very small, since the spherical aberration of the cylindrical lens causes most of the light from the outer zones to be ineffective in producing illumination in the scattering tube. Previously Rank[8] had measured ρ_n for a number of typical Raman lines using the photoelectric spectrograph. Intensity measurements with the photoelectric spectrograph are obtainable with many times the accuracy possible by means of photographic photometry. These results showed that, when properly used, the cylindrical lens method introduced only very small convergence errors. The $\Delta\nu=459$ line of CCl_4 can be used as an example. Cleveland[4] gives $\rho_n=0.072$ after empirically correcting for convergence error. Rank[8] obtained $\rho_n=0.064$ uncorrected for convergence error. Douglas and Rank[7] obtained $\rho_n=0.013$ by the method of polarized incident light which is free of convergence error to the third order of approximation.

The modification of the method of polarized incident light of Douglas and Rank[7] used by SK is essentially a differential method in its operation and is free of the vicissitudes of quantitative photographic photometry, convergence error, and the transmission factor of the spectrograph for the two kinds of plane polarized light. The theory demands only that one know which lines are more strongly polarized except in the case where all lines may belong to polarized classes. In this event quatitative ρ values are desirable and should be obtained by means of a good experimental method essentially free of convergence error.

ZMCD have tried to interpret the line observed at 201 cm^{-1} by SK as being a blend of 260 cm^{-1} excited by λ4347 and 1780 cm^{-1} by λ4078 and thus not as a real molecular frequency. It may be pointed out that λ4347 is very weak in the low-pressure "Toronto type" lamps which are now almost universally used in the more modern laboratories. Even without the use of any filter, excitation by λ4078 is weaker than that of λ4358 by an order of magnitude. We have used a $NaNO_2$ filter in an efficient manner as was pointed out above in the discussion of the proper use of cylindrical lens filters in conjunction with polarization methods.

An additional argument in support of interpreting the frequency at 201 cm^{-1} as a real molecular frequency and not as a blend is that, while the frequency at 201 cm^{-1} increases in intensity with an increase of temperature, the bands at 260 and 1780 cm^{-1} decrease in intensity.

We feel that the most conspicuous features of the spectrum of oxalyl chloride are the existence of very broad bands in both the Raman and infrared spectra, and the large variation in the intensity of these bands with temperature. Unless these effects are explained, the assignments may not be correct. It would appear that there are too many Raman lines for a completely *trans*-structure which requires only six active fundamentals. There are also a few coincidences, all of which may not be accidental. The assignment made with the help of the normal coordinate treatment is not entirely satisfactory as it proposes a strongly depolarized frequency for an A_g fundamental, a strongly polarized frequency for the B_g fundamental, and considers a very strong band in the infrared at 1058 cm^{-1} as a combination band, and a fairly strong Raman band at 189 cm^{-1} as a difference band.

We believe that further experimental work is needed to elucidate the structure of this molecule.

[1] Ziomek, Meister, Cleveland, and Decker, J. Chem. Phys. **21**, 90 (1953).
[2] B. D. Saksena and R. E. Kagarise, J. Chem. Phys. **19**, 987 (1951).
[3] Rank, Shull, and Saksena, Disc. Faraday Soc. **9**, 187 (1950).
[4] F. F. Cleveland, J. Chem. Phys. **13**, 101 (1945).
[5] R. E. Kagarise and D. H. Rank, Trans. Faraday Soc. **48**, 394 (1952).
[6] R. W. Wood and D. H. Rank, Phys. Rev. **48**, 63 (1935).
[7] A. E. Douglas and D. H. Rank, J. Opt. Soc. Am. **38**, 281 (1948).
[8] D. H. Rank, J. Opt. Soc. Am. **37**, 798 (1947).

Absorption of 3.3-cm Microwaves in Chloroform and Ethylene Dichloride in the Liquid State

S. C. SIRKAR, *Optics Department, Indian Association for the Cultivation of Science, Jadavpur, Calcutta, India*

and

D. K. GHOSH, *Department of Physics, University of Calcutta, Calcutta, India*

(Received July 7, 1953)

IT is well known that many simple molecules in the vapor state exhibit absorption bands in the microwave region owing to rotational transitions. In the case of chloroform, for instance, the rotational bands lie in the region 26 417–37 554 Mc/sec.[1,2] In the liquid state, however, these rotational transitions are damped, but the angular motion of the molecules is controlled by the coefficient of viscosity which determines the relaxation time τ of the liquid. It was observed by previous workers[3] that owing to the presence of such a relaxation time many organic liquids show anomalous absorption of radio waves of wavelengths of the order of a few meters. Recently, Sen[4] studied such absorption in many liquids in the region 250–550 Mc/sec by the optical method and observed some absorption peaks, the positions and heights of which depend on the temperature of the liquid. Kastha[5] and Ghosh[6] extended these investigations to the region 550–920 Mc/sec.

We have studied the absorption of microwaves of wavelength 3.33 cm in chloroform and ethylene chloride in the liquid state at different temperatures up to the freezing points of the liquids. A klystron oscillator of type 723 A–B was used in the range 8702–9548 Mc/sec, and the absorption at the radio waves coming out through a wave guide of cross section 2.3 cm×1 cm was studied by optical method, using another wave guide and a crystal detector. The difficulties due to formation of standing waves were avoided by shifting the position of the absorption cell placed between the two wave guides till maximum deflection in the microammeter connected in series with the crystal was observed. The cell containing the liquid was placed in baths at different temperatures, and the absorption coefficient was calculated from the deflections observed with the empty cell and the cell filled with the liquid at different temperatures placed between the two wave guides at proper positions. The values of absorption coefficient were plotted against temperatures of the cell and the temperature at which the absorption was maximum was found out.

The values of τ, the relaxation time, were calculated from the frequency of the waves and the values of dielectric constant ϵ_0 and ϵ_1 for infinite and zero frequencies respectively from Debye's theory. The value of a, the radius of the rotor, was also calculated with the help of extrapolated values of η, the coefficient of viscosity. The results are given in Table I.

TABLE I. $\omega=56\,540$ Mc/sec.

Liquid	T°K for max abs	ϵ_1	ϵ_0	$\tau\times10^{11}$	$\eta\times100$	$a\times10^{8}$ cm
Chloroform	228	6.12	2.094	1.523	1.12	1.5
Ethylene-chloride	263	12.7	2.084	1.214	1.20	1.426

It can be seen from Table I that the values of a are of the order of the C−Cl distance. So the rotor is a single molecule in both cases. Evidently, in the case of $C_2H_4Cl_2$ the rotational orientation is about the C−C axis, and the high value of the dielectric constant indicates a high value of permanent electric moment. Hence the molecule in this case is of *gauche*-type and not of the trans-type even at −10°C. Details will be published elsewhere.

[1] W. V. Smith and R. R. Unterberger, J. Chem. Phys. **17**, 1348 (1949).
[2] Ghosh, Trambarulo, and Gordy, J. Chem. Phys. **20**, 605 (1952).
[3] S. Mizushima, Sci. Papers Inst. Phys. Chem. Research (Tokyo) **5**, 201 (1927).
[4] S. N. Sen, Indian J. Phys. **24**, 163 (1950).
[5] G. S. Kastha, Indian J. Phys. **26**, 103 (1952).
[6] D. K. Ghosh, Indian J. Phys. (to be published).

On the Structure of Oxalyl Chloride

R. E. KAGARISE
Naval Research Laboratory, Washington 25, D. C.
(Received July 1, 1953)

THE question of rotational isomerism in oxalyl chloride has been the subject of two recent papers. Saksena and Kagarise[1] have suggested that the compound is a mixture of two forms, namely, the *trans*- (C_{2h}) and the *cis*- (C_{2v}). From temperature-intensity measurements in the Raman effect, the value of ΔH for the reaction C_{2h} oxalyl chloride→C_{2v} oxalyl chloride in the liquid state was found to be 2.8 kcal/mole. On the basis of these two forms a tentative assignment was made of all fundamental frequencies.

Ziomek, Meister, Cleveland, and Decker[2] have also studied this compound and conclude that the present evidence is greatly in favor of the *trans*-structure for oxalyl chloride. An assignment was made assuming the sample to be in the *trans*-form only. They assert that it would be desirable to investigate the temperature dependence of the infrared spectrum before concluding that the 533-cm^{-1} band is due to the *cis*-structure as suggested by Saksena and Kagarise.[1]

Numerous investigations[3–7] in the past have shown that one of the most convincing ways of demonstrating the phenomenon of rotational isomerism is to study the Raman or infrared spectrum of the crystalline solid. Although the various stable configurations will normally be present in both the gaseous and liquid states, it often happens that only a single isomer occurs in the crystalline solid state, and accordingly a marked simplification of the spectrum occurs upon solidification.

We have investigated the infrared spectrum of oxalyl chloride in the solid phase by means of a low-temperature cell similar to the one described by Lord, McDonald, and Miller.[8] The sample of oxalyl chloride used in this investigation was obtained from the Eastman Kodak Company and was fractionally distilled prior to being used. The spectrum was observed in the rocksalt region by means of a Perkin-Elmer 21 spectrometer, and in the 15–22μ region with the KBr prism instrument of high resolution previously described.[9] The low-temperature cell was filled and sealed, and the spectrum of the liquid at room temperature was obtained. The sample was then frozen by cooling with a dry ice-acetone mixture, and the spectrum of the crystalline solid was observed. These two spectra are shown in Fig. 1. After melting, the spectrum of the liquid was reinvestigated and found to be similar in all respects to that of the initial liquid state.

Figure 1 shows the striking changes that occur upon solidification, the outstanding ones being the complete disappearance of the two bands at 1050 and 533 cm^{-1}, respectively. According to the assignment of Saksena and Kagarise[1] these frequencies are due to the *cis*-form of the molecule and should disappear if only the *trans*-form occurs in the crystalline solid state. On the other hand, it does not appear to be possible to explain these observed temperature and solidification effects on the basis of a single molecular species of symmetry C_{2h} (*trans*-form) or, in fact, by any single molecular species.

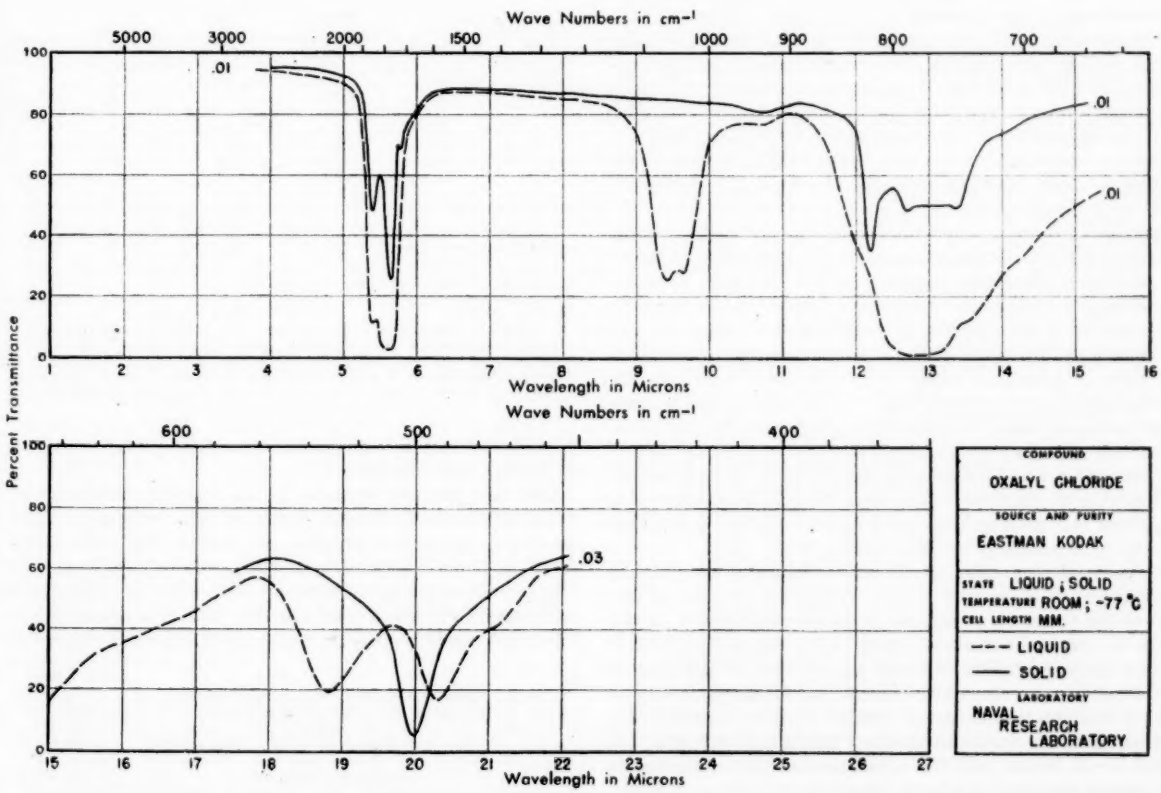

FIG. 1.

In conclusion we should like to emphasize the following points.

1. The temperature-intensity effects observed by Saksena and Kagarise[2] are very pronounced, as evidenced by the calculated energy difference of 2.8 kcal/mole.

2. A marked simplification occurs in the infrared spectrum of oxalyl chloride upon solidification. Since the bands which disappear are strong in both the gaseous and liquid states, one can hardly attribute this effect to the operation of more strict selection rules in the crystal lattice. Axford and Sheppard[10] have pointed out that "since in the crystalline lattice a molecule is in a less symmetrical environment than in the isolated (gaseous) state, it follows that any fundamental internal vibrational mode allowed in the gaseous state will also be allowed in the crystalline state, and in the liquid state also."

3. It appears certain that these observed temperature effects are real and must be an integral part of any satisfactory interpretation of the observed spectra.

[1] B. D. Saksena and R. E. Kagarise, J. Chem. Phys. **19**, 987 (1951).
[2] Zimoek, Meister, Cleveland, and Decker, J. Chem. Phys. **21**, 90 (1953).
[3] Mizushima, Morino, and Noziri, Sci. Papers Inst. Phys. Chem. Research (Tokyo) **29**, 63 (1936).
[4] Rank, Sheppard, and Szasz, J. Chem. Phys. **17**, 83 (1949).
[5] D. W. E. Axford and D. H. Rank, J. Chem. Phys. **18**, 51 (1950).
[6] J. T. Neu and W. D. Gwinn, J. Chem. Phys. **18**, 1642 (1950).
[7] J. K. Brown and N. Sheppard, Disc. Faraday Soc. **9**, 144 (1950).
[8] Lord, McDonald, and Miller, J. Opt. Soc. Am. **42**, 149 (1952).
[9] Nielsen, Crawford, and Smith, J. Opt. Soc. Am. **37**, 296 (1947).
[10] D. W. E. Axford and N. Sheppard, Disc. Faraday Soc. **9**, 210 (1950).

Carbon-Carbon Bond Dissociation Energies in the Cycloalkanes

FRANK H. SEUBOLD, JR.
Department of Chemistry, Northwestern University, Evanston, Illinois
(Received July 13, 1953)

THE current availability of accurate data for the heats of formation of hydrocarbons, the heats of dissociation of chemical bonds, and the energy required for rotational transitions in hydrocarbons makes possible the calculation of the carbon-carbon bond dissociation energies of the cycloalkanes. Although these calculations are obvious, their presentation is deemed appropriate since no unequivocal experimental determinations of these quantities have been published. For example, in the pyrolyses of cyclopentane and cyclohexane, the rates of formation of the products which arise from chain fission exhibit autocatalysis, indicating a chain reaction probably involving the cycloalkyl radicals and vitiating any estimation of D(C−C) from the measured energies of activation.[1] In the case of cyclopropane, Ogg gave a value of 32.9 kcal/mole for D(C−C) from a study of the reaction of the cycloalkane with iodine,[2] but later amended this to about 50 kcal/mole.[3] An electron impact study of cyclopropane provided an estimate of >44 kcal/mole based on the appearance potential of the $C_2H_3^+$ ion,[4] and another unpublished report gave a calculated value of 50 kcal/mole based on the method of group equivalents.[5] Only in the case of cyclobutane does an adequate dissociation energy appear to be available. Walters found the thermal decomposition in the range 430–480°C to be first order and devoid of surface effects, leading almost quantitatively to ethylene.[6] The observed activation energy of 61 kcal/mole is in good agreement with D(C−C) for cyclobutane calculated by the method presented here.

Since heats of formation for the cycloalkanes up to C_9 have been published, it is necessary only to calculate the heat of formation of the bi-radical produced by fission of a carbon-carbon bond for the heat of that dissociation to be known. The heat of formation of the bi-radical is taken as the sum of the heat of formation of the corresponding alkane, the energy necessary to transform it from the staggered configuration to a coiled configuration as in the cycloalkane, the dissociation energy of the terminal C−H bonds, and the association energy of hydrogen.

The energy required to achieve the eclipsed butane configuration (necessary in these calculations once in the case of butane and twice in the case of pentane) is taken as 6 kcal/mole.[7] The methylene interaction energy in the chair form of cyclohexane has been calculated to be 8.4 kcal/mole.[8] This interaction energy has been assumed for hexane coiled to this configuration. In this position, three *gauche*-interactions, accounting for 3×0.8=2.4 kcal/mole[9] of the total energy, are present. The difference, 6.0 kcal/mole, is assumed to arise from the two nonbonded propane type interactions present in the coiled molecule. In the calculations for the seven-, eight-, and nine-membered rings, each such interaction will also be assigned an energy of 3.0 kcal/mole. Thus, the interaction energy of the coiled octane molecule is determined as shown in Fig. 1.

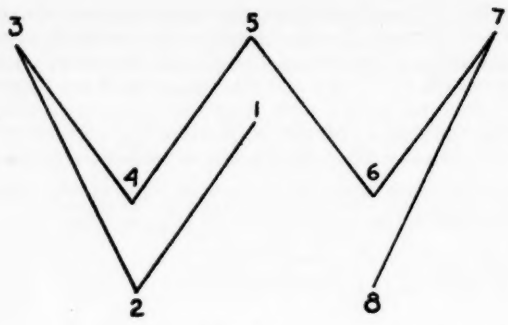

FIG. 1.

Interaction	Energy, kcal/mole
123456	8.4
47	0.8
58	0.8
17	3.0
28	3.0
total	16.0

TABLE I.

C_n	ΔH_f[a] *n*-alkane	IE[b] for *n*-alkane (coiled)	ΔH_f bi-radical	ΔH_f cycloalkane	D(C−C)
3	−24.9[c]	0.0	63.(0)	+12.7[d]	50
4	−29.8	6.0	63.(0)	+ 4.8[e]	58
5	−35.0	12.0	63.(8)	−18.5[e]	82
6	−40.0	8.4	55.(2)	−29.4[e]	85
7	−44.9	12.2	54.(1)	−28.8[f]	83
8	−49.8	16.0	53.(0)	−30.2[f]	83
9	−54.7	19.0	51.(1)	−32.8[g]	84

[a] All values are given in kcal/mole for the perfect gas at 25°C.
[b] Interaction energy.
[c] *Selected Values of Properties of Hydrocarbons* (National Bureau of Standards, Washington, D. C., 1944-1947).
[d] J. W. Knowlton and F. D. Rossini, J. Research Natl. Bur. Standards **43**, 113 (1949).
[e] S. Kaarsemaker and J. Coops, Rec. trav. chim. **71**, 261 (1952).
[f] R. Spitzer and H. M. Huffman, J. Am. Chem. Soc. **69**, 211 (1947).
[g] Reference e, corrected to correspond with the values of the National Bureau of Standards and of Spitzer and Huffman. Where comparable, C_5 through C_8, Coops' values were 2.0 to 2.5 kcal/mole more negative.

In a like manner the other values reported for interaction energies in Table I were obtained.

The last required quantity is the dissociation energy of the terminal carbon-hydrogen bonds of the molecule. Since for methane, ethane, and propane the methyl D(C−H) values are 102.5, 96.9, and 95.5 kcal/mole,[10] respectively, it is most probable that for the succeeding members of the series this quantity is very nearly 95.0 kcal/mole. On this basis, the remainder of the calculation of D(C−C) for cyclo-octane is carried out as follows:

	kcal/mole
$n-C_8H_{18}$ (staggered) → $n-C_8H_{18}$ (coiled)	16.0
$n-C_8H_{18}$ (coiled) → $\cdot(CH_2)_8\cdot + 2H\cdot$	190.0
$2H\cdot \rightarrow H_2$	−103.2
H_2 + cycloC_8H_{16} → $n-C_8H_{18}$ (staggered)	− 19.6
cycloC_8H_{16} → $\cdot(CH_2)_8\cdot$	83.(2)

The other calculations are summarized in Table I.

The accuracy of these calculations rests primarily on the configurational energies as the least well-known quantities, but the latter are believed to be well enough established to give a probable error of no more than ±2 kcal/mole for the dissociation energies, little more than the usual deviation in most experimental determinations.

These calculated values are in accord with the qualitative evidence concerning cycloalkanes: the opening of the cyclopropane ring although cyclobutane is inert under the same conditions; the relative ease of ring opening by hydrogenation of cyclopropane and cyclobutane compared to cyclopentane and cyclohexane; and ring strains calculated on the basis of a strain-free cyclohexane (cyclopropane: 27.4 kcal/mole, cyclobutane: 24.4, cyclopentane: 6.0).

A grant from the Research Corporation in support of the research in connection with which these calculations were made is gratefully acknowledged.

[1] I. Kuchler, Z. physik. Chem. **53**, 307 (1943); A. Eucken, Die Chemie **56**, 342 (1943); G. R. Schultze and G. Wassermann, Z. Elektrochem. **47**, 774 (1941).
[2] R. A. Ogg and W. J. Priest, J. Chem. Phys. **7**, 736 (1939).
[3] Private communication quoted by H. E. Gunning and E. W. R. Steacie, J. Chem. Phys. **17**, 351 (1949).
[4] F. H. Field, J. Chem. Phys. **20**, 1734 (1952).
[5] J. L. Franklin, paper presented at the Seventh Southwest Regional Meeting of the American Chemical Society (unpublished), quoted in reference 4.
[6] C. T. Genaux and W. D. Walters, J. Am. Chem. Soc. **73**, 4497 (1951).
[7] K. Ito, J. Am. Chem. Soc. **75**, 2430 (1953).
[8] P. Hazebroek and L. J. Osterhoff, Discussions Faraday Soc. **10**, 87 (1951).
[9] K. S. Pitzer, J. Chem. Phys. **8**, 711 (1941); Szasz, Sheppard, and Rank, J. Chem. Phys. **16**, 704 (1948).
[10] J. S. Roberts and H. A. Skinner, Trans, Faraday Soc. **45**, 339 (1949)

Random Walk Theory of One-Dimensional Gases*

C. W. Harris, Robert L. Sells, and Eugene Guth
Department of Physics, University of Notre Dame, Notre Dame, Indiana
(Received July 14, 1953)

In a previous communication[1] we have shown that the Born-Green (BG) equation for a one-dimensional gas (of N molecules between two molecules of the same kind fixed at $r=0$ and $r=L$) with nearest neighbor interaction $\varphi(r)$ involving a hard core d and finite range λ,

$$\begin{aligned}\varphi(r)&=\infty\,; \quad r<d=1\\ &=0\,; \quad r>\lambda\end{aligned} \tag{1}$$

has the form:

$$n_2'(r)+\beta n_2^*(r)\varphi'(r)=\beta\Big[n_2(r)\int_0^\infty n_2^*(s)\varphi'(s)ds - \int_0^r n_2^*(s)n_2(r-s)\varphi'(s)ds\Big], \tag{2}$$

where n_2 is the pair distribution function (normalized such that $\int_0^\infty n_2(r)dr=1$), and $\beta=1/kT$. Equation (2) was solved explicitly for hard sphere and square-well interactions.

In contrast to the three-dimensional case, nearest neighbor interaction with hard core permits ordering of the molecules, and then an appropriate rigorously valid superposition principle affects the reduction of n_3 to products of n_2's leading to Eq. (2). The higher distribution functions n_k are simply products of the pair distribution functions.

We also pointed out that, in contrast to the three-dimensional case, the (thermal and caloric) equations of state were determined by $n_2^*(r)$, the distribution function for adjacent molecules. $n_2^*(r)$ satisfies Eq. (2) with the last integral vanishing identically. From this equation we obtain:

$$n_2^*(r)=\frac{e^{-c r-\beta\varphi}}{\int^\infty e^{-cs-\beta\varphi}ds}\,; \quad c=-\beta\int_0^\infty n_2^*(s)\varphi'(s)ds. \tag{3}$$

Independently, Salsburg, Zwanzig, and Kirkwood[2] (SZK) in an interesting paper obtained, by direct integration of the complete phase integral, an expression for $n_2(r)$, extending a method used by Gursey[3] to obtain the partition function and also $n_2^*(r)$. This method involves convolution forms of the Laplace transforms and their inversion. For the square-well interaction, solution (by Laplace transform techniques) of the difference-differential equations to which Eq. (1) reduces and evaluation of this expression naturally involve similar steps and about the same amount of labor.

The purpose of this letter is to point out that *all these problems of a one-dimensional gas are actually special cases of problems of the general one-dimensional random walk.* This observation is almost trivial, nevertheless, it has not been made before in the literature to our knowledge. In the random walk problem each "step" introduces an additional "displacement." Let $P_k(r)dr$ be the (normalized or unnormalized) *a priori* probability that the k'th "step" arrives at a distance r within dr starting at $r=0$. The "steps" are independent. The probability $W_n(R)dR$ that the total "displacement" after n steps will be between R and $R+dR$ is obtained by a method originating with Markoff as

$$W_n(R)=\mathfrak{F}^{-1}\Big\{\prod_{k=1}^{n}\mathfrak{F}P_k(r)\Big\}, \tag{4}$$

where $\mathfrak{F}^{-1}$ and $\mathfrak{F}$ designate inverse and direct Fourier transforms, respectively. Obviously, Laplace ($\mathfrak{L}$) instead of Fourier transforms can be used to obtain for Eq. (4) the alternative form

$$W_n(R)=\mathfrak{L}^{-1}\Big\{\prod_{k=1}^{n}\mathfrak{L}P_k(r)\Big\}. \tag{5}$$

For the one-dimensional gas with nearest neighbor interaction specified by Eq. (1) the pairs of adjacent molecules are the independent "steps." To obtain the partition function $Q_N(R)=W_{N+1}(R)$ one starts with the (unnormalized) probability

$$P_k(r)=P(r)=e^{-\beta\varphi(r)}. \tag{6}$$

Application of Eq. (5) leads at once to Gursey's equation (3.5):

$$\begin{aligned}Q_N(L)&=\mathfrak{L}^{-1}\{[\mathfrak{L}e^{-\beta\varphi(r)}]^{N+1}\}\\ &=(1/2\pi i)\int_{\alpha-i\infty}^{\alpha+i\infty}e^{Ls}[\phi(s)]^{N+1}ds,\end{aligned} \tag{7}$$

where $\phi(s)=\mathfrak{L}[e^{-\beta\varphi(r)}]$. Thus, Gursey's method is actually Markoff's method.

To obtain the pair distribution function $n_2(r)$, one starts with the (normalized) probability:

$$P_k(r)=P(r)=n_2^*(r)=e^{-cr-\beta\varphi}\Big/\int_0^\infty e^{-cs-\beta\varphi}ds. \tag{8}$$

Application of Eq. (5) then leads to $n_2^{(k)}(r)=W_k(r)$, the distribution function for the case that there are $k-1$ molecules between two fixed molecules. [In this notation $n_2^*(r)=n_2^{(1)}(r)$.]

$$n_2^{(k)}(r)=\mathfrak{L}^{-1}\{[\mathfrak{L}n_2^*(r)]^k\}. \tag{9}$$

The second step is simply to sum the $n_2^{(k)}(r)$ to obtain $n_2(r)$:

$$n_2(r)=\sum_{k=1}^{N+1}n_2^{(k)}(r)=\sum_{k=1}^{N+1}\mathfrak{L}^{-1}\{[\mathfrak{L}n_2^*(r)]^k\}. \tag{10}$$

In SZK's notation $\mathfrak{L}[n_2^*(r)]=\Omega(c+u)/\Omega(c)$. Thus, more explicitly Eq. (10) becomes [$S_k(x)=0$ for $x<k$, and $S_k(x)=1$ for $x\geq k$]

$$n_2(r)=\sum_{k=1}^{N+1}S_k(r)\frac{1}{2\pi i}\int_{\alpha-i\infty}^{\alpha+i\infty}e^{ru}\left[\frac{\Omega(c+u)}{\Omega(c)}\right]^k du, \tag{11}$$

where $\alpha=0$ for the interaction of Eq. (1). It is interesting to note that from the $n_2^{(k)}(r)$ only $n_2^{(1)}(r)$ satisfies a (simplified) BG equation, but that the sum of the $n_2^{(k)}(r)$ *does* satisfy the BG integro-differential equation.

Substitution of $c+u=s$ in Eq. (11) leads at once to SZK's Eq. (23b) [we put SZK's $a=1$, and our present definition of $n_2(r)$ differs from SZK's by a factor $\rho=1/la$].

If one uses, with Takahasi,[4] a (p, T) ensemble instead of the $(L, T$ ensemble, one may introduce the generalized partition

function

$$R_N(p, T)=\int_0^\infty Q_N(L, T)e^{-\beta pL}dL=\mathfrak{L}(Q_N). \quad (12)$$

This is related to the Gibbs free energy $G=U-TS+pL$ in the same way as $Q_N(L, T)$ is related to the Helmholtz free energy $F=U-TS$

$$\left.\begin{aligned} G(p, T)&=-kT\ \ln R\\ F(L, T)&=-kT\ \ln Q\end{aligned}\right\}. \quad (13)$$

Then one can introduce immediately (without use of the BG equation)

$$n_2^*(r)=e^{-\beta(p\tau+\varphi)}\Big/\int_0^\infty e^{-\beta(ps+\varphi)}ds, \quad (14)$$

while with the previous method one needs a relation like

$$p=-\int n_2^*(r)\varphi'(r)dr \quad (15)$$

to identify c with p. For $R(p, T)$ we obtain the simple expression

$$R(p, T)=[\Omega(\beta p)]^{N+1}. \quad (16)$$

Random walk methods to derive equations of state for flexible chain molecules were used extensively by James and Guth[5] who also pointed out that use of R is much simpler than the use of Q in such problems.

* Supported in part by U. S. Office of Naval Research.

[1] Sells, Harris, and Guth, J. Chem. Phys. **21** (to be published). In Eq. (3) of this reference $g(s)$ is actually the corresponding distribution function for adjacent molecules. Thus, Eq. (3) is a linear integral equation of the convolution type.

[2] Salsburg, Zwanzig, and Kirkwood, J. Chem. Phys. **21**, 1098 (1953).

[3] F. Gursey, Proc. Cambridge Phil. Soc. **46**, 182 (1950).

[4] H. Takahasi, Proc. Phys.-Math. Soc. Japan **24**, 60 (1942).

[5] H. M. James and E. Guth, J. Chem. Phys. **11**, 455 (1943).

Studies in Molecular Orbital Theory of Valence. II. The Transition State in Walden Inversion Type Reactions*

H. H. JAFFÉ

Venereal Disease Experimental Laboratory, U. S. Public Health Service, School of Public Health, University of North Carolina, Chapel Hill, North Carolina

(Received July 13, 1953)

THE transition state in reactions of the type of the Walden inversion ($AB+C\rightarrow A+BC$) has frequently been described from a valence bond (VB) point of view as resonance between structures I and II.[1] In this paper we shall examine

$$\underset{\text{I}}{A\quad B-C} \qquad\qquad \underset{\text{II}}{A-B\quad C}$$

whether this VB description has an analog in molecular orbital (MO) theory, and what inferences about the nature and energy of the transition states can be drawn from such a MO description. In order to simplify the arguments, we shall deal with a somewhat specific example, although the conclusions can be readily generalized.

The reaction chosen is $ACH_3+A^*\rightarrow A+CH_3A^*$. The transition state then corresponds to a configuration in which A and A^* are equidistant from C. Since it is likely that this transition state is symmetrical, it may be assumed that the central CH_3 group is planar in the xy plane. Because electronic motion is rapid compared with nuclear motion we may assume *that* electronic structure for the CH_3 group which will minimize its energy. Hence the CH bonds will be regarded as formed from the s orbitals of the hydrogen atoms, and sp^2 orbitals of the central carbon atom. Then the p_z orbital of the carbon atom (the ACA^* axis is taken as the z axis) remains available for bond formation with the atoms A and A^*. Each of these atoms will be assumed to have a single atomic orbital with cylindrical symmetry around the z axis available for bonding. These orbitals may be pure p or hybrid s^zp^{1-z} orbitals and will be denoted by σ and σ^*.

On the basis of these assumptions, MO's for AC— and A^*C— bonding can readily be constructed. The orbitals σ and σ^* are combined into group orbitals:[2]

$$\chi_1=(2)^{-\frac{1}{2}}(\sigma+\sigma^*),$$
$$\chi_2=(2)^{-\frac{1}{2}}(\sigma-\sigma^*).$$

χ_2 is of correct symmetry to interact with p_z, leading to the MO's

$$\psi_1=(2+2S)^{-\frac{1}{2}}(p_z+\chi_2)$$
$$\psi_3=(2-2S)^{-\frac{1}{2}}(p_z-\chi_2),$$

where S is the group overlap integral

$$S=\int p_z\chi_2 d\tau=(2)^{\frac{1}{2}}\int p_z\sigma d\tau.$$

χ_1 cannot interact with p_z; hence it is a nonbonding orbital, and will be denoted by ψ_2. The energy of the MO's can readily be seen to increase in the order $\psi_1>\psi_2>\psi_3$. This description of the transition state holds equally if the attacking reagent A is an anion, a free radical, or a cation. The only difference in these three situations is that the nonbonding orbital ψ_2 holds two, one, or no electrons, respectively, in the three cases.

According to this MO description, each CA bond in the transition state is a one-half bond, with a bond order of $(2)^{-\frac{1}{2}}$. Hence extrapolation from published curves[3] should permit a rough estimate of the bond lengths and energies involved. The activation energy for the reaction, i.e., the difference of the energy of initial and transition state can then be estimated. It is equal to the difference between the energy of a simple single covalent AB bond, and twice the energy of the AB half-bond of the transition state. A correction for the change in hybridization of the CH bonding orbitals must be included. This correction is readily available as three times the difference of CH bond energy of CH bonds in saturated and unsaturated (ethylenic) compounds. Finally a further correction term is necessary. Since the CH bond energy and the CA half-bond energy are obtained from compounds with entirely different electronic structures, it seems likely that corrections for electron-repulsion energy are necessary. An evaluation of this last correction factor appears to be a major difficulty. It might be neglected as a first approximation, particularly when interest is focused on comparison of reactions of compounds of similar structure. Further, its importance might be evaluated from comparison of reactions involving A^-, $A\cdot$, and A^+, where the electronic repulsion terms apparently determine the differences of activation energies completely.

One complication further needs some consideration. We have treated the CH_3 group implicitly as formed from localized MO's consisting of carbon sp^2 and hydrogen s orbitals. An explicit nonlocalized MO description of this group would involve, among others, the following MO:

$$\psi_4=A[s_H(1)+s_H(2)+s_H(3)]+Bs_C,$$

where A and B are constants, the $s_H(n)$ are the $1s$ orbitals of the hydrogen atoms, and s_C the $2s$ orbital of the carbon atom. This orbital ψ_4 is of the same symmetry class as ψ_2, and hence may interact with it. Such interaction would lead to slight weakening of the CH bonds and strengthening of the CA bonds. However, the energy of ψ_4 is probably sufficiently lower than that of ψ_2 so that the interaction may well be neglected in the first approximation.

The MO description presented here is essentially equivalent to the customary description of the transition state. However, it appears that the MO description given here is much more detailed than the VB description and permits more straightforward estimation of geometry and energies of the transition state. In particular it appears that relative values for activation energies could be calculated for closely related reactions such as the radioactive exchanges of A (F, Cl, Br, I, OH, NH_2), either for anions A^- or free radicals $A\cdot$. Unfortunately the experimental data for testing predictions from such calculations are not available.

* For paper I of this series see J. Chem. Phys. **21**, 156 (1953). See also H. H. Jaffé, J. Chem. Phys. **21**, 1287 (1953).

[1] M. J. S. Dewar, *Electronic Theory of Organic Chemistry* (Clarendon Press, Oxford, 1949), p. 25; G. W. Wheland, *The Theory of Resonance* (John Wiley and Sons, Inc., New York, 1944), p. 218.

[2] This process assumes that σ and σ^* are so distant that their interaction can be neglected safely.

[3] C. A. Coulson, J Phys. Chem. **56**, 311 (1953).

Paramagnetism in a Thermochromic Compound*

WALTER G. NIELSEN AND GEORGE K. FRAENKEL
Department of Chemistry, Columbia University, New York 27, New York
(Received July 18, 1953)

THE change of color with temperature of numerous organic compounds, the phenomenon known as thermochromism, has been of interest for many years. Grubb and Kistiakowsky[1] and Theilacker, Kortüm, and Friedheim,[2] performed spectroscopic investigations and were led to the conclusion that in solutions of certain of these compounds there exist two interconvertible isomeric forms in thermal equilibrium with each other. Each of the two forms gives rise to an absorption spectrum and the dependence of the color on temperature is accounted for by the changes with temperature, due to a shift of the equilibrium, in the relative number of molecules in the two states. In the particular case of bianthrone,

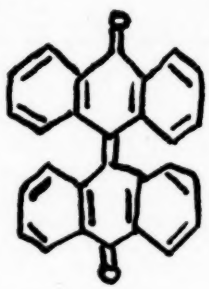

an energy difference between the two forms of 3.5 kcal/mole was found. Certain of these compounds were also found to give rise to the same absorption spectra, when irradiated with ultraviolet light at low temperatures, as when heated.[3] On the basis of chemical evidence, Schönberg[4] proposed that the upper state has a betaine structure, but Grubb and Kistiakowsky[1] and Theilacker, *et al.*,[2] concluded from their spectroscopic data that the higher energy form is a triplet (di-radical) state energy and the lower energy form is a singlet state.

In order to test conclusively the triplet state hypothesis, magnetic measurements are required. In this note, measurements are reported on the paramagnetic resonance absorption of bianthrone,[5] over a range of temperatures, in the crystalline state and in solution with various solvents.[6] Under appropriate conditions, both the crystalline bianthrone and the solutions are found to be paramagnetic. The measurements in solution are qualitatively consistent with the spectroscopic data.

The apparatus used in these experiments has been partially described elsewhere.[7] In addition, the equipment was provided with low-frequency modulation of the magnetic field.

Bianthrone is ordinarily a light yellow crystalline solid. If it is heated to about 265°C, it first turns light green and then, after continued heating at this temperature, turns a darker green without changing its crystalline appearance. The samples heated to 265°C showed a paramagnetic absorption at this temperature and also after cooling to room temperature. The paramagnetism and color of the heated samples appear to persist indefinitely at room temperature; the first sample treated is still paramagnetic after five months. Samples of bianthrone which had never been heated above 190°C did not show any detectable paramagnetic absorption. The spectroscopic splitting factor (g value) measured at room temperature was the same, within the experimental error of 0.1 percent, as that of 2,2′-diphenyl-1-picryl hydrazil ($g=2.0036$).[8] The line width as measured between points of maximum slope is approximately 10 gauss.

Paramagnetic resonance absorption was also observed in solutions of bianthrone in decalin and dimethylphthalate. The solutions were prepared by dissolving the samples at temperatures ranging from 130° to 250°C and varied in concentration from 3.7 to 9.0 grams per 1000 grams of solvent. In most of the samples a paramagnetic absorption was observed in the range from 140° to 200°C. In the more concentrated samples, the intensity of the absorption was found to decrease with decreasing temperature down to a temperature where it could no longer be detected. In the more dilute samples, however, it was only possible to observe that no absorption could be detected below a certain temperature, usually in the range from 100° to 150°C. In one of the more concentrated solutions in dimethylphthalate, an absorption was observed in the supersaturated solution at 88°C. The g value and line widths in solution were measured in only a few cases and generally appeared to be the same as for the solid samples. Paramagnetic absorption was also observed in solutions with acetophenone as solvent.

It was considered possible that the relatively high temperatures which were required to dissolve and detect the paramagnetic absorption may have caused some decomposition of the bianthrone. No direct evidence of decomposition was observed, however, and the paramagnetism was found to be qualitatively reversible with temperature.

It is concluded from these observations that bianthrone exists partially in a paramagnetic state in solution, that the population of this state increases with temperature, and that, at high enough temperatures, the solid is transformed into a paramagnetic state. No direct magnetic evidence is available to indicate that the paramagnetic form is a triplet state.

Additional experiments are planned on solutions of other thermochromic compounds in a variety of solvents, and it is hoped to improve the reproducibility of the measurements sufficiently to obtain approximate values of the change in the heat content and free energy for the transition. Further investigations are also under way on the transformations observed in the solid state.

* Supported in part by the Squier Signal Laboratory, U. S. Army Signal Corps.
[1] W. T. Grubb and G. B. Kistiakowsky, J. Am. Chem. Soc. **72**, 419 (1950).
[2] Theilacker, Kortüm, and Friedheim, Chem. Ber. **83**, 508 (1950).
[3] Y. Hirshberg and E. Fischer, J. Chem. Soc. **1953**, 629.
[4] Schönberg, Ismail, and Asker, J. Chem. Soc. **1946**, 442.
[5] The authors are indebted to Mr. John Arents for the bianthrone sample. The bianthrone was twice recrystallized from a 2:1 (by weight) mixture of acetic acid and methyl salicylate, washed with acetone and dried. The melting point was above 330°C as determined by introducing the sample into a preheated copper block.
[6] All solvents were high quality commercial solvents and were redistilled.
[7] Hirshon, White, and Fraenkel, Rev. Sci. Instr. **23**, 772 (1952).
[8] Holden, Kittel, Merritt, and Yager, Phys. Rev. **77**, 147 (1950).

Multiple Reversible Color Changes Initiated by Irradiation at Low Temperature

YEHUDA HIRSHBERG AND ERNST FISCHER
The Daniel Sieff Research Institute, The Weizmann Institute of Science, Rehovoth, Israel
(Received July 8, 1953)

IN a series of publications[1–4] the authors have described the phenomenon of photochromism, i.e., the *reversible* transformation of certain colorless compounds into colored modifications when the respective solutions are irradiated with ultraviolet light at temperatures in the vicinity of 173°K. It has been then shown that in those compounds which exhibit both thermochromism and photochromism the thermochromic and the photochromic colors are in each case spectroscopically identical.

By extending our investigations to still lower temperatures, we could now show that, when irradiation is carried out at about 105°K (in a solvent mixture of methylcyclohexane and petrol ether), compounds of the spiropyran series are *reversibly* converted into new types of colors (see column B in Table I).

When these colors are slowly heated to about 123°K, they go over spontaneously into a second colored modification, which is also produced when the original colorless solutions are irradiated at 123°K (column C).

On further heating of these colored solutions, to about 163°K, spontaneous conversion into a third colored modification occurs (column D). This modification is identical with the color formed

TABLE I.

A	B	C	D	E
	Color resulting from irradiation:			
Compound	at 103°K	at 123°K (also formed spontaneously from B.)	at 163°K (also formed spontaneously from C.)	Luminescence of modification C.
Dibenzospiropyran	green	wine-red	rose-mauve	yellow
Benzo-β-naphthospiropyran (I)	rose	blue-violet	rose-mauve	red
3:methyl-(I)	rose	blue-violet	rose-mauve	red
3′:methyl-(I)	blue-green	rose	mauve	orange
3:3′-trimethylene-di-β-naphthospiropyran	green	rose	mauve	brick-red

as a result of irradiation of the colorless form at this temperature, as described previously.[3]

At higher temperatures (but in all cases below 273°K) all colors disappear, the original colorless modifications being re-formed.

Luminescence studies of the various modifications described above showed that only the second colored modification in each case (column C) exhibits pronounced luminescence on excitation with the 365-m group of the mercury arc (column E).

If one assumes that low-temperature irradiation results in complete conversion into the various colored modifications, the spectrophotometric data yield calculated molar extinction coefficients of 10 000 to 100 000 for all the colors observed. It therefore seems likely that, in the photochemical-equilibrium mixture established in each case, a considerable fraction of the respective compounds is in its colored form.

A full account of the investigation of photochromism in the spiropyran series will be published shortly.

[1] Y. Hirshberg, Compt. rend. **231**, 903 (1950).
[2] E. Fischer and Y. Hirshberg, J. Chem. Soc. **1952**, 4522.
[3] Y. Hirshberg and E. Fischer, J. Chem. Soc. **1953**, 629.
[4] Hirshberg, Frei, and Fischer, J. Chem. Soc. **1953** (to be published).